Environmental Chemistry for a Sustainable World 32

Nandita Dasgupta
Shivendu Ranjan
Eric Lichtfouse *Editors*

Environmental Nanotechnology Volume 4

Springer

Environmental Chemistry for a Sustainable World

Volume 32

Other Publications by the Editors

Books
Environmental Chemistry
http://www.springer.com/978-3-540-22860-8

Organic Contaminants in Riverine and Groundwater Systems
http://www.springer.com/978-3-540-31169-0

Sustainable Agriculture
Volume 1: http://www.springer.com/978-90-481-2665-1
Volume 2: http://www.springer.com/978-94-007-0393-3

Book series
Environmental Chemistry for a Sustainable World
http://www.springer.com/series/11480

Sustainable Agriculture Reviews
http://www.springer.com/series/8380

Journals
Environmental Chemistry Letters
http://www.springer.com/10311

More information about this series at http://www.springer.com/series/11480

Nandita Dasgupta • Shivendu Ranjan
Eric Lichtfouse
Editors

Environmental Nanotechnology Volume 4

Springer

Editors
Nandita Dasgupta
Department of Biotechnology
Institute of Engineering and Technology
Lucknow, Uttar Pradesh, India

Shivendu Ranjan
Faculty of Engineering and Built Environment
University of Johannesburg
Johannesburg, South Africa

Eric Lichtfouse
Aix Marseille University, CNRS, IRD
INRA, Coll France, CEREGE
Aix-en-Provence, France

ISSN 2213-7114 ISSN 2213-7122 (electronic)
Environmental Chemistry for a Sustainable World
ISBN 978-3-030-26667-7 ISBN 978-3-030-26668-4 (eBook)
https://doi.org/10.1007/978-3-030-26668-4

This Springer imprint is published by the registered company Springer Nature Switzerland AG.
The registered company address is: Gewerbestrasse 11, 6330 Cham, Switzerland

Contents

1 **Nanotechnology for Water and Wastewater Treatment Using Graphene Semiconductor Composite Materials** 1
Francis Opoku, Ephraim M. Kiarii, and Penny P. Govender

2 **Dyes Depollution of Water Using Porous TiO_2-Based Photocatalysts** 35
Bénédicte Lebeau, Florian Jonas, Pierrick Gaudin, Magali Bonne, and Jean-Luc Blin

3 **Application of Nanobiosensor for Food Safety Monitoring** 93
H. V. Raghu, Thulasiraman Parkunan, and N. Kumar

4 **Functional Properties of Nanoporous Membranes for the Desalination of Water** 131
Jananisree Ganesan, Madhangi Priyadharshini Gandhi, Maheswari Nagendran, Bin Li, Vaishakh Nair, and Padmanaban Velayudhaperumal Chellam

5 **Nanotechnology in Wheat Production and Protection** 165
Prem Lal Kashyap, Sudheer Kumar, Poonam Jasrotia, Devendra Pal Singh, and Gyanendra Pratap Singh

6 **Nanoparticles for New Pharmaceuticals: Metabolites from Actinobacteria** 195
Dávila Costa, José Sebastián, Cintia Mariana Romero, María Cecilia Rasuk, Julian Pereyra, Daiana Guerrero, and Analía Álvarez

7 **Titanium Oxide-Based Nanomaterials with Photocatalytic Applications in Environmental Chemistry** 215
Amel Boudjemaa and Santiago Gómez-Ruiz

8 Polymer Nanocomposites: Synthesis and Characterization 265
Anil Arya and A. L. Sharma

9 Application of Nanotechnology in Agriculture 317
Pragati Pramanik, P. Krishnan, Aniruddha Maity, N. Mridha, Anirban Mukherjee, and Vikas Rai

10 Nanomaterials Based Sensors for Air Pollution Control 349
Pradip Kar

Index 405

About the Editors

Nandita Dasgupta has completed her BTech and PhD from VIT University, Vellore, India. She is Elected Fellow (FBSS) of Bose Science Society. She has major working experience in micro-/nanoscience and is currently working as Assistant Professor at the Department of Biotechnology, Institute of Engineering and Technology, Lucknow, India. Earlier at LV Prasad Eye Institute, Bhubaneswar, India, she has worked on mesenchymal stem cell-derived exosomes for the treatment of uveitis. She has exposure of working at university, research institutes, and industries including VIT University, Vellore, Tamil Nadu, India; CSIR-Central Food Technological Research Institute, Mysore, India; Uttar Pradesh Drugs & Pharmaceutical Co. Ltd., Lucknow, India; and Indian Institute of Food Processing Technology (IIFPT), Thanjavur, Ministry of Food Processing Industries, Government of India. At IIFPT, Thanjavur, she was involved in a project funded by a leading pharmaceutical company, Dr. Reddy's Laboratories, and has successfully engineered micro-vehicles for model drug molecules. Her areas of interest include micro/nanomaterial fabrication and its applications in various fields – medicine, food, environment, agriculture and biomedicine.

She has published 13 edited books and 1 authored book with Springer, Switzerland. She is an Associate Editor of *Environmental Chemistry Letters* – a Springer journal with an impact factor of 3.2.

Shivendu Ranjan has completed his BTech and PhD in Biotechnology from VIT University, Vellore, India, and has expertise in nano(bio)technology. He is Elected Fellow of Bose Science Society (FBSS) and is currently working as Head of Research & Technology Development at E-Spin Nanotech Pvt. Ltd., SIDBI Center, Indian Institute of Technology, Kanpur, India. After joining E-Spin Nanotech, IIT, Kanpur, he has successfully developed prototypes for many products and three patents. He is also serving as a Senior Research Associate (Adjunct) at the Faculty of Engineering and Built Environment, University of Johannesburg, Johannesburg, South Africa. He is also mentoring Atal Innovation Centre, Bhubaneswar, Odisha, and giving his technical inputs to the center. Atal Innovation Centre is the part of Atal Innovation Mission of the NITI Aayog, Government of India. He is also Reviewer of Iran National Science Foundation (INSF), Tehran, Iran, and Jury at Venture Cup, Denmark, from the past three consecutive years. He had founded and drafted the concept for the first edition of the "VIT Bio Summit" in 2012, and the same has been continued till date by the university. He has worked in CSIR-CFTRI, Mysuru, India, as well as in UP Drugs and Pharmaceutical Co. Ltd., India, and IIFPT, Thanjavur, MoFPI, Government of India. At IIFPT, Thanjavur, he was involved in a project funded by a leading pharmaceutical company, Dr. Reddy's Laboratories, and has successfully engineered micro-vehicles for model drug molecules.

His research interests are multidisciplinary which includes micro-/nanobiotechnology, nano-toxicology, environmental nanotechnology, nanomedicine, and nanoemulsions. He is an Associate Editor of *Environmental Chemistry Letters* – a Springer journal with an impact factor of 3.2. He has published six edited books and one authored book with Springer, Switzerland, and many scientific articles in international peer-reviewed journals, and has authored many book chapters as well as review articles. He has also received several awards and recognitions from different national and international organizations.

Eric Lichtfouse PhD, born in 1960, is an Environmental Chemist working at the University of Aix-Marseille, France. He has invented carbon-13 dating. He is teaching scientific writing and communication and has published the book *Scientific Writing for Impact Factor Journals*, which includes a new tool – the micro article – to identify the novelty of research results. He is Founder and Chief Editor of scientific journals and series in environmental chemistry and agriculture. He founded the European Association of Chemistry and the Environment. He received the Analytical Chemistry Prize by the French Chemical Society, the Grand Prize of the Universities of Nancy and Metz, and a Journal Citation Award by the Essential Indicators.

Contributors

Analía Álvarez Planta Piloto de Procesos Industriales Microbiológicos (PROIMI-CONICET), Avenida Belgrano y Pasaje Caseros, Tucumán, Argentina
Facultad de Ciencias Naturales e Instituto Miguel Lillo, Universidad Nacional de Tucumán, Tucumán, Argentina

Anil Arya Department of Physical Sciences, Central University of Punjab, Bathinda, Punjab, India

Jean-Luc Blin Université de Lorraine, Laboratoire Lorrain de Chimie Moléculaire UMR CNRS 7053 L2CM, Vandoeuvre-lès-Nancy, France

Magali Bonne Université de Haute Alsace, CNRS, IS2M UMR 7361, Mulhouse, France
Université de Strasbourg, Strasbourg, France

Amel Boudjemaa Centre de Recherche Scientifique et Techniqueen Analyses Physico-Chimiques (CRAPC), Bou-Ismail, Tipaza, Algeria

Dávila Costa Planta Piloto de Procesos Industriales Microbiológicos (PROIMI-CONICET), Avenida Belgrano y Pasaje Caseros, Tucumán, Argentina

Madhangi Priyadharshini Gandhi Centre for Research, Department of Biotechnology, Kamaraj College of Engineering and Technology, Virudhunagar, Tamil Nadu, India

Jananisree Ganesan Centre for Research, Department of Biotechnology, Kamaraj College of Engineering and Technology, Virudhunagar, Tamil Nadu, India

Pierrick Gaudin Université de Lorraine, Laboratoire Lorrain de Chimie Moléculaire UMR CNRS 7053 L2CM, Vandoeuvre-lès-Nancy, France

Santiago Gómez-Ruiz Departamento de Biología y Geología, Física y Química Inorgánica, E.S.C.E.T. Universidad Rey Juan Carlos, Móstoles, Spain

Penny P. Govender Department of Applied Chemistry, University of Johannesburg, Johannesburg, South Africa

Daiana Guerrero Facultad de Bioquímica, Química y Farmacia, Universidad Nacional de Tucumán, Tucumán, Argentina

Poonam Jasrotia ICAR-Indian Institute of Wheat and Barley Research (IIWBR), Karnal, India

Florian Jonas Université de Lorraine, Laboratoire Lorrain de Chimie Moléculaire UMR CNRS 7053 L2CM, Vandoeuvre-lès-Nancy, France

Pradip Kar Department of Chemistry, Birla Institute of Technology, Mesra, Ranchi, Jharkhand, India

Prem Lal Kashyap ICAR-Indian Institute of Wheat and Barley Research (IIWBR), Karnal, India

Ephraim M. Kiarii Department of Applied Chemistry, University of Johannesburg, Johannesburg, South Africa

P. Krishnan Division of Agricultural Physics, ICAR-IARI, New Delhi, India

N. Kumar Dairy Microbiology Division/National Referral Centre, ICAR-National Dairy Research Institute, Karnal, India

Sudheer Kumar ICAR-Indian Institute of Wheat and Barley Research (IIWBR), Karnal, India

Bénédicte Lebeau Université de Haute Alsace, CNRS, IS2M UMR 7361, Mulhouse, France
Université de Strasbourg, Strasbourg, France

Bin Li Shandong Key Laboratory of Marine Ecology Restoration, Shandong Marine Resource and Environment Research Institute, Yantai, China

Aniruddha Maity Department of Soil and Crop Sciences, Texas A&M University, College Station, TX, USA
Division of Seed Technology, ICAR_IGFRI, Jhansi, Uttar Pradesh, India

N. Mridha Division of Agricultural Physics, ICAR-IARI, New Delhi, India

Anirban Mukherjee Division of Agricultural Extension, ICAR-IARI, New Delhi, India

Maheswari Nagendran Centre for Research, Department of Biotechnology, Kamaraj College of Engineering and Technology, Virudhunagar, Tamil Nadu, India

Vaishakh Nair Institute of Physical Chemistry, Polish Academy of Sciences, Poznań, Poland

Francis Opoku Department of Applied Chemistry, University of Johannesburg, Johannesburg, South Africa

Padmanaban Velayudhaperumal Chellam Centre for Research, Department of Biotechnology, Kamaraj College of Engineering and Technology, Virudhunagar, Tamil Nadu, India

Thulasiraman Parkunan Animal Physiology Division, ICAR-National Dairy Research Institute, Karnal, India

Julian Pereyra Facultad de Bioquímica, Química y Farmacia, Universidad Nacional de Tucumán, Tucumán, Argentina

Pragati Pramanik Division of Agricultural Physics, ICAR-IARI, New Delhi, India

H. V. Raghu Dairy Microbiology Division/National Referral Centre, ICAR-National Dairy Research Institute, Karnal, India

Vikas Rai Division of Agricultural Physics, ICAR-IARI, New Delhi, India

María Cecilia Rasuk Planta Piloto de Procesos Industriales Microbiológicos (PROIMI-CONICET), Avenida Belgrano y Pasaje Caseros, Tucumán, Argentina

Cintia Mariana Romero Planta Piloto de Procesos Industriales Microbiológicos (PROIMI-CONICET), Avenida Belgrano y Pasaje Caseros, Tucumán, Argentina
Facultad de Bioquímica, Química y Farmacia, Universidad Nacional de Tucumán, Tucumán, Argentina

José Sebastián Planta Piloto de Procesos Industriales Microbiológicos (PROIMI-CONICET), Avenida Belgrano y Pasaje Caseros, Tucumán, Argentina

A. L. Sharma Department of Physical Sciences, Central University of Punjab, Bathinda, Punjab, India

Devendra Pal Singh ICAR-Indian Institute of Wheat and Barley Research (IIWBR), Karnal, India

Gyanendra Pratap Singh ICAR-Indian Institute of Wheat and Barley Research (IIWBR), Karnal, India

Chapter 1
Nanotechnology for Water and Wastewater Treatment Using Graphene Semiconductor Composite Materials

Francis Opoku, Ephraim M. Kiarii, and Penny P. Govender

Contents

1.1 Introduction 2
1.2 Semiconductors Overview 3
1.2.1 Basic Principles and Mechanism for Photocatalytic Pollutant Removal 4
1.2.2 Fundamentals of Semiconductor-Based Photocatalyst Materials 6
1.3 Factors Controlling Photocatalytic Pollutant Removal 7
1.4 Characterization of Nanomaterials 7
1.4.1 Charge Carrier Transfer Kinetics 8
1.4.2 Band Structure and Light Absorption 8
1.4.3 Surface Reaction 9
1.5 Synthesis of Nanomaterials 9
1.6 Graphene 10
1.6.1 History of Graphene 10
1.6.2 Properties and Structure of Graphene 11
1.6.3 Synthesis of Graphene 11
1.6.4 Characterization of Graphene 12
1.6.5 Adsorption Mechanism of Graphene 13
1.7 Progress on Graphene and Semiconductor Composites 13
1.7.1 Graphene/Semiconductor Composites as Adsorbents 14
1.7.2 Graphene-Based Photocatalyst Materials for Water Treatment 16
1.8 Principles of Graphene/Semiconductor Composites 21
1.9 Conclusion 23
References 25

Abstract Recently, contamination of water resources has become a persistent problem to human due to advanced industrialization and rapid population growth. The major causes of water pollution are dye effluents from textile dyeing, pharmaceuticals, and paper printing industries. Therefore, cost-effective technologies, such as membrane filtration, adsorption, coagulation, microbial degradation, and chemical oxidation, are adopted for the removal of pollutants from water effluents. Graphene-based materials have gained much consideration as a novel material for

F. Opoku · E. M. Kiarii · P. P. Govender (✉)
Department of Applied Chemistry, University of Johannesburg, Johannesburg, South Africa
e-mail: pennyg@uj.ac.za

N. Dasgupta et al. (eds.), *Environmental Nanotechnology Volume 4*, Environmental Chemistry for a Sustainable World 32, https://doi.org/10.1007/978-3-030-26668-4_1

addressing the global environmental issues due their high mechanical strength, excellent electron mobility, large surface area, and high thermal conductivity. Semiconductor photocatalysis has received much interest as a promising technology for water treatment owing to its cost-effective, easy operation, high-efficiency, and convenience. Therefore, the design and fabrication of graphene support with semiconductor photocatalyst are promising as multifunctional catalysts. This book chapter evaluates the recent design of graphene-based materials as adsorbent and photocatalytic materials in environmental remediation. The theoretical outcomes in water treatment using graphene/semiconductor composites are also summarized. A brief outlook on the challenges and new strategies is provided for developing effective water/wastewater treatment techniques using graphene-based materials.

Keywords Nanotechnology · Water treatments · Photocatalyst · Semiconductor · Composites

1.1 Introduction

The release of municipal, agricultural, industrial, and domestic waste effluents into water resources has certainly given rise to a lot of toxic contaminants (Marahel et al. 2015). Heavy metal ions and dyes have attracted serious concern owing to their non-biodegradable, high toxicity and tend to accumulate in the tissues of living organisms (Fu and Wang 2011a). The highly toxic and non-biodegradable of most dye molecules is due to the aromatic ring in their structure (Hou et al. 2012). Furthermore, dyes add adverse color to water resources, which prevent the penetration of sunlight to retard photosynthetic reactions, thereby affecting aquatic life (Marahel et al. 2015). Therefore, the recycling and reuse of wastewater effluents are necessary to enhance the limited fresh water supply (Qu and Fan 2010). Hence, it is essential to minimize dyes and heavy metal ions to acceptable limits before being discharged to water bodies. During the past few decades, several techniques have been realized to design feasible wastewater/water treatment technologies (Gupta et al. 2012). For example, biological treatments are designed to successfully remove various forms of pollutants from water/wastewater resources; nonetheless, this technique also usually produce secondary pollution (Ganzenko et al. 2014), as well as health-threatening bacteria, and soluble refractory organic compounds, which are difficult to remove (Ray et al. 2013). Therefore, developing green, nondestructive, and sustainable technologies for water/wastewater treatment is of much importance.

As a green, nondestructive, and promising technology, heterogeneous semiconductor photocatalysis has recently received broad interest for wastewater/water treatment owing to its effectiveness to remove harmful bacteria and pollutants (Yang et al. 2010). Mostly, the semiconductors can be photoactivated by a photon, which has an energy equal to or greater than its band gap (E_g) (Fageria et al. 2014). As a renewable and safe energy source, the solar energy is the best energy supply

needed for the activation process (Chang 2014). To effectively use the natural sunlight to handle water pollution problems, it is of significant interest to discover new visible light-driven photocatalysts.

Since the initial study by Fujishima and Honda (Fujishima and Honda 1972), several semiconductor materials, such as metal-free semiconductors (Cao et al. 2015), plasmonic metals (Sun et al. 2015), metal oxides (Li et al. 2015), metal sulfides (Zhang and Guo 2013), and metal (oxy)nitrides (Hitoki et al. 2002), are available for multifunctional and diversified applications (Wang et al. 2013d). Nevertheless, some of these semiconductor photocatalysts cannot completely satisfy the practical applications due to their short lifetime of photogenerated charge carriers and wide band gap (Li et al. 2015). Therefore, it is significant to design highly stable and efficient photocatalysts with visible light-driven activity by optimizing the existing approaches by incorporating them with nanocarbon (Zhou et al. 2014b). Recently, activated carbons with a high surface area are considered as a conventional adsorbent for water purification (Bhatnagar et al. 2013). Nonetheless, the column fouling and high production cost are the major disadvantages of using activated carbons as an adsorbent. In the last decade, graphene has been promising adsorbents for water treatment owing to its fast adsorption kinetics, excellent electronic property, large surface area, and low-cost compared to the well-developed activated carbons (McAllister et al. 2007; Xu et al. 2013b; Zhu et al. 2011). In this book chapter, much effort has been made to comprehensively review the properties, synthesis, characterization techniques, and application of graphene/semiconductor composites for the removal of water pollutants, such as organic molecules, waterborne pathogens, and heavy metal ions. The theoretical outcomes in water treatment using graphene/semiconductor composites are also summarized. A brief outlook on the challenges and new strategies is provided for developing effective water/wastewater treatment techniques using graphene-based materials.

1.2 Semiconductors Overview

A semiconductor is a crystalline structure, which has a few free electrons at room temperature (Rahman 2015). Semiconductors are the basic building block of modern electronics, such as transistors, solar cells, light-emitting diodes, analog, and digital integrated circuits (Rahman 2015). The semiconductor properties depend on the quantum physics to explain the migration of electron–hole pairs in a lattice and crystal structure (Feynman et al. 2013). A semiconductor has an electrical conductivity property between that of an insulator (e.g., glass) and a conductor (e.g., copper) (Feynman et al. 2013). Semiconductor devices show beneficial properties, such as sensitivity to heat/light and variable resistance (Rahman 2015). Semiconductors can be used for energy conversion, switching, and amplification since their electrical properties can be tuned by applying electrical fields or doping. An *n-type* semiconductor is a doped semiconductor containing free electrons, while *p-type* is a semiconductor containing free holes. Semiconductor heterogeneous photocatalysis is

mostly suited for the degradation of water/wastewater containing low concentrations of pollutants (Schneider et al. 2014). For water/wastewater purification, the oxidizing radicals can degrade the pollutants by reduction and oxidation reactions (Friedmann et al. 2010). The inherent electronic band structure of semiconductors is mostly characterized by its valence band (VB), conduction band (CB), band-gap energy, and Fermi level (Sze 2008). The VB is formed by the interactions of the highest occupied molecular orbital, while the CB is formed by the interactions of the lowest unoccupied molecular orbital. The band gap is the energy difference between the conduction band minimum (CBM) and the valence band maximum (VBM). The band structure is very important as it determines the redox ability and visible light-driven activity of semiconductor-based photocatalyst materials.

1.2.1 Basic Principles and Mechanism for Photocatalytic Pollutant Removal

A typical photocatalytic system comprises of two components: a catalytically active site and light-harvesting center to aid the pollutant degradation process (Gao et al. 2017). To enhance the activity of both components, their interactions that depend on the charge kinetics upon photoexcitation and behaviors in a photocatalytic system are of significant interest. The light-harvesting center in a heterogeneous photocatalytic system is mostly a semiconductor. The series of reductive and oxidative reactions that occur during the photocatalytic process has been widely proposed.

Under properly simulated light irradiation with photon energy greater than or equal to the semiconductor band-gap energy, electrons (e^-) and holes (h^+) are generated as shown in Eq. (1.1) and Fig. 1.1.

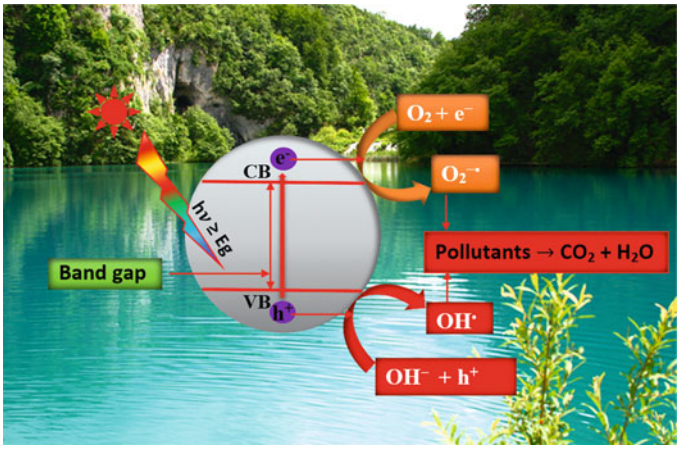

Fig. 1.1 Photodegradation mechanism of organic pollutants in water resources

$$\text{Photocatalyst} + h\nu \rightarrow h^+ + e^- \tag{1.1}$$

At the semiconductor surface, electrons then migrate from the valence band to the conduction band, forming holes (h^+) in the valence band. The three main active species that usually partake in the photocatalytic reactions are the superoxide radical anion ($O_2^{-\bullet}$), hydroxyl ($HO^\bullet$) radical, and h^+ with the $HO^\bullet$ radical as the main oxidant involved in the photodegradation of contaminant in an aqueous medium. The thermodynamics of the photocatalytic reduction and oxidation reactions are determined using the band edge positions of a given photocatalyst. Therefore, during the photodegradation reaction, it is essential to consider the reduction and oxidation potentials of the substrate and several other intermediate reactions that will occur. The electrons can combine with the oxygen (O_2) molecule to produce the $O_2^{-\bullet}$, which further forms the hydroxyl radicals only if the reaction is thermodynamically favorable (Eqs. 1.2, 1.3, and 1.5).

$$e^- + O_2 \rightarrow O_2^{-\bullet} \tag{1.2}$$

$$O_2^{-\bullet} + H^+ \rightarrow HOO^\bullet \tag{1.3}$$

$$2HOO^\bullet \rightarrow O_2 + H_2O_2 \tag{1.4}$$

$$H_2O_2 + h\nu \rightarrow 2HO^\bullet \tag{1.5}$$

Concurrently, the h^+ then interacts with water (H_2O) or hydroxyl ion (OH^-) to generate the $HO^\bullet$ radicals (Eqs. 1.6 and 1.7).

$$h^+ + HO^- \rightarrow HO^\bullet \tag{1.6}$$

$$h^+ + H_2O \rightarrow HO^\bullet + H^+ \tag{1.7}$$

The resulting $HO^\bullet$ radical serves as a strong oxidizing agent, which then combine with the organic pollutants in the water matrices to form an intermediate product, which then produces CO_2, H_2O, and other products (Eq. 1.8).

$$\text{Pollutant} + HO^\bullet \rightarrow CO_2 + H_2O + \text{Degradation product(s)} \tag{1.8}$$

Furthermore, depending on the oxidation conditions and catalyst type, the photogenerated holes are broadly regarded as an oxidant to directly degrade the organic pollutants (Chong et al. 2010). Thus, in the absence of hole or electron scavenger, the photoinduced electrons can recombine with holes after their generation. Therefore, the presence of specific scavengers is essential for restraining the charge recombination rate to enhance the photocatalytic efficiency.

To develop a semiconductor photocatalyst material capable of utilizing a wider part of the solar energy effectively, the semiconductor must have a (1) smaller band gap to absorb a broad region of the electromagnetic spectrum, (2) a favorable VB edge position for the generation of h^+ and hydroxyl radicals (Casbeer et al. 2012), (3) high stability, and (4) efficient charge separation and migration (Qu and Duan 2013).

1.2.2 Fundamentals of Semiconductor-Based Photocatalyst Materials

Thermodynamics of Heterogeneous Semiconductor Photocatalyst

Thermodynamically, the relative energy bands of graphene and semiconductors play a key role in attaining enhanced photocatalytic performance. The reduction and oxidation reactions at the semiconductor surface are driven by the photoinduced charge carriers only if their potentials straddle the CB and the VB edge positions. Thus, to achieve a high photodegradation of a given pollutant, the photoinduced holes and electrons must have a favorable oxidation and reduction ability to combine with the species adsorbed on the semiconductor surface to generate free radicals, which can act as reactive species during the photodegradation process (Chen et al. 2010). Therefore, the more positive valence band edges are helpful for an oxidation reaction, while the more negative conduction band edges are favorable for a reduction reaction. The potentials of selected species are shown in Table 1.1 (Bard et al. 1985).

Kinetics of Heterogeneous Semiconductor Photocatalyst

Generally, the thermodynamic properties, such as narrow band gap and suitable band edge positions, do not allow high performance of the semiconductor photocatalysts since the overall photocatalytic activity is affected by other factors. These include interface/surface morphology, structure at nano- and microlevels, crystallinity, composition, and adsorption capacity of the materials (Li et al. 2015). The complicated surface reaction kinetics and charge carrier dynamics in the multistep process of photocatalysis result in a low quantum yield (Pasternak and Paz 2013). The underlying mechanism of photocatalysis comprises (Pasternak and Paz 2013) (1) light harvesting, (2) charge separation, (3) charge migration/recombination, and (4) charge utilization. Kinetically, the rapid recombination rate of charge carriers is a limiting factor in achieving enhanced photocatalytic activity (Li et al.

Table 1.1 Standard redox potential for selected active species involved in the photodegradation of pollutants (Bard et al. 1985)

Reaction	E^0 (V vs. normal hydrogen electrode at pH = 0)
$e^- + O_2 \rightarrow O_2^{-\bullet}$	−0.330
$2e^- + O_2 + H_2O \rightarrow HO_2^- + OH^-$	−0.065
$e^- + O_2 + H^+ \rightarrow HO_2^\bullet$	−0.046
$e^- + HO_2^- + H_2O \rightarrow HO^\bullet + OH^-$	0.184
$e^- + O_2^- + H_2O \rightarrow HO_2^- + OH^-$	0.200
$2e^- + O_2 + 2H^+ \rightarrow H_2O_2$	0.695
$4h^+ + 2H_2O \rightarrow O_2 + 4H^+$	1.229
$h^+ + OH^- \rightarrow HO^\bullet$	2.690
$4h^+ + 4OH^- \rightarrow O_2 + 2H_2O$	0.401

2015). Moreover, the agglomeration of nanostructured particles and the low specific surface area not only increases the diffusion barriers of the reagents but also decreases the surface oxidation and reduction kinetics, which reduces the photocatalytic performance. Thus, several factors, such as surface reaction kinetics, charge carrier kinetics, diffusion, and adsorption, are kinetically significant in designing highly efficient photocatalyst materials.

1.3 Factors Controlling Photocatalytic Pollutant Removal

A major concern with the heterogeneous photocatalytic process for organic synthesis by oxidation is the highly oxidizing environment and non-selectivity, with products being lost due to complete mineralization. Although semiconductor photocatalysts have potential applications, they still have unwanted disadvantages, such as the wide band gap that limits wider use of solar energy, large interfacial area that induces slow charge carrier migration, nanoscale features, and single phase that causes fast recombination of photogenerated charge carriers. Their effectiveness to the photocatalytic reaction is influenced by factors (Friedmann et al. 2016), such as the excitation of charge carriers from the bulk to the surface, as well as the separation/recombination of charge carriers that occurs in the bulk or at the surface. Besides the band structures and diffusion kinetics, other factors, such as surface properties, crystallinity, morphological architecture, and material choice, must be considered when designing stable and efficient visible light-driven photocatalytic materials (Mori and Yamashita 2010). Thus, choosing the right semiconductor is quite significant, because it determines the visible light photocatalytic performance (Yan et al. 2014). Moreover, the right morphological architecture between the redox reaction center and the photogenerated charge carriers junction can effectively enhance the separation and migration of charge carrier (Yan et al. 2014). The high degree of crystallinity with crystal defects will minimize the recombination rate at the interface, thereby enhancing the efficiency of the photoinduced charge carriers to partake in the redox reaction (Gu et al. 2014). The surface area, which relies on the geometrical shape and porosity of the photocatalysts, influences the photocatalytic performance (Zhu et al. 2010). The adsorption capacity of the semiconductor photocatalysts toward pollutant degradation increases if there are more atoms present on the surface. The absence of well-designed porous interconnected network assembly at larger length scales may unfavorably affect the overall photocatalytic performance.

1.4 Characterization of Nanomaterials

To show the behavior of charge carriers in the photocatalytic material, it is vital to analyze the charge kinetic via several characterization techniques with emphasis on spectroscopic techniques. Currently, several characterization techniques have been

developed to check the charge kinetics behavior at the photocatalysis process. Explicitly, the photogenerated charge carriers are examined by characterizing the band structure and light absorption. Based on charge separation and migration, the characterization techniques are mostly concentrated on charge dynamics (photoexcited charge carrier separation and lifetime efficiency). Moreover, several advanced techniques have been widely designed to check surface reactions, such as the molecular desorption/adsorption, reaction paths, reactant dissociation, and intermediate product.

1.4.1 Charge Carrier Transfer Kinetics

Besides charge transfer kinetics, the charge separation, migration, and recombination processes normally occur in an ultra-small timescale. The transient absorption spectroscopy, which measures the signals for charges at the ground/excited state, and the recombination rate of photogenerated charge carriers, has been broadly utilized in a photocatalytic mechanism study (Berera et al. 2009). However, transient absorption spectroscopy cannot fully reflect the photocatalytic process under simulated solar light irradiation owing to the robust pulsed laser used as excitation sources (Berera et al. 2009). Therefore, photoelectrochemical measurements have been used to check the charge kinetics behavior and average dynamic parameters of a photocatalytic system (Sato 1998). Moreover, the recombination of photogenerated carriers is measured by the time-resolved/steady-state photoluminescence spectroscopy (Anpo and Kamat 2010). Generally, the low intensity in the steady-state photoluminescence spectroscopy shows a low chance of recombination rate of charge carrier. For time-resolved photoluminescence spectroscopy, a rapid photoluminescence degeneration with a short lifetime shows a low recombination of electrons with holes.

1.4.2 Band Structure and Light Absorption

Ultraviolet-visible diffuse reflectance spectroscopy is used to quantify the optical band gaps of semiconductors and light absorption of semiconductor photocatalyst materials. In contrast to ultraviolet-visible spectroscopy, the synchrotron-based soft X-ray spectroscopy is used to measure the electronic structure of complex materials, wherein the VBM and CBM are measured by the X-ray emission and absorption spectroscopy, respectively (Kapilashrami et al. 2014). Synchrotron radiation-based X-ray spectroscopy provides the ability to analyze the band structure of photocatalyst materials, while modifying the wavelength of the incident light allows the study of element-selective photocatalyst materials (Vayssieres 2010).

1.4.3 Surface Reaction

Upon obtaining the charge transfer kinetics and band structures, an in-depth insight of charge dynamics in the photocatalytic reaction on the semiconductor surface is vital for completing the photocatalyst design (Osgood 2006). To measure the surface reaction, several characterization techniques have been established as powerful tools to detect the reaction pathways, products, and intermediate, as well as the activation and adsorption sites of the redox reaction. Infrared (IR) spectroscopy is widely used to check surface reactions. Explicitly, the Fourier transform IR spectroscopy is used to investigate the nature of adsorbed species and the surface properties of photocatalyst systems (Chen et al. 2007). Separately, time-resolved infrared spectroscopy can precisely measure the charge kinetics of the adsorbed species (Chen et al. 2007). Thermal desorption spectroscopy (TDS) is used to measure the thermodynamic and kinetic reaction of desorption and adsorption processes on the photocatalyst surface (Yuan et al. 2013). The defect sites on the photocatalyst surface can be measured by electron spin resonance spectroscopy, X-ray absorption spectroscopy, X-ray absorption fine structure, and positron annihilation spectroscopy (Bai et al. 2015).

1.5 Synthesis of Nanomaterials

Up to now, several semiconductor heterostructures have been successfully designed and synthesized. Mostly, the three-dimensional nano−/microcomposites are synthesized via the self-assembly of nanosized building blocks, such as nanowires, nanosheets, and nanoparticles (Li et al. 2016). Nonetheless, it is extremely challenging to design and synthesize several types of photocatalyst materials with controlled morphologies. Therefore, it is essential to design a simple and low-cost technique to prepare photocatalyst materials with hierarchical and high crystallinity nanostructures. Up to now, hierarchical semiconductor photocatalysts are prepared via template-free methods (chemically induced self-transformation, self-template strategy, and in situ template-free assembly), template method (in situ template-sacrificial dissolution and two-step template method), and post-synthetic treatment method (Li et al. 2016). The template method is one of the most often used technique to fabricate hierarchical nanostructured photocatalysts due to its good reproducibility, abundant types of physical templates, and large-scale synthesis (Liu et al. 2013b). The in situ template-sacrificial dissolution technique has drawbacks, such as the high cost of template, the presence of heterogeneous impurities, tedious synthetic procedures, and sudden morphological changes during template removal (Li et al. 2016). All these limit the large-scale synthesis of photocatalyst materials (Lou et al. 2006). The self-template method is among the most effective and simple techniques to synthesize several photocatalyst materials (Cai et al. 2009). The

chemically induced self-transformation (Qi et al. 2016) method has been used to synthesize several hierarchical hollow microspheres, such as $CaCO_3$, TiO_2, Al_2O_3, SnO_2, and WO_3. The mechanism of the in situ template-free assembly differs from the chemically induced self-transformation (Li et al. 2016). The chemically induced self-transformation involves the creation of hollow interiors through chemical etching of the primary particles, while the in situ template-free assembly involves the self-assembly of nanosized building blocks around the nuclei (Yu et al. 2006).

1.6 Graphene

Nanomaterials with unique properties can be used to design new technologies, as well as improving the performance of existing processes due to their nanoscale dimensions. Nanomaterials have been used to solve major environmental issues, such as contaminant sensing, energy production, and water treatment (Qu et al. 2013). The latest nanomaterials to capture the interest of researchers is graphene (GR), which is a two-dimensional (2D) layer of carbon (C) atoms arranged in a honeycomb crystalline structure (Geim 2009). The interest is due to its unique and notably exceptionally large surface area, physicochemical properties, excellent mechanical strength, thermal and electron mobility.

1.6.1 History of Graphene

Graphene is a thin layer hexagonal crystal structure comprising a 2D monolayer planar sheet of sp^2-bonded C atoms. Graphene is the building block of graphite with the π-stacking sheets holding the lamellar graphite structure (Hontoria-Lucas et al. 1995). The interlayer spacing between the sheets was recorded at 3.34 Å (Hontoria-Lucas et al. 1995). Through a micromechanical cleavage route, graphene was initially synthesized from graphite (Novoselov et al. 2004). This method permits easy fabrication of high-quality GR crystallites, which can lead to massive experimental process (Katsnelson 2007). Under ultrahigh vacuum (<1010 torr) and elevated temperatures, monolayer flakes of carbon with graphene structure were obtained via the epitaxial sublimation of silicon from silicon carbide (SiC) monolayer (Van Bommel et al. 1975). The term "graphene" was described as a single-atom carbon sheet by Boehm et al. (1986). This graphene sheet showed a transparent, flat, and monolayer sheetlike honeycomb structure comprising a single layer of sp^2-bonded C atoms with a C–C bond length of 1.42 Å. The 2D crystals of graphene were thermodynamically unstable under ambient conditions (Yusuf et al. 2015). However, Novoselov et al. (2004) successfully isolated and characterized a mechanically exfoliated graphene monolayer.

1.6.2 Properties and Structure of Graphene

Graphene is a zero band-gap semiconductor, and its unique electronic properties show a low absorption ratio of 2.3% of light and an unpredictably high cloudiness of atomic monolayer (Kuzmenko et al. 2008). Fundamentally, graphene shows fascinating properties, such as high charge carrier mobility (100,000 $cm^2\ V^{-1}\ s^{-1}$), large surface area (2630 $m^2\ g^{-1}$), Young's modulus (~1100 GPa), high thermal conductivity (2000–5000 $W\ m\ K^{-1}$), large electric current density ($10^8\ A\ cm^{-2}$), and superb mechanical strength (2.4 ± 0.4 TPa) (Upadhyay et al. 2014). These unique properties makes graphene an interesting material for several applications in liquid crystal devices, solar cells, capacitors, sensors, batteries, and water treatment (Upadhyay et al. 2014). Graphene is the basic building blocks for several C allotropes, such as fullerenes (0 D), graphite (3 D), and carbon nanotubes (1 D) (Fu and Wang 2011a). Two sub-lattices of C atoms in the graphene lattice are linked with the s and p orbitals of each C atom in the lattice, and this contributes to the electron delocalization network. Graphene's structure is defect-free since similar types of atoms are bonded by flexible and strong bonds, which contributes to the extraordinary properties of graphene.

1.6.3 Synthesis of Graphene

Using a Scotch tape, graphene was initially prepared using the manual mechanical cleavage of graphite (Novoselov et al. 2004), and since then several synthetic techniques have been reported (Allen et al. 2009). These techniques are the bottom-up and top-down methods (Allen et al. 2009). The bottom-up method is the direct fabrication of graphene from molecules or atoms through chemical reactions. Some typical examples of the bottom-up methods includes chemical vapor deposition (CVD) on the surface of metal foil, solvothermal, organic synthesis, and epitaxial growth on single crystals of silicon carbide (Emtsev et al. 2009). However, the bottom-up approaches are not broadly used owing to their high cost and complexity of the substrates. Currently, high-quality GR sheet with a distinct molecular structure has been fabricated by the top-down approaches, such as electrochemical synthesis (Guo et al. 2009), unzipping of carbon nanotubes (Jiao et al. 2010), chemical exfoliation of graphite (Park et al. 2009), arc discharge (Subrahmanyam et al. 2009), micromechanical cleavage (Schedin et al. 2007), liquid phase exfoliation of graphite (Zhou et al. 2014a), thermal exfoliation (McAllister et al. 2007), electrostatic deposition (Tung et al. 2009), and chemical reduction of graphene oxides (Compton and Nguyen 2010). The synthesis techniques of graphene for environmental remediation application must be simple, efficient on a large scale, and cost-effective. However, not all these techniques are possible for water/wastewater treatment. Up to now, there have been a few reports on the fabrication of pristine graphene for water/wastewater treatment. Through a facial

liquid phase exfoliation, Li et al. (2011b) synthesized a monolayer graphene sheet from wormlike graphite. The as-synthesized graphene was utilized to adsorb fluoride from aqueous solution after 1-methyl-2-pyrrolidinone was removed at 200 °C. The epitaxial growth technique of graphene can be realized by heating a honeycomb crystals of SiC at 2400 K (McAllister et al. 2007). For example, the vacuum graphitization technique was used to fabricate epitaxial graphene via the thermal decomposition of SiC at 2400 K (Berger et al. 2006). The mechanical exfoliation method was the first method used for the synthesis of graphene (Novoselov et al. 2004). In this method, an extremely oriented pyrolytic graphite was entrenched in photoresist materials, and the graphene layers were peeled off using adhesive tape. Recently, the Hummers' method/modified Hummers' method is found as the most highly and commonly used technique (Hummers and Offeman 1958). In this method graphite is oxidized into graphene oxide using strong acids (e.g., $KMnO_4$ and H_2SO_4) to form a stable graphene oxide solution dispersed in water (Some et al. 2012), which are then reduced using hydrazine (Li et al. 2008). The CVD method was used to fabricate graphene using a metal substrate under high temperature and ultrahigh vacuum (Tung et al. 2009). In this process, graphene was deposited on the metal substrate surface, such as Cu and Ni with a vapor-rich hydrocarbon heated at ~1073 K. Liquid-phase exfoliation of graphite oxide is among the most practical methods for industrial fabrication of GR owing to its low-cost and scalability (Zhou et al. 2014a). This process encompasses the sonication of graphite oxide/graphite powders in aqueous solution.

1.6.4 Characterization of Graphene

The identification of graphene monolayers is a major issue faced during the characterization of graphene. Up to now, several techniques including the X-ray diffraction, scanning electron microscopy, thermogravimetric analysis, Raman spectroscopy, Fourier transform infrared spectroscopy, transmission electron microscopy, X-ray photoelectron spectroscopy, and atomic force microscopy have been used to characterize graphene. Since it is difficult for a single technique to offer all the essential information, there is the need to combine two or more tools to precisely characterize the intrinsic properties, texture, morphology, and crystal structure of graphene (Guo and Dong 2011). Transmission electron microscopy (Hernandez et al. 2008) images was used to measure the thickness and the number of graphene sheets. Raman spectroscopy analysis is a nondestructive technique, which uses monochromatic laser excitation to investigate the structure of graphene (Machado and Serp 2012). There are three response peaks (D peak = ~1350 cm^{-1}, 2D peak ~2700 cm^{-1}, and G peak = ~1580 cm^{-1}) equal to different phonon/vibrational modes in graphene (Ferrari et al. 2006). The D peak appears strongly in disorderly graphite, which indicates the degree of graphene disorder. Based on the position, shape, and width of the 2D peak, the quality and number of graphene layers can be investigated using Raman spectroscopy (Ferrari et al. 2006). The crystalline structure of graphene sheets is determined

using X-ray diffraction. The diffraction peak of graphene is linked to the A–B stacking order, which correlated with the [002] reflection (Machado and Serp 2012). The [002] reflection occurred at $2\theta \approx 26^\circ$ for pristine graphite, and after oxidation, the layers were shifted to $2\theta \approx 11^\circ$ (Machado and Serp 2012). The number of layers is evaluated using the line broadening by the Lorentzian fitting of the [002] reflection and the Scherrer equation (Rao et al. 2009). Currently, atomic force microscopy is among the most effective technique used to detect few-layer and single-layer crystals (Blake et al. 2007). Therefore, the atomic force microscopy can measure elastic, magnetic, electrical, and mechanical properties of graphene (Singh et al. 2011). The scanning electron microscopy images are used to determine the presence of defects and morphology of graphene, as well as acquiring atomically resolved images of graphene sheets (Machado and Serp 2012).

1.6.5 Adsorption Mechanism of Graphene

The adsorption properties of graphene are influenced by surface properties, such as distribution, surface area, and pore size (Yusuf et al. 2015). Thus, the surface area largely influences the adsorption of adsorbate on the adsorbent since the surface area per unit volume of the adsorbate determines the adsorption ability of the adsorbent (Yusuf et al. 2015). During the adsorption process, a larger surface induces a large surface area of active sites exposed to the adsorbate (Yusuf et al. 2015). Hence, an adsorbent with a small grain size distribution and high porosity increases the adsorption ability and the total surface area (Mohanty et al. 2008). However, graphene exhibited no porosity and an ultrahigh specific surface. The adsorption capacity of graphene can be enhanced by combining with other porous materials (Zhang et al. 2011a).

1.7 Progress on Graphene and Semiconductor Composites

There has been much interest in the fabrication of graphene/semiconductor composites due to the variety of functional semiconductor nanoparticles (Lü et al. 2012). During the pollutant removal process, graphene can often tune the properties of semiconductors. In particular, magnetic Fe_3O_4 nanoparticles have been used as magnetic separation in large-scale industrial application and to address several problems related to gravitational separation, filtration, and centrifugation of graphene. Coupling graphene with a semiconductor is an attractive material for photocatalytic applications since graphene has a zero band gap, high conductivity of electron in storage, and migration of electrons. The nanoparticles on the graphene surface prevent the aggregation of GR sheets to some degree in the composites, which further increases the exposed area for the elimination of pollutants from water/wastewater resources.

1.7.1 Graphene/Semiconductor Composites as Adsorbents

Rapid population growth, industrial, and agricultural activities have given rise to a large number of contaminants being released into the environment, which represent a major public health and environmental concern (Lubchenco 1998). Heavy metal pollutants from municipal waste, industrial waste, corrosion of pipes, and soldered joints are common contaminants that can unpleasantly enter drinking water sources and aquatic environments (USEPA 2014). Therefore, much effort has been made to develop a technology, which can effectively remove pollutants from water. Among them, adsorption is the most effective technology for water/wastewater treatment owing to its inexpensive, low-cost, and efficacy for pollutant removal from aquatic environments (Ali and Gupta 2006). Adsorption involves the capturing of pollutants (adsorbate) by nanomaterials (adsorbents) through a physicochemical interaction (Dąbrowski 2001). Ideally, graphene with a large surface area (2630 $m^2\ g^{-1}$) makes it an attractive adsorbent for the decomposition of pollutants (Ramesha et al. 2011) compared to the conventional adsorbents, such as mesoporous and activated carbons. Moreover, the large π–π conjugation on the surface of graphene could be used for the adsorption of different reactants during the photocatalytic reaction. Moreover, the semiconductor has a large surface-to-volume ratio. Therefore, coupling a graphene sheet with a semiconductor can effectively improve the adsorption capacity and surface area of the composite. Graphene/magnetic nanoparticle composites exhibited enhanced adsorption activity and improved the number of binding sites for heavy metal ions and the surface area of the nanoparticle (Zhu et al. 2011). This is due to the combined effect of adsorption sites on the graphene layer and the metal complexation on the nanoparticles (Zhu et al. 2011). Among the magnetic semiconductor, Fe_3O_4 is the most used semiconductor for water purification owing to its extraordinary biocompatibility (Chandra et al. 2010). Higher conductivity and surface area influence the deionization activity of semiconductors (Wang et al. 2013a). Fortunately, graphene shows both properties, which makes it suitable for the deionization of semiconductors (Zhang et al. 2012a). Wang et al. (2012a) observed a reduction in conductivity from 86.9 to 10.2 μS cm^{-1} after 120 min when graphene was used as an electrode for the deionization of sodium chloride solution. The magnetic graphene/Fe_3O_4 nanocomposites, which was fabricated using a facile one-pot technique, was utilized as an adsorbent to eliminate rhodamine B (RhB) dye from wastewater (Lü et al. 2014). The as-fabricated nanocomposite displays high ability to extract organic pollutants. Thus, the magnetic graphene/Fe_3O_4 adsorbent allows efficient separation of pollutants from wastewater. Zhu et al. (2011) revealed that a complete removal of Cr(IV) by the magnetic graphene composite in acidic pH ranges from 1 to 3. Similarly, a high acidic pH solution can also inhibit the adsorption ability of metal ions by the composites (Alyüz and Veli 2009). The Fe_3O_4/graphene composite with the covalent binding between graphene and Fe_3O_4 showed high adsorption capacity of 190.14 and 140.79 mg g^{-1} for methylene blue (MB) and neutral red dyes, respectively (He et al. 2010). Through a chemical reduction process, a magnetic Fe_3O_4/graphene

composite was fabricated and used to remove Congo red and MB dyes from wastewater media (Yao et al. 2012). The magnetic iron composite showed enhanced adsorption capacities of 33.66 and 45.27 mg g^{-1} for Congo red and MB dyes, respectively. Thus, the composite had a high potential as an efficient adsorbent for removing dyes from aqueous solution. A magnetic nanocomposite was reported to have a high adsorption of fuchsine dye with about 96% of fuchsine dye adsorbed (Wang et al. 2011a). This enhanced adsorption was due to the van der Waals interactions between the honeycomb packed C atoms and the aromatic backbone of fuchsine dye molecule, as well as the delocalized π-electron of the graphene sheet and the π–π stacking interactions of the aromatic part of fuchsine dye. A magnetic $CoFe_2O_4$/graphene composite was prepared by the hydrothermal treatment of exfoliated GR monolayers and inorganic salts (Li et al. 2011a). The as-prepared nanocomposites showed adsorption high capacity (71.54 mg g^{-1}) to effectively remove methyl orange (MO) dye. The SiO_2/graphene composite, which was fabricated via a two-step technique, exhibited a high adsorption capacity (113.6 mg g^{-1}) toward Pb^{2+} ion removal with reference to divalent ions, such as Cd^{2+}, Ni^{2+}, Co^{2+}, Cu^{2+}, and Cr^{3+} (Hao et al. 2012). Nonetheless, the adsorption capacity of SiO_2/graphene composite was suppressed by the addition of KNO_3. The effect of hydrothermal treatment period on the adsorption performance of TiO_2/graphene composite was investigated by Lee and Yang (2012) for the effective elimination of Pb^{2+}, Cd^{2+}, and Zn^{2+} ions. They found that the exposure area of the composite was improved from 88.97 to 132.74 m^2 g^{-1} and the adsorption capacity from 45.0 ± 3.8 to 65.6 ± 2.7 mg g^{-1} for Pb^{2+}, 44.8 ± 3.4 to 88.9 ± 3.3 mg g^{-1} for Zn^{2+}, and 65.1 ± 4.4 to 72.8 ± 1.6 mg g^{-1} for Cd^{2+} upon prolonging the hydrothermal treatment period from 6 to 12 h. A graphene nanosheet/Fe_3O_4 composite, which was synthesized by a facile one-step solvothermal route, showed fast adsorption rates and excellent removal capacity of MB dye in water (Ai et al. 2011). This enhancement was ascribed to the π–π interaction between the aromatic ring of graphene and the MB dye, as well as electrostatic attraction between the cationic MB and the negative surface of oxygen-containing groups. This study shows that the as-synthesized composite could be used as efficient adsorbents for water purification. A detailed investigation of the δ-MnO_2/graphene composite before and after adsorption of lead and copper ions was performed by Ren et al. (2012), and they found that the metal ions not only interpolate in the interlayer of δ-MnO_2 but also get adsorbed on the composite surface. Moreover, the δ-MnO_2/graphene composite displayed high cycling, and the as-prepared composite can be utilized for at least four times, without any significant loss in the adsorption capacity. The adsorption of Ni ions on graphene/δ-MnO_2 composite showed enhanced adsorption capacity from 46.55 to 60.01 mg g^{-1}, and this was 15 and 1.5 times higher than graphene nanosheets and δ-MnO_2, respectively (Ren et al. 2011).

A graphene-based Fe_3O_4 magnetic nanoparticle was used as adsorbent for magnetic solid-phase extraction of prometon, atrazine, prometryn, and propazine (Zhao et al. 2011). They established that the adsorbent was efficiently removed from aqueous solution by an external magnet. A magnetic graphene/Fe_3O_4 nanocomposite, which was fabricated by chemical precipitation method, had been

used as a novel adsorbent for the preconcentration of carbofuran, metolcarb, pirimicarb, diethofencarb, and isoprocarb (Wu et al. 2011b). The as-fabricated nanocomposite showed excellent super paramagnetic properties and adsorption capacity. A magnetic microsphere Fe_3O_4/SiO_2/graphene composite was fabricated as a new adsorbent for the preconcentration of di-*n*-propyl-phthalate, diallyl phthalate, dicyclohexyl phthalate, benzyl butyl phthalate, and diethylhexyl phthalate in soybean milk and water samples (Wang et al. 2013c). The Fe_3O_4/graphene nanocomposite prepared by solvothermal route effectively removed aniline from their aqueous solution within 60 mins (Chang et al. 2012). The composites showed a promising adsorbent for phthalate esters with potential applications. A magnetic Fe_3O_4/graphene composite was used for the extraction of some sulfonamides (sulfamerazine, sulfapyridine, sulfamonomethoxine sodium, sulfameter, sulfadoxine, and sulfachloropyridazine) from the water (Luo et al. 2011). The composite exhibited efficient extraction media for the enhancement of sulfonamide antibiotics in water resources.

1.7.2 Graphene-Based Photocatalyst Materials for Water Treatment

Although adsorption can eliminate pollutants from water/wastewater, this method cannot completely remove pollutants (Chong et al. 2010). Complete mineralization of pollutants can be achieved through a photocatalytic technique (Chong et al. 2010). Recently, semiconductor photocatalyst materials have received global interest in water remediation application (Hoffmann et al. 1995). Nonetheless, the fast recombination of charge carriers results in a low quantum efficiency, which limits its potential visible light applications. Hence, reducing the recombination rate of charge carriers is significant to enhance the photoactivity of semiconductor photocatalysts. The most significant characteristics of graphene sheet for photodegradation of pollutants are due to its ability to tune the band gap and absorption edge of semiconductor photocatalyst materials. The ultrahigh electron conductivity of GR allows the transfer of electrons from the semiconductor to the graphene surface, and this contributes to the reduced recombination rate, thus improving the photocatalytic activity of conventional photocatalysts, such as TiO_2 (Liu et al. 2010). Therefore, composites that combine semiconductor photocatalysts and graphene might offer a desired efficiency for separating the charge carriers. Due to its strong oxidizing activity and low-cost, TiO_2 is the most often used semiconductor for the photodegradation of pollutants. The popularity of TiO_2 is explained by its commercial availability, such as P90 and P25, which serves as reference reagents for the fabrication of graphene-based TiO_2 photocatalyst composites (Liu et al. 2010). Coupling graphene sheets with TiO_2 improved the photoactivity of the composites. Apart from TiO_2, several metal oxides, such as WO_3 (An et al. 2012), ZnO (Min et al. 2012), CuO (Yusoff et al. 2013), Cu_2O (Gao et al. 2012a), SnO_2 (Seema et al.

2012), Mn_2O_3 (Chandra et al. 2012), $BiVO_4$ (Yan et al. 2013), $ZnWO_4$ (Bai et al. 2012), Bi_2WO_6 (Gao et al. 2011), Bi_2MoO_6 (Wang et al. 2012b), $CoFeO_4$ (Fu et al. 2012), and $BaCrO_4$ (Gawande and Thakare 2013), have been used in combination with graphene to serve as a photocatalyst. Theoretically, these semiconductor photocatalysts are characterized by their electronic band structure, which composes of an empty CB and filled VB (Xiang et al. 2012). The P25/graphene nanocomposites, which was fabricated using the hydrothermal route exhibited a higher capacity to degrade MB dye compared to pure P25 nanoparticles (Zhang et al. 2009). The graphene sheet enhances the ability to adsorb organic contaminants, as well as improving the charge separation/migration rate, and visible light absorption of P25/graphene nanocomposites (Zhang et al. 2009). Coupling a semiconductor with graphene reduces its band gap through the hybridization of O *np* (n = 2, 3, 4, 6, 7) and C *2p* atomic orbitals to form a new VB (Li et al. 2013a). The amount of graphene loading to the semiconductor should be carefully tuned to achieve efficient photocatalyst–support interaction. Hence, the amount of graphene sheets plays a significant role in the photocatalytic activity of the composites. Generally, increasing the graphene sheet content in composites enhances the photocatalytic performance but beyond the permissible limit reduces the photocatalytic performance (Yoo et al. 2011). The graphene/TiO_2 composite, which was prepared using the in situ method showed 2.5 times improved photocatalytic degradation of MB dye with reference to Degussa P25 TiO_2 (Wang et al. 2010). When the graphene content was increased to 20% in the $ZnFe_2O_4$/graphene composite, a higher degradation of MB dye was observed compared to $ZnFe_2O_4$ (Fu and Wang 2011b). Through a hydrothermal reaction of CeO_2/TiO_2 nanoparticles with graphene oxide in ethanol, a CeO_2/TiO_2/graphene nanocomposite was prepared (Ghasemi et al. 2012). The performance of CeO_2/TiO_2/graphene nanocomposites decreases with an increase in the graphene sheet content. The CeO_2/TiO_2/graphene composite exhibited high photocatalytic activity compared to the CeO_2/TiO_2/carbon composite owing to the unique electronic and structural properties of the graphene sheet. The influence of graphene loading on the photocatalytic performance of TiO_2/graphene composite showed that a 0.05 threshold weight percent (wt%) of graphene exhibited the maximum activity (Wang et al. 2012c). Using reduced graphene oxide and titanium isopropoxide as Ti-precursors, a series of graphene/TiO_2 composites were fabricated by a sol–gel route (Liu et al. 2013a). The as-fabricated composite showed improved degradation of MB dye compared to pure TiO_2 with graphene/TiO_2 composite exhibiting a higher activity than that of graphene/TiO_2(P25). Through a facile sonochemical approach, the Ag_2Se/graphene/TiO_2 composite was fabricated (Meng et al. 2012). The as-prepared composites demonstrated improved visible light absorption, high adsorptivity of RhB dye, and excellent separation of charge carriers. The high performance was ascribed to the synergetic effects of the absorption edge in the visible light region and high charge carrier mobility of Ag_2Se/graphene/TiO_2 composite. Khalid et al. (2012a) prepared a composite of Fe-doped TiO_2 with graphene toward the photocatalytic degradation of MO dye. Due to the reduced charge carrier recombination, the synergistic effect of enhanced adsorptivity of MO dye, and improved visible light absorption, the as-synthesized showed tenfold photocatalytic

performance compared to the bulk TiO_2. Min et al. (2013) successfully fabricated N-TiO_2/graphene composite for the photocatalytic decomposition of benzoic acid. The as-fabricated composites showed high photocatalytic activity over pristine TiO_2. The photodegradation activity of MB dye by TiO_2/graphene is two and six times faster than that of TiO_2/graphene oxide and P25, respectively (Ismail et al. 2013). This improvement was ascribed to the effective charge transfer from TiO_2 to graphene layers, as well as the better contact between TiO_2 and graphene. The good contact of graphene with TiO_2 nanoparticles enhances the photoelectron conversion of TiO_2 by reducing the charge carriers' recombination rate (Guo et al. 2011). Through, the hydrothermal process, novel graphene/TiO_2 composite efficiently photodegrades MO dye over pure TiO_2 (Khalid et al. 2013a). The efficient charge separation due to the 2D planar structure and π-conjugation system of graphene, as well as the high adsorptivity of MO dye, influences the enhanced performance of the composite. The TiO_2/graphene composite nanosheets, which was fabricated via a facile one-pot solvothermal route, showed improved adsorption capacity and much enhancements toward the photocatalytic decomposition of MB dye compared to P25 (Zhang et al. 2012c). The superiority of graphene sheets compared to carbon nanotubes toward the photocatalytic activity of TiO_2 was investigated (Zhang et al. 2011c). Comparison between carbon nanotubes/TiO_2 and graphene/TiO_2 reveals the prominent advantage of graphene over carbon nanotubes on both enhancing the photocatalytic activity and controlling the morphology of TiO_2. Using a sol–gel method, Fe-doped TiO_2 photocatalyst nanowire arrays were embedded on the surface of functionalized graphene sheets (Farhangi et al. 2011). The photocatalytic performance improved with increasing the Fe-doping concentration between 0.6 and 0.8% of Fe. The as-fabricated composites exhibited high a photodegradation of 17β-estradiol over Fe-doped TiO_2 and TiO_2/functionalized graphene sheet composites. Moreover, surface modification of graphene/semiconductor composite with metal ions, such as Au (Wang et al. 2013b), Pt (Neppolian et al. 2012), Nd (Khalid et al. 2013b), Ag (Tang et al. 2012), and Fe (Khalid et al. 2012a), can enhanced their photocatalytic performance. These metals can enhance the lifetime of charge carriers by restraining their recombination rate. Wang et al. (2013e) revealed that coupling SnO_2 with graphene promoted the performance of SnO_2 for the photodegradation of pendimethalin. This improvement was ascribed to the excitation of an electron from pendimethalin at the excited states to SnO_2 at the interface and the large potential difference between SnO_2 and pendimethalin. The underlying mechanism behind the photocatalytic performance of ZnO/graphene sheet composite was investigated by Xu et al. (2011). They observed that the presence of $O_2^{-\bullet}$, OH, and h^+ active species is responsible for the photocatalytic decomposition toward methylene blue dye. Li and Cao (2011) observed that the ZnO/graphene composite revealed a high photoactivity toward the decomposition of RhB dye. The incorporation of graphene on the semiconductor surface promotes the performance and stability of the semiconductor photocatalysts by reducing their photo-corrosion (Fan et al. 2012). The photocatalytic activity of a semiconductor is influenced by the morphology of the photocatalyst. One-dimensional WO_3/graphene nanorod composites exhibited three

times an improvement in the photocatalytic performance compared to the commercial WO_3 (An et al. 2012). Gao et al. (2011) observed a threefold increase in the performance of Bi_2WO_6/graphene composite toward the degradation of RhB dye compared to pure Bi_2WO_6. This improvement is due to the Fermi energy level shift and efficient transfer of photoinduced electrons at the Bi_2WO_6/graphene interface. The visible photocatalytic activity of $ZnWO_4$ hybridization with graphene sheet was attributed to the efficient transfer of charge carriers at the $ZnWO_4$/graphene interface (Bai et al. 2012). Moreover, carbon free radicals, which was found along with the $O_2^{-\bullet}$ and $HO^{\bullet}$ radicals, did not directly partake in the photodegradation reaction but to some degree enhanced their lifetime for the oxidative reactions. Zhang et al. (2011b) showed 1.87 times photocatalytic performance of $InNbO_4$/graphene compared to pure $InNbO_4$ for the degradation of MB dye. Iron nanoparticles/graphene composites, which was successfully fabricated using graphene oxide as a supporting matrix, showed a higher elimination capacity to decolorize methylene blue dye (Guo et al. 2012). The graphene/Mn_2O_3 nanocomposite with a uniform distribution of Mn_2O_3 nanoparticles throughout the surface of graphene sheet showed ~60, ~80, and ~84% degradation of RhB, eosin, and MB dyes, respectively (Chandra et al. 2012). The graphene/Cu_2O composites, which were fabricated at room temperature using a one-pot solution route, altered the surface charge of the composites from positive to negative (Gao et al. 2012a). This favors the adsorption and photocatalytic degradation of MB dyes under simulated visible light irradiation. Through a simple solvothermal route, graphene/CdS composite was fabricated (Gao et al. 2012b). The as-fabricated composites showed an effective migration of photoinduced electrons from CdS to graphene sheet, as well as enhanced visible light photodegradation activity for RhB dye degradation. The CeO_2/TiO_2/graphene composites synthesized by the sol–gel process exhibited a higher photocatalytic degradation of 2,4-dichlorophenoxyacetic acid and Reactive Red 195 dye in aqueous solution (Ghasemi et al. 2012). A $BiVO_4$/graphene composite was fabricated via a one-step hydrothermal route (Fu et al. 2011). The as-fabricated composite showed enhanced photoactivity for the decomposition of MO, RhB, MB, and active black BL-G dyes in water. This improvement was attributed to the effective separation of charge carriers and the concerted effects of pure $BiVO_4$ and graphene sheet. Through a hydrothermal method, copper oxide was effectively decorated with functionalized graphene sheets (Yusoff et al. 2013). Due to the enhanced synergy interactions between copper oxide and functionalized graphene sheets, the nanocomposite demonstrated higher photoactivity toward the degradation of MB dye. The SnO_2/graphene and Cu_2O/SnO_2/graphene nanocomposites fabricated by simple sol–gel growth route showed a higher photodegradation of pendimethalin than pure SnO_2 and pristine graphene (Wang et al. 2013e). The novel graphene/Sb_2S_3 composites prepared using a facile solvothermal method revealed improved photodegradation activity toward RhB dye due to the negative surface charge, efficient electrons transfer from Sb_2S_3 to the graphene sheet, and smaller Sb_2S_3 particles size (Tao et al. 2013). Within the two-step hydrothermal approach, the La-TiO_2/graphene composites have better charge separation ability and enhanced photodegradation of MB dye with reference to pure TiO_2 (Khalid et al. 2012b). The high performance

was ascribed to the higher adsorptivity of the MB dye, excellent electrical properties of graphene, increased charge separation efficiency, more π–π interactions between the composite and the pollutants, as well as the large surface contact between La-TiO_2 nanoparticles and graphene. The particle size, graphene contents, and targeted pollutants for the different graphene/semiconductor composites are presented in Table 1.2.

Table 1.2 Graphene and semiconductor composites for photocatalytic degradation of pollutants

Graphene composites	Particle size (nm)	Graphene contents (wt.%)	Pollutants	References
TiO_2/graphene	10–30	3	MB	Kim et al. (2012)
TiO_2/graphene	5–40	1	2,4-dichlorophenoxyacetic acid and reactive red 195	Ghasemi et al. (2013)
TiO_2/graphene	–	1–10	MO	Khalid et al. (2013a)
TiO_2/graphene	10–15	10.8	RhB	Lei et al. (2012)
TiO_2/graphene	5 nm pore diameter	1	RhB and norfloxacin	Li et al. (2012)
TiO_2/graphene	20–200	–	MB	Pan et al. (2012)
TiO_2/graphene	12.3–41.0	–	Butane	Štengl et al. (2011)
TiO_2/graphene	18	–	RhB	Wang et al. (2011b)
ZnO/Ag/graphene	∼200		RhB	Xu et al. (2013a)
CdSe/graphene/TiO_2	–	34.22	MO and RhB	Ghosh et al. (2013a)
ZnO/graphene	20	–	MB and MO	Ahmad et al. (2013b)
ZnO/graphene	6	–	MB	Fu et al. (2013)
Graphene/ZnO	∼10	–	RhB	Saravanakumar et al. (2013)
Graphene/Ag-ZnO	32	10	MB, RhB and MO	Ahmad et al. (2013a)
CdSe/graphene	∼10	54.08	MO and RhB	Ghosh et al. (2013b)
PbS-graphene/TiO_2	∼15–19 for TiO_2 ∼20–25 for PbS	–	MB	Ullah et al. (2014)
$ZnFe_2O_4$/graphene	5	–	RhB, MO and MB	Lu et al. (2013)

(continued)

Table 1.2 (continued)

Graphene composites	Particle size (nm)	Graphene contents (wt.%)	Pollutants	References
Graphene/$InNbO_4$	5	–	MB and 2,4-dichlorophenol	Zhang et al. (2011b)
Graphene/γ-Bi_2MoO_6	10	1.0	MB	Zhou et al. (2011)
Graphene/Bi_2MoO_6	–	–	Reactive brilliant red dye	Wang et al. (2012b)
Graphene/$La_2Ti_2O_7$	400	–	RhB	Wu et al. (2011a)
$BiVO_4$/graphene	88	–	MB	Gawande and Thakare (2012)
Ag_3PO_4/graphene	250	–	RhB, MO, and MB	Yang et al. (2013b)
Graphene/BiOBr	–	~1.0	Sulforhodamine 640 dye	Zhang et al. (2012b)

1.8 Principles of Graphene/Semiconductor Composites

The low efficient "trial-and-error" approach immensely increased the workload of some experimental research. However, there has been extreme demand for theoretical guided design of better photocatalyst materials to ease the burden of experimental "trial-and-error" approach. The ability of photocatalytic materials in charge generation and light absorption relies greatly on its electronic band structures. Complementary to these effects, theoretical simulations have been indispensable in evaluating structural stabilities, electronic properties, work functions, charge transfer, and carrier effective mass of several semiconductor photocatalyst materials. In analyzing the charge generation ability of photocatalysts, first-principle simulations using quantum mechanics, such as density functional theory (DFT) and ab initio calculations, are able to explore the optical and electronic properties of semiconductor photocatalysts without experimental parameters. Generally, theoretical calculations can offer a perfect understanding for designing photocatalysts from the perspective of mechanisms. The ab initio prediction of semiconductors requires a precise theoretical explanation of many-body systems, and this has been the biggest problem in solid-state sciences (Li et al. 2017). The electronic Schrödinger equation can be explicitly solved using the Hartree–Fock method by expanding the wave function in the Slater determinant (Szabo and Ostlund 2012). However, this method normally neglects the electron correlation with the underestimation of the bond energies. The electron correlation corrections have been included using the post Hartree–Fock method with expanded determinants, but it is only limited to simple

systems (Szabo and Ostlund 2012). Moreover, the complicated N-electron wave function has proved to be unnecessary, and the total electron density can check the ground-state properties (Hohenberg and Kohn 1964; Kohn and Sham 1965). The DFT method proposed by Hohenberg, Kohn, and Sham decreases the complexity of the many-body Schrödinger equation into a series of Kohn–Sham single particle (Li et al. 2017). In the Kohn–Sham Hamiltonian, everything is known, apart from the exchange–correlation functional (Li et al. 2017). Therefore, the accuracy of DFT is due to its consideration of the exchange–correlation functional. Among the several types of the exchange–correlation functional that have been used in photocatalysis, the generalized gradient approximation (Perdew 1986) and the local density approximation (Kohn and Sham 1965) are the most common ones. The local density approximation works well for metallic systems but not for insulators and semiconductors, for which band gaps are underestimated (Li et al. 2017). The generalized gradient approximation (Becke 1988) is more accurate than the local density approximation since the generalized gradient approximation considers the inhomogeneity of electron density. Higher-order derivatives of electron density with the meta-generalized gradient approximation functionals can enhance the chemical accuracy of photocatalyst systems with severe variations of electron density (Li et al. 2017). Nonetheless, the delocalized effects of the generalized gradient approximation and meta-generalized gradient approximation are intrinsically localized (Li et al. 2017). The delocalized effects are treated by replacing the exchange–correlation energy with the exact Hartree–Fock exchange–correlation energy. The hybrid Heyd–Scuseria–Ernzerhof functional (Heyd et al. 2003) mixes the nonlocal Hartree–Fock exchange with the local/semi-local density functional theory exchange which enhances the accuracy of electronic structures (Muscat et al. 2001). Moreover, adding a Hubbard parameter (U) to the generalized gradient approximation and the local density approximation (DFT + U) calculation also improves the band structure depending on the choice of several empirical parameters (Anisimov et al. 1997). The DFT + U and hybrid Heyd–Scuseria–Ernzerhof functional have been more robust and reliable with progress in solid-state materials science, solid-state physics, chemistry, and chemical engineering (Lejaeghere et al. 2016). Hence, new photocatalyst materials with several structural characteristics, electronic structure (band structure, electron density distributions, the density of state, and charge population), and compositions are continuously studied using DFT calculations. For example, Geng et al. (2013b) carried out DFT calculations to understand the influence of interface structure on the photocatalytic property of ZnO/graphene composites. The authors established that the weak interactions between ZnO monolayer and graphene sheets have no influence on the electronic properties of graphene. Moreover, stronger binding energies and larger charge transfers were observed for thick ZnO slabs with polarized surfaces on the graphene sheet. Coupling graphene sheets on the surface of ZnO with O termination showed lower work function and p-type conductivity, while graphene sheets on the surface of ZnO with Zn termination exhibited higher work function and n-type conductivity. Through the conjugate gradient minimization method with the norm-conserving pseudopotential and the double-zeta plus polarization basis sets,

the synergistic effect of TiO_2/graphene/MoS_2 ternary nanocomposites was investigated (Yuan et al. 2015). It was discovered that the electron excites from TiO_2 cluster to graphene to reduce the band gap of the nanocomposites. Within the local density approximation scheme with the norm-conserving pseudopotential and the plane-wave basis set, the improved absorption of TiO_2(001)/graphene nanocomposites in the visible region was influenced by the graphene hybridization (Gao et al. 2013). The energy bands and the projected density of state results offer much information on the photocatalytic mechanism with electron migrations from O 2p state to the C 2p state of the nanocomposites. The improved charge migration and visible light absorption of graphene/Bi_2WO_6(010) (Ren et al. 2016), graphene/rutile TiO_2 (Du et al. 2011; Long 2013), graphene/anatase TiO_2 (Li et al. 2013b), and ZnO (Pengtao et al. 2013) nanocomposites were ascribed to the large interfacial work function difference. The interfacial interaction between graphene and ZnO (Pengtao et al. 2013), $SrTiO_3$ (Yang et al. 2015), and Ag_3PO_4 (Xu et al. 2014) nanocomposites was due to van der Waal interactions based on the DFT-D2 approach proposed by Grimme (2004, 2006). A higher stability was found in the Fe-doped TiO_2/graphene nanocomposite compared to the TiO_2/GR nanocomposite (Nasrin et al. 2014). This is due to the higher charge carrier transfer from Fe-doped TiO_2 to the GR sheets. The adsorption of TiO_2 on pristine graphene nanoribbons and functionalized graphene was also studied using the generalized gradient approximation functional of the Perdew–Wang 91 and projector augmented wave method (Ayissi et al. 2013). A large physical adsorption was found for the nanocomposites on all the chemical adsorption sites of the graphene sheets and functionalized graphene nanoribbons. Using the semi-core pseudopotential method and the hybrid HSE06 functional, the chemical and electronic structures of titania/graphene and titania/graphdiyne (GD) nanocomposites with different titania facets were explored (Yang et al. 2013a). Higher oxidation properties and charge separation of TiO_2(001)/GD composite compared with the TiO_2(001)/GR and TiO_2(001) composite were observed. Geng et al. (2013a) used DFT to investigate the enhanced photocatalytic performance of TiO_2/graphene composites. The TiO_2 clusters were coupled with monovacancy graphene (V-G), epoxy graphene (O-G), and pristine graphene (P-G). The stability of TiO_2 coupled with V-G and O-G was higher than the P-G based on the binding energy and geometric configurations results. The improved photoactivity of the nanocomposites was as a result of the reduced electrons and holes recombination rate, as well as the decrease excitation energy in the visible region.

1.9 Conclusion

During the past decades, much effort has been made to comprehend how graphene-based materials can be utilized to solve water remediation issues. The inherent properties of graphene, such as large surface area, excellent electron mobility, high mechanical strength, and large thermal conductivity, have opened new opportunities

to enhance the activity of several semiconductors. In this book chapter, several types of graphene/semiconductor composites have been discussed for environmental remediation application. We have selectively discussed the fundamentals, basic principles, and mechanism of semiconductor photocatalysts. In addition, the preparation, properties, characterization techniques, and applications of graphene-based materials in water purification have also been emphasized. The photocatalytic performance toward the removal of heavy metal ions and degradation of contaminants was synergistically improved when graphene was coupled with semiconductors. The size-dependent properties of semiconductors together with the unique properties of graphene induce further functionalities, such as the prolonged visible light absorption edge, enhanced charge separation properties, high adsorption capacity, and stability of the composites.

We have illustrated how theoretical studies have used to explain the photocatalytic behavior of semiconductor. Electronic structure calculations have shown how interface is significant to determine the photocatalytic activity and adsorption behavior of semiconductor photocatalyst materials. This book chapter mentions how first-principle studies can be applied routinely to study charge transfer and electronic properties of materials, which are often challenging to study experimentally.

Several fabrication methods have developed for both in situ and ex situ processing of semiconductor nanoparticles on the graphene sheet; however, some pressing issues must be addressed before large-scale application of these nanocomposites can be effectively achieved. Thus, the technology for fabricating high-quality graphene is still at the fundamental stage; further improvements are needed since the accurate control of the final product in terms of defect sites, reaggregation, purity, the number of layers, and control of defects is yet to be established. Moreover, large surface area architectures (graphene-based xerogels and aerogels) must be applied for heavy metal ions removal using the adsorption technique because the high surface area, nanoporosity, and microstructures of graphene show excellent adsorption capabilities of pollutants and heavy metal ions.

The design and fabrication of novel photocatalyst materials are one of the key research goals. The existing photocatalytic materials have several drawbacks, such as high cost, large band gaps, low active surface area, etc. It is of great significance to find cost-effective and advanced materials to prepare composite photocatalysts for practical applications. A perfect material for engineering composites should fulfill several requirements, such as visible light activity, high solar conversion efficiency, proper band-gap structure for redox reactions, high photostability for long-term applications, and scalability for commercialization.

Currently, the hybrid HSE06 functionals, which can precisely describe the electronic structures, cannot clearly offer a solution to the long-range van der Waals interaction in graphene-based composite materials. Thus, new functionals and codes, which can precisely address both the van der Waals interactions and electron correlation effects, are significant. This will become a key tool for hastening the design of advanced materials for water purification.

Acknowledgments The authors would like to acknowledge the financial contributions from the Faculty of Science: University of Johannesburg, South Africa, Department of Applied Chemistry and the National Research Foundation (TTK14052167682). FO acknowledges the financial support from the Global Excellence and Stature (GES) Doctoral Scholarship: University of Johannesburg, South Africa. EMK also acknowledges the financial support from National Research Foundation (NRF).

References

Ahmad M, Ahmed E, Hong ZL, Khalid NR, Ahmed W, Elhissi A (2013a) Graphene–Ag/ZnO nanocomposites as high performance photocatalysts under visible light irradiation. J Alloys Compd 577:717–727. https://doi.org/10.1016/j.jallcom.2013.06.137

Ahmad M, Ahmed E, Hong ZL, Xu JF, Khalid NR, Elhissi A, Ahmed W (2013b) A facile one-step approach to synthesizing ZnO/graphene composites for enhanced degradation of methylene blue under visible light. Appl Surf Sci 274:273–281. https://doi.org/10.1016/j.apsusc.2013.03.035

Ai L, Zhang C, Chen Z (2011) Removal of methylene blue from aqueous solution by a solvothermal-synthesized graphene/magnetite composite. J Hazard Mater 192:1515–1524. https://doi.org/10.1016/j.jhazmat.2011.06.068

Ali I, Gupta V (2006) Advances in water treatment by adsorption technology. Nat Protoc 1:2661–2667

Allen MJ, Tung VC, Kaner RB (2009) Honeycomb carbon: a review of graphene. Chem Rev 110:132–145

Alyüz B, Veli S (2009) Kinetics and equilibrium studies for the removal of nickel and zinc from aqueous solutions by ion exchange resins. J Hazard Mater 167:482–488

An X, Jimmy CY, Wang Y, Hu Y, Yu X, Zhang G (2012) WO_3 nanorods/graphene nanocomposites for high-efficiency visible-light-driven photocatalysis and NO_2 gas sensing. J Mater Chem 22:8525–8531

Anisimov VI, Aryasetiawan F, Lichtenstein A (1997) First-principles calculations of the electronic structure and spectra of strongly correlated systems: the LDA + U method. J Phys Condens Matter 9:767–808

Anpo M, Kamat P (2010) Environmental benign photocatalysts. In: Applications of titanium oxide-based materials. Springer, New York, pp 1–501

Ayissi S, Charpentier PA, Farhangi N, Wood JA, Palotás K, Hofer WA (2013) Interaction of titanium oxide nanostructures with graphene and functionalized graphene nanoribbons: a DFT study. J Phys Chem C 117:25424–25432. https://doi.org/10.1021/jp403835m

Bai X, Wang L, Zhu Y (2012) Visible photocatalytic activity enhancement of $ZnWO_4$ by graphene hybridization. ACS Catal 2:2769–2778

Bai S, Jiang J, Zhang Q, Xiong Y (2015) Steering charge kinetics in photocatalysis: intersection of materials syntheses, characterization techniques and theoretical simulations. Chem Soc Rev 44:2893–2939

Bard AJ, Parsons R, Jordan J (1985) Standard potentials in aqueous solution, vol 6. CRC press, New York, pp 1–829

Becke AD (1988) Density-functional exchange-energy approximation with correct asymptotic behavior. Phys Rev A 38:3098–3100

Berera R, van Grondelle R, Kennis JT (2009) Ultrafast transient absorption spectroscopy: principles and application to photosynthetic systems. Photosynth Res 101:105–118

Berger C, Song Z, Li X, Wu X, Brown N, Naud C, Mayou D, Li T, Hass J, Marchenkov AN (2006) Electronic confinement and coherence in patterned epitaxial graphene. Science 312:1191–1196

Bhatnagar A, Hogland W, Marques M, Sillanpää M (2013) An overview of the modification methods of activated carbon for its water treatment applications. Chem Eng J 219:499–511
Blake P, Hill E, Castro Neto A, Novoselov K, Jiang D, Yang R, Booth T, Geim A (2007) Making graphene visible. Appl Phys Lett 91:063124
Boehm H, Setton R, Stumpp E (1986) Nomenclature and terminology of graphite intercalation compounds. Carbon 24:241–245
Cai W, Yu J, Mann S (2009) Template-free hydrothermal fabrication of hierarchically organized γ-AlOOH hollow microspheres. Microporous Mesoporous Mater 122:42–47
Cao S, Low J, Yu J, Jaroniec M (2015) Polymeric photocatalysts based on graphitic carbon nitride. Adv Mater 27:2150–2176
Casbeer E, Sharma VK, Li X-Z (2012) Synthesis and photocatalytic activity of ferrites under visible light: a review. Sep Purif Technol 87:1–14
Chandra V, Park J, Chun Y, Lee JW, Hwang I-C, Kim KS (2010) Water-dispersible magnetite-reduced graphene oxide composites for arsenic removal. ACS Nano 4:3979–3986
Chandra S, Das P, Bag S, Bhar R, Pramanik P (2012) Mn_2O_3 decorated graphene nanosheet: an advanced material for the photocatalytic degradation of organic dyes. Mater Sci Eng B 177:855–861
Chang Y-C (2014) ZnO nanopinecone arrays with enhanced photocatalytic performance in sunlight. RSC Adv 4:20273–20280
Chang Y-P, Ren C-L, Qu J-C, Chen X-G (2012) Preparation and characterization of Fe_3O_4/graphene nanocomposite and investigation of its adsorption performance for aniline and p-chloroaniline. Appl Surf Sci 261:504–509. https://doi.org/10.1016/j.apsusc.2012.08.045
Chen T, Feng Z, Wu G, Shi J, Ma G, Ying P, Li C (2007) Mechanistic studies of photocatalytic reaction of methanol for hydrogen production on Pt/TiO_2 by in situ Fourier transform IR and time-resolved IR spectroscopy. J Phys Chem C 111:8005–8014
Chen C, Ma W, Zhao J (2010) Semiconductor-mediated photodegradation of pollutants under visible-light irradiation. Chem Soc Rev 39:4206–4219
Chong MN, Jin B, Chow CW, Saint C (2010) Recent developments in photocatalytic water treatment technology: a review. Water Res 44:2997–3027
Compton OC, Nguyen ST (2010) Graphene oxide, highly reduced graphene oxide, and graphene: versatile building blocks for carbon-based materials. Small 6:711–723
Dąbrowski A (2001) Adsorption—from theory to practice. Adv Colloid Interf Sci 93:135–224
Du A, Ng YH, Bell NJ, Zhu Z, Amal R, Smith SC (2011) Hybrid graphene/titania nanocomposite: Interface charge transfer, hole doping, and sensitization for visible light response. J Phys Chem Lett 2:894–899. https://doi.org/10.1021/jz2002698
Emtsev KV, Bostwick A, Horn K, Jobst J, Kellogg GL, Ley L, McChesney JL, Ohta T, Reshanov SA, Röhrl J (2009) Towards wafer-size graphene layers by atmospheric pressure graphitization of silicon carbide. Nat Mater 8:203–207
Fageria P, Gangopadhyay S, Pande S (2014) Synthesis of ZnO/Au and ZnO/Ag nanoparticles and their photocatalytic application using UV and visible light. RSC Adv 4:24962–24972
Fan H, Zhao X, Yang J, Shan X, Yang L, Zhang Y, Li X, Gao M (2012) ZnO–graphene composite for photocatalytic degradation of methylene blue dye. Catal Commun 29:29–34
Farhangi N, Chowdhury RR, Medina-Gonzalez Y, Ray MB, Charpentier PA (2011) Visible light active Fe doped TiO_2 nanowires grown on graphene using supercritical CO_2. Appl Catal B 110:25–32
Ferrari AC, Meyer J, Scardaci V, Casiraghi C, Lazzeri M, Mauri F, Piscanec S, Jiang D, Novoselov K, Roth S (2006) Raman spectrum of graphene and graphene layers. Phys Rev Lett 97:187401
Feynman RP, Leighton RB, Sands M (2013) The Feynman lectures on physics, desktop edition volume I, vol 1. Basic books, New York, pp 1–52
Friedmann D, Mendive C, Bahnemann D (2010) TiO_2 for water treatment: parameters affecting the kinetics and mechanisms of photocatalysis. Appl Catal B 99:398–406

Friedmann D, Hakki A, Kim H, Choi W, Bahnemann D (2016) Heterogeneous photocatalytic organic synthesis: state-of-the-art and future perspectives. Green Chem 18:5391–5411

Fu F, Wang Q (2011a) Removal of heavy metal ions from wastewaters: a review. J Environ Manag 92:407–418

Fu Y, Wang X (2011b) Magnetically separable $ZnFe_2O_4$–graphene catalyst and its high photocatalytic performance under visible light irradiation. Ind Eng Chem Res 50:7210–7218

Fu Y, Sun X, Wang X (2011) $BiVO_4$–graphene catalyst and its high photocatalytic performance under visible light irradiation. Mater Chem Phys 131:325–330. https://doi.org/10.1016/j.matchemphys.2011.09.049

Fu Y, Chen H, Sun X, Wang X (2012) Combination of cobalt ferrite and graphene: high-performance and recyclable visible-light photocatalysis. Appl Catal B 111:280–287

Fu D, Han G, Yang F, Zhang T, Chang Y, Liu F (2013) Seed-mediated synthesis and the photodegradation activity of ZnO–graphene hybrids excluding the influence of dye adsorption. Appl Surf Sci 283:654–659. https://doi.org/10.1016/j.apsusc.2013.07.003

Fujishima A, Honda K (1972) Electrochemical photolysis of water at a semiconductor electrode. Nature 238:37–38

Ganzenko O, Huguenot D, Van Hullebusch ED, Esposito G, Oturan MA (2014) Electrochemical advanced oxidation and biological processes for wastewater treatment: a review of the combined approaches. Environ Sci Pollut Res 21:8493–8524

Gao E, Wang W, Shang M, Xu J (2011) Synthesis and enhanced photocatalytic performance of graphene-Bi_2WO_6 composite. Phys Chem Chem Phys 13:2887–2893

Gao Z, Liu J, Xu F, Wu D, Wu Z, Jiang K (2012a) One-pot synthesis of graphene–cuprous oxide composite with enhanced photocatalytic activity. Solid State Sci 14:276–280

Gao Z, Liu N, Wu D, Tao W, Xu F, Jiang K (2012b) Graphene–CdS composite, synthesis and enhanced photocatalytic activity. Appl Surf Sci 258:2473–2478. https://doi.org/10.1016/j.apsusc.2011.10.075

Gao H, Li X, Lv J, Liu G (2013) Interfacial charge transfer and enhanced photocatalytic mechanisms for the hybrid graphene/Anatase TiO_2(001) nanocomposites. J Phys Chem C 117:16022–16027. https://doi.org/10.1021/jp403241d

Gao C, Wang J, Xu H, Xiong Y (2017) Coordination chemistry in the design of heterogeneous photocatalysts. Chem Soc Rev 46:2799–2823

Gawande SB, Thakare SR (2012) Graphene wrapped $BiVO_4$ photocatalyst and its enhanced performance under visible light irradiation. Int Nano Lett 2:1–7. https://doi.org/10.1186/2228-5326-2-11

Gawande SB, Thakare SR (2013) Synthesis of visible light active graphene-modified $BaCrO_4$ nanocomposite photocatalyst. Int Nano Lett 3:1–8

Geim AK (2009) Graphene: status and prospects. Science 324:1530–1534

Geng W, Liu H, Yao X (2013a) Enhanced photocatalytic properties of titania–graphene nanocomposites: a density functional theory study. Phys Chem Chem Phys 15:6025–6033

Geng W, Zhao X, Liu H, Yao X (2013b) Influence of interface structure on the properties of ZnO/graphene composites: a theoretical study by density functional theory calculations. J Phys Chem C 117:10536–10544

Ghasemi S, Setayesh SR, Habibi-Yangjeh A, Hormozi-Nezhad MR, Gholami MR (2012) Assembly of CeO_2–TiO_2 nanoparticles prepared in room temperature ionic liquid on graphene nanosheets for photocatalytic degradation of pollutants. J Hazard Mater 199:170–178. https://doi.org/10.1016/j.jhazmat.2011.10.080

Ghasemi S, Esfandiar A, Rahman Setayesh S, Habibi-Yangjeh A, Iraji zad A, Gholami MR (2013) Synthesis and characterization of TiO_2–graphene nanocomposites modified with noble metals as a photocatalyst for degradation of pollutants. Appl Catal A 462:82–90. https://doi.org/10.1016/j.apcata.2013.04.029

Ghosh T, Cho K-Y, Ullah K, Nikam V, Park C-Y, Meng Z-D, Oh W-C (2013a) High photonic effect of organic dye degradation by CdSe–graphene–TiO_2 particles. J Ind Eng Chem 19:797–805. https://doi.org/10.1016/j.jiec.2012.10.020

Ghosh T, Ullah K, Nikam V, Park C-Y, Meng Z-D, Oh W-C (2013b) The characteristic study and sonocatalytic performance of CdSe–graphene as catalyst in the degradation of azo dyes in aqueous solution under dark conditions. Ultrason Sonochem 20:768–776. https://doi.org/10.1016/j.ultsonch.2012.09.005

Grimme S (2004) Accurate description of van der Waals complexes by density functional theory including empirical corrections. J Comput Chem 25:1463–1473

Grimme S (2006) Semiempirical GGA-type density functional constructed with a long-range dispersion correction. J Comput Chem 27:1787–1799

Gu L, Wang J, Zou Z, Han X (2014) Graphitic-C_3N_4-hybridized TiO_2 nanosheets with reactive {001} facets to enhance the UV- and visible-light photocatalytic activity. J Hazard Mater 268:216–223

Guo S, Dong S (2011) Graphene nanosheet: synthesis, molecular engineering, thin film, hybrids, and energy and analytical applications. Chem Soc Rev 40:2644–2672

Guo H-L, Wang X-F, Qian Q-Y, Wang F-B, Xia X-H (2009) A green approach to the synthesis of graphene nanosheets. ACS Nano 3:2653–2659

Guo J, Zhu S, Chen Z, Li Y, Yu Z, Liu Q, Li J, Feng C, Zhang D (2011) Sonochemical synthesis of TiO_2 nanoparticles on graphene for use as photocatalyst. Ultrason Sonochem 18:1082–1090

Guo J, Wang R, Tjiu WW, Pan J, Liu T (2012) Synthesis of Fe nanoparticles@graphene composites for environmental applications. J Hazard Mater 225:63–73. https://doi.org/10.1016/j.jhazmat.2012.04.065

Gupta VK, Ali I, Saleh TA, Nayak A, Agarwal S (2012) Chemical treatment technologies for waste-water recycling-an overview. RSC Adv 2:6380–6388

Hao L, Song H, Zhang L, Wan X, Tang Y, Lv Y (2012) SiO_2/graphene composite for highly selective adsorption of Pb (II) ion. J Colloid Interface Sci 369:381–387. https://doi.org/10.1016/j.jcis.2011.12.023

He F, Fan J, Ma D, Zhang L, Leung C, Chan HL (2010) The attachment of Fe_3O_4 nanoparticles to graphene oxide by covalent bonding. Carbon 48:3139–3144

Hernandez Y, Nicolosi V, Lotya M, Blighe FM, Sun Z, De S, McGovern IT, Holland B, Byrne M, Gun'Ko YK, Boland JJ, Niraj P, Duesberg G, Krishnamurthy S, Goodhue R, Hutchison J, Scardaci V, Ferrari AC, Coleman JN (2008) High-yield production of graphene by liquid-phase exfoliation of graphite. Nat Nanotechnol 3:563–568. http://www.nature.com/nnano/journal/v3/n9/suppinfo/nnano.2008.215_S1.html

Heyd J, Scuseria GE, Ernzerhof M (2003) Hybrid functionals based on a screened Coulomb potential. J Chem Phys 118:8207–8215

Hitoki G, Ishikawa A, Takata T, Kondo JN, Hara M, Domen K (2002) Ta_3N_5 as a novel visible light-driven photocatalyst ($\lambda < 600$ nm). Chem Lett 31:736–737

Hoffmann MR, Martin ST, Choi W, Bahnemann DW (1995) Environmental applications of semiconductor photocatalysis. Chem Rev 95:69–96

Hohenberg P, Kohn W (1964) Inhomogeneous electron gas. Phys Rev 136:B864–B671

Hontoria-Lucas C, López-Peinado A, López-González JD, Rojas-Cervantes M, Martin-Aranda R (1995) Study of oxygen-containing groups in a series of graphite oxides: physical and chemical characterization. Carbon 33:1585–1592

Hou H, Zhou R, Wu P, Wu L (2012) Removal of Congo red dye from aqueous solution with hydroxyapatite/chitosan composite. Chem Eng J 211:336–342

Hummers WS, Offeman RE (1958) Preparation of graphitic oxide. J Am Chem Soc 80:1339–1339. https://doi.org/10.1021/ja01539a017

Ismail AA, Geioushy R, Bouzid H, Al-Sayari SA, Al-Hajry A, Bahnemann DW (2013) TiO_2 decoration of graphene layers for highly efficient photocatalyst: impact of calcination at different gas atmosphere on photocatalytic efficiency. Appl Catal B 129:62–70

Jiao L, Wang X, Diankov G, Wang H, Dai H (2010) Facile synthesis of high-quality graphene nanoribbons. Nat Nanotechnol 5:321–325

Kapilashrami M, Zhang Y, Liu Y-S, Hagfeldt A, Guo J (2014) Probing the optical property and electronic structure of TiO_2 nanomaterials for renewable energy applications. Chem Rev 114:9662–9707

Katsnelson MI (2007) Graphene: carbon in two dimensions. Mater Today 10:20–27

Khalid N, Hong Z, Ahmed E, Zhang Y, Chan H, Ahmad M (2012a) Synergistic effects of Fe and graphene on photocatalytic activity enhancement of TiO_2 under visible light. Appl Surf Sci 258:5827–5834

Khalid NR, Ahmed E, Hong Z, Ahmad M (2012b) Synthesis and photocatalytic properties of visible light responsive La/TiO_2-graphene composites. Appl Surf Sci 263:254–259. https://doi.org/10.1016/j.apsusc.2012.09.039

Khalid N, Ahmed E, Hong Z, Sana L, Ahmed M (2013a) Enhanced photocatalytic activity of graphene–TiO_2 composite under visible light irradiation. Curr Appl Phys 13:659–663. https://doi.org/10.1016/j.cap.2012.11.003

Khalid N, Ahmed E, Hong Z, Zhang Y, Ullah M, Ahmed M (2013b) Graphene modified Nd/TiO_2 photocatalyst for methyl orange degradation under visible light irradiation. Ceram Int 39:3569–3575

Kim CH, Kim B-H, Yang KS (2012) TiO_2 nanoparticles loaded on graphene/carbon composite nanofibers by electrospinning for increased photocatalysis. Carbon 50:2472–2481

Kohn W, Sham LJ (1965) Self-consistent equations including exchange and correlation effects. Phys Rev 140:A1133–A1138

Kuzmenko A, Van Heumen E, Carbone F, Van Der Marel D (2008) Universal optical conductance of graphite. Phys Rev Lett 100:117401

Lee Y-C, Yang J-W (2012) Self-assembled flower-like TiO_2 on exfoliated graphite oxide for heavy metal removal. J Ind Eng Chem 18:1178–1185

Lei Z, Ghosh T, Chong-Yeon P, Ze-Da M, Won-Chun O (2012) Enhanced sonocatalytic degradation of rhodamine B by graphene-TiO_2 composites synthesized by an ultrasonic-assisted method. Chin J Catal 33:1276–1283

Lejaeghere K, Bihlmayer G, Björkman T, Blaha P, Blügel S, Blum V, Caliste D, Castelli IE, Clark SJ, Dal Corso A, de Gironcoli S, Deutsch T, Dewhurst JK, Di Marco I, Draxl C, Dułak M, Eriksson O, Flores-Livas JA, Garrity KF, Genovese L, Giannozzi P, Giantomassi M, Goedecker S, Gonze X, Grånäs O, Gross EKU, Gulans A, Gygi F, Hamann DR, Hasnip PJ, Holzwarth NAW, Iuşan D, Jochym DB, Jollet F, Jones D, Kresse G, Koepernik K, Küçükbenli E, Kvashnin YO, Locht ILM, Lubeck S, Marsman M, Marzari N, Nitzsche U, Nordström L, Ozaki T, Paulatto L, Pickard CJ, Poelmans W, Probert MIJ, Refson K, Richter M, Rignanese G-M, Saha S, Scheffler M, Schlipf M, Schwarz K, Sharma S, Tavazza F, Thunström P, Tkatchenko A, Torrent M, Vanderbilt D, van Setten MJ, Van Speybroeck V, Wills JM, Yates JR, Zhang G-X, Cottenier S (2016) Reproducibility in density functional theory calculations of solids. Science 351:1–7

Li B, Cao H (2011) ZnO@graphene composite with enhanced performance for the removal of dye from water. J Mater Chem 21:3346–3349

Li D, Müller MB, Gilje S, Kaner RB, Wallace GG (2008) Processable aqueous dispersions of graphene nanosheets. Nat Nanotechnol 3:101–105

Li N, Zheng M, Chang X, Ji G, Lu H, Xue L, Pan L, Cao J (2011a) Preparation of magnetic $CoFe_2O_4$-functionalized graphene sheets via a facile hydrothermal method and their adsorption properties. J Solid State Chem 184:953–958. https://doi.org/10.1016/j.jssc.2011.01.014

Li Y, Zhang P, Du Q, Peng X, Liu T, Wang Z, Xia Y, Zhang W, Wang K, Zhu H (2011b) Adsorption of fluoride from aqueous solution by graphene. J Colloid Interface Sci 363:348–354

Li K, Chen T, Yan L, Dai Y, Huang Z, Guo H, Jiang L, Gao X, Xiong J, Song D (2012) Synthesis of mesoporous graphene and tourmaline co-doped titania composites and their photocatalytic activity towards organic pollutant degradation and eutrophic water treatment. Catal Commun 28:196–201

Li K, Chen T, Yan L, Dai Y, Huang Z, Xiong J, Song D, Lv Y, Zeng Z (2013a) Design of graphene and silica co-doped titania composites with ordered mesostructure and their simulated sunlight photocatalytic performance towards atrazine degradation. Colloids Surf A Physicochem Eng Asp 422:90–99

Li X, Gao H, Liu G (2013b) A LDA + U study of the hybrid graphene/anatase TiO_2 nanocomposites: interfacial properties and visible light response. Comput Theor Chem 1025:30–34. https://doi.org/10.1016/j.comptc.2013.10.006

Li X, Yu J, Low J, Fang Y, Xiao J, Chen X (2015) Engineering heterogeneous semiconductors for solar water splitting. J Mater Chem A 3:2485–2534
Li X, Yu J, Jaroniec M (2016) Hierarchical photocatalysts. Chem Soc Rev 45:2603–2636
Li Y, Li Y-L, Sa B, Ahuja R (2017) Review of two-dimensional materials for photocatalytic water splitting from a theoretical perspective. Catal Sci Technol 7:545–559. https://doi.org/10.1039/C6CY02178F
Liu J, Bai H, Wang Y, Liu Z, Zhang X, Sun DD (2010) Self-assembling TiO_2 Nanorods on large graphene oxide sheets at a two-phase Interface and their anti-recombination in photocatalytic applications. Adv Funct Mater 20:4175–4181
Liu S, Sun H, Liu S, Wang S (2013a) Graphene facilitated visible light photodegradation of methylene blue over titanium dioxide photocatalysts. Chem Eng J 214:298–303
Liu Y, Goebl J, Yin Y (2013b) Templated synthesis of nanostructured materials. Chem Soc Rev 42:2610–2653
Long R (2013) Understanding the electronic structures of graphene quantum dot Physisorption and chemisorption onto the TiO_2 (110) surface: a first-principles calculation. ChemPhysChem 14:579–582
Lou XW, Wang Y, Yuan C, Lee JY, Archer LA (2006) Template-free synthesis of SnO_2 hollow nanostructures with high lithium storage capacity. Adv Mater 18:2325–2329
Lü K, Zhao G, Wang X (2012) A brief review of graphene-based material synthesis and its application in environmental pollution management. Chin Sci Bull 57:1223–1234
Lu D, Zhang Y, Lin S, Wang L, Wang C (2013) Synthesis of magnetic $ZnFe_2O_4$/graphene composite and its application in photocatalytic degradation of dyes. J Alloys Compd 579:336–342. https://doi.org/10.1016/j.jallcom.2013.06.098
Lü W, Wu Y, Chen J, Yang Y (2014) Facile preparation of graphene–Fe_3O_4 nanocomposites for extraction of dye from aqueous solution. CrystEngComm 16:609–615
Lubchenco J (1998) Entering the century of the environment: a new social contract for science. Science 279:491–497
Luo Y-B, Shi Z-G, Gao Q, Feng Y-Q (2011) Magnetic retrieval of graphene: extraction of sulfonamide antibiotics from environmental water samples. J Chromatogr A 1218:1353–1358
Machado BF, Serp P (2012) Graphene-based materials for catalysis. Catal Sci Technol 2:54–75
Marahel F, Khan MA, Marahel E, Bayesti I, Hosseini S (2015) Kinetics, thermodynamics, and isotherm studies for the adsorption of BR2 dye onto avocado integument. Desalin Water Treat 53:826–835
McAllister MJ, Li J-L, Adamson DH, Schniepp HC, Abdala AA, Liu J, Herrera-Alonso M, Milius DL, Car R, Prud'homme RK (2007) Single sheet functionalized graphene by oxidation and thermal expansion of graphite. Chem Mater 19:4396–4404
Meng Z-D, Zhu L, Ghosh T, Park C-Y, Ullah K, Nikam V, Oh W-C (2012) Ag_2Se-graphene/TiO_2 nanocomposites, sonochemical synthesis and enhanced photocatalytic properties under visible light. Bull Kor Chem Soc 33:3761–3766
Min Y, Zhang K, Chen L, Chen Y, Zhang Y (2012) Ionic liquid assisting synthesis of ZnO/graphene heterostructure photocatalysts with tunable photoresponse properties. Diam Relat Mater 26:32–38
Min Y, He G, Li R, Zhao W, Chen Y, Zhang Y (2013) Doping nitrogen anion enhanced photocatalytic activity on TiO_2 hybridized with graphene composite under solar light. Sep Purif Technol 106:97–104
Mohanty K, Das D, Biswas MN (2008) Treatment of phenolic wastewater in a novel multi-stage external loop airlift reactor using activated carbon. Sep Purif Technol 58:311–319
Mori K, Yamashita H (2010) Progress in design and architecture of metal nanoparticles for catalytic applications. Phys Chem Chem Phys 12:14420–14432
Muscat J, Wander A, Harrison N (2001) On the prediction of band gaps from hybrid functional theory. Chem Phys Lett 342:397–401
Nasrin F, Serge A, Paul AC (2014) Fe doped TiO_2–graphene nanostructures: synthesis, DFT modeling and photocatalysis. Nanotechnology 25:1–11

Neppolian B, Bruno A, Bianchi CL, Ashokkumar M (2012) Graphene oxide based Pt–TiO_2 photocatalyst: ultrasound assisted synthesis, characterization and catalytic efficiency. Ultrason Sonochem 19:9–15

Novoselov KS, Geim AK, Morozov SV, Jiang D, Zhang Y, Dubonos SV, Grigorieva IV, Firsov AA (2004) Electric field effect in atomically thin carbon films. Science 306:666–669

Osgood R (2006) Photoreaction dynamics of molecular adsorbates on semiconductor and oxide surfaces. Chem Rev 106:4379–4401

Pan X, Zhao Y, Liu S, Korzeniewski CL, Wang S, Fan Z (2012) Comparing graphene-TiO_2 nanowire and graphene-TiO_2 nanoparticle composite photocatalysts. ACS Appl Mater Interfaces 4:3944–3950

Park S, An J, Jung I, Piner RD, An SJ, Li X, Velamakanni A, Ruoff RS (2009) Colloidal suspensions of highly reduced graphene oxide in a wide variety of organic solvents. Nano Lett 9:1593–1597

Pasternak S, Paz Y (2013) On the similarity and dissimilarity between photocatalytic water splitting and photocatalytic degradation of pollutants. ChemPhysChem 14:2059–2070

Pengtao X, Qing T, Zhen Z (2013) Structural and electronic properties of graphene–ZnO interfaces: dispersion-corrected density functional theory investigations. Nanotechnology 24:1–7

Perdew JP (1986) Density-functional approximation for the correlation energy of the inhomogeneous electron gas. Phys Rev B 33:8822–8824

Qi L, Cheng B, Yu J, Ho W (2016) High-surface area mesoporous Pt/TiO_2 hollow chains for efficient formaldehyde decomposition at ambient temperature. J Hazard Mater 301:522–530

Qu Y, Duan X (2013) Progress, challenge and perspective of heterogeneous photocatalysts. Chem Soc Rev 42:2568–2580

Qu J, Fan M (2010) The current state of water quality and technology development for water pollution control in China. Crit Rev Environ Sci Technol 40:519–560

Qu X, Alvarez PJ, Li Q (2013) Applications of nanotechnology in water and wastewater treatment. Water Res 47:3931–3946

Rahman MA (2015) A review on semiconductors including applications and temperature effects in semiconductors. Am Sci Res J Eng Technol Sci 7:50–70

Ramesha G, Kumara AV, Muralidhara H, Sampath S (2011) Graphene and graphene oxide as effective adsorbents toward anionic and cationic dyes. J Colloid Interface Sci 361:270–277

Rao C, Biswas K, Subrahmanyam K, Govindaraj A (2009) Graphene, the new nanocarbon. J Mater Chem 19:2457–2469

Ray S, Takafuji M, Ihara H (2013) Peptide-based surface modified silica particles: adsorption materials for dye-loaded wastewater treatment. RSC Adv 3:23664–23672

Ren Y, Yan N, Wen Q, Fan Z, Wei T, Zhang M, Ma J (2011) Graphene/δ-MnO_2 composite as adsorbent for the removal of nickel ions from wastewater. Chem Eng J 175:1–7

Ren Y, Yan N, Feng J, Ma J, Wen Q, Li N, Dong Q (2012) Adsorption mechanism of copper and lead ions onto graphene nanosheet/δ-MnO_2. Mater Chem Phys 136:538–544

Ren F, Zhang J, Wang Y, Yao W (2016) A graphene-coupled Bi_2WO_6 nanocomposite with enhanced photocatalytic performance: a first-principles study. Phys Chem Chem Phys 18:14113–14121. https://doi.org/10.1039/C6CP00458J

Saravanakumar B, Mohan R, Kim S-J (2013) Facile synthesis of graphene/ZnO nanocomposites by low temperature hydrothermal method. Mater Res Bull 48:878–883. https://doi.org/10.1016/j.materresbull.2012.11.048

Sato N (1998) Electrochemistry at metal and semiconductor electrodes. Elsevier, Amsterdam, pp 1–397

Schedin F, Geim A, Morozov S, Hill E, Blake P, Katsnelson M, Novoselov K (2007) Detection of individual gas molecules adsorbed on graphene. Nat Mater 6:652–655

Schneider J, Matsuoka M, Takeuchi M, Zhang J, Horiuchi Y, Anpo M, Bahnemann DW (2014) Understanding TiO_2 photocatalysis: mechanisms and materials. Chem Rev 114:9919–9986

Seema H, Kemp KC, Chandra V, Kim KS (2012) Graphene–SnO_2 composites for highly efficient photocatalytic degradation of methylene blue under sunlight. Nanotechnology 23:1–8

Singh V, Joung D, Zhai L, Das S, Khondaker SI, Seal S (2011) Graphene based materials: past, present and future. Prog Mater Sci 56:1178–1271

Some S, Kim Y, Hwang E, Yoo H, Lee H (2012) Binol salt as a completely removable graphene surfactant. Chem Commun 48:7732–7734

Štengl VC, Popelková D, Vláčil P (2011) TiO_2–graphene nanocomposite as high performance photocatalysts. J Phys Chem C 115:25209–25218

Subrahmanyam K, Panchakarla L, Govindaraj A, Rao C (2009) Simple method of preparing graphene flakes by an arc-discharge method. J Phys Chem C 113:4257–4259

Sun Y, Zhao Z, Dong F, Zhang W (2015) Mechanism of visible light photocatalytic NO_x oxidation with plasmonic Bi cocatalyst-enhanced $(BiO)_2CO_3$ hierarchical microspheres. Phys Chem Chem Phys 17:10383–10390

Szabo A, Ostlund NS (2012) Modern quantum chemistry: introduction to advanced electronic structure theory. McGraw-Hill, New York

Sze SM (2008) Semiconductor devices: physics and technology, 2nd edn. Wiley, New York

Tang Y, Luo S, Teng Y, Liu C, Xu X, Zhang X, Chen L (2012) Efficient removal of herbicide 2,4-dichlorophenoxyacetic acid from water using Ag/reduced graphene oxide co-decorated TiO_2 nanotube arrays. J Hazard Mater 241:323–330

Tao W, Chang J, Wu D, Gao Z, Duan X, Xu F, Jiang K (2013) Solvothermal synthesis of graphene-Sb_2S_3 composite and the degradation activity under visible light. Mater Res Bull 48:538–543. https://doi.org/10.1016/j.materresbull.2012.11.053

Tung VC, Allen MJ, Yang Y, Kaner RB (2009) High-throughput solution processing of large-scale graphene. Nat Nanotechnol 4:25–29

Ullah K, Meng Z-D, Ye S, Zhu L, Oh W-C (2014) Synthesis and characterization of novel PbS–graphene/TiO_2 composite with enhanced photocatalytic activity. J Ind Eng Chem 20:1035–1042. https://doi.org/10.1016/j.jiec.2013.06.040

Upadhyay RK, Soin N, Roy SS (2014) Role of graphene/metal oxide composites as photocatalysts, adsorbents and disinfectants in water treatment: a review. RSC Adv 4:3823–3851

USEPA (2014) Drinking water and groundwater quality standards. USEPA, New York

Van Bommel A, Crombeen J, Van Tooren A (1975) LEED and Auger electron observations of the SiC(0001) surface. Surf Sci 48:463–472

Vayssieres L (2010) On solar hydrogen and nanotechnology. Wiley, New York, pp 1–665

Wang Y, Shi R, Lin J, Zhu Y (2010) Significant photocatalytic enhancement in methylene blue degradation of TiO_2 photocatalysts via graphene-like carbon in situ hybridization. Appl Catal B 100:179–183

Wang C, Feng C, Gao Y, Ma X, Wu Q, Wang Z (2011a) Preparation of a graphene-based magnetic nanocomposite for the removal of an organic dye from aqueous solution. Chem Eng J 173:92–97

Wang Z, Mao F, Huang X, Huang Y, Feng S, Yi J, Zhang C, Wei H, Liu S (2011b) Orthogonal test design for preparation of TiO_2/Graphene composites and study on its photocatalytic activity. Rare Metals 30:271–275

Wang H, Zhang D, Yan T, Wen X, Shi L, Zhang J (2012a) Graphene prepared via a novel pyridine–thermal strategy for capacitive deionization. J Mater Chem 22:23745–23748

Wang P, Ao Y, Wang C, Hou J, Qian J (2012b) A one-pot method for the preparation of graphene–Bi_2MoO_6 hybrid photocatalysts that are responsive to visible-light and have excellent photocatalytic activity in the degradation of organic pollutants. Carbon 50:5256–5264

Wang W, Yu J, Xiang Q, Cheng B (2012c) Enhanced photocatalytic activity of hierarchical macro/mesoporous TiO_2–graphene composites for photodegradation of acetone in air. Appl Catal B 119:109–116

Wang H, Zhang D, Yan T, Wen X, Zhang J, Shi L, Zhong Q (2013a) Three-dimensional macroporous graphene architectures as high performance electrodes for capacitive deionization. J Mater Chem A 1:11778–11789

Wang W, Lu C, Ni Y, Xu Z (2013b) Fabrication of CNTs and GP/AuGP modified TiO_2 photocatalyst with two-channel electron conduction path for significantly enhanced photocatalytic activity. Appl Catal B 129:606–613

Wang W, Ma R, Wu Q, Wang C, Wang Z (2013c) Fabrication of magnetic microsphere-confined graphene for the preconcentration of some phthalate esters from environmental water and soybean milk samples followed by their determination by HPLC. Talanta 109:133–140

Wang W, Yu JC, Xia D, Wong PK, Li Y (2013d) Graphene and g-C_3N_4 nanosheets cowrapped elemental α-sulfur as a novel metal-free heterojunction photocatalyst for bacterial inactivation under visible-light. Environ Sci Technol 47:8724–8732

Wang Z, Du Y, Zhang F, Zheng Z, Zhang X, Feng Q, Wang C (2013e) Photocatalytic degradation of pendimethalin over Cu_2O/SnO_2/graphene and SnO_2/graphene nanocomposite photocatalysts under visible light irradiation. Mater Chem Phys 140:373–381

Wu C, Zhang Y, Li S, Zheng H, Wang H, Liu J, Li K, Yan H (2011a) Synthesis and photocatalytic properties of the graphene–$La_2Ti_2O_7$ nanocomposites. Chem Eng J 178:468–474. https://doi.org/10.1016/j.cej.2011.10.062

Wu Q, Zhao G, Feng C, Wang C, Wang Z (2011b) Preparation of a graphene-based magnetic nanocomposite for the extraction of carbamate pesticides from environmental water samples. J Chromatogr A 1218:7936–7942

Xiang Q, Yu J, Jaroniec M (2012) Graphene-based semiconductor photocatalysts. Chem Soc Rev 41:782–796

Xu T, Zhang L, Cheng H, Zhu Y (2011) Significantly enhanced photocatalytic performance of ZnO *via* graphene hybridization and the mechanism study. Appl Catal B 101:382–387

Xu F, Yuan Y, Wu D, Zhao M, Gao Z, Jiang K (2013a) Synthesis of ZnO/Ag/graphene composite and its enhanced photocatalytic efficiency. Mater Res Bull 48:2066–2070. https://doi.org/10.1016/j.materresbull.2013.02.034

Xu J, Lv H, Yang S-T, Luo J (2013b) Preparation of graphene adsorbents and their applications in water purification. Rev Inorg Chem 33:139–160

Xu L, Huang W-Q, Wang L-L, Huang G-F, Peng P (2014) Mechanism of superior visible-light photocatalytic activity and stability of hybrid Ag_3PO_4/graphene nanocomposite. J Phys Chem C 118:12972–12979

Yan Y, Sun S, Song Y, Yan X, Guan W, Liu X, Shi W (2013) Microwave-assisted in situ synthesis of reduced graphene oxide-$BiVO_4$ composite photocatalysts and their enhanced photocatalytic performance for the degradation of ciprofloxacin. J Hazard Mater 250:106–114

Yan X-G, Xu L, Huang W-Q, Huang G-F, Yang Z-M, Zhan S-Q, Long J-P (2014) Theoretical insight into the electronic and photocatalytic properties of Cu_2O from a hybrid density functional theory. Mater Sci Semicond Process 23:34–41

Yang L-Y, Dong S-Y, Sun J-H, Feng J-L, Wu Q-H, Sun S-P (2010) Microwave-assisted preparation, characterization and photocatalytic properties of a dumbbell-shaped ZnO photocatalyst. J Hazard Mater 179:438–443

Yang N, Liu Y, Wen H, Tang Z, Zhao H, Li Y, Wang D (2013a) Photocatalytic properties of Graphdiyne and graphene modified TiO_2: from theory to experiment. ACS Nano 7:1504–1512. https://doi.org/10.1021/nn305288z

Yang X, Cui H, Li Y, Qin J, Zhang R, Tang H (2013b) Fabrication of Ag_3PO_4-graphene composites with highly efficient and stable visible light photocatalytic performance. ACS Catal 3:363–369

Yang Y-C, Xu L, Huang W-Q, Luo C-Y, Huang G-F, Peng P (2015) Electronic structures and photocatalytic responses of $SrTiO_3$(100) surface interfaced with graphene, reduced graphene oxide, and Graphane: surface termination effect. J Phys Chem C 119:19095–19104. https://doi.org/10.1021/acs.jpcc.5b03630

Yao Y, Miao S, Liu S, Ma LP, Sun H, Wang S (2012) Synthesis, characterization, and adsorption properties of magnetic Fe_3O_4@graphene nanocomposite. Chem Eng J 184:326–332

Yoo D-H, Cuong TV, Pham VH, Chung JS, Khoa NT, Kim EJ, Hahn SH (2011) Enhanced photocatalytic activity of graphene oxide decorated on TiO_2 films under UV and visible irradiation. Curr Appl Phys 11:805–808

Yu JG, Guo H, Davis SA, Mann S (2006) Fabrication of hollow inorganic microspheres by chemically induced self-transformation. Adv Funct Mater 16:2035–2041

Yuan Q, Wu Z, Jin Y, Xu L, Xiong F, Ma Y, Huang W (2013) Photocatalytic cross-coupling of methanol and formaldehyde on a rutile TiO_2 (110) surface. J Am Chem Soc 135:5212–5219

Yuan Y, Gong X, Wang H (2015) The synergistic mechanism of graphene and MoS_2 for hydrogen generation: insights from density functional theory. Phys Chem Chem Phys 17:11375–11381. https://doi.org/10.1039/C5CP00011D

Yusoff N, Huang N, Muhamad M, Kumar S, Lim H, Harrison I (2013) Hydrothermal synthesis of CuO/functionalized graphene nanocomposites for dye degradation. Mater Lett 93:393–396. https://doi.org/10.1016/j.matlet.2012.10.015

Yusuf M, Elfghi F, Zaidi SA, Abdullah E, Khan MA (2015) Applications of graphene and its derivatives as an adsorbent for heavy metal and dye removal: a systematic and comprehensive overview. RSC Adv 5:50392–50420

Zhang K, Guo L (2013) Metal sulphide semiconductors for photocatalytic hydrogen production. Catal Sci Technol 3:1672–1690

Zhang H, Lv X, Li Y, Wang Y, Li J (2009) P25-graphene composite as a high performance photocatalyst. ACS Nano 4:380–386

Zhang N, Qiu H, Si Y, Wang W, Gao J (2011a) Fabrication of highly porous biodegradable monoliths strengthened by graphene oxide and their adsorption of metal ions. Carbon 49:827–837

Zhang X, Quan X, Chen S, Yu H (2011b) Constructing graphene/$InNbO_4$ composite with excellent adsorptivity and charge separation performance for enhanced visible-light-driven photocatalytic ability. Appl Catal B 105:237–242

Zhang Y, Tang Z-R, Fu X, Xu Y-J (2011c) Engineering the unique 2D mat of graphene to achieve graphene-TiO_2 nanocomposite for photocatalytic selective transformation: what advantage does graphene have over its forebear carbon nanotube? ACS Nano 5:7426–7435

Zhang D, Yan T, Shi L, Peng Z, Wen X, Zhang J (2012a) Enhanced capacitive deionization performance of graphene/carbon nanotube composites. J Mater Chem 22:14696–14704

Zhang X, Chang X, Gondal M, Zhang B, Liu Y, Ji G (2012b) Synthesis and photocatalytic activity of graphene/BiOBr composites under visible light. Appl Surf Sci 258:7826–7832

Zhang Z, Yang W, Zou X, Xu F, Wang X, Zhang B, Tang J (2012c) One-pot, solvothermal synthesis of TiO_2–graphene composite nanosheets. J Colloid Interface Sci 386:198–204

Zhao G, Song S, Wang C, Wu Q, Wang Z (2011) Determination of triazine herbicides in environmental water samples by high-performance liquid chromatography using graphene-coated magnetic nanoparticles as adsorbent. Anal Chim Acta 708:155–159

Zhou F, Shi R, Zhu Y (2011) Significant enhancement of the visible photocatalytic degradation performances of γ-Bi_2MoO_6 nanoplate by graphene hybridization. J Mol Catal A Chem 340:77–82. https://doi.org/10.1016/j.molcata.2011.03.012

Zhou M, Tian T, Li X, Sun X, Zhang J, Cui P, Tang J, Qin L-C (2014a) Production of graphene by liquid-phase exfoliation of intercalated graphite. Int J Electrochem Sci 9:810–820

Zhou P, Yu J, Jaroniec M (2014b) All-solid-state Z-scheme photocatalytic systems. Adv Mater 26:4920–4935

Zhu X, Zhang J, Chen F (2010) Hydrothermal synthesis of nanostructures $Bi_{12}TiO_{20}$ and their photocatalytic activity on acid orange 7 under visible light. Chemosphere 78:1350–1355

Zhu J, Wei S, Gu H, Rapole SB, Wang Q, Luo Z, Haldolaarachchige N, Young DP, Guo Z (2011) One-pot synthesis of magnetic graphene nanocomposites decorated with core@double-shell nanoparticles for fast chromium removal. Environ Sci Technol 46:977–985

Chapter 2
Dyes Depollution of Water Using Porous TiO_2-Based Photocatalysts

Bénédicte Lebeau, Florian Jonas, Pierrick Gaudin, Magali Bonne, and Jean-Luc Blin

Contents

2.1 Introduction 36
2.2 Dye Classifications 38
2.3 Titania Photocatalyst 39
2.3.1 Structure and Properties of TiO_2 40
2.3.2 Mechanisms of Photocatalysis and Principle of Pollutant Degradation 47
2.3.3 Parameter Affecting the TiO_2 Photoactivity Efficiency 49
2.4 Porous TiO_2 Photocatalysts 52
2.4.1 Templated Nanostructured TiO_2 52
2.4.2 Nanoparticles and Nanotubes 54
2.4.3 (Nano)composites: TiO_2 Supported on Porous Matrices 56
2.4.4 Doping of TiO_2 61
2.4.5 Shaping 63
2.5 Examples of Processes for Dyes Removal from Water Using TiO_2 Photocatalyst 65
2.5.1 Photocatalytic Membrane Reactors (PMRs) 65
2.5.2 Continuous-Flow Photochemical Micro-Reactor 72
2.6 Titania and Photocatalysis in Industry 76
2.7 Conclusions 77
References 77

Abstract Wastewater discharge from industries is a major environmental issue. Particularly, dyes are a major concern because of their toxicity on human health. Among the different techniques developed to remove these pollutants from water, heterogeneous photocatalysis appears as a promising technology, and it is one of the most studied for the decomposition of dyes in water phase over the few past decades.

B. Lebeau · M. Bonne
Université de Haute Alsace, CNRS, IS2M UMR 7361, Mulhouse, France

Université de Strasbourg, Strasbourg, France
e-mail: benedicte.lebeau@uha.fr; magali.bonne@uha.fr

F. Jonas · P. Gaudin · J.-L. Blin (✉)
Université de Lorraine, Laboratoire Lorrain de Chimie Moléculaire UMR CNRS 7053 L2CM, Vandoeuvre-lès-Nancy, France
e-mail: florian.jonas@univ-lorraine.fr; pierrick.gaudin@univ-lorraine.fr; jean-luc.blin@univ-lorraine.fr

N. Dasgupta et al. (eds.), *Environmental Nanotechnology Volume 4*, Environmental Chemistry for a Sustainable World 32, https://doi.org/10.1007/978-3-030-26668-4_2

Due to its properties, titania has been widely studied in the water treatment processes. However, to be implanted at a large scale, the photocatalytic activity still needs to be enhanced, especially in the visible domain. One way to reach this goal consists in increasing the specific surface area of the photocatalyst. From this point of view, porous TiO_2 are excellent candidates to be considered in the water treatment technologies.

Here we review the use of porous titania-based nanomaterials for the photocatalytic degradation of dyes contained in wastewater, since this process is the most promising. First a short presentation of common dyes used in the industry and their classification is given. The main information concerning TiO_2 as potential good photocatalyst for dye removal from wastewater is then given to remind its structures and properties, describe the mechanisms proposed for pollutant photodegradation, and present the parameters affecting its photoactivity efficiency. These aspects are the bases that orient researches in the synthesis of performant nanostructured TiO_2 photocatalysts. Recent advances related to this topic are reviewed including the shaping and preparation of TiO_2-based (nano)composites materials that have been developed to favor their use and/or integration in a process for potential industrial use. The last part is devoted to the progress of two most promising process for the implementation of viable system to remove dyes from wastewater at a large scale. Finally some patents and the interest of titania and photocatalysis in industry are reviewed.

Keywords Photodegradation · Titania · Nanomaterials · Doping · Membrane process · Flow reactor · Azo dyes

2.1 Introduction

There are several different types of substances that may pollute water, and contamination of surface water, groundwater, and soil is a major problem (Dror et al. 2012). Because of their potential carcinogenic and toxic effects on human health, among the different pollutants such as detergents, fertilizers, volatile organic compounds (VOC), halogenated organic compounds (HOCs), and dyes are a major environmental concern (Kolpin et al. 2002; Chen et al. 2011). Dyes are mainly discharged from pharmaceutics, printing, food coloring, cosmetics, paper, textiles, and many other industries, involving an environmental pollution. Dyes can change the color of water, impact light penetration, and reduce the solubility of gases such as oxygen, and some of them are toxic, which further affect the ecology in the water (Epolito et al. 2005; Nandi et al. 2009). Over 7×10^5 tons of dyes and pigments comprising more than 10,000 different molecules are produced annually worldwide (Dutta et al. 2014). Among the different kinds of dyes, the ones belonging to the azo family (Forgacs et al. 2004) are carcinogenic, resistant to biodegradation, highly toxic, and mutagenic to both human beings and aquatic life (Cai et al. 2017). Because of this toxicity for human health, many efforts have been devoted to remove dyes in

wastewater, and various processes such as filtration, gravity separation, flotation, biodegradation, or photocatalysis have been developed (Forgacs et al. 2004; Gupta and Suhas 2009; Rafatullah et al. 2010; Alventosa-de Lara et al. 2012). Due to its high efficiency and wide applicability, adsorption is the most employed process for removing water-soluble dyes, and activated carbons are known to be efficient adsorbents for the removal of dyes (Forgacs et al. 2004; Mahmoud et al. 2013). However, activated carbons suffer from low adsorption capacity, high-cost production, and regeneration (Cai et al. 2017). Therefore, other adsorbents such as clays and zeolites have been developed (Forgacs et al. 2004; Martorell et al. 2017). But, with this process the dyes are simply transferred from water to another medium causing secondary pollution. Other techniques such as filtration, gravity separation, and flotation have high operating costs and could release toxic secondary pollutants into the ecosystem. Consequently, they are not able to treat the water to meet standards for reuse filtration or coagulation. Biodegradation of synthetic dyes have also been developed (Demarche et al. 2012; Martorell et al. 2017). This process is quite inexpensive, and the end products of complete mineralization are not toxic. However, many of the synthetic dyes are chemically stable and resistant to microbiological attack. In addition, when the discharges have low biodegradable portions, for example, waste discharges of chemical industries, biological treatments are inefficient or insufficient (Oller et al. 2011). The development of an effective process to depollute water is therefore still of great and continuous interest. To reach this goal, the heterogeneous photocatalysis appears a promising technology, and it is one of the most studied for the decomposition of dyes in water phase over the few past decades (Julkapli et al. 2014; Cambié et al. 2016; Karthikeyan et al. 2017; de Lima et al. 2017; Sharma and Feng 2017; Cai et al. 2017). Indeed this technique has some advantages: (1) complete degradation of organic pollutants to CO_2 and water, (2) no solid wastes disposal problem, and (3) only mild temperature and "pressure" conditions are necessary. Photocatalytic degradation usually occurs at room temperature and pressure and may be more cost-effective than other conventional techniques such as activated carbon adsorption and chemical scrubbers, because the semiconductor catalysts are inexpensive and capable of oxidizing most organic compounds effectively. However, for most photocatalyst the activity still needs to be enhanced in particular in the visible domain.

Most of the considered techniques for water treatment require the use of materials for adsorption of the dye prior to its elimination. Thanks to their properties related to their small size such as large surface area, more active surface available, quantum effect, and so on, nanomaterials like nanoparticles, nanotubes, or ordered mesoporous materials are excellent candidates to be integrated into the processes of dyes removal from water (Cai et al. 2017). For example, Lee et al. have shown that the ordered mesoporous silica MCM-41 may be an effective absorbent for basic dyes removal from aqueous solution (Lee et al. 2007). In addition, the nature and the strength of the interaction between the host molecules and the adsorbent can be tuned by functionalizing the surface of these supports (Qin et al. 2009; Donia et al. 2009). Qin et al. have modified MCM-41 by introducing ammonium group, according to the post-synthesis way, for the adsorption of anionic dyes (Qin et al.

2009). Authors have evidenced that the functionalized MCM-41 material has a high affinity for the considered dyes and that the electrostatic interaction was responsible of the colorants adsorption. Among the various nanomaterials, titania-based ones are of particular interest. In fact, TiO_2 is known to be chemically stable, nontoxic, low cost, and reusable. Even more, the main advantages of titania for water treatment concern its photocatalytic properties. Therefore TiO_2 is the most studied and used photocatalyst nowadays (Gaya and Abdullah 2008; Chong et al. 2010; Lazar et al. 2012; Qiu et al. 2012; Lin et al. 2012; Ajmal et al. 2014). As it will be illustrated in this chapter, titanium dioxide represents a good photocatalyst for wastewater treatment. The adsorption and the photocatalytic efficiencies are favored by an increase of the surface area, and from this point of view, porous TiO_2 are excellent candidates to be considered in the water treatment technologies. This chapter will be dedicated to the use of porous titania-based nanomaterials for the photocatalytic degradation of dyes contained in water treatment, since this process is the most promising.

2.2 Dye Classifications

Synthetic dyes exhibit considerable structural diversity (Fig. 2.1). The main dyes employed in the industry are azo, diazo, anthraquinone, sulfur, indigoid, triphenylmethyl, and phthalocyanine derivatives (Forgacs et al. 2004) (Robinson et al. 2001). Among the wide variety of colorants available, azo dyes are the most used and represent over 50% of the colorants used in the industry (Forgacs et al. 2004). Azo dyes can be basic, acid, or sulfur. Azoïc ones are characterized by the presence of a double bond between two nitrogen atoms (–N=N–) where at least one of the two nitrogen atoms is bonded to an aromatic group. In addition to the –N=N– and aromatics functions, dye molecules can possess several other organic functions such as carboxyl, hydroxyl, amino, and sulfoxyl groups. Because of the presence of such organic functions, most of dyes exhibit amphoteric features. The charge of the dye is strongly dependent on the pH. Indeed, the deprotonation of acidic groups lead to the formation of an anionic moiety (Robinson et al. 2001). On the contrary, the protonation of amino functions lead to cationic dye. The dye can also be nonionic, dependently on the pH (Suteu and Malutan 2013). Nonionic dyes refer to dispersed dyes, which do not ionize in water (Robinson et al. 2001).

The chemical structure of dyes can be very different from one to another, and it is not straightforward to classify them only according to one parameter. Based on their general structure, dyes can be classified as anionic, nonionic, and cationic dyes (Robinson et al. 2001). A classification based on their source (natural, synthetic, animal, plants) and on their chemical structure (azo or non-azo dyes) was proposed by Ajmal et al. 2014 (Fig. 2.2).

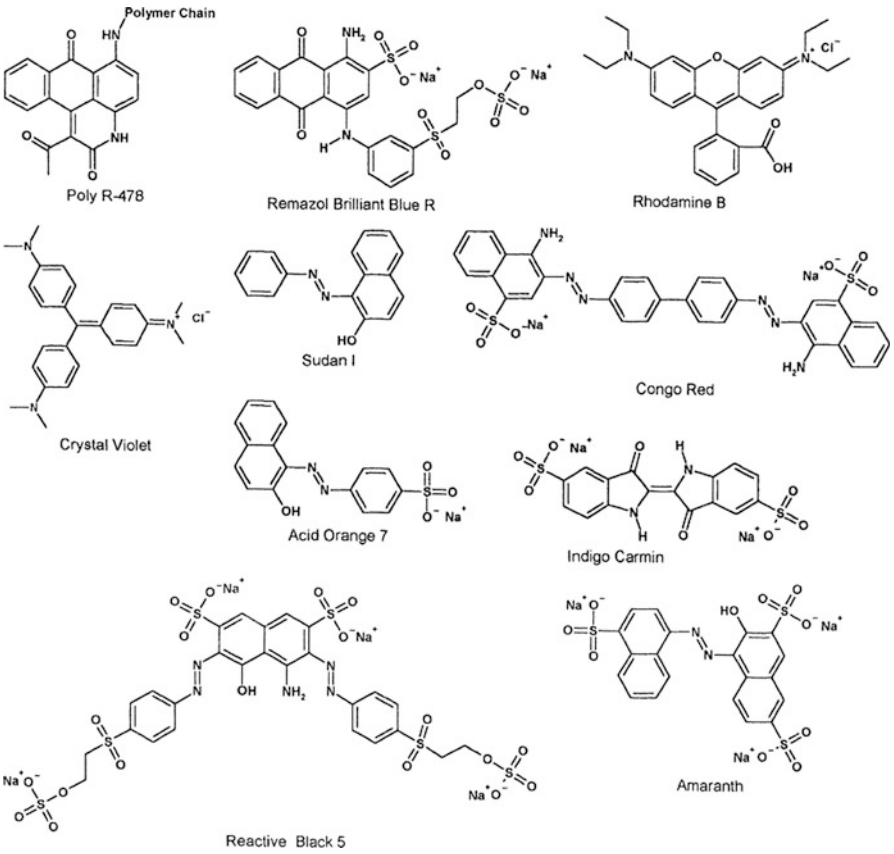

Fig. 2.1 Structure of the main synthetic dyes studied in degradation. Reprinted with permission from Forgacs et al. 2004. Copyright 2004 Elsevier, Environment International

2.3 Titania Photocatalyst

Titanium dioxide is widely used in the formulation of sunscreen and plastics, as pigments, or as catalyst (Carp et al. 2004). For example, when used in catalysis, it enhances the hydrodesulfurization (HDS) of transition metal sulfides (TMS) by transferring electronic density toward the TMS (Castillo-Villalón and Ramírez 2009). More recently, thanks to their good biocompatibility titania-based materials which have attracted much attention for enzyme immobilization. For example, Gao et al. have reported the immobilization of horseradish peroxidase (HRP) in templated titania through the biomimetic titanification process (Jiang et al. 2014). The authors have shown that the encapsulated HRP exhibits improvement of pH and thermal stability as well as tolerance against inactive agents. The encapsulated HRP also presents better removal efficiency than the free enzyme for the removal of both phenol and 2-chlorophenol. Titania is a semiconductor that has received

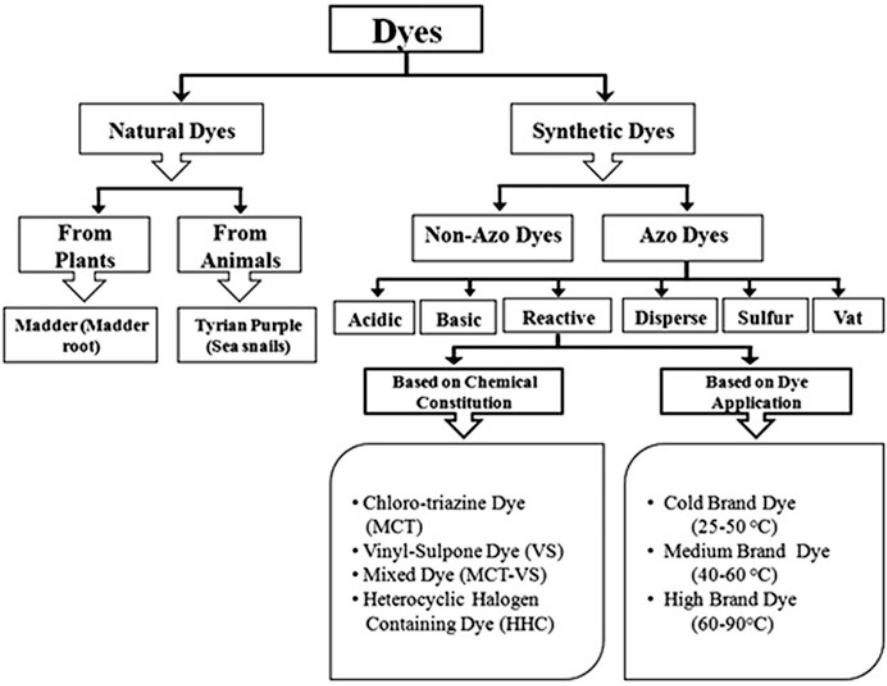

Fig. 2.2 Dye classification on the basis of dye chemical constitution and its application. (Reprinted with permission from Ajmal et al. 2014. Copyright 2014 RSC, RSC Advances)

considerable attention mainly for its applications in electronics, electrochemical systems, including photoelectrochemical solar cells, electrocatalysis, optoelectronic sensors devices, and high-performance photocatalytic films (Fox and Dulay 1993; Hoffmann et al. 1995; Linsebigler et al. 1995; Chen and Mao 2007).

2.3.1 Structure and Properties of TiO_2

TiO_2 exhibits three main polymorphs: anatase, rutile, and brookite (Fig. 2.3) (Landmann et al. 2012; Pelaez et al. 2012). The TiO_6 octahedron is the common primary structural unit of these phases. The structural difference of these phases is due to the different stacking arrangements of their octahedra. Rutile crystallizes in the tetragonal system ($P4_2/mnm$ space group). In rutile, each octahedron has ten neighbors: two share edges and eight share corners. The neighbors share corners along the [110]-type direction. Anatase belongs also to the tetragonal system but to the $I4_1/amd$ space group. It is composed of TiO_6 octahedra sharing faces. The corner-sharing octahedron forms [001] planes. Bulk brookite is a metastable phase, which crystallizes in the orthorhombic system (Pbca space group). At high-

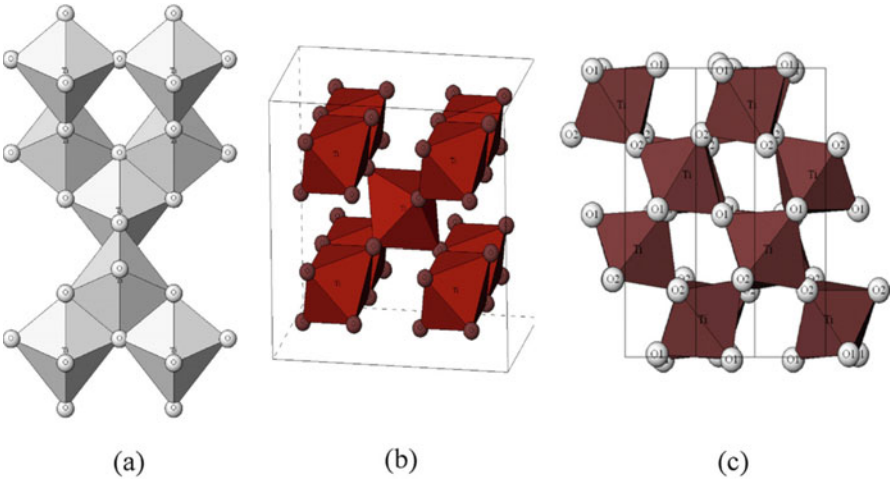

Fig. 2.3 Structure of the main polymorphs of titanium dioxide: anatase (**a**), rutile (**b**), and brookite (**c**). (Reprinted with permission from Pelaez et al. 2012. Copyright 2012 Elsevier, Applied Catalysis B: Environmental)

Table 2.1 Characteristics of the main polymorphs of titanium dioxide

	Anatase	Rutile	Brookite
Crystallographic system	Tetragonal	Tetragonal	Orthorhombic
Space group	$I4_1/amd$	$P4_2/mnm$	Pbca
Cell parameters (Å)	a: 3.793	a: 4.5937	a: 5.456
	c: 9.512	c: 2.9618	b: 5.497
			c: 5.1
Density (cm^3/g)	3.89	4.42	4.12
Band gap (eV)	3.2	3.0	3.4
Refractive index	2.561	2.605	2.581

pressure nonstoichiometric TiO_{2-x}, compounds can also be obtained. The bulk titania rutile structure is the most thermodynamically stable phase. However, at the nanosized level, when the particles size is lower than 11 nm or comprised between 11 and 35 nm, anatase and brookite become the more stable phase, respectively (Zhang and Banfield 2000). The band gap values of bulk rutile, anatase, and brookite are 3.0, 3.2, and 3.4 eV, respectively (Table 2.1). The Raman spectrum of bulk anatase exhibits a very intense band at around 143 cm^{-1} (e.g., band), and this mode shifts to higher wave numbers in nanocrystalline materials (Kelly et al. 1997; Zhang et al. 2000). As depicted in Table 2.2, due to its properties, titania has been widely used in the water treatment processes such as adsorption or photodegradation. In particular, the last one has been widely considered for the removal of either anionic or cationic dye. In this chapter, we will focus on this method for dye removal from

Table 2.2 TiO_2 for dyes removal from water

Dye family	Dye	Materials used for the removal	Depollution water process	Parameters	Lamp informations	Conclusions	References
Anionic dye	Acid black 26	Immobilized TiO_2 nanoparticles	Photodegradation and photocatalytic oxidation	700 mL of acid black 26 solution (0.071 mM) was mixing in a reactor (flow rate: 1 L/min). TiO_2 nanoparticles was immobilized on a sackcloth fiber support	UV lamp with an intensity of 1.8 mW/cm^2	In acidic conditions, with H_2O_2 for oxidation reaction, 80% of dye would be removed from the solution	Vaez et al. (2012)
	Acid blue 25	P25	Photocatalytic oxidation	A solution containing 50 mg/L of dye with various quantity of P25 and H_2O_2	Two UV-C lamp (15 W)	In optimized conditions, the system was able to remove 99% of dye in solution	Mahmoodi and Arami (2009)
	Acid orange 7	S,Cu-codoped TiO_2 nanoparticles	Photodegradation	20 mg/L acid orange 7 aqueous with various masses of catalyst in acidic conditions	Visible light source is 18 W lamp (>447 nm)	In optimized conditions, 60% of dye was converted in the solution	Yi et al. (2014)
	Acid orange 7	Mesoporous ZrO_2/TiO_2	Adsorption	0.01 g of mesoporous powder was mixing with 10 mL of acid orange 7 solution at various concentrations	–	In the better conditions, 101 mg/g of dye would be adsorbed on the materials	Kimling et al. (2017)
	Congo red	TiO_2 nanotubes doped La_2O_3	Adsorption	Adsorption kinetics: 0.20 g of adsorbent was mixing at 200 rpm with a CR aqueous solution of 20 mg/L	–	Equilibrium time is obtained after 10 min of reaction.	Guo et al. (2014)
				Adsorption isotherms: La_2O_3-TiO_2 nanotubes powders were placed in solution of CR at different concentrations (30–120 mg/L)		Langmuir isotherm, thanks to determine the maximum amount adsorbed on the catalysts (up to 140 mg/g)	

	Congo red	TiO_2/ palygorskite composite	Adsorption	0.2 g of adsorbent was introduced in 100 mL of dye solution with a concentration between 200 and 2000 mg/L	–	Langmuir model give a maximum adsorbent on the composite at 518 mg/g	Peng et al. (2013)
	Methyl orange	Mesoporous TiO_2	Adsorption	20 mL aqueous solution containing different concentrations of methyl orange (5–1000 mg/L) is mixing with mesoporous TiO_2 adsorbents during 20 min	–	The maximum adsorption capacities are determined to be 454.5 mg/g using Langmuir adsorption isotherms	Asuha et al. (2010)
	Methyl orange	TiO_2 doped Ag	Photodegradation	10 mg of catalysts were added to a reactor containing 30 mL of 20 mg/L of methyl orange solution	Three lamp (15 W each) : UVA (366 nm), UVB (310 nm), UVC (254 nm)	In each condition, more than 90% of dye discoloration was obtained. After 2 h of reaction, more than 80% of TOC was converted on the solution	Chaker et al. (2016)
	Methyl orange	C, N-modified monolithic TiO_2	Photodegradation	0.05 g of powder was added into 50 mL of methyl orange aqueous solution (12 mg/L)	1000 W xenon lamp	Every sample will be able to remove 90% of dye in solution	Chen et (al. 2010)
	Methyl blue	UiO-66/TiO_2	Photodegradation	45 mL of methylene blue solution with 100 mg of powder	500 W Xe arc lamp with a UV cutoff filter	More than 60% of dye is removed from the solution	Wang et al. (2017)
	Naphthol Green B	Mesoporous ZrO_2-TiO_2	Photocatalytic degradation	50 mL of dye aqueous solution (20 ppm) and variant quantity of ZrO_2-TiO_2 catalysts was mixing	16 W/cm^2 high-pressure mercury lamp (254 nm)	In optimized conditions, >99% of dye could be removed from the solution	Thejaswini et al. (2017)
	Orange II	Mesoporous TiO_2	Adsorption	Adsorption kinetics: 30 mg of adsorbent was introduced in 15 mL of dye solution	–	Equilibrium adsorption is obtained after 400 min of reaction. Langmuir isotherm, thanks to determine the	Abramian and El-Rassy (2009)

(continued)

Table 2.2 (continued)

				(50 mg/L) at different temperature (30, 40, et 50 °C) Adsorption isotherms: same conditions with different dye concentration (50–1500 mg/L)		maximal adsorption capacity at 402.82 mg/g (30 °C)	
	Quinoline yellow	Anatase TiO_2	Photodegradation	Lamp irradiated reactor containing 150 mL of dye solution (8.10^{-5} M) and 9 mg of TiO_2 powder	6 W UV lamp	A complete mineralization of dye is observed using COD analysis	Gupta et al. (2012)
Dye classification	**Dye**	**Reactive materials**	**Depollution water process**	**Parameters**	**Lamp informations**	**Conclusions**	**References**
Cationic dye	Basic blue 41	TiO_2/ palygorskite film	Photodegradation	12 mg of catalyst was introduced in 80 mL of dye solution ($2.5.10^{-5}$ M)	Four lamps with 4 W power each	After 90 min of reaction, more than 80% of dye coloration was removed from the solution	Stathatos et al. (2012)
	Direct red 81	P25	Photodegradation using a continuous-flow reactor	A solution containing 100 mg of P25 powders and $1.5.10^{-5}$ M of dye circulated at a flow rate of 88 mL/min in a reactor containing a photochemical chamber and a continuous source of wave radiation	Fluorescence lamp (max 350 nm) with different intensity (100, 300, 500, et 700 W)	The % photodegradation of dye after 105 min was 100% with the combination of UV/MW (700 W)	Genuino et al. (2012)
	Methylene blue	Mesoporous TiO_2-SiO_2	Adsorption	50 mg of adsorbents was mixed with 5 mL of aqueous dye solution of (0.1–2.5) mmol/L concentration range		Using Langmuir isotherm parameters, maximum adsorption value is 4.79 mmol/g for TiO_2-SiO_2 compound	Messina and Schultz (2006)

	Methylene blue	Mesoporous TiO_2-SiO_2	Photodegradation	0.03 g of powder were added to 300 mL of dye solution (20 mg/L)	500 W mercury lamp (max 365 nm)	99.2% of dye was degraded after 60 min of irradiation. The rate constant is 1.5 times more performed that Degussa P25	Yao et al. (2013)
	Methylene blue	Mn-doped TiO_2 nanoparticles	Photodegradation	100 mg of photocatalysts in 100 mL of solution (10 ppm)	Visible: Osram Dulux lamp 11 W UV: Mercury lamp (310–400 nm) of intensity 4.5 mW/cm^2	In any case, 90% of decolorization can be observed after 60 min of illumination	Binas et al. (2012)
	Methylene blue	TiO_2 coating on HDPE	Photodegradation	TiO_2/HDPE sample disk (surface area : 4.5 cm^2) was placed in the bottom part of a reactor with an aqueous solution (1.10–5 M) of dye	High intensity UV lamp (UVP Blak-Ray B-100AP)	After 6 h of reaction, less than 30% of dye was always in the solution	Kasanen et al. (2011)
	Methylene blue	TiO_2 nanotubes	Photodegradation	0.2 g of titanate nanotubes were dispersed in 100 mL of aqueous solution of MB at 9 mg/L	A 6 W, 254 nm, UV lamp	At equilibrium, 99% of MB was degraded from the solution in 20 min	Lin et al. (2011)
	Methylene blue	Au/TiO_2/SBA-15	Photodegradation	0.1 g of catalyst and 100 mL of dye solution (20 mg/L) were mixing	Visible light (>400 nm)	After 150 min of reaction, 99.8% of dye was removed	Y. Chen et al. (2015)
	Patent blue	Mesoporous TiO_2/apatite	Adsorption Photodegradation	Adsorption and photodegradation: 200 mg of adsorbents were added to 100 mL of a dye solution (20 mg/L)	125 W UV A-B-C lamp (200–600 nm)	In 1 h, adsorption equilibrium was achieved. In optimized conditions, 12 h was used to remove 95% of dye in solution	El Bekkali et al. (2016)

(continued)

Table 2.2 (continued)

	Rhodamine B	Mesoporous TiO_2	Photocatalytic oxidation	50 mg of catalyst was added into a cylindrical glass containing 50 mL of dye solution at 40 ppm	Irradiation lamp was a PLS-SXE 300 300W xenon lamp	After 250 min of irradiation, 90% of dye was removed	Liu et al. (2012)
	Rhodamine B	Ag-modified mesoporous TiO_2	Photodegradation	150 mg of photocatalyst and 300 mL of 8.6.10–3 mM were mixing	125 W high pressure mercury lamp	90% of dye in solution was removed after 60 min of irradiation	Xiong et al. (2011)
	Rhodamine B	Carbon/TiO_2 nanotubes	Photodegradation	25 mg of sample and 20 mL of dye solution (5.10^{-5} M)	Two UV lamps (20 W)	More than 80% of dye concentration was removed after 12 h of reaction	Im et al. (2012)
	Rhodamine B	P25 TiO_2	Photocatalytic oxidation	200 mL of aqueous solution of rhodamine B (5 mg/L) with 5 to 120 mg of P25, pH = 4.5	UV lamp (max 254 nm) with 15 W power and light intensity of 1643 μW/cm^2	96% of dye coloration was removed during the reaction. And 48% of the TOC was take off the solution	de Lima et al. (2017)
	Rhodamine B	Meso-/macroporous TiO_2	Photodegradation	50 mL of aqueous solution of rhodamine B (10^{-5} M) containing 50 mg of TiO_2	300 W mercury lamp	In 8 min of illumination, 97% of dye was removed	Zhao et al. (2016)

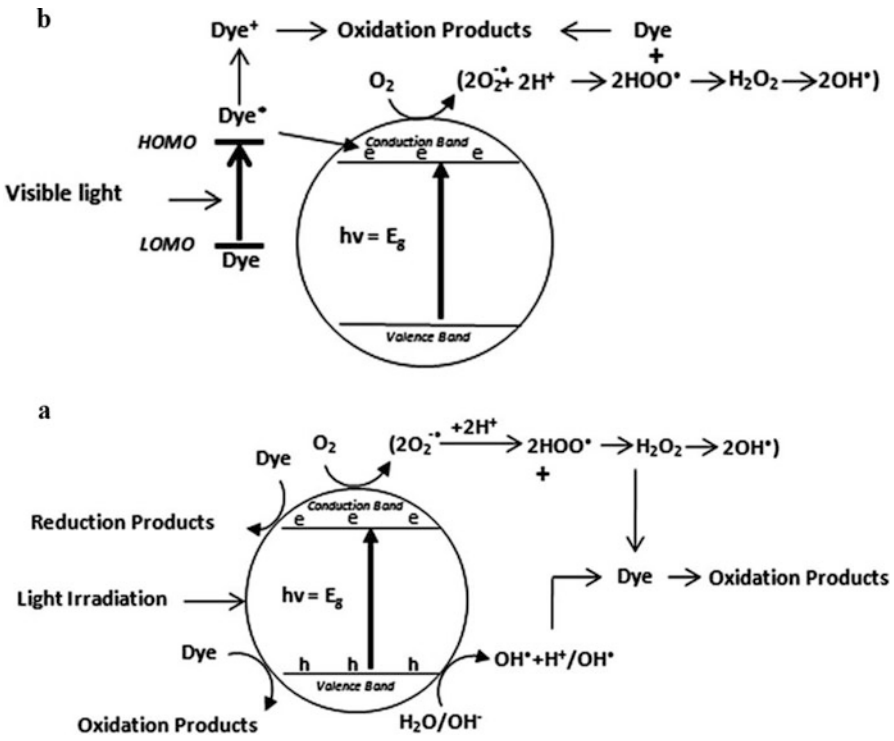

Fig. 2.4 Indirect (**a**) and direct (**b**) dye degradation processes. (Reprinted with permission from Ajmal et al. 2014. Copyright 2014 Royal Society of Chemistry, RSC Advances)

water. For this photocatalytic application, among the common crystalline forms of titania, anatase is generally recognized to be the most active phase.

2.3.2 *Mechanisms of Photocatalysis and Principle of Pollutant Degradation*

Titanium dioxide photocatalysis and photodegradation mechanisms (Fig. 2.4a) are well described in literature (Carp et al. 2004; Gaya and Abdullah 2008; Chong et al. 2010; Ajmal et al. 2014; Dong et al. 2015; Cai et al. 2017). Below we will just give a short overview of the basic principles of both processes. The photocatalytic properties of TiO_2 are evidenced by Fujishima and Honda in 1972 because when the photons energy of incident light is larger than the band gap of the TiO_2 particles, it

can be adsorbed by the semiconductor (Fujishima and Honda 1972). Electrons of the valence band are in an excited state and migrate in the conduction band. This results in the creation of photoelectrons (e^-) and electronic hole (h^+) according to the reaction:

$$TiO_2 + h\nu \rightarrow e^- + h^+$$

Recombination of these electron/hole (e^-/h^+) pairs can occur in the solid; they can also be balanced by a gap or migrate to the TiO_2 particle surface. The latter phenomenon is particularly interesting since oxydo-reduction reactions can take place with the donor or acceptor groups adsorbed at the surface. The strong oxidizing action of the hole (h^+) can involve the formation of highly reactive hydroxyl ($OH^\bullet$) or $R^\bullet$ radicals through the oxidation of water, of the superficial OH groups, or of the organic compounds (R), such as dyes, adsorbed at the TiO_2 surface. These radicals are very powerful oxidizing agents, which can react with the pollutants adsorbed at the material's surface through the following indirect reactions:

$$h^+ + H_2O_{ads} \rightarrow H^+_{ads} + OH^\bullet_{ads}$$
$$h^+ + OH^-_{ads} \rightarrow OH^\bullet_{ads}$$
$$h^+ + R_{ads} \rightarrow R^\bullet_{ads}$$

Electrons (e^-) in the conduction band can also react with electron acceptors such as oxygen to lead to the formation of superoxide radicals $O^\bullet_{2\ ads}$.

$$e^- + O_2 \rightarrow O^\bullet_{2\ ads}$$

This reaction is very important since it prevents the electron/hole recombination. In the absence of appropriated acceptors or donors of electrons, the electron/hole recombination occurs. This process is very fast, in the range of the picosecond.

$$TiO_2 + h^+ + e^- \rightarrow TiO_2$$

The superoxide radical is protonated to form hydroperoxyl radical ($HO^\bullet_2$), and then subsequently hydrogen peroxide (H_2O_2) is formed, which dissociates into two highly reactive hydroxyl radicals.

$$O^\bullet_{2\ ads} + H^+ \rightarrow HO^\bullet_{2\ ads}$$
$$2\ HO^\bullet_{2\ ads} \rightarrow H_2O_{2ads} + O_2$$
$$H_2O_{2ads} \rightarrow 2\ OH^\bullet_{\ ads}$$

The hydroxyl radicals will degrade the pollutant (R).

$$R + OH^{\bullet}{}_{ads} \rightarrow \text{Intermediates of reaction} \rightarrow CO_2 + H_2O$$

Oxidation and reduction processes will also take place at the surface of the photocatalyst:

$$R + h^+ \rightarrow \text{oxidation products}$$
$$R + e^- \rightarrow \text{reduction products}$$

Since the recombination probability is 99.9%, this electron/hole recombination is the limiting factor for the photocatalytic efficiency. They involve a loss of the photoelectrical energy in the form of heat. In addition, only a small fraction of the solar spectrum, around 5%, can effectively be used to degrade pollutants such as dyes. Indeed the band gap of anatase (3.2 eV) requires ultraviolet radiation for photocatalytic activation, but UV light accounts for only 5% of the sun energy compared to the 45% of the visible light (Dong et al. 2015). Thus, many studies are devoted to the shift of TiO_2 band gap toward lower values to induce an optical response of titania in the visible domain. As described in Sect. 4.4, the main way to reach this goal consists in doping titania or associating TiO_2 with another semiconductor such as ZnO. Besides the indirect degradation mechanism, under visible light, direct degradation of the dye (Fig. 2.4b) can also occur (Ajmal et al. 2014). However, the latter is far slower reaction compared to the indirect mechanism (Ma and Yao 1998).

2.3.3 *Parameter Affecting the TiO_2 Photoactivity Efficiency*

The photocatalytic efficiency of TiO_2 in solution depends on several factors such as the pH, the crystal structure, the particle size, the surface area, and the porosity of the photocatalyst (Li et al. 2005; Kim et al. 2007).

At low pH, the TiO_2 surface is positively charged and cannot provide the hydroxyl groups, which are needed for hydroxyl radical formation. However, an acidic solution enhances the amount of $HO^{\bullet}_{2\,ads}$ radicals and hence increases the concentration of H_2O_2, promoting the photocatalysis performance (Paz 2006). On the other hand, more efficient formation of hydroxyl radicals is expected to occur in alkaline solution since a higher pH value can provide a larger concentration of hydroxyl ions to react with the holes to form hydroxyl radicals. However, a too high pH can result in excess radicals, leading to self-quenching (Torres-Martinez et al. 1999).

As mentioned above, the photocatalytic activity of TiO_2 is mainly attributed to its anatase phase, and it is reported that higher crystallinity enhanced drastically the photocatalytic activity of TiO_2 materials (Ohtani et al. 1997; Pelizzetti et al. 1993; Kelly et al. 1997; Zhang et al. 2000). Moreover, small crystallite size is considered to favorably increase the probability of mutual e^-/h^+ recombination at both surface and bulk traps.

It was also reported that the photocatalytic degradation rate of azo dyes in the presence of UV/TiO_2 is strongly dependent on the chemical structure of the dye. Indeed, monoazo dyes are more easily decomposed than triazo dyes since the stability of both triazine nucleus and cyanuric acid intermediates makes triazo dyes difficult to fully oxidize (Reutergadh and Iangphasuk 1997; Minero et al. 1997). Fortunately, such intermediates are not toxic.

Competitive adsorption between water molecules and the target molecules can occur due to photogenerated oxidizing species, which may not migrate far away from their formation centers, explaining that there is no or very slow rate of degradation at few nanometer layers around the catalyst particles surface (Hufschmidt et al. 2002).

According to the configuration of the reactor, light intensity, nature of the dye, and morphology of TiO_2 catalyst, the optimum quantity of the catalyst required for an efficient removal of the dye can change. Several studies have been realized in order to determine this optimum quantity by studying the reaction rate of the photooxidation process. Indeed, when all dye molecules are adsorbed on TiO_2 surface, it clearly appears that the addition of higher quantities of photocatalyst would have no further enhancing effect on the degradation efficiency. Moreover, Zhu et al. reported in their study that the excess of photocatalyst particles may increase opacity of the suspension which may retard the degradation rate (Zhu et al. 2012). Furthermore increasing the quantity of catalyst in the medium will increase particle–particle interaction. In that case, activated molecules can be deactivated by collision with ground-state titanium dioxide particles.

On the other hand, the quantity of the initial dye can also influence the mechanism of photodegradation. Indeed, when increasing dye concentration, dye ions will cover more active sites preventing the formation of OH radicals on the surface of TiO_2 catalyst as described in paragraph 3.2. Several authors described this phenomenon by increasing (Zhu et al. 2012) (Ilinoiu et al. 2013) or decreasing (Kansal et al. 2008) the quantity of initial dye. In order to increase photooxidation rate, adding oxidative species such as hydrogen peroxide (H_2O_2), ammonium persulfate ($(NH_4)_2S_2O_8$), potassium bromate ($KBRO_3$), or potassium peroxydisulfate ($K_2S_2O_8$) (Qamar et al. 2005; Saquib et al. 2008a, b) is often used in the photocatalytic process. Indeed, the electron/hole recombination causes waste of energy, and to avoid this, it is essential to prevent this latter phenomenon. In heterogeneous catalysis, molecular oxygen plays the role of an electron acceptor, so the addition of external oxidant (electron acceptor) in the medium will increase the photocatalytic degradation of contaminants. This phenomenon is well described in literature and based in three steps (Ahmed et al. 2010):

- Removal of the electron-hole recombination
- Increase of the hydroxyl radical concentration and so of the intermediate rate compounds
- Generation of more radicals and other oxidizing species in order to increase the degradation photocatalytic rate of the compounds

The addition of the oxidant species exhibits a dual function: acting as strong oxidants, they will tend to increase the formation of hydroxyl radicals but also inhibit the electron/hole (e^-/h+) pair recombination; however, all the oxidizing agents do not have the same impact on photocatalytic degradation. Indeed, among those cited above, researchers have shown that H_2O_2 is generally the most effective oxidant (Ahmed et al. 2010). In that case, the enhancement of the degradation can be explained as follows (Akpan et al):

$$H_2O_2 + {}^{\bullet}O_2^- \rightarrow {}^{\bullet}OH + OH^- + O_2$$
$$H_2O_2 + hv \rightarrow 2\,{}^{\bullet}OH$$
$$H_2O_2 + e^- \rightarrow {}^{\bullet}OH + OH^-$$

This effect of H_2O_2 has been demonstrated by Chiou et al. in the photocatalytic degradation of phenol where the increase of the removal efficiency is observed (58 to 84% within 3 h with the addition of H_2O_2 from 1.77 mM to 8.82 mM) (Chiou et al. 2008). In this study, they also show the total degradation of phenol within 2.5 h and 1h by increasing the H_2O_2 concentration from 44.1 mM to 88.2 mM.

In addition, it has been generally shown that the UV/TiO_2/oxidant degradation process is more effective in acidic than in basic medium (Ahmed et al. 2010).

Some studies, however, have shown that an optimal concentration of H_2O_2 should be taken into account. In fact, at higher concentrations, for example, the degradation of orange G on N-doped TiO_2 decrease (Akpan and Hameed 2009). This can be explained by the consumption of ${}^{\bullet}OH$ radicals and holes by H_2O_2 itself as described as follows (Mahmoodi et al. 2006; Coleman et al. 2007):

$${}^{\bullet}OH + H_2O_2 \rightarrow HO_2^{\bullet} + H_2O$$
$${}^{\bullet}OH + HO_2^{\bullet} \rightarrow O_2 + H_2O$$
$$h^+ + H_2O_2 \rightarrow O_2 + 2H^+$$

In parallel, the recombination of radicals must be taken into account as a competitive reaction that can occur:

$${}^{\bullet}OH + {}^{\bullet}OH \rightarrow H_2O_2$$

Both ${}^{\bullet}OH$ and h^+ can finally be considered as strong oxidants for organic pollutants, but in the excess of H_2O_2 concentration, the photocatalytic degradation can be inhibited. Moreover, H_2O_2 can be adsorbed on TiO_2 particles that leads to surface modification and thus to the photocatalytic degradation (Tanaka et al. 1989).

However, in various studies many authors have reported adsorption of compounds or intermediates that may acts as poison on the catalyst surface, e.g., a multilayer of dye molecules around the catalyst particles surface which leads to limited interaction between excited dye molecule and the catalyst and thus a decrease in photooxidation process (Bizani et al. 2006).

To develop efficient photocatalysts, the specific surface area is also a crucial parameter that should be considered. Generally, large surface area is likely to exhibit better photocatalytic activity, because a large surface area provides more active sites for adsorbing dyes. Recently, much attention was paid to the synthesis of the nanostructured mesoporous photocatalysts with high surface area and uniform pore size distribution. In this chapter, we will particularly focus on this point.

2.4 Porous TiO_2 Photocatalysts

2.4.1 Templated Nanostructured TiO_2

Usually mesoporous titania are synthesized from the sol-gel process using titanium alkoxides as precursors. For example, using this technique and starting from titanium isopropoxide as precursor and performing a hydrothermal treatment at different temperatures from 40 to 240 °C, Rasalingam et al. have synthesized efficient photocatalysts for the degradation of rhodamine B under visible light irradiation (Rasalingam et al. 2015). Using the sol-gel approach, the textural properties of the TiO_2 materials are mainly controlled by the synthesis conditions such as the pH, the gel composition, the humidity, and so on (Simonsen and Søgaard 2010). The textural properties of the porous TiO_2 can also be enhanced by combining the sol-gel process with the surfactant-templating mechanism, reported for the preparation of the ordered mesoporous silica materials (Li et al. 2014; Bagheri et al. 2015; Kimura 2016). Two methods can lead to the formation of mesostructured TiO_2 mesostructures. The first one is the hard-templating route. In that case, the mesoporous titania is prepared in a confined space, for example, via replication of mesoporous silica. Since the template prevents collapse of the mesostructure upon calcination, the main advantage of this method is the preservation of the ordered mesopore channel array during the crystallization step at high temperature. However, this procedure is time-consuming, non-eco-friendly (it usually requires hydrofluoric acid to remove the hard template), and it is quite difficult to completely fulfill the mesopores of the hard template with the titania precursor. By contrast, the second mechanism labelled the soft-templating pathway is less time-consuming and more eco-friendly. A large variety of structure-directing agents such as ionic liquid, poly(ethylene glycol), diblock copolymer, polyoxyethylene fluoroalkyl ether, cyclodextrins, or homemade block copolymers (BCPs) have been used to prepare the porous titania material though the soft-templating route (Zimny et al. 2010; Veliscek-Carolan et al. 2015; Lannoy et al. 2014; Cao et al. 2016; Preethi et al. 2017). Nevertheless, among these templates, thanks to their large molecular weights, the triblock copolymers such as Pluronic P123 or F127 are the most widely considered for the preparation of porous TiO_2 (Ismail and Bahnemann 2011). Nevertheless, the main difficulty is to control the alkoxide precursor hydrolysis and condensation that are much faster than for silicon. To reach this goal, different strategies have been developed, and, for example, this control can be achieved by the use of mixed

inorganic precursor or hydrolysis controlling agents, such as acetylacetone or hydrogen peroxide (Tian et al. 2002; Tian et al. 2003; Li et al. 2008). For example, in 1995 Antonelli and Ying have reported the first example of mesoporous titania by using tetradecyl phosphate as surfactant and titanium acetylacetonate trisisopropoxide as Ti source. Acetylacetone acts as a hydrolysis controlling agent of the titanium precursor (Antonelli and Ying 1995). The obtained material adopts a hexagonal pore ordering, but the structure partially collapses after the pores are freed from the surfactant by calcination at 350 °C. More recently, we have developed a synthesis procedure of ordered mesoporous materials, having semicrystalline framework and with high specific surface area (>250 m^2/g). Our strategy is based on the evaporation-induced self-assembly method, usually used for the preparation of the mesoporous films and on the liquid crystal templating mechanism (Zimny et al. 2010). The obtained mesostructured TiO_2 materials with semicrystalline framework are effective photocatalyst for dyes degradation such as methyl orange (Zimny et al. 2012; Assaker et al. 2015). The efficiency of the process depends on the working conditions, and the optimal conditions are 1 hour of dark adsorption, a TiO_2 concentration of 0.5 g/L, and a methyl orange concentration of 15 mg/L at acidic pH (pH = 4) with an incident light intensity of 10^{-5} Einstein L^{-1} s^{-1}. The rates of methyl orange decomposition follow Langmuir-Hinshelwood kinetics. The dependence of the reaction rate on the incident light intensity is first order. No change in the activity of the catalyst is observed at the first four cycles, which indicates that the TiO_2 is able to use repeatedly (Blin et al. 2012). We have also succeeded in introducing a second level of porosity, and we have shown that thanks to the synergic effect of the presence of the two mesopore networks, the dual mesoporous titania are more efficient for the photodegradation of methyl orange, used as model dye, than the mono-modal ones (Naboulsi et al. 2017). However, one main drawback still persists: it concerns the limitation of the crystallization temperature around 400 °C, which is far under the required temperature (550 °C) to completely transform amorphous TiO_2 into anatase.

Another dual-templating approach has been reported to produce hierarchical macro-/mesoporous TiO_2 by a bi-template interface-directed deposition mechanism based on a combination of soft-templating with P123 surfactant for mesoporous network and hard-templating with macroporous carbon gabarit (Zhao et al. 2016). Macroporous carbon gabarit was first synthesized and immersed in the precursor solution of the mesoporous TiO_2 network. The resulting hierarchical macro-/mesoporous TiO_2 material presents a regular array of macropores surrounded by ordered mesoporous titania walls composed of well-crystallized anatase nanocrystals. Due to its high specific surface area, high porosity, well-connected channels, and abundant hydroxyl groups, a high capacity of adsorption toward rhodamine B dye was observed. Under stimulated sunlight the rhodamine B was fully decomposed in the presence of this hierarchical macro-/mesoporous TiO_2 in 8 min. The photodecomposition of rhodamine B was slower with two reference catalysts: TiO_2 hollow microsphere arrays and commercial Degussa P25 TiO_2. Macroporosity was also generated by an interesting approach derived from particle-stabilized emulsions to produce macrostructure-controlled titania ceramics

which has been reported by Li et al. (Li et al. 2016). With 3D interpenetrating highly porous structure and uniform 3–18 μm pores, the materials have showed high adsorption capacity and an excellent photocatalytic performance for the degradation of rhodamine B. Interestingly, sucrose has been added in the synthesis medium to produce C-coating on the TiO_2 surface by sintering the solid at 500 °C under N_2. The C-coating of macroporous TiO_2 ceramic has improved both the dye adsorption capacity and the photodegradation rate of rhodamine B.

2.4.2 Nanoparticles and Nanotubes

When TiO_2 materials are synthesized as particles with nanosize, they result in high specific surface area materials with exalted photocatalytic properties. TiO_2 nanoparticles have been widely studied for photodegradation of organic pollutants in aqueous solutions and showed high potential for wastewater treatments. In particular, they have been studied for their ability to decompose organic dyes in aqueous solutions. There are several methods to synthesize TiO_2 nanomaterials such as sol-gel, sol, hydrothermal, solvothermal, and chemical vapor deposition that are well described in the recent review of M. M. Mahlambi et al. (2015). The synthesis method and the experimental conditions are determinant on the structural and textural characteristics such as crystalline phase, crystallinity degree, particle size, and morphology, which directly influence the photocatalytic properties. Nanoparticles can be prepared at low temperature via a sol-gel or sol route, but result in TiO_2 amorphous phase and thus a subsequent thermal treatment has to be applied to get the anatase TiO_2 crystalline phase. W-C. Lin et al. have prepared anatase TiO_2 nanoparticles by using a sol-gel method with titanium isopropoxide (TTIP), isopropanol as solvent, and acetylacetone (AcAc) as stabilizer for TTIP and in the presence of polyethylene glycol that allowed controlling specific surface area (Lin et al. 2012). The synthesis experimental conditions have been optimized with the Taguchi experimental design method ($L_9(3^4)$). The post-synthesis calcination treatment to form pure anatase nanoparticles was also investigated, and a temperature of 550 °C was found optimal. The synthesized nanoparticles processed as powder or as films have been shown to be efficient photocatalyst for the degradation of methyl blue, methyl orange, and indigo dyes in water after 10 h of UV light irradiation. Among the four parameters varied for the experimental design matrix, the molar ratio AcAc/TTIP was found to have the greatest impact on the photocatalytic degradation of dyes in water. It was also observed that the presence of hydroxyl groups can improve the photocatalytic activity. The size of TiO_2 particles is also paramount of importance for photocatalytic efficiency. The influence of the morphology on the photocatalytic activity of TiO_2 nanoparticles has been investigated, and the nanorod shape aroused a particular interest. The sol-gel route allows introducing polymers or block copolymers, amphiphilic, or not, in the synthesis medium to control morphology, particles size, and aggregation. For a practical and an economical point of view, it is highly desired to develop facile

and surfactant/polymer-free methods for the morphology control of TiO_2 nanostructures. Anatase TiO_2 nanorods have been synthesized via a simple two-step method: a hydrothermal treatment of the commercial P25 TiO_2 nanoparticles in a composite-hydroxide eutectic system of 1:1 M KOH/NaOH, followed by acid posttreatment (Hafez 2009). The obtained TiO_2 nanorods have a good crystallinity with the dimensions of 200–300 nm length and of 30–50 nm diameter. Furthermore, they are mesoporous with an average pore size of 6.2 nm and have a BET specific area of 85 m^2/g. Compared to their precursor anatase/rutile TiO_2 P25 and the titanate nanotubes, the pure anatase TiO_2 nanorods are more efficient for the photodegradation of the commercial cibacron red (FN R) textile dye under UV irradiation. Hierarchical rutile TiO_2 superstructures made of nanorods assembled at a water-dichloromethane interface have been prepared by a hydrothermal treatment of dichloromethane solution of $TiCl_4$ (Wang et al. 2009). Size and shape of nanostructures were easily modified by varying the $H_2O/TiCl_4$ molar ratio. The resulting TiO_2 hierarchical superstructures showed higher photocatalytic property to decompose methylene blue under UV light irradiation in aqueous solution (92% in 30 min) compare to that of commercial P25 (47% in 30 min). The hydrothermal synthesis route based on a water-dichloromethane interface has allowed obtaining TiO_2 nanostructures as powder or as freestanding film. The film is composed of greater crystallites, has a lower specific surface area, and shows lower photocatalytic efficiency; however, it offers an easier handling. The synthesis of TiO_2 nanorods has been also realized by a rapid microwave-assisted polyol route from titanium glycolate followed by water treatment under microwave irradiation or calcination at 500 °C (Gerasimova et al. 2016). Following this route or a conventional polyol route, the synthesized nanorods are micro-mesoporous. The post-synthesis water treatment under microwave allowed forming anatase nanocrystallites of 5.4 nm size and increasing specific surface area. The as-synthesized TiO_2 nanorods show a better photocatalytic activity for the removal of rhodamine B (97% decomposition of rhodamine B after 30 min of UV light irradiation). The post-synthesis calcination at 500 °C has resulted in the formation of mesoporous nanorods with bigger anatase crystallites (19.3 nm), a lower specific surface area, and a lower capacity of dye adsorption but having higher photocatalytic efficiency (98% decomposition of rhodamine B after 15 min of UV light irradiation).

Titania nanotubes (TNT) have been also considered for the removal of dyes from aqueous solutions (Lai et al. 2014). The three general approaches in preparing TNT are alkaline hydrothermal route, anodization techniques, and chemical (template) synthesis. The hydrothermal synthesis is recognized as a facile and low-cost method and leads after a first step to titanate nanotubes that can be transformed into anatase TNT by acid posttreatment and calcination (Xu et al. 2011). The obtained mesoporous anatase TNT photocatalyst has shown a good photocatalysis efficiency toward the degradation of acid orange 7 dye. Recently, a single post-acid treatment after hydrothermal synthesis of titanate nanotubes in highly concentrated NaOH solution was reported to be sufficient to obtain anatase nanotubes with high surface OH density (Tsai et al. 2017). The resulting materials are active photocatalysts for the decomposition of Congo red and crystal violet dyes due to their high dye pre-adsorption capacity.

The hydrothermal synthesis of titanate nanotubes with different temperatures and durations and the investigation of their photocatalytic properties for the removal of methylene blue under UV light irradiation from an aqueous environment was reported by Liu et al. (Liu et al. 2015) and Subramaniam et al. (2017). Compared to their P25 TiO_2 nanoparticle precursor, they are mesoporous with larger specific surface area and present both a higher dye absorption capacity and a better photocatalytic performance for the dye decomposition under UV light irradiation in aqueous solutions.

2.4.3 (Nano)composites: TiO_2 Supported on Porous Matrices

Mesoporous TiO_2 are not thermally stable and usually exhibit low porous characteristics, or even a collapse of the mesostructure, after thermal treatment that is necessary to get highly crystalline anatase walls for good photocatalytic efficiency. To overcome these drawbacks, silica-embedded titania and/or titania-silica mixed oxides have been prepared. The introduction of silica is also a way to modulate surface properties for improving the adsorption of dyes and thus the photocatalytic performance of the material. Highly ordered 2D hexagonal mesoporous TiO_2/SiO_2 composite with variable Ti/Si ratios have been prepared by evaporation-induced co-assembly process using titanium isopropoxide and tetraethyl orthosilicate as precursors, triblock P123 copolymer as template, and a large amount of HCl to control co-condensation of precursors (Dong et al. 2007). The obtained TiO_2/SiO_2 nanocomposites have large regular mesopores (6–8 nm) and are ultra thermally stable, over 900 °C when Ti/Si $\leq$ 80/20, with high specific surface area (200–300 m^2/g). Their walls are constituted of anatase nanocrystallites glued by amorphous silica. The photocatalytic activities of these composites for the degradation of rhodamine B in aqueous solution were found excellent and higher than those of commercial TiO_2 P25. The study of their photocatalytic properties has been extended to the degradation of a large variety of anionic and cationic dyes (Dong et al. 2012). It was demonstrated that the surface properties of these TiO_2/SiO_2 nanocomposites can be modulated by varying the Ti/Si ratio and the calcination temperature to adapt them for an optimal adsorption (number of surface hydroxyls) and efficient photodegradation (size and crystallinity of anatase nanocrystals) according to the nature of the dye. Recently, it was reported that the extraction of silica from these TiO_2/SiO_2 nanocomposites leads to stable and reusable three-dimensional interconnected mesoporous anatase photocatalysts. The photocatalytic activity for the degradation of dyes in aqueous solution under UV light irradiation is much higher than the TiO_2/SiO_2 parent materials and commercial P25 (Dong et al. 2017). The departure of silica from the wall has left interlinked mesoporous network that helps the diffusion of dye molecules. The introduction of silica precursor as a stabilizer has been also reported for the solvothermal synthesis of silica-embedded titania rhombic-shaped nanoparticles (Yao et al. 2013). The presence of silica allows growing well-defined anatase crystals with high specific surface area that increases

linearly with the introduced amount of silica and due to textural mesoporosity. Due to the high specific surface area and the high crystallinity, the photocatalytic activity of the optimal silica-embedded titania nanocomposite for methylene blue photodegradation under UV light irradiation is higher than those of pure TiO_2 nanoparticles and commercial P25.

Coupling TiO_2 with another material can be an effective tool to tune the electron/hole recombination. As the photocatalysis mechanism of ZnO is very similar to the one of TiO_2, both oxides are often associated (Jing et al. 2004; Lin et al. 2005). For example, Serpone et al., which have examined many coupled oxides for the photodegradation of aromatic compounds, demonstrated during the reaction that a transfer of electrons and holes happens in the ZnO/TiO_2 (Serpone et al. 1995). This transfer inhibits the recombination of the charge carriers and enhances the photocatalytic activity. Pérez-Larios et al. have reported the preparation of ZnO/TiO_2 mixed oxides by sol-gel method varying the amount of ZnO in the materials between 1 and 10 wt% (Pérez-Larios et al. 2012). They showed that obtained materials present a photocatalytic activity in water splitting six times higher than that presented by the bare TiO_2. Xu et al. (2004, 2005) prepared ZnO/TiO_2 mixed oxides by simple wet impregnation of ZnO precursor on TiO_2 pre-synthesized nanoparticles (Xu et al. 2004, 2005). The authors showed that when ZnO is located on the surface of TiO_2 nanoparticles, it acts as recombination center of charge carriers. Consequently, the photocatalytic activity of obtained materials is enhanced. Shifu et al. investigated the preparation of ZnO/TiO_2 mixed oxides by ball-milling in water (Shifu et al. 2008). These authors tested the effect of the amount of Zn on photocatalytic oxidation of methyl orange and reduction of $Cr_2O_7^{2-}$. They demonstrated that the photocatalytic degradation efficiency of methyl orange decreases with the increase of Zn amount in the ZnO/TiO_2 materials. However, the photocatalytic reduction of $Cr_2O_7^{2-}$ depends on the amount of Zn on the material and reaches its optimum when this amount is of 5 wt. %. They showed also that the materials photocatalytic activity is influenced by the ball-milling time, and the reduction of $Cr_2O_7^{2-}$ is increased when milling time is up to 12 h. Guo et al. explain that high amount of ZnO increases the percentage of voids due to the lack of oxygen in the crystallites of anatase (Guo et al. 2010). These gaps are likely to induce an intermediate energy level close to the conduction band of the anatase phase and therefore to trap photogenerated electrons, by inhibiting the recombination of e^-/h^+, which consequently improves the photocatalytic activity of the material. In the same context, Liao et al. attribute the increase of the photocatalytic activity of the ZnO/TiO_2 compared to TiO_2, to the presence of ZnO particles which cover the surface of TiO_2 (Liao et al. 2008). Thus, an electron (e^-) transfer occurs between the ZnO conduction band and that of the TiO_2 and inversely for the photogenerated holes (h^+), which move from the valence band of TiO_2 to that of ZnO. The separation of charge carriers increases their life and improves the photocatalytic efficiency. In both cases, the presence of ZnO aggregates on the surface of mesoporous TiO_2 reduces the recombination of e^-/h^+ and improves the photocatalytic activity of TiO_2.

The hydrothermal synthesis of mixed porous TiO_2/SnO_2 templated by polystyrene beads was also reported with higher photocatalytical activity toward the

photodegradation of rhodamine B under UV light irradiation than the one of commercial P25 (Wang et al. 2014a, b). However, the correlation between crystalline structures and mesoporous porous structure with photocatalytical activity when molar ratio Ti/Sn is varied was not clearly evidenced.

Concerning TiO_2 nanoparticles, they are highly photocatalytically active for the photodegradation of organic pollutant in solution. However, their morphology makes them difficult for handling and for recovering. To overcome these problems, various strategies to synthesize TiO_2 nanoparticles supported composites as photocatalysts for dye degradation have been developed. Two series of TiO_2–SiO_2 composites have been prepared by post-synthesis impregnation of a TiO_2 precursor onto SBA-15 silica matrices and a subsequent thermal treatment at 400 °C under air (Besançon et al. 2016). The influence of the textural properties (pore size from 4 to 8 nm) of the SBA-15 and the TiO_2 content (20–80 wt%) on the dispersion of TiO_2 and its crystallization in anatase were evaluated. For TiO_2 content superior to 25 wt % and mesopores smaller than 8 nm, the impregnation occurred inside and outside the porosity of the hosts and TiO_2 crystallized as anatase nanoparticles on the SBA-15 particle surface. The quantity of crystallized anatase was determined by XRD using an internal standard when crystalline particles were detected. Their photocatalytic activity was evaluated by following the degradation of methyl orange and compared to commercial TiO_2 references (P25 from Degussa and pure anatase 10 nm from Alfa Aesar). While P25 reference appeared to be the best photocatalyst for the degradation of methyl orange in the used conditions, the photoactivity of the composites containing crystallized anatase was similar to that of Alfa Aesar commercial fully crystallized anatase with a particle size of the same order of magnitude. It clearly appeared that comparing the composites, the one with 44 wt% of crystallized anatase (experimental 80 wt% TiO_2), so more than twice less than commercial anatase references, exhibit the highest methyl orange degradation rate, very closed to the one observed for P25. The presence of the amorphous SiO_2 support has led to a well dispersion of 20 nm well-crystallized anatase particles and assured a high density of hydroxyl groups that consequently improved the catalytic performance of TiO_2-SBA15 composite.

Supported TiO_2 on silica SBA-15 have been also prepared with varied 30–80 wt % TiO_2 loading by a post-synthesis step based on Ti-alkoxide hydrolysis in a support/isopropanol suspension and subsequent calcination 500–900 °C (Yang et al. 2006). The presence of mesoporous SiO_2 amorphous support allowed having high specific area and delaying anatase-to-rutile transformation (only the anatase phase was detected by XRD for calcination temperature up to 800 °C) and controlled-size anatase nanocrystals. As a consequence, the TiO_2-supported SBA-15 composites were found to be more active for the photodegradation under UV irradiation of methylene blue in aqueous solution than the commercial P25. Mesoporous aluminosilicate Al-SBA-15 prepared in supercritical carbon dioxide (Sc-CO_2) was also considered for supporting TiO_2 nanoparticles (Chang et al. 2013). It was observed that TiO_2/Al-SBA-15 composites showed good methylene blue decolorization in aqueous solutions that was much higher than those of TiO_2/SBA-15 and commercial P25 TiO_2. The photocatalytic activity can be mainly related

to a higher dye adsorption capacity due to the enhanced specific surface area when some Si species are substituted by Al species. TiO_2-supported photocatalyst have been also obtained by using microporous supports such as zeolites. Mesoporous TiO_2-supported ZSM-5 zeolite with large specific surface area have been prepared by a direct templating method with P123 as surfactant, 1,3,5-triisopropylbenzene (TIPB) as swelling micelle agent (Znad et al. 2018). The inorganic component is commercially and hydrothermally treated with P123/TIPB aqueous solution to form a multilamellar mesoporous TiO_2/ZSM-5 that is photocatalytically active for the total and fast degradation of methyl orange dye under solar light irradiation in aqueous media. Moreover, the regeneration and the reuse of the photocatalyst were demonstrated. The high photocatalytic efficiency seems to be due in large part to the high specific surface area; however, in this paper the structural and textural characteristics are not clearly exploited and discussed.

Porous titania-supported composites have been also synthesized with the highly stable metal-organic framework (MOF) UiO-66 that has a high specific surface area (Wang et al. 2017). Different amounts of commercial TiO_2 P25 were directly introduced in the precursor solution of the UiO-66. The presence of UiO-66 allowed greatly increasing the methyl orange and rhodamine B dye adsorption in aqueous solutions, and the photocatalytic decomposition under visible light was faster with increasing amount of TiO_2. An optimal molar ratio TiO_2/Zr (from UiO-66) of 49 was found for the most efficient photocatalyst, which correspond to the nanocomposite with the most reduced band gap and recombination of electron-hole pairs. Moreover, the reusability of these TiO_2/MOF photocatalyst has been demonstrated.

Other problems that meet TiO_2 nanoparticles are related to their small size and very active surface that make them prone to deformation and agglomeration during reactions, leading to the loss of their catalytic activity. Besides dispersing TiO_2 nanoparticles on the surface of a solid matrix, another approach consisting in coating them of a mesoporous SiO_2 ($mSiO_2$) layer. A 3D network of core shell P25@$mSiO_2$ has been prepared by a simple surfactant-assisted sol-gel method (Gong et al. 2017). The resulting nanocomposite has shown improved photocatalytic activity for the degradation of methyl orange due to the presence of the $mSiO_2$ coating that stabilizes the nanosized photocatalysts, increases dye adsorption capacity, and binds TiO_2 particles, providing mechanical reinforcement of the nanocomposite. Moreover, it was suggested that hydroxyl radicals (·OH) play a major role in enhancing the performance of P25@$mSiO_2$. A mechanism for the ·OH radical generation and transport in these nanocomposites has been proposed.

Interestingly, since powder materials are difficult to manipulate and to recover from liquid suspension, the introduction of iron oxide phase was realized in TiO_2/SiO_2 composites to allow easy magnetic removal of the catalyst from water after reaction (Fisli et al. 2017). Fe_3O_4/SiO_2/TiO_2 composite has been prepared by the heteroagglomeration method. Fe_3O_4 magnetite nanoparticles were coprecipitated with SiO_2 that forms an amorphous coating. A suspension of commercial TiO_2 nanoparticles dispersed in ammonium sulfate aqueous solution was added to the obtained Fe_3O_4/SiO_2 suspension. TiO_2 nanoparticles are a mixture of anatase and rutile phase. The photocatalytic activity of the Fe_3O_4/SiO_2/TiO_2 composite was

evaluated for the photodegradation of methylene blue in aqueous solution under UV light irradiation. SiO_2 coating plays the role of a barrier between Fe_3O_4 and TiO_2 that improve photocatalytic properties and increase the dye adsorption capacity. Although the photocatalytic activity of the $Fe_3O_4/SiO_2/TiO_2$ composite is slightly lower than the one of the commercial TiO_2 in terms of the amount of degraded methylene blue, it can be easily collected from the aqueous solution after reaction by using a magnetic bar.

For an economical and environmental point of view, the use of natural porous materials as support for TiO_2 nanoparticles can present a great interest. TiO_2-modified kaolin photocatalysts have been prepared by physical mixing with P25 and impregnation with TiO_2 sol (Hajjaji et al. 2016). Good photocatalytic performances for the removal of methylene blue and orange II dyes from aqueous solutions have been reported due to the combination of photocatalytic and adsorption processes. Diatomite, a natural porous silica material, was used as support for producing TiO_2/diatomite composites by a modified sol-gel method and a subsequent calcination step at different 450–950°C temperatures (Wang et al. 2015a, b). The presence of an interfacial anchoring strength between the TiO_2 nanoparticles and diatom skeleton via Si-O-Ti bonds has been shown. The best photocatalytic activity for the photodegradation of rhodamine B was observed for the TiO_2/diatomite composite calcined at 750 °C for 2 h and having 90/10 weight ratio of anatase/rutile. Hydroxyapatite/titania nanocomposites were synthesized by a dissolution/precipitation method from a titanium alkoxide and a natural phosphate. These low-cost photocatalysts were found efficient for the removal of patent blue V and methylene blue dyes from water by combination of adsorption and photodegradation processes. Millimeter-size porous TiO_2/alginate beads have been produced by an ionotropic gelation route with commercial anatase titania powder (Gjipalaj and Alessandri 2017). The composite beads were found good adsorbents for anionic and cationic dyes, such as methyl orange and methylene blue, respectively. However, their photocatalytic efficiencies were observed and reduced compared to the non-aggregated nanopowders. Nevertheless, they have the advantages to be easy to recover and reusable, making them promising materials as green photocatalysts.

Porous carbon matrices such as activated carbon (Gao et al. 2011) or ordered mesoporous carbon (Wei et al. 2014) have also been considered as interesting porous support for TiO_2 nanoparticles because of the chemical inertness and stability in both acid and basic media and tunable textural and chemical properties. The resulting increase in photocatalytic performance for the degradation of organic pollutant such as dyes has been related to their porosity. Larger pores were found preferable to avoid the pore blockage by TiO_2 nanoparticles that results in lower dye adsorption capacity. Nanostructured carbon materials such as carbon nanotubes, fullerenes, graphene, and nanosheets have arisen increasing attention due to their unusual structural and electronical properties (Wang and Zhang 2012). In particular, graphene has emerged as one of the most promising materials to its large surface area that improves dye adsorption capacity and its high electron mobility that reduces the electron-hole pair recombination (Morales-Torres et al. 2012; Giovannetti et al. 2017).

2.4.4 Doping of TiO_2

Another method to limit the e^-/h^+ recombination and thus to enhance the photocatalytic efficiency consists in doping titania (Xu et al. 2005; Chen et al. 2008; Zaleska 2008; Devi et al. 2010; Zhang et al. 2012). The objective of doping is also to shift the band gap of titania in the visible region. In fact, the photocatalytic efficiency of TiO_2 depends partially upon the relative degree of branching of the reactive electron-hole pairs into interfacial charge transfer reactions (Hoffmann et al. 1995). Because of the shift of the band gap of the photocatalyst, the presence of the dopant, such as a metal ion, in the TiO_2 crystalline structure can change both the charge carrier recombination rates and interfacial electron-transfer rates. The dopant can act either as an electron trap or a hole trap. Lee et al. proceeded to doping of TiO_2 with Fe and W and demonstrated that the photocatalytic activity of metal-doped TiO_2 decreased as the concentration of dispersed W or Fe ion in the lattice of TiO_2 was increased (Lee et al. 2001a, b). Xu et al. were the first group preparing zinc ion surface-doped TiO_2 nanoparticles and nanotubes through ligand exchange reaction, proving that the surface-doped materials exhibit a higher photoactivity than the pure ones, by decreasing the electron/hole pair recombination rate (Xu et al. 2004, 2005). Ku et al. demonstrated that an excessive ZnO on the surface of TiO_2 might decrease the photocatalytic activity of the material by serving as recombination centers of electron-hole pairs (Ku et al. 2011). This diminution of the photocatalytic performance at large dopant concentrations (low band gap values) can be explained in terms of charge recombination. For a random distribution of substitutional acceptors/donors of charge dopants, a Gaussian-like density of states appears at the upper/lower part of the valence/conduction band. The corresponding density of states is roughly proportional to the dopant concentration. Nevertheless, high doping concentration (low band gap) may have detrimental effects because tunneling between trapped charges carriers makes a significant contribution to charge (electron hole) recombination. Consequently, the photocatalytic rate constant typically decreases with the shortening of the electron-hole pair distance due to a growing level of dopant (Moser et al. 1987). This trend can be also interpreted in terms of band positions (top of valence band and bottom of conduction band, (ii)). The positions of valence band and conduction band of semiconductor reflect the oxidation ability of hole and reduction ability of electron, respectively. From the thermodynamic point of view, if the conduction band is more negative than the $O_2/O_2^{\cdot-}$ couple, the photogenerated electrons could reduce O_2 to produce $O_2^{\cdot}$. Meanwhile, if the position of the valence band is more positive than the $OH^-/OH^{\cdot}$ couple, the photogenerated holes could oxide OH^- or H_2O to form $OH^{\cdot}$. When the band gap decreases, i.e., for high dopant content titania, the conduction band edge position and the valence band edge position shift downward and upward, respectively. It is now well established that the low conduction band position of doped titania would be the main reason for the low activity in photooxidation of organic molecule for low band gap. The oxidizing potential of the valence band holes remains more positive than the standard potential of $OH^-/OH^{\cdot}$ couple, and the reduction potential of the conduction band electrons becomes less negative than the potential of $O_2/O_2^{\cdot}$. This indicates that

photogenerated holes could react with chemisorbed OH^- or H_2O to produce $OH^{\cdot}$. However, the electrons transferred to the surface of semiconductor particles could not interact with O_2 to form $O_2^{\cdot}$. This accelerates the recombination of the photogenerated electrons and holes, thus reducing the formation rate of $OH^{\cdot}$. Therefore, only a low degradation rate is observed for these photocatalysts. Different strategies such as addition of metal salt into the TiO_2 colloid, sol-gel, ion implantation, impregnation, and chemical vapor deposition have been tested for the syntheses of metal-doped titania (Zaleska 2008). For example, through a post-synthesis treatment Tayade et al. have doped mesoporous titania with different transition metal ions (Tayade et al. 2006). The authors have first prepared the TiO_2 by the hydrolysis of titanium isopropoxide in the absence of surfactant, and thus no mesopore ordering was obtained. In a second step, the metal was introduced by using the wet impregnation method. The obtained doped materials have been tested for the degradation of acetophenone and nitrobenzene present in aqueous solution. The authors have demonstrated that the photocatalytic activity of the silver metal ion impregnated TiO_2 photocatalyst has the highest initial rate of photocatalytic degradation for both compounds due to the interstitial position of impregnated silver metal ion in the TiO_2 lattice. Among the different strategies to introduce the metal ion dopant, the direct sol gel way is of particular interest (Zaleska 2008; Chauhan et al. 2012). Indeed, this technique does not required complicated instruments, since it is simple and easy. In addition, the incorporation of an active dopant in the sol during the gelation stage allows the doping element to have a direct interaction with the support. Mesoporous TiO_2 was also modified with silver nanoparticles that were photogenerated during the wet impregnation by $AgNO_3$ of the preformed TiO_2 (Xiong et al. 2011). The Ag particles formed on the TiO_2 surface were assumed to increase the affinity of the surface to oxygen, which is supposed to be the major role in enhancing the photocatalytic degradation of rhodamine B under UV light irradiation. The doping by metal such as bismuth has also been considered for mesoporous TiO_2/MCM-41 SiO_2 nanocomposites to enhance photocatalytic activity under visible light for methylene blue removal from water solution (Mohamed et al. 2018). Synergetic effects of interfaces between Bi_2O_3 and TiO_2 were assumed to enhance the catalytic performance of the composite Bi/Ti-MCM-41. Co-doping with N has allowed narrowing the band gap energy of the photocatalysts resulting in greater visible light photocatalytic activity for the degradation of acid Red 85-a, a fabric dye (Thejaswini et al. 2016). Co-doping with metal such as Zr and Si can affect anatase phase stability, crystallinity, particle size, and optical properties of TiO_2, resulting in enhanced photocatalytical activity in the photodegradation of methyl orange in aqueous solution under visible light (Ilkhechi and Kaleji 2014).

Nonmetal doping of TiO_2 with boron, carbon, sulfur, fluorine, or nitrogen has also been reported. For example, N-doped TiO_2 have been prepared by treating powder TiO_2 in a NH_3 gas flow (Zhang et al. 2010). In that case, N-doping induces oxygen vacancies and contributes to the absorption as well as photoactivity in the visible region. It is also reported that modified N-doped TiO_2 such as C-N-TiO_2 usually shows favorable effects for improving the photocatalytic activity in the visible compared to N-doped TiO_2 (Zhang et al. 2010). The photocatalytic activity

toward degradation of rhodamine B dye under visible light was enhanced by doping with nonmetal dopants, N, N/S, and N/F hierarchical macro-/mesoporous TiO_2 and combining with water-mediated adsorption (Pan et al. 2013). Besides the advantage to make the TiO_2 photocatalyst active under visible light, the doping with nonmetal such as carbon could also benefit for increasing dye adsorption capacity and improve the photocatalyst activity for dye removal by combination of adsorption and degradation (Xu et al. 2016). Doping with sulfur creates acid sites on the photocatalyst surface that enhance photocatalytic activity for the degradation of organic molecules such as dyes. Sulfur is usually introduced in the synthesis medium with thiourea (Guo et al. 2010), but the use of elemental sulfur was also reported and claimed to be less harmful (Galenda et al. 2017). The main drawback of the nonmetal doping concerns the long-term instability of the photocatalyst. Co-doping with nonmetal and metal dopants have been explored for getting synergetic effect from the two dopants. For producing photocatalyst highly active in the visible, co-doping with S and Cu has been achieved to get advantage of S to lower band gap of TiO_2 and of Cu to trap the electrons in the conduction band of TiO_2 in order to prevent charge recombination of electrons with holes (Yi et al. 2014).

It is noteworthy that other strategies such as encapsulation of photosensitive molecules within porous photocatalysts have been developed to improve photocatalytic properties in the visible. Heteropolytungstic acid (HPA) that is photosensitive has been incorporated by direct synthesis in SBA-15 and Ti-SBA-15 materials (Anandan and Yoon 2007). The photodegradation of methyl orange in aqueous solution under visible light was observed faster in the presence of HPA-TiSBA-15 than those in HPA-SBA-15 and Ti-SBA-15.

2.4.5 Shaping

Most of the TiO_2 photocatalysts are synthesized as nano- or micro-sized particles and are powdered materials that is limiting for their applicative use. The shaping to integrate them in processes that can be developed at the industrial scale is necessary and often remains a challenge since properties of the photocatalysts have to be preserved. Processing photocatalysts as films has been explored according to different strategies. TiO_2 nanoparticles prepared by a sol-gel method in presence of polyethylene glycol have been processed as thin films by spin-coating the obtained TiO_2 sol on glass substrates and applying a subsequent thermal treatment (Lin et al. 2012). The film thickness was varied by repeating the film deposition procedure. The obtained films have been shown to be efficient for the photodegradation of methylene blue, methyl orange, and indigo in water under UV light irradiation. Increasing film thickness results in increasing degradation rate to a certain extent. Indeed the photocatalytic reactions were found to occur mainly on the surface of TiO_2 thin films. For thick films, the TiO_2 particles in the interior region are less active because of the difficulty to access for the reactant and the low diffusion in solution for the reaction by-products. Moreover, an increase in opacity and light scattering was observed for thick films that decreases the light transmission in the film.

Microfibrous palygorskite clay was mixed to a precursor nanocrystalline TiO_2 sol containing Triton X-100 nonionic surfactant, and the resulting mixture was spread on a glass slides by dip-coating (Stathatos et al. 2012). A subsequent thermal treatment at 500 °C was applied to remove organic component. Highly nanostructured porous palygorskite/TiO_2 composite films with variable quantities of palygorskite were produced and tested as catalysts for the photodecomposition of basic blue azo dye in water under UV light irradiation. The film with an optimal palygorskite/TiO_2 weight ratio of 3/2 was found the most effective photocatalyst. It was observed that palygorskite has a low photocatalytic activity under UV illumination probably due to the presence of light-activated oxides such as Fe_2O_3 and TiO_2 present in the clay, and it is assumed that the coexistence of MgO and CaO helps to a better hydroxylation of the surface or to slower charge recombination. The photocatalytic activities of the composites are due to a synergetic effect of the palygorskite clay and anatase nanoparticles. The reusability of the palygorskite/TiO_2 composite films have been evidenced for four cycles. An interesting approach is the immobilization of TiO_2 nanoparticles on macroporous alumina (or clay) disk (or tubular) membranes for filtration. Titania and titania-silica sols were deposited on macroporous alumina disk membranes (Tajer-Kajinebaf et al. 2014). To get anatase with the most favorable crystallite size of 10 nm, a thermal treatment at 400 °C was optimal for both TiO_2-alumina and TiO_2/SiO_2-alumina membranes. The membrane composites have been successfully used for removing methyl orange from aqueous solution by coupling membrane separation process with photocatalytic technique. Since the presence of silica delays the phase transformation of anatase to rutile and inhibits grain growth of anatase, the TiO_2/SiO_2-alumina membranes were assumed to have great potential for efficient water treatment. TiO_2 nanoparticles have been also incorporated polysulfone (PSf) ultrafiltration membrane for a selective degradation of methylene blue (Melvin Ng et al. 2017). First, commercial P25 TiO_2 nanoparticles were modified and molecularly imprinting with methylene blue as template in a polymer matrix. The imprinted TiO_2 was then introduced in the precursor mixture of the PSf membrane. The photocatalytic and selective properties of TiO_2 entrapped in PSf membrane were successfully evidenced in an integrated photodegradation-ultrafiltration system. The incorporation of photoactive TiO_2 nanoparticles onto textile fibers has been studied for self-cleaning (Wang et al. 2015a, b). It is an interesting approach for water treatment since TiO_2-supported onto textile can facilitate the photocatalyst recovery from reaction medium. The use of textile such as sackcloth for TiO_2 photocatalyst support offers the opportunity to produce a composite highly active to photodegrade acid black 26, a dye used in the textile, and stable for applications in water treatment (Vaez et al. 2012). Embedding of titania nanoparticles into porous cellulose aerogel is also attractive for water treatment since the composite is like a textile felt that can be easily handled and used for filtration (Jiao et al. 2015). The obtained anatase TiO_2/cellulose aerogel showed a high photocatalytic activity for indigo carmine dye degradation in aqueous solution under UV light and maintained the well-define shape throughout the radiation process. Another interesting shaping is the production of TiO_2 nanofibers by electrospinning that can be used as reactive filtration materials for water treatment applications (Nalbandian et al. 2015).

2.5 Examples of Processes for Dyes Removal from Water Using TiO_2 Photocatalyst

In most of processes developed for photocatalytic water treatment, TiO_2 is usually introduced as slurry in the reactor. This can lead to several problems of filtration and/or micro-reactor clogging and light transport in the reaction medium (Bouguer-Lambert-Beer law) (Cambié et al. 2016). Up to now, the main drawback of industrial TiO_2-based advanced oxidation processes is due to postoperational separation of the catalyst (filtration, coagulation-flocculation-sedimentation) from the reaction medium (Wang et al. 2014a). This drawback can be overcome, thanks to processes such as sedimentation, membrane filtration, or cross-flow filtration, which allow the physical separation of particles from the slurry (Molinari et al. 2002a, b; Fernández-Ibáñez et al. 2003; Doll and Frimmel 2005). An alternative is to use a packed-bed reactor, but in this case, the light is not able to reach the center of the reactor. Another alternative allows overcoming such limitation by coating a thin catalyst layer on the reactor's walls of a continuous-flow photochemical micro-reactor.

2.5.1 Photocatalytic Membrane Reactors (PMRs)

Membrane Process

Membrane process is a separation technique extensively implemented in numerous industries such as cosmetics, chemical, electronic, food, pharmaceutical, as well as for desalination and wastewater treatment industries. The main advantages of membrane-based processes lie in the low energy cost, suitability for implementing continuous processes, low-cost maintenance, the production of stable quality of water almost independent of the wastewater composition, and the easy scale-up by simply increasing the number of membrane modules (Mozia 2010). On the other hand, among the main drawbacks of such technology, one can specify the membrane lifetime and the membrane fouling with particles and colloids present in the feed.

The two main technologies used are the pressure-driven membrane processes and those where the concentration difference is the driving force (dialysis, pervaporation, and direct contact membrane distillation) (Mozia 2010). In the case of pressure-driven membrane processes, the smaller the pore size is, the smaller the molecules separated are. Pore sizes can be classified as follows: microfiltration (MF) > ultrafiltration (UF) > nanofiltration (NF) > reverse osmosis (RO). MF membranes allow the separation of particles >0.1 μm; UF membranes are efficient for particles >2 nm, and NF membrane allows the separation of particles <2 nm. In reverse osmosis process, almost all salts, metal ions, and small organic molecules are separated (Koros et al. 1996). As expected, decreasing the pore size leads to an increase of the resistance of the membrane, and consequently the pressure to apply in the process increases while decreasing the pore size.

Membrane processes can be implemented either in a dead-end mode, cross-flow mode, and submerged membranes (Chin et al. 2007a, b; Huang et al. 2007; Choo et al. 2008a, b; Fu et al. 2006a, b). In the dead-end mode, the membrane acts as a simple filter, and all the feed flowed through the membrane. The main drawback of this configuration is the accumulation of particles, colloids, and other substance on the membrane, leading to the formation of a cake, which can clog the pores of the membrane. Consequently, such a configuration is not suitable for large-scale industrial applications. The submerged mode is close to the dead-end configuration, but the design of the reactor allows reducing the membrane fouling. In the cross-flow configuration, the incoming feed moves parallel to the membrane surface that limits the deposition of foulants on the membrane surface since the feed flowing tangentially to the membrane removes partially the deposit (Mozia 2010).

Generalities About Photocatalytic Membrane Reactors (PMRs)

Photocatalytic membrane reactors (PMRs) are a promising technology to remediate drawbacks such as separation of the photocatalyst as well as products/by-products from the reaction medium in the field of wastewater treatment (Ollis 2003; Augugliaro et al. 2006; Mozia 2010). In such technology, photocatalysis is coupled with a membrane process. The role of the membrane is to act as a simple barrier for the photocatalyst and a selective barrier for the molecules to be degraded (Molinari et al. 2002a, b).

Some advantages of membrane reactors with respect to conventional ones are (1) the confining of the photocatalyst in the reaction environment by means of the membrane, which allows the implementation of a continuous process with simultaneous catalyst and product separation from the reaction environment and (2) the control of the residence time of molecules in the reactor. As a result, postoperational separation of the catalyst from the reaction medium involving coagulation-flocculation-sedimentation operations is avoided. This allows reducing energy cost and sizing the installation.

As for conventional (photo) catalytic processes, two kinds of PMRs can be distinguished: (1) reactors where the catalyst is suspended in the reaction mixture and (2) those where the catalyst is immobilized on/in the membrane (photocatalytic membrane) (Augugliaro et al. 2006; Ma et al. 2010; Mozia 2010). In the first configuration (catalyst is suspended in the reaction mixture), the main drawback is the membrane fouling by the catalyst particles, especially in the case of pressure-driven processes and more particularly in the cases of microfiltration and ultrafiltration. Photocatalytic membranes, where the photocatalytic reaction occurs on the external surface and within the pores of the membrane, allow overcoming such drawback. However, the membrane has to be resistant to UV irradiation, and the coating of the catalyst on and/or in the membrane results in a decrease of surface area and consequently of the photocatalytic activity.

As expected, when the pore size of the membrane increases (microfiltration (MF) > ultrafiltration (UF) > nanofiltration (NF) > reverse osmosis (RO)), the

amount of organics products in the permeate increases as well (Tomaszewska et al. 1998; Molinari et al. 2004; Mozia et al. 2006), and the pressure to be applied decreases.

Most of the photocatalytic membrane reactors studied in the literature combine photocatalysis with membrane process, involving microfiltration (Erdei et al. 2008; Shon et al. 2008; Benotti et al. 2009), ultrafiltration (Sun et al. 2004; Fu et al. 2006a, b; Tsarenko et al. 2006), and nanofiltration (Augugliaro et al. 2005; Molinari et al. 2006: Molinari et al. 2008

In order to overcome the fouling phenomenon, new types of PMRs combining membrane reactors with direct contact membrane distillation (Mozia et al. 2008; Mozia et al. 2009a, b), pervaporation (Camera-Roda and Santarelli 2005), and dialysis (Azrague et al. 2007) were developed more recently.

Photocatalytic Membranes

TiO_2 Immobilized on/in the Membrane

In such configuration, the light source is located in a way to ensure the irradiation of the membrane (Fig. 2.5). The photodegradation of dyes occurs at the surface and/or within the pores of the membrane. Two asymmetric configurations (Figs. 2.6a and 2.6b) of membrane reactors can be found (Mozia 2010). In the first one, the photoactive separation layer is deposited on a non-photocatalytic support. The membrane acts as both a filter and a photocatalyst. The light source is located in the photoactive separation layer (photocatalytic membrane) side.

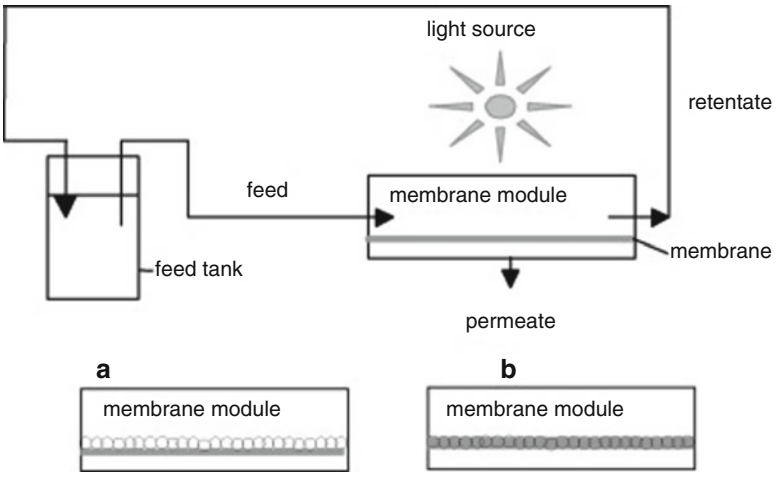

Fig. 2.5 Scheme of an experimental setup working with a photocatalytic membrane (TiO_2 immobilized in or on the membrane). (Reprinted with permission from Mozia 2010. Copyright 2010 Elsevier, Separation and Purification Technology)

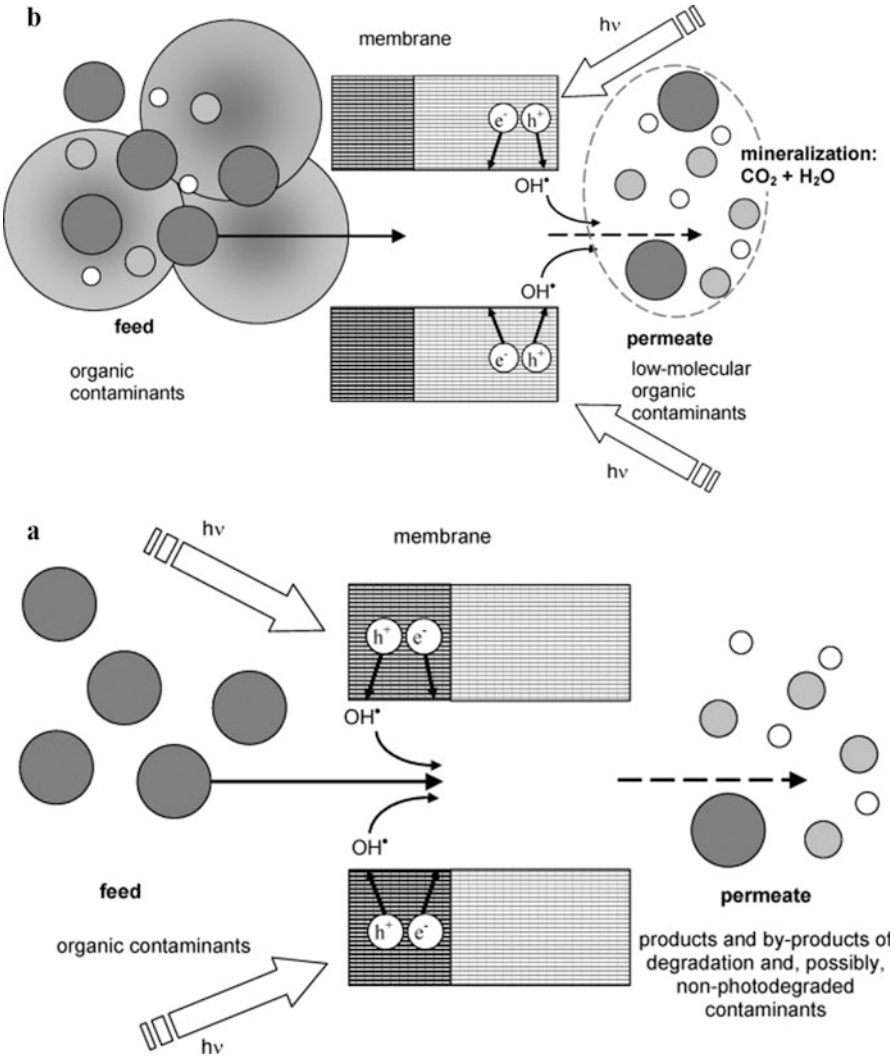

Fig. 2.6 Operating principle of a photocatalytic membrane with photoactive separation layer (**a**) and with photocatalytic membrane with non-photoactive separation layer and photoactive support (**b**). (Reprinted with permission from Mozia 2010. Copyright 2010 Elsevier, Separation and Purification Technology)

In such configuration, the main advantage is that the organic compounds present in the solution are decomposed on/in the membrane, thus preventing cake formation and membrane fouling (Tsuru et al. 2001). The main drawback is that the membrane can be damaged by UV radiations (Ollis 2003) (Chin et al. 2006). Actually the membrane resistance to UV radiation depends on its composition and manufacturing (Molinari et al. 2000; Chin et al. 2006). This limitation can be overcome by the use

of ceramic (Alem et al. 2009; Romanos et al. 2013) or metallic (Bellobono et al. 2005) membranes, but the main drawback of such membranes is their cost.

In the second configuration, the non-photoactive separation layer is deposited on a photoactive support. The light source is located in the photoactive support side. In such configuration, filtration (membrane) and photocatalysis (photoactive support) are separated. Such configuration allows obtaining a higher permeate quality and prevents the membrane degradation by UV radiation (Mozia 2010). The main drawbacks are that only the permeate is purified, the possible fouling of the non-photoactive membrane and the non-degradation of high molecular weight organics. Indeed, such large molecules are blocked by the pore size of the membrane and thus cannot cross the membrane to reach the photocatalytic support. Both configurations were compared by Bosc et al. by using mesoporous TiO_2 -based membranes for the photocatalytic degradation of methylene blue (Bosc et al. 2005). Romanos et al. even implemented "double-side active photocatalytic ultrafiltration (UF) membranes" which consists in coating and irradiating both sides of the membrane (Romanos et al. 2013). From their results on the photocatalytic degradation of methyl orange, authors claimed that such a process exhibits similar performances as compared to the highly efficient standard nanofiltration and with the advantages such as lower energy consumption without the generation of toxic by-products.

Several studies report dye photodegradation through photocatalytic membranes (TiO_2 immobilized on/in the membrane) (Zhang et al. 2006a; Wang et al. 2008; Papageorgiou et al. 2012; Mendret et al. 2013; Romanos et al. 2013; Zhang et al. 2014).

Zhang et al. reported the synthesis of a TiO_2 hollow fiber-based membrane, which was evaluated for the photocatalytic degradation of acid orange 7 (Zhang et al. 2014). The influence of the calcination temperature was found to strongly influence membrane properties: the higher the calcination temperature, the smaller the pore size and the photocatalytic activity, the higher the mechanical robustness. The best calcination temperature was reported to be 900 °C, which allows removing 90.2% of organics at a water flux of 12.2 $L.m^{-2}.h^{-1}$.

Alem et al. reported the synthesis of a multilayer mesoporous TiO_2 coated on alumina membrane with a high surface area (83 $m^2.g^{-1}$ and a pore size of 4 nm) for the photodegradation of methyl orange (Alem et al. 2009). Such membrane allows increasing the photocatalytic activity by 60% without sacrificing its permeation compared to colloidal monolayer membrane. Mendret et al. reported the photodegradation of acid orange 7 on a TiO_2/Al_2O_3 membrane (Mendret et al. 2013). They found that such a process enhances ceramic membrane wettability and allows preventing membrane fouling while improving flux stability. Moreover, membrane cleaning was performed by irradiating membrane surface under static conditions, without chemicals. Papageorgiou et al. 2012 implemented photocatalytic/ultrafiltration process using a composite of AEROXIDE® TiO_2 P25 and alginate polymer fiber-based membrane which were found to be threefold more efficient than conventional membrane for the photocatalytic degradation of methyl orange (Papageorgiou et al. 2012).

TiO_2 Suspended in the Reaction Mixture

In such configuration, the photocatalytic process is ensured by TiO_2 introduced as a slurry in the incoming feed and the membrane acts as a filter for TiO_2 particles, thus ensuring the permeate to be free of TiO_2 particles. Indeed, most of the studies report the high efficiency of the membrane filtration resulting in a very low concentration of TiO_2 particles in the permeate (Meng et al. 2005; Huang et al. 2007; Mozia and Morawski 2009). For reactors where the catalyst is suspended in the reaction mixture, three main configurations can be distinguished: irradiation of the feed tank, irradiation in a specific module (photoreactor) located between the feed tank and the membrane, and irradiation of the membrane.

One advantage of such process is the photocatalytic efficacy given that TiO_2 particles are not embedded in the membrane, allowing a higher surface area available for the photocatalytic process. It also allows obtaining a higher permeate quality and prevents the membrane degradation by UV radiation. On the other hand, the main drawbacks are membrane fouling, especially by TiO_2 particles, leading to the decline of the permeate flow (Molinari et al. 2006; Molinari et al. 2008). As a general trend, the higher the TiO_2 particles concentration is, the fastest the fouling of the membrane is (Sopajaree et al. 1999a, b; Shon et al. 2008). The membrane fouling strongly depends on the pressure and flow applied in the process (Sopajaree et al. 1999a, b). A high flow allows preventing the formation of the cake by removing continuously TiO_2 particles. Under such conditions (high flow) the influence of the pressure on the fouling of the membrane is negligible. However at low flow, the influence of the transmembrane pressure becomes predominant, and membrane clogging can occur. One alternative is the implementation of submerged membrane process, which is less sensitive to membrane fouling (Chin et al. 2007a, b; Molinari et al. 2008). Low permeate flux results in higher residence time that favors the process efficiency (Molinari et al. 2000; Rivero et al. 2006; Chin et al. 2007b). Other parameters such as pH or ionic strength will also affect the process (Mozia 2010). Especially, the pH strongly influences TiO_2 particles agglomeration (Xi and Geissen 2001; Paz 2006). Also, the presence of humic acid was found to render the cake more resistant to the flow (backpressure increase) (Lee et al. 2001a, b). However, one can expect the photodegradation of organic products of the cake by the application of UV light (Choo et al. 2008a, b), especially with the configuration where the membrane is irradiated. The shaping of the catalyst also impacts the membrane clogging. Indeed, by using a ball-shaped TiO_2/SiO_2 catalyst, the fouling phenomenon was found to be reduced as compared to the standard Degussa P25 (Fu et al. 2006a, b). The batch mode is generally found to be more effective than the continuous mode, but the latter is better suited for industrial scale applications (Li and Zhao 1999; Molinari et al. 2002a, b).

Others processes such as dialysis, pervaporation, or direct contact membrane distillation also exist. For example, Azrague et al. developed a photocatalytic membrane process where the mass transport through the membrane is not achieved by transmembrane pressure but thanks to the difference of concentration (dialysis). The main advantage of such process is that it prevents the fouling of the membrane observed with pressure-driven processes (Azrague et al. 2007). Authors observed that under their conditions, the rate-limiting step is the mass transport rather than the

photodegradation. Camera-Roda et al. have also reported a process combining pervaporation and photocatalysis (Camera-Roda and Santarelli 2005). They reported that the integration of photocatalysis to the pervaporation process improved its efficiency. However, in the process presented, the photocatalyst remains in the treated wastewater. Finally, direct contact membrane distillation coupled with photocatalysis process was implemented for the removal of dyes (Mozia et al. 2005, 2007a, b, c; Mozia and Morawski 2006, 2009) as well as for other pollutants (Mozia et al. 2014). In such process, the feed flows through the membrane under gas phase. In this case, the process is driven by the vapor pressure difference between the two sides of the membrane. The main advantage of this technology is that membrane fouling does not occur, even after 180 h of stream and independently of the TiO_2 source (Mozia 2010). Another advantage is that, theoretically, 100% of the nonvolatile compounds such as salts, dyes, or other large organic molecules are separated (Tomaszewska et al. 1998; Curcio et al. 2010). As a result, permeate was found to be of high quality. However, such process suffers from several drawbacks among which high-energy consumption and a low flux as compared to pressure-driven processes.

Several studies report dye treatment using TiO_2 particles in suspension in the reaction mixture (Molinari et al. 2002a, b, 2004; Ryu et al. 2005; Cui et al. 2006; Jiang et al. 2010; Damodar et al. 2010). For example, Molinari et al. reported the removal of Congo red and patent blue from wastewater through a pressure-driven membrane process using the reference TiO_2 Degussa P25 catalyst in suspension in the feed (Molinari et al. 2004). A comparison between suspended and entrapped TiO_2 as well as the influence of different parameters such as system configuration, irradiating source and its position, the pressure in the membrane cell and the initial concentration of the substrates, and the recirculation rate were studied. It was found that the photodegradation rate of Congo red was 50 times higher with the immersed UV lamp than that found with the external lamp. Also, as discussed above, the use of the photocatalyst in suspended form was more efficient than TiO_2 entrapped in a polymeric membrane. Damodar et al. developed a process coupling a polytetrafluoroethylene membrane with a TiO_2/UV slurry reactor that was implemented for the degradation of reactive black 5 (Damodar et al. 2010). Such a system was found capable of removing 75–82% TOC, operating efficiently for long periods with high removal efficiency, as well as efficiently recycling of the catalyst. Jiang et al. reported the photocatalytic degradation of acid Red B in a slurry photocatalytic membrane reactor (Jiang et al. 2010). It was observed that the TiO_2 loading and the initial dye concentration strongly influence the reaction rate.

Cui et al. studied the performances of a slurry photocatalytic reactor coupled with a membrane for the photodegradation of methyl orange (Cui et al. 2006). They found that the degradation rate is higher as compared to a cylindrical reactor, and the rejection rate of the TiO_2 photocatalyst particles reaches 99.9%.

Additionally to the dyes, numerous pollutants such as sodium dodecylbenzene sulfonate (H. Zhang et al. 2006b), trichloroethylene (Choo et al. 2008a, b) biologically treated sewage effluent (Shon et al. 2008), fulvic acids (Fu et al. 2006a, b), para-chlorobenzoate (Huang et al. 2007), bisphenol A (Chin et al. 2007a, b),

lincomycin (Augugliaro et al. 2005, 2006), and others (Choo et al. 2008a, b) can be decontaminated through photocatalytic membrane reactors.

An alternative process to membrane reactors which emerged the past years consists in implementing photocatalytic micro-reactors.

2.5.2 *Continuous-Flow Photochemical Micro-Reactor*

Flow Reactors

A micro-reactor (or flow reactor, microfluidic reactor) is a chemical reactor where the reaction occurs in a confined channel with a diameter below 1 mm (Zhang et al. 2017). Such micro-reactors and their applications undergone intense development and were extensively reviewed the past years (Hartman and Jensen 2009; Jensen et al. 2014; Gemoets et al. 2015; Cambié et al. 2016; Rossetti and Compagnoni 2016: Heggo and Ookawara 2017; Jensen 2017; Zhang et al. 2017). Thanks to their small size, micro-reactors exhibit a high surface-to-volume ratio, which favors mixing, heat, and mass transfer (Gemoets et al. 2015; Zhang et al. 2017). Consequently, flow reactors allow favoring heterogeneous reactions such as liquid-liquid, liquid-gas, liquid-solid, and gas-liquid-solid reactions by favoring the contact area between reactants and catalyst. Indeed, it was reported that specific interfacial areas can reach values as high as liquid–liquid, 1000–10,000 m^2/m^3 and gas–liquid, 160–1300 m^2/m^3, thus improving mass transfer as compared to conventional batch reactors (Nieves-Remacha et al. 2012, 2013). Mass transfer coefficients were found to be liquid–liquid, 1.9–41 s^{-1} and gas–liquid, 0.2–3 s^{-1} (Yue et al. 2009; Woitalka et al. 2014). As a result, the general trend is that the use of micro-reactors results in a better efficiency as compared to conventional ones (Anderson 2012; Mizuno et al. 2016; Cambié et al. 2016). Moreover, thanks to the small reactor volume, safety of the process is improved, even for harsh conditions (Hessel et al. 2011; Gutmann et al. 2015). Indeed, such reactors allow implementing high-temperature and/or high-pressure reactions, as well as explosive reactants/products. Additionally, micro-reactors also present many advantages from a point of view of green chemistry since they allow improving the safety of the process, the energy efficiency, higher yields, and reduced wastes (Newman and Jensen 2013; Rossetti and Compagnoni 2016). The reproducibility and low-cost scale-up are often spotlighted among advantages of micro-reactors. Indeed, it is often claim that the scaling up simply consists of multiplying the number of reactors, but the reality is not as straightforward (Rossetti and Compagnoni 2016). Indeed, the fluid distribution to ensure an accurate control of the flow and the cost of scaling up still represent a major challenge. Three main scaling-up strategies were reported in the literature: parallel numbering-up (reactors in parallel), consecutive numbering-up (reactors in series), and scale-out by suitable dimension enlarging (Zhang et al. 2017; Kuijpers et al. 2017). Flow reactors can be made of glass, polymer, silicon, ceramic, or metal

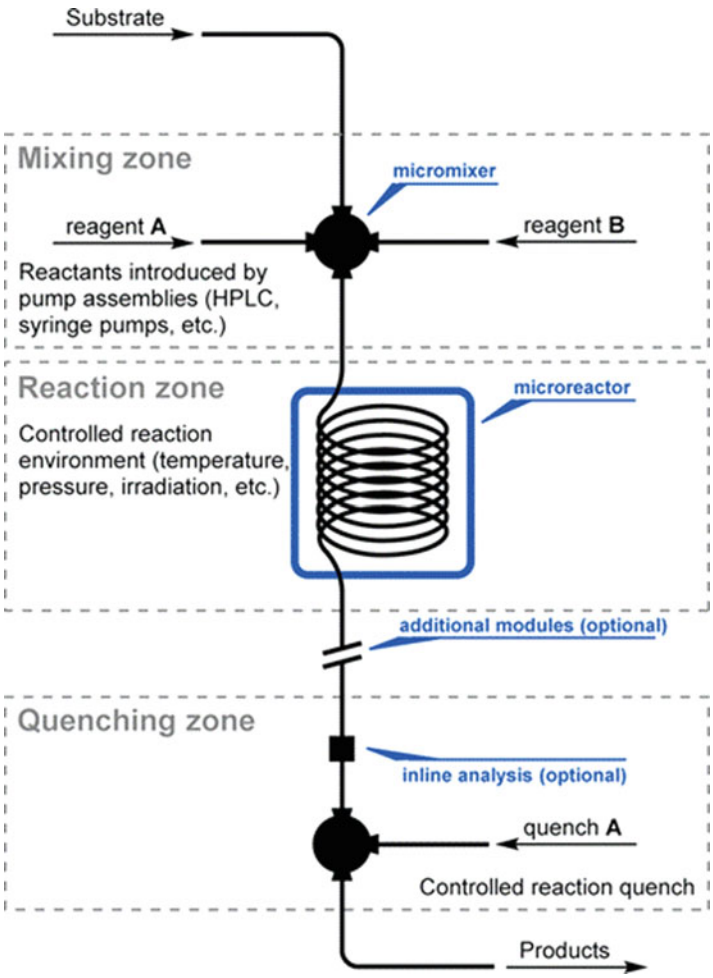

Fig. 2.7 Operating principle of a micro-reactor. (Reprinted with permission from Cambié et al. 2016. Copyright 2016 ACS, Chemical Review)

(Anderson 2012; Heggo and Ookawara 2017). They can be used in numerous configurations and can be coupled with sonochemistry, microwave, and photocatalysis (Wegner et al. 2011).

Photochemical Flow Reactors

Photochemical micro-reactors result from the coupling of a micro-reactor with photocatalytic process (photocatalyst + irradiation source) (Van Gerven et al.

2007; Coyle and Oelgemöller 2008; Su et al. 2014; Heggo and Ookawara 2017). The operating principle of such reactors is schematized in the Fig. 2.7.

The implementation of photochemical micro-reactors allows overcoming some drawbacks of conventional batch reactors, more especially the attenuation effect of photon transport, which makes the scale-up difficult, by ensuring a uniform irradiation of the reaction mixture and/or of the catalyst (Colina-Márquez et al. 2010; Wang et al. 2014a; Cambié et al. 2016). Indeed, their high surface-to-volume ratio results in a high accessible photocatalytic surface area. It was evidenced that mass transfer from the reaction medium to the catalyst is improved (Gorges et al. 2004; Wang et al. 2014a).

The separation of the catalyst from the reaction medium can be overcome by coating a thin photocatalyst layer on the reactor's walls of a continuous-flow photochemical micro-reactor (Heggo and Ookawara 2017). Thus, the catalyst can be fully irradiated. However, such a coating of the catalyst results in a decrease of the accessible surface area (Mozia 2010; Cambié et al. 2016). Fortunately, this phenomenon is compensated, thanks to the high surface-to-volume ratio (up to 11,667 $m^2.m^{-3}$) of micro-photoreactors compared to conventional slurry photoreactors (2631 $m^2.m^{-3}$) (Gorges et al. 2004).

Micro-reactors can be implemented according to different configurations among which slurry-bubble reactor, monolith reactor, membrane reactor, fluidized bed reactor, falling film reactor, planar reactor, microchannel and capillary reactors, silicon reactors, and multiphase micro-droplet reactors.

Flow photoreactors are mostly implemented in organic photochemical reactions and, in a minor extent, TiO_2-based photocatalytic degradation of dyes degradation (Gutmann et al. 2015; Mizuno et al. 2016).

Dye Degradation Using Photochemical Flow Reactors

Several examples of photocatalytic dye degradation in micro-reactors are reported in the literature. Most of them use methylene blue as a model dye. Some studies focus on immobilization of the catalyst on the inner walls of the reactor. For example, Li et al. reported that by using TiO_2-SiO_2 coated walls of a micro-reactor, the degradation rate of methylene blue was increased by more than 150 times as compared to conventional system (Li et al. 2003). In another work, methylene blue was photodegraded both on TiO_2-P25 and TiO_2-graphène photocatalysts deposited on the walls of a glass chip micro-reactor (Padoin et al. 2016). The degradation rate of methylene blue was found to be one order of magnitude higher than with equivalent macroscopic reactor. In order to increase the photocatalytic efficiency for the methylene blue degradation, Lindstrom et al. coated a mesoporous anatase film with a high surface area on the inner walls of the reactor (Lindstrom et al. 2007). As a general feature of micro-reactors, they found that the rate-limiting parameter for the photodegradation of methylene blue is not the catalyst surface area, neither the adsorption properties but the oxygen concentration in the water phase, meaning that the reaction is not limited by heat and mass transfer in such conditions. Lin et al.

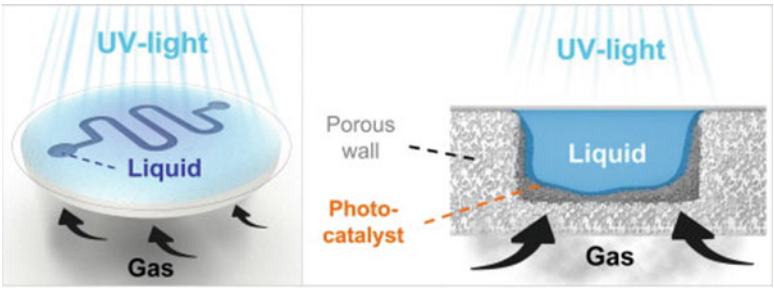

Fig. 2.8 Photocatalytic membrane-based triphasic flow reactor implemented by Aran et al. (Reprinted with permission from Aran et al. 2011. Copyright 2011 Elsevier, Journal of Photochemistry and Photobiology A: Chemistry)

studied the influence of light and TiO_2 doping for the photodegradation of methylene blue while comparing micro-channel and planar photocatalytic micro-reactors (Lin et al. 2016). The planar micro-reactor was found to be more efficient than the micro-channel one, and doped TiO_2 were reported to be more efficient than TiO_2 under natural sunlight.

The influence of reaction parameters on the photodegradation rate and the global process efficiency are strongly dependent on the reactor technology. Zhang et al. reported that the photocatalytic degradation rate of methylene blue in a TiO_2 packed bed micro-reactor was increased by 520 as compared to a conventional bulk container of 15 mL (Zhang et al. 2013). The implementation of a TiO_2 coated monolith in a micro-reactor for the photocatalytic degradation of methylene blue was reported by Teekateerawej et al. (Teekateerawej et al. 2005). Additionally to the TiO_2 coating method, which influences the photocatalyst efficiency, they found that, in such configuration, irradiation light angle is the main parameter governing the catalytic reaction rate given that the light does not cross the monolith. Yang et al. compared three mini-fluidized bed reactors for the photocatalytic degradation of methylene blue (Yang et al. 2016). The first one with Fe^{3+}/TiO_2 photocatalyst coated on the inner wall of the reactor, the second one where the Fe^{3+}/TiO_2 photocatalyst is coated on the surface of fluidized particles (glass beads), and an third one with Fe^{3+}/TiO_2 photocatalyst coated both on the wall of the reactor and on the fluidized glass beads. The fluidization of glass beads allows increasing mass transfer coefficient by 11–13, and apparent reaction rate constant is multiplied by 4.9. The third reactor combining the two forms of catalyst (Fe^{3+}/TiO_2 photocatalyst coated both on the wall of the reactor and on the fluidized glass beads) was found to be 5 to 35% more efficient as compared to the two other configurations.

Interestingly, Aran et al. reported a gas–liquid–solid heterogeneous photocatalytic process by coupling a micro-reactor with a TiO_2-based photocatalytic membrane (Fig. 2.8) whose role is to ensure a continuous delivery of oxygen in the aqueous feed (Aran et al. 2011). Advantageously, such a triphasic system implemented at the microscale improves gas–liquid–solid interface. Authors reported that the photocatalytic degradation rate of phenol was increased, thanks to

oxygen supply. However, no significant effect was observed for the degradation of methylene blue, likely due to the lower initial concentration that lowers the amount of oxygen required for its degradation.

Even if such a technology is promising, there is still a lack of knowledge to develop the scale up of the process at the industrial scale.

2.6 Titania and Photocatalysis in Industry

Up to now titania-based systems for the water treatment by photocatalysis remain mainly at the laboratory stage, and efforts are mainly focused on the preparation of efficient photocatalysts. Besides the different studies reported in academic publications and cited in this chapter, some patents also exist (Park et al. 2002; Willmer and Ranjit 2002; Toledo et al. 2014; Balaya et al. 2015). For example, Willmer et al. have patented the preparation method of doped TiO_2 with lanthanide metal. Materials are obtained by the acid-catalyzed sol-gel process, and the obtained photocatalysts exhibit an enhanced efficiency for the photochemical degradation of the organic substrates such as p-chlorophenoxyacetic acid than the unmodified TiO_2 (Willmer and Ranjit 2002). To implant such material at the industrial scale, much attention should be paid on the shaping. As a matter of fact, the main drawback of using titania is due to the fact that powder form of TiO_2 is considered and that a filtration step is required. This filtration step is a drawback for the economic viability of photocatalysis process based on titania. Nevertheless, it should be noted that several company such as Clearwater Industries, Photox Bradford Ltd., Lynntech Inc., and Ishihara Sangyo Kaisha Ltd. have products at the development stage for water purification using semiconductor photocatalyst (Butters and Powell 1996, 2000; Gonzalez-Martin et al. 1998; Gonzalez-Martin et al. 2000). For example, the Lynntech Inc. company has patented a method and an apparatus based on the photocatalytic oxidation method using a porous titanium dioxide membrane for the mineralization of organic contaminants in water (Gonzalez-Martin et al. 1998). The photocatalytic reactor operates effectively at ambient temperature and low pressures. A packed-bed photoreactor using photocatalyst coated particles is also proposed (Gonzalez-Martin et al. 2000). More recently, Kisalius and Kinsinger have patented a method for synthesis of doped or undoped titania with controlled size, phase, morphology, and porosity (Kisalius and Kinsinger 2017). The prepared photocatalysts are integrated in a device for water treatment. The few examples reported above concerning water treatment allow to conclude that photodegradation of dyes by porous titania is a promising technology that will grow in the future and that it can reach the commercialization stage if we succeed to control the shaping of the photocatalysts.

2.7 Conclusions

Because of their potential toxic effects on human health, water pollution by dyes is a major issue, and many efforts are devoted to solve it. Among the different methods considered to remove dye, photodegradation is one of the most promising methods since it leads to the complete mineralization of the organic pollutants to CO_2, water, and mineral acids. In addition, such process avoids the production of solid wastes, and only mild temperature and pressure conditions are required. Thanks to its properties, titania has been widely considered as photocatalyst for dyes removal, and many efforts have been devoted to increase the specific surface area since this parameter is crucial for the photocatalytic activity.

Various types of porous TiO_2 nanomaterials such as powder mesostructured titania, nanoparticles, nanotubes, or nanorods have been successfully used for dyes photodegradation such as methylene blue, rhodamine B, or methyl orange. However, up to now, these materials are barely incorporated in a process, and most of the tests are performed at the laboratory scale. Many efforts are devoted to their shape modeling to integrate these materials in processes, and formation of films and the immobilization of TiO_2 on support such as membrane disks have been considered.

Properties of titania and in peculiar the specific surface area can also be tuned by associating it with another material to get nanocomposites. By the way both the specific surface area and the thermal stability are increased. As a consequence, in comparison with the performances of commercial titania such as P25, the photocatalytic efficiency of the composites is enhanced. Coupling TiO_2 with another material can also induce a decrease of the band gap, which allows enhancing the activity under the visible light. This can also be achieved by doping, which limits the electron/hole recombination and therefore favors the photocatalytic activity.

Up to now, membrane-based photocatalytic process is one of the most studied techniques to remove dyes from water at a large scale. Nevertheless, micro-reactors also appear as a promising technology for wastewater treatment. The main challenge that still persists is to implant the porous titania in these processes and to develop them at the industrial scale.

References

Abramian L, El-Rassy H (2009) Adsorption kinetics and thermodynamics of azo-dye Orange II onto highly porous titania aerogel. Chem Eng J 150:403–410. https://doi.org/10.1016/j.cej.2009.01.019

Ahmed S, Rasul MG, Martens WN, Brown R, Hashib MA (2010) Heterogeneous photocatalytic degradation of phenols in wastewater: a review on current status and developments. Desalination 261:3–18. https://doi.org/10.1016/j.desal.2010.04.062

Ajmal A, Majeed I, Malik RN, Idriss H, Nadeem MA (2014) Principles and mechanisms of photocatalytic dye degradation on TiO_2 based photocatalysts: a comparative overview. RSC Adv 4:37003–37026. https://doi.org/10.1039/c4ra066584

Akpan UG, Hameed BH (2009) Parameters affecting the photocatalytic degradation of dyes using TiO_2-based photocatalysts: a review. J Hazard Mater 170:520–529. https://doi.org/10.1016/j.jhazmat.2009.05.039

Alem A, Sarpoolaky H, Keshmiri M (2009) Sol–gel preparation of titania multilayer membrane for photocatalytic applications. Ceram Int 35:1837–1843. https://doi.org/10.1016/j.ceramint.2008.10.034

Alventosa-de Lara E, Barredo-Damas S, Alcaina-Miranda MI, Iborra-Clar MI (2012) Ultrafiltration technology with a ceramic membrane for reactive dye removal: optimization of membrane performance. J Hazard Mater 209:492–500. https://doi.org/10.1016/j.jhazmat.2012.01.065

Anandan S, Yoon M (2007) Photocatalytic degradation of Methyl Orange using heteropolytungstic acid-encapsulated TiSBA-15. Sol Energy Mater Sol Cells 91:143–147. https://doi.org/10.1016/j.solmat.2006.07.009

Anderson NG (2012) Using continuous processes to increase production. Org Process Res Dev 16:852–869. https://doi.org/10.1021/op200347k

Antonelli MM, Ying JY (1995) Synthesis of hexagonally packed mesoporous TiO_2 by a modified sol–gel method. Angew Chem Int Ed Eng 34:2014–2017. https://doi.org/10.1002/anie.199520141

Aran HC, Salamon D, Rijnaarts T, Mul G, Wessling M, Lammertink RGH (2011) Porous Photocatalytic Membrane Microreactor (P2M2): a new reactor concept for photochemistry. J Photochem Photobiol A Chem 225:36–41. https://doi.org/10.1016/j.jphotochem.2011.09.022

Assaker K, Benamor T, Michelin L, Lebeau B, Marichal C, Stébé MJ, Blin JL (2015) Mesoporous titania with anatase walls by flash induction calcination. Microporous Mesoporous Mater 201:43–49. https://doi.org/10.1016/j.micromeso.2014.09.028

Asuha S, Zhou XG, Zhao S (2010) Adsorption of Methyl Orange and Cr(VI) on mesoporous TiO_2 prepared by hydrothermal method. J Hazard Mater 181:204–210. https://doi.org/10.1016/j.hazmat.2010.04.117

Augugliaro V, García-López E, Loddo V, Malato-Rodríguez S, Maldonado I, Marcì G, Molinari R, Palmisano L (2005) Degradation of lincomycin in aqueous medium: coupling of solar photocatalysis and membrane separation. Sol Energy 79:402–408. https://doi.org/10.1016/j.solener.2005.02.020

Augugliaro V, Litter M, Palmisano L, Soria J (2006) The combination of heterogeneous photocatalysis with chemical and physical operations: a tool for improving the photoprocess performance. J Photochem Photobiol C: Photochem Rev 7:127–144. https://doi.org/10.1016/j.jphotochemrev.2006.12.001

Azrague K, Aimar P, Benoit-Marquié F, Maurette MT (2007) A new combination of a membrane and a photocatalytic reactor for the depollution of turbid water. Appl Catal B Environ 72:197–204. https://doi.org/10.1016/j.apcatb.2006.10.007

Bagheri S, Hir ZAM, Yousefi AT, Hamid SBA (2015) Progress on mesoporous titanium dioxide: synthesis, modification and applications. Microporous Mesoporous Mater 218:206–222. https://doi.org/10.1016/j.micromeso.2015.05.028

Balaya P, Krishnamoorthy A, Kuppan S (2015) Crystalline mesoporous titaniumdioxide and the use in electrochemical device. US patent US 8,968,931 B2

Bekkali CE, Bouyarmane H, Saoiabi S, Karbane ME, Rami A, Saoiabi A, Boujtita M, Laghzizil A (2016) Low-cost composites based on porous titania-apatite surfaces for the removal of Patent Blue V from water: effect of chemical structure of dye. J Adv Res 7:1009–1017. https://doi.org/10.1016/j.jare.2016.05.001

Bellobono IR, Morazzoni F, Bianchi R, Mangone ES, Stanescu R, Costache C, Tozzi PM (2005) Solar energy driven photocatalytic membrane modules for water reuse in agricultural and food industries. Pre-industrial experience using s-triazines as model molecules. Int J Photoenergy 7(2):87–94. https://doi.org/10.11155/S1110662X05000139

Benotti MJ, Stanford BD, Wert EC, Snyder SA (2009) Evaluation of a photocatalytic reactor membrane pilot system for the removal of pharmaceuticals and endocrine disrupting compounds from water. Water Res 43:1513–1522. https://doi.org/10.1016/j.watres.2008.12.049

Besançon M, Michelin L, Josien L, Vidal L, Assaker K, Bonne M, Lebeau B, Blin JL (2016) Influence of the porous texture of SBA-15 mesoporous silica on the anatase formation in TiO_2–SiO_2 nanocomposites. New J Chem 40:4386–4397. https://doi.org/10.1039/c5nj02859k

Binas VD, Sambani K, Maggos T, Katsanaki A, Kiriakidis G (2012) Synthesis and photocatalytic activity of Mn-doped TiO_2 nanostructured powders under UV and visible light. Appl Catal, B 113:79–86. https://doi.org/10.1016/j.apcatb.2011.11.021

Bizani E, Fytianos K, Poulios I, Tsiridis V (2006) Photocatalytic decolorization and degradation of dye solutions and wastewaters in the presence of titanium dioxide. J Hazard Mater 136:85–94. https://doi.org/10.1016/j.jhazmat.2005.11.017

Blin JL, Stébé MJ, Roques-Carmes T (2012) Use of ordered mesoporous titania with semi-crystalline framework as photocatalyst. Colloids Surf A Physicochem Eng Asp 407:177–185. https://doi.org/10.1016/j.colsurfa.2012.05.029

Bosc F, Ayral A, Guizard C (2005) Mesoporous anatase coatings for coupling membrane separation and photocatalyzed reactions. J Membr Sci 265:13–19. https://doi.org/10.1016/j.memsci.2005.04.039

Butters BE, Powell AL (1996) Advanced filtration technique for fluid purification US patent 5,589,078

Butters BE, Powell AL (2000) System and method for photocatalytic treatment of contaminated media

Cai Z, Sun Y, Liu W, Sun P, Fu J (2017) An overview of nanomaterials applied for removing dyes from water. Environ Sci Pollut Res 24:15882–15904. https://doi.org/10.1007/s11356-017-9003-8

Cambié D, Bottechia C, Straathof NJW, Hessel V, Noël T (2016) Applications of continuous-flow photochemistry in organic synthesis, material science and water treatment. Chem Rev 116:10276–10341. https://doi.org/10.1021/acs.chemrev.5b00707

Camera-Roda G, Santarelli F (2005) Intensification of water detoxification by integrating photocatalysis and pervaporation. J Sol Energy Eng 129:68–73. https://doi.org/10.1115/1.2391204

Cao S, Zhao Y, Qu T, Wang P, Guan S, Xu Y, Rao F, Li Y, Chen A, Lyoda T (2016) Ordered mesoporous crystalline titania with high thermal stability from comb-like liquid crystal block copolymers. RSC Adv 6:55834–55841. https://doi.org/10.1039/C6RA10352A

Carp O, Huisman CL, Reller A (2004) Photoinduced reactivity of titanium dioxide. Prog Solid State Chem 32:33–177. https://doi.org/10.1016/j.progsolidstchem.2004.08.001

Castillo-Villalón P, Ramírez J (2009) Spectroscopic study of the electronic interactions in Ru/TiO_2 HDS catalysts. J Catal 268:39–48. https://doi.org/10.1016/j.jcat.2009.08.014

Chaker H, Chérif-Aouali L, Khaoulani S, Bengueddach A, Fourmentin S (2016) Photocatalytic degradation of Methyl Orange and real wastewater by silver doped mesoporous TiO2 catalysts. J Photochem Photobiol, A 318:142–149. https://doi.org/10.1016/j.photochem.2015.11.025

Chang F, Wang G, Xie Y, Zhang M, Zhang J, Yang HJ, Hu X (2013) Synthesis of TiO_2 nanoparticles on mesoporous aluminosilicate Al-SBA-15 in supercritical CO_2 for photocatalytic decolorization of Methylene Blue. Ceram Int 39:3823–3829. https://doi.org/10.1016/j.ceramint.2012.10.223

Chauhan R, Kumar A, Chaudhary RP (2012) Structural and optical characterization of Zn doped TiO_2 nanoparticles prepared by sol–gel method. J Sol Sci Technol 61:585–591. https://doi.org/10.1007/s10971-011-2664-8

Chen X, Mao SS (2007) Titanium dioxide nanomaterials: synthesis, properties, modifications, and applications. Chem Rev 107:2891–2959. https://doi.org/10.1021/cr0500535

Chen J, Yao M, Wang J (2008) Investigation of transition metal ion doping behaviors on TiO_2 nanoparticles. J Nanopart Res 10:163–171. https://doi.org/10.1007/s11051-007-9237-3

Chen C, Weimin C, Mingce L, Jingyi Z, Baoxue Z, Yahui W, Deyong W (2010) Template-free sol-gel preparation and characterization of free-standing visible light responsive C,N-Modified porous monolithic TiO_2. J Hazard Mater 178:560–565. https://doi.org/10.1016/j.jhazmat.2010.01.121

Chen C, Gunawan P, Xu R (2011) Self-assembled Fe_3O_4-layered double hydroxide colloidal nanohybrids with excellent performance for treatment of organic dyes in water. J Mater Chem 21:1218–1225. https://doi.org/10.1039/c0jm01696a

Chen Y, Wang J, Li W, Ju M (2015) Microwave-assisted hydrothermal synthesis of Au/TiO_2/SBA-15 for enhanced visible-light photoactivity. Mater Lett 159:131–134. https://doi.org/10.1016/j.matlet.2015.04.030

Chin SS, Chiang K, Fane AG (2006) The stability of polymeric membranes in a TiO_2 photocatalysis process. J Membr Sci 275:202–211. https://doi.org/10.1016/j.memsci.2005.09.033

Chin SS, Lim TM, Chiang K, Fane AG (2007a) Hybrid low-pressure submerged membrane photoreactor for the removal of bisphenol A. Desalination 202:253–261. https://doi.org/10.1016/j.desal.2005.12.062

Chin SS, Lim TM, Chiang K, Fane AG (2007b) Factors affecting the performance of a low-pressure submerged membrane photocatalytic reactor. Chem Eng J 130:53–63. https://doi.org/10.1016/j.cej.2006.11.008

Chiou CH, Wu CY, Juang RS (2008) Influence of operating parameters on photocatalytic degradation of phenol in UV/TiO_2 process. Chem Eng J 139:322–329. https://doi.org/10.1016/j.cej.2007.08.002

Chong MN, Jin B, Chow CWK, Saint C (2010) Recent developments in photocatalytic water treatment technology: a review. Water Res 44:2997–3027. https://doi.org/10.1016/j.watres.2010.02.039

Choo KH, Chang DI, Park KW, Kim MH (2008a) Use of an integrated photocatalysis/hollow fiber microfiltration system for the removal of trichloroethylene in water. J Hazard Mater 152:183–190. https://doi.org/10.1016/j.jhazmat.2007.06.117

Choo KH, Tao R, Kim MJ (2008b) Use of a photocatalytic membrane reactor for the removal of natural organic matter in water: effect of photoinduced desorption and ferrihydrite adsorption. J Membr Sci 322:368–374. https://doi.org/10.1016/j.memsci.2008.05.069

Coleman HM, Vimonses V, Leslie G, Amal R (2007) Degradation of 1,4-dioxane in water using TiO_2 based photocatalytic and H_2O_2/UV processes. J Hazard Mater 146:496–501. https://doi.org/10.1016/j.jhazmat.2007.04.049

Colina-Márquez J, Machuca-Martínez F, Puma GL (2010) Radiation absorption and optimization of solar photocatalytic reactors for environmental applications. Environ Sci Technol 44:5112–5120. https://doi.org/10.1021/es100130h

Coyle EE, Oelgemöller M (2008) Micro-photochemistry: photochemistry in microstructured reactors. The new photochemistry of the future? Photochem Photobiol Sci 7:1313–1322. https://doi.org/10.1039/B808778D

Cui P, Zhao X, Zhou M, Wang L (2006) Photocatalysis-membrane separation coupling reactor and its application. Chin J Catal 27:752–754. https://doi.org/10.1016/S1872-2067(06)60041-7

Curcio E, Ji X, Di Profio G, Sulaiman AO, Fontananova E, Drioli E (2010) Membrane distillation operated at high seawater concentration factors: role of the membrane on $CaCO_3$ scaling in presence of humic acid. J Membr Sci 346:263–269

Damodar RA, You S-J, Ou S-H (2010) Coupling of membrane separation with photocatalytic slurry reactor for advanced dye wastewater treatment. Sep Purif Technol 76:64–71. https://doi.org/10.1016/j.seppur.2010.09.021

De Lima LB, Pereira LO, de Moura SG, Magalhães F (2017) Degradation of organic contaminants in effluents-synthetic and from the textile industry-by Fenton, photocatalysis and H_2O_2 photolysis. Environ Sci Pollut Res 24:6299–6306. https://doi.org/10.1007/s11356-016-6973-x

Demarche P, Junghanns C, Nair RR, Agathos SN (2012) Harnessing the power of enzymes for environmentalstewardship. Res Rev Pap Biotechnol Adv 30:933–953. https://doi.org/10.1016/j.biotechadv.2011.05.013

Devi LG, Kottam N, Murthy BN, Kumar SG (2010) Enhanced photocatalytic activity of transition metal ions Mn^{2+}, Ni^{2+} and Zn^{2+} doped polycrystalline titania for the degradation of Aniline Blue under UV/solar light. J Mol Catal A 328:44–52. https://doi.org/10.1016/j.molcata.2010.05.021

Doll TE, Frimmel FH (2005) Cross-flow microfiltration with periodical back-washing for photocatalytic degradation of pharmaceutical and diagnostic residues–evaluation of the long-term stability of the photocatalytic activity of TiO_2. Water Res 39:847–854. https://doi.org/10.1016/j.watres.2004.11.029

Dong W, Sun Y, Lee CW, Hua W, Lu X, Shi Y, Zhang S, Chen J, Zhao D (2007) Controllable and repeatable synthesis of thermally stable anatase nanocrystal-silica composites with highly ordered hexagonal mesostructures. J Am Chem Soc 129:13894–13904. https://doi.org/10.1021/ja073804o

Dong W, Sun Y, Ma Q, Zhu L, Hua W, Lu X, Zhuang G, Zhang S, Guo Z, Zhao D (2012) Excellent photocatalytic degradation activities of ordered mesoporous anatase TiO_2–SiO_2 nanocomposites to various organic contaminants. J Hazard Mater 229–230:307–320. https://doi.org/10.1016/j.jhazmat.2012.06.002

Dong H, Zeng G, Tang L, Fan C, Zhang C, He X, He Y (2015) An overview on the limitations of TiO_2-based particles for photocatalytic degradation of organic pollutants and the corresponding countermeasures. Water Res 29:128–146. https://doi.org/10.1016/j.watres.2015.04.038

Dong W, Yao Y, Li L, Sun Y, Hua W, Zhuang G, Zhao D, Yan S, Song W (2017) Three-dimensional interconnected mesoporous anatase TiO_2 exhibiting unique photocatalytical performance. Appl Catal B Environ 217:293–302. https://doi.org/10.1016/j.apcatb.2017.05.083

Donia AM, Atia AA, Al-amrani WA, El-Nahas AM (2009) Effect of structural properties of acid dyes on their adsorption behaviour from aqueous solutions by amine modified silica. J Hazard Mater 161:1544–1550. https://doi.org/10.1016/j.jhazmat.2008.05.042

Dror I, Jacov OM, Cortis A, Berkowitz B (2012) Catalytic transformation of persistent contaminants using a new composite material based on nanosized zero-valent iron. ACS Appl Mater Interfaces 4:3416–3423. https://doi.org/10.1021/am300402q

Dutta R, Nagarjuma TV, Mandavgane SA, Ekhe JD (2014) Ultrafast removal of cationic dye using agrowaste-derived mesoporous adsorbent. Ind Eng Chem Res 54:18558–18567. https://doi.org/10.1021/ie5030003

Epolito WJ, Lee YH, Bottomley LA, Pavlostathis SG (2005) Characterization of the textile anthraquinone dye Reactive Blue 4. Dyes Pigments 67:35–46. https://doi.org/10.1016/j.dyepig.2004.10.006

Erdei L, Arecrachakul N, Vigneswaran S (2008) A combined photocatalytic slurry reactor–immersed membrane module system for advanced wastewater treatment. Sep Purif Technol 62:382–388. https://doi.org/10.1016/j.seppur.2008.02.003

Fernández-Ibáñez P, Blanco J, Malato S, de las Nieves FJ (2003) Application of the colloidal stability of TiO_2 particles for recovery and reuse in solar photocatalysis. Water Res 37:3180–3188. https://doi.org/10.1016/S0043-1354(03)00157-X

Fisli A, Ridwan R, Krisnandi YK, Gunlazuardi J (2017) Preparation and characterization of Fe_3O_4/SiO_2/TiO_2 composite for Methylene Blue removal in water. Int J Technol 1:76–84. https://doi.org/10.14716/ijtech.v8i1.2888

Forgacs E, Cserháti T, Oros G (2004) Removal of synthetic dyes from wastewaters: a review. Environ Int 30:953–971. https://doi.org/10.1016/j.envint.2004.02.001

Fox M, Dulay M (1993) Heterogeneous. Photocatalysis. Chem Rev 93:341–357. https://doi.org/10.1021/cr00017a016

Fu J, Ji M, Wang Z, Jin L, An D (2006a) A new submerged membrane photocatalysis reactor (SMPR) for fulvic acid removal using a nano-structured photocatalyst. J Hazard Mater 131:238–242. https://doi.org/10.1016/j.jhazmat.2005.09.039

Fu J, Ji M, Zhao Y, Wang L (2006b) Kinetics of aqueous photocatalytic oxidation of fulvic acids in a photocatalysis–ultrafiltration reactor (PUR). Sep Purif Technol 50:107–113. https://doi.org/10.1016/j.seppur.2005.11.017

Fujishima A, Honda K (1972) Electrochemical photolysis of water at a semiconductor electrode. Nature 238:37–38. https://doi.org/10.1038/238037a0

Galenda A, Visentin F, Gerbasi R, Battiston S, El Habra N (2017) Effective and low-cost synthesis of sulphur-modified TiO_2 nanopowder with improved photocatalytic performances in water

treatment applications. Water Air Soil Pollut 228:416. https://doi.org/10.1007/s11270-017-3600-5
Gao B, Yap PS, Lim TM, Lim T-T (2011) Adsorption-photocatalytic degradation of Acid Red 88 by supported TiO2: effect of activated carbon support and aqueous anions. Chem Eng J 171:1098–1107. https://doi.org/10.1016/j.cej.2011.05.006
Gaya UI, Abdullah AH (2008) Heterogeneous photocatalytic degradation of organic contaminants over titanium dioxide: a review of fundamentals, progress and problems. J Photochem Photobiol C 9:1–12. https://doi.org/10.1016/j.photochemrev.2007.12.003
Gemoets HPL, Su Y, Shang M, Hessel V, Luque R, Noël T (2015) Liquid phase oxidation chemistry in continuous-flow microreactors. Chem Soc Rev 45:83–117. https://doi.org/10.1039/C5CS00447K
Genuino HC, Hamal DB, Fu Y-J, Suib SL (2012) Synergetic effects of ultraviolet and microwave radiation for enhanced activity of TiO_2 nanoparticles in degrading organic dyes using a continuous-flow reactor. J Phys Chem C 116:14040–14051. https://doi.org/10.1021/jp3040192
Gerasimova TV, Evdokimova (Galkina) OL, Kraev AS, Ivanov VK, Agafonov AV (2016) Micro-mesoporous anatase TiO_2 nanorods with high specific surface area possessing enhanced adsorption ability and photocatalytic activity. Microporous Mesoporous Mater 235:185–194. https://doi.org/10.1016/j.micromeso.2016.08.015
Giovannetti R, Rommozzi E, Zannotti M, D'Amato CA (2017) recent advances in graphene based TiO2 nanocomposites (GTiO2Ns) for photocatalytic degradation of synthetic dyes. Catalysts 7:305–339. https://doi.org/10.3390/catal7100305
Gjipalaj J, Alessandri I (2017) Easy recovery, mechanical stability, enhanced adsorption capacity and recyclability of alginate-based TiO_2 macrobead photocatalysts for water treatment. J Environ Chem Eng 5:1763–1770. https://doi.org/10.1016/j.jece.2017.03.017
Gong Y, Wang DP, Wu R, Gazi S, Soo HS, Sritharan T, Chen Z (2017) New insights into the photocatalytic activity of 3-D core-shell P25@silica nanocomposites: impact of mesoporous coating. Dalton Trans 46:4994–5002. https://doi.org/10.1039/C7DT00797C
Gonzalez-Martin A, Murphy OJ, Hodko D (1998) Photocatalytic oxidation of organics using a porous titanium dioxide membrane and an efficient oxidant US patent 5,779,912
Gonzalez-Martin A, Murphy OJ, Hodko D (2000) Photocatalytic oxidation of organics using a porous titanium dioxide membrane and an efficient oxidant US patent 6,136,86
Gorges R, Meyer S, Kreisel G (2004) Photocatalysis in microreactors. J Photochem Photobiol A Chem 167:95–99. https://doi.org/10.1016/j.jphotochem.2004.04.004
Guo J, Li J, Yin A, Fan K, Dai W (2010) Photodegradation of Rhodamine B on sulfur doped ZnO/TiO_2 nanocomposite photocatalyst under visible-light irradiation. Chin J Chem 28:2144–2150. https://doi.org/10.1002/cjoc.201090355
Guo J, Jianhua C, Wen W, Zishan Z, Dongfang W (2014) Adsorption behavior of Congo Red from aqueous solution on La_2O_3-doped TiO_2 nanotubes. Korean J Chem Eng 20:3081–3088. https://doi.org/10.1016/j.jiec.2013.11.047
Gupta VK, Suhas (2009) Application of low-cost adsorbents for dye removal: a review. J Environ Manag 90:2313–2342. https://doi.org/10.1016/j.jenvman.2008.11.017
Gupta VK, Rajeev J, Shilpi A, Arunima N, Meenakshi S (2012) Photodegradation of hazardous dye Quinoline Yellow catalyzed by TiO_2. J Colloid Interface Sci 366:135–140. https://doi.org/10.1016/j.jcis.2011.08.059
Gutmann B, Cantillo D, Kappe CO (2015) Continuous-flow technology – a tool for the safe manufacturing of active pharmaceutical ingredients. Angew Chem Int Ed 54:6688–6728. https://doi.org/10.1002/anie.201409318
Hafez HS (2009) Synthesis of highly-active single-crystalline TiO2 nanorods and its application in environmental photocatalysis. Mater Lett 63:1471–1474. https://doi.org/10.1016/j.matlet.2009.03.057
Hajjaji W, Andrejkovicova S, Pullar RC, Tobaldi DM, Lopez-Galindo A, Jammousi F, Rocha F, Labrincha JA (2016) Effective removal of anionic and cationic dyes by kaolinite and TiO_2/kaolinite composites. Clay Miner 51:19–27. https://doi.org/10.1180/claymin.2016.051.1.02
Hartman RL, Jensen KF (2009) Microchemical systems for continuous-flow synthesis. Lab Chip 9:2495–2507. https://doi.org/10.1039/B906343A

Heggo D, Ookawara S (2017) Multiphase photocatalytic microreactors. Chem Eng Sci 169:67–77. https://doi.org/10.1016/j.ces.2017.01.019

Hessel V, Cortese B, de Croon MHJM (2011) Novel process windows-concept, proposition and evaluation methodology, and intensified superheated processing. Chem Eng Sci 66:1426–1448. https://doi.org/10.1016/j.ces.2010.08.018

Hoffmann M, Martin S, Choi W, Bahnemann D (1995) Environmental applications of semiconductor photocatalysis. Chem Rev 95:69–96. https://doi.org/10.1021/cr00033a004

Huang X, Meng Y, Liang P, Qian Y (2007) Operational conditions of a membrane filtration reactor coupled with photocatalytic oxidation. Sep Purif Technol 55:165–172. https://doi.org/10.1016/j.seppur.2006.11.018

Hufschmidt D, Bahnemann D, Testa JJ, Emilio CA, Litter MI (2002) Enhancement of the photocatalytic activity of various TiO_2 materials by platinisation. J Photochem Photobiol A Chem 148:223–231. https://doi.org/10.1016/S1010-6030(02)00048-5

Ilinoiu EC, Pode R, Manea F, Colar LA, Jakab A, Orha C, Ratiu C, Lazau C, Sfarloaga P (2013) Photocatalytic activity of a nitrogen-doped TiO_2 modified zeolite in the degradation of reactive Yellow 125 Azo Dye. J Taiwan Inst Chem Eng 44:270–278. https://doi.org/10.1016/j.jtice.2012.09.006

Ilkhechi NN, Kaleji BK (2014) High temperature stability and photocatalytic activity of nanocrystalline anatase powders with Zr and Si co-dopants. J Sol-Gel Sci Technol 69:351–356. https://doi.org/10.1007/s10971-013-3224-1

Im JH, Seung JY, Chang HY, Chong RP (2012) Simple fabrication of carbon/TiO_2 composite nanotubes showing dual functions with adsorption and photocatalytic decomposition of Rhodamine B. Nanotechnology 23:1–10. https://doi.org/10.1088/0957-4484/23/3/035604

Ismail AA, Bahnemann DW (2011) Mesoporous titania photocatalysts: preparation, characterization and reaction mechanisms. J Mater Chem 21:11686–11707. https://doi.org/10.1039/C1JM10407A

Jensen KF (2017) Flow chemistry-microreaction technology comes of age. AICHE J 63:858–869. https://doi.org/10.1002/aic.15642

Jensen KF, Reizman BJ, Newman SG (2014) Tools for chemical synthesis in microsystems. Lab Chip 14:3206–3212. https://doi.org/10.1039/C4LC00330F

Jiang H, Zhang G, Huang T, Chen J, Wang Q, Meng Q (2010) Photocatalytic membrane reactor for degradation of Acid Red B wastewater. Chem Eng J 156:571–577. https://doi.org/10.1016/j.cej.2009.04.011

Jiang Y, Tang W, Gao J, Zhou L, He Y (2014) Immobilization of horseradish peroxidase in phospholipid-templated titania and its applications in phenolic compounds and dye removal. Enzym Microb Technol 55:1–5. https://doi.org/10.1016/j.enzmictec.2013.11.005

Jiao Y, Wan C, Li J (2015) Room-temperature embedment of anatase titania nanoparticles into porous cellulose aerogels. Appl Phys A Mater Sci Process 120:341–347. https://doi.org/10.1007/s00339-0159192-2

Jing LQ, Wang BQ, Xin BF, Li SD, Shi KY, Cai WM, Fu HG (2004) Investigations on the surface modification of ZnO nanoparticle photocatalyst by depositing Pd. J Solid State Chem 177:4221–4227. https://doi.org/10.1016/j.jssc.2004.08.016

Julkapli N, Bagheri S, Hamid SBA (2014) Recent advances in heterogeneous photocatalytic decolorization of synthetic dyes. Sci World J. Article ID 692307, 25 pages. https://doi.org/10.1155/2014/692307

Kansal SK, Singh M, Sud D (2008) Studies on TiO_2/ZnO photocatalysed degradation of lignin. J Hazard Mater 153:412–417. https://doi.org/10.1016/j.jhazmat.2007.08.091

Karthikeyan N, Sivaranjani T, Dhanavel S, Gupta VK, Narayanan V, Stephen A (2017) Visible light degradation of textile effluent by electrodeposited multiphase $CuInSe_2$ semiconductor photocatalysts. J Mol Liq 227:194–201. https://doi.org/10.1016/j.molliq.2016.12.019

Kasanen J, Salstela J, Suvanto M, Pakkanen TT (2011) Photocatalytic degradation of methylene blue in water solution by multilayer TiO_2 coating on HDPE. Appl Surf Sci 258:1738–1743. https://doi.org/10.1016/j.apsusc.2011.10.028

Kelly S, Pollak FH, Tomkiewicz M (1997) Raman spectroscopy as a morphological probe for TiO_2 aerogels J. Phys Chem B 101:2730–2734. https://doi.org/10.1021/jp962747a

Kim DS, Han SJ, Kwak SY (2007) Synthesis and photocatalytic activity of mesoporous TiO_2 with the surface area, crystallite size, and pore size. J Colloid Interface Sci 316:85–91. https://doi.org/10.1016/j.jcis.2007.07.037

Kimling MC, Dehong C, Caruso RA (2017) Temperature-induced modulation of mesopore size in hierarchically porous amorphous TiO_2/ZrO_2 beads for improved dye adsorption capacity. J Mater Chem 3:3768–3776. https://doi.org/10.1039/C4TA06289B

Kimura T (2016) Evaporation-induced self-assembly process controlled for obtaining highly ordered mesoporous materials with demanded morphologies. Chem Rec 16:445–457. https://doi.org/10.1002/tcr.201500262

Kisalius D, Kinsinger N (2017) Methods of making metal-oxides and uses thereof for water treatment ans energy applications. US patent US 9,670,069 B2

Kolpin DW, Furlong ET, Meyer MT, Thurman EM, Zaugg SD, Barber LB, Buxton HT (2002) Pharmaceuticals, hormones, and other organic wastewater contaminants in US streams, 1999–2000: a national reconnaissance. Environ Sci Technol 36:1202–1211. https://doi.org/10.1021/es011055j

Koros WJ, Ma YH, Shimidzu T (1996) Terminology for membranes and membrane processes (IUPAC Recommendations 1996). Pure Appl Chem 68:1479–1489. https://doi.org/10.1351/pac199668071479

Ku Y, Huang YH, Chou YC (2011) Preparation and characterization of ZnO/TiO_2 for the photocatalytic reduction of Cr(VI) in aqueous solution. J Mol Catal A Chem 342-343:18–22. https://doi.org/10.1016/j.molcata.2011.04.003

Kuijpers KPL, Dijk MAH, van Rumeur QG, Hessel V, Su Y, Noël T (2017) A sensitivity analysis of a numbered-up photomicroreactor system. React Chem Eng 2:109–115. https://doi.org/10.1039/C7RE00024C

Lai CW, Juan JC, Ko WB, Abd Hamid SB (2014) An overview: recent development of titanium oxide nanotubes as photocatalyst for dye degradation. Int J Photoenergy 2014:1–14. https://doi.org/10.1155/2014/524135

Landmann M, Rauls E, Schmidt WG (2012) The electronic structure and optical response of rutile, anatase and brookite TiO_2. J Phys Condens Matter. 24:Article Number: 195503. https://doi.org/10.1088/0953-8984/24/19/195503

Lannoy A, Bleta R, Machut C, Monflier E, Ponchel A (2014) Block copolymer–cyclodextrin supramolecular assemblies as soft templates for the synthesis of titania materials with controlled crystallinity, porosity and photocatalytic activity. RSC Adv 4:4061–4070. https://doi.org/10.1039/c4ra05994h

Lazar MA, Varghese S, Nair SS (2012) Photocatalysis water treatment by titanium dioxide: recent updates. Catalysts 2:572–601. https://doi.org/10.3390/catal2040572

Lee SA, Choo KH, Lee CH, Lee HI, Hyeon T, Choi W, Kwon HH (2001a) Use of ultrafiltration membranes for the separation of TiO_2 photocatalysts in drinking water treatment. Ind Eng Chem Res 40:1712–1719. https://doi.org/10.1021/ie000738p

Lee SS, Kim HJ, Jung KT, Kim HS, Shuf YG (2001b) Photocatalytic activity of metal Ion (Fe or W) doped titania. Korean J Chem Eng 18:914–918. https://doi.org/10.1007/BF02705618

Lee CK, Liu SS, Juang LC, Wang CC, Lin KS, Lyu MD (2007) Application of MCM-41 for dyes removal from wastewater. J Hazard Mater 147:997–1005. https://doi.org/10.1016/j.jhazmat.2007.01.130

Li XZ, Zhao YG (1999) Advanced treatment of dyeing wastewater for reuse. Water Sci Technol 39:249–255. https://doi.org/10.1016/S0273-1223(99)00285-1

Li X, Wang H, Inoue K, Uehara M, Nakamura H, Miyazaki M, Abe E, Maeda H (2003) Modified micro-space using self-organized nanoparticles for reduction of Methylene Blue. Chem Commun 0:964–965. https://doi.org/10.1039/B300765K

Li Z, Hou B, Wu D, Sun Y (2005) Hydrothermal synthesis, characterization, and photocatalytic performance of silica-modified titanium dioxide nanoparticles. J Colloid Interface Sci 288:149–154. https://doi.org/10.1016/j.jcis.2005.02.082

Li H, Shi JL, Liang J, Li X, Li L, Ruan M (2008) Synthesis of well-ordered mesoporous titania powder with crystallized framework. Mater Lett 62:1410–1413. https://doi.org/10.1016/j.matlet.2007.08.072

Li W, Wu Z, Wang J, Elzatahry AA, Zhao D (2014) A perspective on mesoporous TiO_2 materials. Chem Mater 26:287–298. https://doi.org/10.1021/cm4014859

Li Y, Li J, Wang X, Ma Y, Guan W, Qian T (2016) Macrostructure-controlled titania ceramics derived from particle-stabilized emulsions: preparation and photochemical performance. Mater Chem Phys 182:402–408. https://doi.org/10.1016/j.matchemphys.2016.07.048

Liao DL, Badour CA, Liao BQ (2008) Preparation of nanosized TiO_2/ZnO composite catalyst and its photocatalytic activity for degradation of Methyl Orange. J Photochem Photobiol A Chem 194:11–19. https://doi.org/10.1016/j.jphotochem.2007.07.008

Lin C, Liu M, Yang Z (2016) Performance of a metal ion-doped titania-coated planar photocatalytic microreactor. Chem Eng Technol 39:88–96. https://doi.org/10.1002/ceat.201400776

Lin HF, Liao SC, Hung SW (2005) The dc thermal plasma synthesis of ZnO nanoparticles for visible-light photocatalyst. J Photochem Photobiol A Chem 174:82–87. https://doi.org/10.1016/j.jphotochem.2005.02.015

Lin WC, Yang WD, Chung ZJ, Chueng HJ (2011) Preparation and application of titanate nanotubes on Methylene Blue degradation from aqueous media. Appl Mech Mater 117:786–789. https://doi.org/10.4028/AMM.117-119.786

Lin WC, Yang WD, Jheng SY (2012) Photocatalytic degradation of dyes in water using porous nanocrystalline titanium dioxide. J Taiwan Inst Chem Eng 43:269–274. https://doi.org/10.1016/j.jtice.2011.10.010

Lindstrom H, Wootton R, Iles A (2007) High surface area titania photocatalytic microfluidic reactors. AICHE J 53:695–702. https://doi.org/10.1002/aic.11096

Linsebigler A, Lu G, Yates J (1995) Photocatalysis on TiO_2 Surfaces: principles, mechanisms, and selected results. Chem Rev 95:735–758. https://doi.org/10.1021/cr00035a013

Liu F, Liu CL, Hu B, Kong WP, Qi CZ (2012) High temperature hydrothermal synthesis of crystalline mesoporous TiO_2 with superior photocatalytic activity. Appl Surf Sci 258:7448–7454. https://doi.org/10.1016/j.apsusc.2012.04.059

Liu R, Yang WD, Chueng HJ, Ren BQ (2015) Preparation and application of titanate nanotubes on dye degradation from aqueous media by UV irradiation. J Spectrosc. https://doi.org/10.1155/2015/680183

Ma Y, Yao JN (1998) Photodegradation of Rhodamine B catalyzed by TiO_2 thin films. J Photochem Photobiol A Chem 116:167–170. https://doi.org/10.1016/S1010-6030(98)00295-0

Ma N, Zhang Y, Quan X, Fan X, Zhao H (2010) Performing a microfiltration integrated with photocatalysis using an Ag-TiO_2/HAP/Al_2O_3 composite membrane for water treatment: evaluating effectiveness for humic acid removal and anti-fouling properties. Water Res 44:6104–6114. https://doi.org/10.1016/j.watres.2010.06.068

Mahlambi MM, Ngila CJ, Mamba BB (2015) Recent developments in environmental photocatalytic degradation of organic pollutants: the case of titanium dioxide nanoparticles – a review. J Nanomater. https://doi.org/10.1155/2015/790173

Mahmoodi NM, Arami M (2009) Degradation and toxicity reduction of textile wastewater using immobilized titania nanophotocatalysis. J Photochem Photobiol B 94:20–24. https://doi.org/10.1016/j.jphotobiol.2008.09.004

Mahmoodi NM, Arami M, Limaee NY, Tabrizi NS (2006) Kinetics of heterogeneous photocatalytic degradation of reactive dyes in an immobilized TiO_2 photocatalytic reactor. J Colloid Interface Sci 295:159–164. https://doi.org/10.1016/j.jcis.2005.08.007

Mahmoud HR, El-Molla SA, Saif M (2013) Improvement of physicochemicalproperties of Fe_2O_3/MgO nanomaterials by hydrothermal treatment for dye removal from industrial wastewater. Powder Technol 249:225–233. https://doi.org/10.1016/j.powtec.2013.08.021

Martorell MM, Pajot HF, de Figuerosa LIC (2017) Biological degradation of reactive black 5 dye by yeast trichosporon alkiyoshidainum. J Environ Chem Eng 5:5987–5993. https://doi.org/10.1016/j.jece.2017.11.012

Melvin Ng HK, Leo CP, Abdullah AZ (2017) Selective removal of dyes by molecular imprinted TiO_2 nanoparticles in polysulfone ultrafiltration membrane. J Environ Chem Eng 5:3991–3998. https://doi.org/10.1016/j.jece.2017.07.075

Mendret J, Hatat-Fraile M, Rivallin M, Brosillon S (2013) Hydrophilic composite membranes for simultaneous separation and photocatalytic degradation of organic pollutants. Sep Purif Technol 111:9–19. https://doi.org/10.1016/j.seppur.2013.03.030

Meng Y, Huang X, Yang Q, Qian Y, Kubota N, Fukunaga S (2005) Treatment of polluted river water with a photocatalytic slurry reactor using low-pressure mercury lamps coupled with a membrane. Desalination 181:121–133. https://doi.org/10.1016/j.desal.2005.02.015

Messina PV, Schultz PC (2006) Adsorption of reactive dyes on titania-silica mesoporous materials. J Colloid Interface Sci 299:305–320. https://doi.org/10.1016/j.jcis.2006.01.039

Minero C, Maurino V, Pelizzetti E (1997) Heterogeneous photocatalytic transformation of s-triazine derivatives. Res Chem Intermed 23:291–310

Mizuno K, Nishiyama Y, Ogaki T, Terao K, Ikeda H, Kakiuchi K (2016) Utilization of microflow reactors to carry out synthetically useful organic photochemical reactions. J Photochem Photobiol C: Photochem Rev 29:107–147. https://doi.org/10.1016/j.jphotochemrev.2016.10.002

Mohamed SK, Amr IA, Mousa AA, Betiha MA, El-Sharkawy EA, Hassan HMA (2018) Facile fabrication of ordered mesoporous Bi/Ti-MCM-41 nanocomposites for visible light-driven photocatalytic degradation of Methylene Blue and CO oxidation. Sep Purif Technol 195:174–183. https://doi.org/10.1016/j.seppur.2017.12.008

Molinari R, Mungari M, Drioli E, Di Paola A, Loddo V, Palmisano L, Schiavello M (2000) Study on a photocatalytic membrane reactor for water purification. Catal Today 55:71–78. https://doi.org/10.1016/S0920-5861(99)00227-8

Molinari R, Borgese M, Drioli E, Palmisano L, Schiavello M (2002a) Hybrid processes coupling photocatalysis and membranes for degradation of organic pollutants in water. Catal Today 75:77–85. https://doi.org/10.1016/S0920-5861(02)00047-0

Molinari R, Palmisano L, Drioli E, Schiavello M (2002b) Studies on various reactor configurations for coupling photocatalysis and membrane processes in water purification. J Membr Sci 206:399–415. https://doi.org/10.1016/S0376-7388(01)00785-2

Molinari R, Pirillo F, Falco M, Loddo V, Palmisano L (2004) Photocatalytic degradation of dyes by using a membrane reactor. Chem. Eng. Process Process Intensif 43:1103–1114. https://doi.org/10.1016/j.cep.2004.01.008

Molinari R, Pirillo F, Loddo V, Palmisano L (2006) Heterogeneous photocatalytic degradation of pharmaceuticals in water by using polycrystalline TiO_2 and a nanofiltration membrane reactor. Catal Today 118:205–213. https://doi.org/10.1016/j.cattod.2005.11.091

Molinari R, Caruso A, Argurio P, Poerio T (2008) Degradation of the drugs Gemfibrozil and Tamoxifen in pressurized and de-pressurized membrane photoreactors using suspended polycrystalline TiO_2 as catalyst. J Membr Sci 319:54–63. https://doi.org/10.1016/j.memsci.2008.03.033

Morales-Torres S, Pastrana-Martinez LM, Figueiredo JL, Faria JL (2012) Design of graphene-based TiO2 photocatalysts – a review. Environ Sci Pollut Res 19:3676–3687. https://doi.org/10.1007/s11356-012-0939-4

Moser J, Gratzel M, Galley R (1987) Inhibition of electron-hole recombination in substitutionally doped colloidal semiconductor crystallites. Helv Chim Acta 70:1596–1604. https://doi.org/10.1002/hlca.19870700617

Mozia S (2010) Photocatalytic membrane reactors (PMRs) in water and wastewater treatment. A review. Sep Purif Technol 73:71–91. https://doi.org/10.1016/j.seppur.2010.03.021

Mozia S, Morawski AW (2006) Hybridization of photocatalysis and membrane distillation for purification of wastewater. Catal Today 118:181–188. https://doi.org/10.1016/j.cattod.2005.12.003

Mozia S, Morawski AW (2009) Integration of photocatalysis with ultrafiltration or membrane distillation for removal of Azo Dye Direct Green 99 from water. J Adv Oxid Technol 12:111–121. https://doi.org/10.1515/jaots-2009-0114

Mozia S, Tomaszewska M, Morawski AW (2005) A new photocatalytic membrane reactor (PMR) for removal of azo-dye Acid Red 18 from water. Appl Catal B Environ 59:131–137. https://doi.org/10.1016/j.apcatb.2005.01.011

Mozia S, Tomaszewska M, Morawski AW (2006) Removal of azo-dye Acid Red 18 in two hybrid membrane systems employing a photodegradation process. Desalination 198:183–190. https://doi.org/10.1016/j.desal.2006.01.024

Mozia S, Tomaszewska M, Morawski AW (2007a) Photocatalytic membrane reactor (PMR) coupling photocatalysis and membrane distillation-Effectiveness of removal of three azo dyes from water. Catal Today 129:3–8. https://doi.org/10.1016/j.cattod.2007.06.043

Mozia S, Toyoda M, Inagaki M, Tryba B, Morawski AW (2007b) Application of carbon-coated TiO_2 for decomposition of Methylene Blue in a photocatalytic membrane reactor. J Hazard Mater 140:369–375. https://doi.org/10.1016/j.jhazmat.2006.10.016

Mozia S, Toyoda M, Tsumura T, Inagaki M, Morawski AW (2007c) Comparison of effectiveness of methylene blue decomposition using pristine and carbon-coated TiO_2 in a photocatalytic membrane reactor. Desalination 212:141–151. https://doi.org/10.1016/j.desal.2006.10.007

Mozia S, Morawski AW, Toyoda M, Inagaki M (2008) Effectiveness of photodecomposition of an azo dye on a novel anatase-phase TiO_2 and two commercial photocatalysts in a photocatalytic membrane reactor (PMR). Sep Purif Technol 63:386–391. https://doi.org/10.1016/j.seppur.2008.05.029

Mozia S, Morawski AW, Toyoda M, Inagaki M (2009a) Application of anatase-phase TiO_2 for decomposition of azo dye in a photocatalytic membrane reactor. Desalination 241:97–105. https://doi.org/10.1016/j.desal.2007.12.048

Mozia S, Morawski AW, Toyoda M, Tsumura T (2009b) Effect of process parameters on photodegradation of Acid Yellow 36 in a hybrid photocatalysis–membrane distillation system. Chem Eng J 150:152–159. https://doi.org/10.1016/j.cej.2008.12.012

Mozia S, Darowna D, Szymański K, Grondzewska S, Borchert K, Wróbel R, Morawski AW (2014) Performance of two photocatalytic membrane reactors for treatment of primary and secondary effluents. Catal Today 236:135–145. https://doi.org/10.1016/j.cattod.2013.12.049

Naboulsi I, Lebeau B, Michelin L, Carteret C, Vidal L, Bonne M, Blin JL (2017) Insights into the formation and properties of templated dual mesoporous titania with enhanced photocatalytic activity. ACS Appl Mater Interfaces 9:3113–3122. https://doi.org/10.1021/acsami.6b13269

Nalbandian MJ, Greenstein KE, Shuai D, Zhang M, Choa YH, Parkin GF, Myung NV, Cwiertny DM (2015) Tailored synthesis of photoactive TiO_2 nanofibers and Au/TiO_2 nanofiber composites: structure and reactivity optimization for water treatment applications. Environ Sci Technol 49:1654–1663. https://doi.org/10.1021/es502963t

Nandi BK, Goswami A, Purkait MK (2009) Removal cationic dyes from aqueous solutions by kaolin; kinetic and equilibrium studies. Appl Clay Sci 42:583–590. https://doi.org/10.1016/j.clay.2008.03.015

Newman SG, Jensen KF (2013) The role of flow in green chemistry and engineering. Green Chem 15:1456–1472. https://doi.org/10.1039/C3GC40374B

Nieves-Remacha MJ, Kulkarni AA, Jensen KF (2012) Hydrodynamics of liquid-liquid dispersion in an advanced-flow reactor. Ind Eng Chem Res 51:16251–16262. https://doi.org/10.1021/ie301821k

Nieves-Remacha MJ, Kulkarni AA, Jensen KF (2013) Gas-liquid flow and mass transfer in an advanced-flow reactor. Ind Eng Chem Res 52:8996–9010. https://doi.org/10.1021/ie4011707

Ohtani B, Ogawa Y, Nishimoto S (1997) Photocatalytic activity of amorphous-anatase mixture of titanium(IV) oxide particles suspended in aqueous solutions. J Phys Chem B 101:3746–3752. https://doi.org/10.1021/jp962702+

Oller I, Malato S, Sánchez-Pérez JA (2011) Combination of advanced oxidation processes and biological treatments for wastewater decontamination – a review. Sci Total Environ 409:4142–4166. https://doi.org/10.1016/j.scitotenv.2010.08.061

Ollis DF (2003) Integrating photocatalysis and membrane technologies for water treatment. Ann N Y Acad Sci 984:65–84. https://doi.org/10.1111/j.1749-6632.2003.tb05993.x

Padoin N, Andrade L, Ângelo J, Mendes A, Moreira RFPM, Soares C (2016) Intensification of photocatalytic pollutant abatement in microchannel reactor using TiO_2 and TiO_2-graphene. AICHE J 62:2794–2802. https://doi.org/10.1002/aic.15262

Pan L, Zou JJ, Wang S, Huang ZF, Zhang X, Wang L (2013) Enhancement of visible-light-induced photodegradation over hierarchical porous TiO_2 by nonmetal doping and water-mediated dye sensitization. Appl Surf Sci 268:252–258. https://doi.org/10.1016/j.apsusc.2012.12.074

Papageorgiou SK, Katsaros FK, Favvas EP, Romanos GE, Athanasekou CP, Beltsios KG, Tzialla OI, Falaras P (2012) Alginate fibers as photocatalyst immobilizing agents applied in hybrid photocatalytic/ultrafiltration water treatment processes. Water Res 46:1858–1872. https://doi.org/10.1016/j.watres.2012.01.005

Park SE, Hwang JS, Chang JS, Kim JM, Kim DS, Chai HS (2002) Titania photocatalyst and its preparing method US patent application publication 2002/0098977 A1

Paz Y (2006) Preferential photodegradation – why and how? C R Chimie 9:774–787. https://doi.org/10.1016/j.cri.2005.03.032

Pelaez M, Nolan NT, Pillai SC, Seery MK, Falaras P, Kontos AG, Dunlop PSM, Hamilton JWJ, Byrne JA, O'Shea K, Entezari MH, Dionysiou DD (2012) A review on the visible light active titanium dioxide photocatalysts for environmental applications. Appl Catal B Environ 125:331–349. https://doi.org/10.1016/j.apcatb.2012.05.036

Pelizzetti E, Minero C, Borgarello E, Tinucci L, Serpone N (1993) Photocatalytic activity and selectivity of titania colloids and particles prepared by the sol-gel technique: photooxidation of phenol and atrazine. Langmuir 13:2995–3001. https://doi.org/10.1021/la00035a043

Peng YG, Chen DJ, Ji JL, Kong Y, Wan HX, Yao C (2013) The preparation of titanium dioxide/palygorskite composite and its application in the adsorption of Congo Red. Environ Prog 32:1090–1095. https://doi.org/10.1002/ep.11717

Pérez-Larios A, Lopez R, Hernández-Gordillo A, Tzompantzi F, Gómez R, Torres-Guerra LM (2012) Improved hydrogen production from water splitting using TiO_2–ZnO mixed oxides photocatalysts. Fuel 100:139–143. https://doi.org/10.1016/j.fuel.2012.02.026

Preethi P, Padmapriya MP, Abarna B, Rajarajeswari GR (2017) Choline chloride–zinc chloride ionic liquid as a green template for the sol–gel synthesis of mesoporous titania. RSC Adv 7:10081–10091. https://doi.org/10.1039/C6RA28478G

Qamar M, Saquib M, Muneer M (2005) Titanium dioxide mediated photocatalytic degradation of two selected azo dye derivatives, Chrysoidine R and Acid Red 29 (chromotrope 2R), in aqueous suspensions. Desalination 186:255–271. https://doi.org/10.1016/j.desal.2005.05.021

Qin Q, Ma J, Liu K (2009) Adsorption of anionic dyes on ammonium-functionalized MCM-41. J Hazard Mater 162:133–139. https://doi.org/10.1016/j.jhazmat.2008.05.016

Qiu J, Zhang S, Zhao H (2012) Nanostructured TiO_2 photocatalysts for the determination of organic pollutants. J Hazard Mater 211-212:381–388. https://doi.org/10.1016/j.jhazmat.2011.10.093

Rafatullah M, Sulaiman O, Hashim R, Ahmad A (2010) Adsorption of Methylene Blue on low-cost adsorbents: a review. J Hazard Mater 177:70–80. https://doi.org/10.1016/j.jhazmat.2009.12.047

Rasalingam S, Wu CM, Koodali RT (2015) Modulation of pore sizes of titanium Dioxide photocatalysts by a facile template free hydrothermal synthesis method: implications for photocatalytic degradation of Rhodamine B. ACS Appl Mater Interfaces 7:4368–4380. https://doi.org/10.1021/am508883f

Reutergadh LB, Iangphasuk M (1997) Photocatalytic decolourization of reactive azo dye: a comparison between TiO_2 and us photocatalysis. Chemosphere 35:585–596. https://doi.org/10.1016/S0045-6535(97)00122-7

Rivero MJ, Parsons SA, Jeffrey P, Pidou M, Jefferson B (2006) Membrane chemical reactor (MCR) combining photocatalysis and microfiltration for grey water treatment. Water Sci Technol 53:173–180. https://doi.org/10.2166/wst.2006.090

Robinson T, McMullan G, Marchant R, Nigam P (2001) Remediation of dyes in textile effluent: a critical review on current treatment technologies with a proposed alternative. Bioresour Technol 77:247–255. https://doi.org/10.1016/S0960-8524(00)00080-8

Romanos GE, Athanasekou CP, Likodimos V, Aloupogiannis P, Falaras P (2013) Hybrid ultrafiltration/photocatalytic membranes for efficient water treatment. Ind Eng Chem Res 52:13938–13947. https://doi.org/10.1021/ie303475b

Rossetti I, Compagnoni M (2016) Chemical reaction engineering, process design and scale-up issues at the frontier of synthesis: flow chemistry. Chem Eng J 296:56–70. https://doi.org/10.1016/j.cej.2016.02.119

Ryu J, Choi W, Choo K-H (2005) A pilot-scale photocatalyst-membrane hybrid reactor: performance and characterization. Water Sci Technol 51:491–497

Saquib M, Tariq MA, Faisal M, Muneer M (2008a) Photocatalytic degradation of two selected dye derivatives in aqueous suspensions of titanium dioxide. Desalination 219:301–311. https://doi.org/10.1016/j.desal.2007.06.006

Saquib M, Tariq MA, Haque MM, Muneer M (2008b) Photocatalytic degradation of disperse Blue 1 using UV/TiO_2/H_2O_2 process. J Environ Manag 88:300–306. https://doi.org/10.1016/j.desal.2007.06.006

Serpone N, Maruthamuthu P, Pelizzetti P, Hidaka H (1995) Exploiting the interparticle electron transfer process in the photocatalysed oxidation of Phenol, 2-Chlorophenol and pentachlorophenol: chemical evidence for electron and hole transfer between coupled semiconductors. J Photochem Photobiol A Chem 85:247–255. https://doi.org/10.1016/1010-6030(94)03906-B

Sharma VK, Feng M (2017) Water depollution using metal-organic frameworks-catalyzed advanced oxidation processes: a review. J Hazard Mater 372:3–16. https://doi.org/10.1016/j.jhazmat.2017.09.043

Shifu C, Wei Z, Wei L, Sujuan Z (2008) Preparation, characterization and activity evaluation of p–n junction photocatalyst p-ZnO/n-TiO_2. Appl Surf Sci 255:2478–2484. https://doi.org/10.1016/j.jhazmat.2009.08.007

Shon HK, Phuntsho S, Vigneswaran S (2008) Effect of photocatalysis on the membrane hybrid system for wastewater treatment. Desalination 225:235–248. https://doi.org/10.1016/j.desal.2007.05.032

Simonsen ME, Søgaard EG (2010) Sol–gel reactions of titanium alkoxides and water: influence of pH and alkoxy group on cluster formation and properties of the resulting products. J Sol-Gel Sci Technol 53:485–497. https://doi.org/10.1007/s10971-009-2121-0

Sopajaree K, Qasim SA, Basak S, Rajeshwar K (1999a) An integrated flow reactor-membrane filtration system for heterogeneous photocatalysis. Part I: Experiments and modelling of a batch-recirculated photoreactor. J Appl Electrochem 29:533–539. https://doi.org/10.1023/A:1026418208733

Sopajaree K, Qasim SA, Basak S, Rajeshwar K (1999b) An integrated flow reactor-membrane filtration system for heterogeneous photocatalysis. Part II: Experiments on the ultrafiltration unit and combined operation. J Appl Electrochem 29:1111–1118. https://doi.org/10.1023/A:1003633309224

Stathatos E, Papoulis D, Aggelopoulos CA, Panagiotaras D, Nikolopoulou A (2012) TiO_2/palygorskite composite nanocrystalline films prepared by surfactant templating route: synergistic effect to the photocatalytic degradation of an azo-dye in water. J Hazard Mater 211:68–76. https://doi.org/10.1016/j.jhazmat.2011.11.055

Su Y, Straathof NJW, Hessel V, Noël T (2014) Photochemical transformations accelerated in continuous-flow reactors: basic concepts and applications. Chem Eur J 20:10562–10589. https://doi.org/10.1002/chem.201400283

Subramaniam MN, Goh PS, Abdullah N, Lau WJ, Ng BC, Ismail AF (2017) Adsorption and photocatalytic degradation of Methylene Blue using high surface area titanate nanotubes (TNT) synthesized via hydrothermal method. J Nanopart Res 19:220–232. https://doi.org/10.1007/s11051-017-3920-9

Sun D, Meng TT, Loong TH, Hwa TJ (2004) Removal of natural organic matter from water using a nano-structured photocatalyst coupled with filtration membrane. Water Sci Technol 49:103–110

Suteu D, Malutan T (2013) industrial cellolignin wastes as adsorbent for removal of Methylene Blue dye from aqueous solutions. Bioresources 8:42–446

Tajer-Kajinebaf V, Sarpoolaky H, Mohammadi T (2014) Sol-gel synthesis of nanostructured titania-silica mesoporous membranes with phot-degradation and physical separation capacities for water purification. Ceram Int 40:1747–1757. https://doi.org/10.1016/j.ceramint.2013.07.074

Tanaka H, Hisanaga T, Harada K (1989) Efficient photocatalytic degradation of chloral hydrate in aqueous semiconductor suspension. J Photochem Photobiol A Chem 48:155–159. https://doi.org/10.1016/1010-6030(89)87098-4

Tayade RJ, Kulkarni RG, Jarsa RV (2006) Transition metal ion impregnated mesoporous TiO_2 for photocatalytic degradation of organic contaminants in water. Ind Eng Chem Res 45:5231–5238. https://doi.org/10.1021/ie051362o

Teekateerawej S, Nishino J, Nosaka Y (2005) Photocatalytic microreactor study using TiO_2-coated porous ceramics. J Appl Electrochem 35:693–697. https://doi.org/10.1007/s10800-005-1623-x

Thejaswini TVL, Prabhakaran D, Maheswari MA (2016) Soft synthesis of Bi Doped and Bi–N co-doped TiO_2 nanocomposites: a comprehensive mechanistic approach towards visible light induced ultra-fast photocatalytic degradation of fabric dye pollutant. J Environ Chem Eng 4:1308–1321. https://doi.org/10.1016/j.jece.2016.01.031

Thejaswini TVL, Prabhakaran D, Maheswari MA (2017) Synthesis of mesoporous worm-like ZrO_2-TiO_2 monoliths and their photocatalytic applications towards organic dye degradation. J Photochem Photobiol A 344:212–222. https://doi.org/10.1016/j.jphotochem.2017.05.015

Tian B, Yang H, Liu X, Xie S, Yu C, Fan J, Tu B, Zhao D (2002) Fast preparation of highly ordered nonsiliceous mesoporous materials via mixed inorganic precursors. Chem Commun 17:1824–1825. https://doi.org/10.1039/B205006D

Tian B, Liu X, Tu B, Yu C, Fan J, Wang L, Xie S, Stucky GD, Zhao D (2003) Self-adjusted synthesis of ordered stable mesoporous minerals by acid-base pairs. Nat Mater 2:159–163. https://doi.org/10.1038/nmat838

Toledo JA, Chavez CA, Jacome MAC, Ramirez FA, Morales YR, Torres GF, Ortiz LFF, Salinas EL, Lozada y Cassou M (2014) Nanostructured titanium oxide materials and its synthesis procedure US patent 8,658,126 B2

Tomaszewska M, Gryta M, Morawski AW (1998) The influence of salt in solutions on hydrochloric acid recovery by membrane distillation. Sep Purif Technol 14:183–188. https://doi.org/10.1016/S1383-5866(98)00073-2

Torres-Martinez CL, Nguyen L, Kho R, Bae W, Bozhilov K, Klimov V, Mehra RK (1999) Biomolecularly capped uniformly sized nanocrystalline materials: glutathione-capped ZnS nanocrystals. Nanotechnology 10:340–354. https://doi.org/10.1088/0957-4484/10/3/319

Tsai CY, Liu CW, Chan YH, Chang TY, Chen BC, His HC (2017) Development of HCl-treated titania nanotube photocatalysts for dye photodegradation and low-concentration elemental mercury removal. Catal Today 297:113–123. https://doi.org/10.1016/j.cattod.2017.04.061

Tsarenko SA, Kochkodan VM, Samsoni-Todorov AO, Goncharuk VV (2006) Removal of humic substances from aqueous solutions with a photocatalytic membrane reactor. Colloid J 68:341–344. https://doi.org/10.1134/S1061933X06030124

Tsuru T, Toyosada T, Yoshioka T, Asaeda M (2001) Photocatalytic reactions in a filtration system through porous titanium dioxide membranes. J Chem Eng Jpn 34:844–847. https://doi.org/10.1252/jcej.34.844

Vaez M, Abdolsamad ZM, Niyaz MM (2012) Decolorization and degradation of acid dye with immobilized titania nanoparticles. Process Saf Environ Prot 90:56–64. https://doi.org/10.1016/j.psep.2011.07.005

Van Gerven T, Mul G, Moulijn J, Stankiewicz A (2007) A review of intensification of photocatalytic processes. Chem Eng Process Process Intensif 46:781–789. https://doi.org/10.1016/j.cep.2007.05.012

Veliscek-Carolan J, Knott R, Hanley T (2015) Effects of precursor solution aging and other parameters on synthesis of ordered mesoporous titania powders. J Phys Chem C 119:7172–7183. https://doi.org/10.1021/jp5127927

Wang F, Zhang K (2012) Physicochemical and photocatalytic activities of self-assembling TiO2 nanoparticles on nanocarbons surface. Curr Appl Phys 12:346–352. https://doi.org/10.1016/j.cap.2011.07.030

Wang WY, Irawan A, Ku Y (2008) Photocatalytic degradation of Acid Red 4 using a titanium dioxide membrane supported on a porous ceramic tube. Water Res 42:4725–4732. https://doi.org/10.1016/j.watres.2008.08.021

Wang C, Shao C, Liu Y, Li X (2009) Water-dichloromethane interface-controlled synthesis of hierarchical rutil TiO_2 superstructures and their photocatalytic properties. Inorg Chem 48:1105–1113. https://doi.org/10.1021/ic8018138

Wang N, Zhang X, Wang Y, Yu W, Chan HLW (2014a) Microfluidic reactors for photocatalytic water purification. Lab Chip 14:1074–1082. https://doi.org/10.1039/C3LC51233A

Wang Y, Yan Z, Wang X (2014b) Photocatalytic degradation of Rhodamine B Dye over novel porous TiO_2-SnO_2 nanocomposites prepared by hydrothermal method. Int J Photoenergy. https://doi.org/10.1155/2014/928519

Wang B, Condi de Godoi F, Sun Z, Zeng Q, Zheng S, Frost RL (2015a) Synthesis, characterization and activity of an immobilized photocatalyst: natural porous diatomite supported titania nanoparticles. J Colloid Interface Sci 438:204–211. https://doi.org/10.1016/j.jcis.2014.09.064

Wang J, Zhao J, Sun L, Wang X (2015b) A review on the applications of photocatalytic materials on textiles. Text Res J 85:1104–1118. https://doi.org/10.1177/0040517514559583

Wang Y, Huijin L, Manling Z, Wubiao D, Bo L (2017) A dual-functional UiO-66/TiO_2 composite for water treatment and CO_2 capture. RSC Adv 7:16232–16237. https://doi.org/10.1039/C7RA00028F

Wegner J, Ceylan S, Kirschning A (2011) Ten key issues in modern flow chemistry. Chem Commun 47:4583–4592. https://doi.org/10.1039/C0CC05060A

Wei W, Yu C, Zhao Q, Qian X, Li G, Wan Y (2014) Synergy effect in photodegradation of contaminants from water using ordered mesoporous carbon-based titania catalyst. Appl Catal B Environ 146:151–161. https://doi.org/10.1016/j.apcatb.2013.04.048

Willmer I, Ranjit K (2002) Photocatalysts for the degradation of organic pollutants. US patent 6,365,001 B1.

Woitalka A, Kuhn S, Jensen KF (2014) Scalability of mass transfer in liquid-liquid flow. Chem Eng Sci 116:1–8. https://doi.org/10.1016/j.ces.2014.04.036

Xi W, Geissen S (2001) Separation of titanium dioxide from photocatalytically treated water by cross-flow microfiltration. Water Res 35:1256–1262. https://doi.org/10.1016/S0043-1354(00)00378-X

Xiong Z, Jizhen M, Wun JN, Waite TD, Zhao XS (2011) Silver-modified mesoporous TiO_2 photocatalyst for water purification. Water Res 45:2095–2103. https://doi.org/10.1016/j.watres.2010.12.019

Xu JC, Shi YL, Huang JE, Wang B, Li HL (2004) Doping metal ions only onto the catalyst surface. J Mol Catal A Chem 219:351–355. https://doi.org/10.1016/j.molcata.2004.05.018

Xu JC, Lu M, Guo XY, Li HL (2005) Zinc ions surface-doped titanium dioxide nanotubes and its photocatalysis activity for degradation of Methyl Orange in water. J Mol Catal A Chem 226:123–127. https://doi.org/10.1016/j.molcata.2004.09.051

Xu S, Ng J, Zhang X, Bai H, Sun DD (2011) Adsorption and photocatalytic degradation of Acid Orange 7 over hydrothermally synthesized mesoporous TiO_2 nanotube. Coll Surf A: Physicochem Eng Aspects 379:169–175. https://doi.org/10.1016/j.colsurfa.2010.11.032

Xu S, Gao Y, Sun X, Yue M, Yue Q, Gao B (2016) Facile one-pot synthesis of carbon incorporated three-dimensional hierarchical TiO_2 nanostructure for highly efficient pollutant removal. RSC Adv 6:101198–101207. https://doi.org/10.1039/c6ra20188a

Yang J, Zhang J, Zhu L, Chen S, Zhang Y, Tang Y, Zhu Y, Li Y (2006) Synthesis of nanotitania embedded in mesoporous SBA-15: characterization and photocatalytic activity. J Hazard Mater B 137:952–958. https://doi.org/10.1016/j.jhazrdmat.2006.03.017

Yang Z, Liu M, Lin C (2016) Photocatalytic activity and scale-up effect in liquid-solid mini-fluidized bed reactor. Chem Eng J 291:254–268. https://doi.org/10.1016/j.cej.2016.01.050

Yao X, Chunbao Z, Ru H, Xiaoheng L (2013) Highly crystalline and silica-embedded titania rhombic shaped nanoparticles with mesoporous structure and its application in photocatalytic degradation of organic compound. Mater Chem Phys 141:705–712. https://doi.org/10.1016/j.matchemphys.2013.05.067

Yi W, Chunyan Y, Peng Y, Faqiang L (2014) A new perspective for effect of S and Cu on the photocatalytic activity of S, Cu-codoped Nano TiO_2 under visible light irradiation. J Sol-Gel Sci Technol 69:386–396. https://doi.org/10.1007/s10971-013-3231-2

Yue J, Luo L, Gonthier Y, Chen G, Yuan Q (2009) An experimental study of air-water Taylor flow and mass transfer inside square microchannels. Chem Eng Sci 64:3697–3708. https://doi.org/10.1016/j.ces.2009.05.026

Zaleska A (2008) Doped-TiO_2: a review. Recent Patents Eng 2:157–164. https://doi.org/10.2174/187221208786306289

Zhang H, Banfield JF (2000) Understanding Polymorphic Phase Transformation Behavior during Growth of Nanocrystalline Aggregates: insights from TiO_2. J Phys Chem B 104:3481–3487. https://doi.org/10.1021/jp000499j

Zhang WF, He YL, Zhang MS, Yin Z, Chen Q (2000) Raman scattering study on anatase TiO_2 nanocrystals. J Phys D Appl Phys 33:912–916. https://doi.org/10.1088/0022-3727/33/8/305

Zhang H, Quan X, Chen S, Zhao H, Zhao Y (2006a) Fabrication of photocatalytic membrane and evaluation its efficiency in removal of organic pollutants from water. Sep Purif Technol 50:147–155. https://doi.org/10.1016/j.seppur.2005.11.018

Zhang H, Quan X, Chen S, Zhao H, Zhao Y (2006b) The removal of sodium dodecylbenzene sulfonate surfactant from water using silica/titania nanorods/nanotubes composite membrane with photocatalytic capability. Appl Surf Sci 252:8598–8604. https://doi.org/10.1016/j.apsusc.2005.11.090

Zhang J, Wu Y, Xing M, Leghari SAK, Sajjad S (2010) Development of modified N doped TiO_2 photocatalyst with metals, nonmetals and metal oxides. Energy Environ Sci 3:715–726. https://doi.org/10.1039/b927575d

Zhang R, Wang Q, Liang J, Li Q, Dai J, Li W (2012) Optical properties of N and transition metal R (R=V, Cr, Mn, Fe, Co, Ni, Cu, and Zn) codoped anatase TiO_2. Physica B 407:2709–2715. https://doi.org/10.1016/j.physb.2012.03.068

Zhang H, Wang JJ, Fan J, Fang Q (2013) Microfluidic chip-based analytical system for rapid screening of photocatalysts. Talanta 116:946–950. https://doi.org/10.1016/j.talanta.2013.08.012

Zhang X, Wang DK, Lopez DRS, Diniz da Costa JC (2014) Fabrication of nanostructured TiO_2 hollow fiber photocatalytic membrane and application for wastewater treatment. Chem Eng J 236:314–322. https://doi.org/10.1016/j.cej.2013.09.059

Zhang J, Wang K, Teixeira AR, Jensen KF, Luo G (2017) Design and scaling up of microchemical systems: a review. Annu Rev Chem Biomol Eng 8:285–305. https://doi.org/10.1146/annurev-chembioeng-060816-101443

Zhao T, Yuan R, Jianping Y, Lianjun W, Wan J, Elzatahry AA, Abdulaziz A, Yonghui D, Dongyuan Z, Luo W (2016) Hierarchical ordered macro/mesoporous titania with a highly interconnected porous structure for efficient photocatalysis. J Mater Chem A 4:16446–16453. https://doi.org/10.1039/C6TA06849A

Zhu H, Jiang R, Fu Y, Guan Y, Yao J, Xiao L, Zeng G (2012) Effective photocatalytic decolorization of Methyl Orange utilizing TiO_2/ZnO/Chitosan nanocomposite films under simulated solar irradiation. Desalination 286:41–48. https://doi.org/10.1016/j.desal.2011.10.036

Zimny K, Ghanbaja J, Carteret C, Stébé MJ, Blin JL (2010) Highly ordered mesoporous titania with semi crystalline framework templated by large or small nonionic surfactants. New J Chem 34:2113–2117. https://doi.org/10.1039/c0nj00488j

Zimny K, Roques-Carmes T, Carteret C, Stébé MJ, Blin JL (2012) Synthesis and photoactivity of ordered mesoporous titania with a semicrystalline framework. J Phys Chem C 116:6585–6594. https://doi.org/10.1021/jp212428k

Znad H, Abbas K, Hena S, Md AR (2018) Synthesis a novel multilamellar mesoporous TiO_2/ZSM-5 for photo-catalytic degradation of Methyl Orange dye in aqueous media. J Environ Chem Eng 6:218–227. https://doi.org/10.1016/j.jece.2017.11.077

Chapter 3
Application of Nanobiosensors for Food Safety Monitoring

H. V. Raghu, Thulasiraman Parkunan, and N. Kumar

Contents

3.1 Introduction 94
3.2 Quality and Safety Issues 96
3.2.1 Chemical Contaminants 96
3.2.2 Microbiological Contaminants 99
3.3 Detection 100
3.3.1 Chemical Contaminants 100
3.3.2 Microbial Contaminants 100
3.4 Biosensors 101
3.5 Nanobiosensors 102
3.5.1 Nanomaterials 103
3.6 Applications of Nanobiosensors 105
3.6.1 Antibiotic Residues 105
3.6.2 Aflatoxin M1 107
3.6.3 Heavy Metals 110
3.6.4 Adulterants 111
3.6.5 Pesticide Residues 112
3.6.6 Microbial Safety and Quality 115
3.6.7 Packaging 117
3.7 Challenges 119
3.8 Conclusion 120
References 120

Abstract Dairying is a major sector for the development of socioeconomic conditions in India. The milk production in India mainly comes from millions of small farmers, and 35% of milk produced in India is pasteurized predominantly by state cooperatives, multinational companies, or government dairy plants. There are many factors that may affect the quality and safety of milk including pathogen contamination and growth, chemical contaminants, and nutrient degradation. FSSAI has

H. V. Raghu (✉) · N. Kumar
Dairy Microbiology Division/National Referral Centre, ICAR-National Dairy Research Institute, Karnal, India

T. Parkunan
Animal Physiology Division, ICAR-National Dairy Research Institute, Karnal, India

N. Dasgupta et al. (eds.), *Environmental Nanotechnology Volume 4*, Environmental Chemistry for a Sustainable World 32, https://doi.org/10.1007/978-3-030-26668-4_3

established a regulatory standard for microbial and non-microbial contaminants in milk and milk products. Therefore, dairy industries or food business operators (FBOs) are needed to follow these standards during the manufacture, marketing, retails, and distribution of various dairy products. Since consumption pattern of dairy foods by the consumers and the demand for quality and safe food is increasing, the industries are under tremendous pressure to meet the requirement in one working day. Hence the need of the hour is to develop novel methods which are real-time, accurate, cost-effective, selective, no interference with other contaminants, etc. Many studies have revealed the various applications of biosensors, including environmental and bioprocess control and quality and safety control of dairy products. At present, the biosensors are applied to a large variety of samples including dairy products, food, environmental samples, etc. Further, these biosensors are integrated into nano-molecules for the development of nanobiosensor in order to improve the performance of the system in both the existing and potential sensing applications. We reviewed that the nanobiosensors are naturally sensors which are made up of nanomaterials and interestingly these are not the specialized sensors which can detect the nanoscale events and happenings. The nanobiosensors are developed by using specific recognition molecules which are integrated on a surface of the nanowire/nanotube for making a specifically sensitive to the target. The Wide spectrum of recognition molecule like single-stranded DNA, an antibody, aptamer, enzymes, protein which shows an affinity toward a target, or a protein that specifically interact with another biological molecule. These nanobiosensors are having wide application in the field of microbial quality and safety monitoring in dairy industry including antibiotics, pesticides, heavy metals, aflatoxin, and adulterants, microbial contamination including foodborne pathogens, *and* packaging material integration with nanobiosensor as an indicator of quality and safety of the products. Furthermore, the development of lab-on-a-chip technique by integration of analyte onto a microfluidic chip to develop an electromechanical system would provide new avenue field of nanobiosensor. However, there are still several challenges to overcome, which limit the progress of technology transfer and commercialization, mainly related to the difficulties in the integration of all the components into a single portable platform. Yet, there is still a long road ahead for this emerging technology to be fully adapted to a filed application.

Keywords Nanobiosensor · Food safety · Detection · Chemical and microbial

3.1 Introduction

Dairying is one of the finest instrumentals for the development of socioeconomic condition in India. In India, there are 400 million milk-producing animals (FAOSTAT, 2005) providing 146.3 million tons of milk per year as per economic survey in 2014–2015. Among the total milk productions in India, around 54.5% comes from Buffalo followed by 41% from cow and remaining 4.5% from goats

(Hemme et al. 2003). The milk production in India mainly comes from millions of small farmers, dispersed throughout the rural areas, and these farmers are holding average herd size of one or two milch animals which comprises of cow and/or buffaloes. About 35% of milk produced in India is pasteurized predominantly by state cooperatives, multinational companies, or government dairy plants (India in Business 2008). There are many factors that may affect the quality and safety of milk including pathogen contamination and growth, chemical contaminants, and nutrient degradation. Among them, biological hazards are of major concerned in dairy sector due to the fact that milk is an ideal medium for the growth and activity of bacterial pathogens including zoonotic pathogens such as *Salmonella*, *Escherichia coli* O157: H7, *Listeria monocytogenes*, *Staphylococcus aureus*, *Campylobacter jejuni*, *Yersinia enterocolitica*, *Bacillus cereus*, *Clostridium botulinum*, *Mycobacterium bovis*, *Brucella abortus*, and *Brucella melitensis*.

Chemical hazards can be unintentionally introduced into milk and milk products, making them unsafe and unsuitable for consumption. One possible way of getting chemical contamination is by milking the animals which consume feed and/or water that contain chemicals. Chemical contaminants in milk comprise chemical hazards that may introduce during milk production, dairy processing, or packaging. Antibiotic residues, aflatoxins, pesticides, heavy metals, and radionuclides are some chemical contaminants that can come into animal foodstuffs and secreted as residues in milk. Among these, the most combative residues that occur in milk are antimicrobial drugs that may cause risks to the consumers (Khiniki 2006).

In the year 2008, the Government of India has established an authority known as FSSAI (Food Safety and Standards Authority of India) for providing quality and safe food to the consumer. Accordingly, FSSAI has developed a regulatory standard for microbial and non-microbial contaminants in milk and milk products. Indian dairy industries or food business operators (FBOs) are needed to follow these standards during the manufacture, marketing, retails, and distribution of various dairy products. In recent years, consumer preferences and awareness's regarding quality and safety issues in dairy products are also increasing. Therefore, industries are under tremendous pressure to provide these dairy products, within a period of 24 h. or one working day with utmost care regarding quality and safety. Hence the need of the hour is to develop novel methods which are real-time, accurate, cost-effective, selective, no interference with other contaminants, etc. Many studies revealed the various applications of biosensors, including environmental and bioprocess control and quality and safety control of dairy products. At present, the biosensors are applied to a large variety of samples including dairy products, food, environmental samples, etc. Further, these biosensors are integrated into nano-molecules for the development of nanobiosensor in order to improve the performance of the system in both the existing and potential sensing applications. Therefore in this chapter, we have been extensively discussing the applications of nanobiosensors in the dairy industry for the monitoring of dairy processing, shelf-life extension, quality and safety of dairy products, etc.

3.2 Quality and Safety Issues

3.2.1 Chemical Contaminants

Milk is a perishable food commodity having rich source of readily available nutrient including lactose, fat, proteins, mineral, vitamins, etc. If milk is not handled properly, it may lose its natural quality during production, processing, and distribution (Awasthi et al. 2012). The major contaminants that come across in milk and milk products during milk production, dairy processing, or packaging are veterinary drugs/drug residues, heavy metals, radionuclides, mycotoxins, pesticides, etc., which may enter through water, animal feed, and other environmental sources.

Antibiotic Residues

The most combative residues that arise in milk are antibiotic residues that may have both technological and public health importance. Many of the antibiotic residues were used in the treatment of dairy cattle which involves intra-mammary infusion as well as the parenteral route of administering drugs to control mastitis, metritis, etc. In addition, some drugs are administered to control endo- and ectoparasites and several illnesses and to boost milk production (Korsrud et al. 1998). In animal husbandry, antibiotics are extensively used for therapeutics, prophylaxis, and metaphylaxis and as a growth promoter (Woolhouse et al. 2015; Rushton et al. 2014). Antibiotics which are commonly used as feed additives include tetracycline, nitrofurans, and sulfonamides (DeVries 1997). Many biologically active metabolites of antimicrobial in milk and dairy products could result in anaphylaxis and allergic shock in sensitized individuals (Gustafson 1991). The most commonly used antimicrobials in dairy cattle include β-lactams, tetracyclines, amino glycosides, macrolides, and sulfonamides (Mitchell et al. 1998). These drugs are also administered to animals through different routes such as parenteral (intravenous, intramuscular, subcutaneous, intramammary, intrauterine, etc.), oral (in the food/water), topical (on the skin), inhalation, and rectal. Theoretically, in lactating cow administration of drugs through all of the above routes may lead to an appearance of residues in milk and dairy products (Mitchell et al. 1998). These measurable levels of the antibiotic are usually detectable in the milk for a few days after the last administration of the drug (EU/Codex Alimentarius commission). Regulations have recommended the maximum residues limits (MRLs) for some/many drugs in milk (European Commission 1997). Primary concerns associated with antimicrobial residues in milk and dairy products are expressed by the dairy processors who found that contaminated milk inhibits the starter cultures used in the production of cheeses, yogurt, and other fermented dairy products as well as it influences the results of the dye reduction tests used for milk quality at the time of reception of raw milk (Jensen 1995). The main apprehension of veterinary drug residues is the possible transmission of antibiotic resistance gene-containing bacteria from milk and dairy products to human population (Hao et al.

2014). On the other hand, plants and agricultural products serve as a reservoir for many microbes which are nonpathogenic to plants whereas pathogenic to animals and humans (Schikora et al. 2012; Gu et al. 2011). Antibiotics can cause some disruptions like aplasia of the bone marrow (e.g., chloramphenicol) (Mitchell et al. 1998) and carcinogen (e.g., oxytetracycline and furazolidone). Therefore, the use of antibiotics in livestock sector may accelerate the development of antibiotic-resistant microbial pathogens, leading to potentially muddling treatment for both animals and humans diseases.

Pesticides

Pesticides are widely used in agriculture to protect the crop from insects/pests, but, through water, forages, and the environment, they become a part of the milk causing contamination and thus confer a health risk (Bo et al. 2011). Chlorinated pesticides, organophosphate, carbaryl, and related compounds such as DDT, endosulfan, polychlorinated biphenyls (PCBs), and dioxins are some of the pesticides that can enter milk and dairy products (Mukerjee 1998). On ingestion, around 20% of an ingested chlorinated hydrocarbon is excreted in milk, adhering to milk fat and butter (Hubbert et al. 1996). DDT is a lipophilic compound; hence it can accumulate in fatty tissues and can transfer into milk and dairy products. Pesticides, such as hexachlorocyclohexane (HCHs), can cause damage to central nervous system, reproductive system, and endocrine system (Alvarado and Perez 1998). Universally, all organochlorine pesticides are characterized by their high lipophilicity and long elimination half-lives. Disruption of normal endocrine-regulated functions by these chemicals represents an important consideration in risk assessment (Mukerjee 1998). In view of the potential health hazards, there are around 13 pesticides which are restricted for use in India since 1997 such as DDT, lindane, methyl parathion, endosulfan, monocrotophos, aluminum phosphate, dieldrin, etc. Residues of such compounds may persist in the environment and cause contamination through the food chain (Wong and Lee 1997).

Aflatoxin M1

Aflatoxins are a group of highly toxic secondary metabolic products of molds such as *Aspergillus flavus and Aspergillus parasiticus*, which infect the cereals and oil seeds, the major constituents of dairy cattle feed, during their pre- and postharvest management. Molds occur in these agro-products, during the growth of plants, maturity, harvesting, and processing of grains. Their presence is influenced by various factors like temperature, relative humidity, oxygen availability, and damaged or broken grain kernels (Lanyasunya et al. 2005). Aflatoxin M1 (AFM1) may be found in the milk of animals that are fed with aflatoxin B1 (AFB1)-contaminated feed (Kangethe and Langa 2009). The concentration of AFM1 in milk is entirely dependent on the presence of the precursor AFB1 in the

ration of dairy cattle, and it can numerically express as a feed to milk ratio. The AFM1 in milk is a carcinogenic metabolite of aflatoxin B1. The generation of AFM1 by the metabolites of AFB1 occurs in the liver and its secrets into milk in the mammary gland of dairy cows (Khiniki 2006) may lead to increase in the risk of liver cancer. The International Agency for Research on Cancer (IARC) of WHO included AFB1 as primary and AFM1 as secondary groups of carcinogenic compounds. Heat treatments like pasteurization, boiling, and UHT treatment were not effective in lowering the development of AFM1 (Khiniki 2006). These findings indicated that AFM1 with altered levels could be available in dairy products made from unclean milk. Consequently, this subject is a serious problem for the public health for all the age groups, including infants and children who consume the milk-containing products worldwide. For this reason, milk and dairy products have to be evaluated uninterruptedly for AFM1 contamination at least twice a year. Beside this, it is important to have low levels of AFM1 in the feeds of dairy animals, and in order to achieve this purpose, feeds of dairy cows should be kept away from contamination as much as possible (Bakirci 2001; Khiniki 2006). Due to the potent carcinogenicity of aflatoxin, most countries regulate the presence of aflatoxin in both feed and milk. The tolerance level for AFM1 in milk varies among countries from 0.05 μg kg^{-1} in Europe to 0.5 μg kg^{-1} in the USA (Saitanu 1997; WHO 2002). In India, FSSAI has also established a standard for aflatoxin M1 (0.5 ppb) in milk.

Heavy Metals

Heavy metals enter the human and animal body mainly through inhalation and ingestion. Heavy metals produce toxic effects by replacing essential metal ions existing in the chelates present in the body. The intake via ingestion depends upon food habits (Aytenfsu et al. 2016). The metals, namely, copper (Cu) and zinc (Zn), are essential micronutrients and have a variety of biochemical functions in all living organisms (Licata et al. 2004). While Cu and Zn are essential, they can be toxic when taken in excess; both toxicity and necessity vary from element to element. It is well established that lead (Pb) and cadmium (Cd) are toxic for human especially children who are more sensitive to these metals than adults. Milk is the fundamental food for infants, and the daily intake of the heavy metals Pb, Cd, Cu, and Zn can be determined by different age groups of infants through different milks and baby foods. Heavy metals can enter to milk and dairy products and affect the health of people who have consumed contaminate milk and dairy products. The health implications from heavy metals lead to kidney damage, cardiovascular diseases, and induction of hypertension, growth inhibition, and interference in hemoglobin synthesis and irreversible changes in the brain and nerve cells, and also some of these residues are known to be carcinogenic in nature. The pulmonary and nervous systems and skins are the main target organs of arsenic contamination. Cadmium is associated with kidney damage, and lead is considered to be associated with learning deficits in children. Copper and zinc are essential micronutrients but in higher amount may influence metallic taste to the product resulting unacceptability

of the product (Raghunath et al. 1997). With increasing environmental pollution, a heavy metal exposure assessment study is necessary (Ikeda et al. 1996, Raghunath et al. 1997)

3.2.2 Microbiological Contaminants

The presence of foodborne pathogens in milk and milk products is due to direct contact with contaminated sources in the dairy farm environment, infected animals, and improper personnel hygiene (Zeinhom and Abdel-Latef 2014). The microbiological quality of milk and dairy products is influenced by the initial flora of raw milk, the processing conditions, and post-heat treatment contamination (Rajagopal et al. 2005). Today's context, food spoilage is a big economic problem worldwide. Undesirable microbes in the milk can cause spoilage of dairy products which include Gram-negative psychrotrophs, coliforms, lactic acid bacteria, yeasts, and molds. In addition, various bacteria of public health concern such as *Salmonella* spp., *L. monocytogenes*, *C. jejuni*, *Y. enterocolitica*, pathogenic strains of *E. coli*, and enterotoxigenic strains of *S. aureus* may also be found in milk and dairy products. In industrialized countries like India, the percentage of the population suffering from foodborne diseases each year has been reported to be up to 30%. Though there are various foodborne pathogens that have been identified for foodborne illness, *Campylobacter*, *Salmonella*, *L. monocytogenes*, *and E. coli* O157:H7 have been generally found to be responsible for the majority of foodborne outbreaks (Alocilja and Stephen 2003; Chemburu et al. 2005). In the last two decades, other infectious agents have been either newly defined or newly concomitant with foodborne transmission. *L. monocytogenes*, *E. coli* O157:H7, *C. jejuni*, *Staphylococcus intermedia*, *Enterobacter sakazakii*, and *Salmonella enteritidis* are examples of newly described pathogens that often are foodborne. The most dangerous among them are enterohemorrhagic *E. coli* strains, especially serotype O157:H7. *E. coli* O157:H7 has become a pathogen of major concern in dairy industries, and to the public, because of its ability to cause severe illness, in particular hemorrhagic colitis, hemolytic uremic syndrome, and thrombotic thrombocytopenic purpura (Picozzi et al. 2005 and Reuben et al. 2013). Foodborne salmonellosis has been recognized due to consumption of raw or improperly pasteurized milk and milk products (Karshima et al. 2013). Recently CDC has reported an incidence of *L. monocytogenes* in pasteurized milk, Mexican cheeses, and pasteurized cheeses (FDA 2010; CDC 2012/2013/2014; CDC NORS 2012), *Salmonella braenderup* (OHA 2010) and *Salmonella java* in pasteurized cheddar cheese, *Salmonella Montevideo* in pasteurized shredded cheeses, *Salmonella newport* in pasteurized milk, *Salmonella typhimurium* in pasteurized milk, *Campylobacter jejuni* in pasteurized milk and cheese curd, and *Staphylococcus aureus* in powdered milk and pasteurized cheese (CDC NORS 2012).

3.3 Detection

3.3.1 Chemical Contaminants

The accessibility of rapid and sensitive approaches to determine chemical contaminants in dairy products is critical in food safety control laboratories. In countries like the USA, there is a practice to analyze individual farm milk supply for chemical contaminants before allowing to pool with the bulk milk (Kumar et al. 2012). To detect contaminants in milk, different methods have been developed which include screening methods and chromatographic techniques to detect as many contaminants as possible. The screening methods are based on the susceptibility of bacteria to different contaminants including antibiotics (Mitchell et al. 2002). They are very cost-effective, and in contrast to, for example, immunological or receptor-based tests, they have the potential to cover the entire spectrum within one test. However, these methods have their drawbacks as they do not enable specific identification that limits their use. They are highly sensitive to specific groups of contaminants but evidently less sensitive (Navratilova´ 2008). Quantitative confirmatory methods such as high-performance liquid chromatography (HPLC) (Zhou et al. 2009), gas chromatography–mass spectrometry (GC–MS) (Azzouz et al. 2010, 2011), thin-layer chromatography (TLC) (Grzelak et al. 2009), and mass spectrometry (MS) (Blascoa et al. 2009) have been commonly used for the detection of contaminants having safety concern. However, again each method has one or more limitations in terms of precision, accuracy, sensitivity, infrastructural requirement, and ease of method (Kumar et al. 2012).

3.3.2 Microbial Contaminants

Presently, the conventional testing methods that are considered as gold standard tests are among the first choice of the quality control laboratory. These conventional methods generally involve isolation and confirmation procedures for the detection of the microbes and other platform tests that are carried to determine non-microbial contaminants of the milk which are often time-consuming and laborious to perform. The other associated problem with such tests is that the product needs to be hold till the results come. This adds up to working capital of the industry because the holding infrastructure has to be created. Moreover, the perish ability of the milk and milk products further adds up to the problem of storage of these products. In such circumstances the milk and milk products are often pushed into the market without screening. The only thing the industry can do is banning the product and recalling the product. To overcome this unmanageable situation, dairy industry is looking for alternatives to conventional methods. The methods that are rapid, cost-effective, and easy to perform and significantly validated with approved standard methods are the need of the hour (Thakur et al. 2013).

3.4 Biosensors

The biosensor can be defined as "a sensing device or a measurement system designed specifically for the estimation of a material using the biological interactions and then assessing these interactions into a readable form with the help of a transduction and electro-mechanical interpretation" (Malik et al. 2013). In general, three different assay formats are used in biosensors – the direct and the indirect (competitive or noncompetitive) assay. In the case of the direct assay, the analyte is bound by its biorecognition element, which is detected directly (Vasilescu et al. 2016). This can be an antigen binding to its antibody, a hormone binding to a receptor, or a substrate reacting with its enzyme and producing a product (Eijkelkamp et al. 2009). The detection of these binding events is limited to the event itself and can be changed in mass, refractive index, impedance, pH, etc. (Griffin et al. 2014). In contrast, in indirect format, an additional reaction has to occur in order to detect the binding of analyte and biorecognition element. This additional reaction can either be competitive or noncompetitive. In both cases, a label is typically used for subsequent detection and quantification (Ramírez et al. 2009). The detection scheme is much less limited than in the case of the direct approach and depends on the nature of the label. This label can be optical, electrochemical, or mass related and thus permits the use of any transduction principle with indirect assay formats in contrast to the constraints given by the direct assay, which is limited by the nature of the analyte itself (Baeumner 2003). Based on the publication in reputed science journals, different methods which are applied in detection of many foodborne bacterial pathogens were compared by Lazcka et al. (2007) as shown in Fig. 3.1. The most popular methods are, by far, those based on culture and colony counting methods (Leoni and Legnani 2001) and the polymerase chain reaction, PCR (Bej et al. 1991). This can be explained on the grounds of selectivity and reliability of both techniques. Culture and colony counting methods are much more time-consuming than PCR methods, but both provide conclusive and unambiguous results. On the other hand, recent advances in PCR technology, namely, real-time PCR (Levi et al. 2003), now enable obtaining results in a few hours.

Biosensor technology comes with promises of equally reliable results in much smaller times, which is perhaps why they are currently drawing a lot of interest. However, there is still much work to do before biosensors become a real alternative. Figure 3.1 suggests that biosensor technology may soon move ahead of traditional ELISA-based methods and their potential market (Alocilja and Stephen 2003) is very encouraging too. Many biosensors rely on either specific antibodies or DNA as biomolecules to provide specificity.

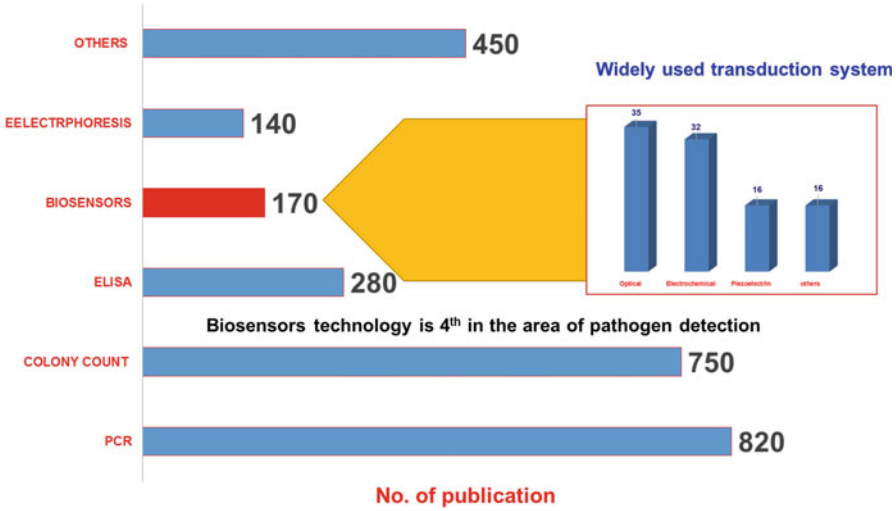

Fig. 3.1 Number of articles using different techniques to detect and identify pathogenic bacteria. Time series of the number of works published on detection of pathogen bacteria over the last 20 years. (Source: ISI web of science, Adapted from Lazcka et al. 2007)

3.5 Nanobiosensors

Nanotechnology is a new branch of science that deals with the generation and alteration of materials to nanosize (10^{-9} m) (Sagadevan and Periasamy 2014). Nanobiosensor is basically the sensors which are made up of nanomaterials, and interestingly these are not the specialized sensors which can detect the nanoscale events and happenings (Malik et al. 2013). A specific recognition group can be used to coat the surface of the nanowire/nanotube, making the device specifically sensitive only to a particular target. This recognition group could be a single-stranded DNA (capable of recognizing its complementary strand), an antibody (that recognizes a particular antigen), an aptamer that shows an affinity for a unique target, or a protein that specifically interacts with another biological molecule. The presence of this recognition group on the nanowire surface gives to the device high specificity and exclusivity toward its target (Thompsons Research Groups) (Fig. 3.2).

Nanomaterials are intended to be used in making biosensors which are going to drive a significant difference in the nanobiosensors technology. The physical properties of nan-materials used during the preparation of sensor will make them a very special due to their constituent atoms located at or near their surface increases the surface area for the interaction of biomolecule with the target material. These nanomaterials having all the vital physicochemical properties (Gatoo et al. 2014) such as size, surface area, surface chemistry, surface roughness, the dispersion medium, and ability to agglomerate will play a vital role in nanobiosensor. Metallic and inorganic nanomaterial having nanoscale in size may demonstrate new research avenue for scientists and researchers working the field of biosensors. Nanomaterials

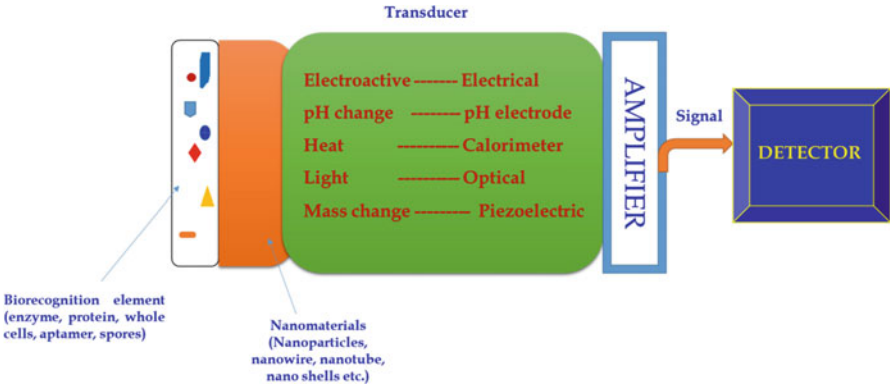

Fig. 3.2 Nanobiosensors

or nanoparticles reveal unique properties in terms of particle aggregation; photoemission; electrical, magnetic, and luminescent activity, heat conductivity; and catalytic activity (Rai et al. 2012). These properties have recently been applied in different biological studies like foodborne pathogen detection, biomolecule detection, sample separation, purification and concentration, signal transduction, and amplification (sensors) (Jain 2007). These nanoparticles further enhance the detection sensitivity of microbial monitoring, degradation, and recovery efficiency of chemicals (Urban and Meas 2008).

3.5.1 Nanomaterials

A nanosized material having at least one external dimension in the size ranges from 1 to 100 nanometers. Nanoscale materials are defined as a set of substances where at least one dimension is less than approximately 100 nanometers. Nanomaterials (NMs) are of interest because at this scale unique optical, magnetic, electrical, and other properties emerge (Alagarasi 2011). NMs include nanoparticles (NPs), nanostructured materials and ultrafine particles, and their agglomerates and aggregates. According to US EPA (USEPA 2007), there are four main types of nanomaterials including carbon-based, metal-based, dendrimers and composites.

Carbon-based nanomaterials are composed mostly of carbon, most commonly taking the form of hollow spheres, ellipsoids, or tubes. Spherical and ellipsoidal carbon nanomaterials are referred to as fullerenes, while cylindrical ones are called nanotubes (Roy and Jayanta 2015). These particles have many potential applications, including improved films and coatings, stronger and lighter materials, and applications in electronics. Metal-based nanomaterials include quantum dots, nanogold, nanosilver, and metal oxides, such as titanium dioxide (Ranganathan 2015). A quantum dot is a closely packed semiconductor crystal comprised of hundreds or thousands of atoms and whose size is on the order of a few nanometers to a few

hundred nanometers. Changing the size of quantum dots changes their optical properties. Dendrimers are nanosized polymers built from branched units. The surface of a dendrimer has numerous chain ends, which can be tailored to perform specific chemical functions. This property could also be useful for catalysis. Also, because three-dimensional dendrimers contain interior cavities into which other molecules could be placed, they may be useful for drug delivery. Composites combine the nanoparticles with other nanoparticles or with larger, bulk-type materials. Nanoparticles, such as nanosized clays, are already being added to products ranging from auto parts to packaging materials, to enhance mechanical, thermal, barrier, and flame-retardant properties.

Physicochemical Properties

The physicochemical properties of these nanomaterials are electrical, optical, catalytic, magnetic, mechanical, thermal, or imaging features that are highly desirable for applications in commercial, medical, food science, food safety, military, and environmental sectors.

The main parameters of interest with respect to nanoparticle safety are:

1. Physical properties
   (a) Size, shape, specific surface area, aspect ratio
   (b) Agglomeration/aggregation state
   (c) Size distribution
   (d) Surface morphology/topography
   (e) Structure, including crystallinity and defect structure
   (f) Solubility
2. Chemical properties
   (a) Structural formula/molecular structure
   (b) Composition of nanomaterial (including degree of purity, known impurities or additives)
   (c) Phase identity
   (d) Surface chemistry (composition, charge, tension, reactive sites, physical structure, photocatalytic properties, zeta potential)
   (e) Hydrophilicity/lipophilicity

The principal parameters of nanoparticles are their shape (including aspect ratios), size, and the morphological substructure of the substance (Williams 2014). Nanoparticles are presented as an aerosol (mostly solid or liquid phase in air), a suspension (mostly solid in liquids) or an emulsion (two liquid phases) (Scientific Committee on Emerging and Newly-Identified Health Risks (Sutariya and Pathak 2014; SCENIHR 2006). In the presence of chemical agents (surfactants), the surface and interfacial properties may be modified. Indirectly such agents can stabilize against coagulation or aggregation by conserving particle charge and by modifying

the outmost layer of the particle. Depending on the growth history and the lifetime of a nanoparticle, very complex compositions, possibly with complex mixtures of adsorbates, have to be expected. In the typical history of a combustion nanoparticle, for example, many different agents are prone to condensation on the particle, while they cool down and are exposed to different ambient atmospheres (Singh et al. 2011). Complex surface chemical processes are to be expected and have been identified only for a small number of particulate model systems. At the nanoparticle–liquid interface, polyelectrolytes have been utilized to modify surface properties and the interactions between particles and their environment. They have been used in a wide range of technologies, including adhesion, lubrication, stabilization, and controlled flocculation of colloidal dispersions (Liufu et al. 2004).

3.6 Applications of Nanobiosensors

3.6.1 Antibiotic Residues

Nanobiosensors for the detection of antibiotic residues in milk by different biomolecules such as antibody, aptamer, enzymes, etc. are in conjugation with gold, silver, or iron nanoparticles based on their change in SPR properties (LSPR, localized surface plasmon resonance) reinforcing the signal by means of electronic coupling of surface and the NP plasmons (Lyon et al. 1998). A gold nanoparticle label is an ideal one in biotechnological systems due to its inherent advantages, such as easy preparation, good biocompatibility, and so on (Sapsford et al. 2013). As far back as the 1970s, colloidal gold particles were used as an immune-staining and contrast agent for electron microscopy (Faulk and Taylor 1971). Nowadays, gold nanoparticles have been extensively employed as the labels for different biological receptors, e.g., enzyme, DNA, antigen/antibody, and other biomolecules (Ghosh et al. 2008; Ambrosi et al. 2007). More significantly, gold nanoparticles can be also used as catalysts in a number of chemical reactions. Yang and Tang (Tang et al. 2011) designed two types of ultrasensitive electrochemical immunoassay using nanometer gold labels as catalysts. The catalytic properties mainly derived from the catalytic reduction of 4-nitrophenol by gold nano-labels (Zhang et al. 2013). Based on the characteristic of surface plasmon resonance absorption of gold nanoparticles, Zhu et al. (2011) constructed an optical sensor for detection of antibiotics by using UV–vis absorbance spectrometry.

Natan's group was one of the first research teams demonstrating the potential of nano-gold probes for signal enhancement. They employed *secondary nano-gold probes* (anti-IgG coupled to AuNP) to detect human IgG in a sandwich format (Lyon et al. 1998). Regarding low molecular weight analytes, few papers report signal enhancement using 10–40 nm *secondary nano-gold probes*. The enhancement allowed reducing the concentration of primary antibody (i.e., from 10 to 1 μg mL^{-1}) and improved the detectability (i.e., LOD from 0.1 to 0.007 μg L^{-1} for benzaldehyde) (Yuan et al. 2007, 2008; Mitchell and Lowe 2009). Jiang et al.

conjugated the primary antibody to AuNP allowing to improve the LOD of estriol from 0.2 to 0.03 μg L^{-1}, but no data is shown comparing the performance of this strategy in respect to the use of *secondary gold probes.*

Frasconi et al. (2010) functionalized the Au nanoparticles (NPs) with thioaniline electropolymerizable groups and (mercapto-phenyl) boronic acid wherein antibiotic substrates neomycin (NE), kanamycin (KA), and streptomycin (ST) include vicinal diol functionalities which were specifically bound to the boronic acid ligands leading to electropolymerization of the functionalized Au NPs onto Au surfaces yields bisaniline-cross-linked Au-NP composites that, after removal of the ligated antibiotics, provide molecularly imprinted matrixes which reveal high sensitivities toward the sensing of the imprinted antibiotic analytes (detection limits for analyzing NE, KA, and ST correspond to 2.00 ± 0.21 pM, 1.00 ± 0.10 pM, and 200 ± 30 fM, respectively).

Another researcher has discovered a selective kanamycin-binding single-strand DNA (ssDNA) aptamer (TGGGGGTTGAGGCTAAGCCGA) through in vitro selection using affinity chromatography with kanamycin-immobilized sepharose beads (Song et al. 2011). The SS DNA Aptamer linked with gold nanoparticle for the selective detection of kanamycin and its derivatives such as kanamycin B and tobramycin with a detection limit of 25 nM by visual observation or by colorimetric method. A colorimetric and fluorescence quenching aptasensors for detection of streptomycin in milk based on double-stranded DNA and gold nanoparticles have been attempted by Emrani et al. (2016). The aptamer/FAM-labeled complementary dsDNA strand is stable, resulting in the aggregation of AuNPs by salt and an obvious color change from red to blue and strong emission of fluorescence in the absence of streptomycin (Emrani et al. 2016). In the presence of streptomycin, aptamer binds to its target, and FAM-labeled complementary strand adsorbs on the surface of AuNPs. Therefore, the well-dispersed AuNPs continue to be stable against salt-induced aggregation with a wine-red color, and the fluorescence of FAM-labeled complimentary strand is efficiently quenched by AuNPs. The colorimetric and fluorescence quenching aptasensors showed excellent selectivity toward streptomycin with the limit of detections as low as 73.1 and 47.6 nM, respectively.

Other efforts by Font et al. (2008) have developed two direct enzyme-linked immunosorbent assays (ELISAs) which have been developed for detection of sulfonamide antibiotic residues in milk samples using magnetic nanoparticles (MNP) for target capture/enrichment (Ab-MNP-ELISA) and further assay performed using microtiter plates. In this assay, selective polyclonal antibodies were raised against 5-[6-(4-amino-benzenesulfonylamino)-pyridin-3-yl]-2-methyl-pentanoic acid (SA1), used in combination with an enzyme tracer prepared with the same hapten, so has to achieve a limit of detection (LOD) lower than 0.5 μg L^{-1} by both ELISA formats. Sulfapyridine, sulfamethoxypyridazine, sulfathiazole, and sulfachloropyridazine are detected below the maximum residue limits established by the European Union for these antibiotics in milk (100 μg L^{-1}). Silver nanoparticle that enhanced the fluorescence of europium (III) for detection of tetracycline in milk has been investigated by Tan and Chen (2012) based on the coordination of Tc with europium functionalized on the surface of AgNPs to become EuTc complex for the

emission of strong fluorescence due to an intramolecular energy transfer from Tc to Eu3+. The fluorescence intensity of this probe displayed a good linear response to Tc concentrations in the range of 10 nM to 10 μM with a detection limit of 4 nM and was applied successfully to determine the levels of Tc in milk with a high selectivity.

3.6.2 Aflatoxin M1

Aflatoxins are secondary metabolites when ingested by animals, and higher vertebrates cause diverse health effects and disease called aflatoxicosis (Adegoke and Puleng 2013). Aflatoxin-contaminated/aflatoxin-containing agricultural and dairy products meet great economic losses (Cleveland et al. 2003). Studies by various researchers have shown that in the storage processes or cultivation of grains showed different levels of contamination, especially with aflatoxin B1 (AFB1) (Caldas et al. 2002). AFB1 is a powerful genotoxic carcinogen for humans and many animal species, including rodents, nonhuman primates, and fish (EC 2012). The main target of this carcinogen is the liver, although tumors may also develop in other organs, such as the lungs, kidney, and colon (Gelderblom et al. 1996). The current maximum residue levels for aflatoxins set by the European community (EC) are 20 μg/kg for AFB1 and 40 μg/kg for total aflatoxins in groundnuts, nuts, dried fruits, and cereals for direct human consumption (EC 2006). Aflatoxin M1 (AFM1), as the hydroxylated metabolite of aflatoxin B1 (AFB1), is usually present in the animal milk contaminated by AFB1. Because of their stronger toxic effects than AFB1 on public health, many governments have provided maximum acceptable limits for residual AFM1 in foodstuffs, especially in milk products (Kadir and Tothill 2010). For example, according to FSSAI standards, aflatoxin M1 content cannot exceed 0.5 μg/kg in milk, whereas the European–USA has higher regulations of 50 ng/kg. Thus, the food administration agencies in almost all countries have dedicated much effort to developing sensitive analytical methods for monitoring ultra-trace levels of AFM1 (<0.05 μg/kg) in foods (Hansmann et al. 2009). Current strategies for ultrasensitive detection of AFM1 are based mainly on thin-layer chromatography (TLC), high-performance liquid chromatography (HPLC), or UV light spectroscopy after extraction and clean-up procedures (Amine et al. 2003). These methods are adequately sensitive and accurate; however, they often require sophisticated, expensive, and heavy instruments that may not be available in laboratories with fewer resources; these methods are especially not fit for mass screening (Gan et al. 2013). The Zhang group developed a rapid method for detection of aflatoxin M1 by coupling superparamagnetic beads with gold labels (Zhang et al. 2013). The recent development of nanobiosensors has roused their application also to aflatoxin analysis. Many examples are reported, like DNA biosensor (Tombelli et al. 2009), electrochemical immune sensor (Linting et al. 2012), an electrochemical sensor (Liu et al. 2006), and the fluorometric biosensor (Carlson et al. 2000). Advantages of nanobiosensors techniques are a reduction of extraction, clean-up analytical steps, and global time of analysis (1 min or only a few seconds), the possibility of online

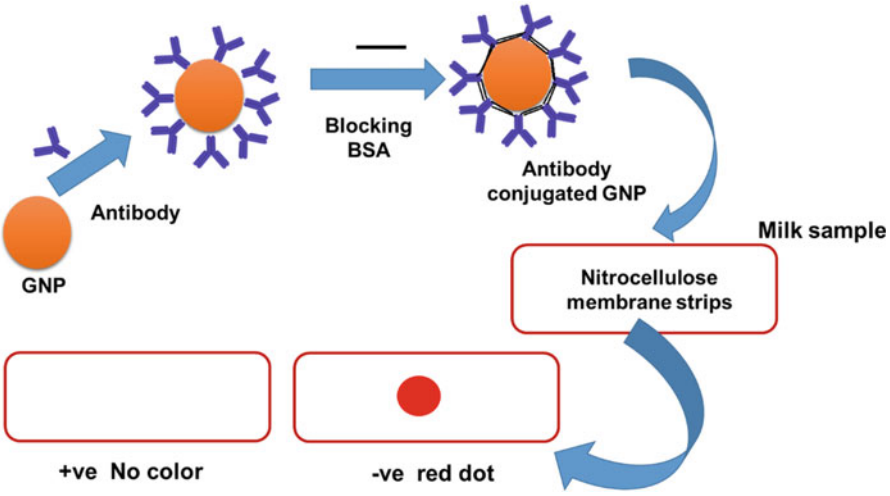

Fig. 3.3 DIGFA sensor for detection of AFB1 in feed

automated analysis, low cost, and no requirement of skilled personnel. On the other side, enhanced sensitivity and their improved stability allow long-term use. Because of the ease of use of these devices, many commercial systems continue to develop not only for aflatoxins but also for all mycotoxins (Eldin et al. 2014).

At the regional center for Food and Feed, ARC, Egypt, by Eldin and coworkers, a dot-immunogold chromatography flow-through assay (DIGFA) was developed for detection of AFB1 in food and feed samples using colloidal gold nanoparticles (AuNPs). AuNPs are being extensively used in various applications due to its stability and controlled geometrical, optical, and surface chemical properties. AuNPs-Anti AFB1 conjugates were designed by physical conjugation wherein AuNPs can be used as a probe for AFB1 detection with acceptable sensitivity and specificity compared to HPLC technique. The FAB1 present in feed and food samples is binding on AuNPs-Anti AFB1 conjugates DIGFA sensor (Fig. 3.3) Constructed DIGFA sensor detects AFB1 with high sensitivity (5 ng/mL) which is validated by HPLC. An assay is rapid (test completion time is 2 min) and reproducible and doesn't require any equipment.

Dynamic light scattering (DLS) coupled with superparamagnetic beads for the detection of AFM1 in milk using gold nanoparticle probe has been developed (Zhang et al. 2013). The nanoprobes were synthesized by the conjugate of AFM and bovine serum albumin (AFM-BSA), BSA, and gold nanoparticles. Magnetic beads-based immunosorbent assay (MBISA) is used to measure the concentration of AFM1 by through competition between AFM1 and nanoprobes. DLS was used to determine the concentration of unattached nanoprobes that was positively proportional to the concentration of AFM in the sample. Compared to conventional ELISA, MBISA could effectively reduce the detection time to 15 min in buffer solution and

completely eliminate the color development step, thus simplifying the analysis of AFM. A linear relationship was observed between the inhibition values and the concentrations of AFM in both buffer solution (0–1000 $ng \cdot L^{-1}$) and spiked milk samples (0–400 $ng \cdot L^{-1}$). The limit of detection was found to be 37.7 $ng \cdot L^{-1}$ for AFM in buffer solution and 27.5 $ng \cdot L^{-1}$ in milk samples.

An ultrasensitive electro-chemiluminescent immunoassay (ECLIA) for aflatoxins M1 (AFM1) in milk using magnetic Fe_3O_4-graphene oxides (Fe-GO) as the absorbent and antibody-labeled cadmium telluride quantum dots (CdTe QDs) as the signal tag (Gan et al. 2013). Firstly, Fe_3O_4 nanoparticles are immobilized on graphene oxides to fabricate the magnetic nanocomposites, which are used as absorbent to AFM1. Secondly, aflatoxin M1 antibody (primary antibody, AFM1 Ab1) is attached to the surface of the CdTe QDs-carbon nanotubes nanocomposite to form the signal tag (AFM1 Ab1/CdTe-CNT). Thirdly, Fe-GO was employed for extraction of AFM1 in milk wherein it can adsorb AFM1 efficiently and selectively within a large extent of pH from 3.0 to 8.0. Adsorption processes reached 95% of the equilibrium within 10 min (Gan et al. 2016). Lastly, the AFM1 with a serial of concentrations absorbed on Fe-GO was conjugated with AFM1 Ab1/CdTe-CNT signal tag based on sandwich immunoassay. The immuno-complex can emit a strong ECL signal whose intensity depended linearly on the logarithm of AFM1 concentration from 1.0 to 1.0×10^5 pg/mL, with the detection limit (LOD) of 0.3 pg/mL (S/N = 3). The method was more sensitive for AFM1 detection compared to the ELISA method.

Pal et al. (2015) have developed a multi-platform detection of AFM1 based on hafnia nanoparticles based on immunochemistry. The fine-grained nanocrystal ceramic powder samples of HfO_2NP_2 were prepared, and they are highly specific to the monoclonal antibody immobilized onto HfO_2 surface using chemical modification and cross-linking chemistry. Further, nanobiosensors were evaluated based on chemiluminescent sandwich enzyme-linked immunosorbent assay followed by photometric measurement of particles with a detection limit of 200–0.5 pg/ml. the multi-platform detection having a good linearity with a limit of detection 6.25 pg/ml, sensitivity, selectivity, and stability.

An electrochemical immune sensor for the detection of ultra-trace amounts of aflatoxin M1 (AFM1) in food products has been developed by Paniel et al. (2010). The sensor was based on a competitive immunoassay using horseradish peroxidase (HRP) as a tag. Magnetic nanoparticles coated with antibody (anti-AFM1) were used to separate the bound and unbound fractions. The samples containing AFM1 were incubated with a fixed amount of antibody and tracer [AFM1 linked to HRP (conjugate)] until the system reached equilibrium. Competition occurs between the antigen (AFM1) and the conjugate for the antibody. Then, the mixture was deposited on the surface of screen-printed carbon electrodes, and the mediator [5-methylphenazinium methyl sulfate (MPMS)] was added. The enzymatic response was measured amperometrically. A standard range (0, 0.005, 0.01, 0.025, 0.05, 0.1, 0.25, 0.3, 0.4 and 0.5 ppb) of AFM1-contaminated milk from the ELISA kit was used to obtain a standard curve for AFM1. To test the detection sensitivity of the sensor, samples of commercial milk were supplemented at 0.01, 0.025, 0.05, or

0.1 ppb with AFM1. Results revealed that the immune sensor has a low detection limit (0.01 ppb), which was under the recommended level of AFM1 [0.05 μg L^{-1} (ppb)], and has good reproducibility.

A new DNA-based biosensor for detection of aflatoxin M1 has been developed by Dinckaya et al. (2011) based on an immobilization of thiol-modified single-stranded DNA (ss-HSDNA) probe that specifically binds to aflatoxin M1, a self-assembled monolayer (SAM) of cysteamine and gold nanoparticles on the SAM on gold electrodes, layer-by-layer. The assembly processes of cysteamine, gold nanoparticles, and ss-HSDNA were monitored with the help of electrochemical impedance spectroscopy (EIS) and cyclic voltammetry (CV) techniques using potassium ferrocyanide as a redox probe for electrochemical measurements. The biosensor provided a linear response to aflatoxin M1 over the concentration range of 1–14 ng/mL with a standard deviation of ±0.36 ng/ml.

3.6.3 Heavy Metals

Heavy metal ions, such as lead, mercury, cadmium, chromium, and arsenic, are hazardous, contributing to water and soil pollution. Through water and soil, these metal residues reach daily foods. Heavy metals are known to cause irreversible changes in protein structures, affecting cell functions. Excessive intake of such substances can result in adverse health conditions including neurological disorders, renal degradation, and bone lesions (Kim et al. 2012). The nanobiosensing methods for the detection of heavy metal ions can be divided into several subcategories according to biorecognition molecule. Chen has developed an AuNPs-based dual-labeling colorimetric method for Hg^{2+} detection using a specific thymine–Hg^{2+}–thymine (T-Hg-T) (Tedsana et al. 2015) as a recognition system and dual-labeling strategy for signal amplification; without using any instruments, they obtained a LOD of 0.025 nM, competitive to other rapid detection methods (Dheng et al. 2015). The target ions aid in assembling AuNPs modified with different Raman labels, leading to different enhancements of Raman signal (Li et al. 2015). Saran and Liu (2016) have used DNAzyme (recognition group and amplifier) for the development of label-free catalytic biosensing platform for the detection of Pb^{2+} and Ag^{+} based on stabilization of AgNCs (signal reporter) with DNA wherein these metals act as a cofactor of DNAzyme activity (Gong et al. 2015). A study by Zhou et al. (2016) for the specific detection of Cd^{2+} and Pb^{2+} by using amino acids because of the functional side chain (like cysteine) wherein graphene oxide nanoparticles were being used based on the change of the electrochemical signal. An approach by Fu et al. (2015) for the detection of heavy metals (Cd^{2+}) by the use of antibody based on core–shell AuNPs/AgNPs enhanced Raman scattering.

Sener et al. (2013) have developed a colorimetric assay based on the aggregation of gold nanoparticles (AuNPs) in the presence of Hg^{2+}. The detection limit of this colorimetric assay is 2.9 nM, which is below the limit value (10 nM) defined by the US Environmental Protection Agency. The colorimetric response of AuNPs in the

presence of lysine is very selective to the Hg^{2+}. Another attempt by Childress et al. (2012) is by the use of dye-doped polymer nanoparticles that are able to detect mercury in aqueous solution at parts per billion (ppb) levels via fluorescence resonance energy transfer (FRET). The polymer NPs are synthesized by re-precipitation of highly fluorescent conjugated polymers in water followed by doping with rhodamine spirolactam dyes that are nonfluorescent until they encounter mercury ions, which promote an irreversible reaction that converts the dyes to fluorescent rhodamines. The rhodamine dyes act as FRET acceptors for the fluorescent nanoparticles, and the ratio of nanoparticle-to-rhodamine fluorescence intensities functions as a radio/ratiometric fluorescence chemodosimeter for mercury. The light-harvesting capability of the conjugated polymer nanoparticles enhances the fluorescence intensity of the rhodamine dyes by a factor of 10, enabling sensitive detection of mercury ions at levels as low as 0.7 ppb.

3.6.4 Adulterants

Some manufacturers and farms engage in food fraud for increasing profit margin, and such ill practices often lead to devastating results. Melamine, a chemical adulterant, is sometimes illegally added to milk powder to improve the apparent protein content (Niu et al. 2015). A melamine aptamer derived from a basic-site-containing triplex molecular beacon (tMB) has been proposed for sensitive recognition of melamine by integrating tMBs and fluorescent AgNCs (Wang et al. 2015). Nitrite is harmful to humans and is widely used as an additive and preservative in food service industry. A biosensor toward nitrite was developed based on the direct electrochemistry of myoglobin on a reduced GOx-multi-walled CNTs-platinum NPs nanocomposite (Mani et al. 2014). ZnO NPs are frequently considered to design biosensing strategies for the detection of bisphenol A, a ubiquitous environmental contaminant found in food products and aquatic ecosystems (Najafi et al. 2014; Zhang et al. 2014). As H_2O_2 is a kind of unlawful decolorizer for food, a biosensing method toward H_2O_2 was developed based on the H_2O_2 enlarging AuNPs that induced significant fluorescence quenching of BSA-AuNCs.

A highly sensitive acetylcholinesterase cyclic voltammetric biosensor based on zinc oxide nanospheres modified Pt electrode has been successfully developed for the simultaneous determination of melamine and urea in cow milk sample (Ezhilan et al. 2017). The fabricated bioelectrode showed 100% permeability to the binary mixture of melamine and urea, which in turn enhanced selectivity. The developed Pt/ZnO/AChE/chitosan bioelectrode detected melamine and urea over a range of 1–20 nM with a limit of detection of 3 pM and 1 pM, respectively. The sensor exhibited good recovery in the range of 99.96–102.22%, thus providing a promising tool for analysis of melamine and urea in cow milk samples. Gold nanoparticles functionalized with cyanuric acid compounds selectively bind to melamine, an adulterant used to enhance the measured proteins content of infant food formulas (Ai et al. 2009).

3.6.5 Pesticide Residues

Various kinds of nanoparticles, such as quantum dots (QDs) and AuNPs, have been used for the development of electrochemical enzyme biosensors. An enzyme biosensor was developed for the amperometric detection of trichlorfon using poly (N-vinyl-2-pyrrolidone) (PVP)-capped CdS QDs (Li et al. 2006). The formation of PVP-QD nanostructures on the electrode surface provided a favorable microenvironment and led to a highly sensitive and stable electrochemical detection of the enzymatically generated thiocholine product. The detection limit was 4.8 × 10–8 M. Another kind of nanoparticles is AuNPs. Their unique property to provide a suitable microenvironment for immobilization of biomolecules retaining their bioactivity is a major advantage for the preparation of biosensors. Moreover, AuNPs facilitate direct electron transfer between immobilized redox proteins and the electrode surface (Pingarron et al. 2008). An electrochemical biosensor based on the colloidal AuNP-modified sol–gel interface was developed for the detection of monocrotophos, carbaryl, and methyl parathion (Du et al. 2008a). The assembled AuNPs on a sol–gel-derived silicate network provided a conductive pathway to electron transfer and favored the interface enzymatic hydrolysis reaction, increasing the sensitivity of the amperometric response. This biosensor presented good stability, retaining 90% of its initial current response after a 30-day storage period. Recently, an efficient biosensor for the detection of monocrotophos was developed by combining the unique properties of AuNPs with those of QDs. This new electrochemical system based on CdTe QD-AuNP electrode was more sensitive than those based on QDs or AuNPs alone (Du et al. 2008b).

Recently, an electrochemical immune sensor was developed for rapid screening of diuron, a substituted phenyl urea herbicide (Sharma et al. 2011). Low-cost ablated electrodes fabricated on polystyrene substrate were modified with Prussian Blue (PB)-AuNP film. The electrodeposition of PBAuNP film enhanced electron transfer in the vicinity of the gold electrode increasing the sensitivity of the system as compared to unmodified gold electrodes. A conductometric immune sensor for the detection of atrazine was also developed using antibodies labeled with nanoparticles (Valera et al. 2008). The authors showed that AuNPs amplify the conductive signal and hence allow the detection of atrazine by means of DC measurements.

Nanoparticles have also been used for the development of efficient optical biosensors (Lin et al. 2006). QDs are candidates to replace conventional fluorescent markers. These semiconductor particles are more photostable than an organic fluorophore. Moreover, QDs exhibit higher fluorescence quantum yields than conventional organic fluorophores, allowing higher sensitivity. Recently, an optical biosensor was developed for the detection of monocrotophos using CdTe as fluorescence probe (Sun et al. 2011). Using positively charged chitosan, CdTe and acetylcholinesterase were assembled onto a quartz surface by a layer-by-layer technique. In the absence of pesticide, acetylcholine was bio-catalytically hydrolyzed inducing the production of choline and acetic acid. The released acid resulted in pH decrease that was sensed by the immobilized pH indicator (CdTe).

The presence of monocrotophos induced a change of the fluorescence intensity that was related to the pesticide concentration. Optical properties of AuNPs have been exploited for the development of localized SPR (LSPR) sensor (Fu et al. 2009). The resonance frequency of the LSPR is highly dependent upon the local environment of the nanoparticle and more specifically upon the binding events that occur to the functionalized NPs. The LSPR was used to develop a biosensor for the detection of paraoxon by immobilizing AChE onto AuNPs layer using a self-assembling technique (Lin et al. 2006). In the presence of pesticides, the enzymatic activity was inhibited causing a change of the light attenuation. The detection limit with optimal conditions was 0.2 ppb. The biosensor retained 94% of its original activity after 6 cycles of inhibition with 500 ppb paraoxon followed by reactivation of AChE with 0.5 mM 2-pyridine aldoxime methiodide. In addition, the sensor retained its activity after 2 months storage in the dry state at 4 °C.

Carbon nanotubes (CNTs) consist of cylindrical graphene sheets with diameter in nanometer diameters. They present unique mechanical, physical, and chemical properties. CNTs include both single-walled and multi-walled structures. Since their discovery, CNTs have been used in nanoelectronics, biomedical engineering, biosensing, and bioanalysis. Recently, CNTs have been used for the development of biosensors based on the inhibition of AChE activity (Du et al. 2007; Oliveira and Mascaro 2011; Firdoz et al. 2010). An amperometric biosensor based on layer-by-layer assembly of single-walled CNT-poly(diallyldimethylammonium chloride) and AChE was developed for the analysis of carbaryl (Firdoz et al. 2010). The biosensor showed good sensitivity and stability toward the monitoring of pesticides in water. The detection limit was 4.9 × 10–15 M. In some cases, the authors developed efficient biosensors for the detection of pesticides by associating the properties of CNTs with those of nanoparticles (Du et al. 2010).

A simple and selective aptamer-based colorimetric assay for the detection of omethoate has been developed by Wang et al. (2016). The principle of the assay is that single-stranded DNA (ssDNA)-wrapped gold nanoparticles (AuNPs) are resistant to salt-induced aggregation. By employing an "artificial antibody" organophosphorus pesticide-binding aptamer (OBA) as the recognition element, aptamer-wrapped AuNPs (Au-apta) show high selectivity toward omethoate, resulting in the disconnection of aptamers from AuNPs and the aggregation of AuNPs. As there is a significant color change from the interparticle plasmon coupling during the aggregation of AuNPs, the established assay showed good linearity between 0.1 and 10 μmol/L, with a low detection limit of 0.1 μmol/L.

A novel nanohybrid composite with good electrochemical responses was developed by Xu et al. (2017), and it was prepared by the esterification reaction of hydroxyl-terminated polybutadiene (HTPB) with MWCNT-COOH, followed by atom transfer radical polymerization of 4-acryloyloxybutyl(ethyl) ferrocene carboxylates with different spacers. The nanohybrid composites were characterized by FTIR, TGA, Raman, XRD, XPS, SEM, and TEM techniques. Cyclic voltammetry (CV) determination showed that a longer spacer between the side ferrocene groups and main chains endowed the electrochemically modified electrodes with active electron response, obvious redox current, and reversible electrochemical properties

because of the faster electron transfer rates. The modified electrode sensor with a longer spacer was used to detect melamine and trichlorfon residues by CV and differential pulse voltammetry (DPV) techniques. The sensor had a good linear relationship over a wide concentration range, a maximal recovery of ca. 112.4% and a low detection limit of about 1.5×10^{-7} and 3.5×10^{-8} mol L^{-1}, respectively.

Turan et al. (2016) have used an innovative approach for the fabrication of a biosensor utilizing a conducting polymer and silver nanowires. To obtain immobilization platform for butyrylcholinesterase (BChE), a graphite electrode was modified with the poly(5,6-bis(octyloxy)-4,7-di(thieno[3][3,2-b]thiophen-2-yl)benzo[c][1,2,5]oxoadiazole) (PTTBO) which has a hydrophobic alkyl chain as the pendant group providing hydrophobic nature to the matrix. Since biomolecules contain both hydrophobic and hydrophilic parts in their structure, alkyl chains interact with the proteins which provide an enhanced stability. Biosensor performance was improved through the deposition of silver nanowires on the polymer-coated surfaces which enhances the charge transfer rate. This enabled the development of rapid, highly sensitive, and stable amperometric sensors for the quantitative determination of organophosphorus pesticide, paraoxon. Fabricated biosensor showed two linear ranges between 0.5–8 μM and 10–120 μM with a low detection limit of 0.212 μM when butyrylthiocholine iodide is used as the substrate.

Zhang et al. (2013) have developed novel nanobiosensing principles for organophosphorus pesticides. Thiocholine generation by AChE catalysis leads to the aggregation of AuNPs, resulting in the recovery of fluorescence resonance energy transfer (FRET) between AuNPs and NaYF4: Yb, upconversion NPs (Long et al. 2015). Immobilization of AChE in fenugreek hydrogel-agarose matrix with AuNPs results in high enzyme retention efficiency of 92% and a significantly prolonged half-life of the AChE (55 days) (Kestwal et al. 2015). Apart from AChE, pesticides can also inhibit other enzyme activity such as trypsin and tyrosinase (Yan et al. 2015). Trypsin easily hydrolyzes protamine covered on the surface of AuNPs, leading to fluorescence quenching of QDs.

Electrochemical and photochemical properties of pesticides such as omethoate, malathion, lindane, carbofuran, carbaryl, etc. are being used for the development of nanobiosensors (Yang et al. 2016). Nanobiosensors based on copper oxide nanowires-CNTs, AgNPs decorated polyaniline-nanocrystalline zeolite organic-inorganic hybrid material, cobalt oxide (CoO)-reduced GOx, zirconia-ordered macroporous polyaniline, and other nanosystems, have already been reported to improve the sensitivity of the nanosensors (Huo et al. 2014; Kaur et al. 2015, Wang et al. 2014, 2015; Wu et al. 2014). In addition to electrochemical methods, a few NP-enhanced surface-enhanced Raman spectroscopy (SERS) methods have been developed, but these methods have limitations in terms of low affinity. Such problems can be overcome by optimizing metal NPs, for example, the type, molecular linker, surface coverage, and laser excitation wavelength of NPs (Kubackova et al. 2015).

Immunoassay-based nanobiosensing systems are most widely being used in the detection of pesticides (Belkhamssa et al. 2016; Sun et al. 2015; Xiao et al. 2016). The application of nanometal organic framework and other materials can greatly

reduce the LOD (Deep et al. 2015). Pesticides are known to hinder certain photo-physical as well as photo-chemical functions of nanomaterial, through specific recognition of pesticides by antibodies immobilized on nanomaterial surfaces may lead to discovery of many excellent phenomena, for example, pentachlorophenol obstructs electrochemiluminescence of Au nanoclusters/graphene hybrid (Luo et al. 2014), acetamiprid decreases enhanced photocurrent produced by electron donor of quercetin in Co-doped ZnO diluted magnetic semiconductor, thiram quenches blue luminescence of Cu^{2+} decorated NaYF4:Yb/Tm up conversion NPs fixed on filter paper (monitored by the smartphone camera through a self-written Android program) (Mei et al. 2016).

3.6.6 Microbial Safety and Quality

Rapid detection of foodborne pathogens is a key step in the control of food-related diseases. Conventional methods for the detection of food pathogens, although typically sensitive, often require multiple time-consuming steps such as extraction, isolation, enrichment, counting, etc., prior to measurement, resulting in testing times which can be days (Paul et al. 2013). There is an urgent necessity to develop rapid and sensitive detection methods. To overcome these limitations, several examples of innovative integration of microbial biosensors with recent nanotechnologies have been proposed in the past decade. For instance, microfluidic systems showed many advantages by minimizing the sample and reagent volumes required, shortening analysis time with high resolution and repeatability, and demonstrating multiple assays on a chip in a high-throughput manner (Kim et al. 2014). In addition, it was demonstrated that microfluidic systems cannot only provide microorganisms with an ideal cell culture microenvironment that is close to in vivo (Shaw and Kado 1986) but also enable high portability and more rapid analysis compared to conventional methods (Joyner and Lindow 2000). The nano-fabrication showed a remarkable potential for microbial biosensors with the following features (Fujimoto et al. 2006):

1. Enhanced optical and electrochemical measurements
2. Improved immobilization and automated culture environments
3. High portability and more practical applications

Nano-based sensing approaches include the use of nanoparticles (NPs) and nanostructures to enhance sensitivity and selectivity, design new detection schemes, improve sample preparation, and increase portability (Bülbül et al. 2015). Recently, nanotechnology allowed for the design of nanosensors for identification of foodborne pathogens or toxins.

The poly(dimethylsiloxane) (PDMS) immune-sensing chips have been developed by Dong et al. (2006) with reinforced, supported, fluid bilayer membranes (r-SBMs) and specific antibodies to the toxin for the detection of with S*taphylococcus* enterotoxin B. Rivas et al. (2006) developed universal G-liposomal nanovesicles based on immune-magnetic bead sandwich assay to detect *E. coli* O157: H7, *Salmonella* sp.,

and *L. monocytogenes* in food. Other pathogenic microorganisms were detected with a specific type of immunosorbent assay using universal protein G-liposomal nanovesicles (Chen and Durst 2006). Furthermore, nanoparticles have been used as nano-sieves to filter out bacteria. On the other hand, detection of bacterial toxins using nanoparticle technology was recently reported (Zhu et al. 2014). Yang et al. (2009) reported a capacitive immune sensor for the detection of *Salmonella* spp. which was fabricated by immobilizing an Au nanoparticle monolayer onto a glassy carbon electrode and then the Salmonella monoclonal antibodies through physical adsorption. It was found that the Au nanoparticles can effectively improve the sensitivity and stability of the immune sensors, which can detect the *Salmonella* spp. concentrations in the range of $1.0 \times 10^2 - 1.0 \times 10^5$ cfu·mL^{-1} with the detection limit of 1.0×10^2 cfu·mL^{-1}. In addition to Au nanoparticles, metal-oxide nanoparticles which possess high surface area and thermally stable, chemically inert, nontoxic inorganic oxide have been also used in the development of bacterial biosensors. Huang et al. (2010) used Fe_3O_4 nanoparticles to immobilize monoclonal antibodies in the construction of electrochemical impedimetric immune sensors for the rapid detection of *Campylobacter jejuni*. The Fe_3O_4 nanoparticle-based immune sensor showed good performance with respect to simplicity of use, fast response, wide linear range, acceptable reproducibility, and long stability. In addition to nanoparticles, nanowires have been attracted much scientific interest in analytical chemistry, especially in biosensing technologies. This is due to their unique semiconductive properties associated with the nanostructures, and they are believed to be ultrasensitive in performing single-molecule sensing. Wang et al. (2009) developed a TiO_2 nanowire bundle microelectrode-based impedimetric immune sensor for rapid and sensitive detection of *L. monocytogenes*. TiO_2 nanowire bundle was connected to gold microelectrodes using mask welding, and then monoclonal antibodies were immobilized on the surface of a TiO_2 nanowire bundle to specifically capture bacteria. Impedance changes caused by the nanowire-antibody-bacteria complex were measured and correlated to the bacterial number. Since the TiO2 nanowires can be highly oriented on substrates or form free-standing membranes, the fabricated electrode showed a large specific surface area, good biocompatibility, good chemical and photochemical stabilities, and negligible protein denaturation. This nanowire bundle-based immune sensor also exhibited a good performance that can detect as low as 10^2 cfu·mL^{-1} of *L. monocytogenes* in 1 h without significant interference from other foodborne pathogens. Ali et al. (2014) have developed a sensitive colorimetric method for the detection of *E.coli* O157:H7 using conjugated gold nanoparticles anti-*E. coli* O157:H7. The key point of gold nanoparticle-based visual detection assay is to control dispersion and aggregation of colloidal nanoparticles by targets of interest *E. coli* O157:H7. The existence of the target molecules can be translated into optical signals and monitored by the naked eye resulting in a dramatic color change from red to blue (Table 3.1).

Table 3.1 Nanobiosensors for detection of microbial quality of food products

Nanomaterials	Microorganisms	Electrode	Detection range	References
Au nanoparticles (NPs)	Sulfate-reducing bacteria	Foam Ni electrode	2.1×10^1 – 2.1×10^7	Wan et al. (2010)
Fe3O4 NPs	*C. jejuni*	GCE	10^{-3} – 10^{-7}	Huang et al. (2010)
AU NPs	*Salmonella* spp.	GCE	10^2 – 10^7	Yang et al. (2009)
Magnetic nanoparticles	*E. coli* O157:H7	IDAM	Pure culture (10^4 – 10^7)	Varshney and Li (2007)
Magnetic nanoparticles	*E. coli*	Pt. plate electrode	10–10^4	Maalouf et al. (2008)

Adopted from Bülbül et al. (2015)

3.6.7 Packaging

The use of nanomaterials in food packaging is already a reality. Nanotechnology can be used in plastic food packaging to make it stronger, lighter, or perform better. Antimicrobials such as nanoparticles of silver or titanium dioxide can be used in packaging to prevent spoilage of foods. Another addition is the introduction of nanoparticles of clay into packaging to block oxygen, carbon dioxide, and moisture from reaching the food and also aids in preventing spoilage. Chemical giant Bayer produces a transparent plastic film called Durethan which contains nanoparticles of clay. Durethan is an engineering plastic based on polyamide 6 and polyamide 66; these particles offer an excellent combination of properties which include high strength and toughness, abrasion resistance, chemical resistance, and resistance to cracking. Durethan is used in various industries and applications, including packaging film for the medical field and food packaging. The nanoparticles are spread throughout the plastic and are able to block oxygen, carbon dioxide, and moisture from reaching fresh meats or other foods. The advantage of using nanoclay is it also makes the plastic lighter, stronger, and more heat-resistant. Durethan film material with nanoparticles combines the advantages of polyamide 6 and ethylene vinyl alcohol (EVOH) to produce an inexpensive but still very airtight packaging material. The embedded nanoparticles prevent gases from penetrating the film and also keeping moisture from escaping. An example is bottles made with nanocomposites which minimize the leakage of carbon dioxide out of the bottle; by minimizing the leakage of CO_2 in the bottle, this will cause an increase in the shelf life of a carbonated beverage without having to use heavier glass bottles or more expensive cans. Another example is food service bins made out of silver nanoparticles embedded in the plastics. The silver nanoparticles kill bacteria from any food previously stored in the bins, which will minimize harmful bacteria.

Generally, nanobiosensors are placed in food packaging to control internal and external conditions of food (Ramachandraiah et al. 2015). From a microbiological point of view, the main objective of nanosensors is to reduce pathogen detection time

from days to hours or even minutes (Fuertes et al. 2016). These nanomaterials are used in the detection of molecules, gases, and microorganisms and detection by surface-enhanced Raman spectroscopy (SERS) (Duncan 2011); nanosensors in raw bacon packaging for detecting oxygen (Mills 2005); electronic tongue for inclusion in food packaging consisting of an array of nanosensors extremely sensitive to gases released by spoiled food, giving a clear and visible sign if the food is fresh or not (Bowles and Lu 2014); use of fluorescent nanoparticles to detect pathogens and toxins in food (Burris and Stewart 2012), for example, detection of pathogenic bacteria in food (*S. typhimurium*, *Shigella flexneri*, and *E. coli* O157:H7), based on functionalized quantum dots coupled with immunomagnetic separation in milk and apple juice (Burris and Stewart 2012); nanosensors to detect temperature changes (Iliadis and Ali 2011; Lee et al. 2011), where food companies like Kraft Foods are incorporating nanosensors that detect the profile of a food consumer (likes and dislikes), allergies, and nutritional deficiencies (Meetoo 2011); nanosensors for the detection of organophosphate pesticide residues in food (Liu et al. 2008), nanosensors to detect humidity or temperature changes due to moisture (Zhang et al. 2010), sensor for detecting *E. coli* in a food sample, by measuring and detecting scattering of light by cellular mitochondria (Horner et al. 2006); biosensor for instantly detecting Salmonella in foods (Fu et al. 2008) and sensor to detect CO_2 as a direct indicator of the quality of the food (Puligundla et al. 2012); and biosensor for the detection of the pathogen-food, *Bacillus cereus* (Pal et al. 2007).

Scientists at Kraft, as well as at Rutgers University, are working on nanoparticle film concentration and another packaging with embedded sensors that will detect food pathogens. Called "electronic tongue" technology, the sensors can detect substances in parts per trillion and would trigger a color change in the packaging to alert the consumer if a food has become contaminated or if it has begun to spoil (Anonymous 2004).

The intelligent packaging (IP) incorporating nanosensors will have great benefits for the food industry. This NM in the form of tiny chips invisible to the human eye is embedded in food or in containers, for use as electronic bar code, which allows for the monitoring of food in all its phases (production, processing, distribution, and consumption) (Fuertes et al., 2016). Communication between NMs is a promising technology that ensures the development of new devices capable of performing basic and simple tasks at nanolevel (computing, data storage, detection, and triggering). The nanosensors have a limited field of measurement; therefore, the development of the wireless nanosensor networks (WNSNs) is essential for the IP industry. developing nanosensors.

One major drawback is the limited energy that can be stored in a nanosensor speck in contrast to the energy required by the device to communicate. Recently, novel collecting energy mechanisms have been proposed to replenish energy stored in nanodevices. With these mechanisms, WNSNs can overcome the bottleneck and even have infinite life (perpetual WNSNs). For now, the limitations of size and power of nanodevices limit the applicability of wireless communication.

One of the most recent alternatives is based on the use of graphene, a nanomaterial of one atom thickness, which was first obtained experimentally in

2004 (Geim and Novoselov 2007). Graphene enables wireless communication between nanosystems, because of its ability to support surface plasmon polariton (SPP) in the terahertz frequency range (Cabellos-Aparicio et al. 2015). The main difference between classical plasmonic antennas and graphene-based plasmonic antennas is that SPP waves in graphene are observed at frequencies in the terahertz band, for example, two orders of magnitude below SPP waves observed in gold and other noble materials (Jornet and Akyildiz 2014). The SPP waves require less energy making the communication between NMs feasible (Akyildiz et al. 2014).

3.7 Challenges

The main focus of nanosensor researchers from the comparative evaluation of nanosensors and conventional based techniques to designing of commercially viable sensors for its field application. Robust comparisons against traditional technologies would also help address a related challenge, i.e., the substantial inertia involved in encouraging professional analysts to replace older technologies with new methods, a process that is surprisingly difficult even when the new methods promise significant benefits.

Despite what could be regarded as a slow adoption of nanosensor technology into the commercial space, nano-sensing is still a growing field with many exciting possibilities for both the food industry and regulatory authorities. Undoubtedly, many challenges need to be resolved for the effective commercialization of this know-how. However, continued research and development and especially a renewed focus on validation against more established detection methods will help solidify nano-sensing potential role in making the world's food supply healthier, safer, and – possibly – more delicious.

Furthermore, with the development of lab-on-a-chip technique, the integration of analyte onto a microfluidic chip to develop a biotic microelectromechanical system would supply a new research aspect in the field of biosensors because such systems only require minimal amounts of sample and provide good sensitivity in the detection of analytes. Current methods of target immobilization on transducer have limitations which affect cell viability as well as cell function. Physical adsorption suffers from poor stability. A major disadvantage of immobilization is the additional diffusion resistance caused by the entrapment material, which would result in a loss of sensitivity. As the world becomes seriously concerned about the effect of food on public health and the safety against biowar, the aforementioned prospects will be a breakthrough in targets immobilization and identification in biosensor field. However, there are still several challenges to overcome, which limit the progress of technology transfer and commercialization, mainly related to the difficulties in the integration of all the components into a single portable platform. Yet, there is still a long road ahead for this emerging technology to be fully adapted to a filed application.

3.8 Conclusion

Dairy food safety problems frequently are compromised due to antibiotic residues, aflatoxin M1, pesticides, heavy metals, adulterants, microbial foodborne pathogens, etc. These classes of milk and milk product contaminations could not be detected efficiently by conventional methods due to the fact they require longer time for the confirmation. These dairy products cannot be stored for the longer period of time because there may be chances change of chemical nature of the products. Therefore, dairy industries are under tremendous pressure to meet the consumer requirement with quality and safety with in one working day. Therefore, the need of the hour is to development of sensors with the use of nanomaterial in link with specific biorecognition molecules. By the application of nanobiosensor with the use of nanoparticles, various food contaminants including microbial pathogens can be identified accurately. Therefore nanosensors have been widely used in the dairy food quality and safety evaluation. Despite what could be regarded as a slow adoption of nanosensor technology into the commercial space, nano-sensing is still a growing field with many exciting possibilities for both the food industry and regulatory authorities.

References

Adegoke GO, Puleng L (2013) Strategies for the prevention and reduction of mycotoxins in developing countries. In: Mycotoxin and food safety in developing countries, 1st edn. InTech, Rijeka, pp 123–136

Ai K, Liu Y, Lu L (2009) Hydrogen-bonding recognition-induced color change of gold nanoparticles for visual detection of melamine in raw milk and infant formula. J Am Chem Soc 131(27):9496–9497

Akyildiz I, Jornet J (2010) The Internet of nano-things. IEEE Wirel Commun 17(6):58–63

Akyildiz IF, Jornet JM, Han C (2014) Terahertz band: next frontier for wireless communications. Phys Commun 12:16–32

Alagarasi A (2011) Introduction to nanomaterials.. The National Centre for Catalysis Research

Ali MA, Eldin TAS, Moghazy GE, Tork IM, Omara II (2014) Detection of *E. coli* O157: H7 in feed samples using gold nanoparticles sensor. Int J Curr Microbiol App Sci 3(6):697–708

Alocilja EC, Stephen MR (2003) Market analysis of biosensors for food safety. Biosens Bioelectron 18(5):841–846

Alvarado Y, Perez CA (1998) The use of biocides: an environmental problem. Interciencia 23:20–22

Ambrosi A, Castañeda MT, Killard AJ, Smyth MR, Alegret S, Merkoçi A (2007) Double-codified gold nanolabels for enhanced immunoanalysis. Anal Chem 79(14):5232–5240

Amine A, Micheli L, Moscone D, Palleschi G (2003) Rapid online analysis to ensure the safety of milk. In: Smit G (ed) Dairy processing-improving quality. Woodhead Publishing Limited and CRC Press, Cambridge, pp 292–309

Anonymous (2004) Down on the farm: the impact of nano-scale technologies on food and agriculture, ETC Group report

Awasthi V, Bahman S, Thakur LK, Singh SK, Dua A, Ganguly S (2012) Contaminants in milk and impact of heating: an assessment study. Indian J Public Health 56(95):9

Aytenfsu S, Mamo G, Kebede B (2016) Review on chemical residues in milk and their public health concern in Ethiopia. J Nutr Food Sci 6(4):524

Azzouz A, Souhail B, Ballesteros E (2010) Continuous solid-phase extraction and gas chromatography-mass spectrometry determination of pharmaceuticals and hormones in water samples. J Chromatogr A 1217(17):2956–2963

Azzouz A, Jurado-Sanchez B, Souhail B, Ballesteros E (2011) Simultaneous determination of 20 pharmacologically active substances in cow's milk, goat's milk, and human breast milk by gas chromatography mass spectrometry. J Agric Food Chem 59:5125–5132

Baeumner AJ (2003) Biosensors for environmental pollutants and food contaminants. Anal Bioanal Chem 377(3):434–445

Bakirci I (2001) Aflatoxin: a study on the occurrence of aflatoxin M1 in milk and milk products produced in van province of Turkey. Food Control 12:47–51

Bej AK, Dicesare JL, Haff L, Atlas RM (1991) Detection of Escherichia coli and Shigella spp. in water by using the polymerase chain reaction and gene probes for uid. Appl Environ Microbiol 57(4):1013–1017

Belkhamssa N, Justino CIL, Santos PSM, Cardoso S, Lopes I, Duarte AC, Rocha-Santos T, Ksibi M (2016) Label-free disposable immunosensor for detection of atrazine. Talanta 146:430–434

Bernardo F (2004) Micotoxicoses: Gestao de Risco. Prova de agregacao. Faculdade de Medicina Veterinaria, Lisboa, p 172

Blascoa C, Corciab AD, Pico Y (2009) Determination of tetracyclines in multi-specie animal tissues by pressurized liquid extraction and liquid chromatography–tandem mass spectrometry. Food Chem 116(4):1005–1012

Bo LY, Zhang YH, Zhao XH (2011) Degradation kinetics of seven organophosphorus pesticides in milk during yoghurt processing. J Serbian Chem Soc 76:353–362

Bowles M, Lu J (2014) Removing the blinders: a literature review on the potential of nanoscale technologies for the management of supply chains. Technol Forecast Soc Change 82 (1):1900–1198

Bülbül G, Hayat A, Andreescu (2015) Portable nanoparticle-based sensors for food safety assessment. Sensors 15(12):30736–30758

Burris KP, Stewart CN Jr (2012) Fluorescent nanoparticles: sensing pathogens and toxins in foods and crops. Trends Food Sci Technol 28(2):143–152

Cabellos-Aparicio A, Llatser I, Alarcón E, Hsu A, Palacios T (2015) Use of terahertz photoconductive sources to characterize tunable graphene RF plasmonic antennas. IEEE Trans Nanotechnol 14(2):390–396

Caldas ED, Silva SC, Oliveira JN (2002) Aflatoxins and ochratoxin A in food and risks to human health. Rev. Saude Publica

Carlson MA, Bargeron CB, Benson DC, Fraser AB, Phillips TE, Velky JT, Groopman JD, Strickland PT, Ko HW (2000) An automated, handheld biosensor for aflatoxin. Biosens Bioelectron 14:841–848

CDC (2012) Multistate outbreak of listeriosis linked to imported frescolina marte brand ricotta salata cheese (Final update)

CDC (2013) Multistate outbreak of listeriosis linked to crave brothers farmstead cheeses

CDC (2014) Multistate outbreak of listeriosis linked to roos foods dairy products. Available at: http://www.cdc.gov/listeria/outbreaks/cheese-02-14/index.html. CDC 2013. Multistate outbreak of listeriosis linked to crave brothers farmstead cheeses

CDC NORS (2012) Centers for disease control and prevention's (CDC) online food-borne disease outbreak database

Chah S, Fendler JH, Yi J (2002) Nanostructured gold hollow microspheres prepared on dissolvable ceramic hollow sphere templates. J Colloid Interface Sci 250(1):142–148

Chang HC, Ho JAA (2015) Gold nanocluster-assisted fluorescent detection for hydrogen peroxide and cholesterol based on the inner filter effect of gold nanoparticles. Anal Chem 87 (20):10362–10367

Chemburu S, Ebtisam W, Abdel-Hamid I (2005) Detection of pathogenic bacteria in food samples using highly-dispersed carbon particles. Biosens Bioelectron 21(3):491–499

Chen CS, Durst RA (2006) Simultaneous detection of *E. coli* O157:H7, Salmonella spp. and *L. monocytogenes* with an array- based immunosorbent assay using universal protein G-liposomal nanovesicles. Talanta 69(1):232–238

Childress ES, Roberts CA, Sherwood DY, LeGuyader CL, Harbron EJ (2012) Ratiometric fluorescence detection of mercury ions in water by conjugated polymer nanoparticles. Anal Chem 84 (3):1235–1239

Cleveland TE, Dowd PF, Desjardins AE, Bhatnagar D, Cotty PJ (2003) United states department of agriculture—agricultural research service research on pre-harvest prevention of mycotoxins and mycotoxigenic fungi in US crops. Pest Manag Sci 59(6–7):629–642

Deep A, Bhardwaj SK, Paul AK, Kim KH, Kumar P (2015) Surface assembly of nano-metal organic framework on amine functionalized indium tin oxide substrate for impedimetric sensing of parathion. Biosens Bioelectron 65:226–231

DeVries J (1997) Food safety and toxicity. CRC Press, Inc., London, pp 53–57

Dheng Y, Wang X, Xue F, Zheng L, Liu J, Yan F, Xia F, Chen W (2015) Ultrasensitive and rapid screening of mercury (II) ions by dual labeling colorimetric method in aqueous samples and applications in mercury-poisoned animal tissues. Anal Chim Acta 868:45–52

Dinckaya E, Kınık Ö, Sezgintürk MK, Altuğ Ç, Akkoca A (2011) Development of an impedimetric Aflatoxin M1 biosensor based on a DNA probe and gold nanoparticles. Biosens Bioelectron 26 (9):3806–3811

Dong Y, Phillips KS, Cheng Q (2006) Immunosensing of Staphylococcus enterotoxin B (SEB) in milk with PDMS microfluidic systems using reinforced supported bilayer membranes (r-SBMs). Lab Chip 6(5):675–681

Du D, Huang X, Cai J, Zhnag A (2007) Comparison of pesticide sensitivity by electrochemical test based on acetylcholinesterase biosensor. Biosens Bioelectron 23(2):285–289

Du D, Chen S, Cai J, Zhang A (2008a) Electrochemical pesticide sensitivity test using acetylcholinesterase biosensor based on colloidal gold nanoparticle modified sol-gel interface. Talanta 74 (4):766–772

Du D, Chen S, Song D, Li H, Chen X (2008b) Development of acetylcholinesterase biosensor based on CdTe quantum dots/gold nanoparticles modified chitosan microspheres interface. Biosens Bioelectron 24(3):475–479

Du D, Chen W, Zhang W, Liu D, Li H, Lin Y (2010) Covalent coupling of organophosphorus hydrolase loaded quantum dots to carbon nanotube. Au nanocomposite for enhanced detection of methyl parathion. Biosens Bioelectron 25(6):1370–1375

Duncan TV (2011) Applications of nanotechnology in food packaging and food safety: barrier materials, antimicrobials and sensors. J Colloid Interface Sci 363(1):1–24

EC (2006) Council of the European Union 2006a 7775/1/06 REV 1. Brussels

EC (2012) Commission Regulation (EC) No 1881/2006 of 19 December 2006 setting maximum levels for certain contaminants in foodstuffs

Eijkelkamp JM, Aarts HJM, Van der Fels-Klerx HJ (2009) Suitability of rapid detection methods for Salmonella in poultry slaughterhouses. Food Anal Methods 2(1):1–13

Eldin TA, Salah HA, Elshoky and Maha A. A. (2014) Nanobiosensors based on Gold nanoparticles Probe for Aflatoxin B1 detection in food. Int J Curr Microbiol App Sci 3(8):219–230

Emrani AS, Danesh NM, Lavaee P, Ramezani M, Abnous K, Taghdisi SM (2016) Colorimetric and fluorescence quenching aptasensors for detection of streptomycin in blood serum and milk based on double-stranded DNA and gold nanoparticles. Food Chem 190:115–121

European Commission (1997) Regulation laying down a community procedure for the establishment of maximum residue limits of veterinary medical products in foodstuffs of animal origin. Off J 224:1–8

Ezhilan M, Gumpu MB, Ramachandra BL, Nesakumar N, Babu KJ, Krishnan UM, Rayappan JBB (2017) Design and development of electrochemical biosensor for the simultaneous detection of melamine and urea in adulterated milk samples. Sensors Actuators B Chem 238:1283–1292

FAOSTAT (2005) Food and Agriculture Organization, Rome, Italy. www.faostat.org
Faulk WP, Taylor GM (1971) Communication to the editors: an immunocolloid method for the electron microscope. Immunochemistry 8(11):1081–1083
FDA (2010) Queseria Bendita Recalls Queso Fresco, Panela, and Requeson Because of Possible Health Risk. Available at: http://www.fda.gov/safety/recalls/ucm201350.htm
Firdoz S, Ma F, Yue X, Dai Z, Kumar A, Jiang B (2010) A novel amperometric biosensor based on single walled carbon nanotubes with acetylcholine esterase for the detection of carbaryl pestcide in water. Talanta 83(1):269–273
Font H, Adrian J, Galve R, Estévez MC, Castellari M, Gratacós-Cubarsí M, Sánchez-Baeza F, Marco MP (2008) Immunochemical assays for direct sulfonamide antibiotic detection in milk and hair samples using antibody derivatized magnetic nanoparticles. J Agric Food Chem 56 (3):736–743
Frasconi M, Ran T-V, Michael R, Itamar W (2010) Surface Plasmon resonance analysis of antibiotics using imprinted boronic acid-functionalized Au nanoparticle composites. Anal Chem 82(6):2512–2519
Fu J, Park B, Siragusa G, Jones L, Tripp R, Zhao Y, Cho YJ (2008) An Au/Si hetero-nanorod-based biosensor for *Salmonella* detection. Nanotechnology 19(15):155502
Fu X, Huang K, Liu S (2009) A robust and fast bacteria counting method using CdSe/ZnS core/shell quantum dots as labels. J Microbiol Methods 79:367–370
Fu J, Park B, Zhao Y (2015) Limitation of a localized surface plasmon resonance sensor for salmonella detection. Sensors Actuators B 141(1):276–283
Fuertes G, Soto I, Vargas M, Valencia A, Sabattin J, Carrasco R (2016) Nanosensors for a monitoring system in intelligent and active packaging. J Sens
Fujimoto H, Wakabayashi M, Yamashiro H, Maeda I, Isoda K, Kondoh M et al (2006) Whole-cell arsenite biosensor using photosynthetic bacterium *Rhodovulum sulfidophilum*. *Rhodovulum sulfidophilum* as an arsenite biosensor. Appl Microbiol Biotechnol 73:332–338
Gan N, Zhou J, Xiong P, Hu F, Cao Y, Li T, Jiang Q (2013) An ultrasensitive electrochemiluminescent immunoassay for Aflatoxin M1 in milk, based on extraction by magnetic graphene and detection by antibody-labeled CdTe quantum dots-carbon nanotubes nanocomposite. Toxins 5(5):865–883
Gan W, Yang H, Zhang Y, Shi SQ, Lin C, Pan L, Huang Z (2016) Synthesis and characterization of sucrose-melamine-formaldehyde adhesives. Bioresources 11(1):2516–2525
Gatoo MA, Sufia N, Mir YA, Ayaz MD, Khusro Q, Swaleha Z (2014) Physicochemical properties of nanomaterials: implication in associated toxic manifestations. BioMed Res Int
Geim AK, Novoselov KS (2007) The rise of graphene. Nat Mater 6(3):183–191
Gelderblom WCA, Snyman SD, Abel S, Lebepe-Mazur S, Smuts CM, Van der Westhuizen L, Marasas WFO, Victor TC, Knasmüller S, Huber W (1996) Hepatotoxicity and-carcinogenicity of the fumonisins in rats. In: Fumonisins in food. Springer US, pp 279–296
Ghosh P, Gang H, Mrinmoy De Chae KK, Vincent MR (2008) Gold nanoparticles in delivery applications. Adv Drug Deliv Rev 60(11):1307–1315
Gong L, Kuai HL, Ren SL, Zhao XH, Huan SY, Zhang XB, Tan WH (2015) Ag nanocluster-based label-free catalytic and molecular beacons for amplified biosensing. Chem Commun 51:12095–12098
Grzelak EM, Malinowska I, Choma IM (2009) Determination of cefacetrile and cefuroxime residues in milk by thin-layer chromatography. J Li J Liquid Chromatogr Relat Technol 32:2043–2049
Gu G, Hu J, Cevallos-Cevallos JM, Richardson SM, Bartz JA, van Bruggen AHC (2011) Internal colonization of Salmonella enterica serovar Typhimurium in tomato plants. PLoS One 6(11): e27340
Gustafson RH (1991) Use of antibiotics in livestock and human health concerns. J Dairy Sci 74:1428–1432

Haddaoui M, Raouafi N (2015) Chlortoluron-induced enzymatic activity inhibition in tyrosinase/ZnO NPs/SPCE biosensor for the detection of ppb levels of herbicide. Sensors Actuators B Chem 219:171–178

Hansmann T, Sanson B, Stojan J, Weik M, Marty JL, Fournier D (2009) Kinetic insight into the mechanism of cholinesterasterase inhibition by aflatoxin B1 to develop biosensors. Biosens Bioelectron 24:2119–2124

Hao H, Cheng G, Iqbal Z, Ai X, Hussain HI, Huang L et al (2014) Benefits and risks of antimicrobial use in food-producing animals. Front Microbiol 5:288

Hemme T, Garcia O, Saha A (2003) A review of milk production in India with particular emphasis on small-scale producers. PPLPI working paper No. 2. International Farm Comparison Network, Pro-Poor Livestock Policy Initiative, 2003. Available at: http://www.fao.org/ag/againfo/programmes/en/pplpi/docarc/wp2.pdf. Accessed May 2009

Horner SR, Mace CR, Rothberg LJ, Miller BL (2006) A proteomic biosensor for Enteropathogenic *E. coli*. Biosens Bioelectron 21(8):1659–1663

Huang JL, Yang GJ, Meng WJ, Wu LP, Zhu AP, Jiao XA (2010) An electrochemical impedimetric immunosensor for label-free detection of *C. jejuni* in diarrhea patients' stool based on O-carboxymethylchitosan surface modified Fe3O4 nanoparticles. Biosens Bioelectron 25:1204–1211

Hubbert WT, Hagstad HV, Spangler E, Hinton MH, Hughes KL (1996) Food safety and quality assurance (Foods of animal origin), 2nd edn. Iowa State University Press, Ames, pp 171–179, 239–273

Huo DQ, Li Q, Zhang YC, Hou CJ, Lei Y (2014) A highly efficient organophosphorus pesticides sensor based on CuO nanowires-SWCNTs hybrid nanocomposite. Sensors Actuators B Chem 199:410–417

Ikeda M, Zhang ZW, Moon CS, Imai Y, Watanabe T et al (1996) Background exposure of general population to cadmium and lead in Tainan city, Taiwan. Arch Environ Contam Toxicol 30:121–126

Iliadis AA, Ali HA (2011) Properties of fast response room temperature ZnO-Si heterojunction gas nanosensors. IEEE Trans Nanotechnol 10(3):652–656

India in business (2008) Investment and technology promotion and energy security. Ministry of External Affairs, Government of India, 2008, Delhi

Jain KK (2007) Applications of nanobiotechnology in clinical diagnostics. Clin Chem 53 (11):2002–2009. (Jasson, 2010)

Jensen RG (1995) Handbook of milk composition. Academic, London, pp 887–900

Jiang XS, Wang RH, Wang Y, Su XL, Ying YB, Wang JP, Li YB (2011) Evaluation of different micro/nanobeads used as amplifiers in QCM immunosensor for more sensitive detection of *E. coli* O157:H7. Biosens Bioelectron 29:23–28

Jornet JM, Akyildiz IF (2012a) Joint energy harvesting and communication analysis for perpetual wireless nanosensor networks in the terahertz band. IEEE Trans Nanotechnol 11(3):570–580

Jornet JM, Akyildiz IF (2012b) The internet of multimedia nano-things. Nano Commun Netw 3 (4):242–251

Jornet JM, Akyildiz IF (2014) Femtosecond-long pulse-based modulation for terahertz band communication in nanonetworks. IEEE Trans Commun 62(5):1742–1754

Joyner DC, Lindow SE (2000) Heterogeneity of iron bioavailability on plants assessed with a whole-cell GFP-based bacterial biosensor. Microbiology 146:2435–2445

Kadir MKA, Tothill IE (2010) Development of an electrochemical immunosensor for fumonisins detection in foods. Toxins 2:382–398

Kangethe E, Langa K (2009) Aflatoxin B1 and M1 contamination of animal feeds and milk from urban centers in Kenya. Afr Health Sci 9(4):218–226

Karshima NS, Pam VA, Bata SI, Dung PA, Paman ND (2013) Isolation of Salmonella species from milk and locally processed milk products traded for human consumption and associated risk factors in Kanam, Plateau State, Nigeria. J Anim Prod Adv 3(3):69–74

Kaur B, Srivastava R, Satpati B (2015) Silver nanoparticle decorated polyaniline-zeolite nanocomposite material based non-enzymatic electrochemical sensor for nanomolar detection of lindane. RSC Adv 5:57657–57665

Kestwal RM, Bagal-Kestwal D, Chiang BH (2015) Fenugreek hydrogel-agarose composite entrapped gold nanoparticles for acetylcholinesterase based biosensor for carbamates detection. Anal Chim Acta 886:143–150

Khandelwal P, Singh DK, Sadhu S, Poddar P (2010) Study of the nucleation and growth of antibiotic labeled Au NPs and blue luminescent Au-8 quantum clusters for Hg^{2+} ion sensing, cellular imaging and antibacterial applications. Nanoscale 7:19985–20002

Khiniki GRJ (2006) Chemical contaminants in milk and public health concerns: a review. Int J Dairy Sci 2:104–115

Kim K, Kim SH, Kim J, Kim H, Yim J (2012) Glutathione s-transferase omega 1 activity is sufficient to suppress neurodegeneration in a Drosophila model of Parkinson disease. J Biol Chem 287(9):6628–6641

Kim M, Lim JW, Kim HJ, Lee SK, Lee SJ, Kim T (2014) Chemostat-like microfluidic platform for highly sensitive detection of heavy metal ions using microbial biosensors. Biosens Bioelectron 65C:257–264

Korsrud GO, Boison JO, Nouws JFM, MacNeil JD (1998) Bacterial inhibition tests used to screen for antimicrobial veterinary drug residues in slaughtered animals. J AOAC Int 81:21–24

Kubackova J, Fabriciova G, Miskovsky P, Jancura D, Sanchez-Cortes S (2015) Sensitive surface-enhanced Raman spectroscopy (SERS) detection of organochlorine pesticides by alkyl dithiol-functionalized metal nanoparticles-induced plasmonic hot spots. Anal Chem 87:663–669

Kumar N, Raghu HV, Kumar A, Haldar L, Khan A, Rane S, Malik RK (2012) Spore germination based assay for monitoring antibiotic residues in milk at dairy farm. World J Microbiol Biotechnol 28(7):2559–2566

Lanyasunya TP, Warnae LW, Musa HH, Olowofeso O, Lokwaleput IK (2005) The risk of mycotoxins contamination of dairy feed and milk on small holder dairy farms in Kenya. Pak J Nutr 4:162–169

Lazcka O, Javier Del Campo F, Xavier MF (2007) Pathogen detection: a perspective of traditional methods and biosensors. Biosens Bioelectron 22(7):1205–1217

Lee J, Mubeen S, Hangarter CM, Mulchandani A, Chen W, Myung NV (2011) Selective and rapid room temperature detection of H2S using gold nanoparticle chain arrays. Electroanalysis 23 (11):2623–2628

Leoni E, Legnani PP (2001) Comparison of selective procedures for isolation and enumeration of Legionella species from hot water systems. J Appl Microbiol 90(1):27–33

Levi K, Smedley J, Towner KJ (2003) Evaluation of a real-time PCR hybridization assay for rapid detection of Legionella pneumophila in hospital and environmental water samples. Clin Microbiol Infect 9(7):754–758

Li X-H, Zonghong X, Hong M, Chenxin L, Meichuan L, Yuezhong X, Litong J (2006) Development of quantum dots modified acetylcholinesterase biosensor for the detection of trichlorfon. Electroanalysis 18(22):2163–2167

Li S, Xu LG, Ma W, Kuang H, Wang LB, Xu CL (2015) Triple Raman label-encoded gold nanoparticle trimers for simultaneous heavy metal ion detection. Small 11:3435–3439

Licata P, Trombetta D, Cristani M, Giofrè F, Martino D et al (2004) Levels of "toxic" and "essential" metals in samples of bovine milk from various dairy farms in Calabria, Italy. Environ Int 30:1–6

Lin T-J, Huang K-T, Liu C-Y (2006) Determination of organophosphorus pesticides by a novel biosensor based on localized surface plasmon resonance. Biosens Bioelectron 22(4):513–518

Linting Z, Li R, Li Z, Xia Q, Fang Y, Liu J (2012) An immunosensor for ultrasensitive detection of aflatoxin B 1 with an enhanced electrochemical performance based on graphene/conducting polymer/gold nanoparticles/the ionic liquid composite film on modified gold electrode with electrodeposition. Sensors Actuators B Chem 174:359–365

Liu Y, Zonghui Q, Xingfa W, Hong J (2006) Immune-biosensor for aflatoxin B 1 based bio-electrocatalytic reaction on micro-comb electrode. Biochem Eng J 32(3):211–221
Liu S, Yuan L, Yue X, Zheng Z, Tang Z (2008) Recent advances in nanosensors for organophosphate pesticide detection. Adv Powder Technol 19(5):419–441
Liufu S, Xiao H, Li Y (2004) Investigation of PEG adsorption on the surface of zinc oxide nanoparticles. Powder Technol 145(1):20–24
Long Q, Li H, Zhang Y, Yao S (2015) Upconversion nanoparticle-based fluorescence resonance energy transfer assay for organophosphorus pesticides. Biosens Bioelectron 68:168–174
Luo S, Xiao H, Yang S, Liu C, Liang J, Tang Y (2014) Ultrasensitive detection of pentachlorophenol based on enhanced electrochemiluminescence of Au nanoclusters/graphene hybrids. Sensors Actuators B Chem 194:325–331
Lyon LA, Michael DM, Michael JN (1998) Colloidal Au-enhanced surface plasmon resonance immunosensing. Anal Chem 70(24):5177–5183
Maalouf R, Hassen WM, Fournier-Wirth C, Coste J, Jaffrezic-Renault N (2008) Comparison of two innovatives approaches for bacterial detection: paramagnetic nanoparticles and self assembled multilayer processes. Microchim Acta 163:157–161
Malik P, Katyal V, Malik V, Asatkar A, Inwati G, Mukherjee TK (2013) Nanobiosensors: concepts and variations. ISRN Nanomater 2013
Mani V, Dinesh B, Chen SM, Saraswathi R (2014) Direct electrochemistry of myoglobin at reduced graphene oxide-multiwalled carbon nanotubes-platinum nanoparticles nanocomposite and biosensing towards hydrogen peroxide and nitrite. Biosens Bioelectron 2014(53):420–427
Meetoo DD (2011) Nanotechnology and the food sector: from the farm to the table. Emirates J Food Agric 23(5):387–403
Mei QS, Jing HR, Li Y, Yisibashaer W, Chen J, Li BN, Zhang Y (2016) Smartphone based visual and quantitative assays on upconversional paper sensor. Biosens Bioelectron 75:427–432
Mills A (2005) Oxygen indicators and intelligent inks for packaging food. Chem Soc Rev 34 (12):1003–1011
Mitchell JS, Lowe TE (2009) Ultrasensitive detection of testosterone using conjugate linker technology in a nanoparticle-enhanced surface plasmon resonance biosensor. Biosens Bioelectron 24(7):2177–2183
Mitchell JM, Griffiths MW, McEwen SA, McNab WB, Yee AJ (1998) Antimicrobial drug residues in milk and meat: causes, concerns, prevalence, regulations, tests, and test performance. J Food Prot 61:742–756
Mitchell JM, Groffiths MW, Mcewen SA, McNab WB, Yee AJ (2002) Antimicrobial drug residues in milk and meat: causes, concerns, prevalence, regulations, tests and test performance. J Food Prot 61:742–756
Mukerjee D (1998) Health risk of endocrine-disrupting ortho-substituted PCBs emitted from incinerators. Environ Eng Sci 15:157–169
Najafi M, Khafilzadeh MA, Karimi-Maleh H (2014) A new strategy for determination of bisphenol A in the presence of Sudan I using a ZnO/CNTs/ionic liquid paste electrode in food samples. Food Chem 158:125–131
Niu CX, Liu QL, Shang ZH, Zhao L, Ouyang J (2015) Dual-emission fluorescent sensor based on AIE organic nanoparticles and Au nanoclusters for the detection of mercury and melamine. Nanoscale 7:8457–8465
OHA (2010) Salmonella cases prompt recall of Umpqua Dairy milk, juice and drink products. Available at: http://www.oregon.gov/DHS/news/2010news/2010-0818a.pdf
Oliveira AC, Mascaro LH (2011) Evaluation of acetylcholinesterase biosensor based on carbon nanotube paste in the determination of chlorphenvinphos. Int J Anal Chem. Article ID 974216. https://doi.org/10.1155/2011/974216
Pal S, Evangelyn CA, Frances PD (2007) Nanowire labeled direct-charge transfer biosensor for detecting Bacillus species. Biosens Bioelectron 22(9):2329–2336
Pal S, Sharma MK, Chatterjee R, Bhand S (2015) Multi-platform nano-immunosensor for aflatoxin M1 in milk. Mater Res Exp 2(4):045010

Paniel N, Radoi A, Marty J-L (2010) Development of an electrochemical biosensor for the detection of Aflatoxin M_1 in milk. Sensors (Basel, Switzerland) 10(10):9439–9448
Paul C, Li Y, Cui T, Ruan R, Ruan R (2013) Nanoparticles based sensors for rapid detection of foodborne pathogens. Int J Agric Biol Eng 6(1). https://doi.org/10.3965/j.ijabe.20130601.002
Picozzi C, Foschino R, Heuvelink A, Beumer R (2005) Phenotypic and genotypic characterization of sorbitol-negative or slow-fermenting (suspected O157) *E. coli* isolated from milk samples in Lombardy region. Lett Appl Microbiol 40(6):491–496
Pingarron J, Yanez-Sedeno P, Gonzalez-Cortes A (2008) Gold nanoparticles-based electrochemical biosensors. Electrochim Acta 53(19):5848–5866
Puligundla P, Jung J, Ko S (2012) Carbon dioxide sensors for intelligent food packaging applications. Food Control 25(1):328–333
Raghunath R, Tripathi RM, Khandekar RN, Nambi KS (1997) Retention times of Pb, Cd, Cu and Zn in children's blood. Sci Total Environ 207:133–139
Rai M, Gade A, Gaikwad S, Marcato PD, Durán N (2012) Biomedical applications of nanobiosensors: the state-of-the-art. J Braz Chem Soc 23(1):14–24
Rajagopal M, Werner BG, Hotchkiss JH (2005) Low pressure CO2 storage of raw milk: microbiological effects. J Dairy Sci 88:3130–3138
Ramachandraiah K, Han SG, Chin KB (2015) Nanotechnology in meat processing and packaging: potential applications – a review. Asian Australas J Anim Sci 28(2):290–302
Ramírez BN, Salgado AM, Valdman B (2009) The evolution and developments of immunosensors for health and environmental monitoring: problems and perspectives. Braz J Chem Eng 26 (2):227–249
Ranganathan S (2015) Selected topic in chemistry. Laxmi Book Publication, Solapur
Reuben CR, Okolocha EC, Bello M, Tanimu H (2013) Occurrence and antibiogram of *E. coli* O157: H7 in locally fermented milk (Nono) sold under market conditions in Nasarawa State, Nigeria. Int J Sci Res (USR) 2(2):591–598
Rivas GA, Miscoria SA, Desbrieres J, Barrera GD (2006) New biosensing platforms based on the layer-by-layer self-assembling polyelectrolytes on Nafion/carbon nanotubes-coated glassy carbon electrodes. Talanta 71(1):270–275
Roy A, Jayanta B (2015) Nanotechnology in industrial wastewater treatment. IWA Publishing, London
Rushton J, Pinto Ferreira J, Stärk KD (2014) Antimicrobial resistance: the use of antimicrobials in the livestock sector, OECD food, agriculture and fisheries papers. 68. OECD Publishing, Paris. https://doi.org/10.1787/5jxvl3dwk3f0-en
Sagadevan S, Periasamy M (2014) Recent trends in nanobiosensors and their applications – a review. Rev Adv Mater Sci 36:62–69
Saitanu K (1997) Incidence of Aflatoxin M1 in Thai milk products. J Food Prot 60:1010–1012
Santacroce MP, Narracci M, Acquaviva MI, Cavallo RA, Zacchino V, Centoducati G (2011) New development in Aflatoxin research: from aquafeed to marine cells. In: Aflatoxins-detection, measurement and control. InTech, Rijeka
Sapsford KE, Algar WR, Berti L, Gemmill KB, Casey BJ, Oh E, Stewart MH, Medintz IL (2013) Functionalizing nanoparticles with biological molecules: developing chemistries that facilitate nanotechnology. Chem Rev 113(3):904–2074
Saran R, Liu J (2016) A silver DNAzyme. Anal Chem 88:4014–4020
SCENIHR (Scientific Committee on Emerging and Newly-Identified Health Risks) (2006) The appropriateness of existing methodologies to assess the potential risks associated with engineered and adventitious products of nanotechnologies. European Commission Health & Consumer Protection Directorate-General: 05
Schikora A, Garcia A, Hirt H (2012) Plants as alternative hosts for Salmonella. Trends Plant Sci 17 (5):245–249
Sener G, Uzun L, Denizli A (2013) Lysine-promoted colorimetric response of gold nanoparticles: a simple assay for ultrasensitive mercury (II) detection. Anal Chem 86(1):514–520
Sharma P, Sablok K, Bhalla V, Suri CR (2011) A novel disposable electrochemical immunosensor for phenyl urea herbicide diuron. Biosens Bioelectron 26(10):4209–4212

Shaw JJ, Kado CI (1986) Development of a Vibrio bioluminescence gene set to monitor phytopathogenic bacteria during the ongoing disease process in a nondisruptive manner. Biotechnology 4:560–564

Shtykov SN, Rusanova TY (2008) Russ J Gen Chem 78:2521

Singh M, Manikandan S, Kumaraguru AK (2011) Nanoparticles: a new technology with wide applications. Res J Nanosci Nanotechnol 1:1–11

Song KM, Cho M, Jo H, Min K, Jeon SH, Kim T, Han MS, Ku JK, Ban C (2011) Gold nanoparticle-based colorimetric detection of kanamycin using a DNA aptamer. Anal Biochem 415(2):175–181

Sun X, Liu B, Xia K (2011) A sensitive and regenerable biosensor for organophosphate pesticide based on selfassembled multilayer film with CdTe as fluorescence probe. Luminescence 26 (6):616–621. https://doi.org/10.1002/bio.1284

Sun ZH, Wang WH, Wen HB, Gan CF, Lei HT, Liu YJ (2015) Sensitive electrochemical immunoassay for chlorpyrifos by using flake-like Fe_3O_4 modified carbon nanotubes as the enhanced multienzyme label. Anal Chim Acta 899:91–99

Sutariya VKB, Pathak Y (eds) (2014) Biointeractions of nanomaterials. CRC Press, Boca Raton

Tan H, Chen Y (2012) Silver nanoparticle enhanced fluorescence of europium (III) for detection of tetracycline in milk. Sensors Actuators B Chem 173:262–267

Tang J, Tang D, Niessner R, Knopp D (2011) A novel strategy for ultra-sensitive electrochemical immunoassay of biomarkers by coupling multifunctional iridium oxide (IrOx) nanospheres with catalytic recycling of self-produced reactants. Anal Bioanal Chem 400(7):2041–2051

Tedsana W, Tuntulani T, Ngeontae W (2015) A circular dichroism sensor for Ni2+ and Co2+ based on L-cysteine capped cadmium sulfide quantum dots. Anal Chim Acta 867:1–8

Thakur G, Kumar N, Raghu HV, Khan A, Yadav A, Singh N, Singh VK (2013) Spore based biosensors for detection of contaminants in milk: a review. Int J Diary Sci Res 2(2):15–21

Tombelli S, Mascini M, Scherm B, Battacone G, Migheli Q (2009) DNA biosensors for the detection of aflatoxin producing Aspergillus flavus and A. parasiticus. Monatshefte für Chemie-Chemical Monthly 140(8):901–907

Turan J, Kesik M, Soylemez S, Goker S, Coskun S, Unalan HE, Toppare L (2016) An effective surface design based on a conjugated polymer and silver nanowires for the detection of paraoxon in tap water and milk. Sensors Actuators B Chem 228:278–286

USEPA (2007) Classification of nanomaterials. The four main types of intentionally produced nanomaterials

Vakil A, Engheta N (2011) Transformation optics using graphene. Science 332(6035):1291–1294

Valera E, Ramon-Azcon J, Sanchez FJ, Mcro MP, Rodriguez A (2008) Conductometric immunosensor for atrazine detection based on antibodies labelled with gold nanoparticles. Sensors Actuators B 134(1):95–103

Varshney M, Li YB (2007) Interdigitated array microelectrode based impedance biosensor coupled with magnetic nanoparticle-antibody conjugates for detection of Escherichia coli O157:H7 in food samples. Biosens Bioelectron 22:2408–2414

Vasilescu A, Nunes G, Hayat A, Latif U, Marty J-L (2016) Electrochemical affinity biosensors based on disposable screen-printed electrodes for detection of food allergens. Sensors (Basel, Switzerland) 16(11):1863

Wan Y, Zhang D, Wang Y, Hou B (2010) A 3D-impedimetric immunosensor based on foam Ni for detection of sulfate-reducing bacteria. Electrochem Commun 12:288–291

Wang Y, Timothy VD (2017) Nanoscale sensors for assuring the safety of food products. Curr Opin Biotechnol 44:74–86

Wang R, Dong W, Ruan C, Kanayeva D, Lassiter K, Tian R, Li Y (2009) TiO2 nanowire bundle microelectrode based impedance immunosensor for rapid and sensitive detection of Listeria monocytogenes. Nano Lett 9:4570–4573

Wang MY, Huang JR, Wang M, Zhang DE, Chen J (2014) Electrochemical nonenzymatic sensor based on CoO decorated reduced graphene oxide for the simultaneous determination of carbofuran and carbaryl in fruits and vegetables. Food Chem 151:191–197

Wang Y, Sun QQ, Zhu LL, Zhang JY, Wang FY, Lu LL, Yu HJ, Xu ZA, Zhang W (2015) Triplex molecular beacons for sensitive recognition of melamine based on abasic-site-containing DNA and fluorescent silver nanoclusters. Chem Commun 51:7958–7961
Wang P, Wan Y, Ali A, Deng S, Su Y, Fan C, Yang S (2016) Aptamer-wrapped gold nanoparticles for the colorimetric detection of omethoate. Sci China Chem 59(2):237–242
WHO (2002) Evaluation of certain mycotoxins in food. Fifty-sixth report of the Joint FAO/WHO Expert Committee on Food Additives. WHO technical report series 906, Geneva, Switzerland.
Williams D (2014) Essential biomaterials science. Cambridge University Press, Cambridge
Wong SK, Lee WO (1997) Survey of organochlorine pesticide residues in milk in Hong Kong (1993–1995). J AOAC Int 80:1332–1335
Woolhouse M, Ward M, van Bunnik B, Farrar J (2015) Antimicrobial resistance in humans, livestock and the wider environment. Philos Trans R Soc B: Biol Sci 370(1670):20140083
Wu BW, Hou LJ, Du M, Zhang TT, Wang ZH, Xue ZH, Lu XQ (2014) A molecularly imprinted electrochemical enzymeless sensor based on functionalized gold nanoparticle decorated carbon nanotubes for methyl-parathion detection. RSC Adv 4:53701–53710
Xiao TT, Shi XZ, Jiao HF, Sun AL, Ding H, Zhang RR, Pan DD, Li DX, Chen J (2016) Selective and sensitive determination of cypermethrin in fish via enzyme-linked immunosorbent assay-like method based on molecularly imprinted artificial antibody-quantum dot optosensing materials. Biosens Bioelectron 75:34–40
Xu F, Cui ZM, Li H, Luo YL (2017) Electrochemical determination of trace pesticide residues based on multiwalled carbon nanotube grafted acryloyloxy ferrocene carboxylates with different spacers. RSC Adv 7(12):7431–7441
Yan X, Li HX, Han XS, Su XG (2015) A ratiometric fluorescent quantum dots based biosensor for organophosphorus pesticides detection by inner-filter effect. Biosens Bioelectron 74:277–283
Yang GJ, Huang JL, Meng WJ, Shen M, Jiao XA (2009) A reusable capacitive immunosensor for detection of *Salmonella* spp. based on grafted ethylene diamine and self-assembled gold nanoparticle monolayers. Anal Chim Acta 647:159–166
Yang T, Huifen H, Fang Z, Qinlu L, Lin Z, Junwen L (2016) Recent progresses in nanobiosensing for food safety analysis. Sensors 16(7):1118
Yuan J, Oliver R, Li J, Lee J, Aguilar M, Wu Y (2007) Sensitivity enhancement of SPR assay of progesterone based on mixed self-assembled monolayers using nanogold particles. Biosens Bioelectron 23(1):144–148
Yuan J, Oliver R, Aguilar MI, Wu Y (2008) Surface plasmon resonance assay for chloramphenicol. Anal Chem 80(21):8329–8333
Zeinhom MMA, Abdel-Latef GK (2014) Public health risk of some milk borne pathogens. Beni-Suef Univ J Basic Appl Sci 3(3):209–215
Zhang H, Li Z, Wang W, Wang C, Liu L (2010) Na+-doped zinc oxide nanofiber membrane for high speed humidity sensor. J Am Ceram Soc 93(1):142–146
Zhang Z, Lin M, Zhang S, Vardhanabhuti B (2013) Detection of aflatoxin M1 in milk by dynamic light scattering coupled with superparamagnetic beads and gold nanoprobes. J Agric Food Chem 61(19):4520–4525
Zhang J, Zhao SQ, Zhang K, Zhou JQ (2014) Cd-doped ZnO quantum dots-based immunoassay for the quantitative determination of bisphenol A. Chemosphere 95:105–110
Zhou J, Xue X, Li Y, Zhang J, Chen F, Wu L, Chen L, Zhao J (2009) Multiresidue determination of tetracycline antibiotics in propolis by using HPLC-UV detection with ultrasonic-assisted extraction and two-step solid phase extraction. Food Chem 115:1074–1080
Zhou WS, Li CH, Sun C, Yang XD (2016) Simultaneously determination of trace Cd2+ and Pb2+ based on L-cysteine/graphene modified glassy carbon electrode. Food Chem 192:351–357
Zhu Y, Murali S, Stoller MD, Ganesh KJ, Cai W, Ferreira PJ, Pirkle A, Wallace RM, Cychosz KA, Thommes M, Su D (2011) Carbon-based supercapacitors produced by activation of graphene. Science 332(6037):1537–1541
Zhu G, Li Y, Zhang C-Y (2014) Simultaneous detection of mercury (ii) and silver (i) ions with picomolar sensitivity. Chem Commun 50:572–574

Chapter 4
Functional Properties of Nanoporous Membranes for the Desalination of Water

Jananisree Ganesan, Madhangi Priyadharshini Gandhi, Maheswari Nagendran, Bin Li, Vaishakh Nair, and Padmanaban Velayudhaperumal Chellam

Contents

4.1 Introduction 132
4.2 Evolution of Desalinating Techniques 133
4.2.1 Multi-effect Distillation 133
4.2.2 Multistage Flash 134
4.2.3 Reverse Osmosis 135
4.2.4 Electrodialysis 136
4.2.5 Carbon Nanotubes 137
4.3 Nanoporous Desalination 138
4.3.1 Process 138
4.3.2 Nanoporous Membranes 138
4.4 Synthesis Methods 139
4.4.1 Focused Electron Beam Induced Etching 139
4.4.2 Diblock Copolymer Templating 140
4.5 Surface Modification 141
4.5.1 Macromolecule Immobilization 141
4.5.2 Surface Adsorption and Coating 142
4.5.3 Surface Treatment 143
4.5.4 Glycosylation by UV-Induced Polymerization 144
4.5.5 Glycosylation by Polymer Analogous Reactions 144
4.5.6 Glycosylation by Surface-Initiated Living Polymerization 144
4.6 Pore Functionalization 145
4.6.1 Chemical Treatment 145
4.6.2 Plasma Treatment 145
4.6.3 Graft Polymerization 146
4.6.4 Copolymer Templating 146

J. Ganesan · M. P. Gandhi · M. Nagendran · P. Velayudhaperumal Chellam (✉)
Centre for Research, Department of Biotechnology, Kamaraj College of Engineering and Technology, Virudhunagar, Tamil Nadu, India

B. Li
Shandong Key Laboratory of Marine Ecology Restoration, Shandong Marine Resource and Environment Research Institute, Yantai, China

V. Nair
Institute of Physical Chemistry, Polish Academy of Sciences, Poznań, Poland

N. Dasgupta et al. (eds.), *Environmental Nanotechnology Volume 4*, Environmental Chemistry for a Sustainable World 32, https://doi.org/10.1007/978-3-030-26668-4_4

4.7 Process Parameters in Desalination System 146
4.8 Nanoporous Zeolite Membranes 147
4.8.1 Mordenite Framework Inverted-Type Zeolite Membranes 148
4.9 Nanoporous Graphene 151
4.9.1 Synthesis of Nanoporous Graphene 152
4.10 Application of Nanofibers in Desalination 153
4.11 Patents on Nanofibers and Nanomembrane 155
4.12 Future Approach 155
4.13 Conclusion 158
References 159

Abstract Desalination provides a possibility of expanding the freshwater reserves by supplementing it with water from oceans and brackish reservoirs. Conventional desalination technologies like reverse osmosis and thermal distillation have failed to meet the expectancy due to high-energy consumption and low salt rejection. Recent research works prove that nanoporous desalination is efficient than conventional technologies due to its high mechanical–chemical stability and higher water flux. Experimental studies along molecular dynamic simulations justify that nanoporous membranes are capable of 100% salt rejection. In addition to nanomembranes, natural and synthetic nanofibers have also emerged as potential nanomaterials for desalination. This review provides a detailed insight on developments and augmentation techniques in the frontier of nanoporous desalination.

Keywords Desalination · Nanoporous desalination · Membrane separation · Molecular dynamics · Nanoporous graphene · Zeolite membrane · Nanofibers · Membrane synthesis · Patents · Commercialization

4.1 Introduction

Fresh water is becoming an increasingly scarce global resource that influences the long-term health and well-being of the nations. Although 70% of the earth's surface is covered with water, 98% of available water resources is saline water (Goh et al. 2013). High concentration of salinity in the seawater makes it unfit for domestic and industrial purposes. The process of desalination holds the promise to expand the freshwater source by supplementing water from various water bodies, mainly seawater (Cohen-Tanugi et al. 2014). The need of fresh water has given rise to a number of desalination techniques like thermal distillation, reverse osmosis, freezing, and electrodialysis (Mishra and Ramaprabhu 2011). Low salt rejection, high-energy consumption, and high costs are the major obstacles in the conventional desalination technologies, which made the researchers look for an alternative technique. *The rapid development of nanoscience and nanotechnology has reduced the scale limits*

of modern technologies along with increase in their efficiency. The science and technology involved in desalination process is undergoing revolution involving the use of nanotechnology with the development of novel nanoporous membranes. The nanoporous membranes hold the key to solve the drawbacks of the conventional techniques. In contrast with classical RO membranes, where water gets transported slowly through a solution–diffusion process, nanoporous membranes can allow fast convective water flow across well-defined channels. Due to its small dimensions, nanoporous membranes are used as filters working on the basis of molecular size separation; small molecules can pass through them, while larger ones cannot. These pores can also make use of other physical principles, such as charge, hydrophobicity to reject ions, or other molecular solutes. This method is characterized as one of the membrane separation techniques that uses an effective separation membrane crafted by creating nanoscale pores in different materials like zeolites, carbon, and silica (Sint et al. 2008; Surwade et al. 2015). The materials used as nanoporous membranes must be chemically and mechanically stable and flexible with thickness ranging in atomic scale (Cohen-Tanugi et al. 2014; Mishra and Ramaprabhu 2011; Sint et al. 2008; Surwade et al. 2015) Theoretical studies show that the performance of such membranes would be superior to state-of-the-art polymer-based filtration membranes, and experimental studies have recently been conducted to explore their potential (Surwade et al. 2015). This review aims to bring out the potential of nanoporous membrane as efficient separation membranes in desalination.

4.2 Evolution of Desalinating Techniques

Several desalinating methods have been designed and experimented for treating seawater to overcome the water shortage. Most widely, commercially proven desalination technologies fall into two categories, thermal- (evaporative) and membrane-based methods. Membrane methods are less energy intensive than thermal methods, and since energy consumption directly affects the cost-effectiveness, the feasibility of using membrane-based methods for desalination technologies has attracted great attention (Fig. 4.1).

4.2.1 Multi-effect Distillation

The multi-effect distillation (MED) process is the oldest technique for seawater desalination that involves consecutive evaporation and condensation (Ophir and Lokiec 2005). The first report on MED dates back to the middle of the nineteenth century (Van der Bruggen and Vandecasteele 2002). The process is carried out through a series of evaporators called effects that works on the principle of

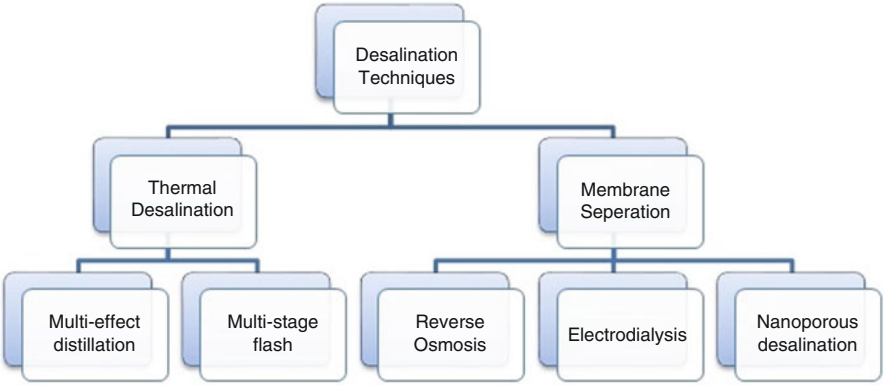

Fig. 4.1 Desalination techniques

decreasing the ambient pressure. Initially, the seawater is fed into the tubes (horizontal or vertical or submerged) and is allowed to undergo repeated boiling without any supplement of additional heat after the first effect where the temperature is raised to its boiling point. It is followed by spraying of seawater that aids in rapid evaporation, and consequently the steam is condensed on the opposite side of the tubes. Only certain quantity of seawater moves into the second effect, the tube bundle. Then these tubes are heated by the vapor produced from the first effect. The process of evaporation and condensation is repeated from one effect to the other based on the conditions of low pressure and temperature (Van der Bruggen and Vandecasteele 2002). In order to increase the performance of MED, heat absorption pumps can be fixed which are used for preheating the tubes. Corrosion and scaling of supersaturated compounds such as $CaSO_2$ and intense contact of steam and brine with the heat exchangers (Van der Bruggen and Vandecasteele 2002) were the major drawbacks of this method. Such problems decrease the performance ratio of MED and limit its use in desalination (Fig. 4.2).

4.2.2 Multistage Flash

Multistage flash (MSF) is a process based on the principle of flash evaporation which came into practice in the early 1960s (Van der Bruggen and Vandecasteele 2002) and became popular due to its reliability and simplicity. The operating system of MSF consists of a series of flash chambers where steam is generated from saline feedwater at a progressively reduced pressure. The generated steam is condensed by heat exchange with a series of closed pipes where the seawater is preheated. The condensate is the desired product with reduced total dissolved salt content which is subjected to further potabilization process. The exhausted brine is recirculated to

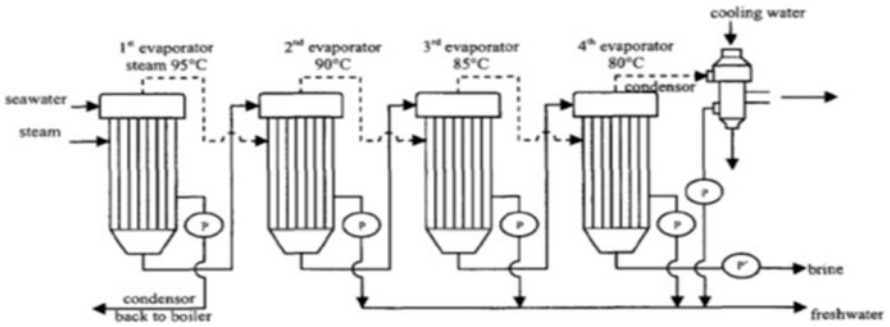

Fig. 4.2 Schematic representation of multi-effect distillation setup (Van der Bruggen and Vandecasteele 2002)

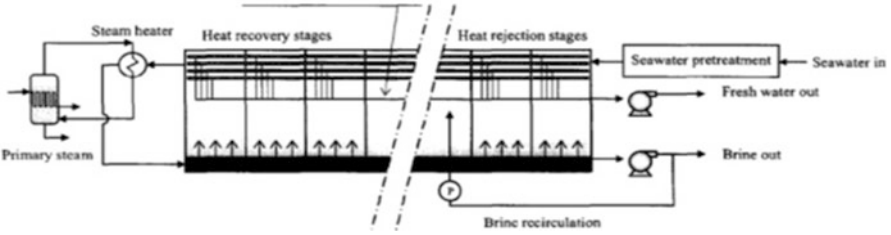

Fig. 4.3 Schematic representation of multistage flash setup (Van der Bruggen and Vandecasteele 2002)

increase the product recovery. The design of MSF was comparatively less complex than MED which contributed in controlling the corrosion, but the lower performance ratio of MSF as well as higher energy consumption made this method undesirable (Othmer 1966; Sadhukhan et al. 1994) (Fig. 4.3).

4.2.3 Reverse Osmosis

Reverse osmosis (RO) is a membrane separation technique in which the seawater is desalinated by passing it through a membrane that restricts the flow of ions present in it. Initially RO was used to desalinate brackish water, which later due to the development of new RO membranes with higher permeability was used for seawater desalination. In the 1980s, RO became a competitive technique with the classical distillation techniques as this method was comparatively less expensive than MED and MSF (Van der Bruggen and Vandecasteele 2002). In the initial step, the feedwater is treated to remove the debris in the seawater and is passed into a cartridge filter where particles with size more than 10 micron are filtered out. Then the treated

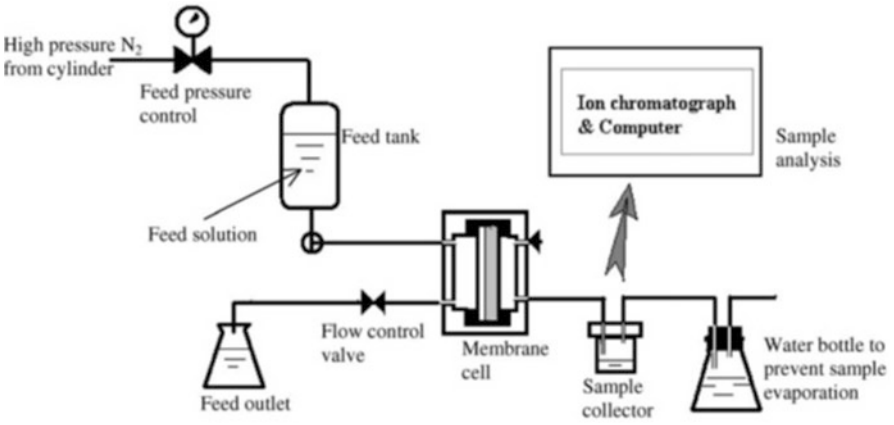

Fig. 4.4 Schematic diagram for desalination of seawater using a reverse osmosis setup (Li et al. 2004)

saline water is forced to permeate through a semipermeable membrane by applying a pressure which is larger than the osmotic pressure of the seawater. In the early days of RO application, the pressure needed for the separation was as high as 120 bar which currently has been reduced to a level around 50 bar. The RO membrane allows the free flow of water but restricts the entry of dissolved salts resulting in the separation of pure water fraction (permeate) from the concentrated fraction (retentate or concentrate) (Wilf and Bartels 2005). The desalinated water that leaves the membrane is subjected to posttreatment where the dissolved gases are removed and pH is adjusted. Fouling of the RO membrane by suspended solids, damage by the presence of oxidizing compounds, organic blooms, and scaling are the major disadvantages of this method which made the researchers look for alternative methods of desalination. However, reverse osmosis remains an important desalination technique even today (Van der Bruggen and Vandecasteele 2002; Othmer 1966; Sadhukhan et al. 1994) (Fig. 4.4).

4.2.4 Electrodialysis

Among the other techniques for seawater or brackish water desalination, electrodialysis (ED) or electrodialysis reversal (EDR) has been characterized as one of the promising techniques of desalination. ED is an electrochemical process for the separation of ions across charged membranes from one solution to another under the influence of an electrical potential difference (Mohammadi and Kaviani 2003). In the method, a stream of saline water is fed into the ED cell setup where the dissolved salts get transported through a stack of cationic and anionic membranes on the application of electric potential, so that a diluted stream is obtained. But this

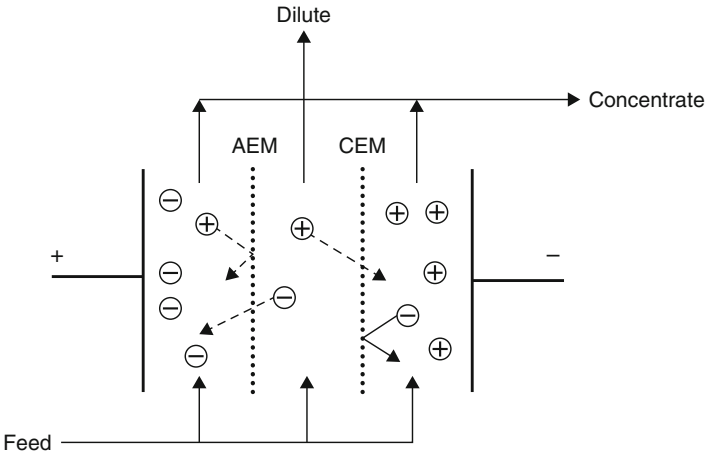

Fig. 4.5 Schematic view of an electrodialysis cell (Sadrzadeh and Mohammadi 2008)

technique is uneconomical for desalination of large salt fractions due to high-energy input (Van der Bruggen and Vandecasteele 2002; Sadrzadeh and Mohammadi 2008; McGovern et al. 2014) (Fig. 4.5).

4.2.5 Carbon Nanotubes

Carbon-based nanomaterials have attracted the attention of scientific community due to their novel properties like large surface area, long range of porosity, good thermal stability, and mechanical strength. Carbon nanotubes (CNTs) have been employed in a range of applications including surface catalysis, power generation, molecular sensing, and desalination due to their unique mechanical, optical, and electrical properties. Simulation studies indicate that single, double, and multi-walled carbon nanotubes of critical pore diameter ~7 Å allow the flow of water molecules but restrict the passage of ions (Corry 2008). Experimental studies shows that, in aligned CNTs, water flows at higher rate and is independent on the length of the nanotubes. The frictionless transport of water through CNTs is facilitated by the weak interaction of the molecules with the hydrophobic walls. Application of external field and chemical modification of CNTs have shown to increase the flow rate. CNTs have also been demonstrated as a useful material for manufacturing electrodes that can be used in the desalination of water using a flow-through capacitor. CNTs are highly efficient against biofouling when compared to polymeric membranes and have a higher salt rejection efficiency which makes them excellent membranes for water filtration (Goh et al. 2013; Tofighy and Mohammadi 2010). However, high cost of CNTs and the difficulty in their synthesis limit their commercial use (Goh et al. 2013; Mishra and Ramaprabhu 2011; Corry 2008) (Fig. 4.6).

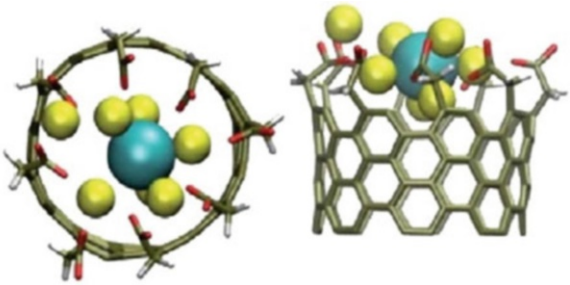

Fig. 4.6 Molecular dynamic simulation illustrating desalination by functionalized CNT (Corry 2011)

The limitations in the above methods stirred the interest among researchers working in the field of desalination to design an alternative and potential method that is capable of complete salt rejection at a lower expense.

4.3 Nanoporous Desalination

4.3.1 Process

Water desalination across nanoporous membranes is based on the elementary concept that salt ions have a larger atomic radius than the actual water molecules (Surwade et al. 2015; Killingsworth 2012). Thus the creation of a hole through which water molecules can pass is the ultimate aim of nanoporous desalination. Using certain principles that are discussed in this review, pores are created in membranes of silica, graphene, and zeolites which allow water molecules to pass through while blocking Na^+ and Cl^- ions which are comparatively larger in size (Sint et al. 2008; Surwade et al. 2015; Xue et al. 2013). The pore diameter is based on the water molecule size which is reported to be 5.5 angstroms (Killingsworth 2012; Cohen-Tanugi and Grossman 2012). Furthermore, research work incorporating functional groups in nanopores has been carried out to maximize the desalination rate (Fig. 4.7).

4.3.2 Nanoporous Membranes

Development of nanoporous membranes has revolutionized the desalination process with superior performance at lower expense. The type of nanoporous membranes used for desalination plays a crucial role in determining the rate of desalination. The nature of the material and the size of the pores are the two basic properties that decide the efficiency of nanoporous desalination (Nicolaï et al. 2014). Nanoporous membranes are developed by the artificial introduction

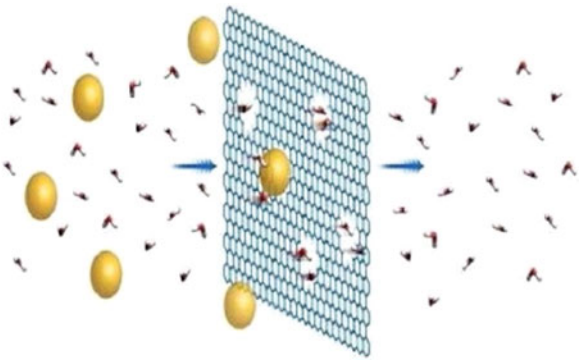

Fig. 4.7 Computational simulation showing the desalination across nanoporous membrane (Wang and Karnik 2012)

of nanosized pores in the synthesized membranes as most of the naturally occurring materials like graphene and MoS_2 are impermeable to water (Surwade et al. 2015; Killingsworth 2012). The ability to adjust pore size in the membrane is a crucial step in nanoporous desalination as a variation of few angstroms in pore size can be the difference between a properly functioning pore and an inefficient one (Killingsworth 2012). Recently, experimental studies have begun to explore a wide variety of methods for introducing nanopores in desalination membranes. Earlier approaches relied on electron beam exposure, but in recent times methods like diblock copolymer templating, helium ion beam drilling, and chemical etching are preferred to achieve both higher porosity and precise pore size distribution (Killingsworth 2012; Chua et al. 2013).

4.4 Synthesis Methods

4.4.1 Focused Electron Beam Induced Etching

In focused electron beam induced etching (FEBIE), a beam of electrons is projected onto the surface of the synthesized membrane. The beam interacts with the pressurized gas on top of the membrane which then bonds with the material's atoms and thus corrodes the surface. FEBIE was considered as a promising tool for the synthesis of nanopores with controlled shape and size (Yemini et al. 2009). The diameter of the pores depends on the pressure of the gas, acceleration voltage (Liebes et al. 2011), and electron beam exposure time (Killingsworth 2012). Pore diameter and peripheral-etched region can be reduced by increasing the applied acceleration voltage (Liebes et al. 2011; Pan et al. 2006). The use of highly focused energetic electron beam as a source makes this method comparably accessible leading to the widespread fabrication of nanopores (Liebes et al. 2011). This technique provides improved lateral resolution at shorter fabrication times when compared to multi-step

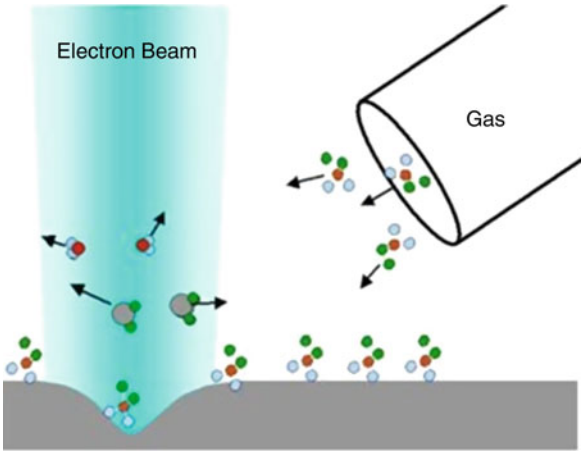

Fig. 4.8 Focused electron beam induced etching (Killingsworth 2012)

chemical, indirect or reactive ion etching-based synthesis techniques (Liebes et al. 2011). However, even though this technique was one of the earlier approaches for the synthesis of nanometer-sized pores, FEBIE is currently not used for wide range of applications because of its inaccuracy in generating uniform-sized pores with functional groups (Fig. 4.8).

4.4.2 Diblock Copolymer Templating

The template method is generally used for synthesizing nanomaterials, especially nanotubes and nanowires (Yu et al. 2003). Diblock copolymer templating is an advanced method to create nanoporous membrane with tunable pore size (Yu et al. 2003), high selectivity, and membrane stability at high pressure (Yang et al. 2008). In this method a suitable template is used in the synthesis of copolymer which is subjected to selective etching (Olson et al. 2007)**.** The pore size and the thickness of the pore in the template membrane can be optimized by this method (Yu et al. 2003). The patterns in the membranes are designed based on its ability to self-assemble into micro-domains, and these patterns can be manipulated by various physical and chemical activations. Inorganic nanoporous membranes like nitrogen-containing mesoporous carbonaceous polymers synthesized using copolymer templating are found to be defect-free which make them suitable for enhanced desalination (McGovern et al. 2014; Yang et al. 2010). Oxygen plasma etching method is done by exposing suspended monolayers to oxygen plasma that causes etching and also allows the size of the pores to be tuned. The intensity of plasma etching is directly proportional to the size and density of pores in the membranes and time of exposure. Maintenance of uniformity is the foremost constraint during the process, and it can be resolved by optimizing the process parameters of the operating system. The resulting membrane exhibits salt rejection rate of nearly 100% with increasing rate

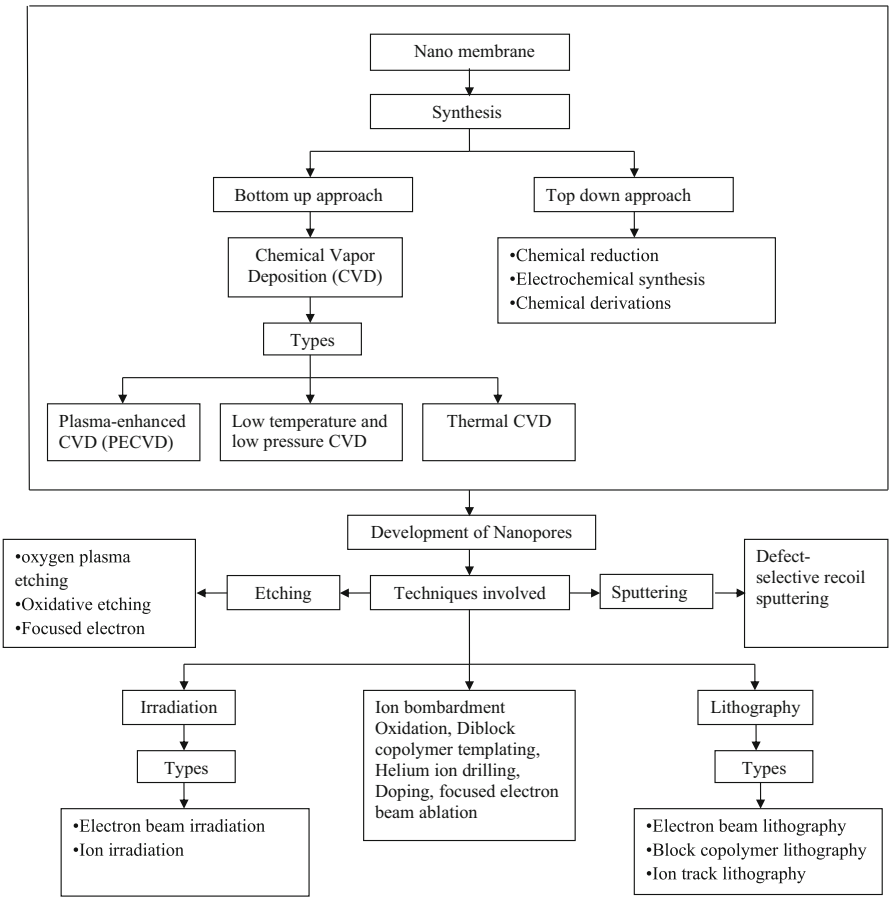

Fig. 4.9 Various methods available for the synthesis of nanoporous membrane

of water flow. There are also several other techniques available for the generation of pores in the membranes which include ion irradiation, electron beam lithography, oxidative etching, electron beam irradiation, and helium ion drilling (Fig. 4.9).

4.5 Surface Modification (Fig. 4.10)

4.5.1 Macromolecule Immobilization

Macromolecule immobilization is a method for introducing a functional layer onto the synthesized membrane surface. The reaction between the macromolecules and the membrane surfaces is classified into three categories as follows: (a) direct reaction between the membrane and the functional groups of the macromolecules,

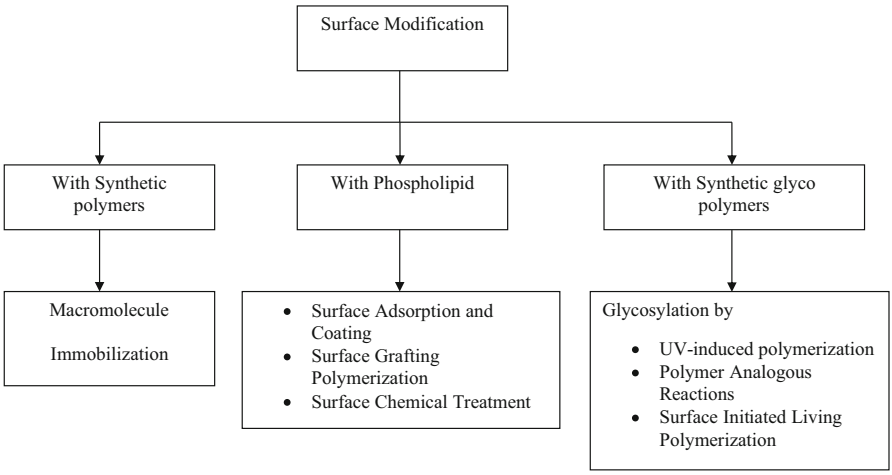

Fig. 4.10 Various methods for the surface modification of nanoporous membrane

(b) membrane functionalization with groups such as amino, carboxyl, and hydroxyl followed by coupling of these groups with the macromolecules, and (c) use of external stimulations such as plasma and UV irradiation which also promote coupling reaction. The method is feasible for the immobilization of macromolecules which are difficult to synthesize artificially, and also it is easy to control the length and structure of the grafted chains (Xu et al. 2009). Limiting flux and antifouling characteristics in a submerged membrane bioreactor (SMBR) for wastewater treatment were improved by the immobilization of poly(N-vinyl-2-pyrrolidone) (PVP) on polypropylene hollow fiber microporous membrane (PPHFMM) through air plasma treatment (Yu et al. 2006). Surface hydrophilicity of asymmetric membranes fabricated from poly(acrylonitrile-co-maleic acid) (PANCMA) was improved by the immobilization of bio-macromolecules such as heparin and/or insulin by the amination of the PANCMA membrane surface with ethylene diamine, followed by the reaction of the amino groups with bio-macromolecules in the presence of 1-ethyl-3-(3-dimethylaminopropyl)carbodiimide (Che et al. 2005).

4.5.2 Surface Adsorption and Coating

Surface adsorption and coating is a physical modification method in which a suitable material is adsorbed or coated on the polymeric membrane directly. The surface of the polymeric membranes can be easily modified with different coating materials to achieve distinct properties while maintaining the substrate properties. The long alkyl chain in the phospholipid increases the hydrophobic interaction with the polymeric membrane and forms a stable film (Xu et al. 2009). Surface modification of the RO membrane by direct coating of nanosilver particles on the membrane sheet and

spacer by chemical reduction showed improved biofouling control in seawater desalination (Yang et al. 2009). In addition, fouling of positively charged nanofiltration membrane can be prevented to some extent by modifying the surface properties such as hydrophilicity, roughness, and charge by adsorbing a layer of water-soluble polymers like dextran and poly(acrylic acid sodium salt) onto the surface in a dynamic manner (Ba et al. 2010).

4.5.3 Surface Treatment

Surface treatments which include techniques like chemical treatment and surface grafting are employed to attain higher desalination rate by utilizing the enhanced properties of surface-modified membranes. Chemical treatment is a covalent binding of phosphorylcholine to the membrane resulting in stable modified surface. The modified membranes exhibited good mechanical property as that of the original membranes, maintained the morphological structure, and showed higher water permeability than the original membranes. The presence of phospholipid side chains also showed high biocompatibility and hydrophilicity (Xu et al. 2009). Dai et al. and Xu et al. proposed an efficient method for attaching phospholipid analogous polymers onto a polypropylene membrane. N,N-dimethylaminoethyl methacrylate (DMAEMA) was photoinduced by graft polymerization onto the membrane surface as ring-opening reagent followed by the ring-opening reaction of grafted poly (DMAEMA) with 2-alkyloxy-2-oxo-1,3,2-dioxaphospholanes (Dai et al. 2004; Xu et al. 2004). Surface grafting polymerization is a chemical tailoring of polymeric membrane with distinct properties while maintaining the substrate properties. Compared with physical coating and adsorption, covalent attachment of phospholipid analogous chain onto polymeric membrane can avoid desorption and maintain a long-term chemical stability. The surface grafting methods include initiator grafting polymerization, photoinduced grafting polymerization, corona irradiation grafting polymerization, and ATRP grafting polymerization (Xu et al. 2009). The hydrophilic character of polyacrylonitrile (PAN) and polysulfone (PSf) ultrafiltration (UF) membranes was improved by graft polymerization of hydrophilic monomers such as 2-hydroxyethyl methacrylate (HEMA) and acrylic or methacrylic acid onto the membrane surfaces by thermal decomposition of peroxides (Ulbricht and Belfort 1996). Polypropylene microfiltration membrane (PPMM) showed improved hydrophilicity after modification by UV photo-assisted and γ-ray pre-irradiation-induced graft polymerization of hydrophilic polymer, poly(N-vinyl-2-pyrrolidone) (Liu et al. 2004).

4.5.4 Glycosylation by UV-Induced Polymerization

Glycosylation of the membrane surface was performed by UV-induced polymerization which results in increased membrane performance. The water flux depends more on surface hydrophilicity than on pore properties as long as the degree of grafting is low. Therefore, during grafting gas flux decreases while the water flux increases (Xu et al. 2009). Antifouling property and hydrophilicity of polyacrylonitrile (PAN) ultrafiltration membrane was improved by grafting a ring-opening glycomonomer d-gluconamidoethyl methacrylate (GAMA) onto the membrane surface by ultraviolet (UV)-initiated grafting polymerization. This resulted in increased flux recovery ratio, indicating that the antifouling of PAN membrane was improved by the glycosylation (Dai et al. 2008).

4.5.5 Glycosylation by Polymer Analogous Reactions

Glycosylation by polymer analogous reaction is a two-step method for the modification of polymer membrane. In polymer analogous reaction, polymers with functional groups were grafted on to the membrane surface, and then the sugars were immobilized on the surface by the reactions between sugar moieties and functional groups. The grafted polymeric chains showed much higher hydrophilicity than in nascent membranes (Xu et al. 2009). Using polymer analogous reaction, acrylamide (AAm) was grafted on the membrane by UV-induced polymerization, and sugars were immobilized by converting amide groups to amine groups by Hofmann rearrangement reaction.

4.5.6 Glycosylation by Surface-Initiated Living Polymerization

Conventional grafting techniques suffer with many disadvantages like lack of control over molecular structure, incapable of further increasing the sugar density, and also glycopolymer chain length may largely affect the recognition activity. In order to overcome the above problems, glycopolymer with a well-defined chain structure and appropriate sugar density was generated which resulted in glycosylated membrane surface with controlled molecular weight and structures. The chain length of the grafted glycopolymer can be controlled by adjusting the polymerization time (Xu et al. 2009). Yang et al. prepared comb-like glycopolymer brushes by grafting poly(2-hydroxyethyl methacrylate) (PHEMA) with hydroxyl groups to the polypropylene microporous membrane surface by UV-induced graft polymerization (Yang et al. 2007).

4.6 Pore Functionalization

Pore functionalization in a nanoporous membrane determines the efficacy of the process by influencing the desalination rate and salt rejection. The type of functional groups (either hydroxyl or hydrogen) used for activation induces the selectivity and determines the orientation of water in the vicinity of the pore which alters the rate of desalination (Sint et al. 2008; Killingsworth 2012; Xue et al. 2013). The principle involved in surface modification techniques served as the base for the development of advanced pore functionalization techniques like chemical treatment, graft polymerization, and copolymer templating which could impart desired characteristics like selectivity by manipulating the pore properties.

4.6.1 Chemical Treatment

Pores of nanoporous membranes can be functionalized by using chemical treatment techniques which include reactions like oxidation, addition, substitution, adsorption, and hydrolysis, respectively. The membrane surface containing pores is exposed to various types of functional groups during the chemical treatment that aids in the manipulation of pore properties. Among these techniques, oxidation plays a dominant role. By implementation of corona discharge and flame treatment methods, oxygen-containing groups like hydroxyl and carboxyl groups are introduced onto the surface of the membrane. This method results in the gain of modified membranes with antifouling property. Jesse et al. reported the functionalization of different metal-organic frameworks by low-pressure hydrogen adsorption to enhance their properties (Rowsell and Yaghi 2006). However chemical treatment is a conventional technique that is now employed as a step in advanced modification processes like copolymer templating for selective functionalization. Ordered mesoporous carbon C-FDU-18 s synthesized by diblock copolymer templating was selectively functionalized by chemical treatment. During oxidative treatment numerous hydrophilic groups are created in the pore channels without destroying the ordered structure of the C-FDU-18 s (Deng et al. 2010). Few research works reported that hydroxylated pores exhibit higher water permeability and hydrogenated pores are more effective in rejection of salt (Killingsworth 2012).

4.6.2 Plasma Treatment

Plasma implantation is a technique in which oxygen or nitrogen groups are attached to the membrane pores by C–C bond breaking to form alcoholic or carbonyl functional groups on its surface. As a result of the functionalization, the wetting properties of the membrane at the pore vicinity can be manipulated to control the

water flux. However, employing this technique limited the range of functional groups that could be attached to the pores. Muller et al. reported that amino functionalization of PVDF microfiltration membranes by direct plasma treatment and plasma pulse technique resulted in modified membranes with improved properties (Müller and Oehr 1999).

4.6.3 Graft Polymerization

Functional groups present on the pore surface are excited upon irradiation of light resulting in the generation of reactive radicals that initiate the grafting process. On using photosensitizer in photochemical grafting, free radicals that generated abstract hydrogen atoms from the base polymer (membrane) form a functionalized pore. Research works state that amino functionalization of PVDF microfiltration membranes by grafting technique was more efficient than plasma modification (Müller and Oehr 1999). Currently grafting technique is being extensively employed in copolymer templating as a functionalization step.

4.6.4 Copolymer Templating

Copolymer templating is one of the most advanced techniques for the synthesis of porous membranes. This technique aids in producing a membrane with uniformly distributed pores of required pore diameter. In addition, this technique also aids in functionalizing the pores. Polymer blocks with patterns containing provision to functionalize the pore region as a result of their ability to self-assemble into microdomains are developed. Further manipulation of these patterns with chemical or physical treatment aids in effective functionalization. Research works have shown that polyethylene oxide (PEO)-functionalized CdSe nanorods were successfully used to functionalize the membrane by assembling the nanorods into the channels and pores of diblock copolymer templates (Zhang et al. 2006). Ryan et al. reported the synthesis of functionalized membrane of PDMA triblock polymer by RAFT (reversible addition–fragmentation chain transfer) polymerization. This membrane was functionalized by converting the PDMA molecules lining the pore into PAA by hydrolysis which enhanced the solute rejection ratio (Mulvenna et al. 2014).

4.7 Process Parameters in Desalination System

Desalination of water through nanopores depends on the physical properties of nanoporous membrane, type of ions in contact with the water molecules, and other process parameters such as pressure, temperature, and water flux. The selective

nature of membrane to allow the movement of water by restricting the passage of ions highly depends on the pore diameter (Cohen-Tanugi and Grossman 2012) which can be easily tuned by various techniques employed during the development of nanopores in single-layer sheets. Movement of ions through nanoporous membrane is also governed by the radius of the ions and charge possessed by the ions and pores. When radii are larger, ions show increased passage rates resulting in the separation of ions from the water molecules (Sint et al. 2008). Nanopores is negatively charged at short oxidation times, whereas at longer oxidation times, the movement of salt is not disturbed, but the transport of large organic molecule is prevented which is an indication of steric size exclusion (O'Hern et al. 2014). During the process, water flux increases linearly with the osmotic pressure of the draw solute resulting in increased rate of salt rejection (O'Hern et al. 2015). Increase in the magnitude of electric field decreases the ion pore binding, but the transport of ions through functionalized nanopores in graphene monolayers is highly selective even in the presence of large electric field due to the existence of coulomb coupling between the ion and the functional groups attached to the polar and charged rim of the nanopores (Sint et al. 2008). Efficacy in mapping and eventual removal of ion shells from water molecules are due to the close contact between the ion and pore rim which leads to the selective removal of ions, as in channel proteins (Sint et al. 2008) in biological membranes. Pore size increases with the increase in temperature, whereas their shape and total porosity remain constant (Santos et al. 2000). An efficient desalination system should maintain constant temperature throughout the process in order to maintain the constant pore size. Movement of water by isothermal evaporation and condensation across the nanopores with pure water on one side and saline water on the other side under a pressure difference across vapor trapping pores results in selective transport of water through the nanopores (Lee and Karnik 2010). Complete removal of ions by nanoporous membrane can be achieved by focusing on the optimization of various process parameters involved in the functioning of the desalination plant (Fig. 4.11).

4.8 Nanoporous Zeolite Membranes

Zeolites are crystalline, hydrated aluminosilicate framework (Breck 1964; Davis 1991; Sklenak et al. 2007) that can act as an excellent absorbent in gas and liquid separation due to their unique surface properties and uniform pore sizes (Kazemimoghadam 2010). As stated in the previous sections, conventional technologies such as polymeric RO membranes are inefficient in desalination due to material instability and membrane fouling (Kazemimoghadam 2010). The need to develop efficient membrane process with superior properties for desalination increased the interest of the researchers and industrial groups toward zeolite membranes since the beginning of the 1980s. From the literatures available on nanoporous zeolite membranes, it has been considered as an economically effective and suitable material for desalination without any substantial pretreatment (Liu and

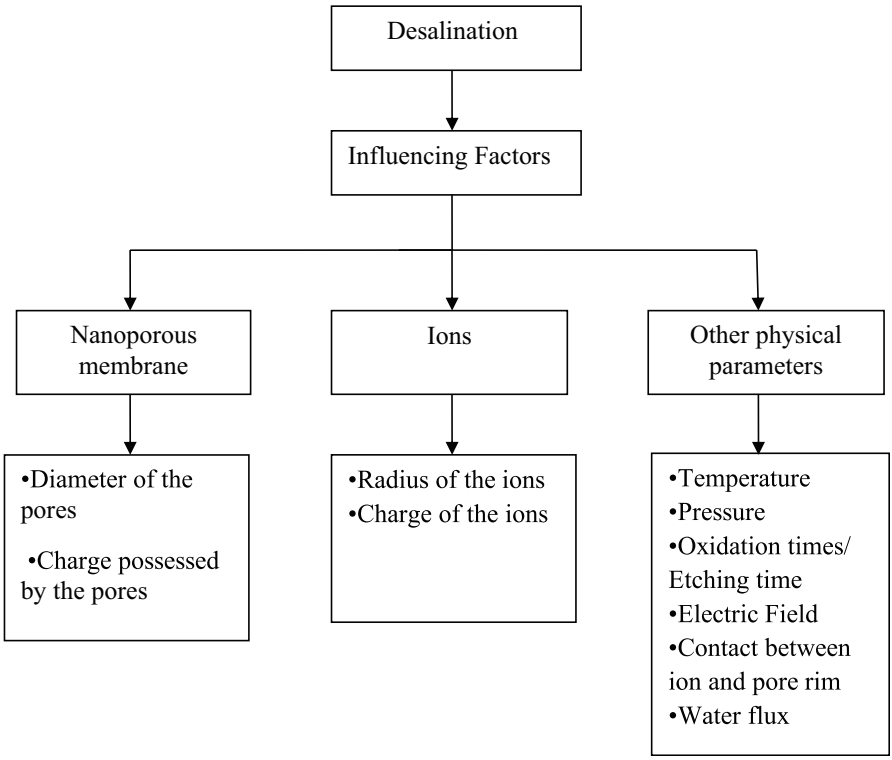

Fig. 4.11 Influencing parameters in desalination system

Chen 2013). These membranes showed much higher fluxes, higher salt rejection rates, and good chemical resistance in desalination system than commercially available polymeric membranes (Mahmoud et al. 2015). Hydrophilic faujasite (FAU) and hydrophobic mordenite framework inverted (MFI) are two types of zeolite membranes that are employed in the reverse osmosis process due to their higher efficiency. The hydrophilic nature of FAU membrane allows it to maintain high water flux through the membrane (Covarrubias et al. 2008).

4.8.1 Mordenite Framework Inverted-Type Zeolite Membranes

Mordenite framework inverted (MFI) membranes are modified zeolite membranes used for effective desalination, as they possess the nanoporous structure required to reject ions. The membrane consists of orthorhombic nearly cylindrical crystal symmetry architecture and ten-membered ring channels with aperture size of approximately 0.56 nm (Zhu et al. 2013a). The ability of MFI-type zeolite membrane

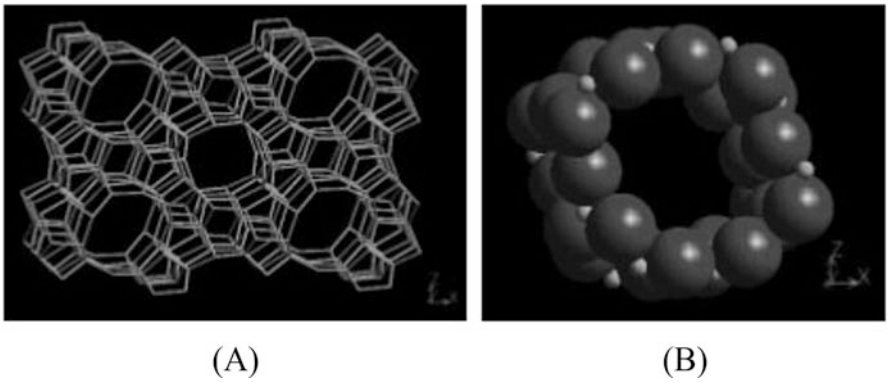

Fig. 4.12 (**a**) Structure of MFI-type zeolite viewed along [010] plane and (**b**) complex of ten rings viewed along [010] plane (Zhu et al. 2013b)

to block the movement of ions is highly efficient because of its smaller aperture size than the size of hydrated ions (Na^+: 0.716 nm, Cl^-: 0.664 nm) but larger than the size of water molecules (0.276 nm) (Zhu et al. 2013a). Structure and the porosity of the zeolite membrane change when subjected to desalination which can be prevented to some extent by incorporating fine techniques available for synthesizing MFI-type zeolite membranes (Fig. 4.12).

MFI-type zeolite membranes are synthesized by various methods like microwave-assisted crystallization (Zhu et al. 2013b), ambient pressure dry-gel conversion (Cai et al. 2010; Naik et al. 2003), chemical vapor-phase method (Kazemimoghadam and Mohammadi 2007), spray seed coating (Kazemimoghadam and Mohammadi 2007), and hydrothermal crystallization, which is further classified as direct in situ hydrothermal crystallization and secondary (seeded) growth hydrothermal crystallization (Zhu et al. 2013b). Irrespective of the method, synthesis of membrane is carried out in the presence of an inorganic porous support (Geus et al. 1992; Caro et al. 2000) whose nature and structure may affect the quality of the zeolite membrane (Kazemimoghadam and Mohammadi 2007). Ceramic materials (alumina, zirconia, titania), metals (stainless steel), and other porous materials (carbon) are used as supports for the preparation of zeolite membrane coatings (Zhu et al. 2013b). Of which, alumina is the most widely used support for the synthesis of zeolite membranes (Zhu et al. 2013b). Optimization of sorption uptake and species selectivity by the membrane is achieved through the modification of Si/Al ratio during the synthesis (Zhu et al. 2014). The properties such as surface charge and surface hydrophobicity which significantly affect the diffusion of electrolytes can be altered by increasing the concentration of alumina (Zhu et al. 2014). As discussed earlier, water flux plays a critical role in desalination system. Al-rich MFI-type zeolite (ZSM-5) membranes deliver higher water fluxes when compared with pure silica (silicalite 1) (Zhu et al. 2014). Among various techniques, porous-supported zeolite membranes are mostly synthesized by direct in situ crystallization method (Zhu et al. 2013b). Besides these methods dry-gel conversion has also

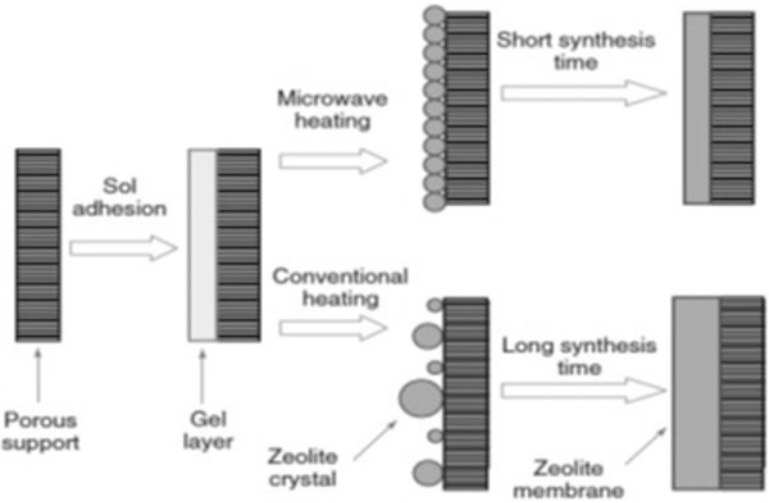

Fig. 4.13 Synthesis of zeolite membrane by microwave heating and conventional heating (Zhu et al. 2013b; Li and Yang 2008)

gained research interest for the synthesis of various composites of zeolites with aluminophosphates and aluminosilicates (Cai et al. 2010). In recent decades microwave-assisted synthesis is used as it is efficient in controlling the distribution of particle size, macroscopic morphology, and phase selectivity (Zhu et al. 2013b). Zeolite membranes with different morphology, orientation, composition, and permeation characteristics can also be synthesized using microwave heating (Zhu et al. 2013b). Augmentation of synthetic methods by coupling microwave heating along with hydrothermal method is one of the promising research areas for the preparation of modified zeolite membranes (Fig. 4.13).

The process of desalination of water involves the monitoring and controlling of certain process parameters such as water flux, osmotic pressure, effective pressure, and ion rejection. Water flux (F) and ion rejection (R) are given by the formulas (Li et al. 2004):

$$F = \frac{Q_w}{A_m \Delta t}$$

$$R = \frac{(C_s)_{\text{feed}} - (C_r)_{\text{perm}}}{(C_s)_{\text{feed}}} \times 100\%$$

where $(C_s)_{\text{feed}}$ and $(C_s)_{\text{perm}}$ are the cation concentrations of feed and permeate solutions, Q_W is the quantity of water collected in time period Δt, and A_m is the effective membrane area (Li et al. 2004).

The rate of desalination is influenced by the process parameters such as water flux, ion rejection, osmotic pressure, and effective pressure. The osmotic pressure

and the effective pressure for different concentrations of NaCl solutions are given by the formulas (Zhu et al. 2013a):

$$\pi = iMRT$$
$$P_{\text{effective}} = P_{\text{total}} - \left(\pi_{\text{feed}} - \pi_{\text{permeate}}\right)$$

where π is the osmotic pressure (atm), i is the dimensionless van't Hoff factor (for NaCl, $i = 1.8$), M is the molarity of the salt in solution, R is the ideal gas constant (0.0821 $\text{L}\cdot\text{atm}\cdot\text{K}^{-1}\cdot\text{mol}^{-1}$), and T is temperature (K). $p_{\text{effective}}$ is the effective pressure (MPa), p_{total} is the applied gauge pressure (MPa), and π_{feed} and π_{permeate} are the osmotic pressures (MPa) for feed and permeate solutions, respectively (Zhu et al. 2013a).

4.9 Nanoporous Graphene

Graphene, sp2-bonded allotropes of carbon (!!! INVALID CITATION !!!), is an ultimately thin single-layered membrane. It acts as a molecular and ionic sieve due to its high selectivity (Mahmoud et al. 2015; D-e et al. 2009), permeability (O'Hern et al. 2012), and transparency (Sint et al. 2008) for both gas-phase and liquid-phase separation processes (O'Hern et al. 2014). Unique and fascinating properties of graphene such as negligible thickness and high mechanical strength make graphene membranes more suitable for purification process than RO membranes (Cohen-Tanugi and Grossman 2012). The material is stated to have high water flux at low pressure. By introducing functionalized pores in the graphene sheets, it would act as a selective filter in desalination system (Konatham et al. 2013; Zhao et al. 2013). Graphene membrane also mimics the function of ion channels by governing the movement of various ions such as Li^+, K^+, Na^+, F^-, Cl^-, and Br^-(Sint et al. 2008) through the nanopores. As previously mentioned, the size of nanopores which significantly influences the performance of the membrane can be easily controlled by employing various techniques available to achieve precise pore size distribution in single-layered graphene lattice (Cohen-Tanugi and Grossman 2012; O'Hern et al. 2014). The resulting nanoporous graphene sheets play a crucial role in the desalination system and are potentially advantageous than other membranes. Experimental studies shows that the usage of CNTs is restricted due to low salt rejection rates (Cohen-Tanugi and Grossman 2012), movement of hydrated ions across the membrane (Sint et al. 2008), and the design of highly aligned denser CNT arrays (Cohen-Tanugi and Grossman 2012). On the contrary zeolites are having relatively low water flux across zeolite membranes due to its complex pore design (Zhu et al. 2013c). Various methods available for the synthesis of nanoporous graphene are elaborately discussed below (Fig. 4.14).

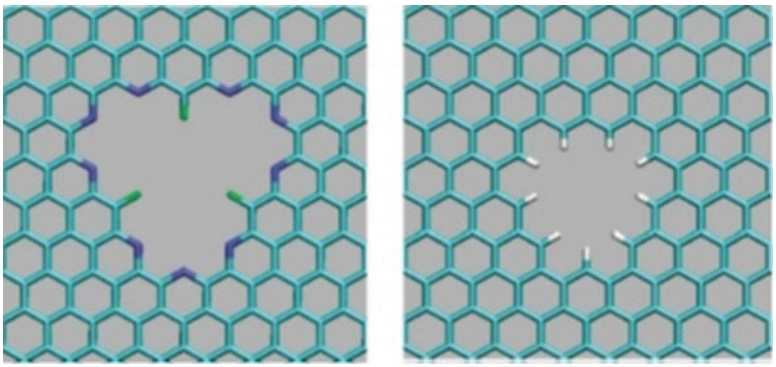

Fig. 4.14 Functionalized graphene nanopores. (**a**) The F-N-terminated nanopore. (**b**) The H-terminated nanopores (Sint et al. 2008)

4.9.1 Synthesis of Nanoporous Graphene

Synthesis of thin-layer nanoporous graphene involves two steps. The first step involves the fabrication of two-dimensional monolayer graphene sheet followed by the development of precise nanometer-sized pores in it. Thin-layer graphene sheets can be synthesized by bottom–up approach like chemical reduction or top–down approach which includes chemical vapor deposition (CVD) and electrochemical synthesis. Nanosized pores are introduced on the graphene sheet by various techniques mentioned in previous sections where the size of the pore is too large to allow the flow of water but too small to block the movement of ions through the pores. Nucleation of isolated and reactive defects in graphene synthesized on copper substrate by low-pressure CVD is performed through ion bombardment followed by oxidative etching which allows the nucleated sites to grow into permeable pores while retaining the structural integrity (O'Hern et al. 2014). Though CVD of graphene is one of the preferable methods, it causes some intrinsic defects during the deposition of graphene on copper and large cuts of size ranging from 100 nm to 200 nm during graphene transfer. In order to achieve selective blocking of defective sites, two-scale multi-step sealing procedure is followed. Intrinsic defects are sealed by the process called atomic layer deposition (ALD), and large defects are sealed by interfacial polymerization reaction (O'Hern et al. 2015). In the preparation of nanoporous graphene, creation of controlled and stable nanometer-sized pores is technically challenging. In recent years creation of nanopores by etching has gained immense interest among the researchers. The potential advantage of oxidative etching technique is that the pore density and its size can be stabilized by optimizing the etch time, which results in selective transport of ions (O'Hern et al. 2014). Charged nanopores formed by ion etching are highly selective in allowing the movement of ions through the pores (Sint et al. 2008). In focused electron beam

induced etching, corroded surface of graphene is obtained by the interaction of electron beam with pressured gas on the graphene layer which results in the growth of nanopores (Killingsworth 2012). By various etching techniques, controlled and stabilized nanopores with high selectivity can be developed on the graphene membrane, but extremely precise-sized pores cannot be obtained through this process. Highly accurate methods like helium ion beam drilling and diblock copolymer templating (Killingsworth 2012) need to be investigated to achieve precise-sized nanopores. Nanoporous graphene membrane with high-density pores contains only uniform-sized nanopores with high salt rejection rate (O'Hern et al. 2015). Nanometer-sized pores can be introduced on graphene sheets by focused electron beam irradiation (Huang et al. 2015). However, this method is inefficient and not suitable for fabricating high-density porous graphene for practical application (Huang et al. 2015). Selection of nanoporous graphene synthesis technique must be based on influencing parameters in order to manufacture thin-layer graphene membrane with size-controlled, high-density pores. Though graphene membrane is efficient and suitable for desalination than other membranes, it has some limitations like creation of size-tunable nanopores in membrane with narrow size distribution and development of a continuous process for its synthesis. Future research works focusing on these obstacles and resolving those uplift the utilization of graphene in desalination process and make it a cost-effective nanoporous membrane.

4.10 Application of Nanofibers in Desalination

Nanofibers are one-dimensional nanomaterial with a diameter of 100 nanometers or less. Nanofibers have been widely used in research and commercial applications due to their outstanding physicochemical properties and characteristics. Among different nanomaterials with promising potential applications, nanofibers stand out from the rest of the materials. Most unique features of nanofibers include high surface-area-to-volume ratio and high porosity, making them robust and attractive material for advanced applications (Lim 2017). In recent decades nanofibers serve as attractive material for various environmental applications including liquid filtration and particulate separation in water treatment (Lim 2017). Nanofibrous structures are used as a filtration material which results in better particulate removal capacity, high separation flux, and lower operational energy (Lim 2017). One of the environmental friendly and cost-effective techniques for removing salt ions from saline water is capacitive deionization which works based on the principles of an electric double-layer capacitor. Hollow carbon nanofibers are used as an effective electrode for brackish water desalination using capacitive deionization process (El-Deen et al. 2014). The specific capacitance of hollow carbon nanofiber is four times greater compared to the specific capacitance of solid carbon nanofibers. Moreover, the surface area of the hollow nanofiber is ten times higher than the solid carbon nanofibers which results in enhanced salt rejection (El-Deen et al. 2014). In addition to hollow nanofibers, nanofiber membrane tailored with carbon nanotubes also

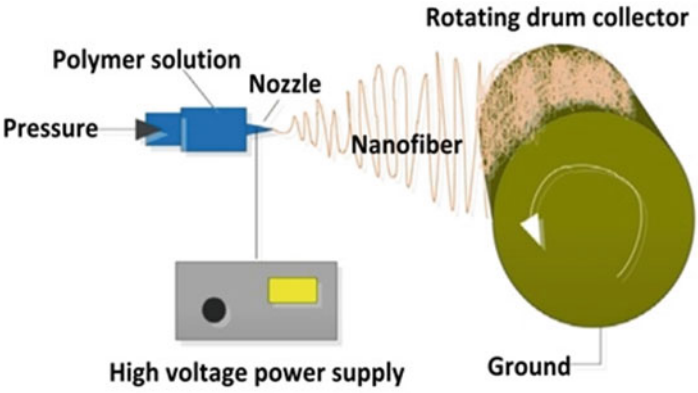

Fig. 4.15 Schematic illustration of the electrospinning setup (Tijing et al. 2016)

demonstrates tremendous potential for direct contact membrane distillation desalination application (Tijing et al. 2016). Carbon nanotubes are used as nanofillers in nanofiber membrane to exhibit additional mechanical and hydrophobic properties (Tijing et al. 2016). Different strategies have been developed for the synthesis of nanofibers, ranging from current methods including self-assembly, polymerization, electrospinning, and template-based synthesis to emerging techniques like electrohydrodynamic writing, solution blow spinning, and centrifugal jet spinning (Lim 2017). Of all current strategies, electrospinning is widely employed for synthesizing one-dimensional nanofiber (Huang et al. 2004). Several variations in conventional electrospinning technique have been employed in order to enhance the productivity. Such variations resulted in needleless, multineedle, and coaxial electrospinning techniques. The needleless and multineedle electrospinning techniques are generally used to increase the productivity of conventional electrospinning. In coaxial electrospinning core–shell and multilayer composite nanofibrous structures with additional functionalities and improved quality can be synthesized (Jiang and Qin 2014) (Fig. 4.15).

In addition to the electrospinning technique, nanofibers are also synthesized using self-assembly technique in solution. The spontaneous and ordered organization of individual macromolecules results in the nanofibers with stable nanoscale supramolecular structures. The nanofibers synthesized using self-assembly have much smaller diameter when compared to the electrospun nanofibers. Though there are various advantages in self-assembly technique, it is a complex and low-throughput method which requires elaborate setup (Lim 2017). In recent years sonochemical method (Casado et al. 2014) and polymerization and template-based synthesis have been used for the synthesis on nanofibers (Bhowmick et al. 2014; Liao et al. 2013).

Various companies like Ad-Nano Technologies, Envision Scientific, E-Spin Nanotech, Nilima Nanotechnologies, and Reinste Nano Ventures operate based on nanotechnology to meet a wide range of applications in India. Out of all these companies in India, E-Spin Nanotech Pvt. Ltd. is the leading company which has

been incorporating translational nanotechnological approaches in the development of the process and products that have been provided to the customers. This company works in the manufacturing of high-quality and cost-effective multifunctional nanofibers that address various needs and issues prevailing in the society. The nanofibers are manufactured by conventional electrospinning methods and reengineered by E-Spin Nanotech that has a series of advanced electrospinning units. Such electrospinning units have been specifically designed to meet the needs of the research organizations and industries. These nanofibers are of several value-added applications such as filtration, automotive, and health care which are also used in various other commercial purposes. Nanofibers play an important role in the application of liquid filtration, where the filter media are composed of highly chemical-resistant nanofibers that are produced from various polymers of geometrically different structures ranging from non-woven web to bulk structures. These nanofibers are either synthetic or biopolymers with which the multiple layers of the filter media are designed to result in a superior filtration performance.

Further the collaboration of this company with the Center for Excellence in Produced Water Management (CEPWM) at the University of Wyoming to develop new membrane material using a combination of nanocomposite and electrospun fiber technology is to be used in nonpressure-driven membrane application. These next-generation membranes will be used to produce clean water from saline water (desalination process) with minimal energy and investments.

4.11 Patents on Nanofibers and Nanomembrane

Patent statistics has been used as an indicator for the economic growth associated to a particular technology or product, its market reach, rate of technological change, and the competitive position among other related technologies. From the statistical data, we can observe that there has been wide range of patents filled on nanomembranes and nanofibers by several industries over the last decade indicating its wide market reach. In recent times several nanomembrane and nanofibers with advanced separation properties like corrosion resistance, selective functionalization, and flux control have been synthesized and patented, indicating the constant enhancement of nano-based separation technologies to fabricate a state-of-the-art separation technique that could address the existing drawbacks (Table 4.1).

4.12 Future Approach

Nanoporous desalination has been characterized as one of the most efficient membrane separation technologies based on computational simulations. Despite the computational simulation results, the real-world implementation of this method requires further research works that modify the technology to withstand the practical

Table 4.1 List of patents on nanomembranes and nanofibers

S. no.	Patent number	Title	Description
Nanomembranes			
1.	KR20170112587 (A)	Acid resistant improved Nanomembrane and manufacturing method thereof	It relates to the method of manufacturing a nanofiber separator having improved acid and temperature resistance
2.	KR101747028 (B1)	Flow rate improved acid-resistant Nanomembrane and manufacturing method thereof	This patent is on acid-resistant nanoseparator exhibiting excellent performance with improved flow rate and corrosion resistance and its novel manufacturing method
3.	RU2418621 (C1)	Method of producing Nanomembrane filters	This patent relates to the process of producing nanomembrane filters of larger area, higher selectivity, and mechanical strength and resistance to higher temperature and chemicals. These nanomembrane filters can be used as superfine fluid and gas cleaning filters or for selective filtration of definite size atoms
4.	WO2017072272 (A1)	Method for manufacturing of a carbon Nanomembrane	This patent proposes a method for the fabrication of carbon nanomembrane by cross-linking monolayers of aromatic molecules with excellent filtration properties
5	US2016151747 (A1)	Porous Nanomembranes	It explains the method of preparing an isolated polymeric nanomembrane comprising pores of different geometric shapes and of controlled size ranging between 10 and 1000 nm, which is larger than the thickness of the membrane
Nanofibers			
6.	CN206873210 (U)	Nanofiber filtration paper	The utility model relates to a nanofiber filtration paper, made of layers of ceramic fiber, bamboo, charcoal, and glass fiber loaded with silver. This structure shows good mechanical strength and filtration with antibacterial properties
7.	CN206881302 (U)	Static spins Nanofiber filter membrane	The utility model relates to a static spin nanofiber filter membrane made of coarse filtering layer, a nanofiber filter

(continued)

Table 4.1 (continued)

S. no.	Patent number	Title	Description
			layer, and PVDF electricity spin fibers. This structure exhibits multistage filtration effect with high strainability
8.	CN107596791 (A)	Composite Nanofiber filter material with Photocatalytic function and preparation method thereof	The filter material consists of a support layer with a nanofiber filter layer attached to its surface, and the nanofiber layer is uniformly filled with photocatalyst. The composite nanofiber filter material with photocatalytic function provided by the invention effectively solves the blocking problem of existing electrospinning needle–nozzle liquid dichargents; has good photocatalytic efficiency on formaldehyde, amine, and toluene; and also exhibits excellent filtration
9.	CN107158969 (A)	Functional Nanofiber filtering material and preparation method and application thereof	This patent deals with the production of functional nanofiber filtering material by processing a polymer spinning solution on a substrate by the electrospinning technique. This functional nanofiber filtering material can be well used in the filtration of organic pollutants, and it exhibits high efficiency with low resistance when being used as an air filtration material. It can greatly improve the air quality
10.	CN107158962 (A)	Preparation method for Nanofiber porous membrane for carrying high-activity Nanometal particles	The invention discloses a preparation method of a nanofiber porous membrane for carrying high-activity nanometal particles by plasma treatment. The nanofiber porous membrane obtained by this preparation method is flexible and therefore is easy to process, and membrane activity gets greatly increased. In addition, the morphology and the size of nanometal particles can be controlled. The synthesized

(continued)

Table 4.1 (continued)

S. no.	Patent number	Title	Description
			membrane has potential application in fields such as filtration, catalysis, bacteria resistance, and surface-enhanced Raman

difficulties that would affect the process potential. The major problem in commercializing nanoporous desalination is the synthesis of nanoporous membranes with perfect pore size and distribution while maintaining its structural integrity. Increasing number of pores and improper pore distribution restrain the mechanical stability of the membrane and prevail as problems which need to be addressed by carrying out extensive research. Recent techniques like oxygen plasma etching and copolymer templating are stated to be highly capable in piercing precisely positioned high-density nanopores in membranes which would help in increasing the efficiency of this technique. For a decade, research works focusing on synthesizing membranes with functionalized nanopores with novel components that enhance both salt rejection and flow rate are major areas of interest in the domain of nanoporous desalination. Future works aim to design membranes that continuously remove the salt that concentrates on the feedside at high permeation rate which prevents membrane fouling. On a practical perspective, we should also consider that the presence of organic and inorganic contaminants in seawater may hinder the efficiency of process. Thus the modification of membrane composition and pore size can assist in preventing membrane incapacitation due to contaminants and may also aid in their removal (Fig. 4.16).

4.13 Conclusion

This review gives a detailed insight on nanoporous desalination which is one of the efficient technologies, showing desalination over 99% based on computational simulation. This paper provides a comprehensive elucidation of the evolution of desalination technologies, advanced synthesis methods involved in the generation of nanoporous membranes, and parameters that influence the efficiency of nanoporous desalination. Membranes perforated with nanometer-sized pores serve as potentially efficient separation membranes than other conventional technologies due to their higher mechanical and chemical stability and higher water flux. Currently, research works focus on enhancing the characteristic nature of the membrane in order to achieve high selectivity meanwhile maintaining equivalent productivity and preserving the performance. Despite the computational simulation results, the real-world implementation of this method requires further research works that modify the technology to withstand the practical difficulties that would affect the process potential. Future works focusing on extending the potential of this method to treat

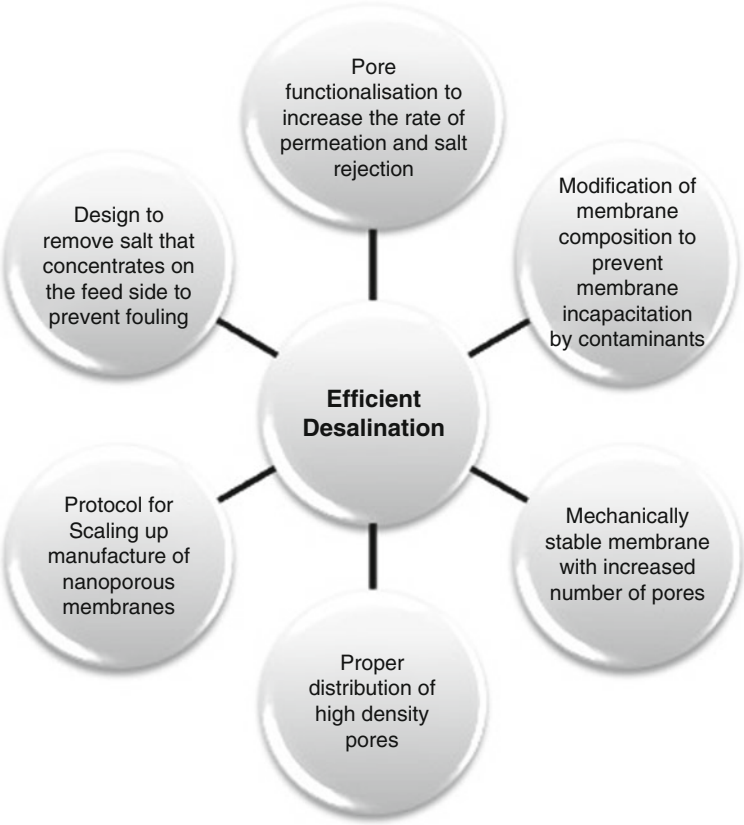

Fig. 4.16 Future perspectives in various domains of desalination technology

polluted water would assist in commercializing an integrated water treatment method.

Acknowledgments The authors are grateful to Prof. Anant Achary, Department of Biotechnology, Kamaraj College of Engineering and Technology, India, for his motivation and support for this contribution to the scientific community.

No Conflict Exists The authors declare that they have no conflict of interest.

References

Ba C, Ladner DA, Economy J (2010) Using polyelectrolyte coatings to improve fouling resistance of a positively charged nanofiltration membrane. J Membr Sci 347(1):250–259

Bhowmick B, Mollick M, Masud R, Mondal D, Maity D, Bain MK, Bera NK, Rana D, Chattopadhyay S, Chakraborty M (2014) Poloxamer and gelatin gel guided polyaniline nanofibers: synthesis and characterization. Polym Int 63(8):1505–1512

Breck DW (1964) Crystalline zeolite Y. Google Patents

Cai R, Liu Y, Gu S, Yan Y (2010) Ambient pressure dry-gel conversion method for zeolite MFI synthesis using ionic liquid and microwave heating. J Am Chem Soc 132(37):12776–12777

Caro J, Noack M, Kölsch P, Schäfer R (2000) Zeolite membranes–state of their development and perspective. Microporous Mesoporous Mater 38(1):3–24

Casado U, Aranguren M, Marcovich N (2014) Preparation and characterization of conductive nanostructured particles based on polyaniline and cellulose nanofibers. Ultrason Sonochem 21(5):1641–1648

Che A-F, Nie F-Q, Huang X-D, Xu Z-K, Yao K (2005) Acrylonitrile-based copolymer membranes containing reactive groups: surface modification by the immobilization of biomacromolecules. Polymer 46(24):11060–11065

Chua YT, Lin CXC, Kleitz F, Zhao XS, Smart S (2013) Nanoporous organosilica membrane for water desalination. Chem Commun 49(40):4534–4536

Cohen-Tanugi D, Grossman JC (2012) Water desalination across nanoporous graphene. Nano Lett 12(7):3602–3608

Cohen-Tanugi D, McGovern RK, Dave SH, Lienhard JH, Grossman JC (2014) Quantifying the potential of ultra-permeable membranes for water desalination. Energy Environ Sci 7(3):1134–1141

Corry B (2008) Designing carbon nanotube membranes for efficient water desalination. J Phys Chem B 112(5):1427–1434

Corry B (2011) Water and ion transport through functionalised carbon nanotubes: implications for desalination technology. Energy Environ Sci 4(3):751–759

Covarrubias C, Garcia R, Arriagada R, Yanez J, Ramanan H, Lai Z, Tsapatsis M (2008) Removal of trivalent chromium contaminant from aqueous media using FAU-type zeolite membranes. J Membr Sci 312(1):163–173

Dai QW, Xu ZK, Wu J (2004) A novel approach for the surface modification of polymeric membrane with phospholipid polymer. Chin Chem Lett 15(8):993–996

Dai Z-W, Wan L-S, Xu Z-K (2008) Surface glycosylation of polyacrylonitrile ultrafiltration membrane to improve its anti-fouling performance. J Membr Sci 325(1):479–485

Davis ME (1991) Zeolites and molecular sieves: not just ordinary catalysts. Ind Eng Chem Res 30(8):1675–1683

Deng Y, Cai Y, Sun Z, Gu D, Wei J, Li W, Guo X, Yang J, Zhao D (2010) Controlled synthesis and functionalization of ordered large-pore mesoporous carbons. Adv Funct Mater 20(21):3658–3665

El-Deen AG, Barakat NA, Khalil KA, Kim HY (2014) Hollow carbon nanofibers as an effective electrode for brackish water desalination using the capacitive deionization process. New J Chem 38(1):198–205

Geus ER, Den Exter MJ, van Bekkum H (1992) Synthesis and characterization of zeolite (MFI) membranes on porous ceramic supports. J Chem Soc Faraday Trans 88(20):3101–3109

Goh PS, Ismail AF, Ng BC (2013) Carbon nanotubes for desalination: performance evaluation and current hurdles. Desalination 308:2–14

Huang Z-M, Zhang Y, Ramakrishna S, Lim C (2004) Electrospinning and mechanical characterization of gelatin nanofibers. Polymer 45(15):5361–5368

Huang L, Zhang M, Li C, Shi G (2015) Graphene-based membranes for molecular separation. J Phys Chem Lett 6(14):2806–2815

Jiang G, Qin X (2014) An improved free surface electrospinning for high throughput manufacturing of core–shell nanofibers. Mater Lett 128:259–262

Jiang D-e, Cooper VR, Dai S (2009) Porous graphene as the ultimate membrane for gas separation. Nano Lett 9(12):4019–4024

Kazemimoghadam M (2010) New nanopore zeolite membranes for water treatment. Desalination 251(1):176–180
Kazemimoghadam M, Mohammadi T (2007) Synthesis of MFI zeolite membranes for water desalination. Desalination 206(1):547–553
Killingsworth B (2012) Water desalination across nanoporous graphene
Konatham D, Yu J, Ho TA, Striolo A (2013) Simulation insights for graphene-based water desalination membranes. Langmuir 29(38):11884–11897
Lee J, Karnik R (2010) Desalination of water by vapor-phase transport through hydrophobic nanopores. J Appl Phys 108(4):044315
Li Y, Yang W (2008) Microwave synthesis of zeolite membranes: a review. J Membr Sci 316(1):3–17
Li L, Dong J, Nenoff TM, Lee R (2004) Desalination by reverse osmosis using MFI zeolite membranes. J Membr Sci 243(1):401–404
Liao Y, Yu D-G, Wang X, Chain W, Li X-G, Hoek EM, Kaner RB (2013) Carbon nanotube-templated polyaniline nanofibers: synthesis, flash welding and ultrafiltration membranes. Nanoscale 5(9):3856–3862
Liebes Y, Hadad B, Ashkenasy N (2011) Effects of electrons on the shape of nanopores prepared by focused electron beam induced etching. Nanotechnology 22(28):285303
Lim CT (2017) Nanofiber technology: current status and emerging developments. Prog Polym Sci 70:1–17
Liu Y, Chen X (2013) High permeability and salt rejection reverse osmosis by a zeolite nano-membrane. Phys Chem Chem Phys 15(18):6817–6824
Liu Z-M, Xu Z-K, Wang J-Q, Wu J, Fu J-J (2004) Surface modification of polypropylene microfiltration membranes by graft polymerization of N-vinyl-2-pyrrolidone. Eur Polym J 40(9):2077–2087. https://doi.org/10.1016/j.eurpolymj.2004.05.020
Mahmoud KA, Mansoor B, Mansour A, Khraisheh M (2015) Functional graphene nanosheets: the next generation membranes for water desalination. Desalination 356:208–225
McGovern RK, Weiner AM, Sun L, Chambers CG, Zubair SM (2014) On the cost of electrodialysis for the desalination of high salinity feeds. Appl Energy 136:649–661
Mishra AK, Ramaprabhu S (2011) Functionalized graphene sheets for arsenic removal and desalination of sea water. Desalination 282:39–45
Mohammadi T, Kaviani A (2003) Water shortage and seawater desalination by electrodialysis. Desalination 158(1):267–270
Müller M, Oehr C (1999) Plasma aminofunctionalisation of PVDF microfiltration membranes: comparison of the in plasma modifications with a grafting method using ESCA and an amino-selective fluorescent probe. Surf Coat Technol 116–119:802–807. https://doi.org/10.1016/S0257-8972(99)00268-6
Mulvenna RA, Weidman JL, Jing B, Pople JA, Zhu Y, Boudouris BW, Phillip WA (2014) Tunable nanoporous membranes with chemically-tailored pore walls from triblock polymer templates. J Membr Sci 470:246–256. https://doi.org/10.1016/j.memsci.2014.07.021
Naik SP, Chiang AS, Thompson R (2003) Synthesis of zeolitic mesoporous materials by dry gel conversion under controlled humidity. J Phys Chem B 107(29):7006–7014
Nicolaï A, Sumpter BG, Meunier V (2014) Tunable water desalination across graphene oxide framework membranes. Phys Chem Chem Phys 16(18):8646–8654
O'Hern SC, Stewart CA, Boutilier MS, Idrobo J-C, Bhaviripudi S, Das SK, Kong J, Laoui T, Atieh M, Karnik R (2012) Selective molecular transport through intrinsic defects in a single layer of CVD graphene. ACS Nano 6(11):10130–10138
O'Hern SC, Boutilier MS, Idrobo J-C, Song Y, Kong J, Laoui T, Atieh M, Karnik R (2014) Selective ionic transport through tunable subnanometer pores in single-layer graphene membranes. Nano Lett 14(3):1234–1241
O'Hern SC, Jang D, Bose S, Idrobo J-C, Song Y, Laoui T, Kong J, Karnik R (2015) Nanofiltration across defect-sealed nanoporous monolayer graphene. Nano Lett 15(5):3254–3260

Olson DA, Chen L, Hillmyer MA (2007) Templating nanoporous polymers with ordered block copolymers†. Chem Mater 20(3):869–890
Ophir A, Lokiec F (2005) Advanced MED process for most economical sea water desalination. Desalination 182(1):187–198
Othmer DF (1966) Evaporation for desalination—scale prevention and removal. Desalination 1(2):194–198
Pan Z, Donthu SK, Wu N, Li S, Dravid VP (2006) Directed fabrication of radially stacked multifunctional oxide heterostructures using soft electron-beam lithography. Small 2(2):274–280
Rowsell JL, Yaghi OM (2006) Effects of functionalization, catenation, and variation of the metal oxide and organic linking units on the low-pressure hydrogen adsorption properties of metal-organic frameworks. J Am Chem Soc 128(4):1304–1315
Sadhukhan H, Ramani M, Misra B, Verma R, Hanra M (1994) Role of evaporative and membrane desalination technology in solving drinking water problems in India. Desalination 96(1):249–258
Sadrzadeh M, Mohammadi T (2008) Sea water desalination using electrodialysis. Desalination 221(1):440–447
Santos L, Santilli CV, Larbot A, Persin M, Pulcinelli SH (2000) Nanopore size growth and ultrafiltration performance of SnO2 ceramic membranes prepared by sol-gel route. J Sol-Gel Sci Technol 19(1–3):621–625
Sint K, Wang B, Král P (2008) Selective ion passage through functionalized graphene nanopores. J Am Chem Soc 130(49):16448–16449
Sklenak S, Dědeček J, Li C, Wichterlová B, Gábová V, Sierka M, Sauer J (2007) Aluminum siting in silicon-rich zeolite frameworks: a combined high-resolution 27Al NMR spectroscopy and quantum mechanics/molecular mechanics study of ZSM-5. Angew Chem Int Ed 46(38):7286–7289
Surwade SP, Smirnov SN, Vlassiouk IV, Unocic RR, Veith GM, Dai S, Mahurin SM (2015) Water desalination using nanoporous single-layer graphene. Nat Nanotechnol 10(5):459–464
Tijing LD, Woo YC, Shim W-G, He T, Choi J-S, Kim S-H, Shon HK (2016) Superhydrophobic nanofiber membrane containing carbon nanotubes for high-performance direct contact membrane distillation. J Membr Sci 502:158–170
Tofighy MA, Mohammadi T (2010) Salty water desalination using carbon nanotube sheets. Desalination 258(1):182–186
Ulbricht M, Belfort G (1996) Surface modification of ultrafiltration membranes by low temperature plasma II. Graft polymerization onto polyacrylonitrile and polysulfone. J Membr Sci 111(2):193–215
Van der Bruggen B, Vandecasteele C (2002) Distillation vs. membrane filtration: overview of process evolutions in seawater desalination. Desalination 143(3):207–218
Wang EN, Karnik R (2012) Water desalination: graphene cleans up water. Nat Nanotechnol 7(9):552–554
Wilf M, Bartels C (2005) Optimization of seawater RO systems design. Desalination 173(1):1–12
Xu Z-K, Dai Q-W, Wu J, Huang X-J, Yang Q (2004) Covalent attachment of phospholipid analogous polymers to modify a polymeric membrane surface: a novel approach. Langmuir 20(4):1481–1488
Xu Z-K, Huang X-J, Wan L-S (2009) Surface engineering of polymer membranes. Springer, Berlin
Xue M, Qiu H, Guo W (2013) Exceptionally fast water desalination at complete salt rejection by pristine graphyne monolayers. Nanotechnology 24(50):505720
Yang Q, Tian J, Hu M-X, Xu Z-K (2007) Construction of a comb-like glycosylated membrane surface by a combination of UV-induced graft polymerization and surface-initiated ATRP. Langmuir 23(12):6684–6690
Yang SY, Park J, Yoon J, Ree M, Jang SK, Kim JK (2008) Virus filtration membranes prepared from nanoporous block copolymers with good dimensional stability under high pressures and excellent solvent resistance. Adv Funct Mater 18(9):1371–1377

Yang H-L, Chun-Te Lin J, Huang C (2009) Application of nanosilver surface modification to RO membrane and spacer for mitigating biofouling in seawater desalination. Water Res 43(15):3777–3786

Yang J, Zhai Y, Deng Y, Gu D, Li Q, Wu Q, Huang Y, Tu B, Zhao D (2010) Direct triblock-copolymer-templating synthesis of ordered nitrogen-containing mesoporous polymers. J Colloid Interface Sci 342(2):579–585

Yemini M, Hadad B, Liebes Y, Goldner A, Ashkenasy N (2009) The controlled fabrication of nanopores by focused electron-beam-induced etching. Nanotechnology 20(24):245302

Yu S, Li N, Wharton J, Martin CR (2003) Nano wheat fields prepared by plasma-etching gold nanowire-containing membranes. Nano Lett 3(6):815–818

Yu H-Y, Xu Z-K, Xie Y-J, Liu Z-M, Wang S-Y (2006) Flux enhancement for polypropylene microporous membrane in a SMBR by the immobilization of poly (N-vinyl-2-pyrrolidone) on the membrane surface. J Membr Sci 279(1):148–155

Zhang Q, Gupta S, Emrick T, Russell TP (2006) Surface-functionalized CdSe nanorods for assembly in diblock copolymer templates. J Am Chem Soc 128(12):3898–3899

Zhao S, Xue J, Kang W (2013) Ion selection of charge-modified large nanopores in a graphene sheet. J Chem Phys 139(11):114702

Zhu B, Kim JH, Na Y-H, Moon I-S, Connor G, Maeda S, Morris G, Gray S, Duke M (2013a) Temperature and pressure effects of desalination using a MFI-type zeolite membrane. Membranes 3(3):155–168

Zhu B, Li B, Zou L, Hill AJ, Zhao D, Lin JY, Duke M (2013b) Functional zeolitic framework membranes for water treatment and desalination. Wiley-VCH, Weinheim

Zhu C, Li H, Zeng XC, Meng S (2013c) Ideal desalination through Graphyne-4 membrane: Nanopores for quantized water transport. arXiv preprint arXiv:13070208

Zhu B, Hong Z, Milne N, Doherty CM, Zou L, Lin Y, Hill AJ, Gu X, Duke M (2014) Desalination of seawater ion complexes by MFI-type zeolite membranes: temperature and long term stability. J Membr Sci 453:126–135

Chapter 5
Nanotechnology in Wheat Production and Protection

Prem Lal Kashyap, Sudheer Kumar, Poonam Jasrotia, Devendra Pal Singh, and Gyanendra Pratap Singh

Contents

5.1 Introduction 166
5.2 Nanomaterials Migration in Wheat Plants 168
5.3 Seed Germination, Growth and Development 170
5.4 Biotic Stress Alleviation 175
5.5 Abiotic Stress Alleviation 177
5.5.1 Drought 177
5.5.2 Salinity 180
5.5.3 Other Abiotic Stresses 181
5.6 Surveillance, Monitoring, and Detection of Wheat Disease and Insect Pests 181
5.7 Controlled and Targeted Release of Fertilizers 182
5.8 Nanotechnology for Storage, Quality Control, and Food Grain Packaging 182
5.9 Toxicity and Adverse Effects of Nanomaterials 184
5.10 Future Challenges and Directions 185
5.11 Conclusion 186
References 187

Abstract Wheat (*Triticum aestivum*) is one of the principal staple food grain crops of the world. Wheat is constantly suffering from plethora of biotic and abiotic stresses leading to huge economic losses. To address these challenges, innovative technologies which have potential to enhance wheat yield and reduce the risk of various biotic and environmental stresses are required to be introduced in modern agriculture. Among these technological advancements, nanotechnology is gathering significant contemplation due to its wide spectrum applications in devising nanofertilizer, nanopesticide, nanoherbicide, nanosensor, and smart delivery systems for controlled and sustained release of agrochemicals in agriculture. So far, both beneficial and negative effects of nanoproducts on agronomic traits, yield, and productivity of plants including modification in the nutritional value of food crops have been observed. The efficacy of nanomaterial also depends on mechanism and pathways of penetration, uptake, and migration of nanoparticles along with

P. L. Kashyap (✉) · S. Kumar · P. Jasrotia · D. P. Singh · G. P. Singh
ICAR-Indian Institute of Wheat and Barley Research (IIWBR), Karnal, India
e-mail: Prem.Kashyap@icar.gov.in

N. Dasgupta et al. (eds.), *Environmental Nanotechnology Volume 4*, Environmental Chemistry for a Sustainable World 32, https://doi.org/10.1007/978-3-030-26668-4_5

application technology to reduce toxicity and adverse effects in wheat. In view of the acclaimed reports on the use of nanotechnology as an emerging tool in wheat research, the present chapter summarizes application of nanomaterial for (i) wheat growth promotion; (ii) protection from biotic and abiotic stresses; (iii) surveillance, monitoring, and detection of wheat pests; and (iv) storage, quality control, and food grain packaging. Here an attempt has also been made to review the challenges, limitations, and future prospects of nanotechnology to combat biotic and abiotic stresses for sustaining wheat production system.

Keywords Agriculture · Biotic stress · Food security · Nanoparticles · Nanotechnology · Nanomaterial · Nanosensor · Production · Protection · Wheat

5.1 Introduction

Wheat (*Triticum aestivum* L.) is a major staple food crop for more than one third of the world population. Currently, wheat is the second highest produced (749 million tons) cereal crop after maize (1.03 billion tons) (Savadi et al. 2018). Chaves et al. (2013) reported that 85% and 82% of the global population depend on wheat for basic calories and protein, respectively. By 2050, the global demand for wheat is expected to incline by 70%, requiring an annual production increase from its present level of 1% to 1.7% (Chenu et al. 2017). Wheat is sensitive to climate change due to direct effects of changes in temperature, precipitation and carbon dioxide concentrations, and also due to indirect effects through changes in soil moisture and the distribution and frequency of infestation by pests and diseases (Abeysingha et al. 2016; Asseng et al. 2014; Ludwig et al. 2009). Naresh Kumar et al. (2014) predicted 6–23% and 15–25% reduction in the wheat yield in India during 2050s and 2080s, respectively, under projected climate change scenarios. Oerke (2006) suggested that the global average of actual yield losses caused by all wheat diseases was about 13% on an annual basis. In Kansas, a study covering 1976–2000 and including analysis of 18 diseases reported annual losses of 10–22% (Bockus et al. 2001). In wheat, Sr31 stem rust resistance has been effective in cultivars for more than three decades, but its breakdown due to newly evolved race Ug99 of *Puccinia graminis* f. sp. *tritici* had been reported. According to estimates, Ug99 race can result in up to 10% yield losses in Asia alone, amounting to one to two billion US dollars per year (Duveiller et al. 2007). An estimate of yield losses of 3.7% due to leaf rust in 22 developing countries growing more than 100 million hectares of wheat has been reported (Marasas et al. 2004). Rust epidemics causing losses exceeding 50 million US dollars per annum occurred during the last decade at least once in all major wheat growing countries where fungicide application is not a routine practice (Shiferaw et al. 2013). Spot blotch caused by *Bipolaris sorokiniana* is reported in about nine million hectares of wheat grown after rice in the Indo-Gangetic Plains, and yield losses of 20% have been observed (Duveiller et al. 2005). The increasing threat of spot blotch pathogen leads to 80% disease severity, and the losses could be as high as 100% under severe

conditions (Kumar et al. 2009). Further, global yield losses due to insect pests in the pre-green revolution era were about 5.1%; however, the losses increased to 9.3% in the post-green revolution in the 1990s (Mondal et al. 2016). However, most likely only 40% of wheat area is actually suffering losses in the range of 5–15% every year, depending on the level and duration of dew and heat stress (Sharma and Duveiller 2004). Therefore, the ability of wheat to tolerate biotic and abiotic stresses is a key aspect of yield resilience. Under such circumstances, nanotechnology certainly holds the potential to rejuvenate wheat farming and is expected to become a dynamic economic force in the near future. Additionally, nanotechnology-based reorientation of wheat cultivation can boost production of quality food in sustainable and environment-friendly manner.

Nanotechnology deals with atomic or molecular aggregates of 1–100 nanometers in size. A vast application in crop production and protection is due to profoundly modified physiochemical properties of nanoparticles associated with smaller size and large surface area (Kashyap et al. 2015, 2018a; Ditta and Arshad 2016; Khot et al. 2012). Nanoparticles of gold, silver, copper, zinc, aluminum, silica, zinc oxide, cesium oxide, titanium dioxide, and magnetized iron have found applications in growth promotion and development of wheat (Jasrotia et al. 2018; Lyu et al. 2017; Iannone et al. 2016; Hafeez et al. 2015; Watson et al. 2015; Jhanzab et al. 2015; Du et al. 2015; Ramesh et al. 2014). The nanoparticles have been used in crop production, protection, and improvement, fertilizer, and irrigation management (Kashyap et al. 2015, 2018b; Mishra et al. 2017). Use of nanoparticles in wheat is consistently increasing. Several beneficial effects of nanomaterials have been observed in wheat plants (Razzaq et al. 2016). Effect of different nanoparticles on germination, growth, physiological activities, fertilizer use efficiency, root growth, branching, biomass, and photosynthetic activity has also been reported (Taran et al. 2017; Siddiqi and Husen 2017; Zaimenko et al. 2014). Wheat seeds treated with metal nanoparticles exhibited enhanced nutrient use efficiency, photosynthetic activity, grain quality, and increased yield (Hafeez et al. 2015). Metal nanoparticles also increase photosynthetic activity and nitrogen metabolism in several crops including wheat (Kole et al. 2013). Improvement in agronomic traits, seed gluten, and starch contents of wheat by exposure to titanium dioxide nanoparticles was also postulated (Jaberzadeh et al. 2013). Application of nanoparticles derived from silicon dioxide and titanium dioxide enhanced germination, growth, and nitrate reductase activity in wheat (Farooqui et al. 2016; Ditta and Arshad 2016). Nanoparticles blended with agrochemicals may provide a more efficient means for delivering pesticides and fertilizers (Kashyap et al. 2015). So far, both detrimental and beneficial effects of nanomaterials on agronomic traits, yield, and productivity of plants including modification in the nutritional value of food crops have been observed. In view of the acclaimed reports on the use of nanotechnology as an emerging tool in wheat research, it is important to understand the course of wheat crop growth in relation to nanotechnology. The recent advances in nanotechnology and its use in growth promotion and stress management are gradually increasing. The present chapter, therefore, attempts to increase understanding of the role of nanotechnology in quality wheat production and protection.

5.2 Nanomaterials Migration in Wheat Plants

Nanomaterials refer to a colloidal particulate system, with size ranging from 1 to 100 nanometer and possessing unique properties such as high surface-to-volume ratio and optical behaviors (Ditta and Arshad 2016; Kashyap et al. 2013). The principle kinds of nanomaterials used in agriculture and allied sector include carbon nanotubes, metal oxides, lipids, zerovalent metals, quantum dots, and nanopolymers and dendrimers with different kinds of features including nanofibers, nanowires, nanosheets, etc. Thus, the field of nanotechnology opens up novel applications in wheat production and protection. Nanoencapsulation is currently the most promising technology for protection of plants against diseases and insect pests. With nanoencapsulation techniques, it is possible to step down the chemical release under controlled situations, reducing the current application dosage and improving efficiency. Nanoparticles have been used in the preparation of new formulations of fungicides, insecticides, herbicides, etc. The beneficial effects of different nanosize metals on wheat cells and seed germination have also been reported.

There are few reports on mechanism of nanomaterial uptake and pathways for their diffusion as nanoparticles and internalization in plants (Yang et al. 2017; Lyu et al. 2017; Chichiriccò and Poma 2015); however, the penetration, uptake, and accumulation of nanoparticles in wheat cells and tissues are not well documented. Generally, the growth cycle of wheat has several stages that include germination, seedling establishment and leaf production, tillering and head differentiation, stem and head growth, head emergence and flowering, and grain filling and maturity. Several studies on wheat showed the ability of metal nanoparticles to penetrate seeds without affecting germination (Larue et al. 2012a). Figure 5.1 depicts the mechanism

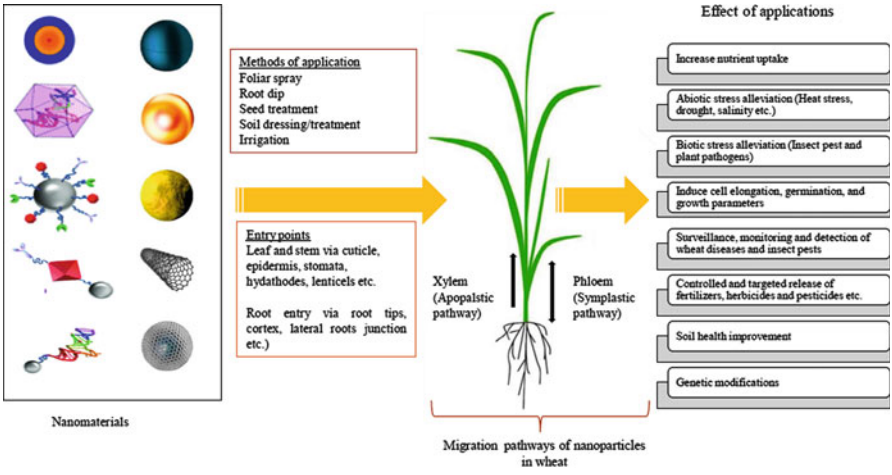

Fig. 5.1 Mechanism of penetration, uptake, and migration of nanoparticles in wheat

and pathways of penetration, uptake, and migration of nanoparticles in wheat plants. Wild and Jones (2009) used two-photon excitation microscopy to observe multi-walled carbon nanotubes piercing the cell wall of wheat roots and reaching the cytoplasm. After root uptake and penetration of the epidermal cells of nanomaterials, further transport requires circulation across the root and to the xylem. Nanoparticles are transported through cell wall pores via apoplastic or symplastic pathway through plasmodesmata and channels that connect adjacent cells (Fig. 5.1). Magnetic carbon-coated nanoparticles of 5–50 nanometers were absorbed by the roots and then translocated to the xylem vessels up to the leaves via trichomes. However, nanoparticle absorption by wheat roots and translocation of nanoparticles in stems and leaves is largely influenced by physicochemical features of nanoparticle, growth stage of plant, and growth medium (Cifuentes et al. 2010). Taran et al. (2017) used nonionic colloidal solutions of nanoparticles (iron, zinc, and manganese) in winter wheat to test concentration in seedlings either arising from pretreated seeds or sprayed with nanoparticles after growth. The outcome of the study provided evidence for the absorption and translocation of manganese and zinc from the foliar epidermis in wheat seedlings. Du et al. (2011) treated wheat plants with titanium dioxide nanoparticles and zinc oxide nanoparticles of 20–100 nanometers in size under field conditions using outdoor lysimeters. Titanium dioxide nanoparticles either agglomerated or adhered to the cell walls of the root periderm, and particles of 50 ± 10 nanometers penetrated the primary epidermis roots and the cortex via apoplast up into cell vacuoles; however, zinc oxide nanoparticles seemed to dissolve and then penetrate the cells in the form of zinc ions. Root uptake of titanium dioxide nanoparticles appears to be size selective (Tripathi et al. 2017). Larue et al. (2012a) postulated that threshold diameters for movement of titanium dioxide nanoparticles through root epidermis of wheat plants should be smaller than 140 nm; thresholds for transferring through parenchyma are 36 nm or less; and for passing through the Casparian band, particle diameters should be smaller than 36 nm. Titanium dioxide nanoparticles smaller than 36 nm could be transported to the stele via two routes: (i) direct penetration of Casparian band and (ii) through plasmodesmata (Larue et al. 2012b). Additionally, titanium dioxide nanoparticles may enter plant cells through endocytosis as nanoparticles have been shown to activate membrane receptors and induce endocytosis (Iversen et al. 2011). Recently, Pradas del Real et al. (2017) investigated the uptake and transfer pathways of silver nanoparticles and sulfidized silver nanoparticles in wheat and the changes in speciation. The results showed that the sulfidation of silver nanoparticles is not a perfect antidote to toxicity and sulfidized silver nanoparticles are not as stable as expected when exposed to plant roots. Moreover, the rhizospheric activity of wheat seedlings partly dissolves silver sulfide causing some impacts on crop quality and yield and more on ecological services. Further, the study illustrated the complexity of the toxicity pattern for plants exposed to silver nanoparticles, where both apoplastic and symplastic transfer of silver in monovalent form in wheat plants (Pradas del Real et al. 2017). Similarly, the effect of citrate-coated iron oxide nanoparticles on hydroponically grown wheat plants was studied by Iannone et al. (2016). The authors mentioned the deposition of

magnetite in epidermal cell wall via apoplastic route. Fairly large quantities of magnetite in the range of 2.01–8.07 mg g^{-1} iron were found in wheat roots. Since no paramagnetic signal was detected in stem and leaves, it suggested that nanoparticles were not translocated through vascular tissues. Nanoparticle penetration into the roots of wheat seedlings have been facilitated by 2–10 nanometer average citrate-coated magnetite nanoparticles, favoring nanoparticle uptake by plants. Nanoparticle uptake might be enhanced by the enlargement of existing pores, induction of new cell wall pores, internalization during endocytosis in the plasma membrane, or crossing the cell membrane using transport carrier proteins or through ion channels (López-Luna et al. 2016).

5.3 Seed Germination, Growth and Development

Nanoparticle containing essential metals is considered in formulations of fertilizers to enhance nutrient absorption in plants with low metal bioavailability. Carbon nanotubes have acquired an important position due to unique mechanical, electrical, thermal, and chemical properties. Carbon nanotubes act as nanotransporters for delivery of DNA and dye molecules into plants cells (Srinivasan and Saraswathi 2010). However, in various studies researchers have reported that multi-walled carbon nanotubes have a unique potential to influence the seed germination and plant growth. Multi-walled carbon nanotubes induce the water and essential calcium and iron nutrient uptake efficiency that could enhance the seed germination and plant growth and development (Villagarcia et al. 2012; Tiwari et al. 2014). Miralles et al. (2012) demonstrated that industrial-grade multi-walled carbon nanotubes enhanced germination and root elongation of wheat. Remarkably, carbon nanotubes were adsorbed onto the root surfaces of wheat without significant uptake or translocation. In another study, Tripathi and Sarkar (2014) noticed that water-soluble carbon nanotubes inside the wheat plants were able to induce the root and shoot growth in light and dark conditions. Hu and Zhou (2014) reported a novel and biocompatible hydrated graphene ribbon could promote germination of wheat seed and enhance resistance to oxidative stress. The metabolomics analysis indicated that hydrated graphene ribbon could upregulate carbohydrate, amino acid, and fatty acid metabolism that determined secondary metabolism, nitrogen sequestration, cell membrane integrity, permeability, and oxidation resistance.

Titanium dioxide nanoparticles are promising as efficient nutrient source for plants to improve biomass production due to enhanced nitrogen assimilation, photoreduction activities of photosystem II and electron transport chain, and scavenging of reactive oxygen species (Lyu et al. 2017; Raliya et al. 2015; Morteza et al. 2013). The exposure of wheat plant to titanium dioxide nanoparticles causes enhancement in root elongation without influencing seed germination, vegetative growth, and photosynthesis. These are short-term effects of titanium dioxide nanoparticles, but during the whole cycle of the plant, it may have some adverse effect (Larue et al. 2012b). Mahmoodzadeh and Aghili (2014) showed that a titanium dioxide nanoparticle at its optimal concentration has a stimulating effect, and high concentrations

have an inhibiting effect on the growth of root and shoot of the wheat. Moreover, the fresh and dry weight of the root is also remarkably affected by titanium dioxide nanoparticles. Jaberzadeh et al. (2013) reported that titanium dioxide nanoparticles augmented wheat plant growth and yielded components under water-deficit stress condition. Titanium dioxide nanoparticle regulates enzyme activity involved in nitrogen metabolism such as nitrate reductase, glutamate dehydrogenase, glutamine synthase, and glutamic-pyruvic transaminase that helps the plants to absorb nitrate and also favors the conversion of inorganic nitrogen to organic nitrogen in the form of protein and chlorophyll that could increase the fresh weight and dry weight of plant (Yang et al. 2006; Mishra et al. 2014).

Riahi-Madvar et al. (2012) reported that foliar application of wheat seedlings with nano-aluminum oxide of less than 50 nanometer diameter decreased the root length, and as result of oxidative stress, the activity of superoxide dismutase and catalase enzymes increased. In another work, Ramesh et al. (2014) reported that lower concentration of zinc oxide nanoparticles exhibited beneficial effect on seed germination of wheat. However, higher dose of nano-zinc oxide impaired seed germination. The effect of nanoparticles on germination depends on concentrations of nanoparticles and varies from plants to plants.

Copper oxide nanoparticles have the potential to enhance growth and yield of wheat, but effect is concentration dependent. Hafeez et al. (2015) revealed that copper nanoparticles do not affect seed germination up to 0.8 parts per million concentration although impair germination at 1 part per million and above. Lower than 1.0 part per million concentration of copper nanoparticles in solution culture and less than 50 parts per million in pots are not toxic for wheat plants. Maximum growth and yield were recorded with 30 parts per million copper nanoparticles in pots.

Cerium oxide nanoparticles have been considered highly stable in environmental and biological surroundings with limited dissolution in soil and plant tissues (Gaiser et al. 2009; Xia et al. 2008). Another report investigated the effects of cerium dioxide exposure on wheat by using hydroponic plant culture. Cerium dioxide nanoparticles have only minor effects, and no growth reduction or toxic response was observed (Schwabe et al. 2013), but catalase and ascorbate peroxidase activity significantly increased.

Mesoporous silica is actually largely used in catalysis, drug delivery, and imaging and thus released in the environment. Recently, Nair et al. (2011) demonstrated that uptake of nonporous silica nanoparticles labeled with fluorescein isothiocyanate had no effect on seed germination at concentrations up to 50 mg L^{-1}. In another study, Hussain et al. (2013) have reported absorption of mesoporous silica nanoparticle functionalized with amine cross-linked fluorescein isothiocyanate by wheat. These nanoparticles have a dimension of approximately 20 nanometers with interconnected pores of around 2 nanometers. The uptake and distribution were examined during seed germination, in roots and leaves of plants. After germination of wheat in solution with nanoparticles, silica nanoparticles were found within cells, in cell wall of roots, and in the xylem and other cells for the transport of elements. Based on the above mentioned reports (Table 5.1), nanomaterials can be used to enhance plant seed germination, growth, and development in a dose-dependent manner.

Table 5.1 Effect of nanomaterials on plant growth promotion of wheat

Nanomaterial	Size (nm)	Mode of application	Concentration used	Type of study	Impact/effect	Reference(s)
TiO_2 NP	11.93–18.67	Soil amendment	20–100 mg kg^{-1}	Pot trial	Increased root and shoot length and total fresh and dry biomass up to 60 mg/kg but decreased at higher concentrations	Rafique et al. (2014)
Colloidal solutions of cu and Zn NP	–	Seed treatment	1 part of colloid solution to 100 parts of water	Green house	Increase in the activity of antioxidative enzymes, reduction in TBARS accumulation, stabilization of photosynthetic pigments	Taran et al. (2017)
Al_2O_3 NP	<100	Foliar spray	100 mgL^{-1}	Pot trial	Increase in root and shoot length	Aliabadi et al. (2016)
CeO_2 NP	8 ± 1	Seed dipping	0, 100, 400 mg kg^{-1}	Petri dish	Changes in microstructure of leaf cells, swollen chloroplasts, squeezed nuclei, bent and loosely arranged thylakoids; decreased chlorophyll contents and exhibits variation in protein content	Rico et al. (2015)
CeO_2 NP	8 ± 1	Soil amendment	0, 125, 250, 500 mg L^{-1}	Field	Changes the amounts of S and Mn in grains, amino acid composition, and linolenic acid contents	Rico et al. (2014)
$nTiO_2$ NP	ND	Seed priming	10, 100, 1000, 1200, 1500, and 1700 ppm	Petri dish	Promote seed germination and seedling growth of wheat in dose-dependent manner	Mahmoodzadeh and Aghili (2014)
CuO NP	<50	Sand amendment	500 mg kg^{-1}	Controlled condition	Inhibition in root and shoot growth; produced oxidative stress possibly due to Cu released from nanoparticles, Cu bioaccumulates	Dimkpa et al. (2012)

TiO_2 NP	< 50	Foliar spray	1000–2000 mg L^{-1}	Greenhouse	Increase in length of root and shoot, malondialdehyde (MDA) and proline content	Aliabadi et al. (2016)
TiO_2 NP	40–60	Seed treatment	250–2000 mg L^{-1}	Petri dish	No phytotoxicity, significant increase in chlorophyll and protein content	Ramesh et al. (2014)
TiO_2 NP	<100	Soil amendments	91 mg kg^{-1}	Field	Reduced biomass, nanoparticles found mostly stick on surface of roots	Du et al. (2011)
TiO_2 NP	54	Seed treatment	200 mg L^{-1}	Petri dish	Promoted growth and encouraged seed germination; higher concentration (>400 mgL^{-1}) cause toxicity	Ullah and Arshad (2014)
ZnO NP	20–50	Seed treatment	250–2000 mg L^{-1}	Petri dish	No phytotoxicity, significant increase chlorophyll and protein content	Ramesh et al. (2014)
ZnO NP	<100	Soil or sand amendment	50 mg kg^{-1}	Field	Reduced plant biomass	Du et al. (2011)
ZnO NP	<100	Soil or sand amendment	500 mg kg^{-1}	Controlled conditions	Reduced root growth, increased reactive oxygen species production	Dimkpa et al. (2012)
Colloidal solution of metal nanoparticles (Zn, Ag, Fe, Mn, and Cu)	–	Seed treatment	1 part of colloid solution to 100 parts of water	Greenhouse	Increase antioxidant properties of cells under phytopathogen stress condition and improve physiological condition of plants	Panyuta et al. (2016)
nFe_3O_4	6.8	Seed treatment	2000 mg L^{-1}	Petri dish	Significantly decreased root growth inhibition and reduced and alleviated oxidative stress induced by the heavy metals	Konate et al. (2017)
MSN	20 and pore diameter 2.78 nm.	Seed treatment	500 and 1000 mg L^{-1}	Petri dish and controlled growth chamber	Enhancement of seed germination, increased plant biomass, total protein and chlorophyll content	Sun et al. (2016)

(continued)

Table 5.1 (continued)

Nanomaterial	Size (nm)	Mode of application	Concentration used	Type of study	Impact/effect	Reference(s)
TiO_2 NP		Seed soaking	0.025%, 0.05%, 0.1%, 0.2%, and 0.5%	Petri dish	Enhanced seed potential by increasing vigor index, root dry matter stress tolerance index, shoot dry matter stress tolerance index, dry matter stress tolerance index, plant height stress tolerance index, root length stress tolerance index, fresh matter stress tolerance index and pigment composition	Shafea et al. (2017)
Fe NP	20	Seedling dip	5 ppm	Pot trial	Stimulatory effects on the germination ratio and plant growth of wheat	Yasmeen et al. (2016)

nm nanometer, *NP* nanoparticles, TiO_2 titanium dioxide, *Fe* iron, ZnO zinc oxide, CeO_2 cerium dioxide, Al_2O_3 aluminum oxide, *CuO* copper oxide, *Ag* silver, *Mn* manganese, *Cu* copper, *MSN* mesoporous silica nanoparticle, *ppm* parts per million, % percent, $mg\ Kg^{-1}$ milligram per Kilogram, $mg\ L^{-1}$ milligram per liter, < less than, > greater than

5.4 Biotic Stress Alleviation

Agrochemicals have changed the face of wheat cultivation, but it has also developed new challenge in the form of resistance against agrochemicals in pathogens and insect pests. Nanoparticles have a great promise for the management and control of insect pest and diseases in wheat (Table 5.2). Mishra et al. (2014) studied the effect of silver nanoparticles in controlling spot blotch disease of wheat caused by *Bipolaris sorokiniana*. The results revealed that application of silver nanoparticles strongly inhibited *B. sorokiniana* infection in wheat. Moreover, decrease in plant growth after pathogen challenge was overcome when wheat plants were treated with silver nanoparticles. Silver nanoparticle-mediated reduction in melanin production might be one of the factors for diminishing the pathogenicity of *B. sorokiniana* on wheat (Mishra and Singh 2015). Similarly, the efficacy of zinc nanoparticles in controlling *Fusarium* head blight and deoxynivalenol formation in wheat was reported by Savi et al. (2015). Savi et al. (2015) demonstrated that zinc oxide nanoparticles efficiently reduced deoxynivalenol (a toxin produced by *F. graminearum*) formation and *F. graminearum* infection in wheat grains even at 100 mM concentration. In another study, Panyuta et al. (2016) studied the effect of pre-sowing seed treatment with metal nanoparticles (silver, iron, manganese, copper, and zinc) on the induction of defense reaction of wheat seedlings infected with *Pseudocercosporella herpotrichoides*. Further, antioxidant effect of nonionic colloidal solutions of biogenic metals via inhibition of the synthesis of lipid peroxidation products has been observed. Besides nanoparticles, antimicrobial activity of nanoparticles loaded with chitosan has been reported to control *Fusarium* head blight of wheat (*Fusarium graminearum*). Kheiri et al. (2016) revealed that chitosan nanoparticles have strong inhibitory effect on the fungal growth, colony formation, and conidial germination of *F. graminearum*. However, plant protection by chitosan nanoparticles is dependent on time period and growth stage of plant.

Nanoproducts have been experimenting as insecticides against different kinds of wheat pests. Nano-silica is one of the widely and universally accepted nanoproduct used as a nanopesticide (Barik et al. 2008). The mechanism of action of nano-silica is based on the fact that insect pests used a variety of cuticular lipids for protecting water barrier and thereby preventing mortality from desiccation. But nano-silica gets absorbed into the cuticular lipids by physio-sorption and thereby causes death of insects by physical means when applied on plant surface. Surface charged modified hydrophobic nano-silica of 3–5 nm size is another product which could be successfully used to control a range of agriculturally important insect pests (Ulrichs et al. 2005). Yang et al. (2009) demonstrated the insecticidal activity of polyethylene glycol-coated nanoparticles loaded with garlic essential oil against adult *Tribolium castaneum* insect found in stored products. It has been observed that the control efficacy against adult *T. castaneum* was about 80%, presumably due to the slow and persistent release of the active components from the nanoparticles. Teodoro et al. (2010) for the first time reported insecticidal activity of nanostructured alumina against major insect pests in stored food grains. The results of the study showed

Table 5.2 Applications of nanomaterials for wheat disease management

Nanomaterial	Size (nm)	Concentration used	Assay	Disease	Pathogen	Type of study	Impact/effect	Reference (s)
ZnO NP	30	100 mM	Foliar spray	Head blight	*Fusarium graminearum*	Field	Reduction in number of CFU of *F. graminearum*	Savi et al. (2015)
Ag NP	10–20	4 μg ml^{-1}	Foliar spray	Spot blotch	*Bipolaris sorokiniana*	Leaf detached assay and greenhouse	Reduced *B. sorokiniana* infection in wheat plants	Mishra et al. (2014)
Colloidal solution of metal nanoparticles (Zn, Ag, Fe, Mn, and Cu)	–	1 part of colloid solution to 100 parts of water	Seed treatment	Eyes pot	*Pseudocercosporella herpotrichoides*	Greenhouse	Increase antioxidant properties of cells under phytopathogen stress condition and improve physiological condition of plants	Panyuta et al. (2016)
Colloidal solution of CS/NPs	225.7 ± 42.81–595.7 ± 81.7	5000 ppm	Spray	Head blight	*F. graminearum*	In vitro assay and greenhouse	Significant inhibitory effects on the fungal growth, colony formation, and conidial germination of *F. graminearum*	Kheiri et al. (2017)
Colloidal solution of CS/NPs	180.9 nm	5000 ppm	Spray	Head blight	*F. graminearum*	In vitro assay and greenhouse	Elevated antifungal activity against *F. graminearum* under in vitro and greenhouse conditions and oxidative activity on plant tissues and cells in the presence of fungus; dehydration and deformation in mycelia growth	Kheiri et al. (2016)

nm nanometer, *NP* nanoparticles, *ZnO* zinc oxide, *Ag* silver, *Fe* iron, *Mn* manganese, *Cu* copper, *CS* chitosan, *ppm* parts per million, *mM* millimolar, *μg* ml^{-1} microgram per milliliter

significant mortality after 3 days of continuous exposure to nanostructured alumina-treated wheat. Recently, Ziaee and Ganji (2016) reported that silicon nanoparticles were also effective in controlling wheat grain pests. The authors revealed that the initial mortality was so high that the impact of food source on delay mortality was unclear in most cases. Overall, it seems that as compared to commercially available insecticides, nanoproducts may provide a cheap and reliable alternative for control of insect pests, and such studies may expand the frontiers for nanoparticle-based technologies in wheat pest management in the future.

5.5 Abiotic Stress Alleviation

Abiotic stresses are the principal limiting factors for decline in wheat productivity (Grayson 2013). Major abiotic stress factors include drought, extreme temperature, salinity and acidic conditions, light intensity, submergence, anaerobiosis, nutrient starvation, etc. (Bailey-Serres and Voesenek 2008; Agarwal and Grover 2006; Nakashima and Yamaguchi-Shinozaki 2006). Drought, flood, salinity, mineral deficiency, acidity, and cold has affected 64%, 13%, 6%, 9%, 15%, and 57% of the global land area (Cramer et al. 2011; Mittler 2006). Out of the world's 5.2 billion hectares of dryland agriculture, 3.6 billion hectares is affected by the problems of erosion, soil degradation, and salinity (Riadh et al. 2010). Ruan et al. (2010) estimated salt-affected soils to impact upon 50% of total irrigated land in the world costing 12 billion US dollars in terms of loss (Flowers et al. 2010). Similarly, global annual cost of land degradation by salinity in irrigated lands could be 27.3 billion US dollars due to loss in crop production (Qadir et al. 2014). Several metal- or metal oxide-based nanoparticles are being studied to assess potential applications in wheat protection from abiotic stresses (Table 5.3), and details of which are summarized in the following sections.

5.5.1 Drought

Drought is a severe environmental stress and the major constraint on wheat productivity with an evident effect on growth (Abid et al. 2017; Nezhadahmadi et al. 2013; Rampino et al. 2006). Global climate models predict changed precipitation patterns with frequent episodes of drought. Although drought impedes wheat performance at all growth stages, it is more critical during the flowering and grain-filling phases (terminal drought) and results in substantial yield losses. For instance, post-anthesis mild

at yields by 1–30 per cent, while prolonged mild drought at flowering and grain filling reduced the grain yields by 58–92% (Farooq et al. 2014). The effects of terminal drought on wheat yields are likely to increase in the near future (Araus et al. 2002; Dias de Oliveria et al. 2013).

Table 5.3 Effect of nanomaterials on abiotic stress management in wheat

Nanomaterial	Size (nm)	Stress	Mode of application	Concentration used	Type of study	Impact/effect	Reference(s)
Colloidal solutions of cu and Zn NPs	–	Drought	Seed treatment	1 part of colloid solution to 100 parts of water	Greenhouse study	Reduction in drought stress on plants, increase in the activity of antioxidative enzymes, reduction in TBARS accumulation, stabilization of photosynthetic pigments, and increase in relative water content of leaves	Taran et al. (2017)
Fe_3O_4 NPs	6.8	Heavy metals (Pb, Zn, cd, and cu)	Seed treatment	2000 mg L^{-1}	Petri dish assay	Significantly decreased root growth inhibition and reduced and alleviated oxidative stress induced by the heavy metals	Konate et al. (2017)
Magnetite NPs	5–20	Heavy metals (cd and Cr)	Sand amendment	1000 mg kg^{-1}	Pot assay	Enhanced in root length and cadmium and chromium accumulation diminished and the metal toxicity alleviated	López-Luna et al. (2016)
Si NP	20–95	UV light	Seedling dip	10 μM	Growth chamber	Effectively alleviated UV-B stresses on wheat seedlings through NO-mediated triggering of antioxidant defense system and counterbalance reactive oxygen species-induced damage to photosynthesis	Tripathi et al. (2017)
Analcite NPs	100	Drought	Soil amendment	500, 1000, and 1500 mg L^{-1}	Pot assay	Increment in seed germination, seedling growth criteria, as well as content of photosynthetic pigments under stress; sharp accumulation of protective antioxidants (flavonoids, carotenoids)	Zaimenko et al. (2014)

Ag NPs	15–29	Salinity	Seed priming	2, 5, and 10 mM	Greenhouse experiment	Enhance salt tolerance in wheat by decreasing the oxidative stress through modification of antioxidant enzyme activities	Mohamed et al. (2017)
Ag NPs	ND	Chilling	Seed priming	30–40 ppm	Petri dish assay	Enhanced seedling vigor, germination percentage, and seedling growth	Bhati-Kushwaha et al. (2013)

nm nanometer, *NP* nanoparticles, Fe_3O_4 iron(II, III) oxide, *Fe* iron, *Zn* zinc, *Si* silicon, *Cd* cadmium, *Pb* lead, *Ag* silver, *Mn* manganese, *Cu* copper, *Cr* chromium, *UV* ultraviolet, *ppm* parts per million, *mg* Kg^{-1} milligram per Kilogram, *mg* L^{-1} milligram per liter, *μM* micromoles, *NO* nitric oxide, *TBARS* thiobarbituric acid reactive substances, *ND* not determined

The effect of the application of nanoparticles of analcite to soil on drought resistance of wheat was observed by Zaimenko et al. (2014). Application of analcite showed enhanced seed germination, seedling growth, as well as content of photosynthetic pigments, while characteristics of water balance less deviated from the normal under water deficit. Moreover, application of analcite nanoparticles induced sharp accumulation of protective antioxidants, e.g., flavonoids and carotenoids, under drought. In another study, Taran et al. (2017) reported that colloidal solution of copper and zinc nanoparticles decreased the negative effect of drought stress on wheat. In particular, increased activity of antioxidative enzymes reduced the level of accumulation of thiobarbituric acid reactive substances and stabilized the content of photosynthetic pigments and increased relative water content in leaves.

5.5.2 Salinity

It is well known that salinity has been considered as a major environmental threat for wheat cultivation. More than 45 million hectares of irrigated land which account to 20% of total land have been damaged by salt worldwide, and 1.5 million hectares are taken out of production every year due to high salinity levels (Negrão et al. 2017; Munns and Tester 2008). Poor germination and poor seedling establishment are the results of soil salinity, which adversely affects plant growth and development and results in to low agricultural production (Miransari and Smith 2007). The effects of salinity at seedling stage of wheat range from reduction in germination percentage and fresh and dry weight of shoots and roots to the uptake of various nutrient ions (Darko et al. 2017; Yang et al. 2014). Salt stress decreases the growth, mineral nutrients, grain yield, chlorophyll content, and gas exchange characteristics in wheat (Rahman et al. 2016). However, application of nanoparticles provided elevated levels of plant growth and improved performance of wheat under salinity stress (Table 5.3). Mohamed et al. (2017) showed that seed priming with silver nanoparticles alleviates the salt stress in wheat by decreasing the oxidative stress through modification of antioxidant enzyme activities depending upon the doses of silver nanoparticle applied. Priming with a lower concentration of silver nanoparticles might be an effective strategy to alleviate the negative effect of salt stress on wheat. Seed priming with silver nanoparticles having 15–29 nm size enhanced the shoot fresh and dry weight of normal and salt-stressed plants. Seed priming with nanoparticles may help the wheat plants to reduce sodium translocation from roots to shoots which ultimately led to increase in plant growth. Moreover, the combined application of silver nanoparticle and salt stress increased the soluble sugars and proline contents, while it decreased catalase activity and increased peroxidase activity.

5.5.3 *Other Abiotic Stresses*

The growth, development, and productivity of wheat plants are adversely affected by other stresses like heavy metal contamination, chilling stress, ultraviolet B radiation, etc. Heavy metal toxicity induced growth inhibition and oxidative stress in wheat crops. Recently, López-Luna et al. (2016) assessed the uptake of citrate-coated magnetite nanoparticles by wheat plants and effect on the bioaccumulation and toxicity of individual and joint cadmium and chromium levels. The toxic effects of individual and mixed cadmium and chromium were markedly diminished when the wheat plants were amended with citrate-coated magnetite nanoparticles, possibly due to reduction of heavy metal phytoavailability upon adsorption onto magnetite nanoparticles. In fact, the stabilization of metals and metalloids by reducing mobility, bioavailability, and bioaccessibility can be achieved by applying immobilizing agents such as nanosized oxides, mainly due to high reactivity and large specific surface area. Moreover, the addition of magnetite nanoparticles enhanced root length of the plants. Konate et al. (2017) investigated the physiological mechanisms of magnetite nanoparticle mitigation of the toxicity of heavy metals (lead, zinc, cadmium, and copper) in wheat seedlings. The addition of magnetite nanoparticles in 1 mM heavy metal solution significantly decreased the growth inhibition and activated protective mechanisms to reduce oxidative stress induced by heavy metals in the wheat seedlings. Moreover, the alleviating effect of magnetite nanoparticle is associated with adsorption capacity of heavy metals and dependent on the increase in the enzyme activity of superoxide dismutase and peroxidase.

Bhati-Kushwaha et al. (2013) suggested that silver nanoparticle confers an increased tolerance of wheat plants to cold stress. The results provided clear evidences that seed priming with silver nanoparticles is one of the suitable methods for increasing seedling vigor and improvement of germination percentage and seedling growth under chilling stress.

Ultraviolet B radiation negatively influenced growth of wheat seedlings through interference in photosynthesis due to decreased levels of antioxidants (superoxide dismutase and peroxidase) and enhanced level of oxidative stress. Recently, Tripathi et al. (2016) reported that pre-addition of 10 μM silicon nanoparticles protects wheat seedlings against ultraviolet B radiation stress by protecting photosynthesis and regulating level of oxidative stress. Silicon nanoparticles protect wheat seedlings through nitric oxide-mediated triggering of antioxidant defense system, which subsequently counterbalance reactive oxygen species-induced damage to photosynthesis.

5.6 Surveillance, Monitoring, and Detection of Wheat Disease and Insect Pests

Rapid detection technologies with high sensitivity and selectivity for plant pathogens and insect pests are essential to prevent disease spread and minimize losses to assure optimal productivity and food security (Kashyap et al. 2016; Sharma et al.

2017a; Kaur et al. 2019). Traditional laboratory techniques used for pest diagnosis are time consuming, labor intensive, and require complex sample handling. The sensitive nature of functionalized nanoparticles can be used to design phytopathogen detection devices with smart sensing capabilities for field use (Kashyap et al. 2017). Singh et al. (2010) used nanogold-based immunosensors that could detect Karnal bunt disease in wheat (*Tilletia indica*) using surface plasmon resonance. Gold nanoparticles have been used in biosensors due to ease in alternation of optical or electrochemical procedures to identify pathogens (Thaxton et al. 2006; Kashyap et al. 2019).

5.7 Controlled and Targeted Release of Fertilizers

Nanofertilizers are new generation of the synthetic fertilizers which contain readily available nutrients in nanoscale range. Nanofertilizers are more soluble and effective than bulk counterparts (DeRosa et al., 2010; Rameshaiah and Jpallavi, 2015). Application of nanofertilizers improves solubility and dispersion of insoluble nutrients in soil, reduces nutrient immobilization (soil fixation), and increases the bioavailability (Naderi and Danesh-Shahraki 2013). Moreover, nanofertilizers can be easily absorbed by plants and provide nutrient supply in soil or on plant for longer duration (Rameshaiah and Jpallavi 2015). Zhang et al. (2006) investigated the effects of controlled release fertilizers cemented and coated by nanomaterials on crop. Interestingly, the synthesized nanocomposites were safe for wheat seed germination, emergence, and growth of seedlings. Moreover, nanocomposites can also provide a regulated, responsive, and on-time delivery of nutrients to plants. Abdel-Aziz et al. (2016) investigated the delivery of chitosan nanoparticles loaded with nitrogen, phosphorus, and potassium for wheat plants by foliar uptake. The results revealed that wheat plants grown on sandy soil with chitosan-based nanofertilizer induced significant increases in harvest index, crop index, and mobilization index of the determined wheat yield variables. Moreover, the life cycle of the nanofertilized wheat plants was shorter than normal-fertilized wheat plants. However, the response of plants to nanofertilizers varies with the type of plant species, growth stages, and nature of nanomaterials.

5.8 Nanotechnology for Storage, Quality Control, and Food Grain Packaging

Nanosensors have potential application in the agricultural and allied sector including food quality assessment, food packaging, food storage, monitoring of food processing, shelf life and viability, indicator of food safety and microbial contamination, and toxin and residual contamination in food grains (Neethirajan et al. 2018;

Srivastava et al. 2018; Dasgupta et al. 2015; Neethirajan and Jayas 2009). Nanosensors based on nanoparticles have been devised to detect moisture content inside a food package (Pathakoti et al. 2017). Such kind of nanosensor is usually based upon carbon-coated copper nanoparticles dispersed in a tenside film (Luechinger et al. 2007). Principally, under humid and moist conditions, swelling of the polymer matrix results in separation of inter-nanoparticle. These changes cause sensor strips to reflect or absorb different colors of light that can be monitored for quick and accurate determination of package moisture levels without invasive sampling. For instance, Neethirajan et al. (2009) developed grain quality monitoring nanosensors by using conducting polymer nanoparticles which respond to analytes and volatiles in the food storage environment and thereby detect the source and the type of spoilage (Neethirajan et al. 2009). Because of the miniaturization and requirement of low power, such type of nanosensors can be designed and deployed into the crevices of grain bulk, where the stored product pests often hide. Jonsson et al. (1997) developed an e-nose with three different complementary sensors (ten gas-sensitive metal oxide semiconductor field effect transistors, four tin dioxide-based sensors, and a carbon dioxide sensor) to test wheat samples with different levels of ergosterol, fungal, and bacterial contamination. In wheat, high degrees of correlation between artificial neural network predictions and measured ergosterol as well as fungal and bacterial colony forming units were observed. Campagnoli et al. (2011) developed electronic nose equipped with metal oxide semiconductor sensors and used it as a screening tool for the recognition of durum wheat naturally contaminated by deoxynivalenol. The e-nose was able to detect durum wheat whole-grain samples naturally contaminated with deoxynivalenol at the concentration level recommended by the European legislation, employing principal component analysis processing and a classifier based on classification and regression trees. Further, Eifler et al. (2011) showed that the metalloporphyrin-based e-nose can be used to qualitatively detect *Fusarium*-infected wheat grains. The developed electronic nose was capable of distinguishing between four wheat *Fusaria* species with an accuracy of more than 80%, which allowing them to be excluded from the food or feed chain. Similarly, Wu et al. (2013) assessed the feasibility of the application of e-nose technology to detect insect infestation in wheat. Wu et al. (2013) used an Alpha MOS FOX-3000 electronic nose equipped with 12 metal oxide semiconductor sensors to evaluate the presence of rusty grain beetle and red flour beetle in wheat. The e-nose detects the presence of red flour beetle in wheat with 20 insects Kg^{-1} of grains at 14–16% moisture content. These results clearly indicated that e-nose could also be used to detect other species of insects, in stored grains.

Nanotechnology offers food safety in terms of packaging for ensuring a longer shelf life by avoiding spoilage or loss of food nutrients (Sharma et al. 2017b). Active packaging has a desirable role in food preservation other than providing an inert barrier to the external conditions (Pathakoti et al. 2017). Active type of packaging includes usage of metal and metal oxide nanoparticles as antimicrobial agents in the form of nanocomposites for food packaging. Several companies like Nanocor Inc. and Southern Clay Products in the USA use montmorillonite as an additive in nanocomposite production. The supplementation of 3–5% montmorillonite makes

plastic lighter, stronger, and more heat resistant and also enhanced barrier properties against oxygen, carbon dioxide, moisture, and volatiles. These characteristics are extremely useful for food packaging applications, and montmorillonite use could enhance the shelf life of food grains including cereals and boil-in-bag food (García et al. 2010). Many advances have been made in the field of food packaging such as the development of a pH sensor embedded in a radio frequency transmitter without batteries, for in situ monitoring of deterioration processes of food grains (Fuertes et al. 2016). With the current application and advancements, nanotechnology will have a great impact on the storage, quality control, and food grain packaging and decide future direction of wheat-based food industries.

5.9 Toxicity and Adverse Effects of Nanomaterials

The major plant physiological indices of the toxic effects of nanomaterials are the germination percentage, root elongation, biomass, and leaf number (Ghosh et al. 2015; Lee et al. 2010). Nanoparticles can have substantial negative effects, such as reduction in seed germination and suppression of plant elongation, and can even cause plant death (Yang et al. 2017). In a recent study, the phytotoxicity and genotoxicity of silver nanoparticles on germinating wheat seedlings were investigated. It was found that silver nanoparticles in the concentration of 10 mg L^{-1} caused the alteration of all sorts of proteins related to cell metabolism (Vannini et al. 2014). The main factors influencing the effects of nanoparticles on plants are the characteristics of the nanomaterials themselves. The characteristics include concentration, size, category, and stability of applied nanomaterial. Additionally, size and species of plant seed, plant growth medium, plant growth stage, and nanoparticle coating material also influenced the action of nanoparticles on plants. For instance, the toxicity and bioavailability of copper nanoparticles were also observed in wheat (Keltjens and Van Beusichem 1998). Wheat crop showed a greater accumulation of copper nanoparticles in its roots due to the roots' morphology, which may be due to the release of cupric ion from copper nanoparticles. Recently, Watson et al. (2015) reported that the phytotoxicity of zinc oxide nanoparticles to young wheat seedlings was dependent on the soil properties. Phytotoxicity of zinc oxide nanoparticles, exhibited as the inhibition of root elongation of wheat, occurred when seedlings were raised in a native acid soil. Inhibition of root elongation due to nanoparticles was also observed when planted in sand (Dimkpa et al. 2013). However, extent of solubility of zinc from the nanoparticles was a 100-fold less in the alkaline than the acid soil; an increased uptake of zinc into the shoots from the nanoparticles occurred in the calcareous alkaline soil (Watson et al. 2015). The sand amended with copper oxide and zinc oxide in the dosage of 500 mg kg^{-1} soil significantly reduced root growth. Dissolved copper from copper oxide nanoparticles showed toxic behavior toward wheat plant, but zinc did not influence the shoot growth. Copper oxide and copper (I)-sulfur complexes were found to be accumulated in the shoot, while zinc was detected as zinc phosphate. Oxidative stress in the nanoparticle-treated plants

was reflected by an increase in lipid peroxidation and oxidized glutathione and higher peroxidase and catalase activities in roots. The solubility of nanoparticles decreased with increasing aggregation causing morphological changes in zinc oxide nanoparticles (Voegelin et al. 2005). It has been shown that the amount of copper and zinc ions released from copper oxide and zinc oxide are almost negligible to cause phytotoxicity to plants. Plants grown with nanoparticles showed increased accumulation of copper and zinc which altered root metabolism in wheat plants. Both copper oxide and zinc oxide nanoparticles have been detected in shoot of the plants. However, the quantitative difference between the two metals is mainly in terms of solubility and diffusion (Siddiqi and Husen 2017). These results indicate that use of zinc oxide nanoparticles as a fertilizer or a pesticide would have to be tuned to the soil being treated to avoid phytotoxic effects yet retain beneficial nanoparticle uptake.

5.10 Future Challenges and Directions

Despite tremendous applications of nanotechnology in wheat production and protection, several issues remain to be resolved in the near future before nanotechnology-based technology reflects significant contributions to the area of sustainable quality wheat production. The major areas that need further attention are enlisted as follows:

- Development of specific hybrid carriers for delivering active agents including fertilizers, pesticides, and nutrients in order to enhance efficiency under field conditions.
- Acquisition of knowledge and developments of methods for risk and life cycle assessment of nanomaterials, nanopesticides, and nanofertilizers as well as assessment of phytotoxic effects on nontarget organisms.
- Vigil and strict regulation policy about the use of nanoproducts. Therefore, future case studies are required in order to address the safety of farmers and consumers with respect to processed wheat grains using nanomaterials and nanoparticles as well as safe for soil health and fertility. Additionally, when developing a nanosensor for sustainable wheat grain production and processing, it is of utmost importance to ensure that the sensing component itself is safe for human health, because otherwise it has no future in its commercialization.
- At present adequate methodologies and tools are not available to understand the dynamics of nanoproducts in the environment, interactions of nanoproducts with target and nontarget organisms, or the occurrence of synergistic effects under field conditions. Therefore, sound and strong implementation of nanotechnology in wheat sector requires the development of tools capable of quantifying engineered nanoparticles at the concentrations present in different environmental compartments.

- Studies on methodologies able to assess possible arise of resistance mechanisms to nanomaterials by pathogens and insect pests should be undertaken. As a whole, the newly developed analytical methodologies would support predictive models to characterize, localize, and quantify engineered nanomaterials in the environments. Under these circumstances, knowledge exchange among researchers from different disciplines would be essential.

5.11 Conclusion

Nanotechnology has the potential to improve growth and yield of wheat under changing climate scenario. Soil and foliar application of nanomaterials may increase wheat yield significantly for meeting the food demand of the growing population. However, comprehensive experimentation is needed to determine the best concentration, mode, and time of application in addition to exploring underlying physiological mechanism responsible for enhanced growth and yield. Despite of these potential benefits, the application of nanotechnology in wheat fertilization and stress management could come with risks to the environment non-target plants, beneficial soil microbes, and other life forms which could be affected if nanomaterials are used injudiciously. Therefore, a better understanding of the agroecological consequences of nanotechnology, especially in context to dose response, release of ions, and nanoparticle-specific effects of mineral nutrients, is important to harness its full dividend. Research on nanosensors for detecting wheat pathogens is yet to be explored specially for its field application. It would be highly valuable for rapid diagnosis and effective disease management especially in case of compound interest diseases like rusts and powdery mildews and seed-borne diseases like loose smut and Karnal bunt. Nanosensors dispersed in the field can detect the presence of wheat pathogens and also the level of soil nutrients. Accelerating plant growth and productivity through the application of nanofertilizers can open new perspectives in resource management practices, because nanotech-based products promise to be a safe way to enrich nutrients to plants without doing significant harm to the environment. Nevertheless, further field studies are needed to study the effect of such concentration on growth and metabolism of wheat plants and to ensure the safety of the nano-treated plants for the use of animals and humans. Regarding the accumulation of nanoparticles in the wheat roots and shoots, quantification and localization of nanoparticles are still very unclear, and further research in this area is necessary. Nanotechnology-based devices will increase the use of sensors for real-time monitoring of wheat fields. However, genetic response of wheat seedlings in the presence of nanoparticles is also a topic of debate. Overall, it may be concluded that nanotechnology has more potential to enhance growth and yield of wheat under stressful environment. However, comprehensive experimentations are needed to determine the proper concentration, mode, and time of application in addition to exploring underlying physiological mechanism responsible for enhanced growth and yield of wheat. The

nanomaterials may be integrated with existing wheat crop production and protection technologies to have better impact and in a cropping system *per se*.

References

Abdel-Aziz HMM, Hasaneen MNA, Omer AM (2016) Nano chitosan-NPK fertilizer enhances the growth and productivity of wheat plants grown in sandy soil. Span J Agric Res 14(1):e0902. https://doi.org/10.5424/sjar/2016141-8205

Abeysingha NS, Singh M, Islam A, Sehgal VK (2016) Climate change impacts on irrigated rice and wheat production in Gomti River basin of India: a case study. Springerplus 5(1):1250. https://doi.org/10.1186/s40064-016-2905-y

Abid M, Shao Y, Liu S, Wang F, Gao J, Jiang D, Tian Z, Dai T (2017) Pre-drought priming sustains grain development under post-anthesis drought stress by regulating the growth hormones in winter wheat (*Triticum aestivum* L.). Planta 246(3):509–524. https://doi.org/10.1007/s00425-017-2698-4

Agarwal S, Grover A (2006) Molecular biology, biotechnology and genomics of flooding-associated low O_2 stress response in plants. Crit Rev Plant Sci 25:1–21. https://doi.org/10.1080/07352680500365232

Aliabadi T, Afshar AS, Nematpour FS (2016) The effects of Nano TiO_2 and Nano aluminium on the growth and some physiological parameters of wheat (*Triticum aestivum*). Iran J Plant Physiol 6 (2):1627–1635

Araus JL, Slafer GA, Reynolds MP, Royo C (2002) Plant breeding and water relations in C_3 cereals: what to breed for? Ann Bot 89:925–940. https://doi.org/10.1093/aob/mcf049

Asseng S, Ewert F, Martre P, Rötter RP, Lobell DB, Cammarano D, Kimball BA et al (2014) Rising temperatures reduce global wheat production. Nat Clim Chang 5(2):143. https://doi.org/10.1038/nclimate2470

Bailey-Serres J, Voesenek LA (2008) Flooding stress: acclimations and genetic diversity. Annu Rev Plant Biol 59:313–339. https://doi.org/10.1146/annurev.arplant.59.032607.092752

Barik TK, Sahu B, Swain V (2008) Nanosilica-from medicine to pest control. Parasitol Res 103 (2):253–258. https://doi.org/10.1007/s00436-008-0975-7

Bhati-Kushwaha H, Kaur A, Malik CP (2013) The synthesis and role of biogenic nanoparticles in overcoming chilling stress. Indian J Plant Sci 2(4):54–62. ISSN: 2319-3824

Bockus WW, Appel JA, Bowden RL, Fritz AK, Gill BS, Martin TJ, Sears RG, Seifers DL, Brown-Guedira GL, Eversmeyer MG (2001) Success stories: breeding for wheat disease resistance in Kansas. Plant Dis 85:453–461. https://doi.org/10.1094/PDIS.2001.85.5.453

Campagnoli A, Cheli F, Polidori C, Zaninelli M, Zecca O et al (2011) Use of the electronic nose as a screening tool for the recognition of durum wheat naturally contaminated by Deoxynivalenol: a preliminary approach. Sensors 11:4899–4916. https://doi.org/10.3390/s110504899

Chaves MS, Martinelli JA, Wesp-Guterres C, Graichen FAS, Brammer S, Scagliusi SM, Da Silva PR, Wiethölter P, Torres GAM, Lau EY et al (2013) The importance for food security of maintaining rust resistance in wheat. Food Secur 5:157–176. https://doi.org/10.1007/s12571-013-0248-x

Chenu K, Porter JR, Martre P, Basso B, Chapman SC, Ewert F, Bindi M, Asseng S (2017) Contribution of crop models to adaptation in wheat. Trends Plant Sci 22(6):472–490. https://doi.org/10.1016/j.tplants.2017.02.003

Chichiriccò G, Poma A (2015) Penetration and toxicity of nanomaterials in higher plants. Nano 5 (2):851–873. https://doi.org/10.3390/nano5020851

Cifuentes Z, Custardoy L, de la Fuente JM, Marquina C, Ibarra MR, Rubiales D, Alejandro Pérez-de-Luque A (2010) Absorption and translocation to the aerial part of magnetic carbon-coated

nanoparticles through the root of different crop plants. J Nanobiotechnol 8:26. https://doi.org/10.1186/1477-3155-8-26

Cramer GR, Urano K, Delrot S, Pezzotti M, Shinozaki K (2011) Effects of abiotic stress on plants: a systems biology perspective. BMC Plant Biol 11:163. https://doi.org/10.1186/1471-2229-11-163

Darko E, Gierczik K, Hudák O, Forgó P, Pál M, Türkösi E et al (2017) Differing metabolic responses to salt stress in wheat-barley addition lines containing different 7H chromosomal fragments. PLoS One 12(3):e0174170. https://doi.org/10.1371/journal.pone.0174170

Dasgupta N, Ranjan S, Mundekkad D, Ramalingam C, Shanker R, Kumar A (2015) Nanotechnology in agro food: from field to plate. Food Res Int 69:381–400. https://doi.org/10.1016/j.foodres.2015.01.005

DeRosa MC, Monreal C, Schnitzer M, Walsh R, Sultan Y (2010) Nanotechnology in fertilizers. Nat Nanotechnol 5(2):91–91. https://doi.org/10.1038/nnano.2010.2

Dias de Oliveria E, Bramley H, Siddique KHM, Henty S, Berger J, Palta JA (2013) Can elevated CO_2 combined with high temperature ameliorate the effect of terminal drought in wheat? Funct Plant Biol 40:160–171. https://doi.org/10.1071/FP12206

Dimkpa CO, McLean JE, Latta DE, Manangón E, Britt DW, Johnson WP, Boyanov MI, Anderson AJ (2012) CuO and ZnO nanoparticles: phytotoxicity, metal speciation, and induction of oxidative stress in sand-grown wheat. J Nanopart Res 14:1–15. https://doi.org/10.1007/s11051-012-1125-9

Dimkpa CO, Latta DE, McLean JE, Britt DW, Boyanov MI, Anderson AJ (2013) Fate of Cuo and ZnO nano- and microparticles in the plant environment. Environ Sci Technol 47:4734–4742. https://doi.org/10.1021/es304736y.E

Ditta A, Arshad M (2016) Applications and perspectives of using nanomaterials for sustainable plant nutrition. Nanotechnol Rev 5(2):209–229. https://doi.org/10.1515/ntrev-2015-0060

Du WC, Sun YY, Ji R, Zhu JG, Wu JC, Guo HY (2011) TiO_2 and ZnO nanoparticles negatively affect wheat growth and soil enzyme activities in agricultural soil. J Environ Monit 13:822–828. https://doi.org/10.1039/c0em00611d

Du WC, Gardea-Torresdey JL, Ji R, Yin Y, Zhu JG, Peralta-Videa JR, Guo HY (2015) Physiological and biochemical changes imposed by CeO_2 nanoparticles on wheat: a life cycle field study. Environ Sci Technol 49:11884–11893. https://doi.org/10.1021/acs.est.5b03055

Duveiller E, Kandel YR, Sharma RC, Shrestha SM (2005) Epidemiology of foliar blights (spot blotch and tan spot) of wheat in the plains bordering the Himalayas. Phytopathology 95:248–256. https://doi.org/10.1094/PHYTO-95-0248

Duveiller E, Singh RP, Nicol JM (2007) The challenges of maintaining wheat productivity: pests, diseases, and potential epidemics. Euphytica 157:417–430. https://doi.org/10.1007/s10681-007-9380-z

Eifler J, Martinelli E, Santonico M, Capuano R, Schild D, Di Natale C (2011) Differential detection of potentially hazardous *Fusarium* species in wheat grains by an electronic nose. PLoS One 6 (6):e21026. https://doi.org/10.1371/journal.pone.0021026

Farooq M, Hussain M, Siddique KHM (2014) Drought stress in wheat during flowering and grain-filling periods. Crit Rev Plant Sci 33(4):331–349. https://doi.org/10.1080/07352689.2014.875291

Farooqui A, Tabassum H, Ahmad A, Mabood A, Ahmad A, Ahmad IZ (2016) Role of nanoparticles in growth and Development of plants: a review. Int J Pharm Bio Sci 7(4):22–37. https://doi.org/10.22376/ijpbs.2016.7.4.p22-37

Flowers TJ, Galal HK, Bromham L (2010) Evolution of halophytes: multiple origins of salt tolerance in land plants. Funct. Plant Biol 37:604–612. https://doi.org/10.1007/s10142-011-0218-3

Fuertes G, Soto I, Carrasco R, Vargas M, Sabattin J, Lagos C (2016) Intelligent packaging systems: sensors and nanosensors to monitor food quality and safety. J Sens 2016:Article ID 4046061. https://doi.org/10.1155/2016/4046061

Gaiser BK, Fernandes TF, Jepson M, Lead JR, Tyler CR, Vicki Stone V (2009) Assessing exposure, uptake and toxicity of silver and cerium dioxide nanoparticles from contaminated environments. Environ Health 8(Suppl 1):S2. https://doi.org/10.1186/1476-069X-8-S1-S2

García M, Forbe T, Gonzalez E (2010) Potential applications of nanotechnology in the agro-food sector. Ciênc Tecnol Aliment Campinas 30(3):573–581

Ghosh M, Bhadra S, Adegoke A, Bandyopadhyay M, Mukherjee A (2015) MWCNT uptake in Allium cepa root cells induces cytotoxic and genotoxic responses and results in DNA hypermethylation. Mutat Res Fundam Mol Mech Mutagen 774:49–58. https://doi.org/10.1016/j.mrfmmm.2015.03.004

Grayson M (2013) Agriculture and drought. Nature 501(7468):S1. https://doi.org/10.1038/501S1a

Hafeez A, Razzaq A, Mahmood T, Jhanzab HM (2015) Potential of copper nanoparticles to increase growth and yield of wheat. J Nanosci Adv Technol 1(1):6–11. https://doi.org/10.24218/jnat.2015.02

Hu X, Zhou Q (2014) Novel hydrated graphene ribbon unexpectedly promotes aged seed germination and root differentiation. Sci Rep 4:3782. https://doi.org/10.1038/srep03782

Hussain HI, Yi ZF, Rookes JE, Kong LXX, Cahill DM (2013) Mesoporous silica nanoparticles as a biomolecule delivery vehicle in plants. J Nanopart Res 15:1–15. https://doi.org/10.1007/s11051-013-1676-4

Iannone MF, Groppa MD, de Sousa ML, Fernández van Raap MB, Benavides MP (2016) Impact of magnetite iron oxide nanoparticles on wheat (*Triticum aestivum* L.) development: evaluation of oxidative damage. Environ Exp Bot 131:77–88. https://doi.org/10.1016/j.envexpbot.2016.07.004

Iversen TG, Skotland T, Sandvig K (2011) Endocytosis and intracellular transport of nanoparticles: present knowledge and need for future studies. Nano Today 6:176–185. https://doi.org/10.1016/j.nantod.2011.02.003

Jaberzadeh A, Moaveni P, Moghadam HRT, Zahedi H (2013) Influence of bulk and nanoparticles titanium foliar application on some agronomic traits, seed gluten and starch contents of wheat subjected to water deficit stress. Not Bot Hortic Agrobot 41:201–207. https://doi.org/10.15835/nbha4119093

Jasrotia P, Kashyap PL, Bhardwaj AK, Kumar S, Singh GP (2018) Scope and applications of nanotechnology for wheat production: a review of recent advances. Wheat Barley Res 10(1):1–14. https://doi.org/10.25174/2249-4065/2018/76672

Jhanzab HM, Razzaq A, Jilani G, Rehman A, Hafeez A, Yasmeen F (2015) Silver nano-particles enhance the growth, yield and nutrient use efficiency of wheat. Int J Agron Agric Res 7(1):15–22

Jonsson A, Winquist F, Schnürer J, Sundgren H, Lundtröm I (1997) Electronic nose for microbial quality classification of grains. Int J Food Microbiol 35:187–193. https://doi.org/10.1016/S0168-1605(96)01218-4

Kashyap PL, Kumar S, Srivastava AK, Sharma AK (2013) Myconanotechnology in agriculture: a perspective. World J Microbiol Biotechnol 29(2):191–207. https://doi.org/10.1007/s11274-012-1171-6

Kashyap PL, Xiang X, Heiden P (2015) Chitosan nanoparticle based delivery systems for sustainable agriculture. Int J Biol Macromol 77:36–51. https://doi.org/10.1016/j.ijbiomac.2015.02.039

Kashyap PL, Rai P, Sharma S, Chakdar H, Kumar S, Pandiyan K, Srivastava AK (2016) Nanotechnology for the detection and diagnosis of plant pathogens. In: Ranjan S et al (eds) Nanoscience in food and agriculture 2, sustainable agriculture reviews 21. Springer, Basel, pp 253–276. https://doi.org/10.1007/978-3-319-39306-3_8

Kashyap PL, Kumar S, Srivastava AK (2017) Nanodiagnostics for plant pathogens. Environ Chem Lett 15:7–13. https://doi.org/10.1007/s10311-016-0580-4

Kashyap PL, Srivastava AK, Tiwari SP, Kumar S (2018a) Microbes for climate resilient agriculture. Wiley, Hoboken, p 349. ISBN: 978-1-119-27592-3

Kashyap PL, Rai P, Kumar R, Sharma S, Jasrotia P, Srivastava AK, Kumar S (2018b) Microbial nanotechnology for climate resilient agriculture. In: Kashyap PL et al (eds) Microbes for climate

resilient agriculture. Wiley, Hoboken, pp 279–344. https://doi.org/10.1002/9781119276050.ch13

Kashyap PL, Kumar S, Jasrotia P, Singh DP, Singh GP (2019) Nanosensors for plant disease diagnosis: current understanding and future perspectives. In: Pudake RN et al (eds) Nanoscience for Sustainable Agriculture. Springer Nature, Switzerland. https://doi.org/10.1007/978-3-319-97852-9_9

Kaur SI, Kashyap PL, Kang SS, Sharma A (2019) Detection and diagnosis of seed-borne viruses and virus-like pathogens. In: Kumar R, Gupta A (eds) Seed borne diseases of agricultural crops: detection, diagnosis & management. Springer Nature, Singapore. https://doi.org/10.1007/978-981-32-9046-4_7

Keltjens W, van Beusichem M (1998) Phytochelatins as biomarkers for heavy metal stress in maize (*Zea mays* L.) and wheat (*Triticum aestivum* L.): combined effects of copper and cadmium. Plant Soil 203:119–126. https://doi.org/10.1023/A:1004373700581

Kheiri A, Moosawi Jorf SA, Malihipour A, Saremi H, Nikkhah M (2016) Application of chitosan and chitosan nanoparticles for the control of *Fusarium* head blight of wheat (*Fusarium graminearum*) *in vitro* and greenhouse. Int J Biol Macromol 93:1261–1272. https://doi.org/10.1016/j.ijbiomac.2016.09.072

Kheiri A, Moosawi Jorf SA, Malihipour A, Saremi H, Nikkhah M (2017) Synthesis and characterization of chitosan nanoparticles and their effect on *Fusarium* head blight and oxidative activity in wheat. Int J Biol Macromol 102:526–538. https://doi.org/10.1016/j.ijbiomac.2017.04.034

Khot LR, Sankaran S, Maja JM, Ehsani R, Schuster EW (2012) Applications of nanomaterials in agricultural production and crop protection: a review. Crop Prot 35:64–70. https://doi.org/10.1016/j.cropro.2012.01.007

Kole C, Kole P, Randunu KM, Choudhary P, Podila R, Ke PC, Rao AM, Marcus RK (2013) Nanobiotechnology can boost crop production and quality: first evidence from increased plant biomass, fruit yield and phytomedicine content in bitter melon (*Momordica charantia*). BMC Biotechnol 13:37. https://doi.org/10.1186/1472-6750-13-37

Konate A, He X, Zhang Z, Ma Y, Zhang P, Alugongo GM, Rui Y (2017) Magnetic (Fe_3O_4) nanoparticles reduce heavy metals uptake and mitigate their toxicity in wheat seedling. Sustainability 9:790. https://doi.org/10.3390/su9050790

Kumar U, Joshi AK, Kumar S, Chand R, Roder MS (2009) Mapping of resistance to spot blotch disease caused by *Bipolaris sorokiniana* in spring wheat. Theor Appl Genet 118:783–792. https://doi.org/10.1007/s00122-008-0938-5

Larue C, Laurette J, Herlin-Boime N, Khodja H, Fayard B, Flank AM et al (2012a) Accumulation, translocation and impact of TiO_2 nanoparticles in wheat (*Triticum aestivum* spp.): influence of diameter and crystal phase. Sci Total Environ 431:197–208. https://doi.org/10.1016/j.scitotenv.2012.04.073

Larue C, Veronese G, Flank AM, Surble S (2012b) Comparative uptake and impact of TiO_2 nanoparticles in wheat and rapeseed. J Toxicol Environ Health A 75(13–15):72–734. https://doi.org/10.1080/15287394.2012.689800

Lee CW, Mahendra S, Zodrow K, Li D, Tsai YC, Braam J, Alvarez PJ (2010) Developmental phytotoxicity of metal oxide nanoparticles to *Arabidopsis thaliana*. Environ Toxicol Chem 29:669–675. https://doi.org/10.1002/etc.58

López-Luna J, Silva-Silva MJ, Martinez-Vargas S, Mijangos-Ricardez OF, González-Chávez MC, Solís-Domínguez FA, Cuevas-Díaz MC (2016) Magnetite nanoparticle (NP) uptake by wheat plants and its effect on cadmium and chromium toxicological behavior. Sci Total Environ 565:941–950. https://doi.org/10.1016/j.scitotenv.2016.01.029

Ludwig F, Milroy SP, Asseng S (2009) Impacts of recent climate change on wheat production systems in Western Australia. Clim Chang 92:495–517. https://doi.org/10.1007/s10584-008-9479-9

Luechinger NA, Loher S, Athanassiou EK, Grass RN, Stark WJ (2007) Highly sensitive optical detection of humidity on polymer/metal nanoparticle hybrid films. Langmuir 23(6):3473–3477. https://doi.org/10.1021/la062424y

Lyu S, Wei X, Chen J, Wang C, Wang X, Pan D (2017) Titanium as a beneficial element for crop production. Front Plant Sci 8:597. https://doi.org/10.3389/fpls.2017.00597

Mahmoodzadeh H, Aghili R (2014) Effect on germination and early growth characteristics in wheat plants (Triticum aestivum L.) seeds exposed to TiO_2 nanoparticles. J Chem Health Risks 4 (1):29–36

Marasas CN, Smale M, Singh RP (2004) The economic impact in developing countries of leaf rust resistance breeding in CIMMYT-related spring bread wheat, Economics Program Paper 04-01. CIMMYT, Mexico

Miralles P, Johnson E, Church TL, Harris AT (2012) Multiwalled carbon nanotubes in alfalfa and wheat: toxicology and uptake. J R Soc Interface 9(77):3514–3527. https://doi.org/10.1098/rsif.2012.0535

Miransari M, Smith DL (2007) Overcoming the stressful effects of salinity on soybean (*Glycine max* L) nodulation and yields using signal molecule genist in under field condition. J Plant Nutr 30:1967–1992. https://doi.org/10.1080/01904160701700384

Mishra S, Singh HB (2015) Silver nanoparticles mediated altered gene expression of melanin biosynthesis genes in *Bipolaris sorokiniana*. Microbiol Res 172:16–18. https://doi.org/10.1016/j.micres.2015.01.006

Mishra S, Singh BR, Singh A, Keswani C, Naqvi AH, Singh HB (2014) Biofabricated silver nanoparticles act as a strong fungicide against *Bipolaris sorokiniana* causing spot blotch disease in wheat. PLoS One 9(5):e97881. https://doi.org/10.1371/journal.pone.0097881

Mishra S, Singh BR, Naqvi AH, Singh HB (2017) Potential of biosynthesized silver nanoparticles using *Stenotrophomonas* sp. BHU-S7 (MTCC 5978) for management of soil-borne and foliar phytopathogens. Sci Rep 7:45154. https://doi.org/10.1038/srep45154

Mittler R (2006) Abiotic stress, the field environment and stress combination. Trends Plant Sci 11:15–19. https://doi.org/10.1016/j.tplants.2005.11.002

Mohamed AKSH, Qayyum MF, Abdel-Hadi AM, Rehman RA, Ali S, Rizwan M (2017) Interactive effect of salinity and silver nanoparticles on photosynthetic and biochemical parameters of wheat. Arch Agron Soil Sci 63(12):1736–1747. https://doi.org/10.1080/03650340.2017.1300256

Mondal S, Rutkoski JE, Velu G, Singh PK, Crespo-Herrera LA, Guzmán C, Bhavani S, Lan C, He X, Singh RP (2016) Harnessing diversity in wheat to enhance grain yield, climate resilience, disease and insect pest resistance and nutrition through conventional and modern breeding approaches. Front Plant Sci 7:991. https://doi.org/10.3389/fpls.2016.00991

Morteza E, Moaveni P, Aliabadi Farahani H, Kiyani M (2013) Study of photosynthetic pigments changes of maize (*Zea mays* L.) under nano TiO2 spraying at various growth stages. Springer Plus 2:247. https://doi.org/10.1186/2193-1801-2-247

Munns R, Tester M (2008) Mechanisms of salinity tolerance. Annu Rev Plant Biol 59:651–681. https://doi.org/10.1146/annurev.arplant.59.032607.092911

Naderi MR, Danesh-Shahraki A (2013) Nanofertilizers and their roles in sustainable agriculture. Int J Agric Crop Sci 5:2229–2232

Nair R, Poulose AC, Nagaoka Y, Yoshida Y, Maekawa T, Kumar DS (2011) Uptake of FITC labeled silica nanoparticles and quantum dots by rice seedlings: effects on seed germination and their potential as biolabels for plants. J Fluoresc 21:2057–2068. https://doi.org/10.1007/s10895-011-0904-5

Nakashima K, Yamaguchi-Shinozaki K (2006) Regulons involved in osmotic stress-responsive and cold stress-responsive gene expression in plants. Physiol Plant 126:62–71. https://doi.org/10.1111/j.1399-3054.2005.00592.x

Naresh Kumar S, Aggarwal PK, Swaroopa Rani DN, Saxena R, Chauhan N, Jain S (2014) Vulnerability of wheat production to climate change in India. Clim Res 59(173–187):5–187. https://doi.org/10.3354/cr01212

Neethirajan S, Jayas DS (2009) Nanotechnology for the food and bioprocessing industries. Food Bioprocess Technol 4:39–47. https://doi.org/10.1007/s11947-010-0328-2

Neethirajan S, Freund MS, Shafai C, Jayas DS, Thomson D J (2009) Development of carbon dioxide sensor for agrifood industry. United States Provisional Patent No. 2009-61/23891

Neethirajan S, Ragavan V, Weng X, Chand R (2018) Biosensors for sustainable food engineering: challenges and perspectives. Biosensors 8(1):23. https://doi.org/10.3390/bios8010023

Negrão S, Schmöckel SM, Tester M (2017) Evaluating physiological responses of plants to salinity stress. Ann Bot 119(1):1–11. https://doi.org/10.1093/aob/mcw191

Nezhadahmadi A, Prodhan ZH, Faruq G (2013) Drought tolerance in wheat. Sci World J:Article ID 610721. https://doi.org/10.1155/2013/610721

Oerke EC (2006) Crop losses to pests. J Agric Sci 144:31–43. https://doi.org/10.1017/S0021859605005708

Panyuta O, Belava V, Fomaidi S, Kalinichenko O, Volkogon M, Taran N (2016) The effect of pre-sowing seed treatment with metal nanoparticles on the formation of the defensive reaction of wheat seedlings infected with the eyespot causal agent. Nanoscale Res Lett 11:92. https://doi.org/10.1186/s11671-016-1305-0

Pathakoti K, Manubolu M, Hwang H-M (2017) Nanostructures: current uses and future applications in food science. J Food Drug Anal 25(2):245–253. https://doi.org/10.1016/j.jfda.2017.02.004

Pradas Del Real AE, Vidal V, Carrière M, Castillo-Michel H, Levard C, Chaurand P, Sarret G (2017) Silver nanoparticles and wheat roots: a complex interplay. Environ Sci Technol 51 (10):5774–5782. https://doi.org/10.1021/acs.est.7b00422

Qadir M, Quillérou E, Nangia V, Murtaza G, Singh M, Thomas RJ et al (2014) Economics of salt-induced land degradation and restoration. Nat Resour Forum 38:282–295. https://doi.org/10.1111/1477-8947.12054

Rafique R, Arshad M, Khokhar MF, Qazi IA, Hamza A, Virk N (2014) Growth response of wheat to titania nanoparticles application. NUST J Eng Sci 7(1):42–46

Rahman MM, Haque MA, Nihad SAI, Akand MMH, Howlader MRA (2016) Morpho-physiological response of *Acacia auriculiformis* as influenced by seawater induced salinity stress. For Syst 25:e071. https://doi.org/10.5424/fs/2016253-09386

Raliya R, Biswas P, Tarafdar JC (2015) TiO_2 nanoparticle biosynthesis and its physiological effect on mung bean (*Vigna radiata* L.). Biotechnol Rep 5:22–26. https://doi.org/10.1016/j.btre.2014.10.009

Ramesh M, Palanisamy K, Babu K, Sharma NK (2014) Effects of bulk & nano-titanium dioxide and zinc oxide on physio-morphological changes in *Triticum aestivum* Linn. J Glob Biosci 3:415–422

Rameshaiah GN, Jpallavi S (2015) Nano fertilizers and nano sensors–an attempt for developing smart agriculture. Int J Eng Res Gen Sci 3:314–320

Rampino P, Pataleo S, Gerardi C, Mita G, Perrotta C (2006) Drought stress response in wheat: physiological and molecular analysis of resistant and sensitive genotypes. Plant Cell Environ 29 (12):2143–2152. https://doi.org/10.1111/j.1365-3040.2006.01588.x

Razzaq A, Ammara R, Jhanzab HM, Mahmood T, Hafeez A, Hussain S (2016) A novel nanomaterial to enhance growth and yield of wheat. J Nanosci Technol 2(1):55–58

Riadh K, Wided M, Hans-Werner K, Chedly A (2010) Responses of halophytes to environmental stresses with special emphasis to salinity. Adv Bot Res 53:117–145. https://doi.org/10.1016/S0065-2296(10)53004-0

Riahi-Madvar A, Rezaee F, Jalili V (2012) Effects of alumina nanoparticles on morphological properties and antioxidant system of *Triticum aestivum*. Iran J Plant Physiol 3(1):595–603

Rico CM, Lee SC, Rubenecia R, Mukherjee A, Hong J, Peralta-Videa JR, Gardea-Torresdey JL (2014) Cerium oxide nanoparticles impact yield and modify nutritional parameters in wheat (*Triticum aestivum* L.). J Agric Food Chem 62:9669–9675. https://doi.org/10.1021/jf503526r

Rico CM, Peralta-Videa JR, Gardea-Torresdey JL (2015) Differential effects of cerium oxide nanoparticles on rice, wheat, and barley roots: a fourier transform infrared (FT-IR) microspectroscopy study. Appl Spectrosc 69:287–295. https://doi.org/10.1366/14-07495

Ruan CJ, da Silva JAT, Mopper S, Qin P, Lutts S (2010) Halophyte improvement for a salinized world. Crit Rev Plant Sci 29:329–359. https://doi.org/10.1080/07352689.2010.524517

Savadi S, Prasad P, Kashyap PL, Bhardwaj SC (2018) Molecular breeding technologies and strategies for rust resistance in wheat (*Triticum aestivum*) for sustained food security. Plant Pathol 67(4):771–791. https://doi.org/10.1111/ppa.12802

Savi GD, Piacentini KC, de Souza SR, Costa MEB, Santos CMR, Scussel VM (2015) Efficacy of zinc compounds in controlling *Fusarium* head blight and deoxynivalenol formation in wheat (*Triticum aestivum* L.). Int J Food Microbiol 205:98–104. https://doi.org/10.1016/j.ijfoodmicro.2015.04.001

Schwabe F, Schulin R, Limbach LK, Stark W, Bürge D, Nowack B (2013) Influence of two types of organic matter on interaction of CeO_2 nanoparticles with plants in hydroponic culture. Chemosphere 91:512–520. https://doi.org/10.1016/j.chemosphere.2012.12.025

Shafea AA, Dawood MF, Zidan MA (2017) Wheat seedlings traits as affected by soaking at titanium dioxide nanoparticles. Environ Earth Ecol 1(1):102–111. https://doi.org/10.24051/eee/6860767

Sharma RC, Duveiller E (2004) Effect of *Helminthosporium* leaf blight on performance of timely and late-seeded wheat under optimal and stressed levels of soil fertility and moisture. Field Crop Res 89:205–218. https://doi.org/10.1016/j.fcr.2004.02.002

Sharma S, Rai P, Rai S, Srivastava M et al (2017a) Genomic revolution in crop disease diagnosis: a review. In: Singh SS (ed) Plants and microbes in an ever changing environment. Nova Science Publishers, Hauppauge, pp 257–293

Sharma C, Dhiman R, Rokana N, Panwar H (2017b) Nanotechnology: an untapped resource for food packaging. Front Microbiol 8:1735. https://doi.org/10.3389/fmicb.2017.01735

Shiferaw B, Smale M, Braun HJ et al (2013) Crops that feed the world 10. Past successes and future challenges to the role played by wheat in global food security. Food Secur 5(3):291–317. https://doi.org/10.1007/s12571-013-0263-y

Siddiqi KS, Husen A (2017) Plant response to engineered metal oxide nanoparticles. Nanoscale Res Lett 12:92. https://doi.org/10.1186/s11671-017-1861-y

Singh S, Singh M, Agrawal VV, Kumar A (2010) An attempt to develop surface plasmon resonance based immunosensor for Karnal bunt (*Tilletia indica*) diagnosis based on the experience of nano-gold based lateral flow immune-dipstick test. Thin Solid Films 519:1156–1159. https://doi.org/10.1016/j.tsf.2010.08.061

Srinivasan C, Saraswathi R (2010) Nano-agriculture-carbon nanotubes enhance tomato seed germination and plant growth. Curr Sci 99:273–275

Srivastava AK, Dev A, Karmakar S (2018) Nanosensors and nanobiosensors in food and agriculture. Environ Chem Lett 16:161. https://doi.org/10.1007/s10311-017-0674-7

Sun D, Hussain HI, Yi Z, Rookes JE, Kong L, Cahill DM (2016) Mesoporous silica nanoparticles enhance seedling growth and photosynthesis in wheat and lupin. Chemosphere 152:81–91. https://doi.org/10.1016/j.chemosphere.2016.02.096

Taran N, Storozhenko V, Svietlova N, Batsmanova L, Shvartau V, Kovalenko M (2017) Effect of zinc and copper nanoparticles on drought resistance of wheat seedlings. Nanoscale Res Lett 12:60. https://doi.org/10.1186/s11671-017-1839-9

Teodoro S, Micaela B, David KW (2010) Novel use of nano-structured alumina as an insecticide. Pest Manag Sci 66(6):577–579. https://doi.org/10.1002/ps.1915

Thaxton CS, Georganopoulou DG, Mirkin CA (2006) Gold nanoparticle probes for the detection of nucleic acid targets. Clin Chim Acta 363(1–2):120–126. https://doi.org/10.1016/j.cccn.2005.05.042

Tiwari DK, Dasgupta-Schubert N, Villaseñor-Cendejas LM, Villegas J, Carreto-Montoya L, Borjas-García SE (2014) Interfacing carbon nanotubes (CNT) with plants: enhancement of growth, water and ionic nutrient uptake in maize (*Zea Mays*) and implications for nanoagriculture. Appl Nanosci 4:577–591. https://doi.org/10.1007/s13204-013-0236-7

Tripathi S, Sarkar S (2014) Influence of water soluble carbon dots on the growth of wheat plant. Appl Nanosci. https://doi.org/10.1007/s13204-014-0355-9

Tripathi DK, Singh S, Singh VP, Prasad SM, Dubey NK, Chauhan DK (2016) Silicon nanoparticles more effectively alleviated UV-B stress than silicon in wheat (*Triticum aestivum*) seedlings. Plant Physiol Biochem 110:70–81. https://doi.org/10.1016/j.plaphy.2016.06.026

Tripathi DK, Singh S, Singh S, Pandey R, Singh VP, Sharma NC et al (2017) An overview on manufactured nanoparticles in plants: uptake, translocation, accumulation and phytotoxicity. Plant Physiol Biochem 110:2–12. https://doi.org/10.1016/j.plaphy.2016.07.030

Ullah S, Arshad M (2014) Exposure-response of *Triticum aestivum* to TNPs application: seedling vigor index and micronuclei formation. Sci Vision 20(1):57–61

Ulrichs C, Mewis I, Goswami A (2005) Crop diversification aiming nutritional security in West Bengal: biotechnology of stinging capsules in nature's water-blooms. Ann Tech Issue of State Agri Technologists Service Assoc, pp 1–18

Vannini C, Domingo G, Onelli E, De Mattia F, Bruni I, Marsoni M, Bracale M (2014) Phytotoxic and genotoxic effects of silver nanoparticles exposure on germinating wheat seedlings. J Plant Physiol 171:1142–1148. https://doi.org/10.1016/j.jplph.2014.05.002

Villagarcia H, Dervishi E, Silva K, Biris AS, Khodakovskaya MV (2012) Surface chemistry of carbon nanotubes impacts the growth and expression of water channel protein in tomato plants. Small 8:2328–2233. https://doi.org/10.1002/smll.201102661

Voegelin A, Pfister S, Scheinost AC, Marcus MA, Kretzschmar R (2005) Changes in zinc speciation in field soil after contamination with zinc oxide. Environ Sci Technol 39:6616–6623. https://doi.org/10.1021/es047962g

Watson JL, Fang T, Dimkpa CO et al (2015) The phytotoxicity of ZnO nanoparticles on wheat varies with soil properties. Biometals 28:101–112. https://doi.org/10.1007/s10534-014-9806-8

Wild E, Jones KC (2009) Novel method for the direct visualization of *in-vivo* nanomaterials and chemical interactions in plants. Environ Sci Technol 43(14):5290–5294. https://doi.org/10.1021/es900065h

Wu J, Jayas DS, Zhang Q, White NDG, York RK (2013) Feasibility of the application of electronic nose technology to detect insect infestation in wheat. Can Biosyst Eng 55:3.1–3.9. https://doi.org/10.7451/CBE.2013.55.3.1

Xia T, Kovochich M, Liong M, Mädler L, Gilbert B, Shi H, Yeh JI, Zink JI, Nel AE (2008) Comparison of the mechanism of toxicity of zinc oxide and cerium oxide nanoparticles based on dissolution and oxidative stress properties. ACS Nano 2(10):2121–2134. https://doi.org/10.1021/nn800511k

Yang JG, Okamoto T, Lchino R, Sarake S, Okido M (2006) A simple way for preparing antioxidation nano-copper powders. Chem Lett 35:648–649

Yang FL, Li XG, Zhu F, Lei CL (2009) Structural characterization of nanoparticles loaded with garlic essential oil and their insecticidal activity against *Tribolium castaneum* (Herbst) (Coleoptera:Tenebrionidae). J Agric Food Chem 57(21):10156–10162. https://doi.org/10.1021/jf9023118

Yang C, Zhao L, Zhang H, Yang Z, Wang H, Wen S, Zhang C, Rustgi S, von Wettstein D, Liu B (2014) Evolution of physiological responses to salt stress in hexaploid wheat. Proc Natl Acad Sci U S A 111(32):11882–11887. https://doi.org/10.1073/pnas.1412839111

Yang J, Cao W, Rui Y (2017) Interactions between nanoparticles and plants: phytotoxicity and defense mechanisms. J Plant Interact 12(1):158–169. https://doi.org/10.1080/17429145.2017.1310944

Yasmeen F, Raja NI, Razzaq A, Komatsu S (2016) Gel-free/label-free proteomic analysis of wheat shoots in stress tolerant varieties under iron nanoparticles exposure. Biochim Biophys Acta, Proteins Proteomics 1864(11):1586–1598. https://doi.org/10.1016/j.bbapap.2016.08.009

Zaimenko NV, Didyk NP, Dzyuba OI, Zakrasov OV, Rositska NV, Viter AV (2014) Enhancement of drought resistance in wheat and corn by nanoparticles of natural mineral analcite. Ecologia Balkanica 6(1):1–10

Zhang F, Wang R, Xiao Q, Wang Y, Zhang J (2006) Effects of slow/controlled-release fertilizer cemented and coated by nano-materials on biology. II. Effects of slow/controlled-release fertilizer cemented and coated by nano-materials on plants. Nano 11:18–26

Ziaee M, Ganji Z (2016) Insecticidal efficacy of silica nanoparticles against *Rhyzopertha dominica* F. and *Tribolium confusum* Jacquelin du Val. J Plant Protect Res 56(3):250–256. https://doi.org/10.1515/jppr-2016-0037

Chapter 6
Nanoparticles for New Pharmaceuticals: Metabolites from Actinobacteria

Dávila Costa, José Sebastián, Cintia Mariana Romero, María Cecilia Rasuk, Julian Pereyra, Daiana Guerrero, and Analía Álvarez

Contents

6.1 Introduction 197
6.2 Mechanisms of Nanoparticle Biosynthesis 199
6.2.1 Intracellular Synthesis 199
6.2.2 Extracellular Synthesis 200
6.3 Actinobacteria: General Features of the Group and Promising Strains for Nanoparticle Biosynthesis 200
6.4 Nanoparticles Toxicity 202
6.5 Methods for Nanoparticle Characterization 203
6.6 Specialized Metabolites in Actinobacteria 205
6.7 Connection Between Primary and Specialized Metabolism: Their Evolution 206
6.8 Extreme *Streptomyces* and *Amycolatopsis* Strains as Source of New Specialized Metabolites 206

Authors José Sebastián and Cintia Mariana Romero have equally contributed to this chapter.

D. Costa · J. Sebastián · M. C. Rasuk
Planta Piloto de Procesos Industriales Microbiológicos (PROIMI-CONICET), Avenida Belgrano y Pasaje Caseros, Tucumán, Argentina

C. M. Romero
Planta Piloto de Procesos Industriales Microbiológicos (PROIMI-CONICET), Avenida Belgrano y Pasaje Caseros, Tucumán, Argentina

Facultad de Bioquímica, Química y Farmacia, Universidad Nacional de Tucumán, Tucumán, Argentina

J. Pereyra · D. Guerrero
Facultad de Bioquímica, Química y Farmacia, Universidad Nacional de Tucumán, Tucumán, Argentina

A. Álvarez (✉)
Planta Piloto de Procesos Industriales Microbiológicos (PROIMI-CONICET), Avenida Belgrano y Pasaje Caseros, Tucumán, Argentina

Facultad de Ciencias Naturales e Instituto Miguel Lillo, Universidad Nacional de Tucumán, Tucumán, Argentina

N. Dasgupta et al. (eds.), *Environmental Nanotechnology Volume 4*, Environmental Chemistry for a Sustainable World 32, https://doi.org/10.1007/978-3-030-26668-4_6

6.9 Patents in the Emerging World of Bio-nanoparticles 208
6.10 Conclusion 209
References 210

Abstract The resistance of common or resurgent pathogens to standard antibiotic therapies is a significant health problem, so the need for new antimicrobial sources is imperative. It is widely known that the most promising source of new drugs remains natural products, mainly those of microbial origin. Such is the case of microbial nanoparticles (NPs) which have unusual physical, chemical, and biological properties like as powerful antibacterial activities. While NPs synthesized by chemical methods involve hazardous and expensive processes, nano-biosynthesis is a green technology by which NPs are obtained through biological processes such as the reduction of a metal salt by the action of biomolecules.

The aim of this chapter is to provide an overview of the continuing central role of natural products like the NPs in the discovery and development of new pharmaceuticals. It is known that *Actinobacteria* are excellent producers of specialized biomolecules, such as NPs. Moreover, it was demonstrated that they have in their genomes many more biosynthetic pathways, which constitute an untapped promising source of new antibacterial molecules and other therapeutic agents. Here, we focus on those heavy metal-resistant strains, due to biogenic NPs are synthesized by simple processes of metal reductions which can naturally occur as part of cellular detoxification mechanisms. In this context, a brief description of the ways of the NPs bioproduction is given. Although extracellular production of metal NPs has more commercial applications in several areas, intracellular production is of the particular dimension and with less polydispersity. This is remarkable due to the control over particle size, and polydispersity is needed to be established for biotechnological purposes. Also, a brief overview of some of the most important methods for nanoparticle characterization is provided. The most applied techniques in NPs characterization are ultraviolet-visible (UV-vis) spectrophotometer, transmission electron microscopy (TEM), scanning electron microscopy (SEM), atomic force microscopy (AFM), dynamic light scattering (DLS), X-ray powder diffraction (XRD), Fourier transform infrared spectroscopy (FT-IR), Zeta potential measurement, particle size analysis (PSA), and energy dispersive X-ray spectroscopy (EDX).

By last, this chapter describes the mechanisms that explain the antimicrobial properties of NPs, and it is believed that the more relevant traits of NPs are related with their surface-reactive groups exposed, leading to the formation of reactive oxygen species (ROS). This is indirectly related to their size, as the size of the particle decreases and its surface area increases and determines the potential number of reactive groups on the particle surface.

Keywords Antibiotic resistance · Microbial nanoparticles · Green technology · Actinobacteria · Antibacterial activity · Metal resistance · Nano-biosynthesis · Characterization techniques · Nanoparticle properties

6.1 Introduction

New drugs, especially antibiotics, are needed to counter the spread of antibiotic-resistant pathogens and to combat several diseases (Payne et al. 2007; Olano et al. 2009). It is widely known that the most promising source of new drugs remain natural products such as biomolecules especially those of microbial origin (Bull and Stach 2007). Members of the *Actinobacteria* group produce about 45% of all microbial bioactive molecules such as secondary metabolites or, more precisely, specialized metabolites (Bérdy 2005; Hoskisson et al. 2015). In particular, *Streptomyces* and *Amycolatopsis* genera produce as part of their normal life cycle specialized metabolites that represent about 65% of the antimicrobial drugs used in clinical (McLean et al. 2016). However, from the study of their genomes, it is known that they have the genetic ability to produce many more of these molecules. Both microbial genera may have between 20 and 50 biosynthetic pathways, but only very few of them are expressed under common laboratory conditions (McLean et al. 2016). It is believed that the biochemical diversity encoded by these "silent" or "unproductive" biosynthetic pathways is an untapped promising source of new antibacterial molecules and other therapeutic agents (Goodfellow and Fiedler 2010). Hence, identification and cloning of clusters of biosynthetic genes encoding potential chemically novel antimicrobial drugs are an emerging technology.

In search of novel biomolecules, nanoscience and nanotechnology are emerging fields which involve the synthesis and application of nanoscale materials such as nanoparticles (NPs) (Golinska et al. 2017). Due to miniaturization (1–100 nm), the change in the physicochemical properties produces novel attributes of nanomaterials. Thus, NP applications are growing on several areas like biomedical, pharmaceutical, catalysis, and drug delivery, among others. The metallic NPs are considered as most promising since they contain remarkable antibacterial properties due to their large surface area related to volume ratio. Metallic NPs which have gained immense attention in recent years are silver, gold, platinum, palladium, titanium, iron, aluminum, and copper. Among the abovementioned metals, silver (Ag) is the most important in NP synthesis since AgNPs have many uses in the medical field. Silver is anti-inflammatory, antitumor (Beeler and Singh 2016), and fundamentally antimicrobial, which arouses great expectations in the search for new sources of AgNPs due to the drastic increase in microbial resistance to antibiotics (WHO 2015).

Researchers are immensely interested in NP synthesis by physical or chemical methods, and these NPs are designated as engineered NPs (ENPs). However, the conventional chemical methods for the synthesis of ENPs use high energy levels, making their production very expensive. Besides, the use of toxic chemicals and nonpolar solvents in the ENPs synthesis limits their applications in clinical areas. Nano-biosynthesis, on the other hand, is a "green technology" by which NPs are obtained through biological processes such as the reduction of a metal salt by the action of biomolecules. In this context, biomolecules (mostly proteins) from plants, algae, bacteria, and fungi can act as reducing and/or stabilizing agents for the formation of monodispersed NPs (Siddiqi and Husen 2016). Nanoparticles

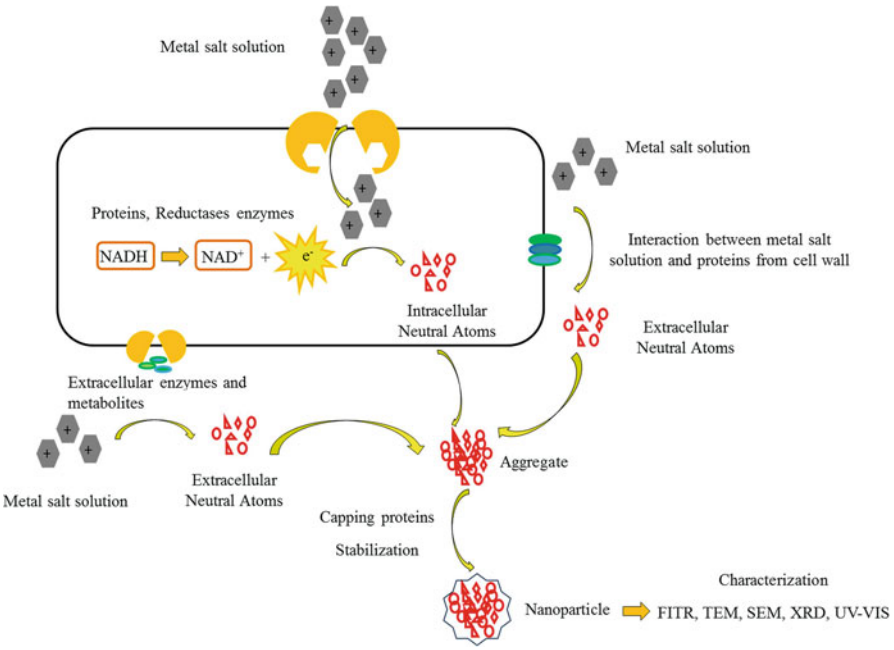

Fig. 6.1 Biosynthesis of nanoparticles (NPs) by a microbial cell. The different possibilities of extracellular and intracellular nano-biosynthesis are represented

developed by biogenic synthesis have advantages over ENPs due to the simplicity of the biological production methods since it does not require high temperatures or pressure. In addition, these processes are inexpensive, relatively easy to scale, and mostly harmless (Borase et al. 2014).

Biogenic NPs are synthesized by simple processes of intra- or extracellular metal reductions which can naturally occur as part of cellular detoxification mechanisms (Siddiqi and Husen 2016). Microbial systems can detoxify the metal ions by either reduction or precipitation of soluble toxic inorganic ions to insoluble nontoxic metal NPs. These NPs can be associated with proteins, which favor their stability, prevent their aggregation, and give NPs exceptional biochemical properties (Golinska et al. 2017) (Fig. 6.1). In this context, microorganisms developed in environments contaminated with metals are an excellent source for the biosynthesis of metallic NPs (Khot et al. 2012).

Cell-free extracts and/or microbial culture supernatants are used as reducers (Gade et al. 2008) for the production of NPs being the extracellular method the most popular because it facilitates the downstream process of recovery of NPs. Thus, by microbial culture, small particles are obtained on a large scale and with relatively high morphology control (Rai et al. 2011). However, NP synthesis depends on many factors such as the microbial species and even the microbial variety (strain), since the formation of NPs is highly dependent on the enzymes and other components produced by the cell capable of reducing, for example, $AgNO_3$ to Ag 0. It has been reported that some

strains of the same species produce more NPs, while others destabilize their formation (Durán et al. 2007). Therefore, it is necessary to make comparisons among microorganisms to identify promising candidates for the synthesis of NPs.

Due to the constant need to improve and optimize human quality of life, scientific world is constantly looking to develop new drugs. In this context, heavy metal-resistant actinobacteria constitute potential biofactories of NPs and source of new specialized metabolites that could be used as novel and effective antimicrobials. This premise is based on the hypothesis that (i) microorganisms isolated from contaminated areas possess in their genomes clusters of genes related to the biosynthesis of specialized biomolecules that allowed them to survive in these extreme environments and (ii) biogenic NPs are synthesized by simple processes of metal reductions which can naturally occur as part of cellular detoxification mechanisms.

The present book chapter compiles and updates the available information about the synthesis of NPs by actinobacteria and discusses about the potential of metal-resistant strains to produce new NPs and specialized metabolites that could be used as novel and effective antimicrobials. In addition, we explore by means of a purely molecular approach the search of new antimicrobials from the genomic analysis. An overview about techniques used for the study and characterization of NPs is also given.

6.2 Mechanisms of Nanoparticle Biosynthesis

Mechanisms of NP biosynthesis are deeply related to the microorganism since each one may reduce and oxidize the metallic precursor of NPs by different ways. In general, methods of biosynthesis show relationship with the specific survival strategies of the microorganism (Bansal et al. 2012). As was previously mentioned, it has been shown that microorganisms utilize defense mechanisms to reduce the environmental toxicity through different ways of NP production. Microbial detoxification can be made either by biomineralization, biosorption, complexation, precipitation, or bioaccumulation. Extracellular production of metal NPs has more commercial applications in several areas. However, since the NP polydispersity is the major concern, it is important to optimize the conditions for monodispersity in a biological process (Jain et al. 2015). In case of intracellular production, the accumulated NPs are of particular dimension and with less polydispersity. Regardless of the biosynthesis mechanism, control over particle size and polydispersity needs to be established for biotechnological purposes.

6.2.1 Intracellular Synthesis

During intracellular NPs synthesis, metallic ions are attracted to the negatively charged functional groups along cell wall and nucleated there, initiating the reduction and synthesis of NPs. Kalabegishvili et al. (2015) demonstrated the biosorption

of metallic ions to the cell wall of a fungus, observing that the ions were heterogeneously distributed according to specific binding sites (AshaRani et al. 2009). Moreover, shape, size, and stability of the NPs are also determined by the binding sites of the cell wall (Asmathunisha and Kathiresan 2013; Erasmus et al. 2014).

For some microorganisms, metallic ions are transferred into the cell via active cellular pumps (ATP-dependent), followed by enzymes that reduce these ions and in occasion cap them. Finally, capping proteins bind to NPs (Fig. 6.1) via open amine groups and cysteine residues, neutralizing its surface charge. Capping proteins also act on preventing the agglomeration and the alteration of NP properties playing an important role as a site for bioconjugation with other molecules. The protein caps provide stability to biologically synthesized NPs that are not otherwise found in ENPs unless that surfactants are included in traditional methods, which are very toxic (El-Deeb et al. 2013). Furthermore, the stability decreases the toxicity of the NPs, making them more environmental friendly (Stark et al. 2015).

6.2.2 Extracellular Synthesis

There are two possible pathways for extracellular NPs synthesis. The first is similar to the intracellular synthesis: ions pass through the cell membrane via active transporters, and then through reductive enzymes, the synthesis of the NPs is initiated. The proteins bind to the NPs during the reductive process, capping and reducing them through active sites. These NPs, after setting their size and form, are transported outside the cell (Bansal et al. 2012). Thus, in some microorganisms, the intracellular and extracellular synthesis of NPs can occur in the same cell (Ramanathan et al. 2011) (Fig. 6.1). The second pathway involves the emission of reducing proteins to the cell solution. This is a result of the whole change in pH in presence of the metallic ions. Upon receiving this signal, the cell emits oxidoreductase enzymes that reduce ions and synthesize NPs. These or other proteins can cap the NPs, adding stability among other properties as mentioned above. Thus, the cell-free supernatant from the microorganism culture contains the biomolecules responsible not only for biosynthesis of NPs but also of its dispersion (Huang et al. 2015).

6.3 Actinobacteria: General Features of the Group and Promising Strains for Nanoparticle Biosynthesis

Actinobacteria is the most diverse group of the *Bacteria* domain. The phylum includes Gram-positive or Gram-variable aerobes, facultative anaerobes, or anaerobes. Most strains are chemoorganotrophs, some with high G + C content and others with low G + C content in their genomes (Ghai et al. 2012). The taxon includes phenotypically diverse microorganisms with a wide variety of morphologies.

Actinobacteria exhibit diverse metabolic properties, such as the production of extracellular enzymes and specialized metabolites (Goodfellow and Fiedler 2010). In fact, the order *Actinomycetales* produce about 45% of all microbial specialized metabolites, with 80% of these compounds being produced by the *Streptomyces* genus (Bérdy 2005). *Actinobacteria* also produce NPs, enzyme inhibitors, phytotoxins, biopesticides, biosurfactants, probiotics, and enzymes involved in the degradation of complex polymers (Manivasagan et al. 2013). The versatility in specialized metabolite production makes actinobacteria important tools for pharmaceutical, medical, and biotechnological applications.

Actinobacteria play important role in remediation of toxic metals, through reduction of metal ions being promising organisms for synthesis of NPs. Consequently, several strains have been isolated from extreme environments and screened for novel bioactive compounds (Alvarez et al. 2017). Biogenic NPs are synthesized by processes of metal reductions inherent to cellular detoxification mechanisms (Siddiqi and Husen 2016). Microbial enzymes and/or specialized metabolites reduce the metal ion in solution synthesizing NPs, which can be stabilized by capping proteins (Fig. 6.1). Therefore, the use of microorganisms that present reductase activities is very relevant for obtaining NPs. For instance, Alani et al. (2012) compared physicochemical properties of AgNPs synthesized intracellularly by a thermoalkalotolerant *Streptomyces* sp. and the fungus *Aspergillus fumigatus*, concluding that the actinobacteria synthesized smaller and monodisperse NPs than *Aspergillus* in a shorter time. This fact becomes relevant considering that among microorganisms, fungi have been reported as one of the best NP producers. The authors explain that different size distributions of NPs may be due to differences in reductases produced by *Streptomyces* sp. and *Aspergillus* or the effects of other proteins coating the NPs. Similarly, Ahmad et al. (2003b) demonstrated formation of AuNPs was faster by *Rhodococcus* sp. (24 h) than the fungus *Verticillium*, when cells of both microorganisms were suspended in an aqueous solution of chloroauric acid. Moreover, the authors highlight the AuNPs synthesized using the fungus were extremely polydisperse. Extracellular synthesis of AgNPs was also demonstrated in a strain of *Streptomyces hygroscopicus* (Sadhasivam et al. 2010) and AuNP synthesis by a strain of *Thermomonospora* sp. (Hulkoti and Taranath 2014).

Some research studied the synergism of AgNPs in combination with antibiotics such as amoxicillin and polymyxin B, founding higher bactericidal activity by binding of AgNPs with antibiotics (Składanowski et al. 2017). For instance, Wypij et al. (2017) obtained AgNPs using the acidophilic actinobacterial strain *Streptomyces kasugaensis* M338-M1^{T}. The AgNPs showed the maximum antimicrobial activity against *E. coli*, followed by *B. subtilis* and *S. aureus*. Further, the synergistic effect of AgNPs in combination with commercial antibiotics (kanamycin, ampicillin, and tetracycline) was also evaluated against bacterial isolates. The antimicrobial efficacy of antibiotics was found to be enhanced in the presence of AgNPs.

The abovementioned research encouraged us to put the focus on a collection of metal-resistant actinobacteria present in the "Laboratory of Biotechnology of Actinobacteria" (PROIMI-CONICET) which bases their resistance to heavy metals in reductase activities. For example, *Streptomyces* sp. MC1 exhibits chromate

reductase activity (Polti et al. 2010), *Amycolatopsis tucumanensis* exhibits cupric reductase activity under different culture conditions (Dávila Costa et al. 2011a), and *Streptomyces* sp. M7 has a chromate reductase whose expression was six times higher in the presence of chromium (Davila Costa, personal communication). This background makes these strains potential large NPs producers. In fact, experiments are currently conducted about this subject and preliminary results are very relevant.

6.4 Nanoparticles Toxicity

The main characteristic of NPs is their size, which falls in the zone between atoms or molecules and the corresponding bulk material. As the size of particle decreases, its surface area increases and also allows a greater proportion of its atoms or molecules to be displayed on the surface rather that the interior of the material. The increase in surface area determines the potential number of reactive groups on the particle surface. Thus, AgNPs show efficient cytotoxic properties compared to other salts due to their extremely large surface area, which provides better contact with microorganisms (Kim et al. 2007).

Nanoparticles, unlike antibiotics, do not target specific traits of bacteria, and antibiotic resistance is often just modification of these traits. There are multiple possible routes for the antimicrobial properties of NPs. Perhaps most importantly, the additional surface-reactive groups exposed in NPs might act as active sites for interactions with molecular dioxygen, which may lead to formation of reactive oxygen species (ROS) including superoxide radical (O2−), hydrogen peroxide (H_2O_2), and hydroxyl radical (OH·) leading to oxidative stress (Ivask et al. 2010). For instance, Dasgupta and Ramalingam (2016) studied the release of intracellular ROS in *E. coli* treated with different concentrations of engineered AgNP. The authors found that the ROS generation was dose-dependent and affects the integrity of bacterial membrane so that cytoplasmic constituents were released. The generality of these mechanisms allows for NPs to bypass the acquired resistance to antibiotics that resistant strains contain.

It is believed that one of the mechanisms by which the NPs present antimicrobial capacity is due to the use of the NPs' negatively charged ions which bind to the microorganism cell wall and break it. Another mechanism that explains NP antimicrobial properties is the passage of smaller NPs through the cell to cause a direct damage to DNA (El-Deeb et al. 2013) (Fig. 6.2). It has been observed that NPs are able to attach to the bacterial cell membrane and produce unrest in its normal functioning. Nanoparticles could be accumulated in the cytoplasm or in the periplasmic space producing the cell membrane disruption and consequently the release of the cell contents (Golinska et al. 2017). The alteration of cell membranes involves the binding of NPs to sulfur-containing proteins present in the plasmatic membrane (Brayner et al. 2006). Similarly, sulfur content of intracellular enzymes and DNA make these molecules the target of the NPs (Raghupathi et al. 2011). In

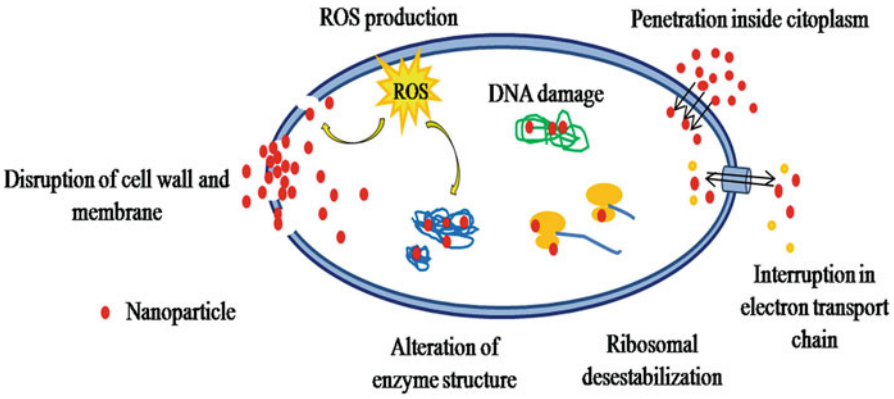

Fig. 6.2 Schematic representation of the different mechanisms of antibacterial activity of nanoparticles (NPs) over a microbial cell

particular, it has been reported that AgNPs especially target pathways of synthesis of bacterial cell wall, nucleic acid, and protein synthesis (Marambio-Jones and Hoek 2010) (Fig. 6.2).

The modification of the structure of the bacteria membrane and the possible damage to DNA caused by the NPs may affect the respiratory chain, cell division, and DNA replication, and finally cell death occurs (Lara et al. 2010). Moreover, silver ions generated from the dissolution of AgNPs could also be involved in the antimicrobial activity since it may complex with electron donor groups (sulfur, oxygen, or nitrogen atoms) present in phosphates, thiols, amino acids, and nucleic acids (Marambio-Jones and Hoek 2010).

Another cellular damage produce by NPs is the denaturation of the 30S subunit of ribosomes. This suppresses the action of enzymes and other proteins necessary for ATP production (Chauhan et al. 2013).

6.5 Methods for Nanoparticle Characterization

Nano (10^{-9} m) is the word employed to name all materials with dimensions below 100 nm. Compared to an identical material in bulk form, the nanomaterial presents new or improved properties based on specific characteristic (Xia et al. 2006). Due to NPs that can be produced in different sizes and shapes, the characterization of NPs is an important step in its biosynthesis. Several techniques are used to study the size, shape, morphology, and dispersion of NPs.

The most applied techniques in NP characterization are ultraviolet-visible (UV-vis) spectrophotometer, transmission electron microscopy (TEM), scanning electron microscopy (SEM), atomic force microscopy (AFM), dynamic light scattering (DLS), X-ray powder diffraction (XRD), Fourier transform infrared

spectroscopy (FT-IR), zeta potential measurement, particle size analysis (PSA), and energy dispersive X-ray spectroscopy (EDX).

The absorption of UV-visible radiation induces an excitation of electrons from lower-energy orbital to higher-energy orbital in a molecule. The UV-visible absorption occurs at a specific wavelength for each molecular structure (Xu et al. 2014). It is a technique widely employed in the study of nanomaterials and can be used as a simple and reliable method for monitoring the stability of NP solutions. The optical absorption spectra of metallic NPs are dominated by surface plasmon resonance (Vaghari et al. 2016). Thus, position and shape of absorption peak depend mainly on factors such as size, shape, and NP polydispersity, surrounding medium, and substances absorbed on its surface (Mahmoudi et al. 2009; Xu and Sun 2013). For example, the appearance of an absorption peak around 400 nm is indicative of the presence of AgNPs (Roduner 2006). Usually, the appearance of this peak is closely associated with color changes of the reaction solution, being the first signal that indicates qualitatively that the NPs have been produced. For the AgNPs the characteristic color change is yellow to brown (Sharma et al. 2015), and for AuNPs the color change is from yellow to purple (Bastús et al. 2014).

The main use of FT-IR in NP characterization is to investigate the presence of biomolecules (such as capping proteins) bound to NPs. For instance, Ahmad et al. (2003a) using FT-IR spectroscopy plus gel electrophoresis hypothesized that certain proteins could be enzymes that reduce chloroaurate ions and cap the AuNPs formed by the actinobacterium *Thermomonospora* sp. It is well known that proteins can bind to NPs either through free amine groups or cysteine residues in the proteins, and therefore, stabilization of the NPs by surface-bound proteins is a possibility.

The most popular tools for the visualization of NPs are electron microscopy techniques. Depending on the technique, resolutions down to the sub-nanometer range can be achieved. Transmission electronic microscopy, SEM, and AFM are most extensively applied techniques not only to visualize the shape of synthesized NPs but also the state of sorption, size, aggregation, dispersion, and structure of NPs (Liu 2006). With TEM and SEM techniques, NPs can be analyzed by its size, morphology, and shape distribution (Chauhan et al. 2016) although generally, imaging of lighter atoms in an electron microscope is more difficult as they scatter electrons less efficiently. Another alternative is to use AFM for analyzing the sample upon liquid conditions. However, it has the disadvantage that particles not fixed to a substrate will float around and eventually can stick to the cantilever, which leads to imaging artifacts (Ghazwani 2015).

Dynamic light scattering is a widely used technique in the characterization of NPs on a simple solvent or biological environment (Wen et al. 2016). In addition, it is one of the methods most employed to quantify size distribution and surface charges of NPs suspended in a liquid. The main advantage of DLS is that measurements are fast and noninvasive when a sample is in its native colloidal state (Xue et al. 2016).

The elemental composition of NPs can be determined by EDX (Shi et al. 2015), while XRD is utilized to determine the crystal structure of the NPs. X-ray powder

diffraction is a good method to measuring interparticle spacing by detecting the interference of waves reflecting on different crystal planes. It is used in mineralogy to determine the crystal structure of mineral particles. Several or some of these techniques are extensively used to characterize many different metal NPs.

6.6 Specialized Metabolites in Actinobacteria

The use of antibiotics to human health care is rather new and emerged from the discovery of penicillin in 1928. After the penicillin, mainly between the 1950s and 1970s, the search of new active molecules resulted in several classes of antibiotic, antifungal, antihelminthic, and anticancer agents. In this period, actinobacteria emerged as excellent bioactive metabolite producers, especially *Streptomyces* and *Micromonospora* genera (Davies and Davies 2010). Discovery of antibiotics led to the perception that these molecules were a kind of "wonder drugs" that killed bad bugs and reduced human deaths by bacterial infections. However, almost immediately after the introduction of these wonder drugs to medicine, bacterial resistance was observed. The apparition of bacterial resistance triggered a race towards the discover of new antibiotics. However, the introduction of new drugs did not avoid the appearance of short-term resistance in pathogens. This natural adaptation in addition to the uncontrolled use of antibiotics in agriculture and medicine turned resistance to antibiotic in a global concern. This problem encouraged researchers, clinicians, industry, and politicians to work together in search of new bioactive molecules using a biological platform actinobacteria.

As we previously mentioned, *Actinobacteria* is a diverse phylum in which the metabolic versatility is a primordial feature (Dávila Costa and Amoroso 2014; Alvarez et al. 2017). Primary metabolism is present in all living organisms and encompasses all essential reactions. Secondary metabolism is more specific, distinctive, and often encompasses species-specific pathways (Hartmann 2008). Species specificity is not an exception for the genera *Bifidobacterium*, *Corynebacterium*, *Mycobacterium*, *Nocardia*, *Amycolatopsis*, *Frankia*, and *Streptomyces*, whereby they have acquired medicinal, agriculture, and industrial importance. Probably, the most specialized genera are *Streptomyces* and *Amycolatopsis*, which are sporulating bacteria with filamentous growth, high G + C content, and linear genomes. Life cycle of these bacteria begins with a unigenomic spore which germinates and grows to form vegetative mycelia that, in response to nutrient limitation, produce aerial hyphae, which subsequently form septa and eventually mature spores. Often, specialized metabolites are produced at the onset of the developmental process. Specialized metabolites synthesized by the genera *Streptomyces* and *Amycolatopsis* are chemically diverse and include lactams, terpenes, nonribosomal peptides, aminoglycosides, and polyketides.

6.7 Connection Between Primary and Specialized Metabolism: Their Evolution

Pathways of central metabolism comprise the primary metabolism and produce macromolecules such as lipids, RNA, DNA, and proteins. Precursors or building blocks for the synthesis of specialized metabolites are also produced during primary metabolism. The importance of primary metabolism is unquestionable; however, cells can dispense with some genes from the core pathways due to "genetic flexibility" (Noda-García and Barona-Gómez 2013). Genetic flexibility provides alternative reactions or isoenzymes to the microorganism for adapting to a new environmental condition and giving an adaptive robustness to metabolism. Interestingly, in *Amycolatopsis* and *Streptomyces* genomes, several genes were annotated to encode the same biochemical function in the central carbon metabolism (Bentley et al. 2002). The evolution and genetic functionality are essential to understand the metabolic versatility that might be useful in biotechnology. Typically, combined functions of genes converge into a specific flux pathway; nevertheless, this is not enough to have a precise idea of the regulation and allostery for the product of each gene. Knowledge of regulation and allostery will help to estimate the impact of these genetic expansions at biochemical level. Hypothetically, cells might use these "redundant genes" in order to gain adaptation and flexibility to changing environments. *Streptomyces* and *Amycolatopsis* possess in their genomes several of these genetic enlargements. This characteristic might justify their ability to produce such diversity of specialized metabolites, since these biosynthetic pathways are often linked to central metabolism and utilize common intermediates. An interesting example of evolution and genetic expansion is the biosynthesis of polyketide in which the multimodular polyketide synthase produces the carbon backbones for the polyketides from carboxylic acid subunits. This carbon assembling system seems to have evolved from fatty acid synthases. Polyketide synthetases possess acyl carrier proteins and highly conserved domains for ketoacyl synthase. Different hypotheses suggest that deletions, horizontal gene transfer, and duplications of these domains gave rise to the variety of polyketides currently known (Jenke-Kodama et al. 2005; Ridley et al. 2008).

6.8 Extreme *Streptomyces* and *Amycolatopsis* Strains as Source of New Specialized Metabolites

Several studies in addition to the previously described above have demonstrated the metabolic versatility of these genera. In turn, this feature made these bacteria important biological tools today. *Streptomyces* and *Amycolatopsis* are the genera from which most of the antibiotics currently used in clinical were obtained. Despite the elevated number of antibiotics produced by these bacteria, it has been predicted

that only about 10% of the total number of natural products that can be synthesized by these organisms have been discovered. Surprisingly, most of the antibiotic-producing bacteria were isolated from non-polluted environments, for instance, *Amycolatopsis balhimycina*, *Amycolatopsis orientalis*, *Streptomyces mediterranei*, and *Streptomyces erythreus* among others. As an interesting hypothesis, actinobacteria isolated from contaminated areas may harbor in their genomes clusters linked to the production of specialized metabolites that allowed them to survive in those extreme environments. Over the last few years, *Amycolatopsis* and *Streptomyces* strains were isolated from highly contaminated areas in the province of Tucumán, Argentina. Resistance to elevated concentrations of heavy metals such as Cu, Cr, and Cd was widely demonstrated in *Streptomyces* sp. MC1 and *Amycolatopsis tucumanensis* (Polti et al. 2007; Dávila Costa et al. 2011a, 2012). These strains, together with *Streptomyces* sp. M7 and *Streptomyces* sp. A5, were also able to degrade toxic organic compounds such as hexachlorocyclohexane, methoxychlor, and phenanthrene among others. Given the potential of these strains for being used in bioremediation processes, their genomes were recently sequenced. As expected, genetic elements involved in mechanisms of resistance to heavy metals and genes related to the degradation of xenobiotics were identified. In addition, genomic bioinformatics analysis of the strains with the software antiSMASH revealed the presence of several genes that may participate in the biosynthesis of specialized metabolites. These clusters include biosynthetic genes for siderophores, terpenes, bacteriocins, butyrolactones, and polyketides (Table 6.1). Certainly, outstanding advances in the field of specialized metabolites produced by actinobacteria were achieved in the last few years. However, as we mentioned above, only about 10% of the total number of natural products synthesized by these bacteria are known. Even more, antimicrobial produced by actinobacteria growing in the presence of toxic compounds were not reported yet.

Although *Streptomyces* and *Amycolatopsis* are well known for producing specialized metabolites, we could postulate that the second one is a rarer genus. Currently, exist 823 species described for the genus *Streptomyces*, while only 71 were described for *Amycolatopsis* so far (http://www.bacterio.net/amycolatopsis.html) (last access October 2017). The genus *Amycolatopsis* was proposed in 1986. These bacteria are characterized to have a type IV cell wall (meso-diaminopimelic acid, arabinose, and galactose in the cell wall); muramic acid in an N-acetyl form; absence of mycolic acids; phosphatidylethanolamine as a diagnostic phospholipid; and a complex mixture of saturated and branched chain fatty acids. Besides, members of this genus are able to metabolize (+)-L-arabinose, (+)-D-cellobiose, (+)-D-fructose, (+)-D-galactose, (+)-D-lactose, (+)-D-mannose, (+)-D-trehalose, and (+)-D-xylose (see Dávila Costa and Amoroso 2014 for a comprehensive review). *Amycolatopsis tucumanensis* was recognized as new species in 2010 (Albarracín et al. 2010), and it is the only heavy metal-resistant member into the genus. Particularly, copper resistance was demonstrated in this bacterium. Copper homeostasis mechanisms include antioxidant molecules and enzymes, production of exopolysaccharide, and cupric reductase activity (Dávila Costa et al. 2011a; b, 2012). The variety of carbon source

Table 6.1 Potential specialized metabolites produced by metalo-tolerant actinobacteria. Metabolites listed in the table were predicted by the software antiSMASH. Most of the biosynthetic gene clusters showed low similarity with already know clusters, suggesting that they could actually produce a similar but not identical metabolite

	Amycolatopsis tucumanensis	*Streptomyces* sp. M7	*Streptomyces* sp. MC1
Specialized metabolites	Amychelin	Oxazolomycin	Polyoxypeptin
	Bacteriocins	Bacteriocins	Bacteriocins
	Clavulanic acid	Meilingmycin	Venezuelin
	Ectoine	Toyocamycin	Ectoine
	Fortimicin	Vicenistatin	Grincamycin
	Frenolicin	Actinomycin	Hopene
	Hopene	Tomaymycin	Alkylresorcinol
	Isorenieratene	Abyssomicin	Informatipeptin
	Lipomycin	Amphotericin	Albaflavenone
	Macrotetrolide	Rabelomycin	Resistomycin
	Nystatin	Grincamycin	Methylenomycin

that can be used by *Amycolatopsis tucumanensis*, the connection between primary metabolism and production of specialized metabolites that we previously discussed, and the cupric reductase activity make this strain a promising tool to produce NPs of Zn, Ag, or Au through the biosynthesis of new specialized metabolites. Interestingly, genes encoding chromate reductase enzymes were found in *Streptomyces* sp. M7 and *Streptomyces* sp. MC1 genomes.

6.9 Patents in the Emerging World of Bio-nanoparticles

In 1873, patents office of USA granted Louis Pasteur the first biotechnological patent related to "a yeast free of disease germs as an article of manufacture." Generally, before 1980 living organisms were not patentable since they were considered "as product of nature." In the same year occurred the famous case known as *Diamond* vs. *Chakrabarty*. The Supreme Court of the United States gave the reason to the latter and established that the bacterium of the genus *Pseudomonas* was patentable. This bacterium met the criteria of patentability: it was a novelty (nonexistent as such in the nature and not obvious to the science of the moment), derived from inventive activity (it had been achieved in the laboratory by transfer of plasmids) and fulfilled the criterion of utility (the object was used in the work of decontamination of oil spills). Then in 1985, a multicellular organism was patented for the first time, while in 1990 occurred the first patenting of a line of cells cultured in vitro. After these series of events arose the historical phrase: patents can be granted "to anything under the sun made by man."

The field of synthesis of bio-nanoparticles is not alien to the patents world. Over the last few years, several patents were granted to different research groups over the world. In 2013, the University of Santiago de Chile requested the patenting of the use of the fungus *Botrytis cinerea* for obtaining gold nanoparticles (WO/2013/143017). Overall, this invention is related to the use of molecules generated by the fungus to produce gold nanoparticles under a specific condition. Recently, similar inventions were also patented. The differences between them consist of the microorganism utilized and expected modifications in the protocol for obtaining the bio-nanoparticle, which depends on the microorganism. Certainly, many of them share the same potential applications (WO/2016/076694; US20120108425A1; US2002/0174743A1; US20090239280A1; US20100055199A1). Patents mentioned here are referred to fungi and Gram-negative bacteria. To our knowledge, processes for the production of bio-nanoparticles by using actinobacteria and specifically those from genus *Streptomyces* were not patented.

Over the years, the nonobviousness criterion required for patenting is more difficult to accomplish; thus certain scientific advances became non-patentable. This is a debatable point since a scientific advance, although non-patentable, may result significant for a biotechnological development. Following a patented process for the production of bio-nanoparticles may result somehow limiting. The metabolic potential of microorganisms, from which depends the organic diversity of bio-nanoparticles, is almost unlimited. The outstanding advances in omics techniques allow predicting the metabolic potential of a microorganism. For instance, combination of genomic and bioinformatics tools is possible to identify clusters of genes related to the synthesis of specialized metabolites that could be the organic portion of a bio-nanoparticle. In addition, the combination of proteomics and metabolomics may give accurate information about how and when to produce a specific specialized metabolite for a bio-nanoparticle. In summary, the advance of science and its techniques can render a patented methodology in a short period of time.

6.10 Conclusion

This chapter resumes updated data about metal NP biogenic synthesis, the techniques used for their study and characterization, and the importance of actinobacteria as producers of new metal NPs to use in clinical, focusing on members of the phylum isolated from polluted environments. Moreover, it is evidenced that these strains are promising sources of new specialized metabolites, mainly with antimicrobial activities, by using genome mining approaches. In this context, it is imperative to conduct deeper studies on the subject, in order to make the biomolecules produced by actinobacteria as effective bioactive products for therapeutic applications, by exploiting their undoubtedly huge potential.

References

Ahmad A, Senapati S, Khan M et al (2003a) Extracellular biosynthesis of monodisperse gold nanoparticles by a novel extremophilic Actinomycete, *Thermomonospora* sp. Langmuir 19:3550–3553. https://doi.org/10.1021/LA026772L

Ahmad A, Senapati S, Khan MI et al (2003b) Intracellular synthesis of gold nanoparticles by a novel alkalotolerant actinomycete, *Rhodococcus* species. Nanotechnology 14:824–828. https://doi.org/10.1088/0957-4484/14/7/323

Alani F, Moo-Young M, Anderson W (2012) Biosynthesis of silver nanoparticles by a new strain of *Streptomyces* sp. compared with Aspergillus fumigatus. World J Microbiol Biotechnol 28:1081–1086. https://doi.org/10.1007/s11274-011-0906-0

Albarracín VH, Alonso-Vega P, Trujillo ME et al (2010) *Amycolatopsis tucumanensis* sp. nov., a copper-resistant actinobacterium isolated from polluted sediments. Int J Syst Evol Microbiol 60:397–401. https://doi.org/10.1099/ijs.0.010587-0

Alvarez A, Saez J, Davila Costa J et al (2017) Actinobacteria: current research and perspectives for bioremediation of pesticides and heavy metals. Chemosphere 166:41–62. https://doi.org/10.1016/J.CHEMOSPHERE.2016.09.070

AshaRani PV, Low Kah Mun G, Hande MP, Valiyaveettil S (2009) Cytotoxicity and genotoxicity of silver nanoparticles in human cells. ACS Nano 3:279–290. https://doi.org/10.1021/nn800596w

Asmathunisha N, Kathiresan K (2013) A review on biosynthesis of nanoparticles by marine organisms. Colloids Surf B Biointerfaces 103:283–287. https://doi.org/10.1016/J.COLSURFB.2012.10.030

Bansal V, Bharde A, Ramanathan R, Bhargava S (2012) Inorganic materials using "unusual" microorganisms. Adv Colloid Interf Sci 179–182:150–168. https://doi.org/10.1016/J.CIS.2012.06.013

Bastús NG, Merkoçi F, Piella J, Puntes V (2014) Synthesis of highly monodisperse citrate-stabilized silver nanoparticles of up to 200 nm: kinetic control and catalytic properties. Chem Mater 26:2836–2846. https://doi.org/10.1021/cm500316k

Beeler E, Singh OV (2016) Extremophiles as sources of inorganic bio-nanoparticles. World J Microbiol Biotechnol 32:156. https://doi.org/10.1007/s11274-016-2111-7

Bentley SD, Chater KF, Cerdeño-Tárraga A-M et al (2002) Complete genome sequence of the model actinomycete *Streptomyces coelicolor* A3(2). Nature 417:141–147. https://doi.org/10.1038/417141a

Bérdy J (2005) Bioactive microbial metabolites. J Antibiot (Tokyo) 58:1–26. https://doi.org/10.1038/ja.2005.1

Borase HP, Salunke BK, Salunkhe RB et al (2014) Plant extract: a promising biomatrix for ecofriendly, controlled synthesis of silver nanoparticles. Appl Biochem Biotechnol 173:1–29. https://doi.org/10.1007/s12010-014-0831-4

Brayner R, Ferrari-Iliou R, Brivois N et al (2006) Toxicological impact studies based on *Escherichia coli* bacteria in ultrafine ZnO nanoparticles colloidal medium. Nano Lett 6:866–870. https://doi.org/10.1021/NL052326H

Bull AT, Stach JEM (2007) Marine actinobacteria: new opportunities for natural product search and discovery. Trends Microbiol 15:491–499. https://doi.org/10.1016/J.TIM.2007.10.004

Chauhan R, Kumar A, Abraham J (2013) A biological approach to synthesis of silver nanoparticles with *Streptomyces* sp. JAR1 and its antimicrobial activity. Sci Pharm 81:607–621. https://doi.org/10.3797/scipharm.1302-02

Chauhan N, Narang J, Jain U (2016) Amperometric acetylcholinesterase biosensor for pesticides monitoring utilising iron oxide nanoparticles and poly(indole-5-carboxylic acid). J Exp Nanosci 11:111–122. https://doi.org/10.1080/17458080.2015.1030712

Dasgupta N, Ramalingam C (2016) Silver nanoparticle antimicrobial activity explained by membrane rupture and reactive oxygen generation. Environ Chem Lett 14:477–485. https://doi.org/10.1007/s10311-016-0583-1

Davies J, Davies D (2010) Origins and evolution of antibiotic resistance. Microbiol Mol Biol Rev 74:417–433. https://doi.org/10.1128/MMBR.00016-10

Dávila Costa JS, Amoroso MJ (2014) Current biotechnological applications of the genus *Amycolatopsis*. World J Microbiol Biotechnol 30:1919–1926. https://doi.org/10.1007/s11274-014-1622-3

Dávila Costa JS, Albarracín VH, Abate CM (2011a) Cupric reductase activity in copper-resistant *Amycolatopsis tucumanensis*. Water Air Soil Pollut 216:527–535. https://doi.org/10.1007/s11270-010-0550-6

Dávila Costa JS, Albarracín VH, Abate CM (2011b) Responses of environmental *Amycolatopsis* strains to copper stress. Ecotoxicol Environ Saf 74:2020–2028. https://doi.org/10.1016/j.ecoenv.2011.06.017

Dávila Costa JS, Kothe E, Abate CM, Amoroso MJ (2012) Unraveling the *Amycolatopsis tucumanensis* copper-resistome. Biometals 25:905–917. https://doi.org/10.1007/s10534-012-9557-3

Durán N, Marcato PD, De Souza GIH et al (2007) Antibacterial effect of silver nanoparticles produced by fungal process on textile fabrics and their effluent treatment. J Biomed Nanotechnol 3:203–208. https://doi.org/10.1166/jbn.2007.022

El-Deeb B, Mostafa NY, Altalhi A, Gherbawy Y (2013) Extracellular biosynthesis of silver nanoparticles by bacteria *Alcaligenes faecalis* with highly efficient anti-microbial property. Int J Chem Eng 30:2051–7858

Erasmus M, Cason ED, van Marwijk J et al (2014) Gold nanoparticle synthesis using the thermophilic bacterium *Thermus scotoductus* SA-01 and the purification and characterization of its unusual gold reducing protein. Gold Bull 47:245–253. https://doi.org/10.1007/s13404-014-0147-8

Gade AK, Bonde P, Ingle AP et al (2008) Exploitation of *Aspergillus niger* for synthesis of silver nanoparticles. J Biobaased Mater Bioenergy 2:243–247. https://doi.org/10.1166/jbmb.2008.401

Ghai R, McMahon KD, Rodriguez-Valera F (2012) Breaking a paradigm: cosmopolitan and abundant freshwater actinobacteria are low GC. Environ Microbiol Rep 4:29–35. https://doi.org/10.1111/j.1758-2229.2011.00274.x

Ghazwani A (2015) Biosynthesis of silver nanoparticles by *Aspergillus niger*, *Fusarium oxysporum* and *Alternaria solani*. Afr J Biotechnol 14:2170–2174

Golinska P, Rathod D, Wypij M et al (2017) Mycoendophytes as efficient synthesizers of bionanoparticles: nanoantimicrobials, mechanism, and cytotoxicity. Crit Rev Biotechnol 37:765–778. https://doi.org/10.1080/07388551.2016.1235011

Goodfellow M, Fiedler H-P (2010) A guide to successful bioprospecting: informed by actinobacterial systematics. Antonie Van Leeuwenhoek 98:119–142. https://doi.org/10.1007/s10482-010-9460-2

Hartmann T (2008) The lost origin of chemical ecology in the late 19th century. Proc Natl Acad Sci U S A 105:4541–4546. https://doi.org/10.1073/pnas.0709231105

Hoskisson PA, Sumby P, Smith MCM (2015) The phage growth limitation system in *Streptomyces coelicolor* a(3)2 is a toxin/antitoxin system, comprising enzymes with DNA methyltransferase, protein kinase and ATPase activity. Virology 477:100–109. https://doi.org/10.1016/J.VIROL.2014.12.036

Huang J, Lin L, Sun D et al (2015) Bio-inspired synthesis of metal nanomaterials and applications. Chem Soc Rev 44:6330–6374. https://doi.org/10.1039/C5CS00133A

Hulkoti N, Taranath T (2014) Biosynthesis of nanoparticles using microbes—a review. Colloids Surfa B Biointerfaces 121:474–483. https://doi.org/10.1016/J.COLSURFB.2014.05.027

Ivask A, Bondarenko O, Jepihhina N, Kahru A (2010) Profiling of the reactive oxygen species-related ecotoxicity of CuO, ZnO, TiO2, silver and fullerene nanoparticles using a set of recombinant luminescent *Escherichia coli* strains: differentiating the impact of particles and solubilised metals. Anal Bioanal Chem 398:701–716. https://doi.org/10.1007/s00216-010-3962-7

Jain N, Bhargava A, Rathi M et al (2015) Removal of protein capping enhances the antibacterial efficiency of biosynthesized silver nanoparticles. PLoS One 10:e0134337. https://doi.org/10.1371/journal.pone.0134337

Jenke-Kodama H, Sandmann A, Müller R, Dittmann E (2005) Evolutionary implications of bacterial polyketide synthases. Mol Biol Evol 22:2027–2039. https://doi.org/10.1093/molbev/msi193

Kalabegishvili TL, Murusidze IG, Kirkesali EI et al (2015) Possibilities of physical methods in development of microbial nanotechnology. Eur Chem Bull 4:43–49. https://doi.org/10.17628/ECB.2015.4.43-49

Khot L, Sankaran S, Maja J et al (2012) Applications of nanomaterials in agricultural production and crop protection: a review. Crop Prot 35:64–70. https://doi.org/10.1016/J.CROPRO.2012.01.007

Kim JS, Kuk E, Yu KN et al (2007) Antimicrobial effects of silver nanoparticles. Nanomedicine 3:95–101. https://doi.org/10.1016/j.nano.2006.12.001

Lara HH, Ayala-Núñez NV, del Ixtepan Turrent LC, Rodríguez Padilla C (2010) Bactericidal effect of silver nanoparticles against multidrug-resistant bacteria. World J Microbiol Biotechnol 26:615–621. https://doi.org/10.1007/s11274-009-0211-3

Liu WT (2006) Nanoparticles and their biological and environmental applications. J Biosci Bioeng 102:1–7. https://doi.org/10.1263/JBB.102.1

Mahmoudi M, Simchi A, Imani M, Häfeli UO (2009) Superparamagnetic iron oxide nanoparticles with rigid cross-linked polyethylene glycol fumarate coating for application in imaging and drug delivery. J Phys Chem C 113:8124–8131. https://doi.org/10.1021/jp900798r

Manivasagan P, Venkatesan J, Sivakumar K, Kim SK (2013) RETRACTED: marine actinobacterial metabolites: current status and future perspectives. Microbiol Res 168:311–332. https://doi.org/10.1016/J.MICRES.2013.02.002

Marambio-Jones C, Hoek EMV (2010) A review of the antibacterial effects of silver nanomaterials and potential implications for human health and the environment. J Nanopart Res 12:1531–1551. https://doi.org/10.1007/s11051-010-9900-y

McLean TC, Hoskisson PA, Seipke RF (2016) Coordinate regulation of antimycin and candicidin biosynthesis. mSphere 1:e00305–e00316. https://doi.org/10.1128/mSphere.00305-16

Noda-García L, Barona-Gómez F (2013) Enzyme evolution beyond gene duplication. Mob Genet Elem 3:e26439. https://doi.org/10.4161/mge.26439

Olano C, Méndez C, Salas JA (2009) Antitumor compounds from marine actinomycetes. Mar Drugs 7:210–248. https://doi.org/10.3390/md7020210

Payne DJ, Gwynn MN, Holmes DJ, Pompliano DL (2007) Drugs for bad bugs: confronting the challenges of antibacterial discovery. Nat Rev Drug Discov 6:29–40. https://doi.org/10.1038/nrd2201

Polti MA, Amoroso MJ, Abate CM (2007) Chromium(VI) resistance and removal by actinomycete strains isolated from sediments. Chemosphere 67:660–667. https://doi.org/10.1016/j.chemosphere.2006.11.008

Polti M, Amoroso M, Abate C (2010) Chromate reductase activity in *Streptomyces* sp. MC1. J Gen Appl Microbiol 56:11–18. https://doi.org/10.2323/jgam.56.11

Raghupathi KR, Koodali RT, Manna AC (2011) Size-dependent bacterial growth inhibition and mechanism of antibacterial activity of zinc oxide nanoparticles. Langmuir 27:4020–4028. https://doi.org/10.1021/la104825u

Rai M, Gade A, Yadav A (2011) Biogenic nanoparticles: an introduction to what they are, how they are synthesized and their applications. In: Metal nanoparticles in microbiology. Springer, Berlin/Heidelberg, pp 1–14

Ramanathan R, O'Mullane AP, Parikh RY et al (2011) Bacterial kinetics-controlled shape-directed biosynthesis of silver nanoplates using *Morganella psychrotolerans*. Langmuir 27:714–719. https://doi.org/10.1021/la1036162

Ridley CP, Lee HY, Khosla C (2008) Evolution of polyketide synthases in bacteria. Proc Natl Acad Sci U S A 105:4595–4600. https://doi.org/10.1073/pnas.0710107105

Roduner E (2006) Size matters: why nanomaterials are different. Chem Soc Rev 35:583. https://doi.org/10.1039/b502142c

Sadhasivam S, Shanmugam P, Yun K (2010) Biosynthesis of silver nanoparticles by *Streptomyces hygroscopicus* and antimicrobial activity against medically important pathogenic microorganisms. Colloids Surf B Biointerfaces 81:358–362. https://doi.org/10.1016/J.COLSURFB.2010.07.036

Sharma K, Singh G, Singh G et al (2015) Silver nanoparticles: facile synthesis and their catalytic application for the degradation of dyes. RSC Adv 5:25781–25788. https://doi.org/10.1039/C5RA02909K

Shi C, Zhu N, Cao Y, Wu P (2015) Biosynthesis of gold nanoparticles assisted by the intracellular protein extract of *Pycnoporus sanguineus* and its catalysis in degradation of 4-nitroaniline. Nanoscale Res Lett 10:147. https://doi.org/10.1186/s11671-015-0856-9

Siddiqi KS, Husen A (2016) Fabrication of metal and metal oxide nanoparticles by algae and their toxic effects. Nanoscale Res Lett 11:363. https://doi.org/10.1186/s11671-016-1580-9

Składanowski M, Wypij M, Laskowski D et al (2017) Silver and gold nanoparticles synthesized from *Streptomyces* sp. isolated from acid forest soil with special reference to its antibacterial activity against pathogens. J Clust Sci 28:59–79. https://doi.org/10.1007/s10876-016-1043-6

Stark WJ, Stoessel PR, Wohlleben W, Hafner A (2015) Industrial applications of nanoparticles. Chem Soc Rev 44:5793–5805. https://doi.org/10.1039/C4CS00362D

Vaghari H, Jafarizadeh-Malmiri H, Mohammadlou M et al (2016) Application of magnetic nanoparticles in smart enzyme immobilization. Biotechnol Lett 38:223–233. https://doi.org/10.1007/s10529-015-1977-z

Wen L, Zeng P, Zhang L et al (2016) Symbiosis theory-directed green synthesis of silver nanoparticles and their application in infected wound healing. Int J Nanomedicine 11:2757–2767. https://doi.org/10.2147/IJN.S106662

WHO (2015) Worldwide country situation analysis: response to antimicrobial resistance. World Health Organization, Geneva

Wypij M, Golinska P, Dahm H, Rai M (2017) Actinobacterial-mediated synthesis of silver nanoparticles and their activity against pathogenic bacteria. IET Nanobiotechnol 11:336–342

Xia T, Kovochich M, Brant J et al (2006) Comparison of the abilities of ambient and manufactured nanoparticles to induce cellular toxicity according to an oxidative stress paradigm. Nano Lett 6:1794–1807. https://doi.org/10.1021/NL061025K

Xu C, Sun S (2013) New forms of superparamagnetic nanoparticles for biomedical applications. Adv Drug Deliv Rev 65:732–743. https://doi.org/10.1016/J.ADDR.2012.10.008

Xu J, Sun J, Wang Y et al (2014) Application of iron magnetic nanoparticles in protein immobilization. Molecules 19:11465–11486. https://doi.org/10.3390/molecules190811465

Xue B, He D, Gao S et al (2016) Biosynthesis of silver nanoparticles by the fungus *Arthroderma fulvum* and its antifungal activity against genera of *Candida*, *Aspergillus* and *Fusarium*. Int J Nanomedicine 11:1899–1906. https://doi.org/10.2147/IJN.S98339

Chapter 7
Titanium Oxide-Based Nanomaterials with Photocatalytic Applications in Environmental Chemistry

Amel Boudjemaa and Santiago Gómez-Ruiz

Contents

7.1 Introduction 216
7.2 Titanium Oxide: Structure and Properties 216
7.2.1 Synthetic Methods for the Preparation of Nanostructures of TiO_2 218
7.3 Environmental Applications in Advanced Oxidation Processes 223
7.3.1 Introduction and Overview 223
7.3.2 Principles of AOP 224
7.3.3 Water Remediation Using Titanium Oxide 227
7.3.4 Water Splitting 234
7.3.5 Hydrogen Production Using Alternative Processes: Photoelectrochemical (PEC) Hydrogen Generation 237
7.3.6 Water Photoreduction 244
7.3.7 Methanol Photoreforming 247
7.4 Conclusions and Outlook 250
References 251

Abstract This chapter reviews the potential applications of photocatalytic processes using titanium oxide-based materials in environmental chemistry. The chapter starts with a short introduction on nanosized titanium oxide discussing its properties, structural features, and the most relevant synthetic methods for its preparation and modification. Subsequently, a section on the applications of titanium oxide nanostructured systems in advanced oxidation processes is presented. In addition, this chapter contains a thorough revision of the latest results on the use of nanosized titanium oxide in water remediation, water splitting, and hydrogen production using photocatalytic or photoelectrocatalytic processes.

A. Boudjemaa
Centre de Recherche Scientifique et Technique en Analyses Physico-Chimiques (CRAPC), Bou-Ismail, Tipaza, Algeria

S. Gómez-Ruiz (✉)
Departamento de Biología y Geología, Física y Química Inorgánica, E.S.C.E.T. Universidad Rey Juan Carlos, Móstoles, Spain
e-mail: santiago.gomez@urjc.es

N. Dasgupta et al. (eds.), *Environmental Nanotechnology Volume 4*, Environmental Chemistry for a Sustainable World 32, https://doi.org/10.1007/978-3-030-26668-4_7

Keywords Titanium dioxide · Nanomaterials · Photocatalysis · Water-splitting · Water remediation · Environmental chemistry

7.1 Introduction

Since the discovery of water-splitting photocatalysis on a titanium oxide electrode under UV light in 1972, a wide variety of materials have been investigated as photocatalysts. However, titanium oxide-based materials are the most widely used heterogeneous catalysts because of their optical and electronic properties, stability, low cost, and low toxicity (Liao et al. 2012; Bahruji et al. 2011; Liu et al. 2008). A lot of effort has been put into their development and implementation in hydrogen and energy production from solar energy.

Titanium oxide, especially in nanosize form, has an ample field of applications, among them, the most important are generally associated with the ceramic industry and its use as cosmetic products and white pigments in paintings. Other more specific applications of this material include, for example, water purification by degradation of organic molecules, gas sensors, gas mixture cleaners, antireflective coatings, antimicrobial photoinduced coating, electrodes for lithium batteries, self-cleaning glasses, and UV absorbers in sun creams. In addition, it has had an important role in bone implants due to its very high biocompatibility which has been studied over the last 20 years (Janczarek et al. 2007; Diebold 2003; Mohammadi et al. 2008). Very recently, titanium oxide has also been used as an angiogenic promoter and may be useful in the future for the treatment of cardiovascular diseases (Nethi et al. 2017).

7.2 Titanium Oxide: Structure and Properties

Titanium dioxide, TiO_2, belongs to the family of transition metal oxides. Usually known as "titania" is a type *n* semiconductor with sensitivity to light. It presents three main crystalline phases: rutile (tetragonal structure), anatase (octahedral structure), and brookite (orthorrombic structure) (Pizarro 2005, Gupta and Tripathi 2011) (Fig. 7.1).

Comparing all the three main phases, rutile is the most thermodinamically stable, and both anatase and brookite phases can be transformed to rutile when they reach a particle size larger than 14 nm, especially at high temperatures. Brookite is a metastable phase, it is a very complex structure with a high cell volume and with a very low density (the lowest of the three main phases), and due to its very low density and subsequent mechanical factor, it is not used in experimental research. However, for nanotechnological approaches anatase is the most suitable phase, due to its low size (usually below 20 nm). In addition, anatase phase is preferred in nanotechnology due to its low dielectric constant, high electronic mobility, and low density. It has also been observed that the (001) face has a higher reactivity than the (101) face in anatase crystals, so that enrichment of the particles in the dimension of

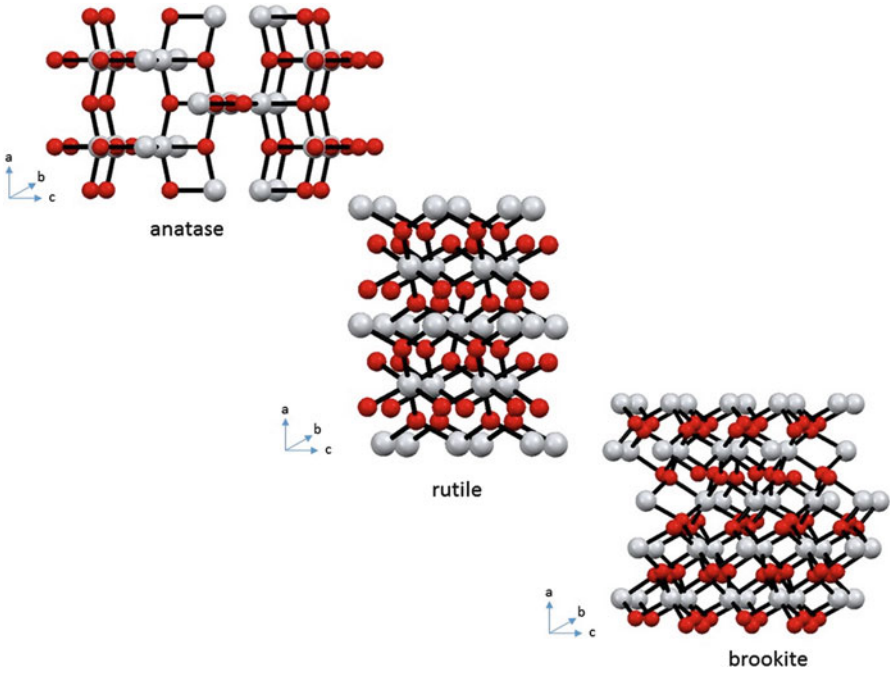

Fig. 7.1 Crystal structure configurations of TiO_2: (**a**) anatase, (**b**) rutile, and (**c**) brookite. (Gupta and Tripathi 2011)

their (001) face leads to more reactive systems with interesting applications in photocatalysis (Gupta and Tripathi 2011).

Owing to the photocatalytic properties, titanium oxide is only active in the near-UV region, as the necessary energy to excite anatase is ca. 3.2 eV while being 3.02 eV for rutile and 2.96 eV for brookite. Despite the need of a more energetic excitation potential for anatase, its larger surface area compared to rutile and brookite facilitates the adsorption of small molecules like hydrophobic organic compounds. The facility of adsorption of molecules by anatase makes the possible electron-hole recombinations more difficult, leading to higher photocatalytic activity compared to that of the other two phases (rutile and brookite).

In this context, recent investigations have shown that the anatase is not the unique photocatalytically active phase as rutile phases can also be photocatalytically active depending on the conditions of its preparation. Thus, a rutile phase with a large surface area can also be active in photocatalytic reactions (Gupta and Tripathi 2011).

There are some limitations in the crystallinity of titanium oxide-based materials which are usually associated with the calcination process; it is well known that the pores in titanium oxide powder may collapse at high calcination temperatures as consequence of the irreversible transformation from anatase to rutile, which is usually associated with a lowering of the external surface area. This phase change with the temperature involves cleavage and formation of Ti–O bonds and crystal nucleation. Crystal-growing phenomena normally occur from 600 up to 800 °C

depending on the starting anatase (Mohammadi et al. 2008; Gupta and Tripathi 2011; Sánchez-Muñoz et al. 2013). Therefore, on raising the calcination temperature, the crystallinity increases (lowering the band-gap); however, the surface area decreases (as the particle size increases and the pores usually collapse).

The resulting photocatalytic activity is dominated by an equilibrium and compensation of crystallinity and surface area. Usually, a high degree of crystallinity is more efficient than a high surface area, because the electron-hole recombination is smaller in more crystalline materials. Indeed, the electron-hole recombination is the biggest problem in most of the photocatalytic reactions in which products have more energy than the reagents (Kudo and Miseki 2009). In addition, the hydroxyl concentration on the external surface area may have a high influence on the photocatalytic activity (Oosawa and Grätzel 1988).

Some authors have recently investigated the phase transformation steps and their relationship with the photocatalytic activity, finding that a higher photocatalytic activity is usually found in crystalline mixtures of rutile and anatase or brookite and anatase when compared with pure anatase (Gupta and Tripathi 2011; Luis et al. 2011).

7.2.1 Synthetic Methods for the Preparation of Nanostructures of TiO_2

There are several methods for the preparation of titanium dioxide, and usually the properties of the obtained materials are dependent on the synthetic route and the calcination parameters (Luis et al. 2011). Indeed, following the same procedure, the particle size may change if a different quantity of starting material is used (Thamaphat et al. 2008).

The photoinduced reactions usually occur on the photocatalyst surface. Therefore, a high surface area is beneficial for the photocatalytic activity, making the use of nanometric titanium oxide interesting (Souvereyns et al. 2013). In recent years, the development of new synthetic methods for an effective reduction of the particle size has been very significant, obtaining mesoporous or nanoporous materials of titanium oxide in the form of nanocrystals, nanopowders, thin films, nanotubes, and nanorods using sol–gel methods either with or without organic surfactants. In addition, homogeneous precipitation, hydrothermal methods, melted salts, or chemical methods in vapor phase have also been recently used (Sánchez-Muñoz et al. 2013; Thamaphat et al. 2008).

Synthetic Methods in Vapor Phase

The synthetic methods in vapor phase are referred to each process in which the materials are condensed in a vacuum chamber to form a solid phase. This kind of processes, without chemical reactions involved, are known as PVD (physical vapor

deposition processes). On the other hand, those that are focused on chemical reactions are usually named CVP (chemical vapor deposition processes) (Chen and Mao 2007).

Among the vapor-phase methods, the flame direct oxidation method is probably the most widely used for the preparation of submicronic anatase particles. This process is based on the combustion (with oxygen) of a mixture of hydrogen and titanium(IV) chloride in a flame. Using this method, the particle size is normally between 10 and 100 nm. This method is usually time-dependent, as long periods of time in the flame give higher particle size.

There are some other methods in vapor phase, such as electric arc-induced plasma, laser- and aerosol-induced methods, (Kho et al. 2011) and electron beams, although all these methods are less extended than the flame oxidation.

During the last 5 years, additional thermal plasma methods have also been applied for the preparation of different phases of titanium oxides with very interesting results, which open up new directions in the search of novel more controlled synthetic methods for the preparation of titanium oxide-based materials (Arif et al. 2017).

Synthetic Methods in Liquid Phase

Liquid-phase synthetic methods offer many advantages compared with the vapor-phase methods, such as a strict control of the stoichiometric conditions, formation of complex forms, production of homogeneous materials, and possibility of preparation of composite materials. However, some disadvantages are also present when using liquid-phase methods, like higher costs of the chemical precursors, presence of carbon as impurities, and longer reaction times (Gupta and Tripathi 2011). In most of the cases, these methods usually have, as an objective, the preparation of nanometric particles with narrow particle size distributions and of extremely high external surface area.

There are a high number of synthetic methods in liquid phase such as hydrothermal, solvothermal, electrodeposition, sonochemical, micellar, inverted micellar, and microwave methods, among others (Chen and Mao 2007). However, the procedures based on the sol–gel technique (Fig. 7.2) are the ones most extended due to their versatility, reproducibility, and ease of the control of the synthetic parameters (Pizarro 2005; Chen and Mao 2007).

Sol–gel methods are based on a physical transition from a system in liquid state (usually a colloidal suspension of nanosized particles, namely, a sol) to a solid phase, namely, a gel (which is a solid constituted of at least two phases with liquid phases trapped and immobilized by the solid phase) (Macwan et al. 2011). The precursors that are usually employed in the preparation of the sol are metallic inorganic salts, such as titanium alkoxides. In a typical sol–gel method (Fig. 7.2), the precursor is hydrolyzed, and a subsequent polycondensation step leads to a colloidal suspension (sol), normally using a base or an acid as catalyst of the reaction. In the system, some very small chains of solid particles are formed in the liquid (organic or aqueous

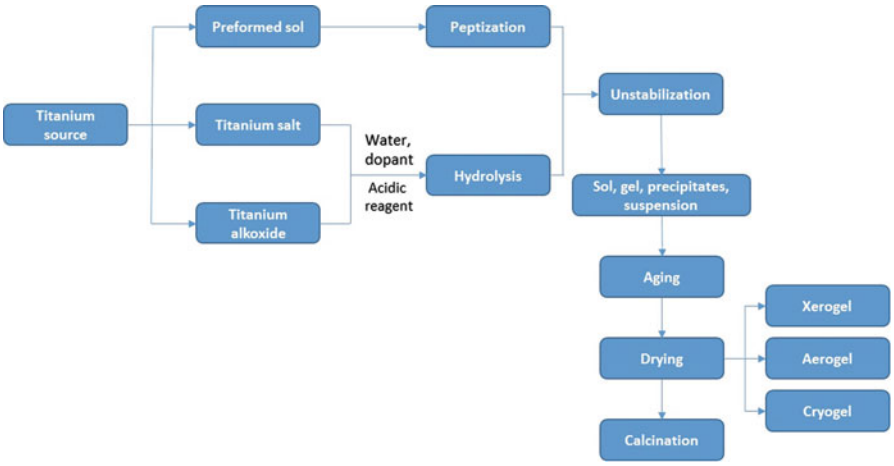

Fig. 7.2 Preparation of titanium oxide photocatalysts via sol–gel methods. (Pizarro 2005; Akpan and Hameed 2010)

solvent). The sol is formed because the particles are very small (1–1000 nm) and the gravitational driving forces are very small compared with the van del Waals and electrostatic forces between the particles that stabilize the colloidal system.

The subsequent transformation of the obtained sol to a gel is usually achieved by a simple drying of the mixture and an additional thermic treatment after drying (calcination), which usually leads to ceramic materials with different morphologies, shapes, and particle sizes, or to formation of thin films of the substrate (Chen and Mao 2007; Macwan et al. 2011).

Sugimoto and coworkers, using a sol–gel method, have carried out some intensive studies on the formation of titanium oxide nanoparticles of different sizes and morphologies, tuning the reaction parameters (Chen and Mao 2007). In this context, Yu and coworkers published in 2002 a very simple synthetic method for the preparation of mesoporous titanium oxide with a control of the 3D structure (Yu et al. 2002) and with a very high thermal stability without the use of surfactants. In addition, some other simple methods with good control of the morphology were used very recently for the preparation of mesoporous agglomerates of nanosized titanium oxide, without the use of a surfactant (Sánchez-Muñoz et al. 2013; Lázaro-Navas et al. 2015; Rico-Oller et al. 2016).

The current trends of the most recently reported sol–gel syntheses for the preparation of porous titanium oxide materials are focused on the use of alkylketene dimers as templates (Takahasi et al. 2017). Additionally, a recent study has compared the effect of sol–gel preparations and solvothermal methods on the final phase and textural properties of titanium oxide (Dastan 2017).

Alternative methods have recently been explored for the preparation of titanium oxide-based materials with enhanced properties using ionic liquids to extend the

applications of the final titanium oxide-based nanomaterials (Grindi et al. 2014; Voepel and Smarsly 2017). Recently, interesting results have been published in this field by using 1-ethyl-3-methylimidazolium for the preparation of titania nanoparticles for ammonia detection (Sali et al. 2017) or 1-hexyl-3-methylimidazolium and 1-octyl-3-methylimidazolium for the synthesis of titanium oxide nanofluids with applications in acaricides detection (Wu et al. 2017).

Modification of Titanium Oxide by Different Synthetic Methods

As explained before, the most important disadvantage of the use of titanium oxide as photocatalyst is its poor absorption of visible light; therefore, for an efficient use of its photocatalytic properties, UV excitation energy is needed, which leads to a higher-energy consumption, and subsequently higher costs, for the UV/TiO_2 system (Janczarek et al. 2007).

To overcome the limitation associated with the energy consumption and to improve the photocatalytic applicability of the titanium oxide-based materials, an increase of the porosity and surface area is beneficial for the system. In addition, a reduction of the band-gap is especially desirable to improve the absorption capacity of titanium oxide materials. Therefore, the modification of titanium oxide absorption spectrum toward visible light has been extensively studied (Janczarek et al. 2007; Sánchez-Muñoz et al. 2013). For example, different methods such as stabilization with dyes (e.g., tionine), doping with metallic ions (using transition metals such as Cu, Co, Ni, Cr, Mn, Mo, Nb, V, Fe, Ru, Zn, Au, Ag, or Pt) or nonmetallic elements (e.g., N, S, C, B, P, I, and F), and coupling with other semiconductors of lower band-gap (e.g., CdS nanoparticles) usually lead to a lower band-gap of the final nanosystem (Gupta and Tripathi 2011; Ni et al. 2007; Zaleska 2008).

It has been experimentally observed that doping with transition metals of the 3d block (one element, various elements, or one element and a co-catalyst) is an efficient and simple method to modulate the band-gap values of the semiconductor due to their ability to act as electron acceptors which minimizes the charge recombination. However, doping is effective only when using a low number of ions as when the optimal quantity is exceeded, the photocatalytic activity may decrease due to the formation of recombination electron-hole centers (Torres-Martínez and Ruiz-Gómez 2011). A consequence of the doping, in the ideal amount, is the modification of the chemical structure of titanium oxide, with a displacement of the absorption maximum to higher wavelengths lowering the band-gap (Janczarek et al. 2007; Sánchez-Muñoz et al. 2013; Calatayud et al. 2012).

In addition, the transition anatase–rutile may be modified due to the presence of certain ions in the growing step of the titanium oxide nanoparticles. It has been established that certain dopants with +4 charge increase the temperature of the anatase–rutile transition, while other dopants with different or variable charge (except Al^{3+}) decrease the temperature of transition anatase–rutile (Torres-Martínez and Ruiz-Gómez 2011). Various authors have studied the doping with interesting

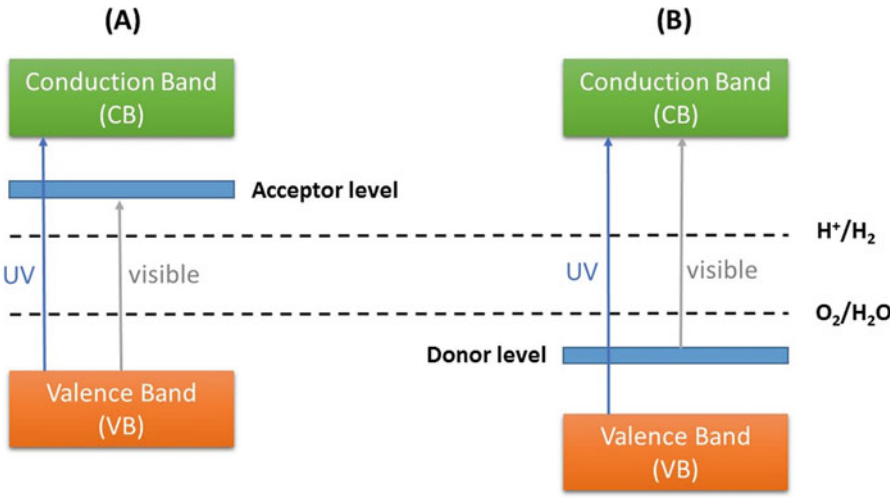

Fig. 7.3 Energy diagram form after doping with different metal ions. (Chen et al. 2010a)

results in the control of the textural and absorption properties of the obtained titanium oxide-based materials; thus, the work of Iishii et al. (2004) Hwangy et al. (2004, 2005) Konta et al. (2004) and Niishiro et al. (2005, 2007) is worthy of highlighting.

In Fig. 7.3, a diagram of the modification of the band-gap, in function of the doping agent, is shown. If the doping metal has an oxidation state higher than +4, it provides an excess of electrons localized in energy levels which are located slightly below the conduction band of titanium oxide (*n*-doping), giving an acceptor level of electrons (A). On the other hand, if the doping metal has an oxidation state lower than +4, due to the lack of electrons, introduces unoccupied energy levels slightly above the valence band of titanium oxide (*p*-doping), giving an electron donor level (B). In both cases, the band-gap is reduced, and the energy radiation needed for the photoactivation is lowered.

The properties of the doped titanium oxide photocatalyst substantially depend on the doping ion nature and its concentration in the medium, the preparation method, the thermal treatment, and some other factors of lower importance (Chen et al. 2010a).

It is important to find new methods with higher simplicity, easily scalable and economically achievable for industry. The use of an abundant and cheap ion, which induces higher photocatalytic activity, is an adequate option for a simple modification of the electronic and absorption properties of pristine titanium oxide.

Attractive dopants such as zinc, fluorine, or nitrogen have extensively been used during the last years (Nethi et al. 2017; Sánchez-Muñoz et al. 2013; Lázaro-Navas et al. 2015; Rico-Oller et al. 2016) with other elements most probably being studied in the future.

7.3 Environmental Applications in Advanced Oxidation Processes

7.3.1 Introduction and Overview

Recently, environmental quality demands have increased with one of the most challenging issues being the presence of recalcitrant compounds in wastewater, due to their potential toxicity. Persistent organic compounds in wastewater can be hazardous or toxic and may cause several problems both in the environment and on human health. Although, the conventional processes such as physical, chemical, or biological are usually efficient for the degradation of pollutants occurring in wastewaters, most of these compounds are, however, not effectively removed. In this context, advanced oxidation processes (AOPs), which are oxidation methods based on the presence of highly reactive species such as hydroxyl radicals, are raising great interest for the removal of those organic pollutants not remediable by conventional methods due to their lack of ability for biodegradation and high chemical stability (Wu et al. 1999; Neyens and Baeyens 2003; Tian et al. 2011).

Over the past decades, AOPs for wastewater treatment has drawn the attention of researchers, as they are one of the most promising advanced technologies to eliminate the total organic content, toxic pollutants, and even microbiological contamination from wastewaters (Bethi et al. 2016). Depending on the chemical structure of the pollutant molecules, AOPs can mineralize some of them into ultimately harmless substances like CO_2 and H_2O, avoiding, therefore, the issue of pollution shifting (Micó et al. 2010).

AOPs have been proposed as alternative methods for the elimination of many toxic organic compounds in wastewater because they can generate less toxic intermediate products during the degradation of organic pollutants. As compared to the conventional treatment techniques, AOPs are more efficient and capable of degrading recalcitrant organic pollutants (Klamerth et al. 2012; Benotti et al. 2009; Babuponnusami and Muthukumar 2014).

In addition, the conventional methods such as biodegradation, chlorination, adsorption, coagulation, etc. cannot remove emergent pollutants such as oxytetracyclines (OTC, Fig. 7.4, a broad-spectrum antibiotic) efficiently due to its bio-resistant property and chemical stability (Liu et al. 2016).

The particular importance of these technologies appears to be in destroying biologically nondegradable chemical structures, as well as ozone-resistant substances such as organic pesticides, dyes, (Cheng et al. 2015; Agustina 2012; Chen and Zhu 2011) aromatic structures, (Karci et al. 2012, 2014) and petroleum constituents (Diya'uddeen et al. 2011) present in the wastewaters. However, the use of AOPs is not cost-effective if mineralizing toxic and recalcitrant compounds in wastewater is intended (Oller et al. 2011).

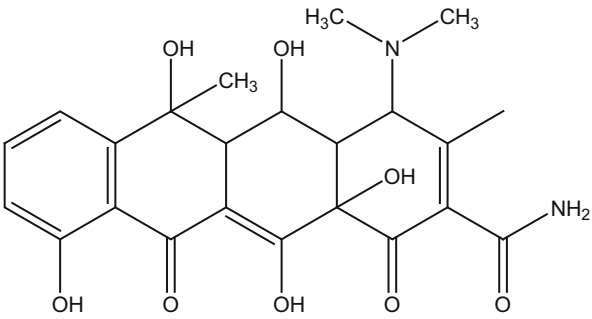

Fig. 7.4 Structure of oxytetracycline, a broad-spectrum antibiotic of the family of tetracyclines

7.3.2 Principles of AOP

The principle of AOPs is to produce hydroxyl radicals (·OH) in water, a very powerful oxidant capable of oxidizing a wide range of organic compounds. AOPs generate extremely reactive ·OH radicals that are responsible for the degradation of pollutants (Shah et al. 2013; He et al. 2014). The main basis of these techniques is the release of high energy (chemical, electrical, or radiating) into water in order to generate highly reactive species such as superoxide radical anions ($O_2-\cdot$) and hydroperoxyl radicals ($HO_2^{\cdot}$) which are involved in the overall reactions.

The most important species are hydroxyl radicals, which have a considerably high oxidation potential, and thus, they can oxidize nonselectively organic pollutants even at ambient temperature. Next in importance as strong oxidation reagents produced by AOP are oxygen radicals, ozone, and hydrogen peroxide. During the activation process, AOPs are able to generate hydroxyl radicals ·OH reactive toward organic compounds in the presence of dissolved oxygen.

AOPs can be considered versatile technologies due to the production of hydroxyl radicals (·OH) by various alternative routes. ·OH are the main desired species due to their nonselective reactivity caused by the high oxidation potential (2.80 V). The first utilizes the natural and artificial light source (e.g., sun light, UV, visible light, etc.). Examples of this are UV/H_2O_2, UV/O_3, UV/TiO_2, and UV/Fenton. In the absence of light, they can be considered to be dark oxidative processes like ozonation (O_3), fenton, and ultrasound.

Heterogeneous Photocatalysis

As one of the most important AOPs, heterogeneous photocatalytic oxidation processes are one of the most important areas in photochemistry, especially when solar light is used. Photocatalysis is defined as a discipline inside chemistry that studies the reactions in which the absorption of light is involved. Thus, in heterogeneous photocatalysis a semiconductor must have the following characteristics:

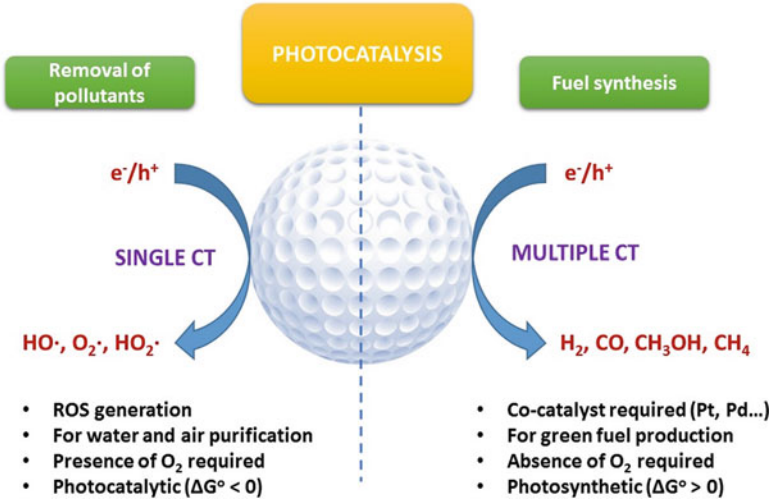

Fig. 7.5 Comparison of photocatalytic reaction features for environmental purification versus solar fuel synthesis. Illustration adapted from Park et al. (2016)

- Appropriate band-gap energy in the range of 1.7–3.2 eV
- Efficient light absorption
- High carrier mobility
- Precise band edge positions that straddle the water redox potentials
- Lack of toxicity and chemical stability (Boudjemaa et al. 2013; Zazoua et al. 2014; Helaili et al. 2015)

In heterogeneous photocatalysis, when photons of energy higher or equal to the band-gap energy are absorbed by a semiconductor, an electron (e^-) from the valence band (VB) is transferred to the conduction band (CB) generating a hole (h^+) in the VB. Thus, the absorption of photons creates electron/hole pairs (e^-/h^+) which can reduce and/or oxidize a compound adsorbed on the photocatalyst surface (Fig. 7.5).

The charge transfer reactions occurring on semiconductor photocatalysts have been applied for two main purposes: (Park et al. 2016)

(i) Environmental applications for the remediation of polluted water and air purification.
(ii) Solar energy storage through the synthesis of solar fuels (eg. hydrogen production from water splitting, CO_2 conversion to hydrocarbons).

Figure 7.5 illustrates how the characteristics of charge transfer in the two processes are different. The former is usually initiated by a single-electron transfer under aerated conditions to generate reactive radical species, whereas the latter proceeds via two or more electron transfers in the absence of molecular oxygen (O_2).

Among the photocatalysts studied to date, TiO_2 is one of the most promising materials because of its relatively low cost, superior photocatalytic performance,

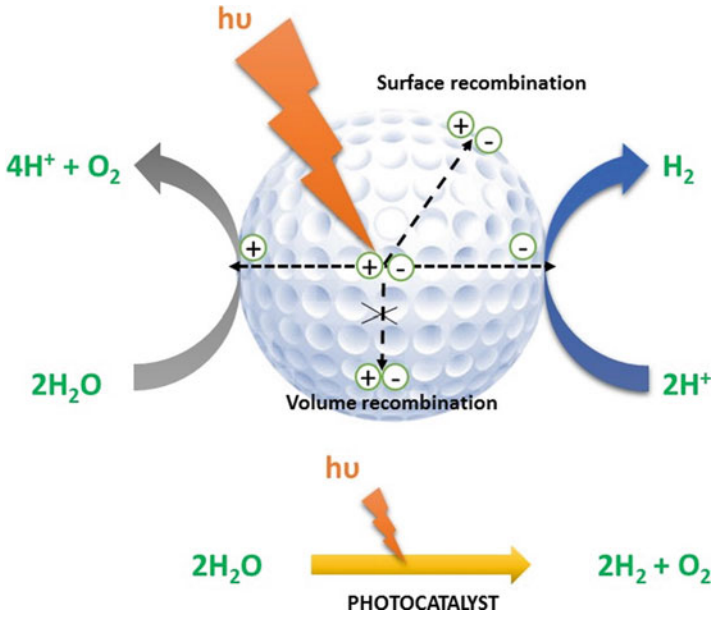

Fig. 7.6 Reactions that may occur over irradiated TiO_2 suspensions under conditions of water splitting. (Illustration adapted from Yang et al. (2013))

long-term stability, and environmental friendliness (Ni et al. 2007). TiO_2, especially in the form of anatase, as photocatalyst is widely used for wastewater treatment and hydrogen generation. TiO_2 exhibits a wide band-gap energy (Eg ~ 3.2 eV) and is a semiconductor corresponding to radiation in the near-UV range. This is one of the advantages compared to other semiconductor photocatalysts. When the TiO_2 surface is irradiated, it is rapidly excited and generates a (e^-/h^+) pair. The hole (h^+) adsorbs the surrounding water molecules and gets oxidized to form a hydroxyl radical. The generation of hydroxyl radical is a cyclic process and initiates the series of reactions on the TiO_2 surface as shown in Fig. 7.6. Some recombination processes, which may reduce the photocatalytic effectivity of titanium oxide are also possible (Fig. 7.6).

As an alternative to titanium oxide in photocatalysis, various TiO_2 nano-architectonic topographies have been extensively studied for enhancing the performance of photoelectrochemical cells (PEC) (Yang et al. 2011; Zhang et al. 2012a; Chen et al. 2013; Wang et al. 2014a; Huang et al. 2015). In general, a predominant PEC cell relies on two factors: the efficient usage of solar energy and the instant transportation/separation of charges. To date, many hierarchical TiO_2 nanostructures based on nanowires (NWs) and nanotubes (NTs) have been synthesized for enhanced photoelectric efficiency in solar energy harvesting, conversion, and pollutants purification (Cho et al. 2011; Lee et al. 2013; Bai et al. 2013).

7.3.3 Water Remediation Using Titanium Oxide

Liquid effluents containing organic contaminants are more difficult to treat using conventional processes such as physicochemical and biological. In this regard, AOPs for the elimination of organic contaminants in an aqueous medium using TiO_2 photocatalysis have been proved to be potentially advantageous for the purification of wastewater, especially for persistent and non-biodegradable contaminants. As a representative photocatalyst based on TiO_2, it is highly stable, resistant to acidic or alkaline conditions, nontoxic, safe, and inexpensive and has a very rich redox reactivity. Thus, TiO_2 is known as the best material for oxidizing organic pollutants (Chi et al. 2013). When the photocatalyst is applied in UV-based oxidation, various organic pollutants can be degraded and/or mineralized into CO_2 and H_2O due to the production of hydroxyl radicals (·OH), which have a strong oxidation potential (2.8 V).

The high importance of TiO_2 as photocatalyst lies in its ability to oxidize many organic compounds into innocuous species such as CO_2 and H_2O, (Carp et al. 2004) although in some other cases, formaldehyde may be the one of the products of the degradation, being, therefore, a target of study (Khanmohammadi et al. 2014). The photodegradation properties of titanium oxide are originated from its suitable electronic band structure. The redox potential for photogenerated holes from TiO_2 is +2.53 V versus the standard hydrogen electrode (SHE) which is positive enough to produce oxygen or ·OH from water. The redox potential for CB electrons is −0.52 V, which is, in principle, negative enough to evolve hydrogen from water and to produce superoxide $O_2^{-\cdot}$ from absorbed oxygen. The generation of ·OH radicals and superoxide $O_2^{-\cdot}$ significantly facilitates the decomposition of organic pollutants (Henderson 2011; Fujishima et al. 2008; Fujishima and Zhang 2006). Textile dyes, compounds of pharmaceutical or industrial origin, or human domestic wastes constitute some of the largest groups of organic compounds that represent an increasing environmental danger. Therefore, this is an interesting topic of study, not only using titanium oxide as semiconductor photocatalyst, but also especially when the degradation process can be activated by visible light (Candal and de la Cruz Martínez 2015). Thus, in recent years a wide variety of hybrid systems based on titanium oxides have been studied for these purposes (Gunti et al. 2017).

Pharmaceutical Compounds

In the environment, pharmaceutical compounds such as nonsteroidal antiinflammatory drugs (NSAIDs), hormones, antibiotics, etc. have been detected in many areas: hospital wastewaters, (Kummerer 2001; Wen et al. 2004) in and out sewage treatment plant effluents, (Carballa et al. 2004) surface water as rivers and lakes, (Boyd et al. 2003) marine waters, (Weigel et al. 2004) and in soil matrices (Scheytt et al. 2006). Pharmaceutical compounds with ng L^{-1} and mg L^{-1} concentrations levels have rarely exceeded the mg/L levels (Chen et al. 2010b; Stumpf et al. 1998; Ternes 1998;

Tixier et al. 2003). However, generally, the concentrations of the pharmaceutical pollutants and photocatalysts used in the laboratories varied from 20 to 200 mg/L and 0.2–1.5 g/L, respectively (Palominos et al. 2009; Mohammadi et al. 2012).

Many pharmaceutical drugs, i.e., ibuprofen (IBP), atenolol (ATL), and carbamazepine (CBZ), are subjects of various studies, (Hapeshi et al. 2010; Georgaki et al. 2014) which employed immobilized TiO_2 systems (Khataee et al. 2013; Sarkar et al. 2015; He et al. 2016). Thus, heterogeneous photocatalysis using TiO_2 nanoparticles has become a promising pathway for elimination of several micropollutants from wastewater (Zhang et al. 2010a; An et al. 2011; Sarkar et al. 2014a, b). Small size nanoparticles provide higher surface to volume ratio and thus offer better surface reactivity.

The influence of some doping atoms on the surface reactivity of titanium oxide-based materials is crucial. For example, it was reported that the 2*p* orbital of nitrogen makes it the most easily binding element with the 2*p* orbital of oxygen among the nonmetal dopants incorporated to titanium oxide. Thus, nitrogen atoms are located in position of oxygen in TiO_2 lattice to form O-Ti-N structure (Schneider et al. 2014). The photocatalytic mechanism of N-doping CNT/TiO_2 under visible light has been proposed by Schneider et al. (2014 and Yuan et al. 2016) The smaller band-gap of N-doping CNT/TiO_2 is mainly resulted from both the polymorphs of TiO_2 and doping with nitrogen, leading to the good separation of (e^-/h^+) pairs under visible light region (Fig. 7.7). The same result was observed by Calza et al. using TiO_2 doped with graphene oxide at various irradiated media under simulated solar irradiation (Calza et al. 2016).

The degradation of IBP by several oxidation processes has already been reported. Lambropoulou et al. studied the TiO_2 photocatalytic degradation of IBP and diclofenac (DCF) pharmaceutical compounds (Lambropoulou et al. 2011). They have suggested that during the application of TiO_2 photocatalysis under UV light, simulated solar, and ultrasound irradiation, numerous transformation products are formed since ·OH does not exhibit selectivity toward various functional groups, while other reactive species (e.g., $O_2^{-\cdot}$, h^+, or e^-) participate in multiple oxido-reductive pathways (Lambropoulou et al. 2011). Different degradation pathways can be put forward, in which hydroxylation, demethylation, decarboxylation, cleavage of isobutyl moiety, and oxidation of hydroxyl groups are described as major steps during the transformation processes (Scheme 7.1) (Michael et al. 2014).

Madhavan et al. studied the photocatalytic degradation of IBP in presence of TiO_2 and reported that the formation of hydroxylated products argued that the hydroxylation process could be the first step of the degradation, followed by a second step of demethylation or decarboxylation with other different by-products with smaller *m/z* values (Madhavan et al. 2010). The formation of hydroxylated products (I) and (II) is observed in all the processes using photocatalysis for degradation. In addition, the products with *m/z* values 133 and 191 corresponding to 4-ethylbenzaldehyde (III) and 4-(1-carboxyethyl)benzoic acid (IV) were also detected (Fig. 7.8).

The relationship between commercial TiO_2 and the photocatalyst activity with the molecular volume of the drugs has been recently studied (da Silva et al. 2015). A

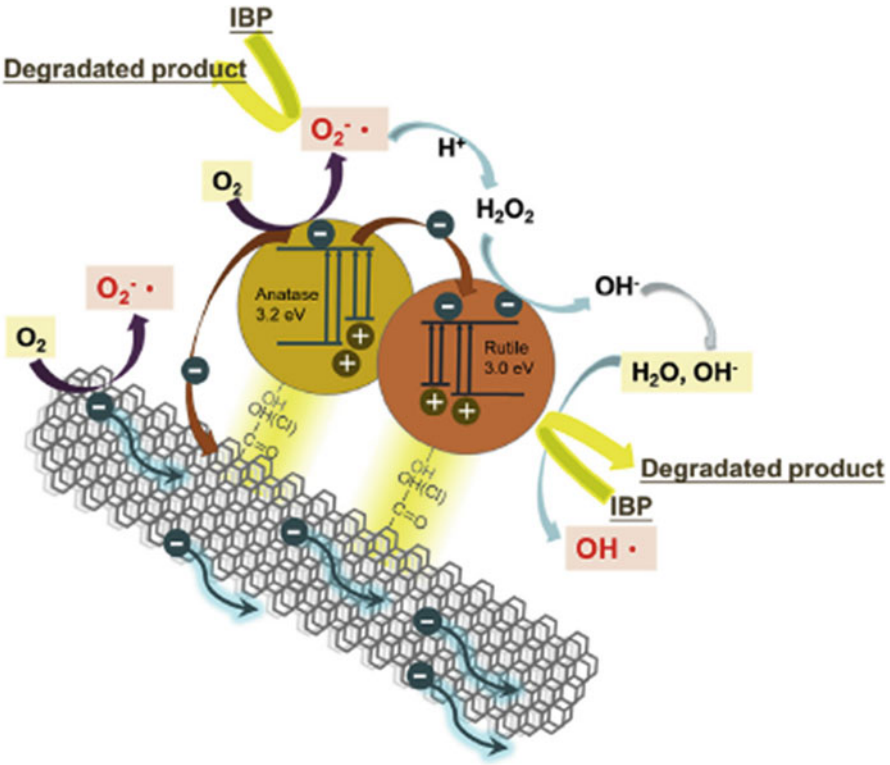

Fig. 7.7 Photocatalytic mechanism of N-doping CNT/TiO_2 irradiated with visible light. Reproduced with permission (Yuan et al. 2016)

series of eleven drugs, namely, diclofenac sodium, atorvastatin calcium, ketoconazole, fluoxetine, ibuprofen, tioconazole, dexamethasone, guaifenesin, valsartan, naphazoline hydrochloride, and paracetamol were comparatively degraded under UV and visible light in the presence of a supported photocatalyst (Fig. 7.9).

The surface charge of particles can vary with aqueous pH which affects the adsorption capacity. The more chemicals adsorbed on the photocatalysts surface, the better photocatalytic performance. Under alkaline conditions, more ·OH formation would offset the repulsion effect although the ·OH anions act as hole (h^+) scavengers to form active ·OH. In a solution with low pH, more H^+ ions are accessible to serve as electron scavengers to produce superoxide radicals and to inhibit the recombination of (e^-/h^+) pairs (Liu et al. 2015a). The higher degradation rate of IBP was therefore found at low-pH solution, probably because the photodegradation is strongly dependent of the contribution of superoxide radicals ($O_2^{-\cdot}$) rather than hydroxyl radicals (·OH) (da Silva et al. 2015).

As explained above, the degradation of IBP is, therefore, one of the most interesting applications of titanium oxide-based materials. However, several other pharmaceutical

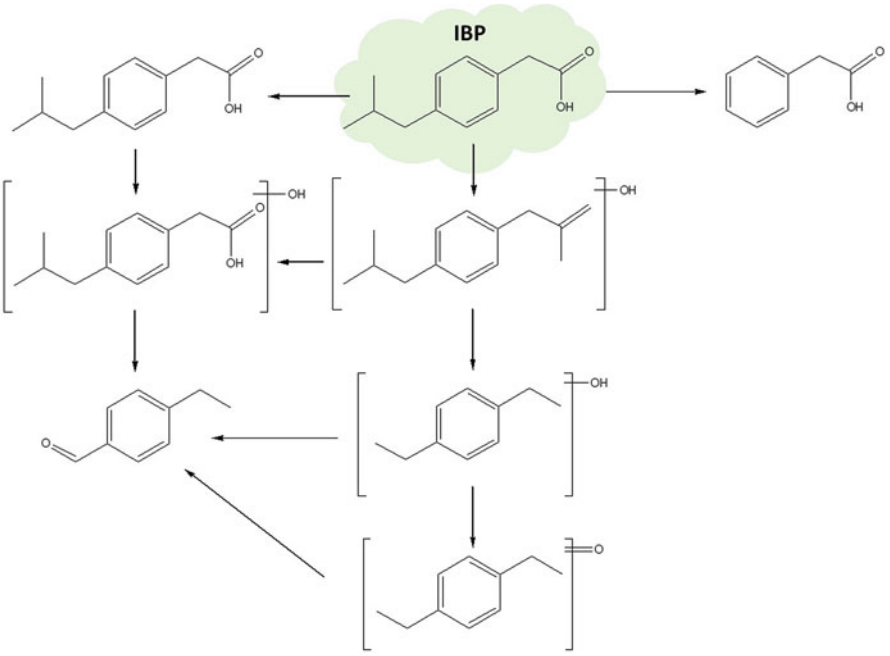

Scheme 7.1 Ibuprofen degradation by photocatalysis under UV light and simulated solar irradiation and sonophotocatalysis. (Michael et al. 2014)

products have been tested (Ahmari et al. 2018), and recent literature revisions on this topic have been published in the last couple of years explaining some more advances in this field (Lee et al. 2017; Li and Yang 2018; Freyria et al. 2018).

Organic Dyes

Recent reports about the preparation and application of TiO_2-based catalysts in the photodegradation of organic dyes are grouped in Table 7.1, which was recently summarized by Wang and coworkers when reviewing the photocatalytical properties of graphene-based hybrid materials (Wang et al. 2013a).

Thus, graphene–TiO_2 composite, as a rising star material, is the most common hybrid photocatalyst for the degradation of dyes (Neppolian et al. 2012; Jiang et al. 2011; Li et al. 2012; Zhang et al. 2012b; Shah et al. 2012; Nguyen-Phan et al. 2012; Morales-Torres et al. 2012; Tan et al. 2012). Because of its nanometer size, TiO_2 showed enhanced photodecomposition efficiency under visible light compared to pristine TiO_2, the commercial TiO_2 (P25) and the physical mixture of graphene and commercial P25. This result may be due to both the large contact surface area and high conductive graphene which reduce the charge resistance and the charge recombination rate.

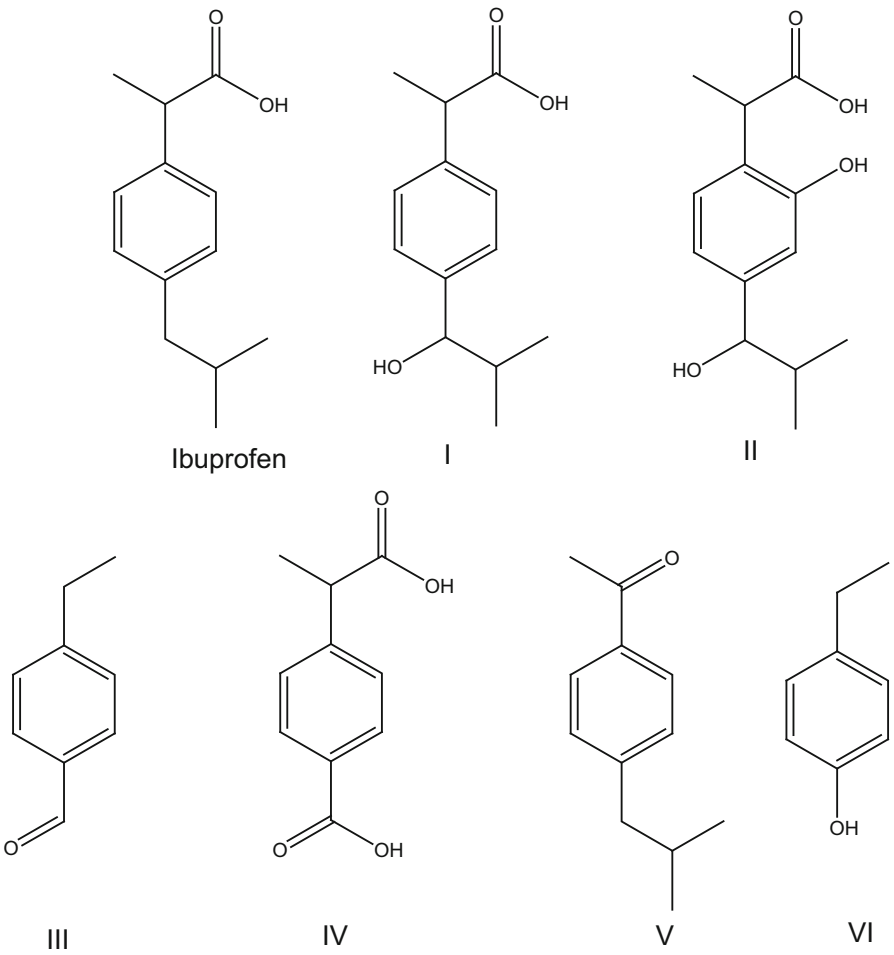

Fig. 7.8 Degradation products observed for ibuprofen during sonolysis, photocatalysis, and sonophotocatalysis

Ag–TiO_2 nanocomposite prepared by a different method, has also been the subject of various reports that show an enhancement of the photocatalytic activity compared with pristine or commercial titanium oxide (Cheng et al. 2010; Xiang et al. 2010). The materials showed enhanced photocatalytic activity on dye degradation, which is probably due to the transfer and separation of photogenerated electrons from TiO_2 shell to the Ag core and to the self-sensitization of the dye molecule.

An extensive work has been carried out in order to prepare ZnO/TiO_2 heterostructures, which show good photocatalytic activity for the degradation of organic dyes, such as methyl orange (MO) (Zhang et al. 2010c), methylene blue (MB) (Arin et al. 2013), rhodamine dye (Liu et al. 2010b; Karunakaran et al. 2011; Xiao 2012), malachite green (Stoyanova et al. 2013) and an azo dye (Sartori et al.

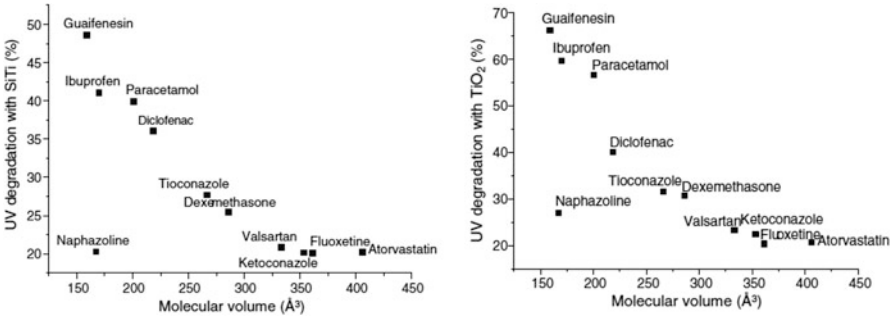

Fig. 7.9 Correlations between the degradation of drugs and molecular volume with a commercial TiO_2 catalyst and under UV radiation. Reproduced with permission (da Silva et al. 2015)

2011). The degradation efficiency is around 98% at acidic medium (pH 2.0), showing a very high degradation efficiency after 30 min and complete mineralization after 60 min. The fabricated ZnO–TiO_2 hollow spheres presented superior photocatalytic activity for the degradation of rhodamine 6G compared with ZnO and TiO_2 hollow spheres (Liu et al. 2010b).

In addition, a porous TiO_2 film modified with RuO_2 by dropping or impregnation methods has been synthesized by Liu and coworkers and has been used as a heterocatalyst (Liu and Li 2011). Modification with an appropriate amount of RuO_2 improved the photocatalytic performance in the degradation of Eosin Y. These materials delayed the recombination (e^-/h^+) and gave much higher efficieny than non-doped systems. It is clear that doping of titania structures is always useful in improving the photocatalytic properties of the materials.

Furthermore, some recent studies have reported that the immobilization of AuNPs on TiO_2 is able to induce visible light-driven photocatalysis for dyes, (Zhang et al. 2011) various volatile organic compounds, (Cojocaru et al. 2011; Wu et al. 2009) and toxic persistent organic pollutants (Alvaro et al. 2010) degradation. In this case, the visible light generated the photoexcited electrons of the AuNPs due to the surface plasmon resonance, and the excited electrons were injected to CB of TiO_2.

Ag@TiO_2 core–shell nanoparticles prepared using hydrazine as reducting agent and a sol–gel method demonstrated significantly higher photocatalytic activities in the degradation of rhodamine B compared to TiO_2 nanoparticles (Chuang and Chen 2009). The enhanced photocatalytic activity was attributed to the formation of Schottky barrier at the core–shell interface as well as to the excitation of the photogenerated electrons from the surface of Ag cores to the conduction band of TiO_2 shells. Photocatalytic activity of TiO_2 modified by Ag has been tested by the degradation of different organic compounds such as methylene blue (MB) (Logar et al. 2010; Chin et al. 2011; Kim et al. 2011). In addition, Kim et al. reported a very high photocatalytic activity in the presence of Ag/TiO_2/carbon nanofibers (Ag–TiO_2/CNF) composites for the degradation of MB under visible light (Kim et al.

Table 7.1 Preparation and application of TiO_2-based photocatalysts in the degradation of organic compounds

Catalysts	Preparation method	Pollutants	References
GO/TiO_2	One-step colloidal blending by the thermal reduction of GO/TiO_2 composite	Methylene blue	Nguyen-Phan et al. (2011)
TiO_2/graphene	One-pot solvothermal	Methylene blue	Zou et al. (2011)
TiO_2/rGO	Hydrothermal	Rhodamine B	Wang and Zhang (2011)
SnO_2/rGO or TiO_2/rGO RGO	Direct redox reaction under the presence of HCl solution	Rhodamine B	Zhang et al. (2011)
TiO_2/graphene	Mixing graphene dispersed solution with $C_{16}H_{36}O_4Ti$, followed by adding deionized water, HCl, and $C_{16}H_{36}O_4Ti$ and then sealed and heated	Methylene blue	Zou et al. (2011)
TiO_2/graphene	Hydrolyzing $Ti(BuO)_4$ in the GO solution, followed by the hydrothermal	Rhodamine B	Liang et al. (2010)
TiO_2/GO	Mixing GO, water, and sodium dodecysulfate, followed by adding $TiCl_3$, Na_2SO_4, and H_2O_2, under modest stirring	Methyl orange	Chen et al. (2010c)
TiO_2/GO TiO_2	Low-temperature hydrolysis	Methylene blue	Liu et al. (2010a)
Kaolinite/TiO_2	Calcined at 200 °C	Methyl orange	Wang et al. (2011a)
TiON/cu/co	Co-modified nitrogen doped titania	Eriochrome black- T (EBT)	Ali et al. (2013a)
CuO-Al_2O_3-ZrO_2-TiO_2	Co-precipitation	Direct sky blue-5B	Ali et al. (2013b)
SnO_2/TiO_2	Sol–gel	Rhodamine B (RhB)	Messih et al. (2013)
TiO_2/graphene	Mixing GO with $Ti(OC_4H_9)_4$ using ethanol as a medium, followed by evaporation and calcination	Methylene blue	Zhao et al. (2012)
SnO_2/TiO_2 composites nanofiber	Electrospinning	Rhodamine B (RhB)	Hwang and Kim (2011)
TiO_2/porous GO	Mixing GO dispersion with $(NH_4)_2TiF_6$ and H_3BO_3, followed by a calcination treatment at 200 °C	Methyl orange	Jiang et al. (2011)
TiO_2/graphene	Mixing GO with ethanol as a medium, followed by evaporation and calcination	Methylene blue	Zhao et al. (2012)
TiO_2/graphene	Non-hydrolytic sol–gel approach	Methylene blue	Lee et al. (2012)
TiO_2	Homogeneous hydrolysis	Methyl orange (MO)	Zhang et al. (2010b)

(continued)

Table 7.1 (continued)

Catalysts	Preparation method	Pollutants	References
TiO_2/graphene	Mixing GO with P25 titania using ethanol as a medium, followed by dip-coating method reactive	Brilliant red dye X-3B	Wang et al. (2012a)
TiO_2/GO	Spin coating under the condition of 3500 rpm for 20 s	Methylene blue	Yoo et al. (2011)
CeO_2/TiO_2/graphene	Hydrothermal reaction with GO in aqueous solution of ethanol	Reactive Red 195	Ghasemi et al. (2012)
CeO_2–TiO_2	2-hydroxyl ethylammonium as room temperature ionic liquid and calcined at different temperatures	Reactive red 195	Ghasemi et al. (2012)
TiO_2	Electrospinning	Rhodamine B	Liu et al. (2010b)
Ti/Si/graphene	Direct sol–gel co-condensation technique and combined with hydrothermal treatment, in the presence of a triblock copolymer non-ionic surfactant P123	Rhodamine B	Li et al. (2012)
TiO_2/Ti-F	Titanium isopropoxide and NaF over an acidic solution of nitric acid at pH 2	Methylene blue	Lázaro-Navas et al. (2015)
TiO_2/Zn	Titanium isopropoxide and zinc nitrate over an acidic solution of nitric acid at pH 2	Methylene blue	Sánchez-Muñoz et al. (2013)
TiO_2/Zn/Pd	Titanium isopropoxide and zinc nitrate over an acidic solution of nitric acid at pH 2. Subsequent reaction with $[Pd(cod)Cl_2]$	Methylene blue	Rico-Oller et al. (2016)

Adapted from Reference (Wang et al. 2013a) and reproduced with permission

2011). This photocatalyst degraded MB 17 times faster than TiO_2/CNF after only 3 h of irradiation. It is important to note that the AgNPs seemed to act as electron acceptors and trapped the photogenerated electrons immediately, which caused an increase in the photodegradation rate and reduced (e^-/h^+) pair recombination.

Some of the most recent studies on the degradation of dyes including the explanation of the effects of the photocatalytic materials, conditions, dye, and textural properties have been recently reviewed by several groups (Thao et al. 2017; Kumar and Pandey 2017; Reza et al. 2017; Giovanetti et al. 2017). These reports constitute very interesting revisions for understanding the correct design of novel nanomaterials with improved photocatalytic activity in the degradation of organic dyes.

7.3.4 Water Splitting

Photocatalytic water splitting using sunlight and particulate semiconductors is a promising technology capable of converting solar energy into hydrogen (Chen et al. 2010a; Walter et al. 2010; Pinaud et al. 2013). H_2 generation from water

splitting by a photocatalytic process is one route that may be used to solve global issues related to renewable energy and environmental pollution. Therefore, it has attracted a great attention in both academic and industrial environments (Zhou et al. 2015a). The water-splitting reaction is first initiated by photon absorption which generates numerous (e^-/h^+) pairs with sufficient potentials. These charge carriers subsequently migrate to the surface of the catalysts and react with surface active sites. Finally, the photogenerated electrons reduce water to hydrogen, and the holes oxidize water molecules to give oxygen. The photogenerated electrons and holes may recombine instantaneously, releasing the energy as photons or heat, when they are not effectively separated. Thus, charge separation is a crucial factor in any photocatalytic activity. If the charges are successfully separated, they migrate to the surface of the semiconductor and participate in oxidation and reduction.

$$H_2O \overset{h\upsilon \geq E_{bg}}{\rightarrow} H_2 + \frac{1}{2}O_2 \tag{7.1}$$

It is well known that TiO_2 is one of the most efficient photocatalyst in terms of stability and photoconversion efficiency among various other semiconductor materials. The band-gap energy of TiO_2 is ca. 3.2 eV which is suitable only for UV radiation absorption, taking only ca. 4% of the total solar light. However, it has some drawbacks whose solution are opening multiple directions for research in TiO_2-based photocatalysis:

1. Rate of (e^-/h^+) recombination in case of an excited charge is very high and is released in form of heat.
2. An absorption response of TiO_2 to the irradiation is very small. This is one of the crucial factors for the low efficiency of the materials.
3. The backward reaction, i.e., combination of H_2 and O_2 to give water, is also possible in these studies.

Furthermore, to achieve the requirement for the water-splitting reaction, the coating on TiO_2 with some electron-rich transport materials and other semiconductors is favored (Jia et al. 2011; Maruthamani et al. 2015). Work has been carried out in order to modify TiO_2-based nanocomposites for effective separation of charge carriers by loading of noble metal nanoparticles such as Au, Ag, and Cu (Maeda and Domen 2010; Sarina et al. 2013; Kochuveedu et al. 2013; Jabbari et al. 2015) that act as electron storage and transport units. Furthermore, some supports may act as reservoirs to store and transport the electrons to the surface of the photocatalyst helping in the reduction of the H^+ from water to give H_2 (Rather et al. 2016; Yu et al. 2013; Wang et al. 2013b). To achieve further enhancement in H_2 production, co-catalysts are loaded onto semiconductors, which are believed to provide active sites and decrease the activation energy for water splitting.

Some noble metals and transition metal oxides such as Ru, Rh, Pd, Pt, Au, Ag, NiO, etc. are used as co-catalysts to improve the hydrogen generation (Kasahara et al. 2002; Le Paven-Thivet et al. 2009). For example, $LaTiO_2N$ has shown better

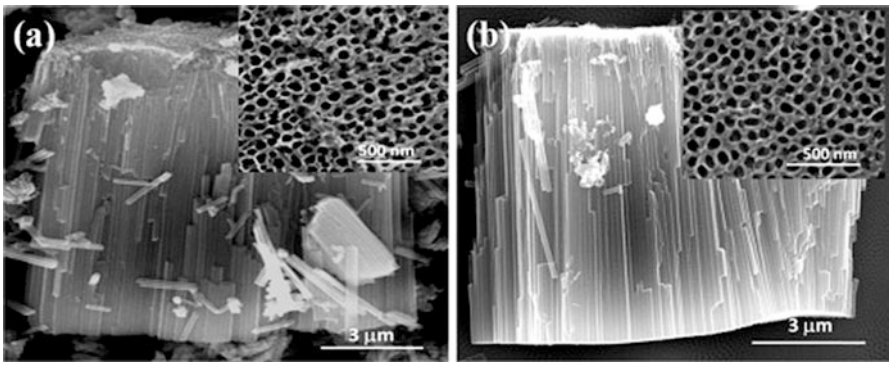

Fig. 7.10 Scanning electron microscopy of as-formed pure TiO_2 nanotube (**a**) and MoO_3–TiO_2 nanotube (**b**). Inset: top morphologies of anodic nanotube arrays. Reproduced with permission from Yang et al. 2016

performance for water oxidation when using RuO_2, IrO_2, CoO_x, or MoO_3 (Fig. 7.10) as co-catalysts (Zhang and Wang 2012; Maegli et al. 2014; Yang et al. 2016; Ran et al. 2014). New advances have been reported when noble metals have been deposited on the surface of TiO_2. These have shown an improvement in the photocatalytic activity by shuttling and storing photogenerated electrons from the photocatalyst to the acceptor (Bahruji et al. 2011; Maicu et al. 2011). In this respect, different studies have demonstrated that metal ions or metal deposited on semiconductors exhibit shifts in the Fermi level bringing it to significantly negative-energy potentials. It must be noted that the Fermi level of deposited precursors (noble metals) are lower than the levels of TiO_2. Thus, the photoexcited electrons can be transferred from the CB to the noble metal particles deposited on TiO_2 surface with the photogenerated holes on the VB remaining unchanged (Rajini et al. 2012).

Nanosized catalysts can enhance the effective transportation of charges and active surface area for catalysis. TiO_2 nanotube arrays have been intensively investigated as TiO_2 catalysts. In comparison to a TiO_2 powder catalyst, the nanotube arrays have specific advantages, including a large surface area, easy retrievability, uniformly ordered structure, and size-dependent properties, all of which make them attractive in wide applications including H_2 generation (Zhou et al. 2015b). It is crucial to note that the amount of active photocatalyst material, the light source, turnover frequency, and catalytic stability is different in each experiment, and, therefore, the hydrogen production should not be estimated as the sole measure of performance in every system.

Some alternatives for hydrogen production by water splitting using different novel photocatalysts have also been recently reported and constitute interesting alternatives to the current materials (Tanigawa and Irie 2016; Wang et al. 2014b; Zhang et al. 2016a; Watanabe 2017).

7.3.5 Hydrogen Production Using Alternative Processes: Photoelectrochemical (PEC) Hydrogen Generation

Honda and Fujishima suggested the possibility of water splitting using TiO_2 as electrode (Fujishima and Honda 1972). Since then, numerous efforts have been made to improve the performance of TiO_2 nanomaterials for hydrogen generation (Chen et al. 2013; Huang et al. 2015; Liu et al. 2014a; Zhao et al. 2014; Zhang and Yang 2013). In general, a predominant PEC cell relies on two factors: the efficient usage of solar energy and the instant transportation/separation of charges (Bard and Fox 1995). Hence, the development of nanosized photoactive semiconductors to satisfy the requirements has been a long-standing objective in the research of PEC cells, especially for one-dimensional TiO_2 due to its superior charge transport property (Lou and Chen 2014).

A PEC process is based on the excitation of the semiconductor by energetic photons ($h\upsilon \geq E_g$) which generate (e^-/h^+) pairs that could be used in the photoredox reactions. A great deal of attention has been paid to hydrogen as a clean fuel with a high-energy density. The stable oxides have a valence band (VB) made up of O_2^-: 2*p* orbital, while the conduction band (CB) derives from metal parentage, thus resulting in a large gap. Such a handicap can be overcome by using a configuration that has the band edges properly matched to the H_2O/H_2 level. A PEC cell is composed of an electrolytic cell: three electrodes (Pt as auxiliary electrode, a saturated calomel electrode (SCE), and the working electrode). When the PEC cell is exposed to the light, a charge transport within the PEC occurs, and there is an evolution of gases at the photoanode or photocathode. The oxygen energy level (O_2/H_2O) should be above the VB of the photoanode to allow electron transfer. For the same reason, the hydrogen energy level (H^+/H_2) should also be below the Fermi level of the metal cathode (or the CB of a semiconducting photocathode, see Fig. 7.11).

Generally, photoelectrode is a *n*- or a *p*-type semiconductor electrode, which conducts the electrons generated by the light-induced chemical reactions initiated at the semiconductor surface. The band-gap energy of the semiconductor must be at least 1.5 eV, higher than the effective redox potential of water (1.23–1.40 eV) (Minggu et al. 2010; Arifin et al. 2013).

Many TiO_2 nanostructures, including nanoparticle films, nanotube, and nanorods, have been used as the photoanodes in PEC for water splitting. Some reports have shown that the control of the composition of the material and their morphology greatly enhances the PEC performance under irradiation. Thus, the effect of the morphology on the performance of the TiO_2 photoanodes in the form of nanotubes, nanoparticles, and nanofilms has been studied by Leng et al. (2010). For TiO_2-based PEC system, a rapid recombination between photogenerated electrons and holes is the major factor in decreasing the photoreactivity. When the surface of TiO_2 nanorods is loaded with metal oxide, the highly dispersed metal nanoparticles not only facilitate the excitation of electrons and generation and

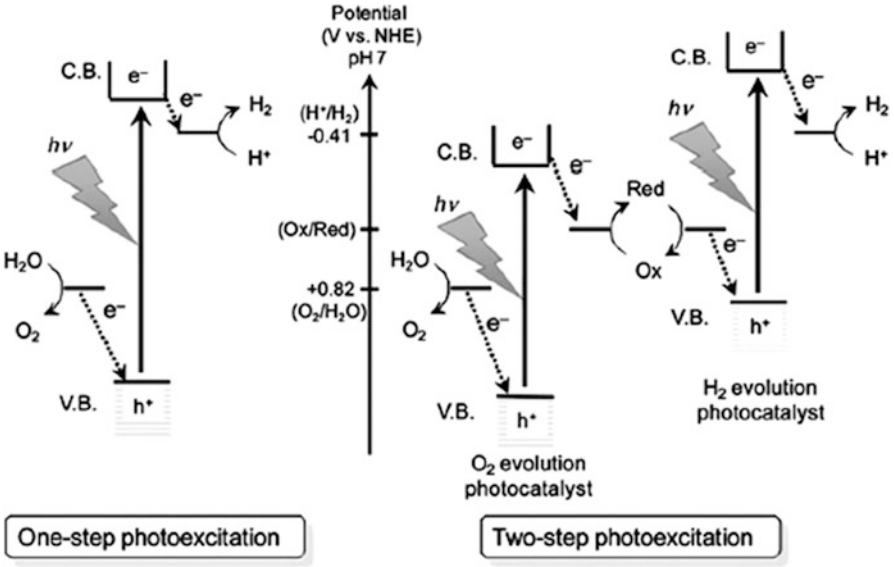

Fig. 7.11 Photocatalytic water splitting for one-step and two-step photoexcitation systems. (Reprinted with permission from Maeda K. et al. (2010)). Efficient Nonsacrificial Water Splitting through Two-Step Photoexcitation by Visible Light using a Modified Oxynitride as a Hydrogen Evolution Photocatalyst. J Am Chem Soc, 132, 5858–5868. Copyright 2010 American Chemical Society (Maeda et al. 2010))

separation of the e^-/h^+ pairs. It is observed that the separation efficiency of photoinduced carrier pairs and water-splitting performance is remarkably improved upon the addition of a metal oxide.

In this context, Zhang and coworkers (2016b) showed that the heterostructured CuO@TiO_2 film has interesting physical properties in PEC water splitting, such as a hierarchical surface, an extended optical absorption range, and a rapid interface charge transfer kinetics (Fig. 7.12). In addition, the generation of a great potential via the water-splitting applications under solar visible light was observed. On the other hand, the PEC efficiency of this material is enhanced because of the positive effect of heterojunctions in which a combination of narrow and wide band-gap semiconductors leads to the separation of e^-/h^+ pairs by the junction electric field (Liu et al. 2011).

TiO_2 nanostructures derived from Ti foil have also been studied because of their lower cost compared to other methods reported by other groups (Liu et al. 2015b; Xu et al. 2014; Mai et al. 2010; Leong et al. 2014). However, Miao and coworkers showed that the photocurrent response of a nanotube-based films was nearly 13.8 $\mu A \cdot cm^{-2}$, which is approximately three times higher than those of nanoflowers-based films (Miao et al. 2015). This indicates that the nanotubes transfer electrons to the surface of the film more successfully. This is probably because nanotubes provide direct pathways for electrons from the point of injection to the Ti foil electrode (Fig. 7.13).

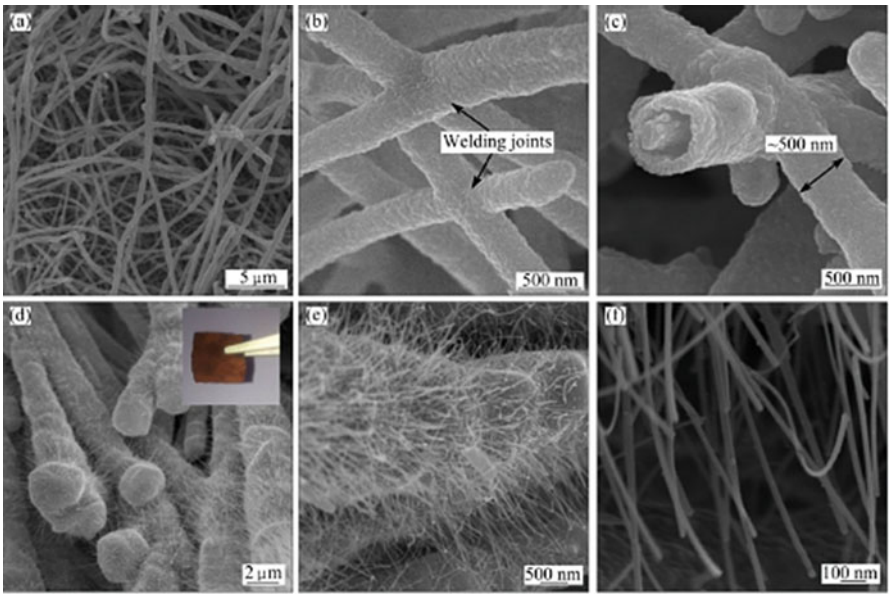

Fig. 7.12 SEM images of nanowires (NWs) film after electroless plating of copper (**a**–**c**), CuO@TiO_2 NWs film (**d**–**f**). (Reproduced with permission (Zhang et al. 2016b))

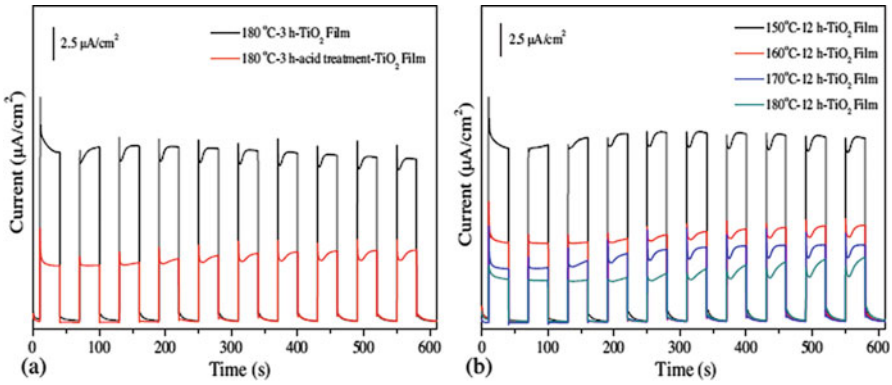

Fig. 7.13 Current–time response curves of TiO_2 nanostructured films (**a**) without/with acid treatment at a hydrothermal treatment temperature of 180 °C for 3 h and (**b**) hydrothermal treatment for 12 h at temperatures of 150, 160, 170, and 180 °C, respectively. (Reproduced with permission (Miao et al. 2015))

The PEC water-splitting behavior under reaction conditions at 100 $mW \cdot cm^{-2}$ for pure TiO_2 and MoO_3–TiO_2 nanotube layers is illustrated in Fig. 7.14. From the photocurrent transient as a function of applied potential, it was found that the MoO_3–TiO_2 nanotubes prepared at 650 °C exhibited higher photocurrent density than that

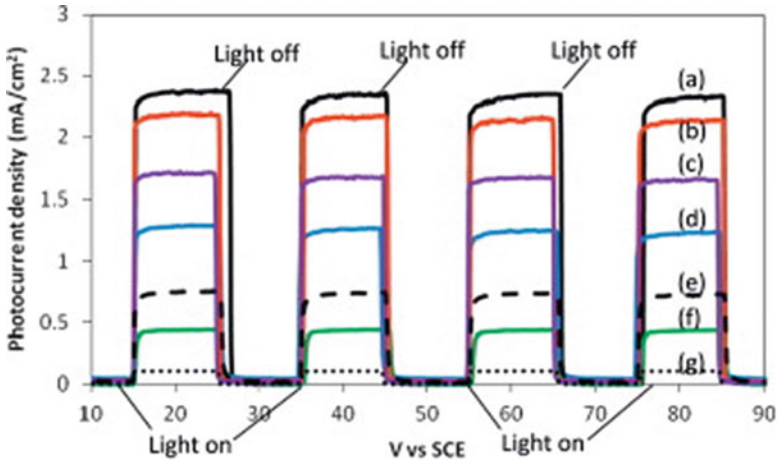

Fig. 7.14 Potentiostatic plot of photocurrent for WO_3-loaded TiO_2 nanotubes subjected to different temperatures: (**a**) 400 °C, (**b**) 500 °C, (**c**) 600 °C, (**d**) 300 °C, (**e**) 700 °C, (**f**) 200 °C, and (**g**) as anodized

of the TiO_2 nanotubes due to lower electron transfer resistance, higher carrier concentration, and enhanced separation efficiency (Yang et al. 2016). In addition, the photocurrent gave a very high value (Lai and Sreekantan 2013), much higher than that of the amorphous material.

Furthermore, noble metals can increase the formation of (e^-/h^+) pairs supported by resonance surface plasmonic effects observing that the Pt loading significantly enhances the sensitivity of TiO_2 nanorods array thin film to light (Atabaev et al. 2016; Atabaev and Atabaev 2016; Wang et al. 2012b). Pt loading is effective for improving the PEC performance of the electrode. The reason for the decrease of current density may be attributed to the fact that excess Pt coating promotes a better interaction at the interface TiO_2/electrolyte (Atabaev et al. 2016; Atabaev and Atabaev 2016; Wang et al. 2012b). Thus Pt is largely used as one of the most suitable co-catalysts for trapping electrons (Yang et al. 2013). It should also be noted that the enhanced photocurrent is not associated with any change in the onset potential, which is not caused by any change in the flat band potential of the semiconductor. Based on these results, the two main reasons for the enhanced photocurrent are a very good (e^-/h^+) separation and the surface plasmon resonance. As the Fermi levels of Pt are lower than the conduction band of TiO_2, photoexcited electrons can be transferred from the CB of TiO_2 to the metal particles deposited on its surface, whereas photogenerated holes remain in the TiO_2 (Atabaev et al. 2016; Atabaev and Atabaev 2016). Under irradiation, (e^-/h^+) pairs are formed on the Pt nanoparticles surface due to surface plasmon resonance, and the introduction of Pt can form the Schottky barrier between titanium dioxide or modified titanium oxide and Pt nanoparticles, which inhibit the photogenerated charge carrier recombination and promote the interfacial charge transfer (Momeni and Nazari 2016).

TiO_2/CdS, TiO_2/CdTe, and TiO_2/CdSTe heterostructured core/shell nanowire have also been successfully synthesized by physical vapor deposition of CdS, CdTe, and the alloyed CdSTe layer onto the hydrothermally pre-grown TiO_2 nanowires (Ai et al. 2015). Compared to CdS- or CdTe-coated TiO_2 NWAs electrode, CdS and CdTe on TiO_2 induce a higher photocurrent density. Moreover, the increase of the photocurrents indicates that the good photoresponse properties of the electrodes are mainly due to a wider light absorption range of the material.

Ai and coworkers reported that TiO_2/CdS_xSe_{1-x} ($0 < x < 1$) core/shell NWAs photoelectrode significantly enhances the PEC hydrogen generation performance, especially in the case of $TiO_2/CdS_{0.52}Se_{0.48}$ composite electrode, due to both an enhanced light absorption and an efficient charge separation. The doping causes an increase in the photocurrent in the PEC cell, which is beneficial for the final hydrogen generation (Zakrzewska et al. 2015). On the other hand, the photoreactivity of TiO_2 codoped was investigated by other authors with different results (Liu and Li 2011; Li et al. 2011). Therefore, the incorporation of metal leads to a decrease in the band-gap energy and increase the light absorption from the UV region to the visible spectral region, leading to enhanced visible light photoreactivity.

Incorporating WO_3 into TiO_2 not only efficiently inhibits the recombination between the photogenerated (e^-/h^+) but also reduces the band-gap energy of TiO_2 (Kobayashi and Katsunori 2007; Yang et al. 2010). WO_3-doped TiO_2 has been used as an efficient photoanode in PEC cells to yield charge carriers with a longer lifetime and enhanced H_2 evolution (Lai and Sreekantan 2013). Hierarchical photoanodes WO_3–TiO_2 nanotube (WTNs) composites have been fabricated by an in situ anodization of titanium in a single-step methodology (Momeni et al. 2015). A method to prepare WTNs composites with a tube diameter of 80–110 nm and a wall thickness of 20–40 nm has also been developed (see Fig. 7.15).

The effect of WO_3 doping becomes clearer from the transient photoresponse behavior (Fig. 7.16a). The potentiostatic plot of TiO_2 modified with different amounts of WO_3 is subjected to on/off cycles of illumination at 0.2 V. All the samples demonstrated stable and instantaneous changes in photocurrent upon illumination on/off cycles. On the other hand, the PEC H_2 evolution using WTNs-2 decreased drastically from 2.14 $mL \cdot cm^{-2}$ compared to WTNs-1 (1.20 $mL \cdot cm^{-2}$) and WTNs-3 (1.72 $mL \cdot cm^{-2}$). These findings agree with the photocurrent density results (Fig. 7.16b).

Recently, the coupling of TiO_2 with carbon materials such as activated carbon, (Hu et al. 2014) C_{60} fullerene, (Grandcolas et al. 2014) carbon nanotubes, (Ong et al. 2013) graphene, (Zhang et al. 2010b; Tan et al. 2013; Xiang et al. 2011) etc. has attracted much attention for the synthesis of efficient photocatalysts. Therefore, all these studies show that the presence of carbon introduces several important effects which improve the photocatalytic efficiency of the hybrid materials. These effects may be due to the stabilization of the TiO_2 in the carbon support improving the charge transport to reduce recombination reactions at the TiO_2/carbon interfaces (Yu et al. 2014). The enhancement in photocatalytic activity of carbon materials is

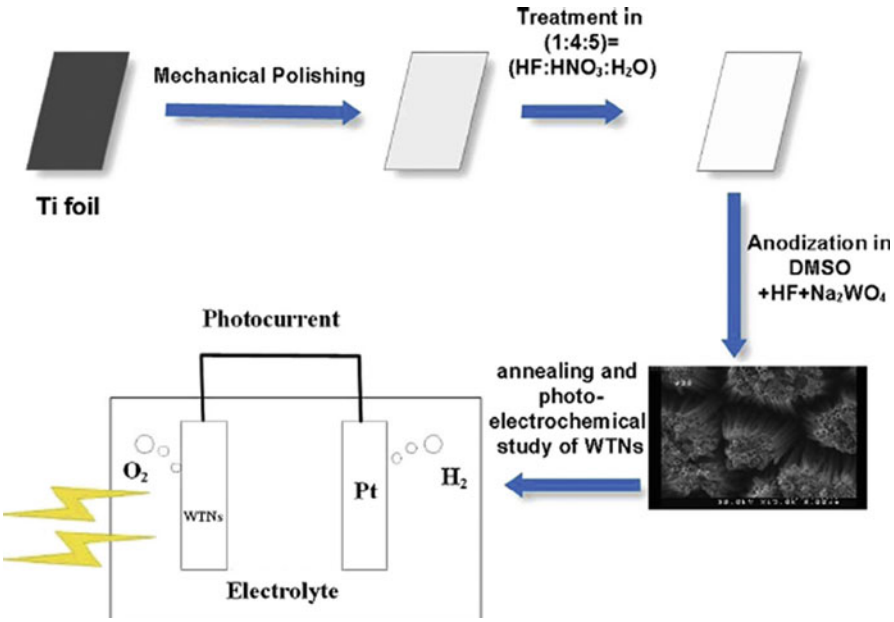

Fig. 7.15 Schematic presentation of the pretreatment method of titanium sheets and process of producing hierarchical WO_3-TiO_2 nanotubes on titanium foils. (Reproduced with permission (Momeni et al. 2015))

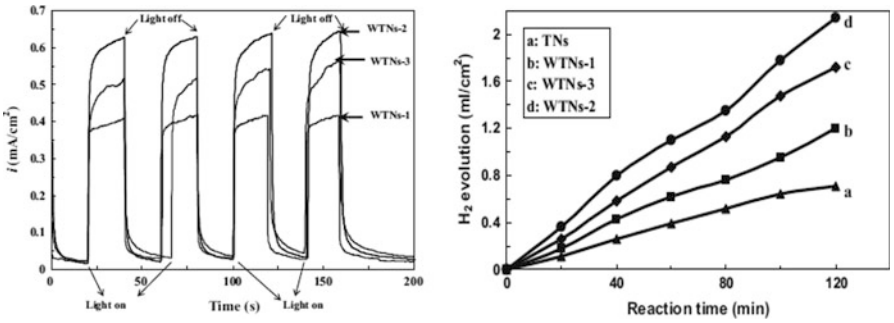

Fig. 7.16 (**a**) Photocurrent density of different WO_3–TiO_2 photoelectrodes and (**b**) quantitative hydrogen generation for pure TiO_2 nanotubes (TNs) and different WO_3–TiO_2 nanotube (WTNs) photoanodes. (Reproduced with permission (Momeni et al. 2015))

also due to the unique physicochemical properties of carbon such as low electrical resistivity, high thermal conductivity, and large surface area (Dillon 2010; Boudjemaa et al. 2015).

Ranganathan and co-authors synthesized some novel films based on composites of the type TiO_2/hollow carbon spheres (HCS) which have been recently used as photoanodes in PEC water-splitting tests. Nitrogen-doped HCSs (NHCSs) and

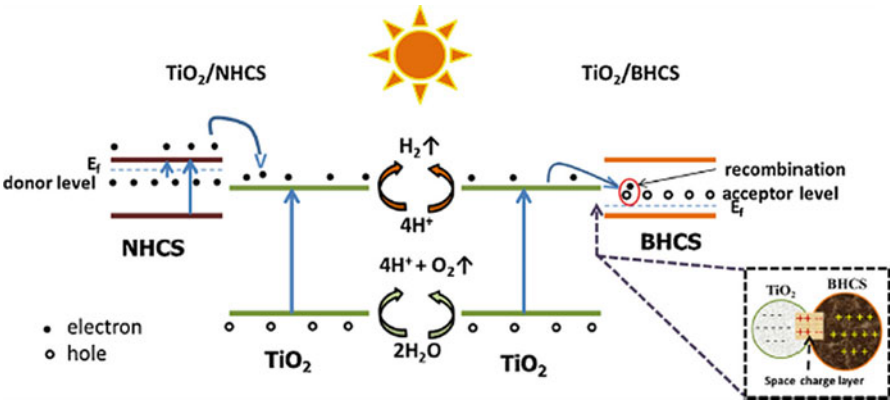

Fig. 7.17 A schematic representation of the electrochemical water-splitting reaction using TiO_2/NHCS and TiO_2/BHCS composite photoanodes under illumination. The inset shows the formation of a space charge layer between the TiO_2 and the BHCS particles. (Reproduced with permission (Ranganathan et al. 2016))

Boron-doped HCSs (BHCSs) were added in the TiO_2 structure and have been compared with pure TiO_2 films with very interesting results (Ranganathan et al. 2016). The TiO_2/NHCS composite electrode showed a good increase (2.4-fold) of the anodic current density compared to the pure TiO_2 electrode. In addition, TiO_2/NHCS gave an enhanced incident photon to current efficiency (IPCE) and a very interesting photoelectrochemical stability over time. Figure 7.17 shows the proposed detailed mechanism for the photoelectrochemical tests catalyzed by these materials (Ranganathan et al. 2016). Moreover, the presence of oxygen and other elemental dopants can modulate the band-gap down to 1.25 eV (Kajen et al. 2012; Jin et al. 2009; Bansal et al. 2012). Doping with HCSs enhances the surface interaction to give a compact film with higher electron density giving a reduced resistance leading to a significant increase of the photocurrent density.

An electron transfer mechanism has also been proposed by Yen et al. for Au/TiO_2 systems (Fig. 7.18). Under illumination, AuNPs absorb visible light generating the energetic active electrons from the process of SP excitation and injecting them into the CB of the adjacent TiO_2 (green arrow). Simultaneously, the UV light is absorbed by TiO_2, producing a photoexcited electron and a hole (black arrow). The plasmon-induced electromagnetic field promotes the separation of photogenerated electrons and holes. Furthermore, the energy bands of anatase and rutile are different, and this provides a driving force to promote electron transfer from anatase to rutile (blue arrow). Finally, the electrons transferred to the cathode (Pt) react with H^+ ions and produce H_2 (pink arrow), whereas the holes present in the anode oxidize H_2O and generate O_2 (Yen et al. 2016).

Additional alternatives have also been recently reported including several systems which can generate hydrogen by other different methods (Agegnehu et al. 2016; Kandiel and Takanabe 2016; Li et al. 2015; Naik et al. 2015; Obregón et al. 2016; Roy et al. 2015; Wang et al. 2016). In addition, a very recent review on the

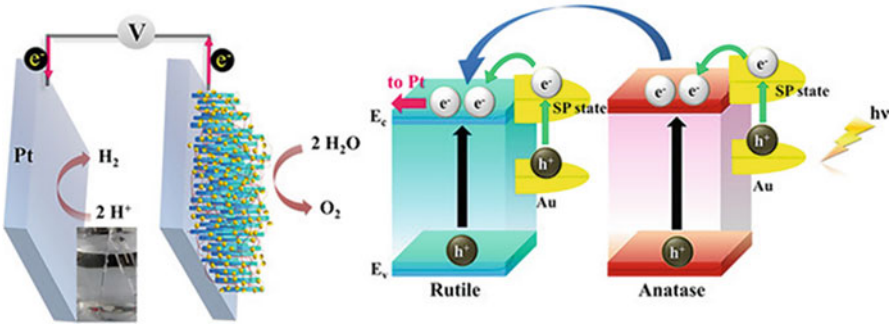

Fig. 7.18 Charge transfer mechanism of Au/TiO_2 ARHN under solar illumination. (Reproduced with permission (Yen et al. 2016))

field covering most of the novel materials and current alternative for photoelectrochemical hydrogen production by using a wide variety of semiconductors including titanium oxide has been published and should be useful for the rational design of new materials which may be of interest for the development of this hydrogen production technology (Joy et al. 2018).

7.3.6 Water Photoreduction

Photocatalytic H_2 production via water photoreduction is different to water splitting. With this process, absorption of energetic photons by semiconductor generates (e^-/h^+) pairs; the electrons migrate to the interface to reduce water into gaseous hydrogen, whereas the holes move into the bulk to react with hole scavenger in the electrolyte preventing the formation of oxygen.

Most of the materials investigated for the water photodecomposition are chemically stable but are of a limited practical use as they have either an unsuitable flat band potential (V_{fb}) or a wide band-gap which inhibits the utilization of the visible region. Moreover, the O_2^-: 2*p* orbital, which constitutes the valence band (VB), lies too far (~2 eV) above the O_2/H_2O level. Accordingly, the CB is positioned at a non-negative enough potential to liberate hydrogen with efficient rates.

One of the methods to increase the photocatalytic performance of the catalyst in heterogeneous photocatalysis is the use of materials as heterojunctions (Wang et al. 2012c). In addition, the combination of ferrites with TiO_2 photocatalysts showed a synergistic effect that produces enhanced photocatalytic activity (Kezzim et al. 2011). Moreover, combining two photocatalysts with different band-gap (Eg) positions effectively causes a greater separation of (e^-/h^+) pairs. When the semiconductor is irradiated with light energy, an electron from the VB is excited to the CB of the photocatalyst, leaving a photogenerated hole. Kezzim and coworkers

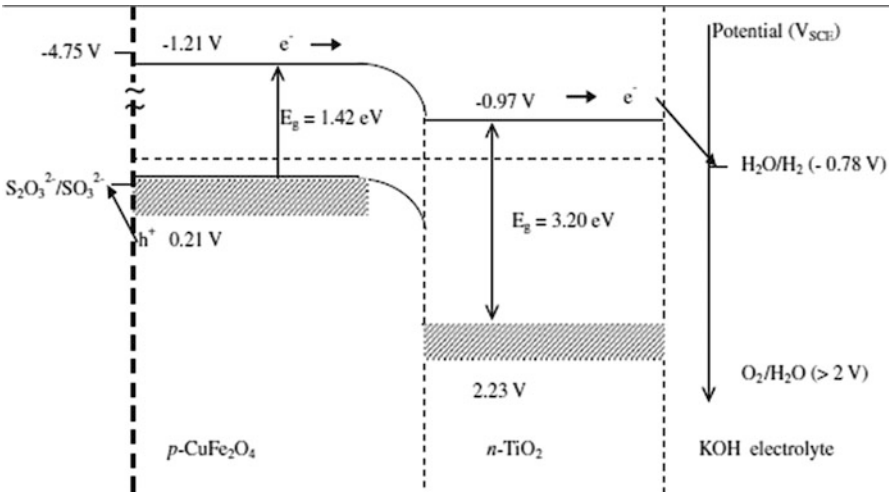

Fig. 7.19 The energy band diagram of the hetero system p-$CuFe_2O_4$/n-TiO_2/electrolyte. (Reproduced with permission (Kezzim et al. 2011))

(Kezzim et al. 2011) have shown that the CB potential positioned below the potential of HER, and this should lead to a spontaneous H_2 evolution even in basic electrolytes (Fig. 7.19).

There are two methods allowing the utilization of visible light irradiation by photocatalysts. The first one consists in doping a photocatalyst (eg. TiO_2) with different elements in order to make it active under visible light (Xu et al. 2015). The second one is the development of photocatalysts characterized by a narrow band-gap allowing a photocatalytic activity under visible light irradiation (Harish et al. 2012; Liu et al. 2014b). The use of polymers as photoelectrodes is of increasing interest, and, among them, polypyrrole (PPy) is promising for solar energy conversion (Wang et al. 2012c). The PEC characterization of PPy has not been extensively investigated, (Deng et al. 2012) and the hydrogen photoevolution has been reported only by Belabed and co-authors (Belabed et al. 2014). PPy/TiO_2 nanocomposites showed better photocatalytic activity than that of neat TiO_2 nanoparticles (see Fig. 7.20).

On the other hand, different strategies have been attempted for improving the efficiency of hetero-system-based PEC cells, where the investigation has not been carried out in detail because of the difficulty of the appropriate tuning of the electronic bands of the semiconductors (Fig. 7.21).

In the case of $ZnFe_2O_4$/$SrTiO_3$ heterojunction, the activation is attributed to an electron transfer from $ZnFe_2O_4$-CB to $SrTiO_3$-CB resulting in HER, while the photoholes in $ZnFe_2O_4$-VB react with a reducing agent: $S_2O_3^{2-}$ being particularly

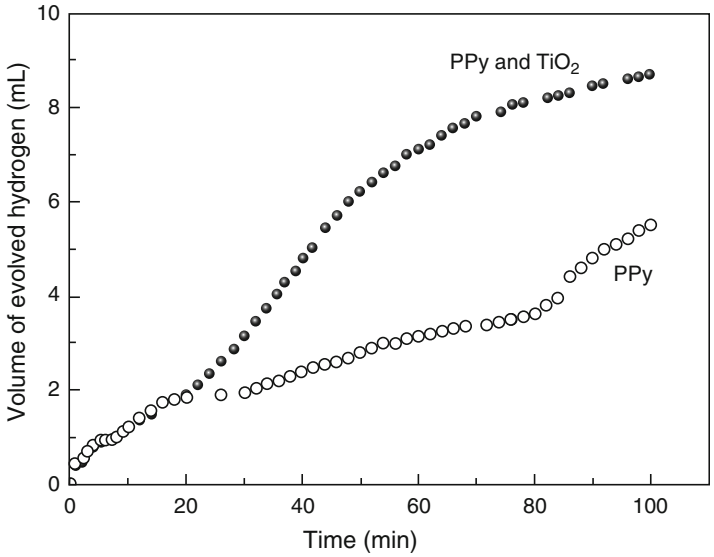

Fig. 7.20 Volume of evolved hydrogen on PPy and PPy/TiO_2 as function of illumination time at pH 6.8 in the presence of $S_2O_3^{2-}$. (Reproduced with permission (Belabed et al. 2014))

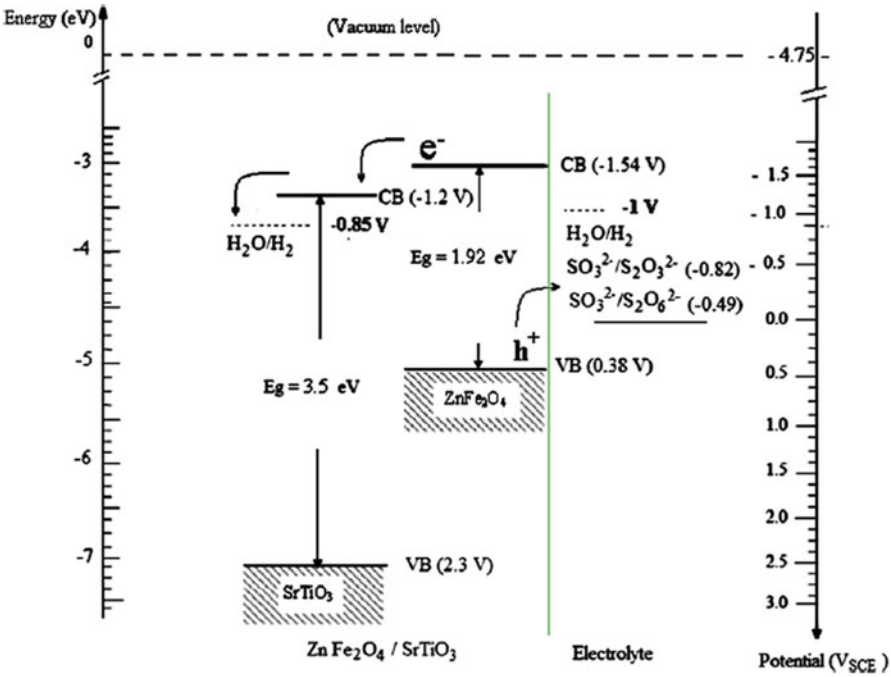

Fig. 7.21 Position of the energy bands at the interface $ZnFe_2O_4/SrTiO_3$/electrolyte. (Reproduced with permission (Boumaza et al. 2010))

favorable to improve the charge separation (Boumaza et al. 2010). Its oxidation to SO_3^{2-} and, subsequently, to $S_2O_2^{-4}$ takes place through hole injection, and the process can be summarized as follows:

$$ZnFe_2O_4 + h\upsilon \rightarrow e^- + h^+ \tag{7.2}$$

$$ZnFe_2O_4(e^- + h^+) + SrTiO_3 \rightarrow ZnFe_2O_4(h^+) + SrTiO_3(e^-) \tag{7.3}$$

$$ZnFe_2O_4CB(e^-) + SrTiO_3CB \rightarrow ZnFe_2O_4 + SrTiO_3(e^-) \tag{7.4}$$

$$SrTiO_3CB + H_2O \rightarrow SrTiO_3 + \frac{1}{2}H_2 + OH^- \tag{7.5}$$

$$S_2O_3^{2-} + 4h^+ + 6OH^- \rightarrow 2SO_3^{2-} + 3H_2O \tag{7.6}$$

$$2SO_3^{2-} + 2h^+ \rightarrow 2S_2O_6^{2-} \tag{7.7}$$

h^+ denotes a positive hole in VB. $ZnFe_2O_4$-CB is appropriately adjusted with respect to $SrTiO_3$-CB which is itself less negative than the H_2O/H_2 potential (-0.85 V) yielding a spontaneous HER. The noticeable enhancement is partly due to intimate contact between $SrTiO_3$ and $ZnFe_2O_4$ which enables a transfer of excited electrons.

In addition to these systems, new methods for the production of hydrogen by photoreduction are being extensively developed over the last 5 years starting from CO_2 and H_2O under visible light, LED light, or sunlight. Titanium oxide is playing a very interesting role as photocatalyst for these methods because of its low cost, and, therefore, the CO_2 and H_2O photoreduction may be an alternative and innovative way to control environmental and energy problems associated with the production of hydrogen by photoreduction methods (Nahar et al. 2017).

7.3.7 Methanol Photoreforming

The overall reaction, which may be described as photoreforming of organic compounds, combines reduction of water and oxidation of the organic substrate into a single process able to produce hydrogen at room temperature and atmospheric pressure. The methanol stream photoreforming approach is based on the ability of methanol generally named and used as sacrificial agents, to donate electrons to the positive holes of the illuminated photocatalyst and to be oxidized generating protons, while the latter are reduced by photogenerated electrons forming hydrogen in the presence of the photocatalyst (Lanese et al. 2013). In addition, to achieve a maximum electron transfer yield, additional sacrificial hole capture agents in the electrolyte, such as ethanol, methanol, or glycerol, are used to enhance the overall H_2 production rate (Yoo et al. 2013). The photocatalytic decomposition of gaseous methanol over Pt-loaded WO_3–TiO_2 composite thin films proceeds through intermediates like CH_2O, CO, H_2O, and finally to CO_2 (Sadale et al. 2012). Therefore,

significantly enhanced H_2 generation rates are obtained by the deposition of Pt nanoparticles on TiO_2, which represent efficient catalytic sites for the recombination of atomic hydrogen to H_2 (Chiarello et al. 2011; Naldoni et al. 2013). In the case of direct hole transfer, the photogenerated holes serve as oxidation sites for the adsorbed methanol molecules, and decomposition reactions may occur (Santato et al. 2001).

The presence of ·OH radical is essential for indirect hole transfer reaction, and water can be generated through this reaction route. In addition to water, the reaction can also produce other intermediates because of a direct hole transfer. In addition, it can clearly be observed that the release of CH_2O and CO as intermediate reaction products, and CO_2 and H^+ as the final decomposition products, is feasible according to the following reactions:

$$H_2O + h^+ \rightarrow \cdot OH + H^+ \tag{7.8}$$

$$CH_3OH + \cdot OH \rightarrow \cdot CH_2OH + H_2O \tag{7.9}$$

followed by

$$\cdot CH_2OH + \cdot OH \rightarrow \cdot CH_2O + H_2O \tag{7.10}$$

$$CH_2O_{(g)} + 2O_a \rightarrow CO_{2_{(g)}} + H_2O_{(g)} \tag{7.11}$$

There are several differences in the use of different photocatalysts. For example, the decomposition of methanol in gas phase over nanocrystalline Pt loaded onto WO_3 thin film occurs via a direct hole transfer reaction. However, a competitive coexistence of direct and indirect hole transfer is observed over Pt-loaded composite thin films of WO_3–TiO_2. In addition, an indirect hole transfer is possibly initiated by ·OH formed at photogenerated Ti^{3+} defect sites on the TiO_2 surface. In this context, Dang and coworkers reported an overall oxidation reaction of the system based on the use of TiO_2 nanotubes (TNTs) as follows (Dang et al. 2013):

$$TNTs \rightarrow TNTs(e^- + h^+) \tag{7.12}$$

$$TNTs(h^+) + CH_3OH + H_2O \rightarrow 6H^+ + CO_2 \tag{7.13}$$

On the other hand, Choi and Kang (2007) tried to go further into the details of the process observing the following reaction, which considered the active role of ·OH (formed from H_2O/OH^- reaction with positive holes):

$$CH_3OH \overset{h\upsilon}{\rightarrow}: CH_2 + H_2O \overset{\cdot OH}{\rightarrow} \cdot CH_2OH \overset{\cdot OH}{\rightarrow} CH_2(OH)_2 \tag{7.14}$$

However, it is interesting to observe that the formation of $CH_2(OH)_2$ may also be explained through other pathways, which consider that the radical species $\cdot CH_2OH$

is still able to react with a positive hole, producing a proton and formaldehyde with the latter capable of generating hydrated compounds by the addition of water.

$$CH_2(OH)_2 \rightarrow CO_2 + H_2O \text{ major decarboxylation} \quad (7.15)$$

$$CH_3OH \leftrightarrow CH_2O + H_2O \rightarrow CO_2 + H_2O \text{ decarboxylation} \quad (7.16)$$

Miwa et al. proposed a mechanism for the organic oxidation (Miwa et al. 2010):

$$CH_3OH + h^+ \rightarrow \cdot CH_2OH + H^+ \quad (7.17)$$

$$\cdot CH_2OH + h^+ \rightarrow CH_2O + H^+ \quad (7.18)$$

$$CH_2O + h^+ + \cdot OH \rightarrow HCOOH + H^+ \quad (7.19)$$

$$HCOOH \rightarrow HCOO^- + H^+ \quad (7.20)$$

$$HCOO^- + 2h^+ \rightarrow CO_2 + H^+ \quad (7.21)$$

Nanoparticles of Pt, Au, Ir, and Pd introduced in TiO_2 and $(CNT\text{-}TiO_2)_{ox}$ by an incipient wetness method have shown an efficient activity for H_2 production from methanol- and saccharide-containing solution (Silva et al. 2015). Compared with the reference TiO_2, composite catalysts presented the highest activity of 485 μmol of H_2 (Pt-loaded composite produced by the one-pot synthesis method being generated after 2 h of irradiation), which contrast with the quantity of 205 μmol of H_2 obtained using Pt/TiO_2 (Table 7.2). Various factors have been observed, which may affect the H_2 evolution efficiency, such as:

(i) The nature and content of the metallic co-catalyst
(ii) The surface, crystallographic and porosity properties of the TiO_2 anatase/rutile support
(iii) The anatase/rutile ratio
(iv) The metal–support interactions
(v) The relative amount of methanol added as a sacrificial reagent (Rosseler et al. 2010)

Table 7.2 Rate of H_2 evolution (r) from water/methanol solution using metal-loaded TiO_2 and $(CNT\text{-}TiO_2)_{ox}$ catalysts reduced at different temperatures (473 or 673 K) and average dimensions of the metal nanoparticles (dM), determined by TEM analysis

	r (μmol·min^{-1}·g$_{cat}^{-1}$)				d_M (nm)			
	TiO_2		$(CNT\text{-}TiO_2)ox$		TiO_2		$(CNT\text{-}TiO_2)ox$	
Co-catalyst	473 K	673 K	473 K	673 K	473 K	673 K	473 K	673 K
Au	0.13	0.45	0.27	0.13	8.4	9.8	9.5	11
Ir	2.2	2.8	2.1	2.2	5.4	4.7	5.0	12
Pd	5.5	0.74	2.7	1.8	6.8	7.6	7.4	8.1
Pt	9.8	1.4	23	1.0	2.6	25	7.2	11

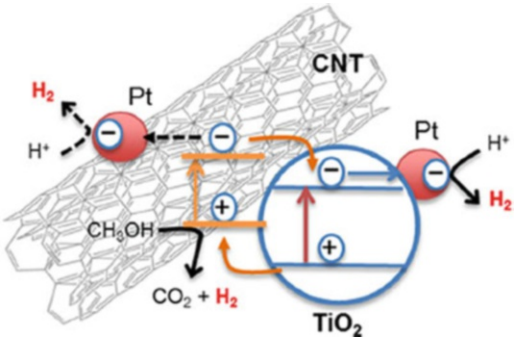

Fig. 7.22 Schematic representation of the photocatalytic mechanism of H_2 generation from water/methanol solutions under near UV to visible light irradiation using $Pt/(CNT\text{-}TiO_2)_{ox}$-473 catalyst. (Reproduced with permission (Silva et al. 2015))

The synergic effect is discussed in terms of the action of carbon nanotubes as dispersing media for TiO_2 particles as well as their action as photosensitizers. The relative efficiency of the catalysts is related to the work function of each metal and the sizes of the metal nanoparticles.

Figure 7.22 describes this effect, as when the material was irradiated with light greater than 365 nm, both TiO_2 and carbon nanotube could be photoexcited. Electrons from the VB of TiO_2 can be excited to the conduction band of the semiconductor and therefore transferred to Pt nanoparticles reducing protons to generate H_2. On the other hand, positively charged holes may migrate to the carbon nanotube phase to oxidize methanol (Silva et al. 2015).

Chiarello and coworkers established that hydrogen can be produced by a photocatalytic process of methanol steam reforming using different noble metals such as Ag, Au, Au–Ag alloy, and Pt-loaded TiO_2 photocatalyst (Chiarello et al. 2011). However, methanol is oxidized to CO_2 via the formation of formaldehyde and formic acid. Wang and coworkers loaded the surface of metal oxide nanocrystals such as TiO_2, ZnO, CuO, etc., observing that these photocatalysts are very effective in liberating hydrogen gas from deionized water at room temperature (Wang et al. 2011b). Very recently, our group has also studied the methanol photoreforming reaction to obtain hydrogen using Zn-doped titanium oxide loaded with 0.5% Pd nanoparticles using a wetness impregnation method. This material gave ca. 1.7 mL hydrogen in 3 h of reaction using ca. 50 mg of catalyst (Rico-Oller et al. 2016). In conclusion, methanol photoreforming may be an alternative method for the solar generation of hydrogen by photocatalytic processes of interest for the industry (Clarizia et al. 2017).

7.4 Conclusions and Outlook

In this chapter, we have reviewed the latest advances on the applications of photocatalytic processes using titanium oxide-based materials with special interest toward their use as environmental solutions in current problems. Thus, we have discussed the potential applications of titanium oxide materials in water remediation

for the elimination of different pollutants and the potential use of pure titanium oxide materials or composites in advanced oxidation processes with special interest in processes such as water splitting and hydrogen production using photocatalytic or photoelectrocatalytic methods. The most recent results in these topics show that simple structural changes and preparation of sophisticated titanium oxide-based composites, together with a sustainable development of the photocatalytic methods, may result in an efficient application and industrial use of these materials as solutions for a wide variety of environmental problems.

References

Agegnehu AK, Pan CJ, Tsai MC, Rick J, Su WN, Lee JF, Hwang BJ (2016) Visible light responsive noble metal-free nanocomposite of V-doped TiO_2 nanorod with highly reduced graphene oxide for enhanced solar H2 production. Int J Hydrog Energy 41:6752–6762

Agustina TE (2012) AOPs application on dyes removal. In: Wastewater reuse management. Springer, Dordrecht, pp 353–372

Ahmari H, Heris SZ, Khayyat MH (2018) The effect of titanium dioxide nanoparticles and UV irradiation on photocatalytic degradation of Imidaclopride. Environ Technol 39:536–547

Ai G, Mo R, Xu H, Chen Q, Yang S, Li H, Zhong J (2015) Vertically aligned TiO_2/(CdS, CdTe, CdSTe) core/shell nanowire array for photoelectrochemical hydrogen generation. J Power Sources 280:5–11

Akpan UG, Hameed BH (2010) The advancements in sol-gel method of doped-TiO_2 photocatalysts. Appl Catal A Gen 375:1–11

Ali Z, Chaudhry MN, Niaz NA, Khalid NR, Ahmed E, Hussain R, Ahmad I, Abbas SM (2013a) Significant effect of graphene on catalytic degradation of methylene blue by pure and Ce-doped TiO_2 at nanoscale. J Nanomater Biostruct 8:1271–1280

Ali Z, Hussain ST, Chaudhry MN, Batool SA, Mahmood T (2013b) Novel nano photocatalyst for the degradation of sky blue 5b textile dye. Int J Phys Sci 8:1201–1208

Alvaro M, Cojocaru B, Ismail AA, Petrea N, Ferrer B, Harraz FA, Parvulescu VI, Garica H (2010) Visible-light photocatalytic activity of gold nanoparticles supported on template-synthesized mesoporous titania for the decontamination of the chemical warfare agent Soman. Appl Catal B 99:191–197

An T, An J, Yang H, Li G, Feng H, Nie X (2011) Photocatalytic degradation kinetics and mechanism of antivirus drug-lamivudine in TiO_2 dispersion. J Hazard Mater 197:229–236

Arif AF, Balgis R, Ogi T, Iskandar F, Kinoshita A, Nakamura K, Okuyama K (2017) Highly conductive nano-sized Magnéli phases titanium oxide (TiO_x). Sci Rep 7:3646

Arifin K, Daud WRW, Kassim MB (2013) Optical and photoelectrochemical properties of a TiO_2 thin film doped with a ruthenium-tungsten bimetallic complex. Ceram Int 39:2699–2707

Arin J, Thongtem S, Thongtem T (2013) Single-step synthesis of ZnO/TiO_2 nanocomposites by microwave radiation and their photocatalytic activities. Mater Lett 96:78–81

Atabaev TS, Atabaev S (2016) Titania coated hematite nanostructures for solar water splitting applications. Nano Life 6:1650004–1650008

Atabaev TS, Hossain MA, Lee D, Kim HK, Hwang YH (2016) Pt-coated TiO_2 nanorods for photoelectrochemical water splitting applications. Results Phys 6:373–376

Babuponnusami A, Muthukumar K (2014) A review on Fenton and improvements to the Fenton process for wastewater treatment. J Environ Chem Eng 2:557–572

Bahruji H, Bowker M, Davies PR, Pedrono F (2011) New insights into the mechanism of photocatalytic reforming on Pd/TiO_2. Appl Catal B Environ 107:205–209

Bai H, Liu L, Liu Z, Sun DD (2013) Hierarchical 3D dendritic TiO_2 Nanospheres building with Ultralong 1D nanoribbon/wires for high performance concurrent photocatalytic membrane water purification. Water Res 47:4126–4138

Bansal T, Mohite AD, Shah HM, Galande C, Srivastava A, Jasinski JB, Ajayan PM, Alphenaar BW (2012) New insights into the density of states of graphene oxide using capacitive photocurrent spectroscopy. Carbon 50:808–814

Bard AJ, Fox MA (1995) Artificial photosynthesis: solar splitting of water to hydrogen and oxygen. Acc Chem Res 28:141–145

Belabed C, Haine N, Benabdelghani Z, Bellal B, Trari M (2014) Photocatalytic hydrogen evolution on the hetero-system polypyrrol/TiO2 under visible light. Int J Hydrog Energy 39:17533–17539

Benotti MJ, Stanford BD, Wert EC, Snyder SA (2009) Evaluation of a photocatalytic reactor membrane pilot system for the removal of pharmaceuticals and endocrine disrupting compounds from water. Water Res 43:1513–1522

Bethi B, Sonawane SH, Bhanvase BA, Gumfekar SP (2016) Nanomaterials-based advanced oxidation processes for wastewater treatment: a review. Chem Eng Process 109:178–189

Boudjemaa A, Bachari K, Trari M (2013) Photoelectrochemical characterization of porous material Fe-FSM-16. Application for hydrogen production. Mater Sci Semicond Process 16:838–844

Boudjemaa A, Mokrani T, Bachari K, Coville NJ (2015) Electrochemical and photoelectrochemical properties of carbon spheres prepared via chemical vapor deposition. Mater Sci Semicond Process 30:456–461

Boumaza S, Boudjemaa A, Bouguelia A, Bouarab R, Trari M (2010) Visible light induced hydrogen on new hetero-system $ZnFe_2O_4/SrTiO_3$. Appl Energy 87:2230–2236

Boyd G, Reemtsma H, Grimm A, Mitra S (2003) Pharmaceuticals and personal care products (PPCPs) in surface and treated waters of Louisiana, USA and Ontario, Canada. Sci Total Environ 311:135–149

Calatayud DG, Rodríguez M, Gallego B, Fernández-Hevia D, Jardiel T (2012) Preparación de Materiales Fotocatalizadores Basados en $Bi_4Ti_3O_{12}$ Dopados con Metales de Transición. Bol Soc Esp Cerám Vidrio 51:55–60

Calza P, Hadjicostas C, Sakkas VA, Sarro M, Minero C, Medana C, Albanis TA (2016) Photocatalytic transformation of the antipsychotic drug risperidone in aqueous media on reduced graphene oxide TiO_2 composites. Appl Catal B Environ 183:96–106

Candal R, de la Cruz Martínez, A (2015) New visible-light active semiconductors. In: Hernández-Ramírez A, Medina-Ramírez I (eds) Photocatalytic semiconductors. Springer, pp 41–67. https://doi.org/10.1007/978-3-319-10999-2_2

Carballa M, Omil F, Lema J, Llompart M, García-Jares C, Rodríguez I, Gómez M, Ternes T (2004) Behavior of pharmaceuticals, cosmetics and hormones in a sewage treatment plants. Water Res 38:2918–2926

Carp O, Huisman CL, Reller A (2004) Photoinduced reactivity of titanium dioxide. Prog Solid State Chem 32:33–177

Chen X, Mao SS (2007) Titanium dioxide nanomaterials: synthesis, properties, modifications, and applications. Chem Rev 107:2891–2959

Chen JX, Zhu LZ (2011) Oxalate enhanced mechanism of hydroxyl-Fe-pillared bentonite during the degradation of Orange II by UV-Fenton process. J Hazard Mater 185:1477–1481

Chen X, Shen S, Guo L, Mao SS (2010a) Semiconductor-based photocatalytic hydrogen generation. Chem Rev 110:6503–6570

Chen L, Zhang X, Xu Y, Du X, Sun X, Sun L, Wang H, Zhao Q, Yu A, Zhang H, Ding L (2010b) Determination of fluoroquinolone antibiotics in environmental water samples based on magnetic molecularly imprinted polymer extraction followed by liquid chromatography-tandem mass spectrometry. Anal Chim Acta 662:31–38

Chen C, Cai W, Long M, Zhou B, Wu Y, Wu D, Feng Y (2010c) Synthesis of visible-light responsive graphene oxide/TiO_2 omposites with p/n heterojunction. ACS Nano 4:6425–6432

Chen B, Hou J, Lu K (2013) Formation mechanism of TiO_2 nanotubes and their applications in Photoelectrochemical water splitting and supercapacitors. Langmuir 29:5911–5919

Cheng B, Le Y, Yu J (2010) Preparation and enhanced photocatalytic activity of Ag@ TiO_2 core-shell nanocomposite nanowires. J Hazard Mater 177:971–977

Cheng G, Lin J, Lu J, Zhao X, Cai Z, Fu J (2015) Advanced treatment of pesticide-containing wastewater using Fenton reagent enhanced by microwave electrodeless ultraviolet. Biomed Res Int 2015:ID 205903, 8

Chi Y, Yuan Q, Li Y, Zhao L, Li N, Li X, Yan W (2013) Magnetically separable Fe_3O_4@SiO_2@TiO_2-ag microspheres with well-designed nanostructure and enhanced photocatalytic activity. J Hazard Mater 262:404–411

Chiarello GL, Aguirre MH, Selli E (2011) Hydrogen production by photocatalytic steam reforming of methanol on noble metal-modified TiO2. J Catal 273:182–190

Chin SF, Pang SC, Dom FEI (2011) Sol gel synthesis of silver/titanium dioxide (Ag/TiO_2) core-shell nanowires for photocatalytic applications. Mater Lett 65:2673

Cho IS, Chen Z, Forman AJ, Kim DR, Rao PM, Jaramillo TF, Zheng X (2011) Branched TiO_2 Nanorods for Photoelectrochemical hydrogen production. Nano Lett 11:4978–4984

Choi HJ, Kang M (2007) Hydrogen production from methanol/water decomposition in a liquid photosystem using the anatase structure of Cu loaded TiO_2. Int J Hydrog Energy 32:3841–3848

Chuang HY, Chen DH (2009) Fabrication and photocatalytic activities in visible UV light region of Ag@TiO_2 and NiAg@TiO_2 nanoparticles. Nanotechnology 20:105704

Clarizia L, Russo D, Di Somma I, Andreozzi R, Marotta R (2017) Hydrogen generation through solar photocatalytic processes: a review of the configuration and the properties of effective metal-based semiconductor nanomaterials. Energies 10:1624

Cojocaru B, Neatu S, Pârvulescu ES, Lévy F, Pârvulescu VI, Garcia H (2011) Influence of gold particle size on the photocatalytic activity for acetone oxidation of Au/TiO_2 catalysts prepared by dc-magnetron sputtering. Appl Catal B 107:140–149

da Silva WL, Lansarin MA, Livotto PR, Henrique Z, dos Santos J (2015) Photocatalytic degradation of drugs by supported titania-based catalysts produced from petrochemical plant residue. Powder Technol 279:166–172

Dang H, Dong X, Dong Y, Zhang Y, Hampshire S (2013) TiO_2 nanotubes coupled with nano-Cu $(OH)_2$ for highly efficient photocatalytic hydrogen production. Int J Hydrog Energy 38:2126–2135

Dastan D (2017) Effect of preparation methods on the properties of titania nanoparticles: solvothermal versus sol–gel. Appl Phys A Mater Sci Process 123:699

Deng F, Li Y, Luo X, Yang L, Tu X (2012) Preparation of conductive polypyrrole/TiO2 nanocomposite via surface molecular imprinting technique and its photocatalytic activity under simulated solar light irradiation. Colloids Surf A Physicochem Eng Asp 395:183–189

Diebold U (2003) The surface science of titanium dioxide. Surf Sci Rep 48:53–229

Dillon AC (2010) Carbon nanotubes for photoconversion and electrical energy storage. Chem Rev 110:6856–6872

Diya'uddeen BH, Ashri Wan Daud WM, Abdul Aziz AR (2011) Treatment technologies for petroleum refinery effluents: a review. Process Saf Environ Prot 89:95–105

Freyria FS, Geobaldo F, Bonelli B (2018) Nanomaterials for the abatement of pharmaceuticals and personal care products from wastewater. Appl Sci 8:170

Fujishima A, Honda K (1972) Electrochemical photolysis of water at a semiconductor electrode. Nature 238(5358):37–38

Fujishima A, Zhang XT (2006) Titanium dioxide photocatalysis: present situation and future approaches. C R Chim 9:750–760

Fujishima A, Zhang X, Tryk DA (2008) TiO_2 photocatalysis and related surface phenomena. Surf Sci Rep 63:515–582

Georgaki I, Vasilaki E, Katsarakis N (2014) A study on the degradation of carbamazepine and ibuprofen by TiO_2 and ZnO photocatalysis upon UV/visible-light irradiation. Am J Anal Chem 5:518–534

Ghasemi S, Setayesh SR, Habibi AY, Hormozi MRN, Gholami MR (2012) Assembly of CeO_2-TiO_2 nanoparticles prepared in room temperature ionic liquid on graphene nanosheets for photocatalytic degradation of pollutants. J Hazard Mater 199–200:170–178

Giovanetti R, Rommozzi E, Zannotti M, D'Amato CA (2017) Recent advances in graphene based TiO_2 nanocomposites ($GTiO_2Ns$) for photocatalytic degradation of synthetic dyes. Catalysts 7:305

Grandcolas M, Ye J, Miyazawa K (2014) Titania nanotubes and fullerenes C60assemblies and their photocatalytic activity under visible light. Ceram Int 40:1297–1302

Grindi IM, Frizzo CP, Bender CR, Tier AZ, Martins MAP, Villetti MA, Machado G, Rodriguez LC, Rodrigues DC (2014) Preparation of TiO_2 nanoparticles coated with ionic liquids: a supramolecular approach. ACS Appl Mater Interfaces 6:11536–11543

Gunti S, Kumar A, Ram MK (2017) Nanostructured photocatalysis in the visible spectrum for the decontamination of air and water. Int Mater Rev 4:257–282

Gupta SM, Tripathi M (2011) A review of TiO_2 nanoparticles. Chin Sci Bull 56:1639–1657

Hapeshi E, Achilleos A, Vasquez MI, Michael C, Xekoukoulotakis NP, Mantzavinos D, Kassinos D (2010) Drugs degrading photocatalytically: kinetics and mechanisms of loxacin and at enolol removal on titania suspensions. Water Res 44:1737–1746

Harish KN, Bhojya Naik HS, Prashanth Kumar PN, Viswanath R (2012) Synthesis, enhanced optical and photocatalytic study of Cd-Zn ferrites under sunlight. Cat Sci Technol 2:1033–1039

He X, Mezyk SP, Michael I, Fatta-Kassinos D, Dionysiou DD (2014) Degradation kinetics and mechanism of b-lactam antibiotics by the activation of H_2O_2 and $Na_2S_2O_8$ under UV-254 nm irradiation. J Hazard Mater 279:375–383

He Y, Sutton NB, Rijnaarts HHM, Langenhoff AAM (2016) Corrigendum to degradation of pharmaceuticals in wastewater using immobilized TiO_2 photocatalysis under simulated solar irradiation. Appl Catal B Environ 182:283

Helaili N, Mitran G, Popescu I, Bachari K, Marcu I-C, Boudjema A (2015) Photoelectrochemical properties of AFe_2O_4 (A = Co, Cu, Zn) ferrospinels for water photoreduction. J Electroanal Chem 742:47–53

Henderson MA (2011) A surface science perspective on TiO_2 photocatalysis. Surf Sci Rep 66:185–297

Hu L, Wei H, Zhang Y, Zhang S, Li B (2014) TiO_2/carbon paper composite materials with hierarchically porous structure for photocatalysis. Mater Lett 119:88–91

Huang W, Wang X, Xue Y, Yang Y, Ao X (2015) Hybrid nanostructures of mixed-phase TiO_2 for Pnhanced Photoelectrochemical water splitting. RSC Adv 5:56098–56102

Hwang SH, Kim C, Jang J (2011) SnO_2 nanoparticles embedded TiO_2 nanofibres-Hightly efficient photocatalyst for the degradation of rhodamine B. J Catal Commun 12:1037–1041

Hwang DW, Kim HG, Jang JS, Bae SW, Ji SM, Lee JS (2004) Photocatalytic decomposition of water-methanol solution over metal-doped layered perovskites under visible light irradiation. Catal Today 93:845–850

Hwang DW, Kim HG, Lee JS, Kim J, Le W, Oh SH (2005) Photocatalytic hydrogen production from water over M-doped $La_2Ti_2O_7$ (M=Cr, Fe) under visible light irradiation ($\lambda > 420$ nm). J Phys Chem B 109:2093–2102

Ishii T, Kato H, Kudo A (2004) Photocatalytic activities of noble metal ion doped $SrTiO_3$ under visible light irradiation. J Phys Chem B 108:8992–8995

Jabbari V, Hamadanian M, Karimzadeh S, Villagran D (2015) Enhanced charge carrier efficiency and solar light-induced photocatalytic activity of TiO_2 nanoparticles through doping of silver nanoclusters and C-N-S nonmetals. J Ind Eng Chem 35:132–139

Janczarek M, Kisch H, Hupka J (2007) Photoelectrochemical characterization of nitrogen-modified TiO_2. Physicochem Probl Mineral Process 41:159–166

Jia F, Yao Z, Jiang Z, Li C (2011) Preparation of carbon coated TiO_2 nanotubes film and its catalytic application for H_2 generation. Catal Commun 12:497–501

Jiang GD, Lin ZF, Chen C, Zhu L, Chang Q, Wang N, Wei W, Tang H (2011) TiO_2 nanoparticles assembled on graphene oxide nanosheets with high photocatalytic activity for removal of polluants. Carbon 49:2693–2701

Jin M, Jeong HK, Yu WJ, Bae DJ, Kang BR, Lee YH (2009) Graphene oxide thin film field effect transistors without reduction. J Phys D Appl Phys 42:135109

Joy J, Mathew J, George SC (2018) Nanomaterials for photoelectrochemical water splitting – review. Int J Hydrog Energy 43(10):4804–4817. https://doi.org/10.1016/j.ijhydene.2018.01.099

Kajen RS, Chandrasekhar N, Pey KL, Vijila C (2012) Trap energy levels in graphene oxide determined by ballistic electron emission spectroscopy. ECS Solid State Lett 1:M27–M28

Kandiel TA, Takanabe K (2016) Solvent-induced deposition of Cu-Ga-In-S nanocrystals onto a titanium dioxide surface for visible-light-driven photocatalytic hydrogen production. Appl Catal B Environ 184:264–269

Karci A, Arslan-Alaton I, Olmez-Hanci T, Bekbölet M (2012) Transformation of 2,4-dichlorophenol by H_2O_2/UV-C, fenton and photofenton processes: oxidation products and toxicity evolution. J Photochem Photobiol A Chem 230:65–73

Karci A, Arslan-Alaton I, Bekbolet M, Ozhan G, Alpertunga B (2014) H_2O_2/UV-C and PhotoFenton treatment of a nonylphenol polyethoxylate in synthetic freshwater: follow-up of degradation products, acute toxicity and genotoxicity. Chem Eng J 241:43–51

Karunakaran C, Biramasundari G, Gomathisankar P, Manikandan G, Anandi V (2011) Preaparation and charactyerization of ZnO-TiO_2 nanocomposite for photocatalytic disinfection of bacteria and detoxification of cyanide under visible light. Mater Res Bull 46:1586–1592

Kasahara A, Nukumizu K, Takata T, Kondo JN, Hara M, Kobayashi H, Domen K (2002) LaTiO2N as a visible-light ($\leq$600 nm)-driven Photocatalyst (2). J Phys Chem B 107:791–797

Kezzim A, Nasrallah N, Abdi A, Trari M (2011) Visible light induced hydrogen on the novel hetero-system CuFe2O4/TiO2. Energy Convers Manag 52:2800–2806

Khanmohammadi M, Garmarudi AB, Elmizadeh H, Roochi MB (2014) Spectrophotometric evaluation of the photocatalytic degradation of formaldehyde by Fe_2O_3-TiO_2 nanohybrid. J Ind Eng Chem 20:1841–1844

Khataee AR, Fathinia M, Joo SW (2013) Simultaneous monitoring of photocatalysis of three pharmaceuticals by immobilized TiO_2 nanoparticles: Chemometric assessment, intermediates identification and ecotoxicological evaluation. Spectrochim Acta A Mol Biomol Spectrosc 112:33–45

Kho YK, Teoh WY, Mädler L, Amal R (2011) Dopant-free, polymorphic design of TiO_2 nanocrystals by flame aerosol synthesis. Chem Eng Sci 66:2409–2416

Kim CK, Kim BH, Yang KS (2011) Visible light-induced photocatalytic activity of Ag-containing TiO_2/carbon nanofibers composites. Synth Met 161:1068–1072

Klamerth N, Malato S, Agüera A, Fernández-Alba A, Mailhot G (2012) Treatment of municipal wastewater treatment plant effluents with modified photofenton as a tertiary treatment for the degradation of micro pollutants and disinfection. Environ Sci Technol 46:2885–2892

Kobayashi M, Katsunori K (2007) WO_3-TiO_2 monolithic catalysts for high temperature SCR of NO by NH_3. Influence of preparation method on structural and physico-chemical properties, activity and durability. Appl Catal B 72:253–261

Kochuveedu ST, Jang YH, Kim DH (2013) A study on the mechanism for the interaction of light with noble metal-metal oxide semiconductor nanostructures for various photophysical applications. Chem Soc Rev 42:8467–8493

Konta R, Ishii T, Kato H, Kudo A (2004) Photocatalytic activities of noble metal ion doped $SrTiO_3$ under visible light irradiation. J Phys Chem B 108:8992–8995

Kudo A, Miseki Y (2009) Heterogeneous photocatalyst materials for water splitting. Chem Soc Rev 38:253–278

Kumar A, Pandey G (2017) A review on the factors affecting the photocatalytic degradation of hazardous materials. Mater Sci Eng Int J 1:00018

Kummerer K (2001) Drugs in the environment: emission of drugs, diagnostic aids and disinfectants into wastewater by hospitals in relation in relation to other sources – a review. Chemosphere 45:957–969

Lai CW, Sreekantan S (2013) Effect of heat treatmenton WO_3-loaded TiO_2 nanotubes for hydrogen generation via enhanced water splitting. Mater Sci Semicond Process 16:947–954

Lambropoulou D, Konstantinou I, Albanis T, Fernández-Alba A (2011) Photocatalytic degradation of the fungicide Fenhexamid in aqueous TiO_2 suspensions: identification of intermediates products and reaction pathways. Chemosphere 83:367–378

Lanese V, Spasiano D, Marotta R, Di Somma I, Lisi L, Cimino S (2013) Hydrogen production by photoreforming of formic acid in aqueous copper/TiO_2 suspensions under UV simulated solar radiation at room temperature. Int J Hydrog Energy 38:9644–9654

Lázaro-Navas S, Prashar S, Fajardo M, Gómez-Ruiz S (2015) Visible light driven photocatalytic degradation of organic pollutants with hybrid palladium-fluorine-doped titanium oxide nanoparticles. J Nanopart Res 17:94

Le Paven-Thivet C, Ishikawa A, Ziani A, Le Gendre L, Yoshida M, Kubota J, Tessier F, Domen K (2009) Photoelectrochemical properties of crystalline perovskite lanthanum titanium oxynitride films under visible light. J Phys Chem C 113:6156–6162

Lee E, Hong JY, Kang H, Jang J (2012) Synthesis of TiO2 nanorod-decorated grapheme sheet and their highly efficient photocatalytic activities under visible light irradiation. J Hazard Mater 219–220:13–18

Lee D, Rho Y, Allen FI, Minor AM, Ko SH, Grigoropoulos CP (2013) Synthesis of hierarchical TiO_2 nanowires with densely-packed and omnidirectional branches. Nanoscale 5:11147–11152

Lee CM, Palaniandy P, Dahlan I (2017) Pharmaceutical residues in aquatic environment and water remediation by TiO_2 heterogeneous photocatalysis: a review. Environ Earth Sci 76:611

Leng WH, Barnes PR, Juozapavicius M, O'Regan BC, Durrant JR (2010) Electron diffusion length in mesoporous nanocrystalline TiO_2 photoelectrodes during water oxidation. J Phys Chem Lett 1:967–972

Leong KH, Gan BL, Ibrahim S, Saravanan P (2014) Synthesis of surface plasmon resonance (SPR) triggered Ag/TiO_2 photocatalyst for degradation of endocrine disturbing compounds. Appl Surf Sci 319:128–135

Li Z, Yang P (2018) Review on physicochemical, chemical, and biological processes for pharmaceutical wastewater. IOP Conf Ser Earth Environ Sci 113:012185

Li Y, Wang W, Qiu X, Song L, Meyer HM III, Paranthaman MP, Eres G, Zhang Z, Gu B (2011) Comparing Cr, and N only doping with (Cr,N)-codoping for enhancing visible light reactivity of TiO_2. Appl Catal B Environ 110:148–153

Li K, Huang Y, Yan L, Dai Y, Xue K, Guo H, Huang Z, Xiong J (2012) Simulated sunlight photodegradation of aqueous atrazine and rhodamine B catalyzed by the ordered mesoporous graphene-titania/silica composite material. Catal Commun 18:16

Li L, Yan J, Wang T, Zhao Z-J, Zhang J, Gong J, Guan N (2015) Sub-10 nm rutile titanium dioxide nanoparticles for efficient visible-light-driven photocatalytic hydrogen production. Nat Commun 6:5881

Liang Y, Wang H, Casalongue HS, Chen Z, Dai H (2010) TiO_2 nanocrystals grown on graphene as advanced photocatalytic hybrid materials. Nano Res 3:701–705

Liao CH, Huang CW, Wu JCS (2012) Hydrogen production from semiconductor-based Photocatalysis via water splitting. Catalysts 2:490–516

Liu P, Li W (2011) Photocatalytic activity enhancement of TiO_2 porous thin film due to homogeneous surface modification of RuO_2. J Mater Res 26:1532

Liu C, Tang X, Mo C, Qiang Z (2008) Characterization and activity of visible-light-driven TiO_2 photocatalyst codoped with nitrogen and cerium. J Solid State Chem 181:913–919

Liu J, Bai H, Wang Y, Liu Z, Zhang X, Sun DD (2010a) Self-assembling TiO_2 Nanorods on large graphene oxide sheets at a two-phase Interface and their anti-recombination in photocatalytic applications. Adv Funct Mater 20:4175–4181

Liu R, Ye H, Xiong X, Liu H (2010b) Fabrication of TiO_2/ZnO composite nanofibers by electrospinning and their photocatalytic property. Mater Chem Phys 121:432–439

Liu L, Chen S, Sun W, Xin J (2011) Enhancing the visible light absorption via combinational doping of TiO_2 with nitrogen (N) and chromium (Cr). J Mol Struct 1001:23–28

Liu R, Zheng Z, Spurgeon J, Yang X (2014a) Enhanced photoelectrochemical water-splitting performance of semiconductors by surface passivation layers. Energy Environ Sci 7:2504–2517

Liu H, Chen Z, Jin Z, Su Y, Wang Y (2014b) A reduced graphene oxide supported Cu3SnS4 composite as an efficient visible-light photocatalyst. Dalton Trans 43:7491–7498

Liu F, Xie Y, Yu C, Liu X, Dai Y, Liu L, Ling Y (2015a) Novel hybrid Sr-doped TiO_2/magnetic $Ni_{0.6}Zn_{0.4}Fe_2O_4$ for enhanced separation and photodegradation of organics under visible light. RSC Adv 48:24056–24063

Liu E, Fan J, Hu X, Hu Y, Li H, Tang C, Sun L, Wan J (2015b) A facile strategy to fabricate plasmonic Au/TiO_2 nano-grass films with overlapping visible light-harvesting structures for H_2 production from water. J Mater Sci 50:2298–2305

Liu Y, He X, Fu Y, Dionysiou DD (2016) Degradation kinetics and mechanism of oxytetracycline by hydroxyl radical-based advanced oxidation processes. Chem Eng J 284:1317–1327

Logar M, Jancar B, Sturm S, Suvorov D (2010) Weak Polyion multilayer-assisted in situ synthesis as a route toward a Plasmonic Ag/TiO_2 Photocatalyst. Langmuir 26:12215–12224

Lou Y, Chen J (2014) Recent developments in one dimensional (1D) nanostructured TiO_2 for photoelectrochemical water splitting. Nanosci Nanotechnol Lett 6:361–371

Luis AM, Neves MC, Mendonc MH, Monteiro OC (2011) Influence of calcination parameters on the TiO_2 photocatalytic properties. Mater Chem Phys 125:20–25

Macwan DP, Dave PN, Chaturvedi S (2011) A review on nano-TiO_2 sol-gel type syntheses and its applications. J Mater Sci 46:3669–3686

Madhavan J, Grieser F, Ashokkumar M (2010) Combined advanced oxidation processes for the synergistic degradation of ibuprofen in aqueous environments. J Hazard Mater 178:202–208

Maeda K, Domen K (2010) Photocatalytic water splitting: recent Progress and future challenges. J Phys Chem Lett 1:2655–2661

Maeda K, Hagashi M, Lu D, Abe R, Domen K (2010) Efficient nonsacrificial water splitting through two-step photoexcitation by visible light using a modified oxynitride as a hydrogen evolution photocatalyst. J Am Chem Soc 132:5858–5868

Maegli AE, Pokrant S, Hisatomi T, Trottmann M, Domen K, Weidenkaff A (2014) Enhancement of photocatalytic water oxidation by the morphological control of LaTiO2N and cobalt oxide catalysts. J Phys Chem C 118:16344–16351

Mai FD, Lee WLW, Chang JL, Liu SC, Wu CW, Chen CC (2010) Fabrication of porous TiO2 film on Ti foil by hydrothermal process and its photocatalytic efficiency and mechanisms with ethyl violet dye. J Hazard Mater 177:864–875

Maicu M, Hidalgo MC, Colón G, Ja N (2011) Comparative study of the Photodeposition of Pt, au and Pd on pre-sulphated TiO_2 for the photocatalytic decomposition of phenol. J Photochem Photob A Chem 217:275–283

Maruthamani D, Divakar D, Kumaravel M (2015) Enhanced photocatalytic activity of TiO_2 by reduced graphene oxide in mineralization of Rhodamine B dye. J Ind Eng Chem 30:33–43

Messih MFA, Ahmed MA, Syhed ASE (2013) Photocatalytic decolorization of Rhodamine B dye using novel mesoporous SnO_2-TiO_2 nano mixed oxides prepared by sol-gel method. J Photochem Photobiol A 260:1–8

Miao H, Hu X, Fan J, Li C, Sun Q, Hao Y, Zhang G, Bai J, Hou X (2015) Hydrothermal synthesis of TiO_2 nanostructure films and their photoelectrochemical properties. Appl Surf Sci 358:418–424

Michael I, Achilleos D, Lambropoulou V, Osorio Torrens S, Pérez M, Petrovic D, Barceló D, Fatta-Kassinos D (2014) Proposed transformation pathway and evolution profile of diclofenac and ibuprofen transformation products during (sono)photocatalysis. Appl Catal B Environ 147:1015–1027

Micó MM, Chourdaki S, Bacardit J, Sans C (2010) Comparison between ozonation and photofenton processes for pesticide methomyl removal in advanced greenhouses. Ozone Sci Eng 32:259–264

Minggu LJ, Daud WW, Kassim MB (2010) An overview of photocells and photoreactors for photoelectrochemical water splitting. Int J Hydrog Energy 3:5233–5244

Miwa T, Kaneco S, Katsumata H, Suzuki T, Ohta K, Verma SC (2010) Photocatalytic hydrogen production from aqueous methanol solution with CuO/Al_2O_3/TiO_2 nanocomposite. Int J Hydrog Energy 35:6554–6560

Mohammadi MR, Fray DJ, Mohammadi A (2008) Sol-gel nanostructured titanium dioxide: controlling the crystal structure, crystallite size, phase transformation, packing and ordering. Microporous Mesoporous Mater 112:392–402

Mohammadi R, Massoumi B, Rabani M (2012) Photocatalytic decompositionof amoxicillin trihydrate antibiotic in aqueous solutions under UV irra-diation using Sn/TiO_2 nanoparticles. Int J Photoenergy 2012:514856

Momeni MM, Nazari Z (2016) Fabrication of new photoanodes for solar-water-splitting photoelectrochemical cells: synergistic effect between platinum and nanocomposite photocatalysts. Mater Res Innov 20:51–57

Momeni MM, Ghayeb Y, Davarzadeh M (2015) Single-step electrochemical anodization for synthesis of hierarchical WO_3-TiO_2 nanotube arrays on titanium foil as a good photoanode for water splitting with visible light. J Electroanal Chem 739:149–155

Morales-Torres S, Pastrana-Martínez LM, Figueiredo JL, Faria JL, Silva AMT (2012) Design of graphene-based TiO_2 photocatalysts-a review. Environ Sci Pollut Res 19:3676–3687

Nahar S, Zain MFM, Kadhum AAH, Hasan HA, Hasan MR (2017) Advances in photocatalytic CO_2 reduction with water: a review. Materials 10:629

Naik B, Moon S, Sang Y, Kim H, Park JY (2015) Enhanced photocatalytic generation of hydrogen by Pt-deposited nitrogen-doped TiO2 hierarchical nanostructures. Appl Surf Sci 354:347–352

Naldoni A, D'Arienzo M, Altomare M, Marelli M, Scotti R, Morazzoni F, Selli E, Santo VD (2013) Pt and Au/TiO_2 photocatalysts for methanol reforming: role of metal nanoparticles in tuning charge trapping properties and photoefficiency. Appl Catal B 130–131:239

Neppolian B, Bruno A, Bianchi CL, Ashokkumar M (2012) Graphene oxide based Pt-TiO2 photocatalyst: ultrasound assisted synthesis, characterization and catalytic efficiency. Ultrason Sonochem 19:9–15

Nethi SK, Aparna N, Rico-Oller B, Rodríguez-Diéguez A, Gómez-Ruiz S, Patra CR (2017) Design, synthesis and characterization of doped-titanium oxide nanomaterials with environmental and angiogenic applications. Sci Total Environ 599–600:1263–1274

Neyens E, Baeyens J (2003) A review of classic Fenton's peroxidation as an advanced oxidation technique. J Hazard Mater 98:33–50

Nguyen-Phan TD, Pham VH, Shin EW, Pham H, Kim S, Chung JS, Kim EJ, Hur SH (2011) The role of grapheme oxide content on the adsorption-enhanced photocatalysis of titanium dioxide/grapheme oxide composites. Chem Eng J 170:226–232

Nguyen-Phan TD, Pham VH, Kweon H, Chung JS, Kim EJ, Hur SH, Shin SH (2012) Uniform distribution of TiO_2 nanocrystal on reduced graphene oxide sheet by the chelating ligands. J Colloid Interface Sci 367:139–147

Ni M, Leung MKH, Leung DYC, Sumathy K (2007) A review and recent developments in photocatalytic water-splitting using TiO_2 for hydrogen production. Renew Sust Energ Rev 11:401–425

Niishiro R, Kato H, Kudo A (2005) Nickel and either tantalum or niobium-codoped TiO_2 and $SrTiO_3$ photocatalysts with visible-light response for H_2 or O_2 evolution from aqueous solutions. Phys Chem Chem Phys 7:2241–2245

Niishiro R, Konta R, Kato H, Chun WJ, Asakura K, Kudo A (2007) Photocatalytic O_2 evolution of rhodium and antimony-codoped rutile-type TiO_2 under visible light irradiation. J Phys Chem C 111:17420–17426

Obregón S, Lee SW, Rodríguez-González V (2016) Loading effects of silver nanoparticles on hydrogen photoproduction using a Cu-TiO_2 photocatalyst. Mater Lett 173:174–177

Oller I, Malato S, Sánchez-Pérez JA (2011) Combination of advanced oxidation processes and biological treatments for wastewater decontamination-a review. Sci Total Environ 409:4141–4166

Ong WJ, Gui MM, Chai SP, Mohamed AR (2013) Direct growth of carbon nanotubes on Ni/TiO_2 as next generation catalysts for photoreduction of CO_2 to methane by water under visible light irradiation. RSC Adv 3:4505–4509

Oosawa Y, Grätzel M (1988) Effect of surface hydroxyl density on photocatalytic oxygen generation in aqueous TiO_2 suspensions. J Chem Soc Faraday Trans 84:197–205

Palominos RA, Mondaca MA, Giraldo A, Peñuela G, Pérez-Moya M, Mansilla HD (2009) Photocatalytic oxidation of the antibiotic tetracycline on TiO_2 and ZnO suspensions. Catal Today 144:10–105

Park H, Kim H, Moon G, Choi W (2016) Photoinduced charge transfer processes in solar photocatalysis based on modified TiO_2. Energy Environ Sci 9:411–433

Pinaud BA, Benck JD, Seitz LC, Forman AJ, Chen Z, Deutsch TG, James BD, Baum KN, Baum GN, Ardo S, Wang H, Miller E, Jaramillo TF (2013) Technical and economic feasibility of centralized facilities for solar hydrogen production via photocatalysis and photoelectrochemistry. Energy Environ Sci 6:1983–2002

Pizarro P (2005) Desarrollo de materiales basados en TiO_2 mesoestructurado con aplicaciones fotocatalíticas. PhD thesis. Universidad Rey Juan Carlos, Spain

Rajini PA, Mathews T, Ramesh C, Murugesan N, Dasgupta A, Dhara S, Dash S, Tyagi AK (2012) Efficient photocatalytic hydrogen generation by Pt modified TiO_2 nanotubes fabricated by rapid breakdown anodization. Int J Hydrog Energy 37:8268–8276

Ran J, Zhang J, Yu J, Jaroniec M, Qiao SZ (2014) Earth-abundant cocatalysts for semiconductor-based photocatalytic water splitting. Chem Soc Rev 43:7787–7812

Ranganathan K, Morais A, Nongwe I, Longo C, Nogueira AF, Coville NJ (2016) Study of photoelectrochemical water splitting using composite films based on TiO_2 nanoparticles and nitrogen or boron doped hollow carbon spheres as photoanodes. J Mol Catal A Chem 422:165–174

Rather RA, Singh S, Pal B (2016) Core-shell morphology of Au-TiO_2@graphene oxide nanocomposite exhibiting enhanced hydrogen production from water. J Ind Eng Chem 37:288–294

Reza KM, Kurny ASW, Gulshan F (2017) Parameters affecting the photocatalytic degradation of dyes using TiO_2: a review. Appl Water Sci 7:1569–1578

Rico-Oller B, Boudjemaa A, Bahruji H, Kebir M, Prashar S, Bachari K, Fajardo M, Gómez-Ruiz S (2016) Photodegradation of organic pollutants in water and green hydrogen production via methanol photoreforming of doped titanium oxide nanoparticles. Sci Total Environ 563–564:921–932

Rosseler O, Shankar MV, Le Du MK, Schmidlin L, Keller N, Keller V (2010) Solar light photocatalytic hydrogen production from water over Pt and Au/TiO_2 (anatase/rutile) photocatalysts: influence of noble metal and porogen promotion. J Catal 269:179–190

Roy A, Lingampalli SR, Saha S, Rao CNR (2015) Effects of morphology and surface area of the oxide nanostructures onthe visible-light induced generation of hydrogen in ZnO(TiO_2)/Cd1-xZnxS and ZnO(TiO_2)/Pt/Cd1-xZnxS heterostructures (x = 0.0, 0.2). Chem Phys Lett 637:137–142

Sadale SB, Noda K, Kobayashi K, Yamada H, Matsushige K (2012) Real-time investigation on photocatalytic oxidation of gaseous methanol with nanocrystalline WO3-TiO2 composite films. Thin Solid Films 520:3847–3851

Sali SM, Joy S, Meenakshisundaram N, Karn RK, Gopalakrishnan C, Karthick P, Jeyadheepan K, Sankaranarayanan K (2017) Phase tuned synthesis of titanium dioxide nanoparticles for room temperature enhanced ammonia detection. RSC Adv 7:37720–37728

Sánchez-Muñoz S, Pérez-Quintanilla D, Gómez-Ruiz S (2013) Synthesis and photocatalytic applications of nano-sized zinc-doped mesoporous titanium oxide. Mater Res Bull 48:250–255

Santato C, Ulmann M, Augustynski J (2001) Photoelectrochemical properties of nanostructured tungsten trioxide films. J Phys Chem B 105:936–940

Sarina S, Waclawik ER, Zhu H (2013) Photocatalysis on supported gold and silver nanoparticles under ultraviolet and visible light irradiation. Green Chem 15:1814–1833

Sarkar S, Chowdhury R, Das R, Chakraborty S, Choi H, Bhattacherjee C (2014a) Application of ANFIS model to optimize the photocatalytic degradation of chlorhe xidinedi gluconate. RSC Adv 4:21141–21150

Sarkar S, Das R, Choi H, Bhattacharjee C (2014b) Involvement of process parameters and various modes of application of TiO_2 nanoparticles in heterogeneous photocatalysis of pharmaceutical wastes – a short review. RSC Adv 4:57250–57266

Sarkar S, Chakraborty S, Bhattacharjee C (2015) Photocatalytic degradation of pharmaceutical wastes by alginate supported TiO_2 nanoparticles in packed bed photoreactor (PBPR). Ecotoxicol Environ Saf 121:263–270

Sartori A, Visentin F, Habra NE, Zorzi CD, Natali M, Garoli D, Gerbasi R, Casarin M, Rossetto G (2011) Preparation of tetrapod-like ZnO/TiO_2 core-shell nanostructures as photocatalytic powder. Cryst Res Technol 46:885–890

Scheytt T, Mersmann P, Heberer T (2006) Mobility of pharmaceuticals carbamazepine, diclofenac, ibuprofen, and propyphenazone in miscible-displacement experiments. J Contam Hydrol 83:53–69

Schneider J, Matsuoka M, Takeuchi M, Zhang J, Horiuchi Y, Anpo M, Bahnemann DW (2014) Understanding TiO_2 photocatalysis: mechanisms and materials. Chem Rev 114:9919–9986

Shah MSAS, Park AR, Zhang K, Park JH, Yoo PJ (2012) Green synthesis of biphasic TiO_2-reduced graphene oxide nanocomposites with highly enhanced photocatalytic activity. ACS Appl Mater Interfaces 4:3893–3901

Shah NS, He X, Khan HM, Khan JA, O'Shea KE, Boccelli DL, Dionysiou DD (2013) Efficient removal of endosulfan from aqueous solution by UV-C/peroxides: a comparative study. J Hazard Mater 263:584–592

Silva CG, Sampaio MJ, Marques RRN, Ferreira LA, Tavares PB, Silva AMT, Faria J (2015) Photocatalytic production of hydrogen from methanol and saccharides using carbon nanotube-TiO_2 catalysts. Appl Catal B Environ 178:82–90

Souvereyns B, Elen K, De Dobbelaere C, Kelchtermans A, Peys N, D'Haen J, Mertens M, Mullens S, Van den Rul H, Meynen V, Cool P, Hardy A, Van Bael MK (2013) Hydrothermal synthesis of a concentrated and stable dispersion of TiO_2 nanoparticles. Chem Eng J 223:135–144

Stoyanova A, Hitkova H, Nedelcheva AB, Iordanova R, Ivanova N, Sredkova M (2013) Synthesis and antibacterial activity of TiO_2/ZnO nanocomposites prepared via nonhydrolytic route. J Chem Technol Metal 48:154–161

Stumpf M, Ternes T, Harbere K, Baumann W (1998) Isolierung von Ibuprofen-Metaboliten und deren Bedeutung als Kontaminanten der aquatischen Umwelt. Vom Wasser 91:291–303

Takahasi R, Matsumoto H, Horie T, Matsuda K (2017) Preparation of porous Titania by Sol–Gel method using Alkylketene dimers as a template. J Chem Eng Jpn 50:450–454

Tan L, Chai S, Mohamed AR (2012) Synthesis and applications of graphene-based TiO_2 photocatalysts. ChemSusChem 5:1868–1882

Tan LL, Ong WJ, Chai SP, Mohamed AR (2013) Reduced graphene oxide-TiO2 nanocomposite as a promising visible-light-active photocatalyst for the conversion of carbon dioxide. Nanoscale Res Lett 8:465

Tanigawa S, Irie H (2016) Visible-light-sensitive two-step overall water-splitting based on band structure control of titanium dioxide. Appl Catal B Environ 180:1–5

Ternes TA (1998) Occurrence of drugs in Germann sewage treatment plants and rivers. Water Res 32:3245–3260

Thamaphat K, Limsuwan P, Ngotawornchai B (2008) Phase characterization of TiO_2 powder by XRD and TEM. Nat Sci 42:357–361

Thao LTS, Dang TTT, Khanitchaidecha W, Channei D, Nakaruk A (2017) Photocatalytic degradation of organic dye under UV-A irradiation using TiO_2-vetiver multifunctional nano particles. Materials 10:122

Tian SH, Yu YT, Chen DS, Chen X, Xiong Y (2011) Degradation of acid orange II at neutral pH using $Fe_2(MoO_4)_3$ as a heterogeneous Fenton-like catalyst. Chem Eng J 169:31–37

Tixier C, Singer H, Oellers S, Müller S (2003) Ocurrence and fate of carbamazepine, ibuprofen, ketoprofen and naproxen in surface waters. Environ Sci Technol 37:1061–1068

Torres-Martínez LM, Ruiz-Gómez MA (2011) Estudio de las propiedades estructurales, texturales y catalíticas de TiO_2 dopado con indio y níquel. Ingenierias UANL (XIV) 53:23–53

Voepel P, Smarsly BM (2017) Synthesis of titanium oxide nanostructures in ionic liquids. Z Anorg Allg Chem 643:3–13

Walter MG, Warren EL, McKone JR, Boettcher SW, Mi Q, Santori EA, Lewis NS (2010) Solar water splitting cells. Chem Rev 110:6446–6473

Wang F, Zhang K (2011) Reduced grapheme oxide-TiO_2 nanocomposite with high photocatalytic activity for the degradation of rhodamine B. J Mol Catal A Chem 345:101–107
Wang C, Shi H, Zhang P, Li Y (2011a) Synthesis and characterization of kaolite/TiO_2 nano-photocatalysts. Appl Clay Sci 53:646–649
Wang H, Chung H, Teng H, Cao G (2011b) Generation of hydrogen from aluminum and water – effect of metal oxide nanocrystals and water quality. Int J Hydrog Energy 36:15136–15144
Wang PF, Ao YH, Wang C, Hou J, Qian J (2012a) Enhanced photoelectrocatalytic activity for dye degradation by grapheme-titania composite film electrodes. J Hazard Mater 223–224:79–83
Wang F, Zheng Z, Jia F (2012b) Enhanced photoelectrochemical water splitting on Pt-loaded TiO_2 nanorods array thin film. Mater Lett 71:141–144
Wang Y, Wei W, Liu X, Gu Y (2012c) Research progress on polymer heterojunction. Sol Energy Mater Sol Cells 98:129–145
Wang H, Yuan X, Wu Y, Huang H, Peng X, Zeng G, Zhong H, Liang J, Ren MM (2013a) Graphene-based materials: fabrication, characterization and application for the decontamination of wastewater and wastegas and hydrogen storage/generation. Adv Colloid Interf Sci 195–196:19–40
Wang B, Sun Q, Liu S, Li Y (2013b) Synergetic catalysis of CuO and graphene additives on TiO_2 for photocatalytic water splitting. Int J Hydrog Energy 38:7232–7240
Wang D, Zhang X, Sun P, Lu S, Wang L, Wang C, Liu Y (2014a) Photoelectrochemical water splitting with rutile TiO_2 nanowires Array: synergistic effect of hydrogen treatment and surface modification with Anatase nanoparticles. Electrochim Acta 130:290–295
Wang Q, Hisatomi T, Ma SSK, Li Y, Domen K (2014b) Core/shell structured La- and Rh-Codoped $SrTiO_3$ as a hydrogen evolution photocatalyst in Z-scheme overall water splitting under visible light irradiation. Chem Mater 26:4144–4150
Wang F, Jin Z, Jiangd Y, Backusb EHG, Bonnb M, Loua SN, Turchinovich D, Amala R (2016) Probing the charge separation process on In_2S_3/Pt-TiO_2 nanocomposites for boosted visible-light photocatalytic hydrogen production. Appl Catal B Environ 198:25–31
Watanabe M (2017) Dye-sensitized photocatalyst for effective water splitting catalyst. Sci Technol Adv Mater 18:705–723
Weigel S, Berger U, Jensen E, Kallenborn R, Thoresen H, Huhnerfuss H (2004) Determination of selected pharmaceuticals and caffeine in sewage and seawater from Tromso/Norway whit emphasis on ibuprofen and its metabolites. Chemosphere 56:583–592
Wen X, Ding H, Huang X, Liu R (2004) Treatment of hospital wastewater using a submerged membrane bioreactor. Process Biochem 39:1427–1431
Wu KQ, Xie YD, Zhao JC, Hidaka H (1999) PhotoFenton degradation of a dye under visible light irradiation. J Mol Catal A Chem 144(1):77–84
Wu XF, Song HY, Yoon JM, Yu YT, Chen YF (2009) Synthesis of Core−Shell Au@TiO2 nanoparticles with truncated wedge-shaped morphology and their photocatalytic properties. Langmuir 25:6438–6447
Wu X, Li X, Yang M, Zeng H, Zhang S, Lu R, Gao H, Xu D (2017) An ionic liquid-based Nanofluid of titanium dioxide nanoparticles for effervescence-assisted dispersive liquid–liquid extraction for acaricide detection. J Chromatogr A 1497:1–8
Xiang Q, Yu J, Cheng B, Ong HC (2010) Microwave-hydrothermal preparation and visible-light photoactivity of plasmonic photocatalyst ag-TiO_2 nanocomposite hollow spheres. Chem Asian J 5:1466–1474
Xiang Q, Yu J, Jaroniec M (2011) Enhanced photocatalytic H2-production activity ofgraphene-modified titania nanosheets. Nanoscale 3:3670–3678
Xiao FX (2012) Construction of highly ordered ZnO-TiO_2 nanotube arrays (ZnO/TNTs) Heterostructure for photocatalytic application. ACS Appl Mater Interfaces 4:7055–7063
Xu Y, Zhang M, Zhang M, Lv J, Jiang X, He G, Song X, Sun Z (2014) Controllable hydrothermal synthesis, optical and photocatalytic properties of TiO2 nanostructures. Appl Surf Sci 315:299–306

Xu Q, Feng J, Li L, Xiao Q, Wang J (2015) Hollow ZnFe2O4/TiO2 composites: high-performance and recyclable visible-light photocatalyst. J Alloys Compd 641:110–118

Yang L, Xiao Y, Liu S, Li Y, Cai Q, Luo S, Zeng G (2010) Photocatalytic reduction of Cr(VI) on WO3 doped long TiO2 nanotube arrays in the presence of citric acid. Appl Catal B 94:142–149

Yang XH, Li Z, Liu G, Xing J, Sun C, Yang HG, Li C (2011) Ultra-thin Anatase TiO_2 Nanosheets dominated with {001} facets: thickness-controlled synthesis, growth mechanism and water-splitting properties. CrystEngComm 13:1378–1383

Yang J, Wang D, Han H, Li C (2013) Roles of cocatalysts in photocatalysis and photoelectrocatalysis. Acc Chem Res 46:1900–1909

Yang M, Zhang L, Jin B, Huang L, Gan Y (2016) Enhanced photoelectrochemical properties and water splitting activity of self-ordered MoO_3-TiO_2 nanotubes. Appl Surf Sci 364:410–415

Yen YC, Chen JA, Ou S, Chen YS, Lin KJ (2016) Plasmon-enhanced photocurrent using gold nanoparticles on a three-dimensional TiO_2 nanowire-web electrode. Nat Sci Rep 7:42524

Yoo DH, Cuong TV, Pham VH, Chung JS, Khoa NT, Kim EJ, Hahn SH (2011) Enhanced photocatalytic activity of grapheme oxide decorated on TiO_2 films under UV and visible irradiation. Curr Appl Phys 11:805–808

Yoo JE, Lee K, Altomare M, Selli E, Schmuki P (2013) Self-organized arrays of single-metal catalyst particles in TiO2 cavities: a highly efficient photocatalytic system. Angew Chem Int Ed 52:7514–7517

Yu JC, Zhang L, Yu J (2002) Rapid synthesis of mesoporous TiO_2 with high photocatalytic activity by ultrasound-induced agglomeration. New J Chem 26:416–420

Yu Z, Meng J, Li Y, Li Y (2013) Efficient photocatalytic hydrogen production from water over a CuO and carbon fiber co-modified TiO_2 nanocomposite photocatalyst. Int J Hydrog Energy 38:16649–11655

Yu H, Zhao Y, Zhou C, Shang L, Peng Y, Cao Y (2014) Carbon quantumdots/TiO_2 composites for efficient photocatalytic hydrogen evolution. J Mater Chem A 2:3344

Yuan C, Hung CH, Li HW, Chang WH (2016) Photodegradation of ibuprofen by TiO_2 co-doping with urea and functionalized CNT irradiated with visible light effect of doping content and pH. Chemosphere 155:471–478

Zakrzewska K, Kollbek K, Sikora M, Cz K, Szlachetko J, Sitarz M, Ziabka M, Radecka M (2015) Importance of the electronic structure of modified TiO_2 in the photoelectrochemical processes of hydrogen generation. Int J Hydrog Energy 40:815–824

Zaleska A (2008) Doped-TiO_2: a review. Recent Patents Eng 2:157–164

Zazoua H, Boudjemaa A, Chebout R, Bachari K (2014) Enhanced photocatalytic hydrogen production under visible light over a material based on magnesium ferrite derived from layered double hydroxides (LDHs). Int J Energy Res 38:2010–2018

Zhang Z, Wang P (2012) Optimization of Photoelectrochemical water splitting performance on hierarchical TiO_2 nanotube arrays. Energy Environ Sci 5:6506–6512

Zhang D, Yang M (2013) Band structure engineering of TiO_2 nanowires by n-p codoping for enhanced visible-light photoelectrochemical water-splitting. Phys Chem Chem Phys 15:18523–18539

Zhang J, Fu D, Xu Y, Liu C (2010a) Optimization of parameters on photocatalytic degradation of chloram phenicol using TiO_2 as photocatalyst by response surface methodology. J Environ Sci 22:1281–1289

Zhang H, Lv X, Li Y, Wang Y, Li J (2010b) P25-Graphene composite as a highperformance photocatalyst. ACS Nano 4:380–386

Zhang M, An T, Liu X, Hu X, Sheng G, Fu J (2010c) Preparation of a high activity ZnO/TiO2 photocatalyst via homogenous hydrolysis method with low temperature crystallization. Mater Lett 64:1883–1886

Zhang N, Liu S, Fu X, Xu YJ (2011) Synthesis of M@TiO_2 (M = Au, Pd, Pt) Core-Shell nanocomposites with tunable photoreactivity. J Phys Chem C 115:9136–9145

Zhang F, Yamakata A, Maeda K, Moriya Y, Takata T, Kubota J, Teshima K, Oishi S, Domen K (2012a) Cobalt-modified porous single-crystalline $LaTiO_2N$ for highly efficient water oxidation under visible light. J Am Chem Soc 134:8348–8351

Zhang Z, Yang W, Zou X, Xu F, Wang X, Zhang B, Tang J (2012b) One-pot, solvothermal synthesis of TiO_2-graphene composite nanosheets. J Colloid Interface Sci 386:198–204

Zhang J, Jin X, Morales-Guzman PI, Yu X, Liu H, Zhang H, Razzari L, Claverie JP (2016a) Engineering the absorption and field enhancement properties of au-TiO2 Nanohybrids via whispering gallery mode resonances for photocatalytic water splitting. ACS Nano 10:4496–4503

Zhang S, Cao X-B, Wu J, Zhu L-W, Gu L (2016b) Preparation of hierarchical CuO@TiO_2 nanowire film and its application in photoelectrochemical water splitting. Trans Nonferrous Metals Soc China 26:2094–2101

Zhao D, Sheng G, Chen C, Wang X (2012) Enhancement photocatalytic degradation of methylene blue under visible irradiation on graphene@TiO_2 dyad structure. Appl Catal B Environ 111–112:303–309

Zhao Y, Chen Q, Pan F, Li H, Xu QG, Chen W (2014) Uniform mesoporous Anatase hollow spheres: An unexpectedly efficient fabrication process and enhanced performance in photocatalytic hydrogen evolution. Chem Eur J 20:1–7

Zhou D, Chen Z, Gao T, Niu F, Qin L, Huang Y (2015a) Hydrogen generation from water splitting on TiO_2 nanotube-array-based photocatalysts. Energy Technol 3:888–895

Zhou M, Glushenkova AM, Kartachova O, Li Y, Chen Y (2015b) Titanium dioxide nanotube films for electrochemical supercapacitors: biocompatibility and operation in an electrolyte based on a physiological fluid. J Electrochem Soc 162:A5065

Zou R, Zhang Z, Yu L, TianQ CZ, Hu J (2011) A general approach for the growth of metal oxide Nanorod arrays on graphene sheets and their applications. Chem Eur J 17:13912–13917

Chapter 8
Polymer Nanocomposites: Synthesis and Characterization

Anil Arya and A. L. Sharma

Contents

8.1 Introduction 266
8.2 Polymer Electrolytes 270
8.3 Materials and Methodology 274
8.3.1 Preparation Methods 274
8.3.2 Characterization Techniques 276
8.4 Recent Updates 281
8.4.1 Nanofiller Dispersed Polymer Nanocomposites 281
8.4.2 Nanoclay Dispersed Polymer Nanocomposites 291
8.4.3 Nanorod–Nanowire Dispersed Polymer Nanocomposites 301
8.4.4 Separator Development: Commercial and Patents 308
8.5 Summary and Conclusions 309
References 312

Abstract This chapter presents the fundamental properties of polymer nanocomposites (PNCs) and their characteristics that play a significant role in deciding their capability for the advanced energy storage devices. The various synthesization methods used for the preparation of polymer electrolytes are described followed by the characterization techniques used for the analysis. The properties of the polymer host, salt, nanofiller, ionic liquid, plasticizer, and nanoclay–nanorod–nanowire are described. Various ion transport mechanisms with different nanoparticle dispersions in polymer electrolytes are highlighted. Various important results are summarized, and a pathway is built to fulfill the dream of the future renewable source of energy that is economical and environmental benign. Chapter motivation is focused on the investigation of the role of polymer host, aspect ratio, surface area, nanoparticle shape, and size in terms of boosting the electrolytic–electrochemical properties of PNC. It will certainly help in order to open new doors toward the development of advanced polymeric materials with overall balancing property for enhancement of the fast solid-state ionic conductor which would revolutionize the energy storage–conversion device technology.

A. Arya · A. L. Sharma (✉)
Department of Physical Sciences, Central University of Punjab, Bathinda, Punjab, India
e-mail: alsharma@cup.edu.in

N. Dasgupta et al. (eds.), *Environmental Nanotechnology Volume 4*, Environmental Chemistry for a Sustainable World 32, https://doi.org/10.1007/978-3-030-26668-4_8

Keywords Li-ion battery · Polymer nanocomposites · Electrical properties · Ion transport mechanism

8.1 Introduction

In the world, most of the energy demand (~75%) of human beings is till now fulfilled by nonrenewable energy resources that include oils, coal, natural gas, etc. They are sufficient to provide us energy for a long period, but two major drawbacks associated with them are lack of time and pollution. The combustion of these nonrenewable sources of energy has fired much increase in the CO_2 emission (32,190 metric ton per year), and one day, that will cross above the global point in which it would become difficult to sustain life on earth. Further, natural disasters such as storms and floods lead to collapsing of buildings and public as well as government properties, and it leads to energy blackout. So it becomes important to resolve this issue and focus on the best alternative. It can be summarized in one line that environmental change is affecting our lives, and it becomes a necessity to look at some other efficient alternative energy resources. The best appropriate alternative which seems to be feasible is the use of renewable energy such as solar energy, wind energy, hydroenergy, electrochemical energy, and nuclear energy. In the last three decades, since Sony commercialized its Li–ion battery in 1991, and a lot of research is being done till 2016 (25th anniversary of LIB introduction) to replace these nonrenewable sources with a renewable one. First-time Prof. Michel Armand in 1970 formulated the idea of the intercalation compounds and highlighted the ion migration in between electrodes (rocking chair battery). The battery is now the crucial part of portable consumer electronics, and its demand is supposed to rise in the coming future. Besides these lithium–ion batteries, electric vehicles will replace cars, buses, and trains to fight against pollution. So, many companies are now front-runners in boosting the e-mobility and plug-in vehicles (Fig. 8.1a). This is an environmentally friendly and safe source that can be used for a longer period (Li et al. 2016; Armand and Tarascon 2008; Lin et al. 2016; Yang et al. 2011; Arya and Sharma 2016).

Figure 8.1b shows the growth of the commercial secondary batteries from 1950 to 2010 by about 3 Wh kg^{-1} per year on average (shown in the dashed line). Dash line shows the progress of the last 80 years, and the solid line represents the development of Li–ion batteries in the last 20 years. This demonstrates that the present energy density (210 Wh kg^{-1}) will reach the target energy densities 500 Wh kg^{-1} and 700 Wh kg^{-1}, which will be realized in years 2110 and 2177, respectively. Further, another step has been taken to enhance the utilization of the Li–ion battery by lowering the prices of the LIB (Fig. 8.1c).

So, to fulfill the demand for renewable source of energy, in 2015, for the first time, Tesla disclosed the stationary storage products for homes that boosted the demand for the batteries. The first step toward the renewable energy source is completed in November 2017; Tesla has completed the construction of the world's biggest Li–ion battery (LIB) with 100 MW capacity just outside the South Australian city of Jamestown (Fig. 8.1d). It will deliver power to 30,000 homes for about an

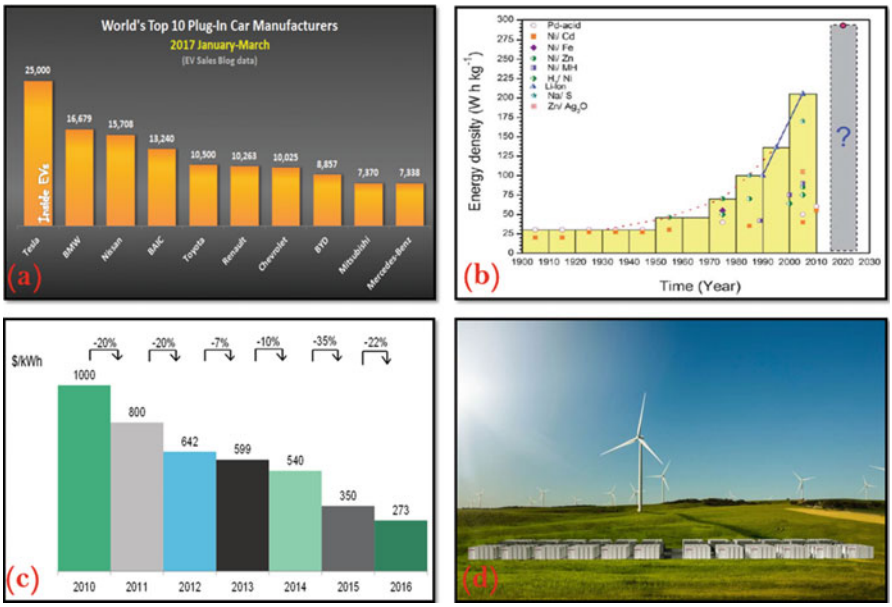

Fig. 8.1 (**a**) The world's top ten plug-in car manufacturers – 2017 March. (Data source: EV Sales Blog) (https://insideevs.com/volkswagens-transform-2025-plan-calls-for-automaker-to-be-1-for-evs/). (**b**) History of development of secondary batteries in view of energy density (Zu and Li 2011). (**c**) BNEF Li–ion battery price survey, 2010–2016 ($/kWh) (https://about.bnef.com/blog/lithium-ion-battery-costs-squeezed-margins-new-business-models/). (**d**) The world's largest grid-scale battery – the Hornsdale Power Reserve battery (https://www.greentechmedia.com/articles/read/tesla-fulfills-australia-battery-bet-whats-that-mean-industry)

hour (https://insideevs.com/volkswagens-transform-2025-plan-calls-for-automaker-to-be-1-for-evs/; Zu and Li 2011; https://about.bnef.com/blog/lithium-ion-battery-costs-squeezed-margins-new-business-models/; https://www.greentechmedia.com/articles/read/tesla-fulfills-australia-battery-bet-whats-that-mean-industry). It opened the doors of future affordable renewable energy source with a lot of possibilities that will revolutionize the energy sector. Another remarkable point with this battery was highlighted in a statement by the Elon Musk, "You can essentially charge up the battery packs when you have excess power when the cost of production is very low and then discharge it when the cost of power production is high, and this effectively lowers the average cost to the end customer."

A battery is a very catchy system where separator–electrolyte is sandwiched between two different counter electrodes (i) cathode (positive electrode) and (ii) anode (negative electrode). The separator–electrolyte provides the path for shuttling the ion between the electrodes, while electrons move via the external circuit. The cathode is generally made of metal oxide ($LiCoO_2$, $LiCoMnO_2$) and the anode of graphite. During discharge, the ions flow from the anode to the cathode (oxidation at the anode; loss of electrons) through the electrolyte and separator; while during the charging process, charge reverses the direction, and the ions flow

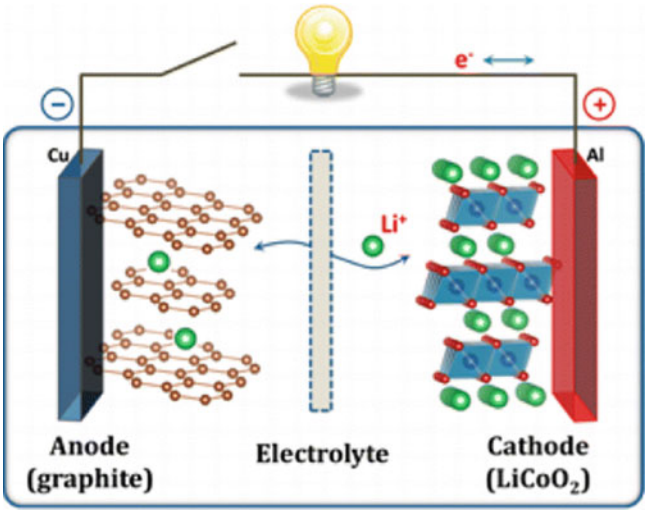

Fig. 8.2 Schematic illustration of the first Li–ion battery ($LiCoO_2$–Li+ electrolyte–graphite). (With permission from (Goodenough and Park 2013) Copyright © 2013 American Chemical Society)

from the cathode to the anode (reduction of the cathode; a gain of electrons) (Goodenough and Park 2013). Figure 8.2 demonstrates the operation of a Li–ion battery and its components cathode, anode, and electrolyte. The role of the electrolyte is to physically separate both electrodes and provide medium for ion migration.

A lot of research is going on the development of both cathode and anodes that may provide large energy density and power density without affecting its stability or cycle life. Besides them, electrolyte is a more interesting candidate as it is placed in between the electrodes, and it remains always in the active state either it is in discharging or charging process. The electrolyte is the heart of the battery and plays a key role in the operation of a battery. Nowadays most of the battery systems are based on liquid electrolyte. Although the battery possesses high ionic conductivity, poor mechanical strength and stability prevent its use in commercial applications. Another critical drawback is the dendrite growth formation that leads to short-circuiting of the battery. Another issue is the capacity fading and the narrow safety window due to the liquid electrolyte. So to overcome all issues faced by the liquid electrolyte-based storage system, the most attractive approach which is adopted nowadays is the use of solid polymer electrolyte (SPE). It prevents the use of separate casing for the electrolyte, and it plays a dual role that automatically reduces both cost and weight. Another fundamental advantage with the SPE is that the dendrite growth formation could be minimized at practical level due to good interface contact with the electrodes (Cheng et al. 2017). SPE is superior in comparison to both liquid polymer electrolyte and gel polymer electrolyte in many aspects such as stability, flexibility, shape variation, safety, and cost. Although SPE is a suitable candidate as an alternative to the conventional electrolyte, still some drawback exists there. Another crucial point is the ease of the preparation. It

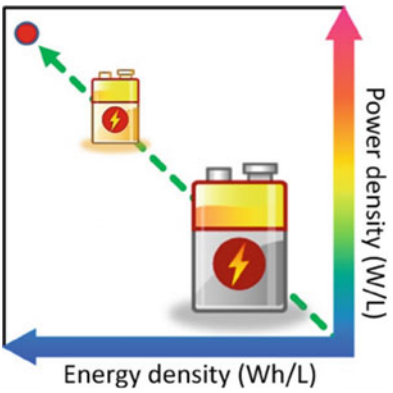

Fig. 8.3 An illustration to the demonstration that future Li–ion batteries should be light and small without any compromise on energy and power. (With permission from (Deng 2015) Copyright © 2015 John Wiley and Sons)

(SPE) involves the dissolution of host polymer having an electron-rich group (polar group), and the salt with bulky anion dissolves in the solvent. The host polymer provides the coordinating sites that favor the fast ion migration and further supported by the segmental motion of the polymer chains. The segmental motion of the polymer chain is linked with the flexibility of the polymer chain, as it pushes the ion from one site to the next and mobility is enhanced. The most important one is the low ionic conductivity as compared to the desire for the practical applications, and the other one is the mechanical stability. So, a new type of solid-state advanced material needs to be developed which can provide us the desirable conductivity value for practical applications ($\sim 10^{-3}$ S cm^{-1}) (Arya and Sharma 2017a, 2018).

Nowadays, due to increased demand for Li–ion batteries globally, it becomes important to develop new technologies which can provide safe and advanced energy storage system, as the nanoparticles (nanofiller, nanorod, nanowire) are attractive candidates for developing all components of the battery. One important point to be noticed here is that the nanomaterial has possibilities to fulfill the dream of the energy storage system with high-energy density and power density, as it is well known that the shape of the nanoparticle influences strongly all properties. Figure 8.3 depicts that the next-generation energy storage system probably of the battery must be of a smaller size with improved performances so that the empty space in energy storage devices can be filled (Deng 2015).

A number of reviews are published till now with a focus on different types of polymer electrolytes (Hallinan Jr and Balsara 2013; Ngai et al. 2016; Miller III et al. 2017; Bhattacharya 2016; Arya and Sharma 2017b). Song et al. highlighted the advantages and characteristics of gel polymer electrolyte for Li–ion batteries. The chapter covered the four plasticized systems with main focus on, i.e., poly(ethylene oxide) (PEO)-, poly(acrylonitrile) (PAN)-, poly(methyl methacrylate) (PMMA)-, and poly(vinylidene fluoride) (PVdF)-based electrolytes (Song et al. 1999). Stephan et al. chapter was geared toward the state of the art of polymer electrolytes in view of their electrochemical and physical properties for the applications in lithium batteries with the main focus on the polymer poly(ethylene oxide) (PEO), poly(acrylonitrile) (PAN), poly(methyl methacrylate) (PMMA), poly(vinylidene fluoride) (PVdF), and

poly(vinylidene fluoride–hexafluoropropylene) (PVdF–HFP) as electrolytes. The cycling behavior of $LiMn_2O_4$–polymer electrolyte (PE)–Li cells is also described (Stephan 2006). Another review by Zhang et al. covered the separators used in liquid electrolyte Li–ion batteries. The classification of separators was done on the basis of the structure and composition of the membranes followed by a discussion on the manufacture, characteristics, performance, and modifications of the separators (Zhang 2007a). Stephan et al. discussed the composite polymer electrolytes (CPEs) with the main focus on electrochemical and physical properties for the applications in lithium batteries. The polymer hosts discussed were poly(ethylene oxide) (PEO), poly(acrylonitrile) (PAN), poly(methyl methacrylate) (PMMA), and poly(vinylidene fluoride) (PVdF) (Stephan and Nahm 2006). The above reviews mostly covered the gel and liquid polymer electrolytes with the main focus on the properties of the polymer electrolytes. To the best of our knowledge, no review articles with the main focus on the shape of the nanofiller in polymer electrolyte have been systematically concluded till now. Polymer nanocomposites are basically the solid polymer electrolytes which are a two-phase system; the first phase acts as host matrix in which different nanoparticles are dispersed (Suthanthiraraj and Johnsi 2017). The polymer nanocomposite enables us to develop polymer electrolyte with improved mechanical, thermal properties, voltage stability window, and electrochemical properties.

In this chapter, a brief summary of polymer nanocomposites (PNCs) with nanoparticles of various shapes is given in detail. First, the status of the LIB technology in the current practical applications is described and followed by the working principle of the battery. Then we discussed the characteristics of the polymer electrolytes and the properties of the constituents used, i.e., polymer host, salt, ionic liquid, plasticizer, nanoclay, nanofiller, nanorod, and nanowire. Then the preparation methods and the common characterization techniques used to identify the suitability of the polymer nanocomposites are discussed followed by the factors influenced by the addition of different nanoparticles. Finally, we have summarized the recent key developments done till now in the field of the solid polymer electrolytes.

8.2 Polymer Electrolytes

In energy storage devices, polymer electrolyte plays the dual role of both electrolytes and separator and is sandwiched between the electrodes. So, the polymer host which is to be used has some special characteristics that make its candidature stronger as compared to the other. The polymer electrolytes are classified into three types, (i) *gel polymer electrolytes*, an organic solvent is added in the polymer matrix; (ii) *solid polymer electrolyte*, polymer matrix acts as host matrix and provides coordinating sites for cation migration and no organic solvent required; and (iii) *composite polymer electrolyte*, here nanoparticle is dispersed in the polymer–salt matrix, also known as polymer nanocomposites. Figure 8.4 depicts the properties that are

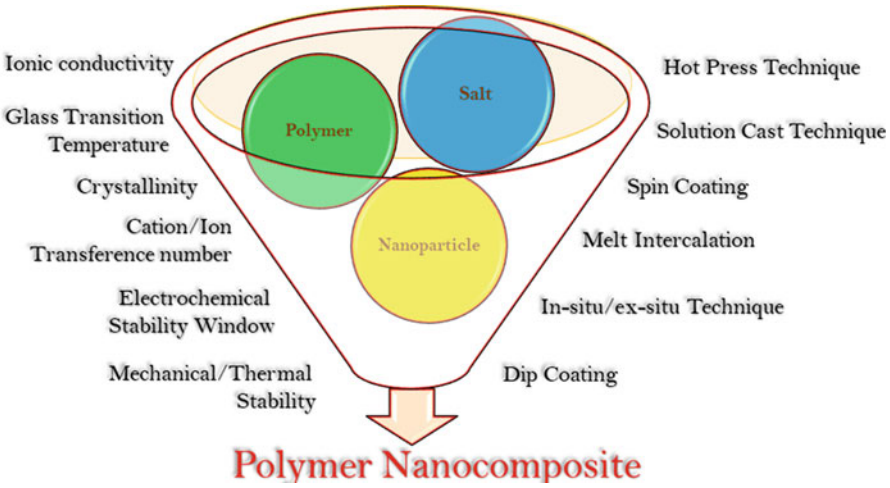

Fig. 8.4 Representation of the properties required for the suitable polymer electrolyte and the synthesization techniques

influenced by the addition of the nanoparticle and the synthesization techniques. These properties are linked with one another. The ionic conductivity is linked to the glass transition temperature and hence the flexibility. As ion transport in the polymer, electrolytes is supposed to occur via the amorphous phase so crystallinity associated with the polymer matrix is minimized by altering the polymer chain rearrangement. The cation transference number and ion transference number are crucial for getting insights of applicability of any system for the battery. As during fabrication, the battery's system is under stress, it needs to be focused on along with the electrical properties (Arya and Sharma 2017a, b; Hallinan Jr and Balsara 2013). There are various synthesization approaches for solid polymer electrolytes. The properties of the polymer nanocomposites are also affected by the preparation method.

For three decades, a lot of research has been done on the salt–ionic liquid–plasticizer-based polymer electrolytes. Although there was a desirable enhancement in the electrical parameters, poor mechanical strength limits their use in commercial applications. So, their alternative was developed, and incorporation of nanoparticle was adopted as the most fascinating approach to develop the advanced polymer electrolytes. The suitable nanoparticles adopted were nanofiller and nanoclay, and they reported enhancement in the electrical as well as thermal–mechanical properties, as nanoparticle shape plays an effective role due to the interconnection of the electrical properties of the nanoparticle shape and surface group. Recently, research is focused toward the development of nanoparticle with the high specific surface area. The two approaches were adopted: one is the addition of nanorod and another is the addition of nanowire. Both are effective nanoparticles as a long continuous path is created that is beneficial for achieving fast ion transport.

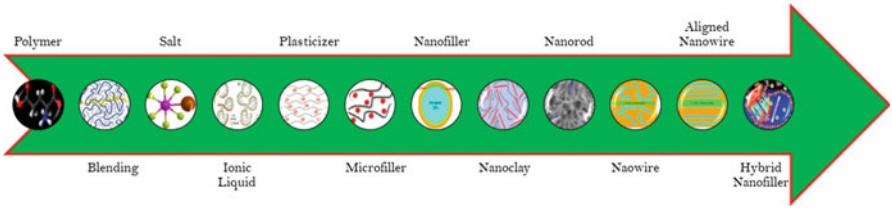

Fig. 8.5 Approaches adopted for the modification of the polymer electrolyte and the progress made till now

Various approaches used for the enhancement of the properties to fulfill the criteria of a solid-state ionic conductor are displayed in Fig. 8.5 (from left to right) as various constituents play a different role in enhancing the electrical properties, thermal properties, and mechanical properties. Table 8.1 shows the important characteristics that are the deciding factors for the selection of appropriate material for preparation of advanced polymer electrolyte.

Polymer Nanocomposites

Polymer nanocomposites (PNCs) are the recently adopted composite polymer electrolyte in the electrolyte community due to various advantages such as high safety, inflammable nature, high reliability, and broad thermal–voltage stability. The synthesization of the composite polymer electrolyte includes the addition of salt in the host polymer matrix and a nanoparticle. The most critical requirement with the PNC is the formation of the amorphous content that will improve the electrode–electrolyte interface (Arya and Sharma 2017a; Bhattacharya 2016). The increased amorphous content also improves the use of full electrode material during cell operation. The two parameters ionic conductivity and the cation transference number are generally observed in deciding the electrolyte in energy storage–conversion devices. The conductivity enhancement can be done by various approaches, such as the addition of nanofiller, nanoclay, nanorod, or nanowire. The main characteristics are that the nanoparticle must have high surface area and oxygen vacancies. The former one results in the formation of a long continuous conducting path for cation migration, while the latter one provides additional coordinating sites for the cation. In the case of nanoclay, the polymer chains get intercalated inside the clay galleries, and this increases the interchain separation as well as gallery spacing. This increase in both parameters leads to overall enhancement in the conductivity. Beside the nanofiller, nanoclay, nanorod/nanowire are attractive candidates being used for the preparation of the polymer nanocomposite. The two advantages of them are the formation of a long conductive continuous network and the presence of oxygen vacancies for ion migration. Then one fundamental requirement for ideal electrolyte is that, cation transference number must be unity. So, the main approach is to imobilise the anion which could prevent the concentration polarization at the electrodes. The anion may be covalently bonded to the polymer backbone or some anion acceptors may be used.

Table 8.1 Characteristics of constituents of polymer electrolytes

Polymer host	**Plasticizer**
Provide fast segmental motion of polymer chain	Low melting point
Low glass transition temperature	High boiling point
High molecular weight	High dielectric constant
Low viscosity	Low viscosity
High degradation temperature	Easily available
High dielectric constant	Economic
Must have electron donor groups	Inert to both electrodes
	Good safety and nontoxic nature
Solvent	**Nanofiller**
Abundant in nature	High polarity
Nonaqueous in nature	Low melting and high boiling point
Low melting point	Safe and nontoxic
Low viscosity	Environmentally friendly and cost-effective
Large flash point	Inert to all cell components
High dielectric constant	Act as Lewis acid for interaction with polymer
Good solubility for polymer and salt	High dielectric constant for better dissociation of salt
Salt	**Nanoclay**
Low lattice energy for more availability of free ions	Layered–unique structure with high aspect ratio (∼1000)
High ionic conductivity	Complex rheological behavior
High mobility	Amorphous behavior with acid-based properties
Broad voltage stability window	Greater ability for intercalation and swelling
Low ion pair formation at high content	Increase solubility of salts
Large anion size	High swelling index (water and polar solvents)
Small cation size for fast migration between the electrodes	High cation exchange capacity (CEC) (∼80 meq/100 g)
High thermal and chemical stability	High external–internal surface area (∼31.82 $m^2\ g^{-1}$)
Large ion transference number	Appropriate interlayer charge (∼0.55)
Inert toward cell components	Adjustable hydrophilic–hydrophobic balance
Ionic liquid	**Nanorod–nanowire–nanobelt**
Good thermal stability	High specific surface area
Wide electrochemical stability	High aspect ratio
Low melting point	Long continuous path
Low viscosity for fast transport	Easily alignment perpendicular to electrodes
Negligible volatility	Oxygen vacancies on the surface for cation
Non-flammability	Less agglomeration at high content
Negligible vapor pressure	High thermal stability
High ionic conductivity	Better chemical stability
High polarity	Long cycle stability
High dielectric constant	

With permission from (Arya and Sharma 2017a) Copyright © 2017 Springer

8.3 Materials and Methodology

8.3.1 Preparation Methods

The preparation of the polymer nanocomposites is done by various methods, such as solution cast technique, in situ polymerization technique, melt intercalation technique, spin coating technique, hot press technique, and dip coating technique.

Solution Cast Technique

It is the traditional method and preferred due to its ease of fabrication and produces polymer film from various thicknesses (50–300 μm). First of all, the specified amount of the polymer host is dissolved in the appropriate solvent by continuous stirring. Then the appropriate salt content is added to the homogenous polymer matrix and again stirred till a homogenous and transparent solution is obtained. Now, to prepare the polymer nanocomposite, firstly, the nanoparticle is added in a solvent, and ultrasonication is performed for better dispersion. Then the obtained solution is added to the polymer–salt solution and stirred till a homogenous solution is obtained. Finally, the viscous solution is casted in the petri dish and kept at room temperature for evaporation of the solvent and then kept in a vacuum oven to completely remove the residual solvent, and film is peeled off from petri dish (Arya and Sharma 2018). The obtained film is kept in a desiccator with silica gel for further characterization and moisture prevention. For high-quality film, the solvent must be free from water content and should dissolve the polymer, salt, and nanoparticle (Karuppasamy et al. 2015).

Spin Coating

This method is almost identical to the solution cast technique. The key advantages of spin coating technique are simplicity and relative ease of preparation and produce uniform films from a few nanometers to a few microns in thickness. In this technique, a small amount of solution is dropped on a substrate and kept on the spin coater which can be rotated at desired speed. The centripetal acceleration spreads the mixture on a substrate followed by heating to evaporate the solvent. One point that must be taken care of is that the substrate spinning axis must be perpendicular to the substrate which is to be coated. The thickness of the film is influenced by (i) viscosity of mixture, (ii) concentration of mixture, (iii) speed of rotation, and (iv) spin time. However, this method is advantageous only for low viscosity mixture not for too high viscosity mixture. For a gel mixture, the spin coater rotation is not enough to spread the mixture droplet to form thin film (Park et al. 2006; Krebs 2009).

Hot Press Technique

Hot press technique is a unique technique with features such as low cost, solvent-free, and a good film with dense materials and is a fast method. The setup consists of a weighing cylinder, heating chamber, basement, and (d) temperature controller. Firstly, the polymer, salt, and nanoparticle are grounded in the agate pestle for the required time. Then the obtained mixture is heated (close to melting temperature of polymer), and the obtained slurry is sandwiched between the stainless steel (SS blocks). Then pressure-controlled system presses the slurry, and obtained film is used for further characterizations (Wilson and Gottesfeld 1992; Agrawal and Chandra 2007).

Dip Coating

The dip coating's unique feature is that it enables us to obtain high-quality film on both sides of the substrate and is a low-cost technique. First of all, the chosen substrate is dipped in the solvent (Brinker and Hurd 1994). The three-step process occurs, immersion, then deposition, and drainage, followed by evaporation of the solvent. In immersion, the substrate is immersed in solution at a desired speed that provides sufficient time for coating. In the next step, deposition and drainage, the substrate remains dipped in the solvent for sufficient time (dwell time) to enable interaction of the substrate with a solvent. Now, the substrate is pulled out slowly at a constant speed that leads to the formation of a thin film on the substrate. Then in the final step, evaporation, the solvent is evaporated, and the substrate may be heated to completely remove the extra solvent. The thickness and quality of the film can be controlled by the speed of removal and density of the solution.

Melt Intercalation Technique

This is an important technique due to advantages such as being environmentally friendly and cost-effective and not needing any solvent. One point to be noted is that for better dispersion of nanoparticle, the optimization of thermal properties needs to be performed as high temperature may alter the surface properties of the nanoparticle and may degrade it. First of all, the annealing of the polymer matrix is done at high temperatures, and then nanoparticle is added, followed by kneading the composite to achieve uniform distribution. In conclusion, the surface modification of clay–nanofiller, compatibility of filler with host polymer, and processing conditions affect the dispersion of nanoparticle (Pavlidou and Papaspyrides 2008; Erceg et al. 2014).

8.3.2 Characterization Techniques

A battery assembly consists of three components: cathode, anode, and electrolyte–separator. The solid polymer electrolyte (polymer nanocomposite) is sandwiched between the two electrodes and plays the dual role of both electrolytes (for ion migration) and separator (for physical separation of electrodes to prevent short-circuit). Thus, the electrolyte plays a key role during the operation of the battery. Keeping in mind the desirable device for practical application, there are some requirements or performance parameters that need to be measured experimentally in any polymer electrolyte cum separator (Sharma and Thakur 2013).

Fourier Transform Infrared Spectroscopy (FTIR)

The salt dissociation capability of the polymer host plays an important role in deciding the suitable polymer electrolyte with balanced properties. The polymer host must have high dissolution capability to boost the salt dissociation into cation and anion and to fulfill the purpose of the fast ionic conductor. The dissociation capability of the host polymer is indicated by the presence of the polar group of polymer ($-O-$, $C \equiv N-$, $C=O$,) and how strongly it gets coordinated with the cation. Another important point is the less tendency of the chain reorganization so that complete polymer chain can effectively participate in separating the cation and anion. Further, the supportive role is played by the salt in deciding the overall solvation ability. The salt must have bulky anion as they have low lattice energy and supports in overcoming the coulombic interaction between ions. The mutual dissolution ability of the polymer and salt leads to the cation migration via the segmental motion of the polymer chains. Besides the polymer chain and the salt, solvent also influences the dissolution ability of all participating species. The solvent must have high dielectric constant and high dipole moment so that the ion association can be hindered. The overall effect of the three key players is the effective number of free ion carriers for transport and elimination of the ion pair as they do not participate in the conduction. So, to achieve the balanced properties, the suitable combination of the polymer, salt, and solvent is a vital requirement for the fast ionic conductor. The properties of the individual polymer, salt, and solvent are discussed in the forthcoming section.

Complex Impedance Spectroscopy (CIS)

As ionic conduction decides the performance of an energy storage system, and ionic conductivity depends on the molecular weight of the polymer, cation–anion size, and viscosity of polymer chains. The polymer electrolyte, therefore, must possess high ionic conductivity and negligible electronic conductivity. As the migration of anions may affect the battery performance, its migration is avoided during the design of any

polymer electrolyte system. The main strategy is to immobilize the anion, and the only cation dominates in the conduction. The ionic conductivity of any polymer electrolyte system (σ) is linked with two parameters: a number of free charge carriers and ion mobility (Eq. 8.1).

$$\sigma = \sum n_i q_i \mu_i \tag{8.1}$$

Here, n_i represents the effective number of charge carriers of type i, q_i is the charge of the charge carriers, and μ_i is the mobility.

An important factor that influences the ionic conductivity is the activation energy. This is the minimum energy that is required for ion migration and is obtained from the conductivity vs. temperature plot (Kumar and Yashonath 2006). Activation energy decreases with the increase of the temperature. Generally, it is supposed that the crystalline phase dominates below the melting temperature, while the amorphous phase is effective above the melting temperature. So, both regions are examined by two conduction mechanisms dependent on temperature: (i) Arrhenius behavior and (ii) Vogel–Tammann–Fulcher (VTF) behavior. The Arrhenius equation describes the relation between logσ and T^{-1}, as shown in Eq. (8.2)

$$\sigma = \sigma_o \exp\left(-\frac{E_a}{kT}\right) \tag{8.2}$$

Here, E_a is the activation energy, which can be calculated from the nonlinear least-squares fitting of the data from plots of log σ vs. T^{-1}. For polymer electrolytes, plots of σ vs. T^{-1} are typically nonlinear, indicating that the conductivity mechanism involves an ionic hopping motion coupled with the relaxation and/or segmental motion of the polymeric chains.

The VTF equation can be derived from the quasi-thermodynamic models with the free volume and configurational entropy, and its behavior can be related with coupled motion with the segmental motion. This can be expressed by Eq. 8.3.

$$\sigma = \sigma_o T^{-1/2} \exp\left(-\frac{B}{T - T_o}\right) \tag{8.3}$$

Here, σ_o is the pre-exponential factor, which is related to the number of charge carriers n_i, B is the pseudoactivation energy of the conductivity, and T_o is the reference temperature associated with the ideal glass transition temperature (zero mobility temperature). For practical aspects, the high ionic conductivity of the order of 10^{-2}–10^{-3} S cm^{-1} and electronic conductivity of the order of 10^{-6}–10^{-10} S cm^{-1} are required. This enhances the charging–discharging rate and cyclic stability (Table 8.2).

Table 8.2 Definition and comparison of the laws governing the transport phenomena in polymer electrolytes

	Arrhenius	Vogel–Tammann–Fulcher (VTF)	WLF (Williams, Landel, and Ferry)
Expression	$\sigma = \sigma_o \exp\left(-\frac{E_a}{kT}\right)$	$\sigma = \sigma_o T^{-1/2} \exp\left(-\frac{B}{T-T_o}\right)$	$\sigma = \sigma_o \exp\left(-\left(\frac{C_1(T-T_{ref})}{C_2+T-T_{ref}}\right)\right)$
Typical values	–	$\sigma_o = 0.4$ S cm^{-1}, $B = 2.210^{-3}$ *K*-1, $T_o = 210$, $K \approx T_g$-50	$C_1 = 17.4$, $C_2 = 52$ *K*, $T_{ref} = T_g = 240$ *K*
Derived from	$k = a \exp\left(-\frac{E_a}{kT}\right)$	Variation of viscosity with T	Scaling factor $a_T$for relaxation:
		$\eta \propto T^{1/2} exp\left(-\frac{B}{T-T_o}\right)$	$\log(a_T) = -\left(\frac{C_1(T-T_{ref})}{C_2+T-T_{ref}}\right)$
Valid relations needed	$y = mx + c$	$D = \frac{kT}{6\pi\eta r}$ Stokes–Einstein	$\sigma = \frac{Ze^2}{kT} D$ Nernst–Einstein
Correspondence VTF↔WLF	$T_o \rightarrow 0$ to in VTF	Neglect $T^{1/2}$ prefactor in σ_o from VTF $C_1C_2 = B$	$C_2 = T_{ref} - T_o$

With permission from (Baril et al. 1997) Copyright ©1997 Elsevier

Table 8.3 Definition and comparison of the transference number in polymer electrolytes

	Cation transference number	Ion transference number
Expression	$t_{cation} = \left(\frac{I_s(V-I_oR_o)}{I_o(V-I_sR_s)}\right)$	$t_{ion} = \left(1 - \frac{I_e}{I_t}\right)$
Symbol depiction	V is the applied dc voltage for sample polarization, I_o and I_s are the currents before and after polarization, and R_o and R_s are the initial and steady-state resistance of the passivation layers	I_t is total initial current due to ions and electrons contribution, and I_e is residual current due to electrons contribution only
Value	~1	~100%

i-t Characteristics (Transference Number)

It is one of the essential parameters that must be close to the unity (~1) for a good ionic conductor and function of the ionic conductivity. One main drawback associated with the polymer electrolytes is concentration polarization (CP) on the electrode interface which hinders the ion migration during cell operation. This affects the overall performance of the device and observed in terms of the low-energy density and power density. So, the main strategy to reduce the CP is to immobilize the anion and keep only the active species as the main hero of the charge transport scenario. This fulfills the idea of the single-state ionic conductor. So, the large value of the cation transference number also plays an effective role in the enhancement of the ionic conductivity. Two approaches are adopted for immobilizing the anion. One approach suggests the anion interaction with the hydrogen of the polymer backbone (hydrogen bond formation); another is the introduction of the anon receptors. Generally, there are two terms here: cation transference number and ion transference number (Table 8.3).

Differential Scanning Calorimetry (DSC)

Glass transition temperature (T_g) is one of the most fundamental properties of the polymer electrolytes that is directly linked to the electrochemical properties. It is influenced by the polymer chain arrangement, crystallinity, viscosity, polymer interactions or polarity, and molecular weight of the polymers as most of the polymers are crystalline in nature. The ionic conduction in case of the polymers is supposed to occur via the amorphous phase and segmental motion of the polymer chains which is further linked with the flexibility of chains. This flexibility criterion is specified by the glass transition temperature (T_g) value. It is defined as a transition temperature at which any system goes from rigid to rubbery–viscous phase. Below $T_{g,}$ there is no ion migration or chain is not moving. While above the T_g, there is a drastic change in the intrinsic properties (density, specific heat, mechanical modulus, mechanical energy absorption, their dielectric and acoustical equivalents) of the polymer that supports the fast segmental motion or less viscosity (Zhang et al. 2016). The differential scanning calorimetry (DSC) measurement is performed to measure the T_g, and it also provides the melting and crystallinity of the used material. The lower value of the T_g indicates enhanced flexibility for the polymer matrix. This increase in flexibility improved the ion swimming rate between electrodes with the coordinating sites of the polymer chains. So, the main strategy for lowering the value of the T_g is to alter the polymer chain arrangement and disruption of the covalent bonding between the polymer chains. This can be done by the addition of nanofiller, plasticizer, nanoclay, etc. Generally, the addition of the above said particles increases the free volume available for the ion migration, and this makes faster ion migration.

Crystallinity

The ordering of the polymer chain (long range and short range) affects the ion migration in a polymer electrolyte as long range order is associated with the crystallinity which in case of the polymer electrolyte must be lower for faster ion migration. So, the crystallinity of any system provides sufficient information regarding the material and how it will play its role during the ion transport. The crystallinity of any polymer material is obtained by the X-ray diffraction (XRD) and the differential scanning calorimetry (DSC). It needs to be mentioned here that the amorphous content supports the fast ion migration in the case of the polymer electrolytes. The amorphous content is achieved by disrupting the crystalline arrangement of the polymer chains. The best approach is the addition of the nanofiller, which alters the arrangement of the Lewis acid–base interaction with polymer chains. The intercalation of the polymer chains in the clay gallery also lowers the crystallinity. This increases the free volume available for the ion migration as now segmental motion of the polymer chains becomes faster and the ion jumps faster from one coordinating site to another. The amorphous content can be

visualized by the field emission scanning electron microscopy (FESEM), transmission electron microscopy (TEM), and atomic force microscopy (AFM).

Linear Sweep Voltammetry (LSV)

For fulfilling the requirement of polymer electrolyte for the application aspects, it must have a broad electrochemical stability window (ESW), which depends on the stability of individual cation–anion. It is defined as the difference between the potentials of the oxidation reaction and reduction reaction. One characteristic a polymer electrolyte must possess is that it must be inert toward both electrodes. For this, the oxidation potential must be higher than the embedding potential of cation (Li^+) in the cathode, and the reduction potential must be lower than that of lithium metal in the anode. The desirable range of the ESW is ~4–5 V and is enough for the commercialized systems.

Thermogravimetric Analysis (TGA)

Thermal stability of a battery device is important to avoid the material decomposition and explosion during cell operation. So, the thermal stability is investigated by TGA to check the safety window of a polymer electrolyte as different materials have different decomposition temperature ranges, and for long-term cycle stability, all material must lie beyond the decomposition range. So, for safe working of the battery system, the thermal stability must be large. The approach for the enhancement of the thermal stability is the addition of nanoparticles in the polymer matrix.

Stress–Strain Curve

During the commercialization of the battery or any energy storage device, one important property is the mechanical stability. So, along with high cation transference number and the ionic conductivity, it must have mechanical property sufficient enough for long-term cycle stability. The mechanical stability is measured by the stress–strain curve in terms of the modulus, stress, and strain, as during the cell packaging, the polymer electrolyte is sandwiched between the two electrodes so it must have the capability to sustain the pressure applied. The polymer electrolyte having poor mechanical strength may short-circuit the electrodes during cell operation. So, the material must be flexible by nature, and brittleness is avoided. It must have inherent characteristics that may absorb the small internal shocks and does not affect the electrodes. There are various strategies that are adopted for the enhancement of the modulus, stress, and strain. The most suitable and the attractive approaches are the dispersion of the nanofiller, nanoclay and nanoparticle it high aspect ratio such as nanorod, nanowire, nanotube. Here these nanoparticles may play

the role of the cross-linking center, and overall enhancement in the mechanical property of the complete polymer matrix is achieved.

8.4 Recent Updates

8.4.1 Nanofiller Dispersed Polymer Nanocomposites

There are various reports toward the addition of different nanofillers in the polymer matrix for improving the electrical, thermal, and mechanical properties. Generally, all nanofiller addition suppresses the crystallinity, and cross-linking alters the polymer chain arrangement. Another effective point is that nanofiller supports salt dissociation via Lewis acid–base interactions and provides additional conducting sites for ion transport. But still, there is lack of availability of a polymer matrix with enhanced amorphous content, and weak polymer–nanofiller interaction results in nanofiller agglomeration. So, Lin et al. (2015) reported the preparation of (PEO)-monodispersed ultrafine SiO_2 ($MUSiO_2$) composite polymer electrolyte (PEO-$MUSiO_2$ CPE) via in situ hydrolysis of tetraethyl orthosilicate(TEOS) in PEO solution. Basically, the advantage with the in situ hydrolysis is that the polymer–nanofiller interaction is more effective in suppressing the crystallinity by linking the polymer chains with the nanofiller surface. Two possible dominant interactions exist here: (i) between the hydroxyl groups at the ends of PEO chains with the surface of SiO_2 and (ii) wrapping and embedding of PEO chains inside SiO_2 spheres.

TEM image evidences that the higher polymer density was for the in situ prepared composites as compared to ex situ and indicates the presence of strong interaction between the polymers and nanofiller (Fig. 8.6 d–f). Further, XRD also evidences the superior evidence of reduction of crystallinity as compared to the ex situ synthesis (Fig. 8.6j). Further FTIR and DSC also evidence the reduction of crystallinity by in situ synthesis. One reason is disruption of the polymer chain reorganization tendency due to the interaction between $MUSiO_2$ spheres and polymer chains. Another reason is improved surface area due to uniformity in size and distribution.

Another remarkable evidence is the increased number of free ion charge carriers (left to right) in Fig. 8.6k–n. The degree of dissociation of salt was higher for the sample synthesized by in situ synthesis following the relation in in situ (98.1%) > ex situ (92.8%) > PEO-fumed SiO_2 CPE (87.4%) > ceramic-free SPE (85.0%). This was attributed to the simultaneous achievement of two parameters, uniform distribution of SiO_2 and increased the segmental motion of polymer chains. The ionic conductivity also shows enhancement for polymer electrolyte synthesized by in situ and is in the range 10^{-4}–10^{-5} S cm^{-1} (at ambient temperature) and 1.2×10^{-3} S cm^{-1} (at 60 °C). Further, the electrochemical stability window was improved for in situ synthesis (>5.5 V) as compared to ex situ synthesis (~4.7 V) and may be due to the strong adsorption effect on anion for in situ synthesis (Park et al. 2003). Further, the rate capability test of solid-state battery (LFP–CPE–Li) displays double capacity

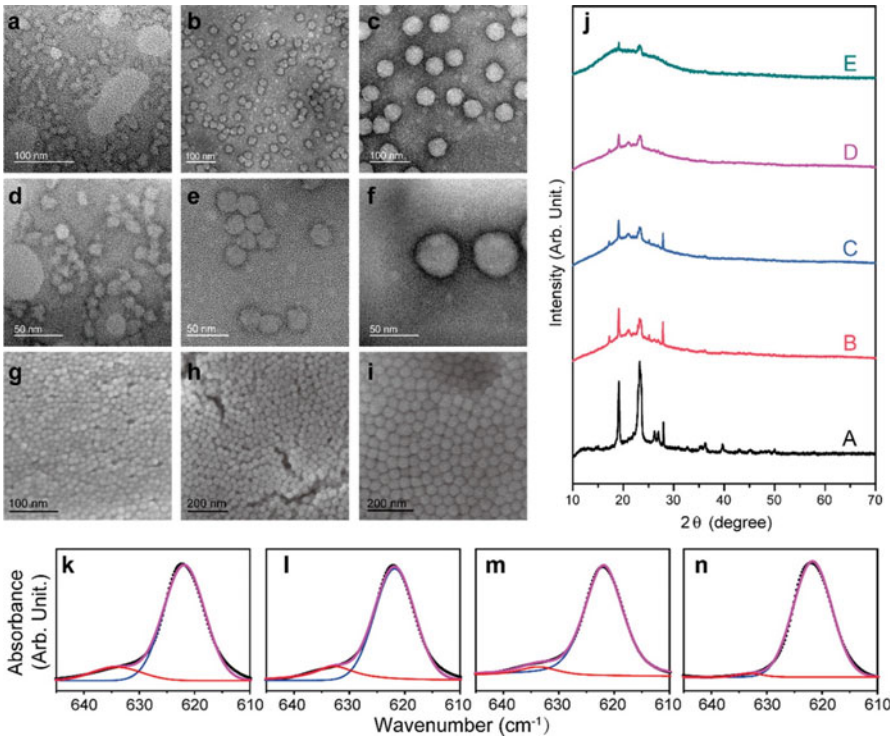

Fig. 8.6 Characterizations of in situ CPE. (**a**–**f**) TEM images of in situ PEO–$MUSiO_2$ composite with different sizes of ~12 nm (**a** and **d**), ~30 nm (**b** and **e**), and ~45 nm (**c** and **f**) PEO was stained with 0.1% phosphotungstic acid to show better contrast. (**g**–**i**) SEM images of as-synthesized corresponding $MUSiO_2$ spheres (without PEO) with various sizes of ~12 nm (**g**), ~30 nm (**h**), and ~45 nm (**i**). (**j**) Comparison on XRD spectra of pure PEO(A), ceramic-free SPE (B), PEO-fumed SiO_2 CPE (C), ex situ CPE (D), and in situ CPE. (E) (**k**–**n**) FTIR spectra at 610–645 cm^{-1} and corresponding Gaussian–Lorentzian fitting of the ClO_4^- absorbance for ceramic-free PEO SPE (**k**), PEO-fumed SiO_2 CPE (**l**), ex situ CPE (**m**), and in situ CPE (**n**). (With permission from (Lin et al. 2015) Copyright © 2016 American Chemical Society)

retention for in situ synthesis (120 $mAhg^{-1}$ at 90 °C and 100 $mAhg^{-1}$ at 60 °C) as compared to ex situ (65 $mAhg^{-1}$), while for ceramic-free, it was 50 $mAhg^{-1}$. For in situ cycle, stability was achieved, and after 80 cycles, capacity delivered was 105 $mAhg^{-1}$. After 80 cycles, a decrease was observed due to the poor interface stability, and dendrite growth may occur.

Pal et al. (Pal and Ghosh 2017) reported the PMMA–$LiClO_4$-based polymer nanocomposite electrolyte with TiO_2 as nanofiller using solution cast technique. XRD diffractograms depict complete dissociation of salt, and PMMA peak broadens with the addition of nanofiller. The addition of 1 wt. % TiO_2 evidences the optimum enhancement of the amorphous content. Further, TEM analysis evidences the nonuniform distribution and clustering, with no effect on particle size with nanofiller loading.

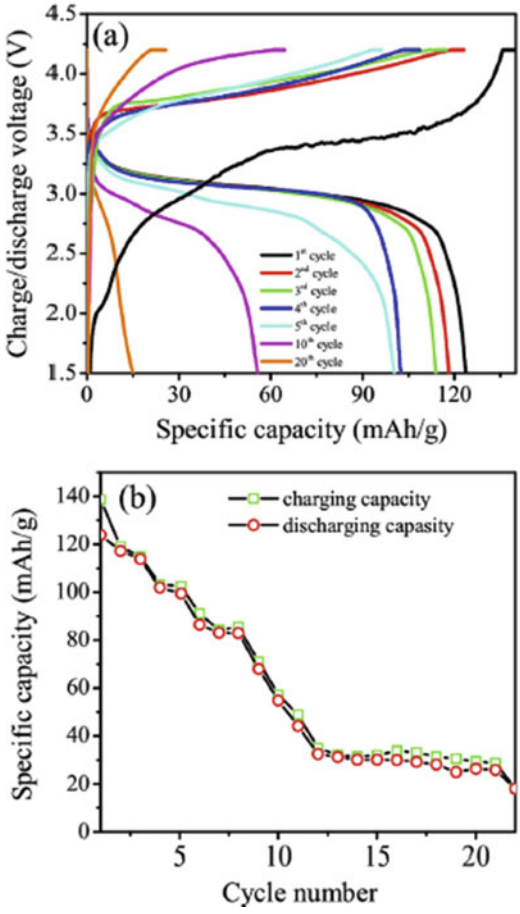

Fig. 8.7 (**a**) Charge–discharge profile at C/16 of graphite-plasticized PMMA–$LiClO_4$-1 wt% TiO_2–$LiCoO_2$ lithium–ion polymer coin cell at 25 °C. (**b**) Cycling performance of plasticized PMMA–$LiClO_4$-1 wt% TiO_2 electrolyte at C/16 at 25 °C. (With permission from (Pal and Ghosh 2017) Copyright © 2018 Elsevier)

The changes in the peak of pure PMMA (1732, 1492, 1444, 1385, 1192, 1150, 988, 966, 844, and 756 cm^{-1}, C=O asymmetric stretching of the carbonyl group, –CH_2 scissoring, O–CH_3 bending, -CH_2 twisting, C–O–C bending, carboxylic acid ester group, C–C symmetric stretching, –CH_2 wagging, –CH_2 asymmetric rocking, and –CH_2 rocking) with the addition of the salt and nanofiller in FTIR spectra confirm the presence of polymer–ion and ion–ion interactions. Also, the number of free charge carriers was more for low clay content and attributed to the cation interaction with electron-rich group of PMMA. DSC analysis shows a decrease of the T_g with the addition of nanofiller, while at high nanofiller content, increase is due to nanofiller cluster formation. TGA analysis shows thermal stability up to 250 °C and is in the desirable range for application purpose. The solid-state battery configuration with PMMA–$LiClO_4$- 1 wt% TiO_2 as electrolyte shows the discharge capacity of 123 $mAhg^{-1}$ for the first cycle and 136 $mAhg^{-1}$ for the first charging cycle with coulombic efficiency 100% (Fig. 8.7).

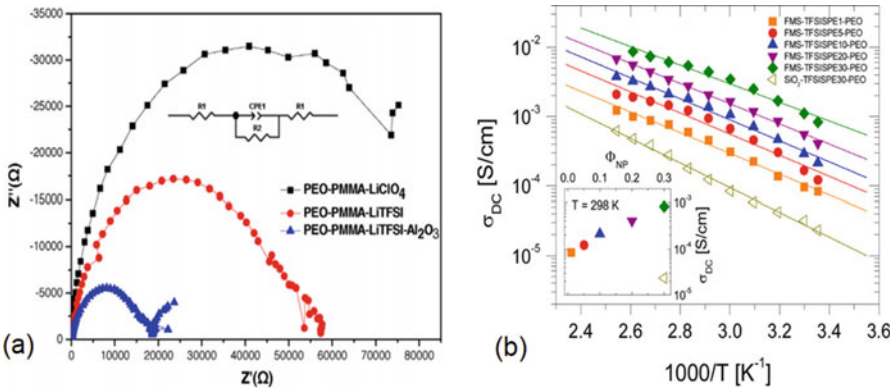

Fig. 8.8 (**a**) Impedance spectrum for the SS–PEO–PMMA–lithium salt (EO–Li^+ = 20)/SS cell at room temperature. With permission from (Liang et al. 2015) Copyright © 2015 Elsevier. (**b**) Temperature dependence of the ionic conductivities σ_{DC} of the nanohybrid electrolyte series (FMS-TFSISPE-PEO, filled symbols) with increasing amount of FMS-TFSISPE nanoparticles, Φ_{NP}, compared with σ_{DC} of the nonporous silica nanoparticle-based electrolytes (SiO_2-TFSISPE30-PEO, open symbols) (σ_{DC} at 298 K vs. Φ_{NP} in the inset). (With permission from (Kim et al. 2017) Copyright © 2017 American Chemical Society)

As a lot of reports are available by the addition of nonporous inorganic nanofiller, mesoporous nanoparticle may be a vital alternative and may fulfill the dream of single-ion conductor. So, the suppression of crystallinity along with immobilization of anion is simultaneously resolved by introducing the bulky imide group. Liang et al. (2015) prepared the PEO–PMMA-based polymer nanocomposites with two salts ($LiClO_4$ or LiTFSI), and nano-Al_2O_3 was used as nanofiller by solution cast technique. FESEM analysis showed the more uniform dispersion for PEO–PMMA–LiTFSIAl_2O_3 and a more even surface morphology which evidences the lowering of the interfacial resistance. Figure 8.8 a shows the impedance spectrum for the polymer-based electrolyte prepared at room temperature. The conductivity was increased with the nanofiller addition and is about 9.39×10^{-7} S cm^{-1}. This increase in the conductivity was due to the increased salt dissociation and increased flexibility. The thermal stability displayed by the TGA graph was above 300 °C and was improved after the addition of the nanofiller. Also, the higher stability was shown with LiTFSI salt as compared to the $LiClO_4$. The temperature dependence of the ionic conductivity follows Arrhenius behavior, and activation energy decreases from 20.10 kJ/mol to 10.96 kJ/mol. The voltage stability window of the prepared system was up to 4.9 V. Further mechanical analysis was analyzed from the stress–strain curves. The tensile strength was 2.84 MPa (PEO–PMMA–$LiClO_4$–Al_2O_3) with an elongation-at-break value at 31.7%. While for PEO–PMMA–LiTFSI–Al_2O_3 electrolyte, the tensile strength increased to 3.26 MPa (elongation-at-break value at 11.7%.) and is higher than the PEO–PMMA–LiTFSI (tensile strength = 2.78 MPa, elongation-at-break value at 9.5%).

Kim et al. (2017) reported the preparation of polymer nanocomposite using the functionalized mesoporous silica (FMS-TFSISPE) nanoparticles (av. size 50 nm)

with PEO as host matrix. The prepared films were transparent and display smooth surface morphology with optimum content 30 wt. %. DSC analysis evidences the single-glass transition temperature, and the absence of melting peak suggests its use in a wide range. Also, for 1 wt. % loading, it shows a comparatively better effect in suppressing the crystallinity as compared to nanofiller and may be due to the uniform distribution which lowers the reorganization of polymer chains. At high content, increase in the T_g was observed and was attributed to the formation of temporary cross-linking due to the high surface area and mobility reduces. The highest ionic conductivity was $\sim 10^{-3}$ S cm^{-1} (At 25 °C) for 30 wt % FMS-TFSISPE ($E_a = 26$ kJ/mol) and was ten times higher as compared to desirable limit (Fig. 8.8b). This was improved than the nonporous silica which displays conductivity $\sim 2 \times 10^{-5}$ S cm^{-1} (At 25 °C) ($E_a = 34$ kJ/mol). Also, the Li^+ transference number ($t_{Li}{}^+$) was ~0.9 and evidences the single-ion conductive matrix. This increase in conductivity and $t_{Li}{}^+$ with the mesoporous silica and porous nature along with large charge carriers overall supports the fast ion conduction. Further, mechanical properties were improved, and modulus was 3×10^4 Pa for 30 wt % FMS-TFSISPE and follows a relative trend with T_g. One attention-grabbing point was that both modulus and conductivity were improved simultaneously. It was concluded that the well-ordered mesoporous channel (high surface area and high pore volume) in the FMS-TFSISPE nanoparticles is superior's candidate for fulfilling the criteria of single-ion conductor where anion is in an immobilized state in the pore wall.

Tang et al. (2012) reported the preparation of polymer nanocomposite by dispersing the hybrid nanofiller (montmorillonite clay−CNT hybrid fillers) into PEO–$LiClO_4$ matrix. XRD analysis demonstrates the disruption of the crystallinity with the addition of nanofiller and may be due to the alteration in polymer chain arrangement. The FTIR evidenced the presence of strong interaction between the polymer matrix and cation and addition of hybrid nanofiller support in the smooth migration of the cation. The FTIR deconvolution evidence that for 10 wt. clay–CNT highest number of free charged were available for condition (Fig. 8.9a). This increase may be due to the negative surface charge layer on CNT and ether group which increases the salt dissociation rate (Fig. 8.9b). Another aspect is that there may be an increase of free volume due to less possibility of chain reorganization. This increase in free volume is linked with faster ion mobility as evidenced by the impedance analysis in terms of conductivity. The highest ionic conductivity was 2.07×10^{-5} S cm^{-1} for the optimum 10 wt. % clay–CNT, and with further increase, hybrid nanofiller aggregation occurs which lowers the conductivity value. The mechanical strength and elongation were also much higher as compared to pure PEO. This may be attributed to the principal characteristics of the hybrid nanofiller: (i) high aspect ratio, and (ii) rough surface. Both parameters lead to an improved interface between the polymer and nanofiller and hence the improved mechanical property.

Zhao et al. (2016) reported the preparation of the composite polymer electrolyte based on PEO–LiTFSI and $Li_{1.5}Al_{0.5}Ge_{1.5}(PO_4)_3$ (LAGP) as nanofiller. The highest ionic conductivity was 6.76×10^{-4} S cm^{-1} (at 60 °C) for LAGP-I, and it also has smaller particle size. Further, DSC analysis shows the lowering of the glass

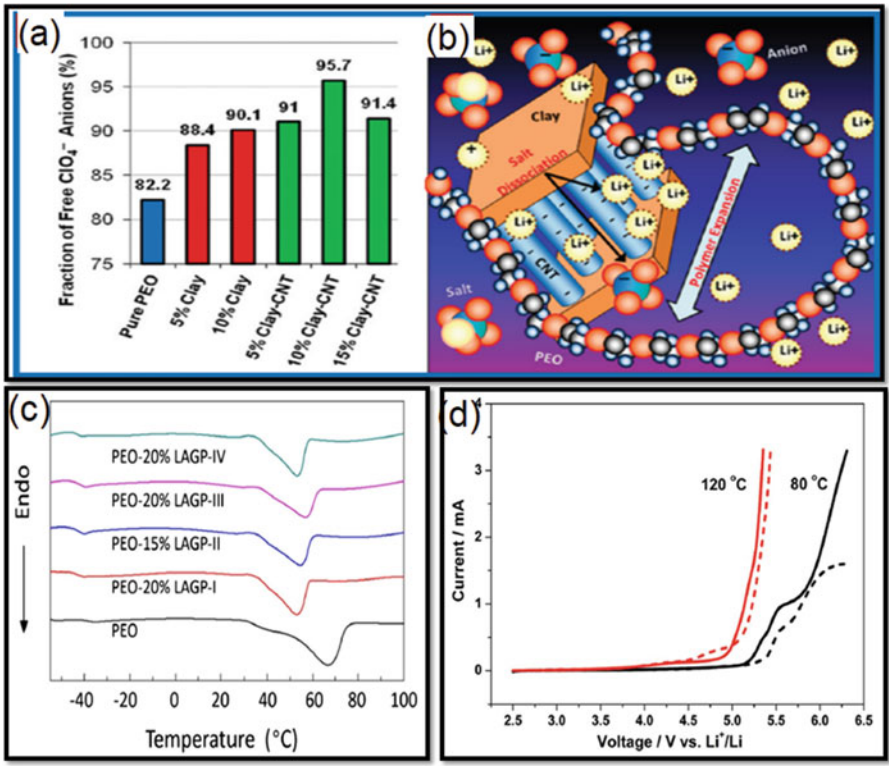

Fig. 8.9 (**a**) Fraction of dissociated salt ions (ClO_4^- anions) based on FTIR analysis of pure and filled PEO electrolyte. (**b**) Schematics of the interactions between clay, carbon nanotubes, polymer chains, and lithium salt ions. With permission from (Tang et al. 2012) Copyright © 2012 American Chemical Society. (**c**) DSC results for the electrolyte membranes. With permission from (Zhao et al. 2016) Copyright © 2016 Elsevier. (**d**) Linear sweep voltammograms of SS/PEO–LiTFSI/Li (solid line) and SS/PEO–MIL-53(Al)-LiTFSI/Li (dotted line) batteries at 80 °C (black) and 120 °C (red). The electrolytes were swept in the potential range from 2.5 V to 6.5 V (vs. Li–Li^+) at a rate of 10 mV s^{-1}. (With permission from (Zhu et al. 2014) Copyright © 2014 Royal Society of Chemistry)

transition temperature and melting temperature (−42 °C and 52.8 °C); this indicates that the increased amorphous content favors faster ion transport (Fig. 8.9c). The cation transference number was >0.36 and is attributed to the anion blockage. Fillers also play the role of the cross-linking network and increase the cation transference number by providing additional conducting pathways. The voltage stability window was 5.3 V for 20 wt. % LAGP-I. The electrochemical analysis of the $LiFePO_4$–PEO-20% LAGP-I–Li cell demonstrates capacities of 166, 155, 143, and 108 mAh g^{-1} at current rates of 0.1, 0.2, 0.5, and 1C, respectively, with capacity retention of cell 44% (after 50 cycles).

Zhu et al. (2014) reported the preparation of solid polymer electrolyte using the metal–organic framework aluminum 1,4-benzenedicarboxylate (MIL-53(Al)) is used as a filler with PEO as host polymer and LiTFSI (EO: Li ratio = 10, 15, 20,

25) as salt. SEM analysis suggests the uniform surface and morphology was unaltered with cylindrical particles. The ionic conductivity was 10 wt. % MIL-53 (Al) content for EO:Li ratio of 15:1 with value 1.62×10^{-5} S cm^{-1} (at 30 °C) and 9.71×10^{-4} S cm^{-1} (at 80 °C). This was also further supported by the lowering of phase transition temperature from 56.9 °C to 50.3 °C with the addition of MIL-53 (Al); and this enhances the amorphous content and hence the improved conductivity. The Li^+ transference number was increased from 0.252 to 0.343 with MIL-53(Al) addition and may be due to the formation of the metal–organic framework which enhances the ion mobility. Then the zeta electric potential measurement shows the pH is about 7, and it indicates that the MIL-53(Al) particles have strong Lewis acidic properties. This helps in the salt dissociation, while anion is coordinated with the Lewis acidic surface of the nanoparticle. The overall effect is the disruption of the crystalline nature and improved ionic conductivity. The electrochemical stability window of the polymer electrolyte was 5.31 V at 80 °C and 5.10 V at 120 °C with nanoparticle and is larger than the nanoparticle-free system which shows 5.15 V at 80 °C and 4.99 V at 120 °C (Fig. 8.9d). The thermal stability analysis evidences the thermal stability of about 200 °C with the first degradation beginning from 195 °C (decomposition of PEO) followed by degradation at 375 °C (decomposition of LiTFSI) (Shodai et al. 1994). Also, the mechanical properties were enhanced with nanoparticle addition and may be due to the formation of crossing-linking centers for PEO. Then the cyclic performance of the solid-state battery (LiFePO4–PEO–MIL-53(Al)-LiTFSI–Li) was tested, and the initial discharge capacity was 127.1 mAhg^{-1} (at 5 C and 80 °C) and 136.4 mA h g^{-1} at 120 °C. After 300 cycles, the discharge capacity was 116.0 mAh g^{-1} at 80 °C and 129.2 mAh g^{-1} at 120 °C. Even after 14 cycles, the retention ratios of 52.4% and 61.3%, respectively, were achieved at 80 °C and 120 °C.

Vignabooran et al. (2014) reported the preparation of the composite polymer electrolyte based on PEO-LiTf-EC-TiO_2. The purpose of this research was to study the combined effect of the plasticizer and the nanofiller, as both influence the polymer matrix in a different manner. The highest ionic conductivity was 4.9×10^{-5} S cm^{-1} for the 10 wt. % TiO_2 (at 30 °C, $E_a = 78.8$ kJ/mol) and was attributed to the Lewis acid–base character of the nanofiller surface. The nanofiller surface can affect in two ways: one is a reduction of the polymer recrystallization tendency and another is an increase of salt dissociation or lowering in ion pairing. Both simultaneously support the fast ion migration. Further addition of the EC increases the conductivity up to 1.6×10^{-4} S cm^{-1} for the 50 wt. % EC (at 30 °C, $E_a = 57.5$ kJ/mol). Further, DSC analysis supports the enhancement in the conductivity as both glass transition temperature (−46 °C to −50 °C) and the melting temperature (60 °C to 50 °C) show a decrease in the signal temperature with addition of the EC in TiO_2-based polymer matrix.

Another report by Klongkan et al. (Klongkan and Pumchusak 2015) investigated the effect of PEG–DOP plasticizer and Al_2O_3 nanofiller on the PEO–$LiCF_3SO_3$-based polymer matrix. DSC spectra shows the decrease of the crystallinity from 37.31% (PEO-15 wt.%$LiCF_3SO_3$) to 23.11% (PEO-15 wt.% $LiCF_3SO_3$-20 wt.% DOP) and 18.61% (PEO-15 wt.% $LiCF_3SO_3$-20 wt.%Al_2O_3). The decrease in

crystallinity on the addition of salt was due to the cation coordination with the PEO, and it alters the polymer chain arrangement and hence the increased segmental mobility. The addition of nanofiller increases slightly the T_g and T_m and that may be due to the cross-linking of the polymer chain while crystallinity reduction is observed (Kumar et al. 2011). The ionic conductivity increases from 1.00×10^{-6} S cm^{-1} to 7.60×10^{-4} S cm^{-1} (PEO-15 wt. % $LiCF_3SO_3$-20 wt.% DOP) and 8.64×10^{-5} S cm^{-1} (PEO-15 wt.% $LiCF_3SO_3$-20 wt.%Al_2O_3). This increase in the conductivity was attributed to increased amorphous phase with the addition of the nanofiller and the plasticizer. Further mechanical analysis supports both DSC and the conductivity data. The stress at maximum load, percentage strain at maximum load, and Young's modulus are 4.4 MPa, 3351%, and 15MPa, respectively, for the polymer matrix (PEO-15 wt% $LiCF_3SO_3$). This decrease was attributed to the disruption of the polymer chain sliding. Further addition of the DOP also lowers the mechanical properties, and that may be attributed to the effective role of the plasticizer which lowers the friction (increase the mobility), and it lowers the mechanical properties (Gondaliya et al. 2013; Ahmed et al. 2010).

Another report using the hybrid nanofiller was by Polu et al. (2017), and it was based on the effect of polyhedral oligomeric silsesquioxane-polyethylene glycol (POSS–PEG($n = 4$)) nanofiller on the physicochemical and electrochemical properties of PEO–LiDFOB-based nanocomposite solid polymer electrolyte. FESEM micrographs depict the change of morphology from rough (of PEO) to smoother on the addition of nanoparticle and may be associated with the complete dissociation of both salt and nanofiller. XRD analysis confirms the insertion of nanofiller in the polymer–salt matrix, and enhancement of amorphous content is achieved. Further DSC analysis confirmed the increased amorphous content and fast segmental motion. The highest ionic conductivity was 7.28×10^{-5} S cm^{-1} for 40 wt. % of the nanoparticle.

This increase may be attributed to the increased free charge carriers and the increased segmental motion of polymer chains. The increase in temperature increases the polymer flexibility and hence the increased conductivity that was evidenced by the reduction of activation energy from 0.594 eV to 0.433 eV with 40 wt. % nanoparticle. The electrochemical stability window of the prepared system was up to 4.7 V and is in the desirable range. The thermal stability window of the prepared PNC was ~200 °C (Fig. 8.10a). The stress–strain curve evidences the increase of stress from 0.076 to 0.099 MPa and elongation break from 472 to 516%. This may be due to the key role of nanofiller as a cross-linking center (Fig. 8.10b). The electrochemical analysis of the cell (Li/PEO:LiDFOB:x wt% POSS–PEG($x = 0$ and 40)/LCO–CBL) shows initial capacity up to 187 $mAhg^{-1}$ (for 0 wt. % nanofiller is 158 $mAhg^{-1}$), and after 50 cycles, discharge capacity was 143 $mAhg^{-1}$ (for 0 wt. % nanofiller is 122 $mAhg^{-1}$) with coulombic efficiency of 99 % at the 25th cycle.

Another report by Wang et al. (2017) explored the role of $Li_{1.5}Al_{0.5}Ge_{1.5}(PO_4)_3$ (LAGP) on the PEO (LiTFSI) in the suppression of Li dendrite growth. XRD evidences the decrease of the crystallinity. Figure 8.11a shows the process for the cell fabrication. Figure 8.11b shows the ion transport mechanism on the addition of

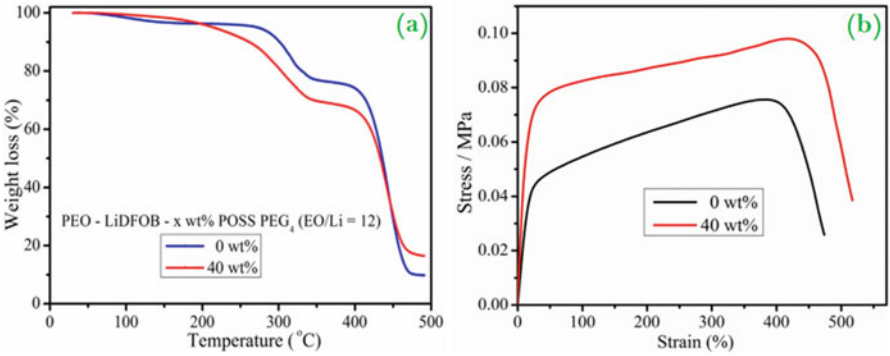

Fig. 8.10 (**a**) TGA heating traces 0 wt. % and 40 wt. % POSS–PEG doped PEO_{12}:LiDFOB electrolyte membranes and (**b**) stress–strain curves of PEO_{12}:LiDFOB and PEO_{12}:LiDFOB:40 wt. % POSS–PEG polymer electrolyte membranes. (With permission from (Polu et al. 2017), Copyright © 2017 Elsevier)

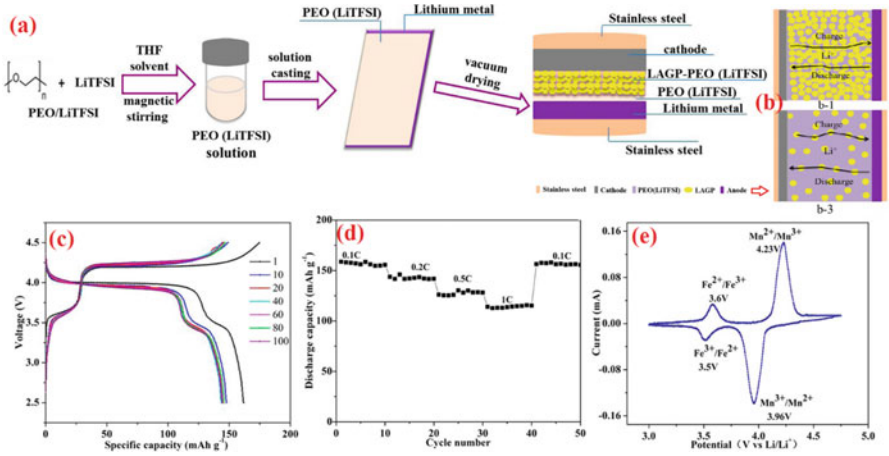

Fig. 8.11 (**a**) All solid-state Li–PEO (LiTFSI)/LAGP–PEO (LiTFSI)/LiMFP cells. (**b**) Li^+ ion transport mechanism in the composite solid electrolyte with different contents of PEO (LiTFSI): (b-1) LAGP–PEO1, (b-3) LAGP–PEO[5], (**c**) charge–discharge curves. (**d**) Rate performance of Li–PEO-500000(LiTFSI)/LAGP–PEO1/LiMFP cell (cutoff voltage: 2.5−4.5 V, 50 °C). (**e**) CV curve of LiMFP at a scan rate of 0.1 mV s^{-1} in 2.5−4.75 V at 50 °C. (With permission from (Wang et al. 2017) Copyright © 2017 American Chemical Society)

LAGP (for two systems), and the preferred path is a path having low activation energy. The voltage stability window was broader (~5.12 V) as compared to pure PEO. The electrochemical performance was investigated for the cell composition Li-PEO (LiTFSI)/LAGP–PEO1/LiMFP within the voltage 2.5−4.5 V (at 0.2 C, at 50 °C) as shown in Fig. 8.11c. The initial discharge capacity was 161.7 mAh g^{-1} (coulombic efficiency of 92.4%), and after 10 cycles, the coulombic efficiency was above 99%. Figure 8.11d shows the rate discharge performance of the Li–PEO-

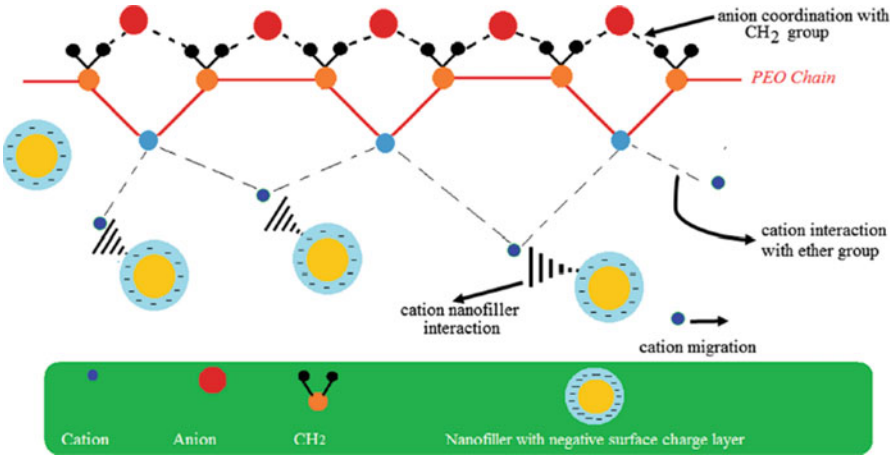

Fig. 8.12 Proposed interaction scheme in the polymer nanocomposite matrix. (With permission from (Arya and Sharma 2017c) Copyright © 2017 Springer)

500000- (LiTFSI)/LAGP–PEO1/LiMFP cell at 50 °C (at 0.1 °C, 0.2 °C, 0.5 °C, and 1.0 °C). Even at a high rate (1.0 °C), the discharge capacity was 115 mAh g^{-1}. Figure 8.11e shows the CV, which confirms the reversible process of Li^+ extraction and insertion. The oxidation peaks at 3.6 and 4.23 V (attributed to Fe^{2+} to Fe^{3+} and Mn^{2+} to Mn^{3+}), and the reduction peaks at 3.5 and 3.96 V (attributed to the reduction of Fe^{3+} to Fe^{2+} and Mn^{3+} to Mn^{2+}) agree well with the charge−discharge plateaus as shown in Fig. 8.11c.

Arya et al. (Arya and Sharma 2017c) investigated the effect of various nanofillers ($BaTiO_3$, CeO_2, Er_2O_3, TiO_2) on the PEO–PVC blend polymer electrolyte. The XRD analysis confirms the polymer nanocomposite formation. FTIR provides evidence of interaction among the functional groups of the polymer with the ions and the nanofiller in terms of shifting and change of the peak profile. The highest ionic conductivity is 2.3×10^{-5} S cm^{-1} with a wide electrochemical stability window of ~3.5 V for 10 wt. % Er_2O_3. Figure 8.12 shows the proposed ion transport mechanism. It depicts that the anion is going to coordinate with the polymer backbone while cation with the ether group of the polymer chain. Nanofiller with the surface group also helps in the salt dissociation, and polymer–ion–nanofiller interaction enhances the overall ion transport. Also, the coordinating interaction of the cation with the polymer chain modifies the polymer chain arrangement, and disorder is produced that evidences the increase in the polymer chain flexibility. The enhanced flexibility is an indication of the enhanced conductivity, and the fast segmental motion of the polymer chain provides a path for ion transport.

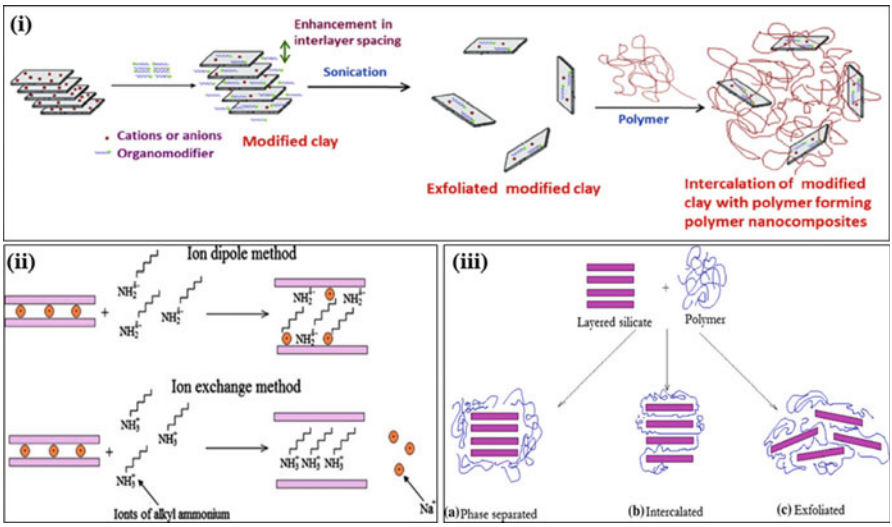

Fig. 8.13 (i) Schematic diagram showing clay modification and intercalation of polymer to form polymer nanocomposites. With permission from (Kotal and Bhowmick 2015) Copyright © 2015 Elsevier. (ii) Principles of modification of clay minerals and (iii) The level of intercalation–exfoliation of nanofiller in a polymeric matrix. (With permission from (Kubišovß et al., 2010) Copyright © 2010 Springer)

8.4.2 Nanoclay Dispersed Polymer Nanocomposites

As studied earlier, the nanofiller enhances the possibility of interaction between polymer–ions via the Lewis acid–base interactions. It alters the polymer chain arrangement, and the more free volume is available for the ion transport. Another important role is played by the surface group of the nanofiller, and it leads to the formation of the conductive continuous network. The overall enhancement is of the amorphous content that is beneficial for a fast solid-state ionic conductor. But with nanofiller, one issue is still there that is of dual-ion conduction. So, an alternative is the use of nanoclay instead of the nanofiller.

One important step before using the clay is its modification in which the covalent bonding between the clay layers is disrupted by the introduction of the surfactants or hydrophobic functional moieties. This increases the dispersion of nanoclay, and the overall aim is to increase the basal spacing so that polymer chain can be intercalated easily (Fig. 8.13a). Two approaches are shown in Fig. 8.13b: (i) ion-dipole method and (ii) ion-exchange reaction (Sharma and Thakur 2011; Kubišovß et al. 2010).

Nanoclay has two advantages: for one, it blocks the anion migration inside clay galleries (the only cation is available for conduction) and another is that polymer chain is intercalated inside the clay galleries so the polymer recrystallization tendency or crystallinity is reduced. Both the above properties lead to enhancement of the ion transport and hence the ionic conductivity. The high cation-exchange capacity of the clay supports the intercalation and swelling of the polymer chains.

The combined effect of them increases the dispersion of the nanoclay with the polymer matrix. By monitoring the separation of layers (basal spacing; d_{001}), four types of polymer nanocomposites with nanoclay are obtained (Fig. 8.13b) (Kotal and Bhowmick 2015; Pinnavaia and Beall 2000; Chen et al. 2008).

1. If there is no change in the basal spacing with the addition of clay and clay layers remain outside, then the PNC is *conventional* PNC.
2. If the basal spacing increases with nanoclay and clay layers are stacked with polymer chain intercalated between layers, then it is called *intercalated* PNC. This type of PNC leads to building up of the nanometric channels for cation transport and disrupts the recrystallization tendency of the polymer chains.
3. If the clay layers are completely in the disordered state as well as the polymer chains, then the PNC is *exfoliated* PNC. This type of PNC lowers the ion-pairing effect.
4. If the long molecular chains get intercalated inside the two or more clay galleries, then it is called *flocculated*-type PNC.

Besides this, the nanoclay such as halloysite nanotube (HN) and montmorillonite (MMT) clay are gaining more intention in the formation of the polymer nanocomposites, and the main influence is on the thermal, electrical, and the mechanical properties. The interaction mechanism behind the nanoclay is the formation of the electrostatic interactions between the charges present on the nanoclay surface and the electron-rich group of the host polymer. This interaction disrupts the weak dipolar and van der Waals forces between clay sheets. As now polymer gets intercalated between the clay sheets and prevents the direct impact on the polymer on heating, the improved properties are achieved (Choudhary and Sengwa 2014; Sengwa and Choudhary 2014a; Fan et al. 2002; Shukla and Thakur 2010; Dam et al. 2015; Fu et al. 2016; Sharma et al. 2008).

In the formation of the PNC, preparation method plays an effective role in altering the chain arrangement. So, Dhatarwal et al. (2017) reported the preparation of the polymer nanocomposite (PNC) solid polymer electrolyte based on PEO–PMMA–$LiBF_4$+ 10 wt.% EC and 3 wt.% MMT clay by solution cast (SC) and the ultrasonic–microwave irradiated (US–MW) solution cast methods. XRD analysis suggests the complete dissolution of the salt as there was no peak corresponding to the salt ($2\theta = 26.33^\circ$) (Figure 8.14). Pure MMT shows the peak at $2\theta = 7.03^\circ$ (001; plane) and is also observed in the PNC prepared by SC technique along with two main peaks of PEO ($2\theta = 19.43^\circ$ and $2\theta = 23.57^\circ$).

Further, for the PNC, the MMT peak shifts toward lower angle by more than 2° as compared to that of the pristine MMT, and the increase of the d-spacing evidence the formation of the intercalated structure. The SC methods display the high intensity of MMT, while US–MW methods show a diffused peak with low intensity. The former one is evidence of the intercalated structure, while the latter one is an indication of the exfoliated structures (Sengwa et al. 2015). It was concluded that the increased basal spacing, crystallite size, and the relative intensities were increased for the PNC prepared by the US–MW method. Further, from the impedance spectra, it was founded that the conductivity was more for the intercalated-type PNC and supports

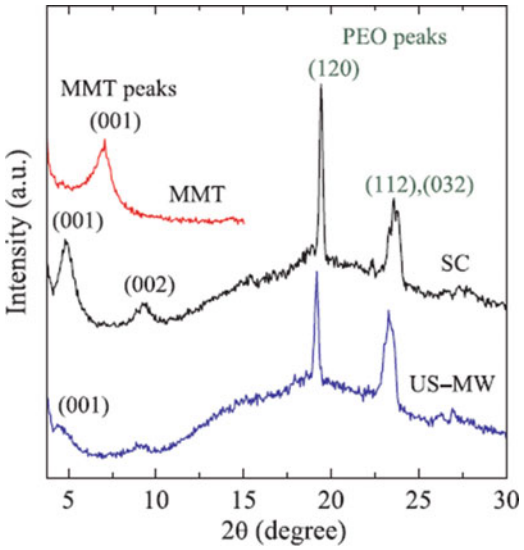

Fig. 8.14 XRD patterns of MMT nanopowder and (PEO–PMMA)–LiBF4–10 wt. % EC–3 wt. % MMT films prepared by SC and US–MW methods. (With permission from (Dhatarwal et al. 2017) Copyright © 2017 Elsevier)

faster ion migration as compared to the exfoliated-type PNC, and hopping mechanism seems to be followed as indicated by the value of n. So, the preparation methods influence the ion mobility, and intercalated type is more beneficial as compared to the exfoliated type which hinders the ion migration.

Erceg et al. (2014) prepared the composite polymer electrolyte based on poly (ethylene oxide)–lithium montmorillonite (PEO–LiMMT) by melt intercalation technique. The small-angle X-ray scattering (SAXS) evidenced the increase of the interlayer spacing due to polymer chain intercalation inside the clay galleries with a maximum of about 1.88 nm, while the interlayer distance was 0.93 nm (maximum). DSC analysis displays the powering of the melting temperature and indicates the disruption of the crystallinity after addition of clay (76.1% to 37.1%). FTIR spectrum evidences the broadening in the spectrum in region 3000 and 2750 cm^{-1} and 1500 cm^{-1} to 2000 cm^{-1}, while some new peaks were observed after clay addition. It confirms the existence of a crystalline phase and gets broadened with clay addition indicating the change of the crystallinity. The highest ionic conductivity was 2.8×10^{-6} S cm^{-1} for 40 wt. % clay content and may be due to the proper dispersion of nanoclay, while at higher content, self-aggregation of clay layers traps the cation and hence the lowering of the ion mobility.

Sengwa et al. (Sengwa and Choudhary 2014b) prepared the solid polymer nanocomposite electrolytes (SPNEs) based on poly(methyl methacrylate) (PMMA) and lithium perchlorate ($LiClO_4$) with varying concentrations of montmorillonite (MMT) clay by solution casting and high-intensity ultrasonic-assisted solution casting methods. XRD analysis evidences the complete dissociation of the salt, and the exfoliation of clay was attributed to the interactions of polymer–salt complex ($C{=}O{-}Li^+$) with the MMT nanosheet surfaces. Impedance analysis suggested that the current carriers are ions which govern the total electrical conductivity of these

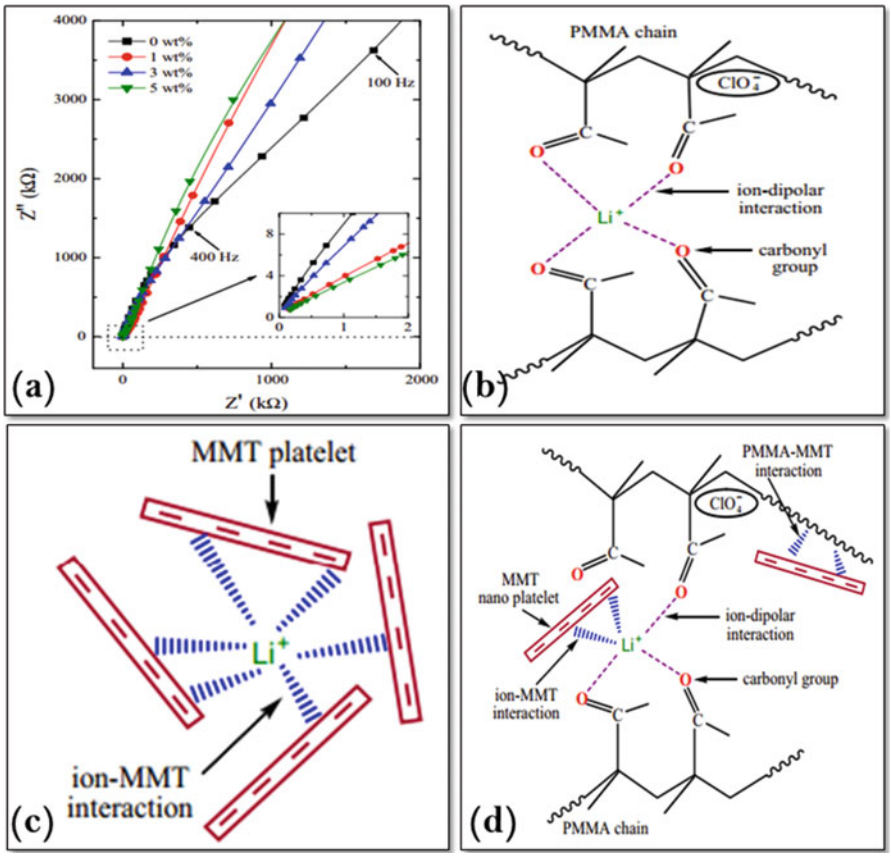

Fig. 8.15 (**a**) Complex impedance plane plots (Z″ vs. Z′) of PMMA–$LiClO_4$–x wt. % MMT films prepared by solution cast (SC) method and schematic illustration of PMMA–LiClO4–MMT interactions: (**b**) C=O–Li^+ complexes, (**c**) Li^+–MMT complexes, and (**d**) C=O–Li^+–MMT complexes. (With permission from (Sengwa and Choudhary 2014b) Copyright © 2014 Elsevier)

electrolytes with value about 10^{-5} S cm^{-1}. Figure 8.15a displays the impedance of the sample prepared by the solution cast method. The proposed mechanism supports the enhancement of the conductivity with the addition of clay. Figure 8.15b shows the cation coordination with the C=O in PMMA–$LiClO_4$ domain, while anion is somewhere in the polymer backbone as an uncoordinated form. Figure 8.15c displays the cation coordination with the MMT domain, and exfoliated structure is observed. Figure 8.15d demonstrates the PMMA–Li^+–MMT interactions.

Lin et al. (2017) reported the preparation of nanocomposite using halloysite nanotube (HNT; 10–50 nm outer diameter and 5–20 nm inner diameter, with a length of 50–1000 nm) clay in PEO–LiTFSI-based polymer matrix. The highest ionic conductivity was 1.11×10^{-4} S cm^{-1}, 1.34×10^{-3} S cm^{-1}, and 2.14×10^{-3} S cm^{-1} at 25, 60, and 100 °C, respectively, for 10 % HNT (Fig. 8.16b). This increase

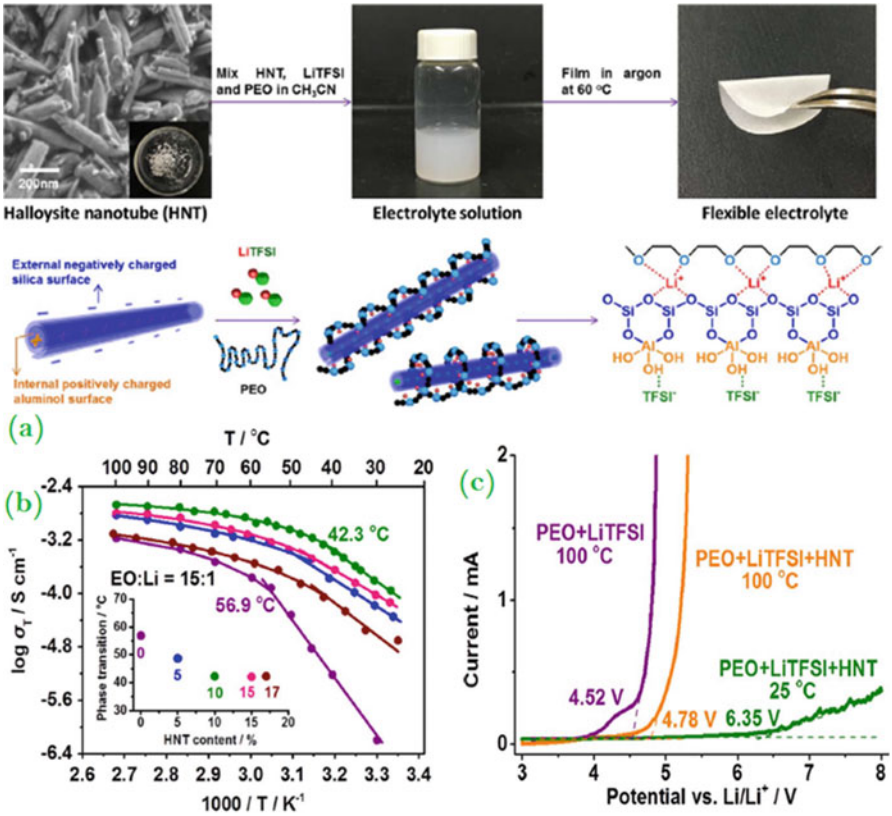

Fig. 8.16 (**a**) Preparation of HNT-modified flexible electrolyte and mechanism of HNT addition for enhanced ionic conductivity. The halloysite nanotube, LiTFSI, and PEO are mixed in the solvent to form a uniform electrolyte solution. The solution is cast in an argon atmosphere to produce a flexible electrolyte thin film and lithium–ion transport for HNT nanocomposite electrolytes. (**b**) Ionic conductivities of the PEO+LiTFSI+HNT films with different HNT contents at EO:Li = 15:1 as a function of temperature inset are the phase transition temperature as a function of HNT content obtained after fitting. (**c**) Linear sweep voltammetry Li–PEO+LiTFSI+HNT–SS cells at 25 °C and 100 °C, and Li–PEO+LiTFSI–SS cells at 100 °C at a rate of 10 mV s^{-1}. (With permission from (Lin et al. 2017) Copyright © 2017 Elsevier)

of the conductivity was evidenced further by the optical images which show the decrease of crystal size with the addition of HNT ($Al_2Si_2O_5(OH)_4$). The Li^+ transference number was also increased from 0.25 to 0.40 on the addition of HNT. The voltage stability window of the composite polymer electrolyte was 6.35 at 25 °C and decreased to 4.78 V at 100 °C (Fig. 8.16c). Figure 8.16b explores the increase of conductivity with the addition of HNT. The HNT has two face surfaces: one has a –Si–O–Si– silica tetrahedral sheet and another has –Al–OH groups from the octahedral sheet known as outer and inner surface, respectively (Figure 8.16a). The presence of opposite charge on the HNT surface separates the ion pairs, and cation

gets associated with the negatively charged silica surface (–Si–O–Si–), while the anion gets associated with the inner surface (–Al–OH). Also, the electron-rich ether group of PEO interacts with the cation, and 3D network formed here supports the ion migration. The overall impact is the disruption of the crystalline phase due to the reduction of the crystallinity and hence the low ion pair formation. Another point mentioned here was that HNT helps in improving the mechanical property with uniform surface. Also, the zeta potential measurements show increase from negative to positive, and this evidences the adsorption of ions on the HNT surface. The thermal stability window was ~400 °C. The stress after the addition of HNT increases from 1.25 MPa to 2.28 MPa with 400% strain and displays good flexibility of the investigated polymer matrix. The initial discharge capacity of the cell was 1350 mAh g^{-1} and with an average value of 745 ± 21 mAh g^{-1} in the 100 discharge–charge cycles, with 87% retention. While at 100 °C, the initial discharge capacity was 1493 mAh g^{-1} and was 386 mAh g^{-1} after the 400 discharge–charge cycles. It was concluded here that the natural HNT clay mineral provides the desirable energy density at low cost with improved safety.

Gomari et al. (2017) reported the preparation of nanocomposite solid polymer electrolyte based on poly(ethylene) oxide (PEO) and lithium perchlorate salt ($LiClO_4$) with pristine graphene (GnP) or polyethylene glycol-grafted graphene (FGnP). From FESEM analysis of the nanocomposite, it was concluded that the rough surface of the pristine PEO changes to smooth on the addition of GnP–FGnP and suggests the better dispersion of both. Another reason behind this may be the presence of the hydrogen interactions between the electron-rich group of host polymer and PEG groups of FGnP. XRD analysis evidences the decrease of the crystallinity with the addition of GnP, and more decrease was observed for the FGnP-based polymer nanocomposite. Further evidence provided by the DSC analysis demonstrates no change in the glass transition–melting temperature with a dispersion of GnP addition, while FGnP dispersion displays shift toward lower temperature of both glass transition–melting temperature. This may be associated with the better dispersion of the FGnP as compared to the GnP which enables sufficient interactions with the PEO. The lowering of the T_g indicates an increase of ion mobility or polymer flexibility owing to the increased free volume. The polarized optical microscopy also supports both XRD and DSC results as suppression of spherulitic growth in the presence of graphene nanosheets was obtained as compared to PEO. Further deconvolution of the anion peak in the FTIR spectra confirmed the increase of free charge carriers with FGnP which participate in conduction and was attributed to the interaction of PEO as well as additional coordinating sites provided by PEG. The ionic conductivity was 8.19×10^{-6} S cm^{-1} for 0.1 % GnP and 2.53×10^{-5} S cm^{-1} for 0.5 % FGnP. The increase in the conductivity was associated with the additional coordinating sites provided by the PEG, and an ion conduction channel formation supports the faster segmental motion. The stress–strain curve reports the increase of stiffness and was 74% and 83% increase for GnP and FGnP at 0.5 wt %, respectively.

Kim et al. (Kim and Park 2007) reported the preparation of the polymer composite electrolyte based on the poly(ethylene oxide) (PEO)–$LiClO_4$ and different

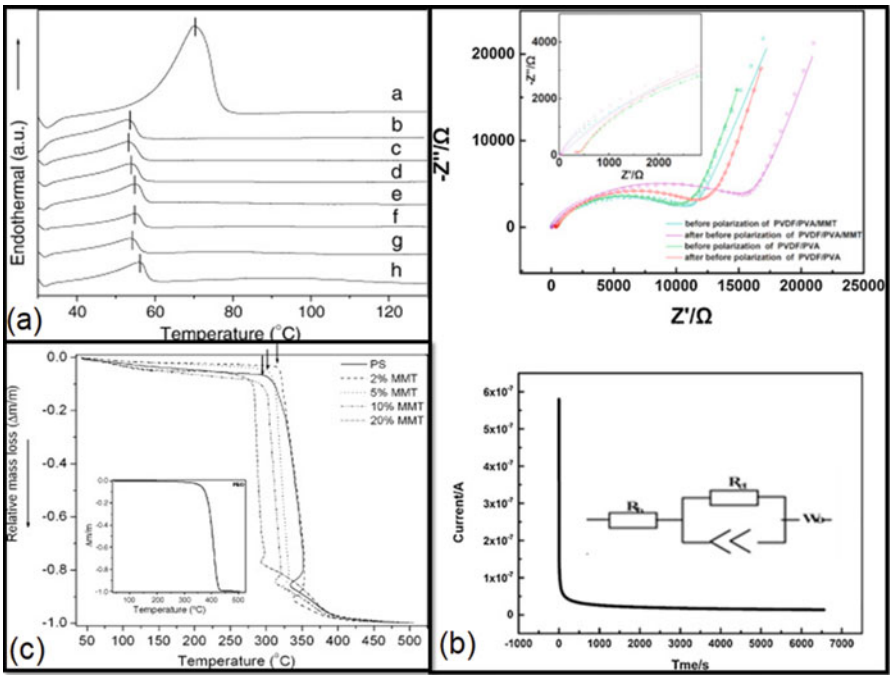

Fig. 8.17 (**a**) DSC curves of (a) pure PEO and PCEs containing (b) 0%, (c) 2%, (d) 5%, (e) 10%, (f) 15%, (g) 20%, and (h) 25% of Li–MMT. With permission from (Kim and Park 2007) Copyright © 2007 Elsevier. (**b**) AC impedance behaviors of polymer electrolytes based on casting PVDF–PVA–MMT CSPE. With permission from (Ma et al. 2016) Copyright © 2016 Elsevier. (**c**) Thermogravimetric analysis (TGA) plots of polymer–salt complex (PS) and polymer-based nanocomposite (PNCE) films having different clay concentrations compared with TGA pattern of pure PEO (inset). (With permission from (Mohapatra et al. 2009) Copyright © 2009 Elsevier)

contents of the lithium–montmorillonite (Li–MMT) clay. The absence of the Na peak in EDS spectra evidences the de-intercalation of Na and the intercalation of the Li–ion. XRD analysis suggested the decrease of the interlayer spacing from 32.43 to 25.66 Å with increase of the clay content from 10 to 25 wt.% and evidences difficult for polymer intercalation in the clay gallery. Further, for 20 wt.% of nanoclay content, fundamental peak of PEO is broadened, and intensity is reduced. It evidences the decrease of the crystallinity value. This was further supported by the DSC data which demonstrates the shift of the melting peak toward lower temperature (for pure PEO 65.4 °C to 52.2 °C) and decrease of crystallinity with lowest for 20 wt. % clay content (for pure PEO 53.97% to 37.73%). Figure 8.17a depicts the DSC results with different clay contents. The thermal stability of the PCE was up to 200 °C. The highest ionic conductivity was obtained for the 20 wt. % clay content and is about 5.3×10^{-6} S cm^{-1}. Further, the temperature variation of the conductivity follows the Arrhenius behavior, and activation energy decreases with the addition of clay content (0.70 to 0.19 eV, below 60 °C). The cation transference number (t_{Li+}) was 0.55, and this high value of cation transference number was attributed to the poor

interaction of cation with ether group of PEO owing to the clay interaction with ether group.

Ma et al. (2016) prepared the composite solid polymer electrolyte (CSPE) based on montmorillonite (MMT) nanoclay fillers, lithium-bis(trifluoromethanesulfonyl) (LiTFSI), polyvinylidene difluoride (PVDF), and polyvinyl alcohol (PVA) copolymer by the casting method. FESEM analysis evidences the porous structure that will be beneficial for the cation transport. Further, the addition of MMT to blend polymer matrix lowers the crystallinity and indicates the increased amorphous content. The ionic conductivity also increases with the addition of MMT, and highest conductivity was 4.31×10^{-4} S cm^{-1} for 4 wt. % clay content. The increase in the conductivity value was due to the high surface area of the nanoclay which increases in the free volume and the amorphous content. These together lead to smoother ion transport and hence high ionic conductivity. The activation energy value decreases with the addition of MMT from 26.46 kJ to 16.22 kJ and evidences the faster ion migration. The cation transference number increased from 0.29 to 0.40 with the addition of the MMT (Fig. 8.17b). The displacement load curve evidenced the increase of the tensile strength from 1.17 MPa to 2.24 MPa with the addition of clay and is attributed to the improved stability. The Li–CSPE–$LiFePO_4$ cells show pretty high specific discharge capacity above 123 mAhg^{-1} along with a coulombic efficiency of 97.1% after 100 cycles.

Mohapatra et al. (2009) reported the preparation of the PEO–$LiClO_4$-based composite polymer electrolyte with organo-modified montmorillonite clay using solution cast technique. XRD analysis evidenced the complex formation, and shift in the peak of the hot matrix shows the effective role played by clay. The decrease of the peak intensity evidences the reduction of the crystallinity due to the polymer and the nanoclay interaction. The d-spacing was almost the same in all systems, while the crystallite size decreases, and clay gallery width was maximum for the 10 wt. % clay content (9 Å). Further, the polymer–salt intercalation in the clay galleries was evidenced and was due to the dipolar interaction. It was concluded from the XRD that the prepared PNCE films have a multiphase combination of crystalline and amorphous PS phases, an amorphous phase boundary, crystalline clay, and amorphous PS inside the clay galleries at the interface of the clay layers and PS matrix. Further, TEM analysis provides strong evidence of the intercalation along with exfoliation at low clay content. At very high clay content (>20 wt. %), clay cluster formation was reported. DSC analysis displayed the lowering of the glass transition temperature (T_g) owing to the enhanced flexibility assisted by intercalation on nanocomposite formation. The highest ionic conductivity was 6.48×10^{-5} S cm^{-1} for 10 wt. % clay content (at 30 °C). TGA analysis shows the thermal stability of the composite polymer electrolyte up to 300 °C and is sufficient for the application purpose (Fig. 8.17c). The cation transference number was 0.50 at 2 wt. % clay content. And voltage stability window was about 3 V. The thermal stability was improved after the polymer chain intercalation inside clay galleries. This may be attributed to the barrier role played by clay layers which prevent the decomposition of the polymer–salt complex. Another reason may be the catalytic effect in which the clay layers accumulated all heat and prevent the decomposition of the polymer slats system.

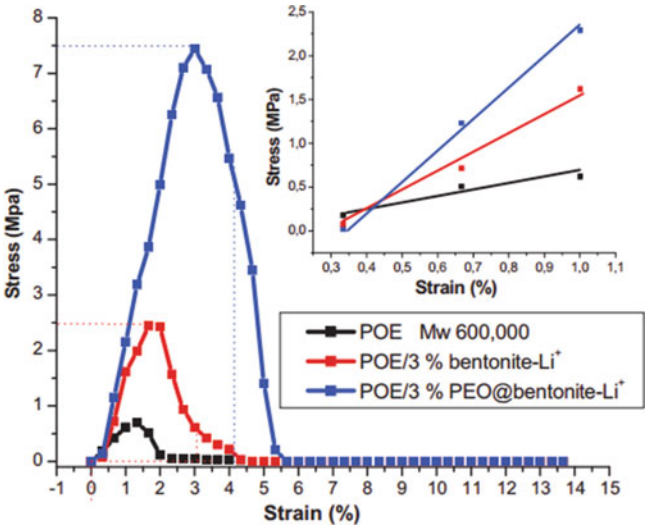

Fig. 8.18 Tensile stress–strain behavior of films of PEO and SPEs with bentonite-Li+ and PEO@bentonite-Li^+ with PEO Mw 600,000. (With permission from (Moreno et al. 2011) Copyright © 2011 Elsevier)

Sharma et al. (Sharma and Thakur 2010) reported the preparation of the polymer nanocomposites based on $(PAN)_8LiCF_3SO_3$ -x wt %DMMT. From XRD analysis, the increase in the interlayer spacing and the clay gallery width was observed. This increase was attributed to the polymer chain intercalation in the clay nanometric clay galleries. The ionic conductivity was highest for the 7.5 wt. % clay content and is about 6.8×10^{-3} S cm^{-1}. The ion transference number was close to unity and evidence the dominance of the ionic nature of the electrolyte. The cation transference number was 0.67 and is an indication of proper dissociation of the salt after polymer chain intercalation inside clay galleries. The voltage stability window was 5.6 V, and thermal stability window was approx. 200 °C.

Moreno et al. (2011) prepared the polymer nanocomposite based on the PEO (with molecular weight 600,000 and 4,000,000) bentonite. XRD analysis demonstrated the absence of peak associated with the bentonite confirmed the polymer intercalation inside clay galleries. Figure 8.18 shows the tensile stress–strain curves for PEO Mw 600,000 SPE films. The Young's modulus and the tensile strength (MPa) of the PEO–PEO@bentonite-Li^+ were 325 ± 32.5 MPa and 7.5 ± 0.75 MPa, while the PEO–bentonite-Li^+ was 247 ± 24.7 MPa and 2.9 ± 0.29 MPa. Compared with the PEO–bentonite-Li^+, the ionic conductivity of the PEO–PEO@bentonite-Li^+ increased from 3.89×10^{-8} to 1.81×10^{-7} S cm^{-1} at 25 °C. It can be seen that the mechanical properties improved after the addition of 3 wt. % bentonite.

Zhang et al. (2015) reported the preparation of solid polymer electrolyte comprising of PEO, LiTFSI, and MMT. The XRD analysis evidences the increase of the interlayer spacing that confirms the polymer intercalation and hence increases of the

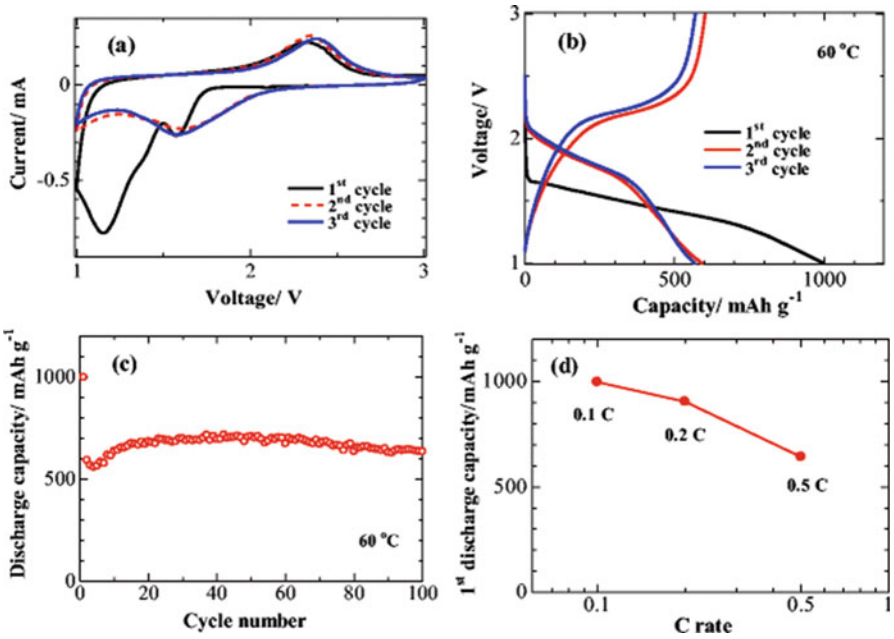

Fig. 8.19 (**a**) Initial CV profiles of all solid-state Li–S cell at 60 °C; the measurement is conducted at a scan rate of 0.1 mV s^{-1} in the voltage range of 1.0 to 3.0 V vs. Li^+–Li; (**b**) Charge–discharge profiles (at 0.1 °C) of all solid-state Li–S cell at 60 °C; (**c**) Cycle performance (at 0.1 °C) of all solid-state Li–S cell at 60 °C; (**d**) Rate capability of all solid-state Li–S cell at 60 °C. (With permission from (Zhang et al. 2015) Copyright © 2014 Springer nature)

amorphous content. The highest ionic conductivity was 3.22×10^{-4} S cm^{-1} at 60 °C for 10 wt. % MMT and cation transport number (t_{Li}^+) was 0.45.

The voltage stability window of the optimized electrolyte was 4 V. The cyclic voltammograms (CV) of the cell show good electrochemical stability in the operating range (Fig. 8.19a). The galvanostatic charge–discharge cycling tests in Fig. 8.19b show the specific capacity of 998 mAh g^{-1} (at first discharge at 0.1 °C) and a reversible capacity of 591 mAh g^{-1} (for second cycle). Figure 8.19c shows the initial increase in capacity which indicates the gradual activation of the electrochemical properties of polymer electrolyte electrochemical and is attributed to the cation dynamics in the polymer matrix. Even after 100 cycles, a high reversible specific discharge capacity (634 mAh g^{-1}) with 63.5 % capacity retention is noticed. Figure 8.19d displays the rate capability of cells (at 0.1, 0.2, and 0.5 °C) and is sufficient for the fabricated cell.

8.4.3 Nanorod–Nanowire Dispersed Polymer Nanocomposites

As a lot of reports are available on the dispersion of nanofiller in the polymer electrolyte matrix which provides in hand the superior properties as compared to the micro fillers there are three fundamental mechanisms which dominate here: (i) creation of percolation pathways, (ii) reduction of polymer reorganization tendency, and (iii) aspect ratio or shape of the nanoparticle. As nanofiller surface has acidic and basic sites which play an effective role in the ion transport or mobility in case of polymer electrolytes, these sites support the formation of conducting pathways for the ion transport. These paths are termed as percolation pathways. As the nanofiller surface groups alter the existing interaction between the polymer chains and the polymer–ion, this lowers the chain reorganization tendency and provides smoother transport. Another key role is played by the aspect ratio of the nanoparticle. As it is well known that the nanofiller have a high aspect ratio as compared to the micro fillers, the aspect ratio is in inverse relation with the percolation threshold. Also, the optimum or critical concentration is lower for the nanoparticles with high aspect ratio due to increased size distribution (Celzard et al. 1996; Liu et al. 2015, 2016, 2017; Do et al. 2012).

The mechanism behind the improved conductivity on the addition of nanofiller highlights the interaction electron-rich group of host polymer with the surface group of nanofiller. This supports the salt dissociation, and more free charge carriers are available for conduction. Another important role played by nanofiller is the disruption of the recrystallization tendency of the polymer chain arrangement, and hence the amorphous content is increased which favors the smoother and faster ion migration. So, the percolation pathways created by the nanofiller are beneficial for the faster ion transport. It can be concluded from here that the larger the percolation path, the faster will be the ion migration due to the long continuous path. This will depend on the coordinating sites (acidic–basic) available to favor the ion mobility and sufficient salt dissociation. Another remarkable point here is that the suitable control over the acidic–basic sites of nanofiller can lead to the improved electrical properties. Also, the alignment of the nanorod and nanowire is important as the aligned nanoparticle parallel to the electrodes limits the perpendicular ion migration. The nanoparticles with the different aspect ratio and shape also alter the mechanical properties that are further altered by the alignment of nanorod–nanowire–nanotube.

Beyond the active–passive nanoparticle, one another attractive approach is the use of 1 D nanofiller for enhancing the electrical properties. So, regarding this, Liu et al. (2015) reported the dispersion of LLTO ($Li_{0.33}La_{0.557}TiO_3$) nanowire in the PAN–$LiClO_4$-based polymer–salt matrix. XRD analysis provides no alteration in the peak of pure PAN with the addition of nanowire, and SEM micrograph displays the uniform distribution of NW and is fully embedded in the polymer matrix evidenced by TEM (Fig. 8.20a–f). The highest ionic conductivity was 2.4×10^{-4} S cm^{-1} (15 wt. % LLTO) and is three orders higher than the polymer–salt matrix without NW. AT high NW, content lowering of conductivity is observed and may be

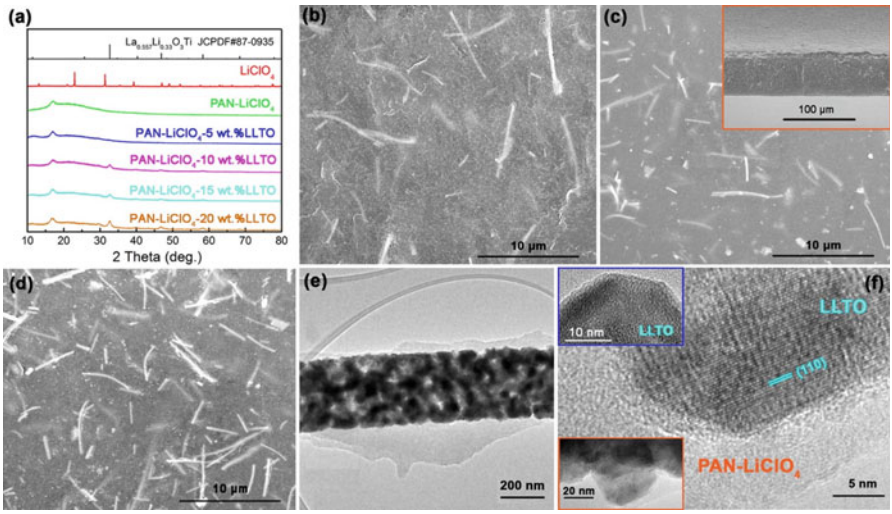

Fig. 8.20 Phase structure and morphology of the composite electrolytes with various contents of LLTO nanowires. (**a**) XRD patterns of the composite electrolytes with various LLTO concentrations of 5−20 wt %. SEM images for the composite electrolytes with (**b**) 10 wt %, (**c**) 15 wt %, and (**d**) 20 wt % nanowire fillers. (**e**) TEM image and (**f**) HRTEM image of the composite electrolyte with 15 wt % nanowires, respectively. In panel f, the upper inset is the HRTEM image for LLTO nanowire, and the bottom one illustrates the individual grain of the nanowires embedded in PAN matrix. (With permission from (Liu et al. 2015) Copyright © 2015, American Chemical Society)

associated with the aggregation of NW and incomplete dissolution of polymer with NW. Further, the dehydration temperature was correlated with the crystallinity, and it was concluded that the disruption of the crystallinity was not the dominant factor for enhancement of the conductivity and is also confirmed by the XRD. This enhancement in the conductivity was explained with the oxygen vacancy-rich surface of the nanowire. These vacancies help in the salt dissociation, and oxygen vacancy helps in smoother ion migration and hence faster ion mobility. The voltage stability window was increased from 4.8 V (for NW free) to 5.5 V (wt. 10 wt. % NW).

So, keeping this in mind, Do et al. (2012) prepared the nanorod (α-Fe_2O_3 nanofiller with aspect ratio 7) so that the desired improvement can be achieved at low critical concentration. For better comparison, both nanoparticle (NP; diameter 20–30 nm) and nanorod (NR; diameter 10–20 m) were dispersed separately as nanorod has a higher aspect ratio which is associated with the longer percolation paths available for the conduction. Figure 8.21 a and b depicts the FESEM image of NR (average length and diameter of 105 $\pm$ 32 and 16 $\pm$ 5.4 nm, aspect ratio 6.6) and NP with average diameter 29 $\pm$ 11 nm. The ionic conductivity variation with the temperature suggests that the maximum conductivity was achieved with NR even at a lower content than the NP (Fig. 8.21c, d). This may be attributed to the formation of a sufficient number of conducting pathways at low concentration owing to the high aspect ratio of NR as compared to NP. Also, at high concentration, there is a

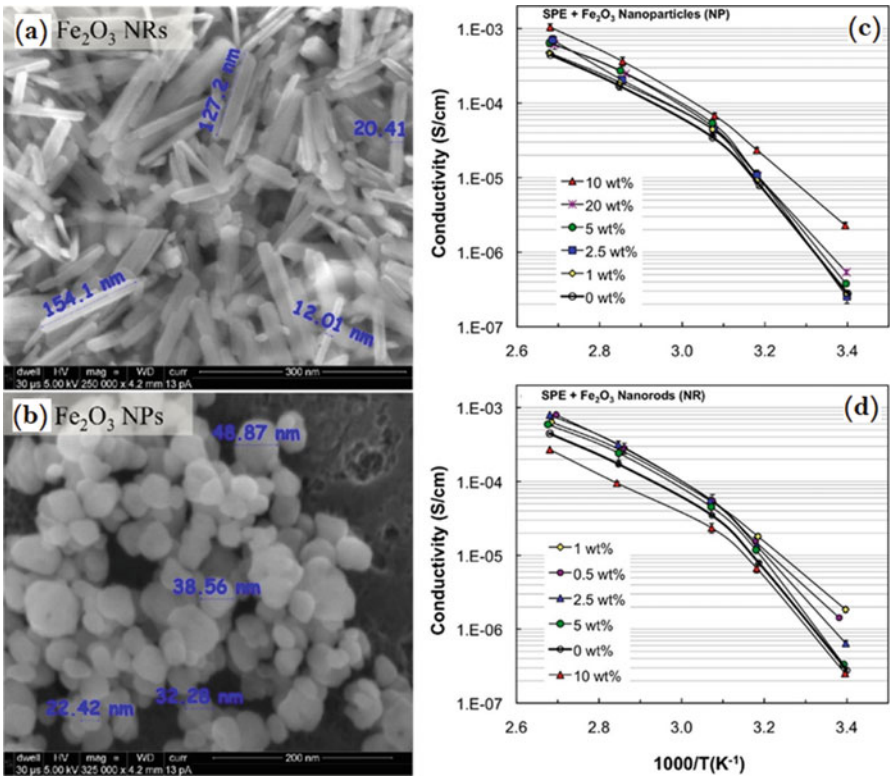

Fig. 8.21 Scanning electron micrographs of (**a**) α-Fe_2O_3 nanorods (NR) with average length 105 ± 32 nm and average diameter 16 ± 5.4 nm and (**b**) α-Fe_2O_3 nanoparticles (NP) with average diameter 29 ± 11 nm. The error represents one standard deviation from the mean and ionic conductivity versus temperature for PEO–$LiClO_4$ SPEs filled with (**c**) α-Fe_2O_3 NPs and (**d**) α-Fe_2O_3 NRs. The symbols represent the average of two measurements, and error represents the largest and smallest measured values. (With permission from (Do et al. 2012) Copyright © 2012, American Chemical Society)

decrease of conductivity and that may be due to the formation of ion traps because of rods aligned in parallel with the electrodes. Above the melting temperature, the enhancement in the conductivity was obtained. From DSC results, it was concluded that the nanofiller does not affect the polymer chain flexibility as no change in glass transition temperature (T_g) was evidenced. This was explained using the activation energy concept and is due to suppression of the crystallinity as evaluated from the melting peak. It was concluded that the recrystallization tendency is more for the NR (1 wt. %) due to more interparticle interaction as compared to the NP. This leads to more aggregation of NR as compared to NP. So, here, it was explained on the basis of the length of conducting pathways of NR.

Another effective approach is to create the positively charged oxygen vacancies on the 1 D nanofiller surface which acts as Lewis acid sites in the composite polymer

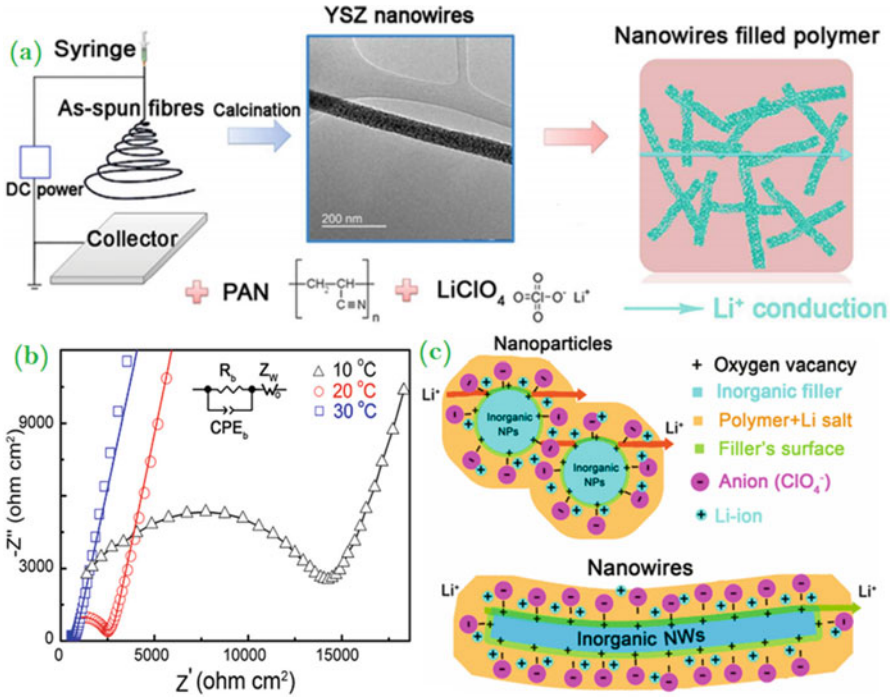

Fig. 8.22 (**a**) Schematic illustration for the synthesis of the solid composite polymer electrolyte. Electrospinning setup for the preparation of the YSZ nanowires, together with a TEM image of calcined nanowires. PAN, $LiClO_4$, and YSZ nanowires constitute the composite polymer electrolyte. Electrical properties of the composite polymer electrolyte filled with the YSZ nanowires. (**b**) Experimental and fitting impedance spectra for the composite electrolyte with YSZ nanowires at different measuring temperatures and equivalent circuit. (**c**) Schematic illustration for Li–ion transport in the composite polymer electrolytes with nanoparticle and nanowire fillers. The positive-charged oxygen vacancies on the surfaces of the fillers act as Lewis acid sites that can interact strongly with anions and release Li–ions. A continuous fast conduction pathway can be seen for nanowires rather than nanoparticles. (With permission from (Liu et al. 2016) Copyright © 2016, American Chemical Society)

electrolyte matrix. Liu et al. (2016) reported the Y_2O_3-doped ZrO_2 (YSZ) nanowire (1 D NW; av. diameter 55 nm) addition in the PAN−$LiClO_4$ polymer electrolyte (Fig. 8.22a). The motto behind the use of nanowire was the formation of effective percolation network across a long distance. SEM micrograph after the NW dispersion demonstrates the smooth morphology and evidences uniform distribution of nanowire in the host polymer matrix. The ionic conductivity was improved from 2.98×10^{-6} S cm^{-1} (YSZ nanoparticle) to 1.07×10^{-5} S cm^{-1} (7 YSZ nanowire) (Fig. 8.22b). This increase was due to the formation of continuous pathways with nanowire dispersion having oxygen vacancies (Fig. 8.22c). This helps in migration of more cations participating in the conduction. Further evidence was obtained from the FTIR deconvolution pattern of the anion (ClO_4^-), and it displays the lowest ion pair for 7 YSZ and hence the highest ionic conductivity. This was in correlation with

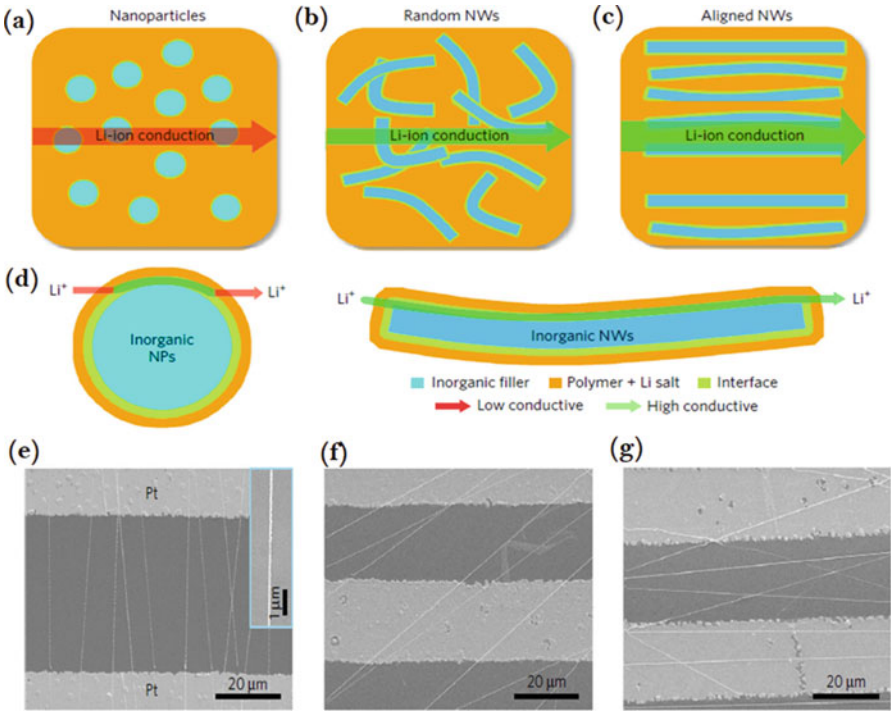

Fig. 8.23 The comparison of possible Li–ion conduction pathways. (**a**–**c**), Li–ion conduction pathways in composite polymer electrolytes with nanoparticles (**a**) random nanowires (**b**) and aligned nanowires (**c**). Compared with isolated nanoparticles, random nanowires could supply a more continuous fast conduction pathway for Li–ion. Compared with random nanowires, aligned nanowires are free of crossing junctions. (**d**) The surface region of inorganic nanoparticles (NPs) and nanowires (NWs) acts as an expressway for Li–ion conduction. (**e**–**g**), SEM images of the aligned nanowires at orientations of 0° (**e**), 45° (**f**) and 90° (**g**). The inset in Figure **d** is a SEM image at high magnification for the aligned nanowires. (With permission from (Liu et al. 2017) Copyright © 2017 Springer Nature)

the increased Li^+ ion transference number from 0.27 to 0.56. From TGA analysis, a correlation of ionic conductivity was built with dehydration temperature, and the lower the dehydration temperature, the higher will be the conductivity and lower crystallinity. The voltage stability window was increased as compared to the polymer–salt matrix.

Although the ionic conductivity was enhanced after the dispersion of the nanowire compared to nanoparticle, one possibility still arise that may affect the ion migration or restrict the effective role of nanowire–nanorod in the polymer matrix. As in the previous reports, the random distribution of the nanowire is investigated, but here, if the nanowire is aligned parallel to the electrodes, then they may show the negative effect by blocking the perpendicular ion migration. So, the alignment of the nanorod–nanowire may play an elective role in enhancing the conductivity further (Fig. 8.23a–d).

So, a recent report by Liu et al. (2017) investigated the effect of alignment of the nanowire (LLTO; $Li_{0.33}La_{0.557}TiO_3$) in the three orientations (0° ± 5°, 45° ± 9°, and 90° ± 8°) w.r.t of electrodes in a PAN–$LiClO_4$- based polymer matrix. SEM analysis depicts that the NW are well embedded in the polymer matrix with an average spacing of 5 μm (Fig. 8.23e–g). The ionic conductivity of randomly aligned NW was 5.40×10^{-6} S cm^{-1} and is higher than when dispersed with the nanoparticle. Further, when the NW were aligned with 0° orientation, then conductivity was increased to 6.05×10^{-5} S cm^{-1}.

This enhancement in the conductivity may be due to the absence of the crossing junctions as in the nanoparticle and aligned NW. For orientation, angle 45° conductivity decreases to 2.24×10^{-5} S cm^{-1} and is due to more continuous length along electrodes as compared to the 0°. While for the 90° orientation, the conductivity was 1.78×10^{-7} S cm^{-1} and is due to the parallel alignment of NW with electrodes. Also, the electronic conductivity was of the order of 10^{-11} S cm^{-1} and is negligible as compared to the ionic conductivity. The dispersion of the nanowire may also increase the polymer chain segmental motion, and that was evidenced by the increased Li^+ transference number from 0.27 to 0.42. Further, the faster relaxation was confirmed by plotting the imaginary part of impedance, and peak shifts toward high-frequency evidence the same. To further verify the experimental conductivity data simulation using the COMSOL Multiphysics (COMSOL), numerical analysis of the current distribution was performed and is in good agreement with experimental data.

Another report by Zhang et al. (2011) demonstrates the synthetization of the composite gel polymer electrolytes by adding SiO_2 nanowires into a P(VDF–HFP) matrix. FESEM analysis concludes that the synthesized nanowires are flexible and of high purity with the diameter and length of the SiO_2 as <50 nm and ~1 μm, respectively. FTIR was performed to check the nanorod formation, and it shows the main absorption band asymmetric bending mode of –Si–O–Si, symmetric bending mode of –Si–O–Si, bending mode of –O–Si–O, and the bending mode of the –Si–OH. FESEM analysis of the composite matrix suggests the effective role in modifying the surface morphology of pure polymer which is favorable for cation transport. Also, the presence of pores suggests the absorption of more electrolyte and hence the more ionic conductivity. FTIR spectrum confirms the interaction between the Si atoms of SiO_2 and F atoms of P(VDF–HFP) chain which helps in ion migration. TGA plot reveals the improved thermal stability (427 °C) as compared to the pure polymer (384 °C) and is due to the interaction between the host polymer matrix and the Si nanowire. Further, DSC analysis shows the reduction in the crystallinity on the addition of nanowire and may be due to the lowering of polymer chain reorganization tendency and enhanced amorphous content. The stress–strain curve shows increased tensile strength from 18.3 MPa (zero % nanowire) to 27.3 MPa for composite polymer electrolyte with 10 wt. % nanowire and is owing to the interaction between the polymer matrix and SiO_2 nanowire. This may be due to the increased chain flexibility on the addition of nanowire which makes it capable to bear high stress and is in agreement with the FTIR. The ionic conductivity was increased by one order and is 1.08×10^{-3} S cm^{-1} (at 30 °C) and may be due to the

weakening of the interaction of cation with fluorine of host polymer matrix. Also, the porous structure as evidenced in FESEM provides some additional conducting pathways in the same volume favorable for ion transport, and space charge region buildup occurs due to the more free charge carriers' availability. At high content, the interpenetrating networks are formed due to the overlapped space charge regions and hence the ion conducting pathways. Also, the transference number of Li^+ was increased from 0.23 to 0.70 on the addition of nanowire and may be due to the increased number of free ions via the dual interaction of acidic sites with fluorine of polymer host as well as an anion (PF_6^-). The electrochemical stability window of the synthesized composite polymer electrolyte was 4.8 V, and no effect of a surface group of the nanofiller was observed on the stability window.

Another report based on $Mg_2B_2O_5$ nanowires (Av. diameter ~270 nm) with PEO–LiTFSI was reported by Sheng et al. (2018). The advantages with $Mg_2B_2O_5$ NWs are the hardness of 15.4 GPa and Young's modulus of 125.8 GPa (Tao and Li 2008). The highest ionic conductivity was 1.53×10^{-4} S cm^{-1} (at 40 °C) and 3.7×10^{-4} S cm^{-1} (at 50 °C) for 10 wt. % $Mg_2B_2O_5$ nanowires. The enhancement was attributed to the coordination interaction of anion ($TFSI^-$) with $Mg_2B_2O_5$ nanowires, and it enhances the salt dissociation which increases the number of lithium–ions for migration (Fig. 8.24a). Another reason may be the reduction of the crystallinity and reorganization tendency after incorporation of NW which promotes faster segmental motion as evidenced by the XRD and DSC analysis. The lithium transference number (t_{Li}^+) was 0.44 and is much higher as compared to pure PEO which ($t_{Li}^+ = 0.19$). The voltage stability window was 4.7 V and is superior to NW free system which shows 4.25 V.

The maximum strength was 2.29 MPa, and mechanical properties were improved after addition of NW. The prepared system shows excellent flame-retardant performance. Figure 8.24–e shows the electrochemical performance of Li–ion battery assembled using PEO–LiTFSI–$Mg_2B_2O_5$. The discharge and charge voltage plateaus are around 3.35 and 3.50 V (at 0.2 °C), and overpotential between charge–discharge plateau increases with the increase of current density (Fig. 8.24b). Figure 8.24 c shows the performance with NW and without NW. The polymer electrolyte system with NW displays the specific discharge capacity of about 158 (at 0.2 °C), 140 (at 0.4 °C), 124 (at 0.8 °C), 117 (at .0 °C), and 72 mAh g^{-1} (at 2.0 °C), while without NW, the specific discharge capacity is 139 (at 0.2 °C), 121 (at 0.4 °C), 92 (at 0.8 °C), 75 (at 1.0 °C), and 37 mAh g^{-1} (at 2.0 °C). It concluded that the addition of NW increases the cyclic stability and capacity independent of current rate. Figure 8.24d shows the impedance study of the battery with and without NW. The addition of NW reduces both charge–transfer resistance (R_{ct}) and ohmic resistance (R_o) which indicates the increase of ionic conductivity with NW. Figure 8.24 e shows the stable specific capacity nearly 120 mAh g^{-1} in 230 discharge−charge cycles (at 1.0 °C, 50 °C) with a coulombic efficiency of 100%. The inset in the Fig. 8.24e shows a lightening LED with present battery (shape of "I").

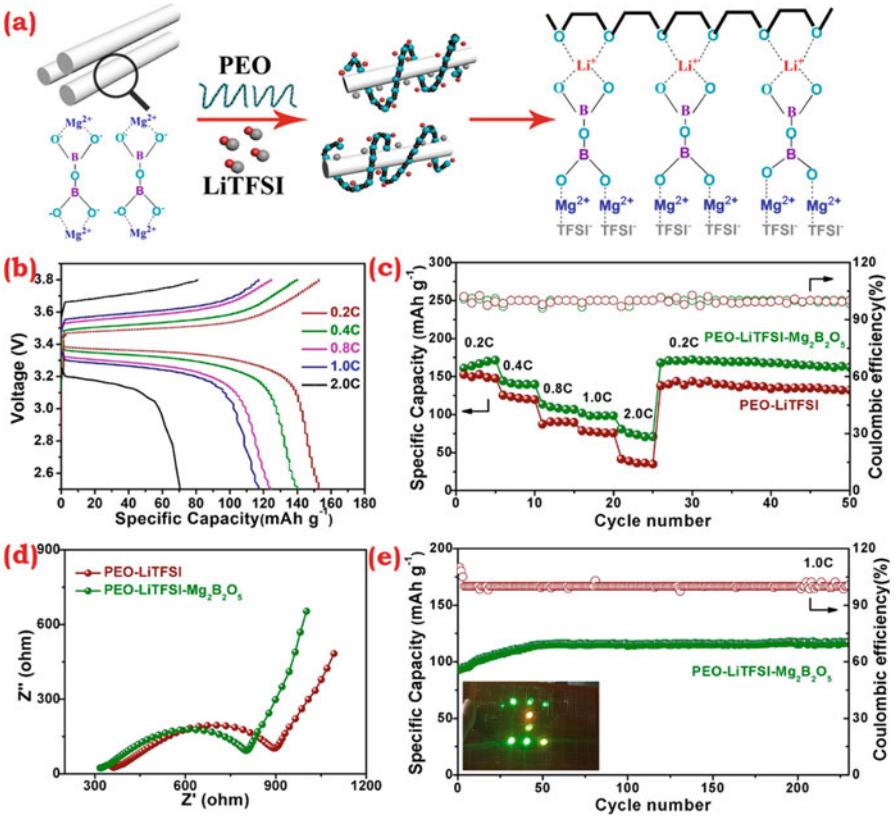

Fig. 8.24 (**a**) Schematics of lithium–ion migration in $Mg_2B_2O_5$ enhanced composite SSEs, (**b**) typical charge–discharge curves of $LiFePO_4$–Li SSLIBs using PEO–LiTFSI-10 wt % $Mg_2B_2O_5$ electrolyte at 50 °C. (**c**) Rate performance of $LiFePO_4$–Li SSLIBs using SSEs with and without $Mg_2B_2O_5$ at 50 °C. (**d**) EIS spectra of battery using SSEs with and without $Mg_2B_2O_5$ at 50 °C. (**e**) Cycling performance of $LiFePO_4$–Li SSLIBs with PEO–LiTFSI-10 wt % $Mg_2B_2O_5$ electrolyte at 1.0 °C and 50 °C. The inset is a digital photograph of LEDs lightened by SSLIBs. (With permission from (Sheng et al. 2018) Copyright © 2018 American Chemical Society)

8.4.4 Separator Development: Commercial and Patents

As the electrolyte–separator is the key component of the battery, the first commercialized battery produced in 1991 by Sony Corporation comprised a porous plastic film soaked typically in $LiPF_6$ dissolved in a mixture of EC–EMC–DEC. The role of the separator is to provide path to ions, (i) cathode to the anode during charging and (ii) anode to cathode during discharging. Table 8.4 summarizes the various manufacturers and composition of the separator, and Table 8.5 (information available on their site) summarizes the properties of commercial separators.

The separator must provide smooth ion migration and should be as thin as possible and lightweight and must prevent electronic conduction. The most crucial

Table 8.4 Major manufacturers of Li–ion battery separators along with their typical products

Manufacturer	Structure	Composition	Process	Trade name
Asahi Kasai	Single layer	PE	Wet	HiPore
Celgard LLC	Single layer	PP, PE	Dry	Celgard
	Multilayer	PP/PE/PP	Dry	Celgard
	PVdF coated	PVdF, PP, PE, PP/PE/PP	Dry	Celgard
Entek Membranes	Single layer	PE	Wet	Teklon
Mitsui Chemical	Single layer	PE	Wet	–
Nitto Denko	Single layer	PE	Wet	
DSM	Single layer	PE	Wet	Solupur
Tonen	Single layer	PE	Wet	Setela
Ube Industries	Multilayer	PP/PE/PP	Dry	U-pore
Targary	–	PE/PP	Wet	NAATBat
Daramic	–	PE	–	
Dry Lyte	–	Solid polymer electrolyte		SEEO
Nanomyte®SE-50	Self-standing (amorphous)	Polymer–ceramic composite Material with Lithium salt	In acetonitrile	NEI Co.
NANOMYTE® H-polymer	Self-standing (amorphous)	PEO-based polymer electrolyte with lithium salt	In acetonitrile	NEI Co.
Ionic materials		Polymer electrolyte		Ionic mat. Inc.

With permission from (Arora and Zhang 2004) Copyright © 2004, American Chemical Society

point is that separator must have good compatibility and less thickness (<25 μm) with the electrodes and possess desirable mechanical, electrochemical, and stability (thermal–voltage) properties (Arora and Zhang 2004; Zhang 2007b). Table 8.6 summarizes the selected patents in polymer electrolytes.

8.5 Summary and Conclusions

This chapter highlighted the recent updates on the solid PNCs with nanoparticle of different shapes and specific surface area. The development of solid polymer electrolyte as an alternative to liquid–gel polymer electrolyte has been the focus of researchers all over the world. From the last three decades, the nanoparticles have gained attention for the preparation of the solid polymer electrolyte for the energy storage systems. Among the various nanoparticles used for dispersion in the polymer matrix, nanoclay and active–passive nanofiller have been most studied. The nanofiller and nanoclay improved the overall properties of the polymer electrolytes. The nanofiller enhanced the electrical properties along with mechanical properties depending on the preparation method, dispersion, surface group interaction with polymer chains, surface area, and dielectric constant. The Lewis acid–base

Table 8.5 Typical properties of some commercial microporous membranes

	Property							
Company	Thickness (average)	Basis weight (g/m^2)	Porosity	Air permeability	Tensile strength	Tensile elongation at break	Puncture resistance	Thermal shrinkage at 120 °C, 1 h
ENTEK	20 μm	10.5	43%	300 s	MD > 1000 kg/cm^2	MD – 90%	550 g	MD – <10%
					TD – 750 kg/cm^2	TD – 300%		TD – <3%
ENTEK EPX	12 μm	5.5	54%	65 s	MD > 1000 kg/cm^2	MD – 90%	300 g	MD – <12%
					TD – 800 kg/cm^2	TD – 230%		TD – <7%
EPENTEK EPH	16 μm	8.4	47%	150 s	MD > 1000 kg/cm^2	MD – 80%	430 g	MD – <10%
					TD – 700 kg/cm^2	TD – 250%		TD – <4%

Table 8.6 Some available patents on electrolytes

Inventor	Polymer used	Patent no.	Year	Conductivity
Bauer et al.	$LiClO_4$ in a 400 MW PEG	4,654,279	1987	4×10^{-4} S cm^{-1} at 25 °C
Kuzhikalail M et al.	PAN, EC, PC, and $LiPF_6$–$LiAsF_6$	5510209	1995	OCV = 2.85 V
Nitash Pervez Balsara et al.	Block copolymer	US 8,889,301 B2	2014	1×10^{-4} S cm^{-1} at 25 °C
Wunder et al.	PEO–POSS–phenyl7 $(BF_3Li)_3$	9680182 B2	2017	1×10^{-4} S cm^{-1} at 25 °C. (for O/Li = 14)
Michael A. Zimmerman	PPS, PPO, PEEK, PPA	2017/0018781 A1	2017	1×10^{-5} S cm^{-1} (At RT)
Russell Clayton Pratt et al.	Perfluoropolyether electrolytes terminated with urethane	9923245	2018	3.6×10^{-5} S Cm^{-1} (at 40 °C)
				1.1×10^{-4} S Cm^{-1} (at 80 °C)
Mohit Singh et al.	Ceramic electrolyte	20110281173	2018	Stability up to 500 cycles

interaction mechanism was elaborated for the understanding of the cation transport. The serious drawback with nanofiller was that at high concentration, it was not able to play its effective role in enhancing the properties may be due to the possibility of aggregation. Also, the lack of a continuous path for cation limits the enhancement in the rate of ion transport. In order to resolve the issue of agglomeration, search of new nanoparticle ended with the nanoclay. The advantage with the nanoclay is that percolation threshold is lower as compared to nanofiller, and it is fit for the elimination of most detrimental factor, i.e., concentration polarization. It may be considered as the first step toward the realization of single-ion solid polymer electrolyte (PNC), as the specific surface area plays an effective role in enhancing the electrical and transport properties along with mechanical properties. So, the research was focused toward the use of nanoparticle with the high specific surface area and sufficient oxygen vacancies that promote the faster ion transport. This leads the development of nanorod and nanowire as the dispersive element in the solid polymer electrolytes. One remarkable advantage with the nanorod was that a long continuous path was available for ion migration. This provides the smoother ion migration between the electrodes along with improved mechanical and thermal properties. The nanowire dispersion is the recent advancement in solid polymer electrolytes. The oxygen vacancies on the nanowire surface provide additional sites to the ion for a long time. This enhances the ionic conductivity and thermal–mechanical properties. But one barrier was the random alignment of the nanowire that hinders the ion migration. This was solved by the alignment of the nanowire, and it provides continuous path to the ion between the electrodes without any constraint. The electrochemical cells fabricated using the nanorod and nanowire promise their launch at a commercial level.

Acknowledgments The author thanks the Central University of Punjab for providing fellowship.

References

Agrawal RC, Chandra A (2007) Ion transport and electrochemical cell performance studies on hot-press-synthesized Ag+ ion conducting electroactive polymeric membranes:(1− x) PEO: x [0.7 (0.75 AgI: 0.25 AgCl): 0.3 MI]. J Phys D Appl Phys 40(22):7024

Ahmed S, Mehmood M, Iqbal R (2010) Influence of dioctyl phthalate (DOP) on the mechanical, optical and thermal properties of formulations for the industrial manufacture of radiation sterilizable medical disposables. Radiat Phys Chem 79:339–342

Armand M, Tarascon JM (2008) Building better batteries. Nature 451(7179):652–657

Arora P, Zhang Z (2004) Battery separators. Chem Rev 104(10):4419–4462

Arya A, Sharma AL (2016) Conductivity and stability properties of solid polymer electrolyte based on PEO-PAN+LiPF6 for energy storage. Appl Sci Lett 2:72–75

Arya A, Sharma AL (2017a) Polymer electrolytes for lithium ion batteries: a critical study. Ionics 23:497–540

Arya A, Sharma AL (2017b) Insights into the use of polyethylene oxide in energy storage/conversion devices: a critical review. J Phys D Appl Phys 50(44):443002

Arya A, Sharma AL (2017c) Effect of variation of different nanofillers on structural, electrical, dielectric, and transport properties of blend polymer nanocomposites. Ionics 24(8):2295–2319. https://doi.org/10.1007/s11581-017-2364-7

Arya A, Sharma AL (2018) Optimization of salt concentration and explanation of two peak percolation in blend solid polymer nanocomposite films. J Solid State Electrochem 22(9):2725–2745

Baril D, Michot C, Armand M (1997) Electrochemistry of liquids vs. solids: polymer electrolytes. Solid State Ionics 94(1–4):35–47

Bhattacharya M (2016) Polymer nanocomposites – a comparison between carbon nanotubes, graphene, and clay as nanofillers. Materials 9(4):262

Brinker CJ, Hurd AJ (1994) Fundamentals of sol-gel dip-coating. J Phys III 4(7):1231–1242

Celzard A, McRae E, Deleuze C, Dufort M, Furdin G, Marêché JF (1996) Critical concentration in percolating systems containing a high-aspect-ratio filler. Phys Rev B 53(10):6209

Chen B, Evans JR, Greenwell HC, Boulet P, Coveney PV, Bowden AA, Whiting A (2008) A critical appraisal of polymer–clay nanocomposites. Chem Soc Rev 37(3):568–594

Cheng XB, Zhang R, Zhao CZ, Zhang Q (2017) Toward safe lithium metal anode in rechargeable batteries: a review. Chem Rev 117(15):10403–10473

Choudhary S, Sengwa RJ (2014) Intercalated clay structures and amorphous behavior of solution cast and melt pressed poly (ethylene oxide)–clay nanocomposites. J Appl Polym Sci 131(4). https://doi.org/10.1002/app.39898

Dam T, Karan NK, Thomas R, Pradhan DK, Katiyar RS (2015) Observation of ionic transport and ion-coordinated segmental motions in composite (polymer-salt-clay) solid polymer electrolyte. Ionics *21*(2):401–410

Deng D (2015) Li-ion batteries: basics, progress, and challenges. Energy Sci Eng 3(5):385–418

Dhatarwal P, Sengwa RJ, Choudhary S (2017) Effect of intercalated and exfoliated montmorillonite clay on the structural, dielectric and electrical properties of plasticized nanocomposite solid polymer electrolytes. Composit Commun 5:1–7

Do NST, Schaetzl DM, Dey B, Seabaugh AC, Fullerton-Shirey SK (2012) Influence of Fe2O3 nanofiller shape on the conductivity and thermal properties of solid polymer electrolytes: nanorods versus nanospheres. J Phys Chem C 116(40):21216–21223

Erceg M, Jozić D, Banovac I, Perinović S, Bernstorff S (2014) Preparation and characterization of melt intercalated poly (ethylene oxide)/lithium montmorillonite nanocomposites. Thermochim Acta 579:86–92

Fan L, Nan CW, Dang Z (2002) Effect of modified montmorillonites on the ionic conductivity of (PEO)16LiClO4 electrolytes. Electrochim Acta 47(21):3541–3544

Fu X, Yu D, Zhou J, Li S, Gao X, Han Y et al (2016) Inorganic and organic hybrid solid electrolytes for lithium-ion batteries. Cryst Eng Commun 18(23):4236–4258

Gomari S, Esfandeh M, Ghasemi I (2017) All-solid-state flexible nanocomposite polymer electrolytes based on poly (ethylene oxide): lithium perchlorate using functionalized graphene. Solid State Ionics 303:37–46

Gondaliya N, Kanchan DK, Sharma P (2013) Effect of a plasticizer on a solid polymer electrolyte. Soc Plastics Eng Plastics Res. https://doi.org/10.2417/spepro.004646

Goodenough JB, Park KS (2013) The Li-ion rechargeable battery: a perspective. J Am Chem Soc 135(4):1167–1176

Hallinan DT Jr, Balsara NP (2013) Polymer electrolytes. Annu Rev Mater Res 43:503–525

https://about.bnef.com/blog/lithium-ion-battery-costs-squeezed-margins-new-business-models/

https://insideevs.com/volkswagens-transform-2025-plan-calls-for-automaker-to-be-1-for-evs/

https://www.greentechmedia.com/articles/read/tesla-fulfills-australia-battery-bet-whats-that-mean-industry

Karuppasamy K, Antony R, Alwin S, Balakumar S, Sahaya Shajan X (2015) A review on PEO based solid polymer electrolytes (SPEs) complexed with LiX (X= Tf, BOB) for rechargeable lithium ion batteries. Mater Sci Forum 807:41–63

Kim S, Park SJ (2007) Preparation and ion-conducting behaviors of poly (ethylene oxide)-composite electrolytes containing lithium montmorillonite. Solid State Ionics 178(13):973–979

Kim Y, Kwon SJ, Jang HK, Jung BM, Lee SB, Choi UH (2017) High ion conducting nanohybrid solid polymer electrolytes via single-ion conducting mesoporous organosilica in poly (ethylene oxide). Chem Mater 29(10):4401–4410

Klongkan S, Pumchusak J (2015) Effects of nano alumina and plasticizers on morphology, ionic conductivity, thermal and mechanical properties of PEO-LiCF3SO3 solid polymer electrolyte. Electrochim Acta 161:171–176

Kotal M, Bhowmick AK (2015) Polymer nanocomposites from modified clays: recent advances and challenges. Prog Polym Sci 51:127–187

Krebs FC (2009) Fabrication and processing of polymer solar cells: a review of printing and coating techniques. Sol Energy Mater Sol Cells 93(4):394–412

Kubišovß H, MěřÝnskß D, Svoboda P (2010) PP/clay nanocomposite: optimization of mixing conditions with respect to mechanical properties. *Polym Bull 65*(5):533–541

Kumar PP, Yashonath S (2006) Ionic conduction in the solid state. J Chem Sci 118(1):135–154

Kumar Y, Hashmi SA, Pandey GP (2011) Lithium ion transport and ion–polymer interaction in PEO based polymer electrolyte plasticized with ionic liquid. Solid State Ionics 201(1):73–80

Li W, Liu J, Zhao D (2016) Mesoporous materials for energy conversion and storage devices. Nat Rev Mater 1:16023

Liang B, Tang S, Jiang Q, Chen C, Chen X, Li S, Yan X (2015) Preparation and characterization of PEO-PMMA polymer composite electrolytes doped with nano-Al 2 O 3. Electrochim Acta 169:334–341

Lin D, Liu W, Liu Y, Lee HR, Hsu PC, Liu K, Cui Y (2015) The high ionic conductivity of composite solid polymer electrolyte via in situ syntheses of monodispersed SiO2 nanospheres in poly (ethylene oxide). Nano Lett 16(1):459–465

Lin X, Salari M, Arava LMR, Ajayan PM, Grinstaff MW (2016) High temperature electrical energy storage: advances, challenges, and frontiers. Chem Soc Rev 45(21):5848–5887

Lin Y, Wang X, Liu J, Miller JD (2017) Natural halloysite nano-clay electrolyte for advanced all-solid-state lithium-sulfur batteries. Nano Energy 31:478–485

Liu W, Liu N, Sun J, Hsu PC, Li Y, Lee HW, Cui Y (2015) Ionic conductivity enhancement of polymer electrolytes with ceramic nanowire fillers. Nano Lett 15(4):2740–2745

Liu W, Lin D, Sun J, Zhou G, Cui Y (2016) Improved lithium ionic conductivity in composite polymer electrolytes with oxide-ion conducting nanowires. ACS Nano 10(12):11407–11413

Liu W, Lee SW, Lin D, Shi F, Wang S, Sendek AD, Cui Y (2017) Enhancing ionic conductivity in composite polymer electrolytes with well-aligned ceramic nanowires. Nat Energy 2:17035

Ma Y, Li LB, Gao GX, Yang XY, You Y (2016) Effect of montmorillonite on the ionic conductivity and electrochemical properties of a composite solid polymer electrolyte based on polyvinylidene difluoride/polyvinyl alcohol matrix for lithium ion batteries. Electrochim Acta 187:535–542

Miller TF III, Wang ZG, Coates GW, Balsara NP (2017) Designing polymer electrolytes for safe and high capacity rechargeable lithium batteries. Acc Chem Res 50(3):590–593
Mohapatra SR, Thakur AK, Choudhary RNP (2009) Effect of nanoscopic confinement on improvement in ion conduction and stability properties of an intercalated polymer nanocomposite electrolyte for energy storage applications. J Power Sources 191(2):601–613
Moreno M, Quijada R, Santa Ana MA, Benavente E, Gomez-Romero P, González G (2011) Electrical and mechanical properties of poly (ethylene oxide)/intercalated clay polymer electrolyte. Electrochim Acta 58:112–118
Ngai KS, Ramesh S, Ramesh K, Juan JC (2016) A review of polymer electrolytes: fundamental, approaches and applications. Ionics 22(8):1259–1279
Pal P, Ghosh A (2017) Influence of TiO2 nano-particles on charge carrier transport and cell performance of PMMA-LiClO4 based nano-composite electrolytes. Electrochim Acta 260:157–167
Park CH, Kim DW, Prakash J, Sun YK (2003) Electrochemical stability and conductivity enhancement of composite polymer electrolytes. Solid State Ionics 159(1):111–119
Park CH, Park M, Yoo SI, Joo SK (2006) A spin-coated solid polymer electrolyte for all-solid-state rechargeable thin-film lithium polymer batteries. J Power Sources 158(2):1442–1446
Pavlidou S, Papaspyrides CD (2008) A review on polymer–layered silicate nanocomposites. Prog Polym Sci 33(12):1119–1198
Pinnavaia TJ, Beall GW (2000) Polymer-clay nanocomposites. Wiley, Chichester
Polu AR, Rhee HW, Reddy MJK, Shanmugharaj AM, Ryu SH, Kim DK (2017) Effect of POSS-PEG hybrid nanoparticles on cycling performance of polyether-LiDFOB based solid polymer electrolytes for all solid-state Li-ion battery applications. J Ind Eng Chem 45:68–77
Sengwa RJ, Choudhary S (2014a) Structural characterization of hydrophilic polymer blends/montmorillonite clay nanocomposites. J Appl Polym Sci 131(16). https://doi.org/10.1002/app.40617
Sengwa RJ, Choudhary S (2014b) Dielectric properties and fluctuating relaxation processes of poly (methyl methacrylate) based polymeric nanocomposite electrolytes. J Phys Chem Solids 75 (6):765–774
Sengwa RJ, Choudhary S, Dhatarwal P (2015) Influences of ultrasonic-and microwave-irradiated preparation methods on the structural and dielectric properties of (PEO–PMMA)–LiCF3SO3–x wt% MMT nanocomposite electrolytes. Ionics 21(1):95–109
Sharma AL, Thakur AK (2010) Improvement in voltage, thermal, mechanical stability and ion transport properties in polymer-clay nanocomposites. J Appl Polym Sci 118(5):2743–2753
Sharma AL, Thakur AK (2011) Polymer matrix–clay interaction mediated mechanism of electrical transport in exfoliated and intercalated polymer nanocomposites. J Mater Sci 46(6):1916–1931
Sharma AL, Thakur AK (2013) Plastic separators with improved properties for portable power device applications. Ionics 19(5):795–809
Sharma AL, Shukla N, Thakur AK (2008) Studies on structure property relationship in a polymer–clay nanocomposite film based on (PAN)8LiClO4. J Polym Sci B Polym Phys 46 (23):2577–2592
Sheng O, Jin C, Luo J, Yuan H, Huang H, Gan Y et al (2018) Mg2B2O5 nanowire enabled multifunctional solid-state electrolytes with high ionic conductivity, excellent mechanical properties, and flame-retardant performance. Nano Lett 18(5):3104–3112. https://doi.org/10.1021/acs.nanolett.8b00659
Shodai T, Owens BB, Ohtsuka H, Yamaki JI (1994) Thermal stability of the polymer electrolyte (PEO)8LiCF3SO3. J Electrochem Soc 141(11):2978–2981
Shukla N, Thakur AK (2010) Ion transport model in exfoliated and intercalated polymer–clay nanocomposites. Solid State Ionics *181*(19):921–932
Song JY, Wang YY, Wan CC (1999) Review of gel-type polymer electrolytes for lithium-ion batteries. J Power Sources 77(2):183–197
Stephan AM (2006) Review on gel polymer electrolytes for lithium batteries. Eur Polym J 42(1):21–42

Stephan AM, Nahm KS (2006) Review on composite polymer electrolytes for lithium batteries. Polymer 47(16):5952–5964

Suthanthiraraj SA, Johnsi M (2017) Nanocomposite polymer electrolytes. Ionics 23:2531–2542

Tang C, Hackenberg K, Fu Q, Ajayan PM, Ardebili H (2012) High ion conducting polymer nanocomposite electrolytes using hybrid nanofillers. Nano Lett 12(3):1152–1156

Tao X, Li X (2008) Catalyst-free synthesis, structural, and mechanical characterization of twinned Mg2B2O5 nanowires. Nano Lett 8(2):505–510

Vignarooban K, Dissanayake MAKL, Albinsson I, Mellander BE (2014) Effect of TiO2 nano-filler and EC plasticizer on electrical and thermal properties of poly (ethylene oxide)(PEO) based solid polymer electrolytes. Solid State Ionics 266:25–28

Wang C, Yang Y, Liu X, Zhong H, Xu H, Xu Z et al (2017) Suppression of lithium dendrite formation by using LAGP-PEO (LiTFSI) composite solid electrolyte and lithium metal anode modified by PEO (LiTFSI) in all-solid-state lithium batteries. ACS Appl Mater Interfaces 9(15):13694–13702

Wilson MS, Gottesfeld S (1992) Thin-film catalyst layers for polymer electrolyte fuel cell electrodes. J Appl Electrochem 22(1):1–7

Yang Z, Zhang J, Kintner-Meyer MC, Lu X, Choi D, Lemmon JP, Liu J (2011) Electrochemical energy storage for green grid. Chem Rev 111(5):3577–3613

Zhang SS (2007a) A review on the separators of liquid electrolyte Li-ion batteries. J Power Sources 164(1):351–364

Zhang SS (2007b) A review on the separators of liquid electrolyte Li-ion batteries. J Power Sources 164(1):351–364

Zhang P, Yang LC, Li LL, Ding ML, Wu YP, Holze R (2011) Enhanced electrochemical and mechanical properties of P (VDF-HFP)-based composite polymer electrolytes with SiO2 nanowires. J Membr Sci 379(1):80–85

Zhang Y, Zhao Y, Gosselink D, Chen P (2015) Synthesis of poly (ethylene-oxide)/nanoclay solid polymer electrolyte for all solid-state lithium/sulfur battery. Ionics 21(2):381–385

Zhang Q, Liu K, Ding F, Liu X (2016) Recent advances in solid polymer electrolytes for lithium batteries. Nano Res:1–36

Zhao Y, Huang Z, Chen S, Chen B, Yang J, Zhang Q et al (2016) A promising PEO/LAGP hybrid electrolyte prepared by a simple method for all-solid-state lithium batteries. Solid State Ionics 295:65–71

Zhu K, Liu Y, Liu J (2014) A fast charging/discharging all-solid-state lithium ion battery based on PEO-MIL-53 (Al)-LiTFSI thin film electrolyte. RSC Adv 4(80):42278–42284

Zu CX, Li H (2011) Thermodynamic analysis on energy densities of batteries. Energy Environ Sci 4(8):2614–2624

Chapter 9
Application of Nanotechnology in Agriculture

Pragati Pramanik, P. Krishnan, Aniruddha Maity, N. Mridha, Anirban Mukherjee, and Vikas Rai

Contents

9.1 Introduction 318
9.2 Applications of Nanotechnology in Agriculture 319
9.2.1 Natural Resource Management 320
9.2.2 Crop Improvement 329
9.2.3 Crop Protection 331
9.2.4 Food Processing/Packaging Processing/Export Potential of Ethnic Foods 332
9.3 Protocols for Risk Assessment/Safety and Education Awareness 335
9.3.1 Protocols for Risk Assessment/Safety of Nanotechnology 337
9.3.2 Recommendation for Safe Nanotechnology for Workplace 338
9.4 Conclusions 342
References 343

Abstract Indian agricultural growth has reduced from about 3.6% in 1985–1995 to less than 2% in 1995–2005. This is far below than the targeted 4% annual growth in agricultural sector for 2020. The major concern is food grain production. Among the many scientific advancements, nanotechnology (NT) has been identified as a potential technology for reviving the agriculture and food industry and can improve livelihood of poor. Various sectors like health care, materials, textile, information and communication technology (ITC), and energy can get huge benefits from nanotechnology. In agricultural sector in particular, nanotechnology plays an important role in crop production, food processing and packaging, food security and water purification, environmental remediation, crop improvement, and plant protection. Agricultural productivity can be improved through nanomaterial-induced genetically improved animals and plants, site-specific drug and gene delivery of molecules

P. Pramanik (✉) · P. Krishnan · N. Mridha · V. Rai
Division of Agricultural Physics, ICAR-IARI, New Delhi, India

A. Maity
Department of Soil and Crop Sciences, Texas A&M University, College Station, TX, USA

Division of Seed Technology, ICAR_IGFRI, Jhansi, Uttar Pradesh, India

A. Mukherjee
Division of Agricultural Extension, ICAR-IARI, New Delhi, India

N. Dasgupta et al. (eds.), *Environmental Nanotechnology Volume 4*, Environmental Chemistry for a Sustainable World 32, https://doi.org/10.1007/978-3-030-26668-4_9

at cellular/molecular levels in animals and plants, and nano-array-based genetic modification in animals and plants in stress conditions. Nanotechnology has the potential of precise delivery of agrochemicals for improving disease resistance, plant growth, and nutrient use. Nanoencapsulated products show the ability of more effective and site-specific use of pesticides, insecticides, and herbicides in an eco-friendly and greener way. It is successfully used in postharvest for maintaining freshness, quality, and shelf life of stored product and preventing disease occurrences in a fairly safer way. The use of nanomaterials is quite new in agriculture and it requires additional research. Social and ethical repercussions of nanotechnology uses in agriculture have to be considered. Before commercialization and field application, toxicity of nanomaterials has to be evaluated.

Keywords Nanotechnology · Agriculture · Precision farming · Nanoremediation · Crop protection · Protocols

9.1 Introduction

Indian agricultural growth is 3.59% in 2004–2014 (Ministry of Finance, Govt of India 2014) which is below than the targeted 4% annual growth in agricultural sector for 2020. The major concern is food grain production. The annual per capita food grain production has reduced from 207 kg in 1991/1995 to only 179 kg in 2014/2017 (Ministry of Agriculture, Govt of India 2017–2018), and these declining trends pose concern for food and nutritional security. With limited water and land resources, targeted agricultural growth can be obtained by increasing per unit natural resources productivity and farm income through judicious use of advanced technologies. During the era of green revolution, potential yields and farm incomes were enhanced manyfold using short-duration improved high-yielding varieties, intensive fertilizer use, irrigation and pesticides, neglecting sustainable and efficient utilization of natural resources. Recently, farm productivity and incomes have shown steady decline. To maintain overall national growth, stabilization of agricultural production is required as livelihood of 60% of Indian population depends on agriculture. The problems are accelerated by deterioration of natural resources like soil, climate, and water. This difficult situation of Indian agriculture is known as "technology fatigue." To overcome the "technology fatigue," focusing on technologies that can increase agricultural production, resource use efficiencies, and product quality is the need of the hour.

Among the many scientific advancements, nanotechnology (NT) has been identified as one of the potential technologies that can revive the agriculture and food industry (Kuzma and VerHage 2006) and can improve livelihood of poor people. The European Commission has identified nanotechnology as one of the six "Key Enabling Technologies" that can play important role in sustainable growth of different fields (EC 2012). The term "nanotechnology" was first used by Norio Taniguchi in 1974. Nanotechnology is the branch of science which studies the

understanding of matter at nanometer dimensions (1–100 nm) (US EPA). It manipulates matter of individual atoms, molecules, and molecular clusters in new structures with new or entirely different properties. It involves varied applications like building, controlling, and structuring of devices and materials of various nature like chemical, physical, and biological at nanoscale level. In order to promote nanotechnology, the US Federal Government introduced the National Nanotechnology Initiative (NNI) in 2001. The NNI defines nanotechnology as the restructuring of matter with at least one dimension ranged from 1 to 100 nanometers. In general the new physical and/or chemical properties of nanoscale device and material provide important functions (ObservatoryNANO FP7 2011) that are used in medicine, electronics, biotechnology, energy sectors, and materials science. As a tool, nanotechnology can handle the world's most critical water, energy, health, agriculture, biodiversity (WEHAB)-related problems. These five critical areas have been identified by the United Nations Johannesburg Summit on Sustainable Development on 2002. UN Survey has identified agricultural productivity enhancement through nanotechnology in developing countries as the second important aspect for achieving millennium development goals, while energy conversion and storage were first with water treatment as the third vital areas of nanotechnology applications.

However at global level as well as in India, application of nanotechnology in agricultural sector and food systems is at nascent stage, and its ultimate success will depend on the acceptance of the stakeholders. Application of nanotechnology in agriculture calls for an effective regulatory and strong governance mechanisms and system with all group of stakeholders' involvement. Thus nanotechnology can provide the much required second green revolution in Indian agricultural sector with emphasis on sustainable production. The applications of nanotechnology have been discussed in detail in the following sections.

9.2 Applications of Nanotechnology in Agriculture

Over time agriculture gets constant benefits from different technological innovations like hybrid varieties and synthetic fertilizers and pesticides. Now agricultural scientists are realizing that smart innovation like nanotechnology is strongly required for agricultural growth, to face global challenges of food security and climate change. The importance of nanotechnology applications in agricultural sector came only in recent years, but the research was started about half a century back (Mukhopadhyay 2014). The uses of nanomaterials are required for increasing fertilization (or fertilizer) use efficiency, yields, and reducing pesticide need; rapid and early pathogens and toxic chemical detection in food items; smart pesticides and fertilizer delivery systems; smart systems used for food packaging and processing; and regulating agricultural food security (Moraru et al. 2003; Chau et al. 2007). Agricultural productivity can be improved through nanomaterial-induced genetically improved animals and plants (Kuzma 2007; Scott 2007), site-specific drug and gene delivery of molecules at cellular/molecular levels in animals and plants

(Maysinger 2007), and nano-array-based genetic modification in animals and plants in stress conditions. Nanofilters or nanocatalysts can degrade and reduce existing pollutants and thereby pollution. In agriculture, nanotechnology can be used to produce slow-release nanofertilizers for fertilizer use by plants; nanoparticles encapsulated pesticides for controlled and on-demand release; site-specific drug and nutrient delivery in fisheries and livestock; nanoparticles, nanobrushes, and nanomembranes for treatment of water and soil; cleaning and maintenance of fishponds; and nanosensors for assessing plant health and soil quality. Some recent breakthrough in nanotechnology in agriculture has been given in Table 9.1.

9.2.1 Natural Resource Management

Soil Fertility Management

Fertilizers are required for maintaining soil fertility and production of food and crop quality particularly after the adoption of high-yielding, hybrid, and fertilizer-responsive cultivars. Conventional fertilizer application methods (like spraying and broadcasting) cause losses by leaching, drifting, runoff water, evaporation, soil moisture-driven hydrolysis, and microbial and photolytic degradation. This causes very less concentration to reach to the targeted site. About 40–70% nitrogen, 80–90% phosphorus, and 50–90% potassium of conventionally applied fertilizers are lost in the environment (Trenkel 1997) resulting the requirement of repeated applications of fertilizers and pesticides. But the excess use of fertilizers and pesticides causes environmental pollution; natural resource degradation; pesticide resistance in pest and pathogens; reduction in soil microflora and nitrogen fixation; and bioaccumulation of pesticides (Tilman et al. 2002). Hence, optimum use of chemical/synthetic fertilizer as per nutritional demand of crop and minimum environmental pollution are the need of the hour. This can be done through application of nanofertilizers. Nanofertilizers also called smart fertilizer are either nanomaterials (NMs) which supply single or multiple nutrients to plants improving development and yield of crops or those which compliments better performance of conventional synthetic fertilizers, without directly supplying nutrients to crops (Liu and Lal 2015). A nanofertilizer is a product in nanometer level that supply nutrients to specific target sites and can improve nutrient use efficiency (NUE) and diminish environmental degradation (Chinnamuthu and Boopathi 2009). Nanoencapsulation of fertilizers is done in three ways: nutrients are (a) encapsulated in nanoporous materials, (b) coated with thin film polymer, or (c) delivered as nanoparticle or nanoemulsions (Rai et al. 2012). Nanomaterial encapsulation on fertilizer binds more strongly the material because of high surface tension (Brady and Weil 1999). The nanoformulation of fertilizer possesses properties like high solubility, controlled and timely release, stability, effectiveness, improved targeted activity by delivering desired concentration, and reduced toxicity with easy, safe distribution and disposal (Torney et al. 2007 and Green and Beestman 2007). The nanoparticles loaded with nutrients are prepared by (a) absorption, (b) ligand-mediated

Table 9.1 Nanotechnology in agricultural sectors

Areas of applications	Uses	References
Crop production		
Plant protection products	Nanoparticles encapsulated pesticides, nanocapsules, and nanoemulsions for controlled and on-demand release for better efficiency and disease pest control of plants	Anjali et al. (2012)
Nanofertilizers	Buckyball fertilizer nanoparticles, nanocapsules, and viral capsids for better nutrients absorption of plants and site-specific nutrient delivery	Anjali et al. (2012)
Precision farming	Nanosensors connected with global positioning system (GPS) navigation system for real-time monitoring of soil environments and crop growth, precise application of fertilizer and pesticide	Kalpana-Sastry et al. (2009)
Soil improvement		
Water/liquid retention	Nanomaterials like zeolites and nanoclays are used to hold water and liquid agrochemicals in soil for their subsequent slow release to plants	http://www.geohumus.com/us/products.html
Water purification		
Water purification and pollutant remediation	Nanomaterials like nZVI nanoclays and carbon nanotubes (CNTs) are used for filtering and binding of toxic substances and their subsequent removal from environments	McMurray et al. (2006)
Diagnostic		
Nanosensors and diagnostic devices	Nanomaterials and nanostructures like electrochemically active CNTs and nanofibers are extremely delicate biochemical sensors used to closely assess environmental conditions, plant status, and growth	Vamvakaki and Chaniotakis (2007)
Livestock and fisheries	Nanoveterinary medicine like nanoparticles, buckyballs, dendrimers, nanocapsules used for drug delivery, nanovaccines; smart herds, cleaning fish ponds	Kalpana-Sastry et al. (2009)
Plant breeding		
Plant genetic modification	Nanoparticles loaded with desired DNA or RNA are delivered to plant cells for their genetic transformation or to trigger defense mechanism activated by pathogens	Torney et al. (2007)
Nanomaterials from plant		
Nanoparticles from plants	Production of nanofibers from bio-nanocomposite and Nanofibers from cotton waste and wheat straw and soy hulls for improved strength of clothing	Kalpana-Sastry et al. (2009)
Food industry	Use of silicate nanoparticles in airtight packaging of food products and nanosensors for contamination and pathogen determination in food	Kalpana-Sastry et al. (2009)

attachment, (c) nanoparticulate polymeric shell encapsulation, (d) polymeric nanoparticles entrapment, and (e) synthesis of nutrient-rich nanoparticles (Solanki et al. 2015). Nanofertilizers when combined with nanodevices for synchronized release of N and P fertilizer prevent unwanted nutrient losses to the environment (DeRosa et al. 2010) by leaching and/or leaking (Veronica et al. 2015). As mentioned in Table 9.2, nanofertilizers show controlled release of chemicals, site-specific delivery, reduced toxicity, and better nutrient utilization (Cui et al. 2010). Nanosized mineral micronutrient formulation can increase solubility besides dispersion of micronutrients in soil, diminishes absorption in addition to fixation, improves bioavailability which leads to increased NUE, and saves fertilizer resource (Naderi and Danesh-Sharaki 2013).

Several studies have already proved the importance of nanofertilizers. Nanoparticles with diameter lesser than the cell wall pores (5–20 nm) can pass into the plant cells straightly through the sieve-like plant cell wall configurations. After dissolution of nanofertilizer in water, soluble nutrient ions are released into the soil. The soluble nutrient ions are like dissolved conventional fertilizers; thus plants take up nutrient ions released from nanofertilizers. The proportion and range of dissolution of nanofertilizers in aqueous medium and soil solution are greater (due to considerable lesser particle dimensions and greater specific surface areas) (Liu and Lal 2015). Corradini et al. (2010) assessed the relations and firmness of chitosan nanoparticle solution comprising N, P, and K fertilizers and obtained improved results. Kottegoda et al. (2011) prepared urea-modified hydroxyapatite (HA) nanoformulation for steady release of nitrogen fulfilling crop growth demand. Initially HA nanoformulation showed surge; however they could release nitrogen up to 60 days of crop growth. Mesoporous silica nanoparticles (150 nm) have been reported to capture urea and had minimum fivefold greater release time (Wanyika et al. 2012). It has been perceived that 15.5% urea was encumbered inside mesoporous silica nanoparticles and exhibited a measured urea discharge in water and soil. Milani et al. 2012 had characterized the solubility and dissolution kinetics of urea and monoammonium phosphate (MAP) coated with ZnO nanoparticles and bulk ZnO particles and found better performance of ZnO nanoparticles.

Precision Farming and Smart Delivery System

Precision farming is defined as performing exact management practices at precise location, at the exact rate, and at perfect time to improve enduring site-specific crop production efficiency and profitability with integrated targeted information and sustainable farming system, whereas decreasing unintended environmental impacts. The success definitely relies on precise assessment of localized crop environmental conditions by identifying the input demands varied by location (Blackmore 1994). A centralized monitoring system to determine crop development and soil conditions, fertilizer, seeding, water, and chemical use can be refined to reduce costs and maximize crop production. These monitoring systems empowered by nanotechnology and/or tiny sensors will have a huge impression on future precision farming

approaches. Traditional method of managing a large area based on some hypothetical mean properties results in gross inaccuracies as agricultural system exists with inherent spatial and temporal heterogeneity with reference to soil, crops, weather, etc. Accurate sensing of location-specific variations regarding management practices, soil properties, and/or environmental conditions within fields, data acquirement, manipulation, storage, and transfer is thus vital in handling this variability to fine-tune management operations accordingly. The revolution in electronics of the last several decades has produced two technologies like Global Positioning System (GPS) and Geographic Information Systems (GIS). Along with GPS and GIS, a wide range of sensors, monitors, and controllers are used to instruct exact motion of equipment, deliver at precise location, apply fertilizers and pesticides, and analyze all data in combination with agronomic, climatic, and other sources of data for precise monitoring of crop environment.

Wireless Nanosensors in Precision Farming

The sensing devices with sensing dimensions (at least one dimension) less than 100 nm are called nanosensors. In precision farming, nanosensors are crucial for (a) monitoring chemical and physical event in crop and soil environment, (b) assessing soil and plant nutrient status, (c) detecting pathogens in crops, etc. Nanosensors are broadly categorized as physical (to measure pressure, mass, displacement, or force), chemical (to determine gas concentration, the occurrence of particular molecular species), and biological (to monitor biomolecular processes) nanosensors. In case of precision farming, wireless nanosensor networks are required for precise and continuous monitoring. A wireless nanosensor network (WNSN) is a group of integrated nanosensor nodes which interact through electromagnetic communication. Some key features of the WNSN can be highlighted as size of the nanosensor devices (one to few hundreds of nm), graphene-based nanoantennas for electromagnetic communication in terahertz frequency, enormously higher bit rate (Terabits/s), and extremely low transmission ranges (tens of millimeters) (Rupani et al. 2015). Unlike classical communication where transmission is based on continuous signal, nanodevice fails to produce high power signals in the nanoscale at terahertz frequency due to size and energy constraint of nanodevices. In WNSN, short pulse-based Time Spread On–Off Keying (TS–OOK) modulation technique is used (Rupani et al. 2015).

Network Architecture of WNSNs

WNSNs are a very exciting research area due its numerous practical utilities impacting our daily lives and changing the society. The association of nanosensor and nanoactuator devices, prevailing wireless communication networks, and eventually the Internet needs to make new networking architectures. WNSN is composed of several components that are nano-nodes, nano-router, nano-micro interface, and

gateway. Nano-nodes perform simple calculation with restricted memory under narrow transmission range. Nano-routers are able to perform larger computations than nano-nodes and regulate the performance of nano-nodes by switching very easy commands (on/off, read, sleep, value, etc.). But, nano-routers are more invasive due to their larger size. Nano-micro interface are able to integrate the nano-router's information and send it in microscale and vice versa. Gateway device is capable of controlling the nanosensor network remotely over the Internet. However, gateway development and organizing and managing network structure over the Internet are very challenging and under open research areas.

Challenges in Nanocommunication

Nanocommunication is a fast developing research area determined for the development of novel communication techniques to be used for nanodevices (Dressler and Kargle 2012) in agriculture. There are several challenging issues in nanocommunication that have to be addressed as the research moves forward such as nanoantennas (length~100 nm) and nanotransceivers. The requirement of higher frequency in nanoantennas, generally greater than 10 terahertz, can be overcome by using graphene or carbon nanotubes to reduce the necessary frequency to 0.1 terahertz. In addition, the quantum effects at nanoscale level need to be considered. There may be two potential frequencies, namely, the megahertz and the terahertz band, which work for networks of wireless nanosensor. In addition, communication for nanosensor would be able to work over longer distances at lower frequencies. Though, the generation of electromagnetic wave in a nanodevice through mechanical process is not energy efficient at all, in contrast, higher-frequency waves can control thousands to millions of nanosensors installed for a larger area. For that nanosensors should essentially communicate in terahertz frequency (0.1–10.0 THz) which is a least probed band of electromagnetic spectrum. Thus, developing the new channel models in the terahertz frequency is primary research challenge for communication of nanosensor device (Akyildiz Ian and Jornet 2010). Another challenge in nanocommunication comprises nanotransceivers. The existing graphene transistors can only switch at 100 GHz, and the electronic noise restricts communication range. So it is very much required to develop faster transistors in the range of 1–10 terahertz and formulation of more accurate models of noise in graphene-based electronics (Dressler and Kargle 2012). The major challenge witnessed in design and analysis of the wireless nanosensor networks is communication between nanodevices. Due to limited energy supply in nanosensor device, energy harvesting and consumption are a big issue in WNSN. Size of the network also affects the network efficiency, as the number of nano-nodes varies with the size of network. These may have different behaviors of packet loss ratio (PLR) and packet delay with various sizes of networks. To manage the size of the network and other parameters of the network, efficient medium access control (MAC) protocol and routing algorithm are required (Rupani et al. 2015).

Possible Applications in Precision Farming

Nanosensor-based devices can be the key players for real-time and automatic monitoring if they perform as per their design and omnipresent wireless sensors will become an indispensable aid of getting this vision of precision agriculture to a maturity. The networked nanosensors distributed throughout the field are anticipated to deliver detailed and comprehensive data on crop and soil environments like soil moisture, nutrient status of soil and crop, soil temperature, weed infestations, insects, and plant diseases and transmit that information in actual time to a distant place (Joseph and Morrison 2006). Such real-time monitoring with wireless nanosensors throughout the crop fields provides crucial data on best sowing and harvesting time of the crops, the precise application of required amount of water and fertilizers, spraying of herbicides and pesticides, and other treatments. This has motivated precision farming to maximize its controlling power. In the near future, more precise water distribution systems can be developed which requires storing of water, in situ water holding capacity (WHC), soil moisture availability at roots, plant's efficiency to absorb water, demand-based release of encapsulated water, and communication with field intelligence through wireless nanosensor networks. As the components of nanodevices such as nanosensors, processor, antenna, and memory consume very less energy, the nanosensor mote provides prolonged battery duration than normal sensor which used to be positioned in the crop plant. Again, smallness of sensor node sharply reduces the chance of damaging the mote (Rohith 2015). Another two important applications are monitoring of soil temperature and soil moisture. In water, being a critical input in agriculture, precise information on water distribution near roots is crucial for developing irrigation controlling systems. Traditional methods though expensive and time-consuming are unable to detect and dispatch real-time information of soil moisture and temperature when required. Development of low-cost sensors based on wireless nanotechnology showed huge potential for moisture detection as well as soil temperature. These sensors are made up of MEMS (microelectromechanical systems) cantilever beams covered with nanopolymer layer sensitive to moisture detection and on-chip piezo-resistive sensor for temperature sensitivity. MEMS sensors based on nanotechnology are capable of sensing as well as responding to variations in the crop and soil environments using microelectronic circuits (Madou 1997). A project called SoilNet focused to develop a sensor network sensitive to soil moisture variations for temporal and spatial monitoring in small catchment area of the Wüstebach (about 26.7 ha) consisting of 12 coordinator nodes along with 286 sub nodes was established. The SoilNet has typical features like dynamic and expansible wireless sensor network using high-level communication protocol (Zigbee), longer battery life, easily accessible database for measured data, and customized configurations for nodes to facilitate adapted measurement arrangements. It was effective in monitoring the soil moisture changes on a 100 by 100 meter forest plot site located on the premises of the Forschungszentrum Jülich equipped with 25 end devices each consisting of 6 vertically arranged soil water content sensors. (http://eprints.dbges.de/57/1/3.pdf).

Precision Agriculture Monitoring System (PAMS)

The basic functionalities of a precision farming system should contain real-time sensing of different crop production parameters likes crop, soil, or environment parameters, etc.; positioning of sensing location and data accumulation; and decision-making using the accumulated data. For precise monitoring of a farming system, sensors are placed in the open crop field outside the control station and positioned on static locations with unique sensor ID for network configuration and deployment. PAMS allows continuous (24 × 7 h) control of environmental data, various thresholds, and health of network and alerts and produces different decisions from aggregated data. Thus, real-time monitoring is possible from anyplace outside the field whenever it is required. Each sink node positioned in different locations in the crop field is wirelessly linked to the central server. Each sink gathers data from the field sensors and transmits a query request to the leader of the cluster which forwards it to sink node in the similar way as event information is forwarded. If it matches, it directs the event data back to the sink along the reverse path (Rohith 2015).

There are some nanotechnology-based advanced concepts for precision farming.

Smart Dust Sensors

The development of autonomous wireless tiny sensors was started in 20 years back by a robotics professor, Kris Pister, at University of California. These motes or "smart dust" sensors utilize silicon etching technology for an onboard power supply, computation abilities, detection, and then communication with other neighborhood motes which make these motes efficient enough to transmit data wirelessly. Presently different companies (Crossbow Technologies with Millennial Net and Ember) are manufacturing "smart dust" sensors, and Motorola, Intel, and Philips are also planning to do so. Scientists are studying wireless sensor networks by installing motes (approx. no. 120) for remote monitoring of microclimates around redwood trees in Sonoma County, California (USA) (ETC report 2004).

Agrinfortronics

The effective blend of information and communication technology (ICT) and mechatronics for agricultural applications is known as agrinfortronics (Opara 2002). It is presumed that the future of agriculture is highly dependent on the knowledge economy which includes sensing, acquirement, analysis, storage, and broadcast of precise and consistent data about the crop production environment (Opara 2002). "Millipede," a new concept of data storage (terrabit) based on scanning probe, is reported by Vettiger et al. (2002) which provides ultrahigh density with very small size and high data rate.

Ambient Intelligence

A very new discipline is emerging today, known as "ambient intelligence." It is an improved version of intelligence aimed at developing smart environments which utilize artificial intelligence (AI) and sensors to foresee the individual needs and react accordingly (Cook et al. 2009).

Smart Delivery Systems

In the near future, nanosensor with unique characteristics could be developed to reform the agricultural systems as "smart." "Smart cards" can be implanted inside plants for optimizing productivity, resource utilization, and product traceability and "smart machines" for attaining higher accuracy, capacity, and appropriateness of the operations. Similarly, smart nano-micro machines can be developed to alleviate the impacts of agriculture in the environment and ecosystems (Opara 2002). As, for example, tiny sensors can be utilized to detect plant diseases before showing visible symptoms and thus can be used for both prevention and early warning through controlled or smart delivery of chemicals in a similar manner for drug delivery of nanomedicine in humans (Khiyami et al. 2014).

The USDA has shown innovative way for developing "Smart Field System" going beyond sensing to autonomous detections, locating, report generation, and application of water, fertilizers, and pesticides. Intel has developed nanoscale sensors and mounted motes in a vineyard in Oregon, USA, for minute-scale temperature measurement with "proactive computing." Similarly, Crossbow Technologies (www.xbow.com) has developed motes which are capable for managing irrigation water in the farm, pesticide application, detecting and warning of frost occurrence, timing to harvest farm produce, bioremediation, and assessing of water quality. For years, researchers are working to develop more efficient fertilizer and pesticide delivery systems for controlled discharge of their cargo responding to various indicators such as electromagnetic fields, moisture, heat, etc. due to the changes in environmental conditions. Agrochemical companies like Syngenta has developed nanoemulsion product named Primo MAXX® plant growth regulator that increases resistance against different stress occurrences during the crop growing period and Karate® ZEON, an encapsulated product that provides control against insect pests of different crops like soybeans, cotton, rice, and peanuts.

Environmental Remediation

Environmental remediation is degradation and sequestration of pollutants. The application of nanomaterials, i.e., nanoremediation for remediation, would be more rapid or cost-effective. Nanoremediation (use of nanoparticles for environmental remediation) can be used to treat ground and surface water (purification disinfection and desalination), wastewater, soil, sediment, or other pollutants (Crane and Scott 2012) and to control air pollution. In nanoremediation, reactive nanomaterials are used to detoxify and transform the pollutants. In this process, reactive nanoparticles are injected into a contaminated aquifer via an injection well. The reactive nanoparticles are carried away with groundwater to the contaminated site. When the nanoparticles come to contact with contaminants, these can sequester through adsorption or complexation, immobilize them, and degrade the contaminants to less toxic and less mobile compounds. Drilling and packing of well are very expensive. Direct push wells are less costly than drilled wells and are the most frequently used

Table 9.2 Uses of different types of nanomaterials for surface and wastewater treatments

Nanomaterial	Advantage/disadvantage	Uses
Nanoadsorbents like carbon nanotubes (CNT), zeolites	High surface area, greater adsorption rates, control release of active ingredients, small footprint, but high production costs and health risk	Point-of-use, removal of organics, highly degradable pollutants, heavy metals and bacteria
Nanometals and nanometal oxides like TiO_2 and nZVI	Little intraparticle diffusion distance compressible, abrasion-resistant, magnetic, bactericidal and low human toxicity, photocatalytic in nature highly reactive but less reusable	Arsenic removal of and radionuclides, groundwater remediation
Membranes and membrane processes like nanoCeram, aquaporins	Reliable, high selectivity, water	All arenas of water and wastewater treatment processes
	Permeability and bactericidal basically automated process comparatively more energy requirement	

Adapted and modified from Gehrke et al. (2015)

tool for remediation with nano-iron. A nanoparticle slurry is also used for site-specific regions (Lowry 2007). Performance of many reactive nanoparticles has been evaluated. Nanoscale zeolites, noble metals, carbon nanotubes (CNT), metal oxides, and titanium dioxide (Table 9.2) are used for environmental remediation.

Nanoscale zerovalent iron (nZVI) is the utmost attractive and usually used material for environmental remediation because of high surface area and reaction rate. nZVI with particle diameter range from 10 to 100 nm are injected into the site for degrading contaminated site by creating a nanoparticle "wall" which cleans water when contaminants pass through nZVI or by using mobile nanoparticles sufficiently small to pass through soil pores (Fig. 9.1). When nZVI is used for remediation of contaminated site, it generates less amount of hazardous compound during the remediation process (Varma and Nadagouda 2009). Bimetallic nanoparticle (BNP) is also used in nanoremediation. BNP consists of iron or other metal elements conjugated with metal catalyst like platinum (Pt), nickel (Ni), gold (Au), and palladium (Otto et al. 2008; Zhang and Elliot 2006). Palladium and iron BNPs are mostly used for TCE (trichloroethane) removal (Zhang and Elliot 2006). Recently, use of carbon nanotubes (CNTs) has been increased because of unique properties. CNTs are nanomaterials that are rolled into a tube and are categorized as single-walled carbon nanotubes (SWNT) and multi-walled carbon nanotubes (MWNTs). They are applied for the removal of heavy metals like Cr^{3+}, Pb^{2+}(Li et al. 2003), and Zn^{2+} (Rao et al. 2007), metalloids like arsenic compounds (Peng et al. 2005), and removing persistent organic pollutant (POP) like dioxin (Long and Yang 2001) and volatile organic compounds (VOCs) (Agnihotri et al. 2005). The use of various nanomaterials like CNTs and TiO_2 shows potential for purification, disinfection, and desalination of surface water (Theron et al. 2008). Common contaminants present in surface waters are heavy metals, organic pollutants, and pathogens. In surface water

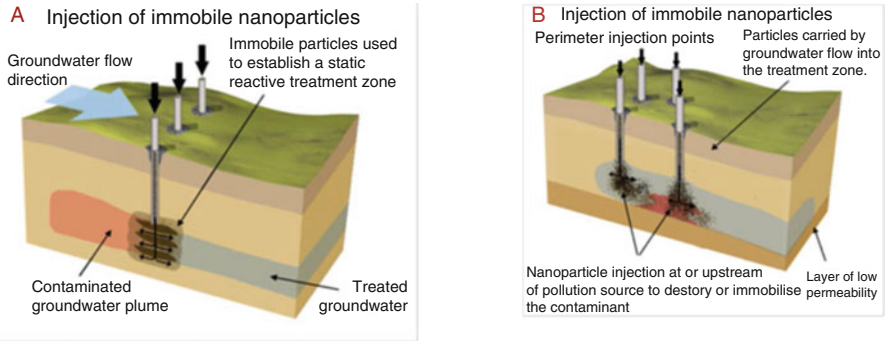

Fig. 9.1 Schematic of how (**a**) immobile nanoparticles and (**b**) mobile nanoparticles are injected into the subsurface for groundwater treatment. (Modified from Crane and Scott 2012)

treatment, nanoparticles may be used as sorbents or reactive agents (like photocatalysts or redox agents). Nanoparticles are also used in membranes for nanofiltration. Nanoparticle-based filtration techniques can be used for controlling air pollution. Automobile tailpipes and factory smokestacks fitted with nanofilters will be able to separate contaminants and will prevent their atmospheric entry. Nanosensors can be used to detect toxic gas leakage even at extremely low concentrations.

9.2.2 Crop Improvement

Nanotechnology has lured scientists to think differently. It has been able to modify the genetic makeup of the crops, which has otherwise been possible through mutation breeding. A nanotech research endeavor in Thailand aimed to modify the characteristics of indigenous rice cultivars, including the famous jasmine rice, at atomic level. It is an endeavor to rule out the controversy over genetically modified organisms (GMOs) as the nanobiotech helps agriculture to avoid the argument of GMOs and to reach to the next level – atomically modified organisms (AMOs). According to BIOTHAI, scientists of nuclear physics lab at Chiang Mai University have stepped forward and have been successful to modify the color of an indigenous rice cultivar, "Khao Kam," using nanotechnology. The meaning of the word "Kam" is deep purple, and the cultivar is known for the purple stem, leaves, and grains. The purple color of the stems and leaves of the cultivar has been changed from purple to green by the scientists using nanotechnology. Scientists of the research group told that their next target is to deal with jasmine rice. They are targeting to breed a modified jasmine cultivar which will be photo-insensitive and can be cultivated throughout the year, having dwarf stems and better color of grain (Anonymous 2004; Prasanna 2007). The researchers at Chiang Mai are using a type of mutation breeding. They are trying to find out an ideal passage through the cell wall and

membrane of plant so that the nanoparticle can penetrate the cell to induce targeted alteration in the genetic makeup without hampering other essential functions of the cell wall and membrane. Crop improvement through mutation breeding and nuclear physics are well-known method, and the United Nations Food and Agriculture Organization/International Atomic Energy Agency program in Vienna have significant contribution in this line since inception of the technology. Since the beginning, scientists have been imposing X-rays, beta rays, and gamma rays on plant cells to modify genetic makeup of crop plants (Anonymous 2004; Prasanna 2007).

Nanobiotechnology is an emerging area of research, in which modern advances in nanotechnology have been integrated into the biology domain, in particular into molecular biology and cell biology. This convergence of technology with biology at the nanolevel is called "nanobiotechnology" which is a highly interdisciplinary field of research. We are just beginning to understand the nanoscale methods used in nature to create self-replicating, self-monitoring, self-controlling, and self-repairing tools, materials, and structures. The term "nanobiotechnology" has been coined by Lynn W. Jelinski who is a biophysicist at Cornell University, USA. Exploiting the unprecedented properties of biological molecules and cell processes, nanotechnologists can achieve many goals that are otherwise difficult or impossible to achieve. Ladder structure of DNA serves as natural platform to nanotechnologists for assembling nanostructures, rather than by building silicon scaffolding. It is possible because of high specificity in bonding properties that assemble atoms together in a predefined arrangement to create a nanostructure. Nanomachines are being structured taking DNA as an indispensable part. Most appropriately, DNA, the information storage molecule, may serve as the basis of the next generation of computers. In the transforming process of microprocessors and microcircuits to nanoprocessors and nanocircuits, microchips are replaced by DNA molecules mounted onto silicon chips. These DNA-based processors or biochips use DNA's amazing capacity of storing information. Nanobiotechnology, in this way, is a promising field of science that converges both nano/microfabrication and biological systems to offer advantage to both. It relates to all applications of genomics including plant, microbial, and mammalian. It helps in designing the basic tools and subsequently the technology for collecting information of sequence and designing innovative devices to address the biologically important issues of the genomic science and the application of this knowledge in diverse fields, particularly medicine and agriculture (Prasanna 2007).

The usage of nanoparticles in seed before sowing is comparatively safe as several metabolic, physiological, and morphological changes occur before the plant biomass or seed production takes place. The high initial vigor, foliage growth, and good germination in thickly sown crop help in suppressing the weeds and enhancing the biomass. Some promoting and promising results have been found regarding enhancement of germination (Khodakovskaya et al. 2009) and yield (Prasad et al. 2012) by nanoparticles (NPs) in different crops. Lu et al. (2002) have proved that nanosized TiO_2 and SiO_2 jointly could enhance several growth-promoting parameters and in fact accelerate its germination and growth. It has also been seen that TiO_2 nanoparticles boost seed germinability and plant growth in spinach (*Spinacia*

oleracea) (Zhang et al. 2005). Zhang et al. (2005) and Hong et al. (2005) reported that nanosized TiO_2 could promote photosynthesis and nitrogen metabolism and consequently improve the growth of spinach at a suitable concentration. But Yang and Watts (2005) concluded that treatment with uncoated alumina nanoparticle inhibit root elongation of cucumber (*Cucumis sativus*), corn (*Zea mays*), cabbage (*Brassica oleracea*), soybean (G. max), and carrot (*Daucus carota*). Zhang et al. (2005) reported that nanosized TiO_2 treatment at 250–4000 ppm, in comparison with bulk TiO_2, improved the germination rate and the germination and vigor indexes of spinach. Gao et al. (2006) revealed that nano-anatase TiO_2 accelerated Rubisco carboxylase activity by 2.67 times in *S. oleracea*. Lee et al. (2008) concluded that the growth rates of *Phaseolus radiatus* and *Triticum aestivum* plants were retarded when exposed to nanoparticles and there was a negative correlation between seedling length and the concentration of nanoparticles. It is clear from different studies that nanoparticles can influence the germination, growth, and yield of different crops. In several experiments (Maity et al. 2016), NPs enhanced germination significantly, but at higher doses, in some cases, it reduced the germination. Regarding yield data at field level, scanty of literatures (Maity et al. 2016, 2018; Srinivasan et al. 2017) have still been produced. Prasad et al. (2012) suggested that the micronutrients like Zn content of seed could be enriched after treating seed with nanoscale ZnO that eventually improves the germination, shoot–root growth, dry weight, and pod yield. In our study, ZnO NPs enhanced seed yield at lower doses whereas decreased it at higher doses, but NPs overtook the control at all doses. Roghayyeh et al. (2010) have also reported that treatment with nano-iron could increase in leaf and pod weight and finally the seed yield of soybean, whereas the growth of *Sesbania* was unaffected by treatment with nano-gold even up to 200 ppm. Musante and White (2010) have reported a reduction in growth of *Cucurbita pepo*, on treatment with silver and copper nanoparticles, whereas Miao et al. (2007) have reported the same trend with silver nanoparticles on phytoplankton growth. Still, limited information is available on the exact mode of action of the nanoparticles on crop plants. Metal nanoparticles provide additional surface area for electron exchange with biomolecules (Shah and Belozerova 2009), and thus, antioxidant status of the treated living materials can be altered by nanoparticles, by virtue of their innate role in cellular redox reactions.

9.2.3 Crop Protection

To meet the food demand of growing population, there is excessive use of pesticide worldwide to combat pests and pathogens. Alternative way of restricting use of pesticide is the need of the hour. Very less amount of pesticides (nearly 0.1%) reaches to the target sites, and the rest are lost to the environment by runoff, spray drift, off-target deposition, and photodegradation, thus increasing environmental and application costs (Castro et al. 2013). Among the latest progress in agricultural sciences, nanomaterials play a very important role in plant protection since it has

distinctive physical and chemical characteristics. Nanotechnological application in plant pathology offers new insights toward crop protection. Nanoparticles stay bound to the pathogen cell wall and causes malformation because of more energy transfer and ultimately causing its death. Nanomaterials accomplish the two vital aspects of disease management: first, efficiency with negligible ecological effect and reduced toxicity to human health (Mousavi and Rezaei 2011). Nanomaterial can be used in plant protection through controlled release of encapsulated pesticide against pests and pathogens, timely detection of plant diseases and pollutants from pesticide residues by nanosensors (Ghormade et al. 2011). Nanomaterials are used efficiently for safe administration of pesticides, herbicides, and fertilizers at lower doses to cover big plant surfaces and thousands of plants (Kuzma and VerHage 2006). Nanopesticide formulations improve the solubility of less soluble active compound and aid in releasing the active compound gradually (Kah et al. 2012). Nanoparticles are packed with pesticides and released gradually depending on the need (Lauterwasser 2005). As nanoscale products are highly reactive as compared to the bulk material, very less amount of nanocides shows improved effect in crop protection (Debnath et al. 2011). Nanoencapsulation of pesticide for measured and effective release to a specific host plant for pest control lets the chemical to be correctly adsorbed by plants (Scrinis and Lyons 2007). The way through which the nanomaterials are absorbed into the plants and their subsequent movement within plant tissues and organs is very important while formulating the nanoproduct. The formulation varies depending on the absorption of active ingredient through leaves or roots of plants. Root can easily absorb nanocides, but if the nanomaterial is imbibed through leaves, then better efficiency will be obtained. Nanosensors can be used to detect soilborne disease through the amount of different oxygen demands of microbes in the soil. The application of nanomaterial in plant protection has been given in Table 9.3.

9.2.4 Food Processing/Packaging Processing/Export Potential of Ethnic Foods

Nanotechnology has immense potential to reform food systems besides agriculture (Rashidi and Khosravi-Darani 2011). The nanoscale level of foods affects efficiency, safety, bioavailability, and nutritive value of novel food products and ingredients (Aguilera 2005). Main areas of nanotechnology application in food science include improving processing and food security, absorbable plant nutrients, taste and nutrition, distribution methods, functionality of diets, pathogen detection, environmental protection, and low-cost storage and dissemination (Rashidi and Khosravi-Darani 2011). The main areas of nanotechnology applications in food production are given in Table 9.4. Application of nanotechnology in food industry (Rashidi and Khosravi-Darani 2011) has been given in Fig. 9.2.

Table 9.3 Application of nanomaterials in plant protection

Nanomaterials	Microbes	Advantages	References
Biopolymer nanoparticle s	*Xanthomonas perforans*	Readily biodegradable, nontoxic, environment-friendly, safe and low-cost materials	Ocsoy et al. (2013)
Chitosan chitosan, chitosan-saponin, and cu-chitosan nanoparticles	*Fusarium solani*	Biodegradable and nontoxic	Ing et al. (2012) and Saharan et al. (2013)
Metallic nanoparticles (silver, silicon, copper, zinc)	Silver nanoparticle – *Colletotrichum* species, *Bipolaris sorokiniana* and	Unique chemical and physical properties, small size, huge surface-to-volume ratio, structural stability, and strong affinity to their targets	Kumar et al. (2010)
			Lamsal et al. (2011)
	Magnaporthe grisea, *Fusarium graminearum*, *Botrytis cinerea*, and *Penicillium expansum*		Jo et al. (2009)
			He et al. (2011)
	Silicon nanoparticle		
Nanocomposites	*Aspergillus Niger*	Strong growth inhibitory action	Pinto et al. (2013)
Nanostructured alumina	*Sitophilus oryzae* L. and *Rhyzopertha dominica* (F.).	Cheap and reliable alternative for pest management	Stadler et al. (2010)
Validamycin-loaded nanosized calcium carbonate	*Rhizoctonia solani*	Better germicidal efficacy	Qian et al. (2011)
Thiamine di-lauryl sulfate (TDS) nanoparticles	*C. Gloeosporioides*	80% growth inhibition	Seo et al. (2011)

Research on encapsulation of active compounds like vitamins, antimicrobials, minerals, drugs, probiotic microorganisms, drugs, and micronutrients with nanomaterial is necessary (Chen et al. 2006; Hsieh and Ofori 2007). Encapsulation is done in food science to veneer aromas or flavors, control interactions and release of active ingredients, confirm accessibility in target at precise rate, and defend them from moistness, heat (Ubbink and Kruger 2006), and chemical and biological deterioration gradation in the course of processing, packaging storage, and distribution (Weiss et al. 2006). Large varieties of delivery methods like emulsions, biopolymer matrices, simple solutions, and association colloids have been industrialized to preserve active compounds for extended time periods (Jelinski 2002). The delivery systems efficiency can be amplified by dendrimer, a unique group of polymer-coated nanoparticles. Fixed and extremely branched three-dimensional organized dendrimers can be used as sensors and catalysts, in drug delivery and in gene therapy (Hughes 2005). It is nontoxic, nonimmunogenetic, and biodegradable (Khosravi-Darani et al. 2007; Aulenta et al. 2003). Multilayered structured cochleates are very small in size and can be used to capture various bioactive constituents with less water solubility, protein and peptide, drugs, and large hydrophilic molecules (Gould-Fogerite et al. 2007). By

Table 9.4 Possible application of nanotechnology in food science

Area of application	Uses
Design of nanotechnology-based materials like particles, emulsions, composites, biocomposites, laminates	Novel product with self-assembling, self-healing, and self-manipulating characteristics
Nanosensors and nanobiosensors for food safety and quality control	Detection of very less concentration of contaminants, checking and labeling of food items, sensor evaluation through electronic nose and tongue, detection of foodborne pathogen through measurement of indicator metabolite of microorganism like nucleic acid and protein
Nanotechnology-based food processing through filtration, enzymatic reactor, heat and mass transfer, fabrication, nanocapsules for alteration of nutrient absorption	Selective path of materials according to shape and size, process understanding, greater high temperature-resistant packaging, nanoceramic pan for less roasting time and oil consumption, increase use of plant oil for reduced trans–fatty acid consumption, incorporation of nanocapsules into food for increased absorption of desired nutrients
Packaging	Nanocomposites are used as barriers, coating, release device, and novel packaging, modifying the permeation behavior of foils, increasing mechanical, thermal, chemical, and microbial properties, improving mechanical and heat-resistance behavior
	Nanomycells are used for nutrition nanotherapy and controlled release of nutrients, proteins, antioxidants, and flavors through nanoencapsulation and nanoscale enzymatic reactor to develop new product and omega-3 fatty acid, haem, lycopene, beta-carotene, phytosterols, DHA/EPA-fortified food items

Adapted and modified from Rashidi and Khosravi-Darani (2011)

altering gas or moisture permeability, nanoparticles can increase mechanical and high temperature-resistant characteristics of food pack and consequently increase shelf life span (Rashidi and Khosravi-Darani 2011). Scientists are trying to develop devices for detection of very minute fractions of pathogens in food by exploiting unique attributes of nanomaterials. Biosensors are used to identify target analytes through alteration in biological reactions. Nanobiosensors may be applied for the detection and identification of pathogens in processing plants and distributors according to food safety standards (Cheng et al. 2006; Helmke and Minerick 2006). Rivas et al. (2006) developed a nanofabricated electrochemical glucose biosensor for identification and quantification of glucose in food items. Development of liposome nanovesicles has helped to detect peanut protein causing allergy in chocolate (Wen et al. 2005). A gold nanoparticle-coated quartz crystal microbalance-based DNA sensor has been developed by Mao et al. (2006) for the detection of *E. coli* O157:H7 synthesized oligonucleotides.

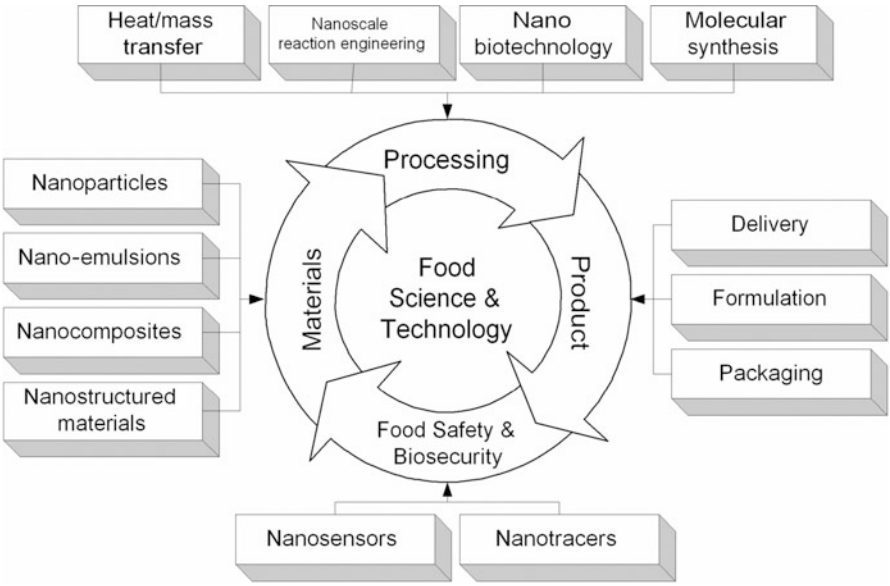

Fig. 9.2 Application areas of nanotechnology in food industry (Ozimek et al. 2010)

9.3 Protocols for Risk Assessment/Safety and Education Awareness

Every technology has light and dark sides. Similarly, the benefits of nanotechnology in agriculture and food security have some ill impacts too. Till today the knowledge is narrow on the implications of nanomaterial exposure on environment and health. But as it is a recent technology, a lot of researches are going on to gather a huge volume of data. Many more are synthesizing the findings of the earlier studies through meta-analysis to come across prudent conclusions (Satterfield et al. 2009). Gradually because of continued development of nanotechnology, people shall recognize its importance and consequences. It will likely to affect public as the mass can largely react like GM crops earlier. The public's willingness to allow research and experiment to precede the uncertain trials may cause hazards to environment and benefits to mankind. In general people reacted more against the consequences might not be aware about the fact properly. They are influenced more by neighbors and friends than facts. Public opinion surveys were conducted to understand the community perception about nanotechnology and its risk in different countries (Dowling et al. (2004) in the UK; Fujita et al. (2006) in Japan; Scheufele et al. (2009) in the USA/EU, Siegrist et al. (2008) in Sweden; Kahan et al. (2009) in the USA). The perception study is critical for any new research arena because the risk perception is not a knowledge deficit but the result of social and psychological factors (Stanovich and West 2008). Another reason is that human behavior is highly influenced by what

they perceive or believe to be correct, because perceptions and biases are not easily altered with new knowledge (Irwin and Wynne 2003). Kahan et al. (2009) reported that peoples' attitudes are prone to be formed by psychological dynamics linked with cultural cognition. Just knowledge dissemination is not enough, but influencing sociopsychological factors and educating people are required to change their attitude, behavior, and belief system toward a new technology. There is need to develop a mechanism for education-led awareness of nanotechnology. Experienced researchers, professors, and teachers should provide accurate information on nanotechnologies and their applications to the public. History has revealed that attempts to fix up risk perceptions with education campaigns may be adverse if the welfares are over highlighted and the hazards are concealed (Satterfield et al. 2009).

Figure 9.3 indicates about the mechanism to make people understand better about the technology. The society is constituted of people having diverse sociopsychological background. The current research proposes that predisposing characteristics such as cultural values, race, gender, and religiosity influence risk perception and welfares associated with a nascent technology are directly related to its effect and indirectly to the interaction of tendency of individuals and effect (Kahan et al. 2009). Accurate information about the potentials and risks of nanotechnology, open access research reports, open discussions, and debates about pros and cons should be made available to the public, and ultimately inclusion of nanotechnology as a subject in school, graduation, and postgraduation educational curriculum should be prioritized. This will make information available to society, and people will be more familiar to the technology, which will result in positive estimations of its applications. Theory says, generally moderate attitudes toward nanotechnology deliver perfect opportunity for superior understandings of risks and benefits (Satterfield et al. 2009).

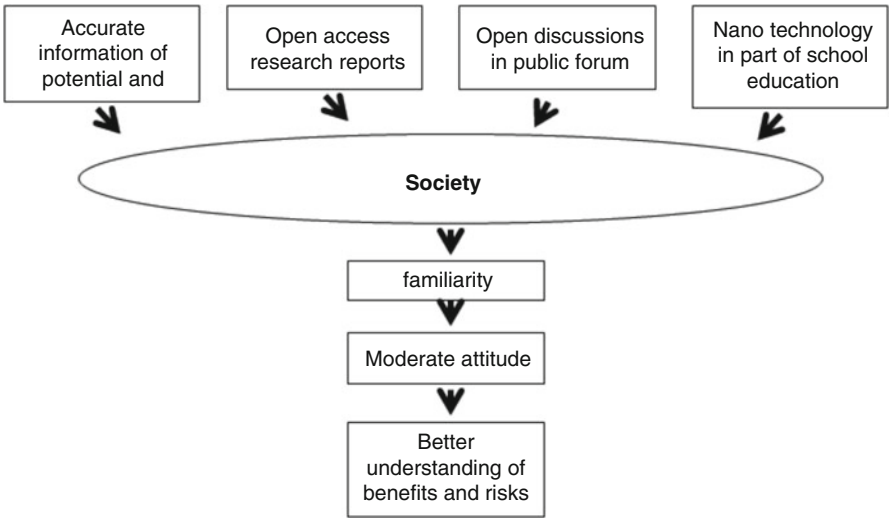

Fig. 9.3 Mechanism for better understanding about nanotechnology

Changing people's attitude is not an easy task. It is depending on the media content, frequency, influence, and above all public exposure to it; hence the government should be proactive.

9.3.1 Protocols for Risk Assessment/Safety of Nanotechnology

There are so many risk perception that researcher are assuming as a result of hazardous nanoparticles. Nanoparticles can go into the human body through ingestion, dermal exposure, and inhalation; and due to high bioavailability, they can pierce the bloodstream, blood–brain barrier, and digestive tract. During regulation development, it should be taken into consideration that nanomaterials exhibit dissimilar chemical properties from their bulk counterparts (Lewinski 2005). Coming to agriculture, nanoparticles can also facilitate deposition of toxins deep into the soil. Because of the larger surface area, nanoparticles can bond with other pollutants and carry them through the soil resulting nano-pollutants to be adsorbed and absorbed deeper and quicker than normal, though many studies didn't find any toxic effect of nanoparticles on soil microbial community (Maity et al. 2016; Srinivasan et al. 2017; Shah and Belozerova 2009). Furthermore, nanoparticles are commonly reactive and may catalyze physical or chemical reactions with the pollutants, which can possibly lead to new toxic compounds. It is still not understandable whether the available alternative approaches are useful at the nanoscale or how much of them have so far been validated for nanomaterials. Before any regulatory decision is brought into effect, some basic questions should be asked addressing the concern dilemma: is the existing regulatory structure adequate? If not, where should the attention be focused for regulating nanotechnology? Therefore, proper risk assessment and safety measures should be taken. In this process science-based policy decisions will help in formulating proper risk assessment protocol. Science helps to take informed policy decisions by availing information of risk and benefit of a technology or a product made out of that.

Risk assessment is required to understand potential hazards, chances of exposure, and its consequent risks to humans and other animals due to nanomaterials. There is a need to determine the level possible risks and implications to the environment. Nanomaterial for mammalian and ecological safety should be characterized and tested properly. Interpretations about potential risk should be made based on scientific evidence and not on speculations. Even though queries exist about the environment, health, and safety consequences of nanomaterials, governments around the globe comprehend that nanomaterials can have significant well-being applications: technologies with improved solar technologies, self-cleaning surfaces, energy efficiency, possibility for application of fewer amounts of a given chemical, substitute to highly toxic chemicals, and the remediation of contaminated sites. It makes a puzzle for regulators or controllers who on the one side may desire to see beneficial

products safe to environment come into the market and on the other side may have several uncertain concerns about its potential risks (Morris et al. 2011).

The US Environmental Defense Fund has suggested that research must be undertaken to examine possible risks all over the nanoproduct life cycle and considering consumer use, employee safety, and environmental effects from product disposal. Nevertheless, this would entail further improvement and modification of the current conventional risk assessment methods. For instance, the mass- or volume-based toxicity standards currently used to evaluate environmental and worker exposure are to be modified. Environmental fate and exposure measurement should be done throughout the experiment, tests, and modeling. Information obtained through such testing must be considered in aggregation with exposure and transformation potential of nanoparticles during life cycle. Combined application of life cycle and risk assessment for nanomaterials has better possibility to provide inclusive answers to questions associated with the risk in their production and use (Christensen and Olsen 2004). Some approaches for managing or preventing nanomaterial risks are redefinition and adaptation of safety policy and necessities, exercising proper level of precaution, qualitative risk assessment, and connecting stakeholders and industry for voluntary cooperation (Murashov and Howard 2009). Conducting such testing in addition to robust characterization of the material being tested requires valid test methods and appropriate dose metrics (Morris et al. 2011).

9.3.2 Recommendation for Safe Nanotechnology for Workplace

The nations have been engaged in framing guidelines for using safe nanotechnology. They are trying to balance between potential hazards to environment and human and the prospect of this technology in daily life. As a result, countries have come out with draft guidelines and precautionary measures to address the issue. Europe, the USA, and other developed and developing countries are on a continuous process to provide logical guidance to its users through monitoring at research as well as consumption level and import and export levels too (Table 9.5). The National Institute for Occupational Safety and Health (NIOSH), USA, has prepared a number of recommendations for safe use of nanotechnology for workplace, and it is an area of emphasis for the Working Party on Manufactured Nanomaterials (WPMN) (http://go.nature.com/rGNFu8). The Federal Institute for Occupational Safety and Health, Germany, and German Chemical Industry Association have made guidelines for the handling and use of nanomaterials in the workplace (http://go.nature.com/8CgPeg). For some of the nanomaterial, it will take substantial time to address the numerous safety questions. Therefore, researchers and risk managers should work in collaboration to develop approaches to limit exposure and identify that specific nanomaterial which may be the source of potential hazards in the future. Industry should come together in this effort.

Table 9.5 Summary of food legislation in EU and some non-EU countries

Country	Responsible organization	Key legislation	Online resources
Europe	European union	Regulation on the Provision of Food Information to Consumers (1169/20119)	http://eur-lex.europa.eu/
		Regulation on Plastic Food Contact Materials and Articles (10/2011);	
		Regulation on Active and Intelligent Materials and Articles (450/2009)	
		Biocidal Products Regulation (528/2012)	
		Cosmetic Products Regulation (1223/2009)	
		Novel Food Regulation (258/97)	
		Registration, Evaluation, Authorisation and Restriction of Chemicals Regulation (1907/2006)	
USA	US Food and Drug Administration (FDA)	Federal Food, Drug, and Cosmetic Act (FFDCA)	http://www.fda.gov/regulatoryinformation/legislation/federalfooddrugandcosmeticactFDCAct/default.htm
	Environmental Protection Agency (EPA)		http://www.fda.gov/Food/default.htm
		Federal Insecticide, Fungicide, and Rodenticide Act (FIFRA)	http://www.epa.gov/oecaagct/lfra.html

(continued)

Table 9.5 (continued)

Country	Responsible organization	Key legislation	Online resources
Canada	Canadian Food Inspection Agency (CFIA)	Food and Drugs Act	http://www.hc-sc.gc.ca/dhp-mps/nano-eng.php
	Public Health Agency of Canada (PHAC)		http://laws-lois.justice.gc.ca/eng/regulations/C.R.C.%2C_c._870/
Australia and New Zealand	Food Standards Australia New Zealand (FSANZ)	Australia New Zealand Food Standards Code	http://www.foodstandards.gov.au/code/Pages/default.aspx
			http://www.nicnas.gov.au/communications/issues/nanomaterials-nanotechnology/nicnas-regulatory-activities-in-nanomaterials
			http://www.foodstandards.gov.au/consumer/foodtech/nanotech/pages/default.aspx
Switzerland	Swiss Federal Office of Public Health (FOPH)		http://www.bag.admin.ch/nanotechnologie/12171/12174/index.html?lang=en
			http://www.bag.admin.ch/nanotechnologie/12171/12176/index.html?lang=en
	Federal Office for the Environment (FOEN)		http://www.bag.admin.ch/themen/lebensmittel/10380/index.html?lang=en
Russia	The Federal Service for the Protection of Consumer Rights and Human Well-Being of the Ministry of Health and Social Development (Rospotrebnadzor)	Sanitary Rules and Regulations ("SanPiN")	http://www.rospotrebnadzor.ru/en/deyatelnost/bilateral.php
Japan	Ministry of Health, Labour and Welfare	Food Sanitation Law	http://www.mhlw.go.jp/english/policy/health-medical/food/index.html
			http://www.jetro.go.jp/en/reports/regulations/
Korea	Ministry of Food and Drug Safety (MFDS)	Food Sanitation Act	http://www.kfda.go.kr/eng/index.do?nMenuCode=61
			http://www.mfds.go.kr/eng/index.do
	Korean food and Drug Administration (KFDA)		http://www.kats.go.kr/english/home/home.asp?OlapCode=ATSU15
	Korean Agency for Technology		

(continued)

Table 9.5 (continued)

Country	Responsible organization	Key legislation	Online resources
	and Science (KATS)		
India	Food Safety Standard Authority of India (FSSAI)	Food Safety and Standards Act (2006)	http://www.fssai.gov.in/AboutFssai/Introduction.aspx?RequestID=kHte14K1h8e3hHK4iHe_doAction=True
China	Ministry of Agriculture	Food Safety Law of China (2009)	http://en.nim.ac.cn/
	Ministry of Health		http://en.nim.ac.cn/division/overview/924
	National Institute of Metrology		
Malaysia	Ministry of Science Technology and Innovation	Food Regulations 1985	http://www.mosti.gov.my/index.php?option=com_content&view=frontpage&Itemid=27&lang=en
		The Food Act 1983	
Iran	Nanotechnology Committee of Food and Drug Organisation		http://nanohealth.ir/pages/static_page.php?id=9&site=1&lang=2
	Iran Nanotechnology Initiative Council (INIC)		http://irannano.org/nano/index.php?ctrl=section&actn=get_section&lang=2&id=22
Thailand	Food and Drug Administration of the Ministry of Public Health	Food Act B. E.2522	http://eng.moph.go.th/index.php/safety
South Africa		Foodstuffs, Cosmetics and Disinfectants Amendment Act (2007)	http://www.sani.org.za/
Brazil	National Agency of Sanitary Surveillance (ANVISA)		http://portal.anvisa.gov.br/wps/portal/anvisa-ingleshttp://www.agricultura.gov.br/
	Ministry of Agriculture, Livestock, and Food Supply (MAPA)		
	Ministry of Health (MS)		

Amenta et al. (2015)

9.4 Conclusions

Nanotechnology plays a role in agriculture, food processing and packaging, food security and water purification, environmental remediation, crop improvement, and plant protection. Nanotechnology has the potential of precise delivery of agrochemicals for improving disease resistance, plant growth, and nutrient use. Nanoencapsulated products show the ability of more effective and site-specific use of pesticides, insecticides, and herbicides in an eco-friendly greener way. It is successfully used in postharvest for maintaining freshness, quality, and shelf life of stored product and check disease occurrences in a fairly safer way. The use of nanomaterials is quite new in agriculture and it requires additional research. Social and ethical repercussions of nanotechnology uses in agriculture have to be considered. Before commercialization and field application, toxicity of nanomaterials has to be evaluated. Nanomaterials may impose negative effects to ecosystem, environment, and humans' health. The possible risks related with released nanomaterials into the ecosystem are quiet vague as perceived by scientists. With advancement in technologies, huge amount of engineered nanomaterials are released into the environment by consumer and commercial commodities. Current vital constraint in application in agriculture is production scale and associated cost. Huge manufacturing of nanomaterials and its efficient use in agriculture will reduce the cost to a radical range.

The potential application of nanomaterials in different agricultural applications needs further research investigation with respect to synthesis, toxicology, and its effective application at field level. In the field of agriculture, there are still many possibilities to explore with new nanoproducts and techniques. Despite these potential advantages of nanotechnology, agricultural applications are very few as compared to other industrial sectors. The success in agriculture is primarily claimed by academic sector. Public opinion and proper regulatory mechanism are very much required for its success at field level. Various regulatory bodies should be involved in safety assessment. Proper labeling on nanoproduct may give negative connotations for a new technology. Consumers may reject nanoproducts after seeing labels. Some studies on consumer preferences demonstrated the overall negative public opinion for nanotechnology. Agro-nanotech pioneering goods are suffering difficulties in getting market, making agriculture still a borderline sector for nanotechnology. This is because of high production costs of nanotechnology-based products, which are requisite in great volumes in the agricultural segment, uncertain technical profits, and legislative doubts, in addition to public opinion. However, the research and development scopes are very hopeful, and the prospects offered by nanotechnology in numerous agricultural uses are being vigorously explored. Moreover, nanotechnology is developing at rapid speed in other arenas. The information achieved in other developing sectors, for example, energy and packaging, may be used, or may deliver spillovers, to agricultural uses too. Precision farming becomes highly advanced and accurate when we choose for synergistic approach of using smart nanosensors, wireless sensor networks with smart dust sensors, ambient intelligence,

agrinfortronics, etc. which allow improved productivity by giving precise information, thus benefiting farmers with superior decisions. Empowering the communication among nanosensors is quite an unresolved challenge. More researches on network size, harvesting of energy, channel modeling, routing algorithm, and more advanced MAC protocol are greatly needed to resolve the challenges and realize this new paradigm.

References

Agnihotri S, Rood MJ, Rostam-Abadi M (2005) Adsorption equilibrium of organic vapors on singlewalled carbon nanotubes. Carbon [Online] 43:2379–2388. Available: web.utk.edu/~enrg/Navigation.../Agnihotri_05_Adsorption_equilibrium. www.springerlink.com/index/u76r1743j02292n3.pdf

Aguilera JM (2005) Why food microstructure? J Food Eng 67(1–2):3–11

Akyildiz Ian F, Jornet JM (2010) Nano Commun Networks 1:3–19

Amenta V, Aschberger K, Arena M, Bouwmeester H, Moniz FB, Brandhoff P et al (2015) Regulatory aspects of nanotechnology in the agri/feed/food sector in EU and non-EU countries. Regul Toxicol Pharmacol 73(1):463–476

Annual report (2017–2018) Ministry of Agriculture, Govt. of India

Anjali CH, Sharma Y, Mukherjee A, Chandrasekaran N (2012) Pest Manag Sci 68:158–163

Anonymous (2004) Antifungal activity of transparent nanocomposite thin films of pullulan and silver against *Aspergillus niger*. http://www.etcgroup.org/es/content/jazzing-jasmine-atomically-modified-rice-asia

Aulenta F, Hayes W, Rannard S (2003) Dendrimers a new class of nanoscopic containers and delivery devices. J Eur Polym 39(9):1741–1771

AZoNanotechnology Article: "Precision Agriculture – Nanotech Methods Used, Such as 'Smart Dust', Smart Fields' and Nanosensors:" http://www.azonano.com/details.asp.ArticleID=1318

Blackmore S (1994) Precision farming: an introduction. Outlook Agric 23(4):275–280

Brady NR, Weil RR (1999) In: Brady NR, Weil RR (eds) The nature and properties of soils. Prentice Hall, Upper Saddle River, pp 415–473

Castro ML, Ojeda C, Cirelli A (2013) Advances in surfactants for agrochemicals. Environ Chem Lett:1–11

Chau C, Wu S, Yen G (2007) The development of regulations for food nanotechnology. Trends Food Sci Technol 18:269–280

Chen H, Weiss J, Shahidi F (2006) Nanotechnology in nutraceuticals and functional foods. J Food Technol 60(3):30–36

Cheng MMC, Cuda G, Bunimovich YL, Gaspari M, Heath JR, Hill HD, Mirkin CA, Nijdam AJ, Terracciano R, Thundat T, Ferrari M (2006) Nanotechnologies for biomolecular detection and medical diagnostics. Curr Opin Chem Biol 10:11–19

Chinnamuthu CR, Boopathi PM (2009) Madras Agric J 96:17–31

Christensen FM, Olsen SI (2004) The potential role of life cycle assessment in regulation of chemicals in the European Union. Int J Life Cycle Assess 9(5):327–332

Cook DJ, Augusto JC, Vikramaditya JR (2009) Ambient intelligence: technologies, applications, and opportunities. Pervasive Mob Comput 5(4):277–298

Corradini E, De Moura MR, Mattoso LHC (2010) A preliminary study of the incorporation of NPK. Express Polym Lett 4:509–515

Crane RA, Scott TB (2012) Nanoscale zero-valent iron: future prospects for an emerging water treatment technology. Nanotechnologies for the treatment of water, air and soil. J Hazard Mater 211–212:112–125

Cui HX, Sun CJ, Liu Q, Jiang J, Gu W (2010) Applications of nanotechnology in agrochemical formulation, perspectives, challenges and strategies. In: International conference on Nanoagri, Sao Pedro, Brazil, pp 28–33

Debnath N, Das S, Seth D, Chandra R, Bhattacharya S, Goswami A (2011) Entomotoxic effect of silica nanoparticles against Sitophilus oryzae (L.). J Pest Sci 84:99–105

DeRosa MC, Monreal C, Schnitzer M, Walsh R, Sultan Y (2010) Nanotechnology in fertilizers. Nat Nanotechnol 5:91

Dowling A, Clift R, Grobert N, Hutton D, Oliver R, O'Neill O, Pethica J, Pidgeon N, Porritt J, Ryan J, Seaton A (2004) Nanoscience and nanotechnologies: opportunities and uncertainties. Royal Society and Royal Academy of Engineering, London

Dressler F, Kargle F (2012) Towards security in Nano-communication: challenges and opportunities. Elsevier Nano Commun Netw 3(3):151–160

EC (2012) Communication from the Commission to the European Parliament, the Council, the European Economic and Social Committee and the Committee of the Regions. A European strategy for Key Enabling Technologies – A bridge to growth and jobs. http://eur-lex.europa.eu/LexUriServ/LexUriServ.do?uri=COM:012:0341:FIN:EN:PDF

ETC group (2004) http://www.etcgroup.org/documents/ETC_DOTFarm2004.pdf. Down on the farm

Fujita Y, Yokoyama H, Abe S (2006) Perception of nanotechnology among the general public in Japan—of the NRI nanotechnology and society survey project. Asia Pacific Nanotechnol Wkly 4:1–2

Gao F, Hong F, Liu C, Zheng L, Su M, Wu X, Yang F, Wu C, Yang P (2006) Mechanism of nano-anatase TiO_2 on promoting photosynthetic carbon reaction of spinach. Biol Trace Elem Res 111:239–253

Gehrke I, Geiser A, Somborn-Schulz A (2015) Innovations in nanotechnology for water treatment. Nanotechnol Sci Appl 8:1–17

Ghormade V, Deshpande MV, Paknikar KM (2011) Perspectives for nano-biotechnology enabled protection and nutrition of plants. Biotechnol Adv 29:792–803

Gould-Fogerite S, Mannino RJ, Margolis D (2007) Cochleate delivery vehicles: applications to gene therapy. Drug Deliv Technol 3(2):40–47

Green JM, Beestman GB (2007) Recently patented and commercialized formulation and adjuvant technology. Crop Prot 26:320–327

He L, Liu Y, Mustapha A, Lin M (2011) Antifungal activity of zinc oxide nanoparticles against *Botrytis cinerea* and *Penicillium expansum*. Microbiol Res 166:207–215

Helmke BP, Minerick AR (2006) Designing a nano-interface in a microfluidic chip to probe living cells: challenges and perspectives. Proc Natl Acad Sci U S A 103:6419–6424

Hong F, Zhou J, Liu C, Yang F, Wu C, Zheng L, Yang P (2005) Effects of Nano-TiO2 on photochemical reaction of chloroplasts of Spinach. Biol Trace Elem Res 105:269–279

Hsieh YHP, Ofori JA (2007) Innovations in food technology for health. Asia Pac J Clin Nutr 16:65–73

http://go.nature.com/8CgPeg

http://go.nature.com/rGNFu8

Hughes GA (2005) Nanostructure-mediated drug delivery. Nanomed Nanotechnol Biol Med 1:22–30

Ing LY, Zin NM, Sarwar A, Katas H (2012) Antifungal activity of chitosan nanoparticles and correlation with their physical properties. Int J Biomater 2012:9

Irwin A, Wynne B (2003) Misunderstanding science?: the public reconstruction of science and technology. Cambridge University Press, Cambridge

Jelinski L (2002) Biologically related aspects of nanoparticles, nanostructured materials, and nanodevices. In: Siegel RW, Hu E, Roco MC (eds) Nanostructure science & technology. A worldwide study, prepared under the guidance of national science and technology council and the interagency working group on nanoscience, engineering, and technology, May 2002. Available online at www.wtec.org/loyola/nano/toc.htm

Jo YK, Kim BH, Jung G (2009) Antifungal activity of silver ions and nanoparticles on phytopathogenic fungi. Plant Dis 93:1037–1043

Joseph T, Morrison M (2006) Nanotechnology in agriculture and food, A Nanoforum report, available for download from www.nanoforum.org

Kah M, Beulke S, Tiede K, Hofmann T (2012) Nanopesticides: state of knowledge, environmental fate, and exposure modeling. Crit Rev Environ Sci Technol 43:1823–1867

Kahan DM, Braman D, Slovic P, Gastil J, Cohen G (2009) Cultural cognition of the risks and benefits of nanotechnology. Nat Nanotechnol 4(2):87–90

Kalpana-Sastry R, Rashmi HB, Rao NH, Ilyas SM (2009) Nanotechnology and agriculture in India: The second green revolution?; Presented at the OECD conference on "Potential environmental benefits of nanotechnology: fostering safe innovation-led growth" Session 7. Agricultural nanotechnology, Paris, France. July 15–17, 2009

Khiyami MA, Almoammar H, Awad YM, Alghuthaymi MA, Abd-Elsalam KA (2014) Plant pathogen nanodiagnostic techniques: forthcoming changes? Biotechnol Biotechnol Equip 28 (5):775–785. https://doi.org/10.1080/13102818.2014.960739

Khodakovskaya ME, Mahmood DM, Xu Y, Li Z, Watanabe F, Biris AS (2009) Carbon nanotubes are able to penetrate plant seed coat and dramatically affect seed germination and plant growth. ACS Nano 3(10):3221–3227

Khosravi-Darani K, Pardakhty A, Honarpisheh H, Rao VSNM, Mozafari MR (2007) The role of high-resolution imaging in the evaluation of nanosystems for bioactive encapsulation and targeted nanotherapy. Micron 38(8):804–818

Kottegoda N, Munaweera I, Madusanka N, Karunaratne V (2011) A green slow-release fertilizer composition based on urea-modified hydroxyapatite nanoparticles encapsulated wood. Curr Sci 101:73–78

Kumar R, Sharon M, Choudhary AK (2010) Nanotechnology in agricultural diseases and food safety. J Phytology 2:83–92

Kuzma J (2007) Moving forward responsibly: oversight for the nanotechnology-biology interface. J Nanopart Res 9:165–182

Kuzma J, VerHage P (2006) Nanotechnology in agriculture and food production: anticipated applications. Project on Emerging Nanotechnologies, Washington, DC

Lamsal K, Kim SW, Jung JH, Kim YS, Kim KS, Lee YS (2011) Application of silver nanoparticles for the control of *Colletotrichum* species *In vitro* and pepper anthracnose disease in field. Mycobiology 39:194–199

Lauterwasser C (2005) Small sizes that matter: opportunities and risks of nanotechnologies. Report in cooperation with the OECD International Futures Programme. http://www.oecd.org/dataoecd/32/1/44108334.pdf

Lee WM, An YJ, Yoon H, Kwbon HS (2008) Toxicity and bioavailability of copper nanoparticles to the terrestrial plants mung bean (Phaseolus radiatus) and wheat (Triticum aestivum): plant agar test for water-insoluble nanoparticles. Environ Toxicol Chem 27:1915–1921

Lewinski N (2005) Nanotechnology policy and environmental regulatory issues. J Eng Public Policy 9:1–37

Li YH, Dinga J, Luanb Z, Dia Z, Zhua Y, Xua C, Wu D, Wei B (2003) Competitive adsorption of Pb2+, Cu2+ and Cd2+ ions from aqueous solutions by multiwalled carbon nanotubes. Carbon [Online] 41(14):2787–2792. Available: http://linkinghub.elsevier.com/retrieve/pii/S0008622303003920

Liu R, Lal R (2015) Potentials of engineered nanoparticles as fertilizers for increasing agronomic productions. A review. Sci Total Environ 514:131–139. https://doi.org/10.1016/j.scitotenv.2015.01.104

Long RQ, Yang RT (2001) Carbon nanotubes as superior sorbent for dioxin removal. J Am Chem Soc [Online] 123(9):2058–2059. Available: www.ncbi.nlm.nih.gov/pubmed/11456830

Lowry GV (2007) Nanomaterials for groundwater remediation. In: Wiesner MR, Bottero J (eds) Environmental nanotechnology. The McGraw-Hill Companies, New York, pp 297–336

Lu CM, Zhang CY, Wen JQ, Wu GR, Tao MX (2002) Research of the effect of nanometer materials on germination and growth enhancement of Glycine max and its mechanism. Soybean Sci 21:168–172. (Chinese Journal)

Madou MJ (1997) Fundamentals of microfabrication. CRC Press, Boca Raton. (Graduate level introduction to microfabrication)

Maity A, Natarajan N, Vijay D, Srinivasan R, Pastor M, Malaviya DR (2016) Influence of metal nanoparticles (NPs) on seed germination and yield of forage oat (*Avena sativa*) and berseem (*Trifolium alexandrinum*). PNAS India Biol Sci B. https://doi.org/10.1007/s40011-016-0796-x

Maity A, Natarajan N, Pastor M, Vijay D, Gupta CK, Wasnik VK, Ghosh PK (2018) Nanoparticles influence seed germination traits and seed pathogen infection rate in forage sorghum (Sorghum bicolor) and cowpea (Vigna unguiculata). Indian J Exp Biol 56:363–372

Mao X, Yang L, Su XL, Li Y (2006) A nanoparticle amplification based quartz crystal microbalance DNA sensor for detection of *Escherichia coli* O157:H7. Biosens Bioelectron 21:1178–1185

Maysinger D (2007) Nanoparticles and cells: good companions and doomed partnerships. Org Biomol Chem 5:2335–2342

McMurray TA, Dunlop P, Byrne J (2006) The photocatalytic degradation of atrazine on nanoparticulate TiO2 films. J Photochem Photobiol A Chem 182:43–51. https://doi.org/10.1016/j.jphotochem.2006.01.010

Miao AJ, Quigg A, Schwehr K, Xu C, Santschi P (2007) Engineered silver nanoparticles (ESNs) in coastal marine environments: bioavailability and toxic effects to the phytoplankton Thalassiosira weissflogii. 2nd International conference on the environmental effects of nanoparticles and nanomaterials, 24–25th September, London UK

Milani N, McLaughlin MJ, Stacey SP, Kirkby JK, Hettiarachchi GM, Beak DG, Cornelis G (2012) Dissolution kinetics of macronutrient fertilizers coated with manufactured zinc oxide nanoparticles. J Agric Food Chem 60:3991–3998

Moraru CI, Panchapakesan CP, Quingrong H, Takhistov P, Liu S, Kokini JL (2003) Nanotechnology: a new frontier in food science. Food Technol 57:24–29

Morris J, Willis J, De Martinis D, Hansen B, Laursen H, Sintes JR, Kearns P, Gonzalez M (2011) Science policy considerations for responsible nanotechnology decisions. Nat Nanotechnol 6(2):73–77

Mousavi SR, Rezaei M (2011) Nanotechnology in agriculture and food production. J Appl Environ Biol Sci 1(10):414–419

Mukhopadhyay SS (2014) Nanotechnology in agriculture prospects and constraints. Nanotechnol Sci Appl 7:63–71. Available online at http://www.ncbi.nlm.nih.gov/pmc/articles/PMC4130717/

Murashov V, Howard J (2009) Essential features for proactive risk management. Nat Nanotechnol 4(8):467–470

Musante C, White JC (2010) Toxicity of silver and copper to Cucurbita pepo: differential effects of nano and bulk-size particles. Environ Toxicol. https://doi.org/10.1002/tox.20667

Naderi MR, Danesh-Sharaki A (2013) Nanofertilizers and their role in sustainable agriculture. Int J Agric Crop Sci 5(19):2229–2232

ObservatoryNANO FP7, European nanotechnology landscape report, 2011. http://www.scor.com/en/sgrc/pac/motor/item/1327-european-nanotechnology-landscape-report.html

Ocsoy I, Paret ML, Ocsoy MA, Kunwar S, Chen T, You M, Tan W (2013) Nanotechnology in plant disease management: DNA-directed silver nanoparticles on graphene oxide as an antibacterial against *Xanthomonas perforans*. ACS Nano 7:8972–8980

Opara LU (2002) Agricultural Engineering education and research in knowledge-based economy. In: Kosutic S (ed) Proceedings of the 30th international symposium on agricultural engineering, Zagreb, Croatia, pp 33–46

Otto M, Floyd M, Bajpai S (2008) Nanotechnology for site remediation. Remediat J [Online] 19(1):99–108

Ozimek L, Pospiech E, Narine S (2010) Nanotechnologies in food and meat processing. Acta Sci Pol Technol Aliment 9(4):401–412

Peng X, Luan Z, Ding J, Di Z, Li Y, Tian B (2005) Ceria nanoparticles supported nanotubes for removal of arsenate in water. Mater Lett [Online] 59(4):399–403. Available: http://linkinghub.elsevier.com/retrieve/pii/S0167577X04007384

Pinto RJ, Almeida A, Fernandes SC, Freire CS, Silvestre AJ, Neto CP, Trindade T (2013) Antifungal activity of transparent nanocomposite thin films of pullulan and silver against Aspergillus niger. Colloids Surf B: Biointerfaces 103:143–148

Prasad TNVV, Sudhakar P, Sreenivasulu Y, Latha P, Munaswamy V, Reddy KR, Sreeprasad TS, Sajanlal PR, Pradeep T (2012) Effect of nanoscale zinc oxide particles on the germination, growth and yield of peanut. J Plant Nutr 35:905–927

Prasanna BM (2007) Nanotechnology in Agriculture. In Parsad R, Gupta VK, Bhar LM, Bhatia VK (ed) Advances in data analytical techniques: module- VI. Indian Agricultural Statistics Research Institute (I.C.A.R.), Library Avenue, New Delhi – 11001. http://www.iasri.res.in/ebook/EBADAT/6-Other%20Useful%20Techniques/10-nanotech_in_Agriculture__BM_Prasanna__1.2.2007.pdf

Qian K, Shi T, Tang T, Zhang S, Liu X, Cao Y (2011) Preparation and characterization of nano-sized calcium carbonate as controlled release pesticide carrier for validamycin against *Rhizoctonia solani*. Microchim Acta 173:51–57

Rai V, Acharya S, Dey N (2012) J Biomat Nanobiotechnol 3:315–324

Rao GP, Lu C, Su F (2007) Sorption of divalent metal ions from aqueous solutions by carbon nanotubes: a review. Sep Purif Technol [Online] 58(1):224–231. Available: https://linkinghub.elsevier.com/retrieve/pii/S1383586606004163

Rashidi L, Khosravi-Darani K (2011) The applications of nanotechnology in food industry. Crit Rev Food Sci Nutr 51:723–730

Rivas GA, Miscoria SA, Desbrieres J, Berrera GD (2006) New biosensing platforms based on the layer-by-layer self-assembling polyelectrolytes on Nafion/carbon nanotubes-coated glassy carbon electrodes. Talanta 71(1):270–275

Roghayyeh SMS, Mehdi TS, Rauf SS (2010) Effects of nano-iron oxide particles on agronomic traits of soybean. Notulae Sci Biol 2:112–113

Rohith RS (2015) Precision farming using Nano based wireless sensor network. Int J Eng Res Gen Sci 3(2):343–350

Rupani V, Kargathara S, Sureja J (2015) A review on wireless nanosensor networks based on electromagnetic communication. Int J Comput Sci Inf Technol 6(2):1019–1022

Saharan V, Mehrotra A, Khatik R, Rawal P, Sharma SS, Pal A (2013) Synthesis of chitosan based nanoparticles and their *in vitro* evaluation against phytopathogenic fungi. Int J Biol Macromol 62:677–683

Satterfield T, Kandlikar M, Beaudrie CE, Conti J, Harthorn BH (2009) Anticipating the perceived risk of nanotechnologies. Nat Nanotechnol 4(11):752–758

Scheufele DA, Corley EA, Shih TJ, Dalrymple KE, Ho SS (2009) Religious beliefs and public attitudes toward nanotechnology in Europe and the United States. Nat Nanotechnol 4(2):91–94

Scott NR (2007) Nanoscience in veterinary medicine. Vet Res Commun 31(Suppl. 1):139–144

Scrinis G, Lyons K (2007) The emerging nano-corporate paradigm: nanotechnology and the transformation of nature, food and agri-food systems. Int J Sociol Food Agric 15:22–44

Seo Y, Cho J, Jeong H, Yim T, Cho K, Lee T (2011) Enhancement of antifungal activity of anthracnose in pepper by nanoparticles of thiamine di-lauryl sulfate. Korean J Med Crop Sci 19:198–240

Shah V, Belozerova I (2009) Influence of metal nanoparticles on the soil microbial community and germination of lettuce seeds. Water Air Soil Pollut 197:143–148

Siegrist M, Stampfli N, Kastenholz H, Keller C (2008) Perceived risks and perceived benefits of different nanotechnology foods and nanotechnology food packaging. Appetite 51(2):283–290

Solanki P, Bhargava A, Chhipa H, Jain N, Panwar J (2015) Nano-fertilizers and their smart delivery system. In: Mahendra Rai, Caue Ribeiro, Luiz Mattoso,·Nelson Duran (ed) Nanotechnologies in food and agriculture pp 81–101

Srinivasan R, Maity A, Singh KK, Ghosh PK, Kumar S, Srivastava MK, Radhakrishna A, Srivastava R, Kumari B (2017) Influence of copper oxide and zinc oxide nanoparticles on fodder cowpea and soil microbiological properties. Range Manag Agrofor 38(2):208–214

Stadler T, Buteler M, Weaver DK (2010) Novel use of nanostructured alumina as an insect. Pest Manag Sci 66(6):577–579

Stanovich KE, West RF (2008) On the relative independence of thinking biases and cognitive ability. J Pers Soc Psychol 94(4):672

Theron J, Moraru JA, Cloete TE (2008) Nanotechnology and Water Treatment: Applications and Emerging Opportunities. Crit Rev Microbiol 34(1):43–69. https://doi.org/10.1080/10408410701710442. ISSN 1040-841X. Retrieved 2014-07-29

Tilman D, Knops J, Wedin D, Reich P (2002) Plant diversity and composition: effects on productivity and nutrient dynamics of experimental grasslands. In: Loreau M, Naeem S, Inchausti P (eds) Biodiversity and ecosystem functioning. Oxford University Press, Oxford, pp 21–35

Torney F, Trewyn BG, Lin VS-Y, Wang K (2007) Mesoporous silica nanoparticles deliver DNA and chemicals into plants. Nat Nanotechnol 2:295–300

Trenkel ME (1997) Controlled-release and stabilized fertilizers in agriculture. International Fertilizer Industry Association, Paris

Ubbink J, Kruger J (2006) Physical approaches for the delivery of active ingredients in foods. Trends Food Sci Technol 17:244–254

Vamvakaki V, Chaniotakis NA (2007) Biosens. Bioelectronics 22:2848–2853

Varma R, Nadagouda MN (2009) Risk reduction vie greener synthesis of noble metal nanostructures and nano composites. Environ Secur [Online] 3:209–217. Available: http://www.springerlink.com/content/l3577386k6q12328/

Veronica N, Tulasi G, Thatikunta R, Reddy NS (2015) Role of Nano fertilizers in agricultural farming. Int J Environ Sci Technol 1(1):1–3

Vettiger P, Cross G, Despont M, Dreschler U, Durig U, Gotsmann B, Haberle W, Lantz MA, Rothuizen HE, Stutz R, Binnig GK (2002) The "millipede" – nanotechnology entering data storage. IEEE Trans Nanotechnol 1(1):39–55

Wanyika H, Gatebe E, Kioni P, Tang Z, Gao Y (2012) Mesoporous silica nanoparticles carrier for urea: potential applications in agrochemical delivery systems. J Nanosci Nanotechnol 12:2221–2228

Weiss J, Takhistov P, McClements DJ (2006) Functional materials in food nanotechnology. J Food Sci 71(9):R107–R116

Wen HW, Borejsza-Wysocki W, DeCory TR, Baeumner AJ, Durst RA (2005) A novel extraction method for peanut allergenic proteins in chocolate and their detection by liposome-based lateral flow assay. Eur Food Res Technol 221:564–569

Yang L, Watts DJ (2005) Particle surface characteristics may play an important role in phytotoxicity of alumina nanoparticles. Toxicol Lett 158:122–132

Zhang WX, Elliot DW (2006) Applications of iron nanoparticle in ground water remediation. Remed J [Online] 16(2):7–21. Available: http://onlinelibrary.wiley.com/doi/10.1002/rem.20078/abstract

Zhang L, Hong F, Lu S, Liu C (2005) Effect of nano-TiO_2 on strength of naturally aged seeds and growth of spinach. Biol Trace Elem Res 106:279–297

Chapter 10
Nanomaterials Based Sensors for Air Pollution Control

Pradip Kar

Contents

10.1 Introduction 350
10.2 Nanomaterials as Receptor for Air Pollutants 353
10.2.1 Inorganic Nanomaterials as Receptor 354
10.2.2 Organic Nanomaterials as Receptor 356
10.2.3 Hybrid Nanomaterials as Receptor 357
10.3 Synthesis of Nanomaterials 360
10.3.1 Synthesis of Inorganic Nanomaterials 360
10.3.2 Synthesis of Organic Nanomaterials 363
10.3.3 Synthesis of Hybrid Nanomaterials 364
10.4 Parameters of Nanomaterials Promising for Sensing 367
10.4.1 Processability 367
10.4.2 Mechanical Strength 368
10.4.3 Stability 369
10.4.4 Transducer Properties 370
10.4.5 Operating Temperature 372
10.5 Sensing of Air Pollutant by Nanomaterials 372
10.5.1 Oxides of Carbon 372
10.5.2 Oxides of Nitrogen 374
10.5.3 Oxides of Sulfur 377
10.5.4 Volatile Organic Compounds 378
10.5.5 Ozone 383
10.5.6 Humidity 385
10.5.7 Ammonia 387
10.5.8 LPG and Hydrocarbons 388
10.5.9 Hydrogen Sulfide 389
10.5.10 Others 390
10.6 Conclusions 391
References 392

P. Kar (✉)
Department of Chemistry, Birla Institute of Technology, Mesra, Ranchi, Jharkhand, India
e-mail: pkar@bitmesra.ac.in

N. Dasgupta et al. (eds.), *Environmental Nanotechnology Volume 4*, Environmental Chemistry for a Sustainable World 32, https://doi.org/10.1007/978-3-030-26668-4_10

Abstract Nowadays air pollution created by chemical gaseous pollutants becomes the major concern for the adverse effect on human health, plant or animal life, or the welfare of man. Thus miniaturized low-cost sensor device based on nanomaterials can be introduced for an observable signal, or warning bell may be set to control the pollution level of outdoor as well as indoor air. Exploring the present state-of-the-art inorganic, organic, or even hybrid nanomaterials used as receptor in chemical sensors to detect the pollutants in the air is briefly considered here.

In that goal, the utility of the various nanomaterials is focused in the sensing of various air pollutants. Among those, the nanomaterials receptors like metal and metal oxide semiconductors, solid electrolytes, insulators, catalytic materials, polymers, etc. including their hybrid nanomaterials have been considered here. The synthesis and required properties of the nanomaterials for the sensing application of specific gaseous pollutants are discussed in brief. The discussion also highlights the activity of nanomaterials for the improvement of sensing performance of existing sensor. Finally the important example of air pollutant sensor based on various nanomaterials is represented elaborately, and challenges for the future development are outlined in this chapter.

Keywords Air pollution · Sensor · Pollution sensor · Environmental sensor · Gas sensor · Nanomaterials · Nanomaterials-based sensor · Nanomaterials sensors

10.1 Introduction

The environment and its related issues have attracted the attention of decision-makers, scientists, and technologists around the globe. This is because environmental issues including climate change, pollution, environmental degradation, resource depletion, etc. must be solved or taken into consideration for the coming generations. Most of the environmental issues are directly or indirectly related to environmental contamination or pollution. Environmental pollution may be defined as the presence of pollutants into the environment adversely altering the natural quality of the environment and causing detrimental effect toward the environment. In addition, the pollutant defines the minimum concentration of exposure that the typical worker can experience without an unreasonable risk of disease or injury. According to the possibility of contaminations in the air, soil, and water, environmental pollution can be divided among the categories of air, soil, and water pollution.

Air pollution may be defined as the presence in the atmosphere of one or more pollutants (or combination thereof) in such quantities and of such durations, which might be injurious to human health, plant or animal life, or the welfare of man. The effects of air pollution are greatly influenced by the type and quantity of pollutants and their possible combinations as well as wind speed and direction, typography, sunlight, precipitation, vertical change in air temperature, photochemical reactions, height at which pollutant is released, etc. Therefore, the complete and timely information regarding the air pollutants would be necessary to achieve healthful

Table 10.1 Common indoor and outdoor air pollutants

Pollution zone	Common air pollutants	Major sources of air pollutants	Important adverse effect
Indoor air pollution	Moisture	Evaporation and boiling of water used	Respiratory
	Oxides of carbon	Combustion of wood, liquefied petroleum gas, coal, kerosene, etc. for cooking, room heating, etc.	Dermal and mucous irritation
	Oxides of nitrogen		
	Oxides of sulfur		Effects on the nervous system
	Liquefied petroleum gas, hydrocarbons		Cardiovascular
	Volatile organic compounds	Cleaning agents, paints, cosmetics, etc.	Effects on the gastrointestinal apparatus
	Ammonia	Urine, cleaning agents, cosmetics, hair color, etc.	Effects on the reproductive system
	Acid	Cleaning agents, detergents, etc.	Infections and intoxication
	Hydrogen sulfide	Vegetable or animal parts thrown in dustbin	
Outdoor air pollution	Moisture	Evaporation of water, snow, dew, etc.	Greenhouse effect
	Oxides of carbon	Combustion of coal, hydrocarbon fuel in refinery, industry, automobile, power plant, refrigerator, air conditioner, volcanic activity, vegetation decay, forest fires, etc.	Global warming
	Oxides of nitrogen		Weather change
	Oxides of sulfur		Depletion of ozone layer
	Hydrocarbons		Photochemical and chemical smog
	Volatile organic compounds	Pharmaceutical, medical, clinical, industrial, refrigerator, air conditioner, etc.	Acid rain
	Ammonia	Decomposition of dead animal, plant, etc.	Adverse effect on plant growth and animal productivity
	Acid		
	Hydrogen sulfide		
	Ozone	Microwave oven, television, electrical discharge, sunlight, etc.	Serious illness

air quality in order to control the air pollution. In general, much attention has been paid to address the outdoor air pollution issues. However, as a person spends average 90% time in a day within indoor environment, indoor pollution issues should be given primary importance. It was not only recently that the international scientific community worried about reducing the indoor air pollution as well. The list and sources of common indoor and outdoor air pollutants are given in Table 10.1. The plants and animals have inbuilt sensor devices for detection of external agencies in their surrounding environments. Electromagnetic type of natural detector is present in plants for sensing against external attacks, and animals are sensing through five

different organs such as the tongue, skin, eye, ear, and nose. However, the sensing of toxic pollutants in the air may create some serious problems like irritation, vomiting, suffocation, illness, etc., or it may be even deadly poisonous for living bodies above the threshold limit value. For example, any animal or plants are not able to live without oxygen. Not only living parts but also the nonliving parts of environment or materials are also badly attacked by air pollutants in their respective life cycle. The simplest example is the rusting of iron in the air. Thus it is better to sense artificially of those hazardous and toxic pollutants before interacting with the living or nonliving parts of environments more efficiently than that the animal detector as well. In order to take timely action over the pollutants, constant analysis is required. Moreover, the threshold limit value can only be detected after the successful sensing of the pollutants in the air. In that goal, the sensing of air pollutants becomes an emerging technological field in the modern period.

A sensor is a device that gives an observable signal by interacting with a particular analyte, viz., physical, chemical, and bio-species. Hence, three types of sensors are known, namely, physical sensors used to measure physical properties like temperature, mass, distance, pressure, etc.; chemical sensors used to analyze chemicals; and biosensors used to analyze biomolecules or bioactivity. The chemical sensors have been categorized into three general groups according to the operating principle: (1) electrochemical sensors (2) optical sensors, and (3) mass sensors. The advantage of sensor is that it measures a physical quantity and converts it into a signal which can be read by an observer or by an instrument consisting of optics, detectors, and electronics. Sensor collects radiation and converts it into some other form suitable for obtaining information in certain pattern (an image, a profile, etc.), a warning, a control signal, or some other signal. Thus using a miniaturized low-cost sensor device, an observable signal or warning bell may be set to control the pollution level of outdoor as well as indoor air. The functioning of simple sensor network is extremely complex. In general, a common sensor consists of a receptor or detection element, a transducing element, and a signal processing element. Such type of simple air pollution sensor setup is shown in Fig. 10.1. The pollutants in the air, i.e., the gaseous pollutants, interact with the receptor or detection element to generate a response. The response from the receptor is read by the transducer part through different transducer principles, followed by amplification and conversion of signal to an interpretable and quantifiable term in the microelectronic signal processor part. In

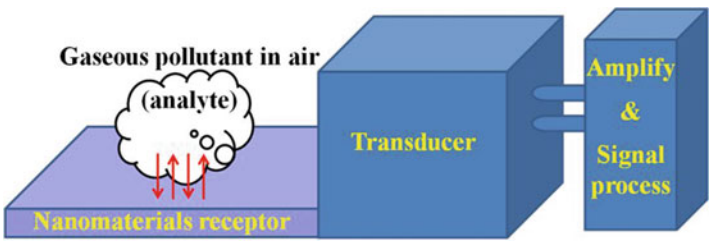

Fig. 10.1 Simple air pollution sensor setup

chemical sensor, various chemical receptors, the heart of the sensor, have been employed like metal and metal oxide semiconductors, solid electrolytes, insulators, catalytic materials, polymers, composites, etc. Among those, exploring the present state-of-the-art nanomaterials used as receptor in chemical sensors to detect the pollutants in the air is our primary goal. The semiconducting metal oxides have been extensively used for this purpose, and some of those are commercialized as well. Recently, the conjugated polymers have been tried to explore as better choice for chemical receptor in sensor. However, the inorganic semiconductors as well as conjugated polymers as receptor for chemical analytes are strongly associated with inherent common serious problems like poor response, poor selectivity, incomplete recovery, higher response and recovery time, low performances, etc. (Adhikari and Kar 2010; Kar et al. 2015). Some of those problems could be easily addressed by simply using the nano-dimensional inorganic semiconductor or conjugated polymers. Moreover, the use of nanohybrids would also open up a new dimension in the field as nanohybrid combination of properties of different materials is possible with keeping properties of nano-dimensional materials.

10.2 Nanomaterials as Receptor for Air Pollutants

The recent development has been directed toward the nanomaterials-based technology as it is well established that the properties of materials change as their size approaches the nanoscale and as the percentage of atoms at the surface of the material becomes significant. The nanomaterials are defined as the materials having one of the dimensions is of the order of a nanometer (10^{-9} miter) and more precisely it should be less than 100 nm. Many important chemical and physical properties of the materials are directly governed by surface area and surface properties, and therefore in nanomaterials the dramatic changes of properties are observed due to having a large surface area for a given volume, i.e., high aspect ratios. In general, these materials classified by their geometries are broadly divided into four classes: zero-dimensional, one-dimensional, two-dimensional, and three-dimensional nanomaterials (Thostenson et al. 2005). The details on classification and their examples are given elsewhere. Various chemical receptors in bulk form or in nanoscale have been employed like metal and metal oxide semiconductors, solid electrolytes, insulators, catalytic materials, polymers, composites, etc. However, the sensing response is distinct and significantly improved in the nano-dimensional materials. For example, the sensing response of hierarchical zinc oxide nanostructured was improved to 59% from 47% observed for micro rods toward 50–200 ppm ethanol at operating temperature of 325 °C (Das et al. 2016). Moreover, according to our scope of discussion, only the nanomaterials or hybrid nanomaterials have been considered here.

The nanomaterials are a generic name given to a vast number of materials, which can have the wide properties and wide applications. These nanomaterials exist in countless numbers because not all the nanomaterials should be used as a receptor for

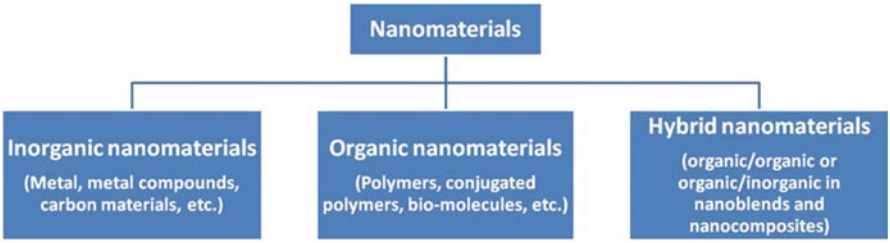

Fig. 10.2 Common types of nanomaterials to be used as sensor receptor

the sensing of air pollutant. These should be categorized to study their synthesis, properties as well as applications elaborately and systematically. The fundamental chemical nature of the materials in chemistry is organic or inorganic. In addition, polymer is a special type of organic or inorganic material with respect to its properties as well as versatility. The mixture of two or more materials may also be included in the classification. Therefore, according to the nature of nanomaterials, there are three types (Fig. 10.2), inorganic nanomaterials, organic nanomaterials, and hybrid nanomaterials, which can be used as receptor for sensing of air pollutants.

10.2.1 Inorganic Nanomaterials as Receptor

As the name suggested, the materials made from rocks and minerals with nano-dimensions are inorganic nanomaterials. The types of inorganic nanomaterials are layered materials, metal, metal oxides, carbon materials, etc. There are almost no reports on the use of metal nanomaterials as sensing receptor for the gaseous air pollutants.

Semiconducting metal oxides are among the most potential candidates to be used as chemical sensors in environmental monitoring, automotive emission monitoring, and aerospace vehicle health monitoring. In principle, semiconducting metal oxide has mainly two types: n-type whose majority carrier is electron such as zinc oxide, tin dioxide, titanium dioxide, ferric oxide, etc. and p-type whose majority carrier is a hole like nickel oxide, cobalt oxide, etc. (Pearce et al. 2003). The chemiresistive gas sensing response of metal oxide sensor generally is recorded at high operating temperature. Initially, oxygen is absorbed on the heated metal oxide film after forming ionic species O^{-2}, O^{-}, and O^{2-} desorbed from the surface at temperatures of 80, 130, and 250 °C, respectively (Labidi et al. 2006; Sahay and Tewari 2005). An increase in the resistance of metal oxide film is observed for n-type semiconducting metal oxide due to decrease in the electron concentration by transferring electron from the conduction band to the chemisorbed oxygen. Alternatively, the resistance of p-type metal oxide is reduced as a hole is created by transferring electron from the conduction band to the chemisorbed oxygen. The gaseous air pollutants can be either oxidizing like nitrogen dioxide, nitric oxide, nitrous oxide, carbon dioxide, etc. or

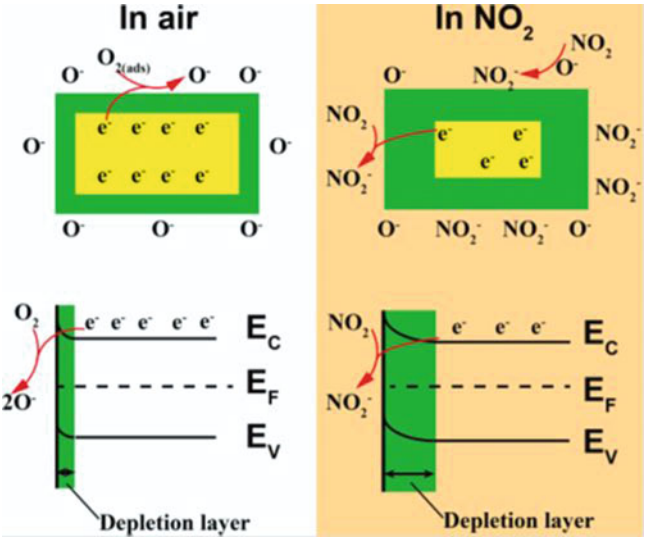

Fig. 10.3 The schematic diagram of the nitrogen dioxide (NO_2) gas sensing by indium oxide nanobricks. (Reprinted with permission of Elsevier from Han et al. 2018)

reducing like hydrogen sulfide, carbon monoxide, ammonia, methane, sulfur dioxide, etc. The concentration of electrons on the surface of metal oxide is decreased during sensing of oxidizing gaseous pollutant as a result of oxidation reaction with adsorbed ionic oxygen species on the metal oxide surfaces. Therefore, the resistance of n-type sensing layer of metal oxide increases, while the resistance of p-type metal oxide surface decreases. In contrast, the electrons are released by the chemisorbed oxygen back to the conduction band due to reduction of gaseous pollutants by the ionic oxygen species on the metal oxide surface. As a result, the resistance of n-type sensing layer of metal oxide decreases and that of p-type metal oxide surface increases. The sensing performance of metal oxide can be limited by limiting analyte or oxygen adsorption–desorption process in bulk morphology and microstructure films. This type of model sensing mechanism is well illustrated in Fig. 10.3 for the sensing of nitrogen dioxide gas by indium oxide nanobricks (Han et al. 2018). Reduction of the bulk surface to nanometer provides high surface area as well as porous networks of metal oxides, and that enhances the uptake/diffusion of analyte or oxygen relative to the bulk surface (Jitianu et al. 2003). For example, the chemisorptions of the reducing gas carbon monoxide and hydrogen gas sensing on the magnesium ferrite were considered as sensing mechanism followed by desorption of the reaction product carbon dioxide or water molecules, respectively, at recovery (Mukherjee et al. 2010).

In the case of carbon nanotube (CNT), the response mechanism is based on changes in electrical properties induced by charge transfer or change adsorption from the molecules of gaseous pollutants. The charge transfer or change adsorption depends on the electron affinity of the gaseous pollutant with respect to the CNT. In

principle, the conductivity of CNT increases by electron withdrawing upon exposure of electron-withdrawing gases such as oxides of nitrogen, phosphorus trichloride, sulfur dioxide, oxygen, etc., and the conductivity decreases by electron donation upon exposure to electron-acceptor gases like hydrogen sulfide, ammonia, hydrazine, methanol, ethanol, etc. Moreover, the main limitation with pristine CNT is its poor sensitivity for minimum charge transfer with analyte molecules and lack of selectivity toward target vapor due to the weak specific interactions (Hatchett and Josowicz 2008).

10.2.2 Organic Nanomaterials as Receptor

The organic materials are made from (or extracted from) plants or animals, and the nano-dimensional organic chemicals are included in this category. The most common organic nanomaterials are nanosized polymers, small organic molecules, etc. Organic polymers are the most widely used versatile materials in the globe due to some serious advantages over the other materials like flexibility, tailorability, processability, environmental stability, low cost, light weight, etc. Polymers are million times bigger than the normal molecules, i.e., macromolecules due to repetitive union (mer unit or repeating unit) of a large number of a reactive small molecule in a regular sequence. The simplest example is polyethylene, where ethylene moiety is the "mer unit" In general, the properties of polymers depend on their chemical composition, molecular structure, molecular weight, molecular weight distribution, and morphology.

Optical sensing principle based on colorimetric, fluorescence, or luminescence effects and on changes in light refraction/propagation on the polymer surface in presence of gaseous analyte has been demonstrated (Adhikari and Kar 2010). However, those optical sensing principles are commonly used for bulk polymer sensing layer as there is no need to introduce the nano-dimensional polymer in order to influence those properties.

Semiconducting organic nanomaterials especially the conjugated polymer semiconductor should be introduced as sensing layer using almost similar sensing principle. As the conducting polymer interacts with gaseous species, the *p*-type conjugated polymer donates electrons to the gaseous analyte, and *n*-type conjugated polymer accepts electrons from the gaseous analyte. Subsequently, the hole conductivity of conjugated polymer increases when it donates electron to the analyte, and conductivity decreases when it accepts electron from the analyte. For that reason, the conductivity of conjugated polymers like polythiophene, polypyrroles, polyaniline, and their derivatives decreases upon exposure to nucleophilic gases such as hydrogen sulfide, ammonia, hydrazine, methanol, ethanol, etc. On the other hand, the opposite effect shown by the electrophilic gases like oxides of nitrogen, phosphorus trichloride, sulfur dioxide, oxygen, etc. having higher electron affinity than the conducting polymer increases the number of charge carriers in the conducting polymer. Alternatively, the pollutants can interact with the polymer by some type

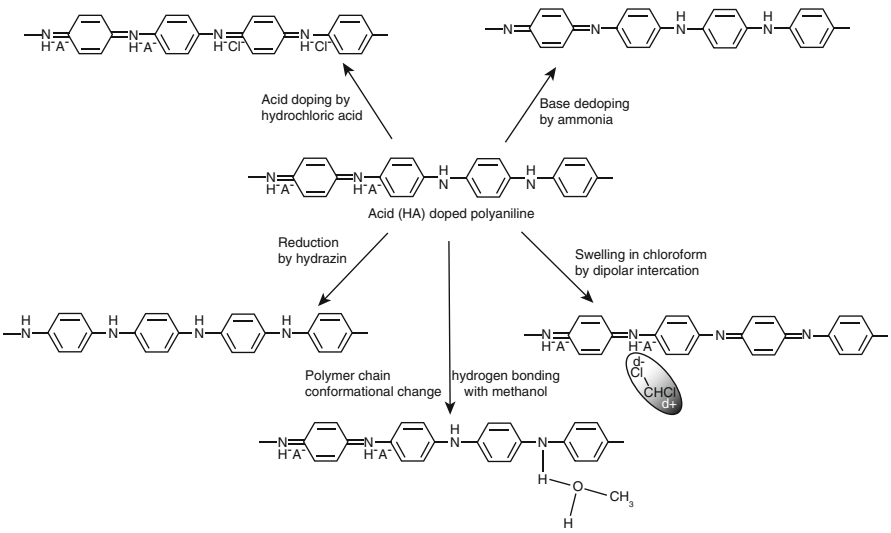

Fig. 10.4 Different sensing mechanisms of polyaniline with different analytes

of weak interaction or even small amount of charge induction in order to influence the conducting properties during sensing. The above statements are reflected in the example that the polyaniline nanofiber sensor for the five different gases was explored to have five different mechanisms: acid doping, base dedoping, reduction, swelling, and polymer chain conformational changes with five different analytes. hydrochloric acid, ammonia, hydrazine, chloroform, and methanol, respectively (Virji et al. 2004). These five types of sensing mechanism are well explained in Fig. 10.4.

10.2.3 Hybrid Nanomaterials as Receptor

Typically, vast varieties of available organic and inorganic nanomaterials have been introduced for the development of hybrid nanomaterials. The mixture of two or more materials, in which one should be at nano-dimension, is considered as hybrid nanomaterials, and it would be nanocomposites or nanoblends. The narrow difference between blends and composites is that the two main constituents in the composites remain recognizable, while these are not recognizable in blends. The examples are the composite of nanomaterials including carbon, graphene, metal, metal oxide, etc. with polymers or metal oxide matrices. The properties of the polymer or ceramic matrices are generally reinforced by the dispersed nanofiller materials in their hybrid; however, the sensing principle for the gaseous pollutants remains the same. As evidence, the same sensing mechanism was considered for n-type nanocrystalline magnesium ferrite (Mukherjee et al. 2010) and its composite

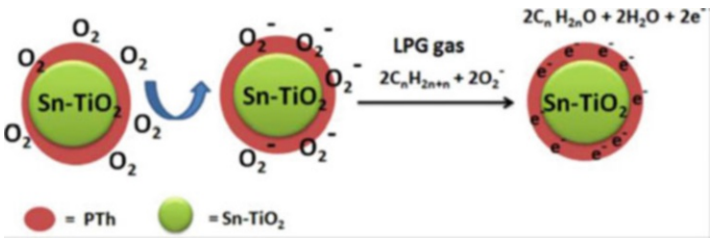

Fig. 10.5 The sensing mechanism of polythiophene–tin–titanium dioxide composite material with LPG. (Reprinted with permission of Elsevier from Chandra et al. 2017)

with zinc ferrite toward (Mukherjee and Majumder 2010) a variety of reducing gases including carbon monoxide, hydrogen, methane, and nitrous oxide. The analytes can interact with the hybrid layer by electron donation or electron withdrawing or some type of weak interaction or even small amount of charge induction (Kar et al. 2015). As described earlier, hole conductivity increases for a p-type nanocomposite by donating electrons to the chemical analyte, and conductivity decreases for n-type nanocomposite by accepting electron from chemical analyte. For example, the liquefied petroleum gas (LPG) exchanges the electrons with the chemisorbed oxygen on the polythiophene–tin–titanium dioxide composite material resulting in decreased conductivity (Fig. 10.5) (Chandra et al. 2017). The sensing performers are often enhanced as good electric properties and catalytic properties of metal nanomaterials can greatly improve the response to particular gas when the materials are added with the other matrix like metal oxide or polymer. For example, the catalytic influence was considered to explain the sensing of methanol or acetone by using conducting polymer nanocomposite with metal nanoparticle like silver, palladium, or copper (Choudhury et al. 2009; Kar and Choudhury 2013; Athawale et al. 2006). Similarly, the selective methanol sensing was reported by the poly(m-aminophenol)–copper nanocomposite through the effective interactions with the polymer matrix as well as with the copper nanoparticles (Bhuyan et al. 2018). As shown in Fig. 10.6, in addition to the hydrogen-bonding interaction with the poly(m-aminophenol) just like sulfuric acid-doped polymer (Kar et al. 2009), the polar interaction was explained with the copper nanoparticles. The formation of heterojunction interface between metal oxide-conjugated polymer and two types of metal oxide in their nanocomposite may have significant effect on the performance of gas sensor. For example, the hetero p–n junction consisted by n-type tin dioxide with p-type conducting polyaniline has been responded upon ammonia exposure due to depletion of change in the junction region (Deshpande et al. 2009). Similarly, the sensing of volatile organic compounds especially ethanol was explained by the chemical adsorption and desorption of gas molecule on the surface of cobalt monoxide–tin dioxide heterojunction (Wang et al. 2018a). In hybrid nanocomposite, the CNT especially functionalized CNT as dispersed secondary material is not only used to reinforce the conducting properties but also used to impart additional interactions with the analyte molecule. The increase of sensing performance of hybrid nanomaterial could also be attributed simply to the synergistic properties of the

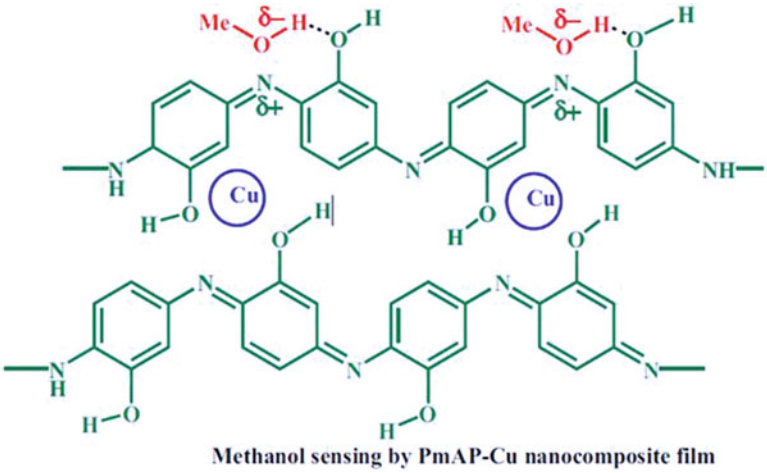

Fig. 10.6 The proposed methanol sensing mechanism of poly(m-aminophenol)–copper nanocomposite. (Reprinted with permission of Springer Nature from Bhuyan et al. 2018)

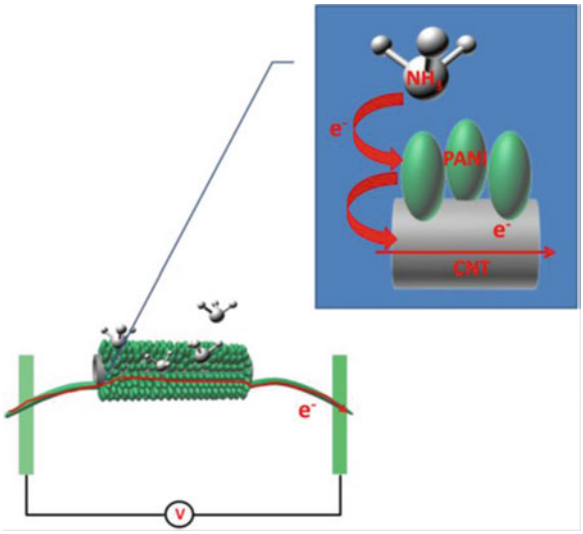

Fig. 10.7 The proposed ammonia gas sensing mechanism of polyaniline–CNT nanocomposite. (Reprinted with permission of Elsevier from Xue et al. 2017)

two components. As shown in Fig. 10.7, the electrons provided from the adsorbed ammonia molecules onto polyaniline transfer easily from polyamine matrix to CNT filler through the interconnected network with lower-energy barrier (Xue et al. 2017). The functionalized CNT may increase the number of interacting sites or increase the intra- and interchain mobility of charge in the polymer chains as matrix or even change the affinity of the nanocomposite toward the electron-donor or -acceptor gases. These types of secondary interactions with the functionalized CNT in their hybrid nanocomposites are helpful to increase the sensitivity of the

analyte or have the selective response for particular analyte. The response of the nanocomposite with carboxylic acid-functionalized multi-walled CNT (MWCNT) sensor toward aliphatic alcohol vapor was significantly improved compared to pristine polymer. The response of nanocomposite sensor was substantially improved toward methanol and ethanol as functionalized MWCNT favorably interacts with the poly(m-aminophenol) chains and subsequently generates a pathway for possible H-bonding/dipole interactions with the alcohol molecules (Verma et al. 2015). The selectivity of the methanol and ethanol vapor was further increased by using sulfonic acid-functionalized MWCNT/poly(m-aminophenol) nanocomposite through hydrogen-bonding interaction with the polymer as well as strong dielectric interaction with the nanofillers (Verma et al. 2017a). The response was observed more selectively toward ethanol only for polymer nanocomposite with amine-functionalized MWCNT due to balancing of hydrogen-bonding/dipole interactions (Verma et al. 2017b). The selective detection of carbon monoxide gas at room temperature using reduced graphene oxide nanocomposite with palladium-loaded tin dioxide nanoparticles was explained by special interactions between palladium-loaded tin dioxide as well as reduced graphene oxide nanosheets having high specific surface area and good conductivity (Shojaee et al. 2018).

10.3 Synthesis of Nanomaterials

Nanomaterials are not simply miniaturization of macro- or micro-materials, but the nano-world lies midway between the scale of atomic and quantum phenomena. The transition from macro- or micro-materials to nanomaterials yields dramatic changes in various properties due to having a large surface area for a given volume, i.e., high aspect ratios. For nanomaterials, the size-dependent properties are observed such as quantum confinement in semiconductor particles, surface plasmon resonance in some metal particles, superparamagnetism in magnetic materials, etc. Thus the synthesis of various nanomaterials should be optimized to obtain nanomaterials with precise size and narrow distribution of size.

10.3.1 Synthesis of Inorganic Nanomaterials

In general, the nanoclay minerals are a class of naturally occurring phyllosilicates and usually formed as a result of environmental process such as chemical weathering, hydrothermal alterations, and sedimentary rock. However, the synthetic nanoclay minerals with well-designed composition and structure can be synthesized in laboratory by inspiring the natural process: (i) synthesis at low temperature close to early earth surroundings and (ii) transformations from natural minerals. The clay nanomaterials are also synthesized by most popular low-temperature, hydrothermal process from primary naturally occurring minerals such as feldspars, albite,

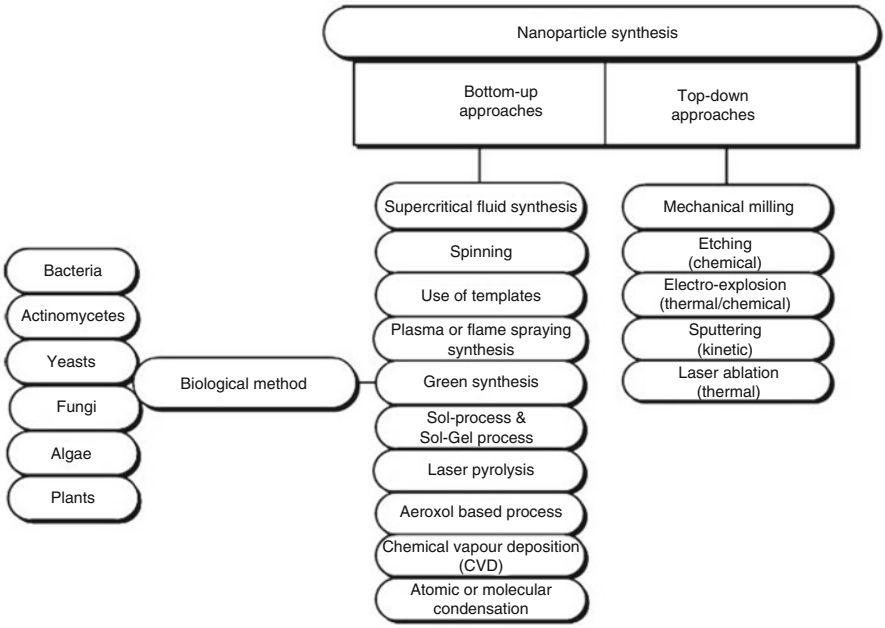

Fig. 10.8 The common methods for the synthesis of inorganic nanomaterials. (Reprinted with permission of Royal Society of Chemistry from Iravani 2011)

muscovite, etc. The routes used to modify the surface of nanoclays are adsorption, ion exchange, binding with inorganic and organic anions, grafting, reaction with acids, pillaring by different types of poly(hydroxo metal) cations, intraparticle and interparticle polymerization, dehydroxylation and calcination, delamination and reaggregation of smectites, lyophilisation, ultrasound, and plasma (Bergaya and Lagaly 2001; dePaiva et al. 2008). The inorganic metal, metal oxide, and metal compound nanomaterials can be made using different approaches in both top–down and bottom–up techniques like homogeneous nucleation from liquid or gas phase, heterogeneous nucleation on a substrate, phase separation through annealing of certain solids or micelle synthesis, thermodynamic equilibrium approach, kinetic approach, etc. In general, the synthesis methods for nanostructured metal oxides or metal compounds can be classified broadly into solution-based and vapor-phase synthesis methods. Important solution phase methods include hydrothermal, sol–gel, electrochemical deposition, precipitation methods, thermolysis, flame spray pyrolysis, etc., and vapor-phase methods are physical vapor deposition, chemical vapor deposition method, arc discharge, laser pyrolysis, etc. (Fig. 10.8) (Iravani 2011). The hydrothermal method is the most popular one. For example, the tin dioxide nanoparticles as well as the same types of metal oxides were reported to have been synthesized by this method (Chiu and Yeh 2007). The tin dioxide nanomaterials were synthesized by hydrothermal method, and the Au nanoparticles were synthesized by reducing hydrogen tetrachloroaurate using sodium borohydride reducing

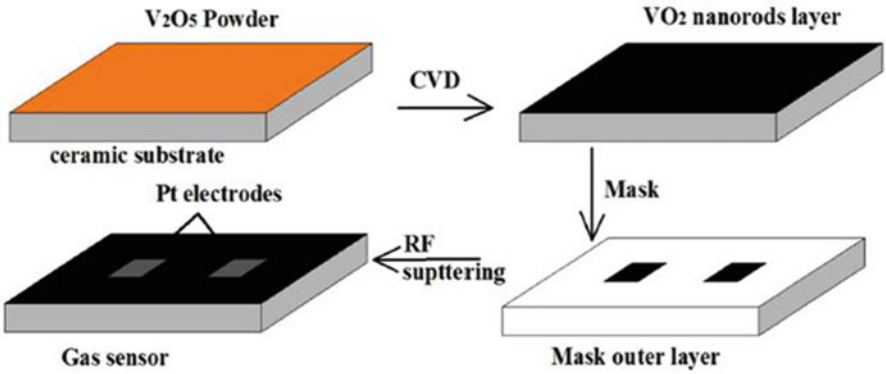

Fig. 10.9 The stepwise growth of vanadium dioxide nanorods following thermal evaporation process. (Reprinted with permission of Elsevier from Li et al. 2016)

agent (Manjula et al. 2011). The nanocrystalline metal oxides such as tin dioxide, indium oxide, and tungsten trioxide were prepared by laser-ablated method (Starke et al. 2002). Microemulsion-based solvothermal method has been used to synthesize both the hierarchical flower-like and one-dimensional tube-like zinc oxide nano-architectures (Chen et al. 2011). The carbothermal reduction method was used to prepare the indium oxide nanowires by reaction between indium oxide and active carbon at 1000 °C under flowing nitrogen atmosphere (Xiangfeng et al. 2004). The synthesis of nanostructured zinc oxide was performed by two different synthetic routes: traditional sol–gel route and a combination of vapor transport process and controlled oxidation methods (Carotta et al. 2009). Even the zinc oxide nanostructures were deposited on glass substrates by the simple aqueous chemical growth technique at low temperature as low as 95 °C (Kenanakis et al. 2007). The simple electrospinning process was also adopted to fabricate the tin dioxide nanofibers by electrospinning the poly(vinyl alcohol)–tin chloride pentahydrate precursor (Zhang et al. 2008). In physical method, vanadium dioxide nanorods were prepared through thermal evaporation technique from vanadium pentoxide powder under 20 Pa and argon gas at a flow rate of 20 sccm transporting vanadium and oxygen atoms. The stepwise process and growth of vanadium dioxide nanorods are shown in Fig. 10.9 (Li et al. 2016).

Another important type of inorganic nanomaterial is carbon nanomaterials such as carbon black, CNT, SWCNT, MWCNT, carbon nanofibers, graphene, etc. The activated carbons or carbon black was generally produced from different precursors like wood, coal, or nutshell (Beguin and Frackowiak 2010). The arc discharge method is the most common and easiest way to prepare the CNT in comparison with other methods like laser ablation method, chemical vapor deposition method, flame synthesis method, silane solution method, etc. (Peter and Harris 1999). After preparation of the nanotubes containing a large amount of impurities such as metal particles, amorphous carbon, multishell, etc., different processes are used like air oxidation, acid refluxing, strong acid refluxing, surfactant-aided sonication,

filtration, and annealing (Peter and Harris 1999) etc. for the purification of the CNT. The CNT was synthesized on iron-coated low-cost alumina substrates using radio-frequency plasma-enhanced chemical vapor deposition technology (Penza et al. 2010). The surface functionalization of CNTs by breaking the covalent linkage of functional entities onto carbon scaffold was employed by various chemical reactions such as fluorination followed by amino, alkyl, and hydroxyl group modification or carbene and nitrene addition, chlorination, bromination, hydrogenation, azomethine ylides, carboxylation, amination, sulfonation, etc. (Yang et al. 2007).

10.3.2 Synthesis of Organic Nanomaterials

Like the preparation of other nanomaterials, the fabrication of polymer nanomaterial approaches either assembling of monomers together to polymer nanomaterials in "bottom–up" process or reassembling (organizing or orienting) of polymer molecules into nanostructure one in "top–down" process (Rao and Geckeler 2011). The names of the important methods of top–down process are (Fig. 10.10) solvent evaporation, salting-out, nanoprecipitation, emulsification–solvent diffusion, supercritical fluid technology, spin coating, lithography, self-assembly, layer-by-layer or Langmuir–Blodgett technique, electrospinning, etc. (Rao and Geckeler 2011). Methods for nanofabrication of polymers by bottom–up process are vigorous bulk polymerization, emulsion polymerization, polymerization using steric stabilizers,

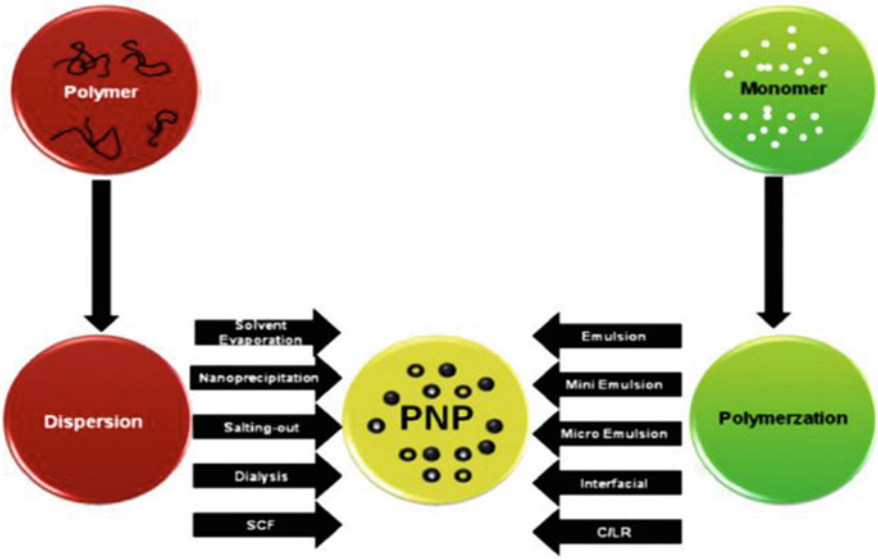

Fig. 10.10 Common techniques for the synthesis of polymeric nanomaterials. (Reprinted with permission of Elsevier from Rao and Geckeler 2011)

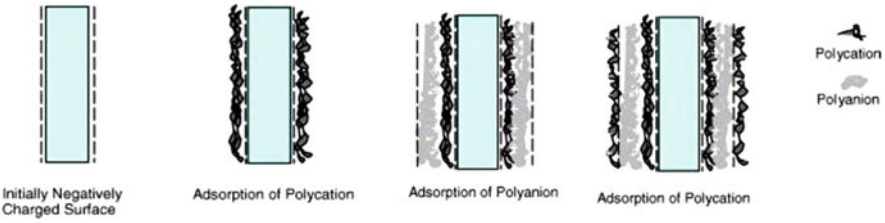

Fig. 10.11 Schematic layer-by-layer assembly to form polymer nanolayer. (Reprinted with permission of Elsevier from Nohria et al. 2006)

template method, interfacial polymerization, controlled/living radical polymerization, etc. (Rao and Geckeler 2011). The third type of mixed technique, which is the combinations of top–down and bottom–up, is also introduced for the nanofabrication of polymers. After the synthesis of polythiophene and its block copolymers with different second blocks, polystyrene, poly(methylacrylate), and poly (n-butylacrylate), the polymers were fabricated to nanofibers by standard photolithography processes (Li et al. 2006a). The ex situ nanolayer fabrication by layer-by-layer deposition nano-assembly method was used for conjugated polymers with suitable electrolytes such as poly(styrene sulfonate)–polypyrrole or poly(styrene sulfonate)–polyaniline. As illustrated in Fig. 10.11, the nanolayer of the conjugated polymer was formed due to self-assembled layer formation on the preassembled polycation through ionic interaction (Nohria et al. 2006). Oriented polyaniline nanowires with average diameters of 100 nm were fabricated on gold electrodes using a nonlithographic deposition process in order to improve the chemical sensing performances (Liu et al. 2004). The synthesis of polyaniline was performed through interfacial polymerization technique in the interface of immiscible organic–aqueous solvent (Huang et al. 2003; Virji et al. 2004; Yan et al. 2007). Another important approach to fabricate the nanowire or nanofiber of the polymer is the use of microchannels as template, for example, the polypyrrole nanofibers with 300 nm diameter and 50–60 μm length were prepared by chemical polymerization of pyrrole inside silicon dioxide-coated alumina template (Hernandez et al. 2007). Similarly, the surface-modified silicon substrates with self-assembled monolayer of amino silane were employed as artificial seeds for self-organization of polyaniline nanofiber during chemical polymerization of aniline (Sutar et al. 2007).

10.3.3 Synthesis of Hybrid Nanomaterials

The hybrid materials are the mixture of two or more materials in a single material having distinct improved properties than the virgin materials, and one of the materials in the mixture should be nano-dimensional within the hybrid nanomaterials. In general, most of the hybrid nanomaterials are mixture of two materials, i.e., one nanomaterial is dispersed within the other material. The examples

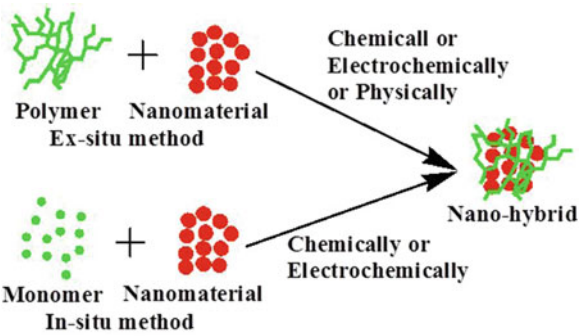

Fig. 10.12 Schematic presentation of ex situ and in situ nanohybrid preparation (polymer matrix based). (Modified after Kar et al. 2015)

of hybrid nanomaterials having mixture of more than two materials are very rare. The hybrid nanomaterials are broadly classified into two categories: nanocomposites and nanoblends. Nanocomposites are combinations of two materials in which the nanomaterial called reinforcing phase is embedded in the other material called the matrix phase. Typically vast varieties of available nanomaterials have been introduced for the development of nanocomposite into (1) metal matrix nanocomposites, (2) ceramic matrix nanocomposites, and (3) polymer matrix nanocomposites. Nanoblends are the mixture of two materials having either of the components with nano-dimensional morphology. In addition, the basic difference between blends and composites is that the two materials in the composites remain in separate phase, while these are miscible in blend.

Preparative methods of hybrid nanocomposites can be broadly classified as ex situ and in situ techniques through physical, chemical, or electrochemical routes (Kar et al. 2015). Those methods are illustrated in Fig. 10.12. In ex situ method, the pre-synthesized nanomaterials are mixed up with other the pre-synthesized materials mostly by physical methods. The chemical and electrochemical techniques are very rarely used in ex situ synthesis method. The in situ method involves the mixing up of nanomaterials with the other materials during the chemical or electrochemical synthesis of either of the materials or both the materials. Here, the physical techniques are very rarely used or not at all used in in situ synthesis method. For example, the tin dioxide–gold ceramic matrix composite was prepared by reducing hydrogen tetrachloroaurate in situ chemically using sodium borohydride to gold nanoparticles within aqueous suspension of pre-synthesized tin dioxide nanoparticle matrix (Manjula et al. 2011). In general, the in situ method for the preparation of nanocomposite is the better approach over the others in terms of disparity of the nanomaterials and hence the positive influence on properties of the nanocomposite. The tin dioxide doped with different weight percentages of samarium oxide nanocomposites was prepared by microwave-induced solution combustion of tin chloride and samarium nitrate solution mixture (Habibzadeh et al. 2010). The simple in situ wet chemical method has been used to prepare the zinc oxide–tin dioxide nanocomposite by hydrolyzing stannous chloride on zinc oxide nanorods (Lu et al. 2012). In order to prepare the crystalline tin dioxide–reduced graphene oxide nanocomposites, simultaneous reduction of tin salt and graphene oxide was

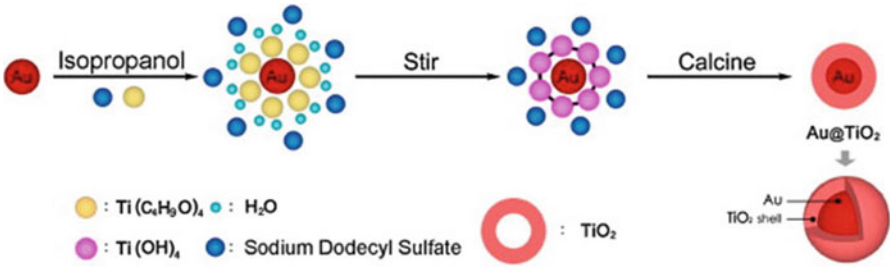

Fig. 10.13 Schematic mechanism for the formation of titanium dioxide shell on gold core nanocomposite. (Reprinted with permission of Elsevier from Zhu et al. 2015)

performed by a one-pot microwave-assisted nonaqueous sol–gel method (Neri et al. 2013). As shown in Fig. 10.13, the titanium dioxide shell on gold core nanocomposite was prepared using the in situ reverse micelle sol–gel method with gold dispersion (Zhu et al. 2015). The composites of inorganic metal oxide nanomaterials with conjugated polymer matrix were mostly prepared by simple in situ techniques. In a typical method, the inorganic metal oxide nanomaterials were dispersed first in the aqueous solution of monomer followed by polymerization of monomer by adding suitable oxidant. For example, the method was followed to prepare the polyaniline nanocomposites with metal oxide nanomaterials such as titanium dioxide, tin dioxide, and indium oxide (Ram et al. 2005; Sadek et al. 2006). The in situ electrochemical polymerization was performed by either of the two methods: (1) the electrochemical polymerization of monomer from solution with nanoparticle dispassion and (2) the electrochemical polymerization of monomer from solution on a pre-coated electrode with the corresponding nanomaterials. For example, the second procedure was followed to prepare the nanocomposite of SWCNT functionalized with polyaniline on the electrode (Zhang et al. 2006). Vapor-phase in situ polymerization was used to fabricate the polypyrrole nanocomposite on the surface of electrospun titanium dioxide–zinc oxide nanofibers (Wang et al. 2009). In in situ method, the preparations of inorganic hybrid nanomaterials were also performed simply by following the same method for the synthesis of inorganic nanomaterials within the dispersion of other matrix. For example, the Au nanoparticles dispersed inside a titanium dioxide−nickel oxide mixed oxide matrix were prepared by the sol−gel method (Gaspera et al. 2010). The coprecipitation of both the components was used to prepare the nanocomposite by in situ chemical method. Following the method tin dioxide/vanadium pentoxide was prepared by simultaneous precipitation technique from aqueous stannous chloride solution and aqueous acidic vanadium pentoxide solution by adding ammonium hydroxide solution drop wise at 60–80 °C for 1 h under constant stirring. Then maintaining a pH of 10, the simultaneously precipitated hydroxides were washed, made chloride-free, and finally calcined at 950 °C for 2 h to get the nanocomposite powders (Das et al. 2008).

10.4 Parameters of Nanomaterials Promising for Sensing

10.4.1 Processability

The fabrication of sensing layers by the nanomaterials to be used as analyte receptor is a very tricky process as well as important process since the sensor sensitivity depends on thickness, chemical composition, crystallinity, morphology, transducer properties, etc. The present state-of-the-art fabrication of sensor layer by various nanomaterials has been extensively studied, and numerous research articles are available in various sensor-related journals and books. The most common names of such processes are electrochemical deposition, pellet preparation, dip coating, drop coating, spin coating, film casting, printing, layer-by-layer deposition, Langmuir–Blodgett film casting, self-assembly techniques, etc. Here the procedure of individual process is not elaborated as those have been briefly discussed elsewhere. There are two main ways in order to fabricate the sensing layer through processing of the nanomaterials by the above techniques, viz., solution processability and thermal processability.

The inorganic nanomaterials are generally thermally very much stable, but melting those nanomaterials at achievable temperature is quite impossible. On the other hand, the thermal melting of organic especially polymer nanomaterials is possible, but they often start to decompose or degrade before melting. For hybrid nanomaterials although the properties are improved as well as influence greatly on the type of materials mixture used, however, the properties should be very close to that of the parent inorganic or organic materials. In other words, the thermal processing of nanomaterials is not used at all or sometimes used but in very rare cases. The modified thermal processing might be used for some inorganic nanomaterials during the synthesis.

The solution processability is quite promising for organic polymer nanomaterials and polymer-based hybrid nanomaterials. This is because the vast organic polymers are soluble in many solvents according to their structural skeleton. However, some structurally rigid polymers like conjugated polymers as well as their hybrid nanomaterials are insoluble or poorly soluble in organic solvent. By following this route, the processing of inorganic nanomaterials is not possible as almost all the inorganic nanomaterials are not soluble in organic solvent. However, the insoluble inorganic nanomaterials are processed from their suspension. For example, the gold–tin dioxide nanocomposite was brush coated onto cylindrical alumina tube by making a paste of powder with water (Manjula et al. 2011). As illustrated in Fig. 10.14, a thick receptor film of most of the inorganic nanomaterials was deposited by painting or coating an aqueous paste of powders on the ceramic interdigitated substrate followed by drying under controlled temperature (Neri et al. 2013). The Langmuir–Blodgett or layer-by-layer deposition method may be used for the inorganic nanomaterials insoluble in the solvent. Even the Langmuir–Blodgett technique was used to deposit SWCNT sensing layer on the pre-deposited cadmium arachidate buffer following the same method (Penza et al. 2005a). Pellet making is found to be the last solution for the processing of infusible and insoluble nanomaterials.

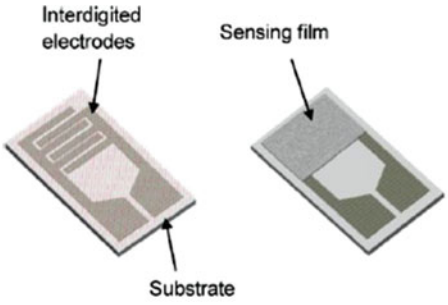

Fig. 10.14 Scheme for the preparation of sensing layer on interdigited substrate. (Reprinted with permission of Elsevier from Neri et al. 2013)

10.4.2 Mechanical Strength

The nanomaterials to be used in a sensor device must possess adequate mechanical strength in order to sustain handling other stresses and durability. Flexible film-based gas sensors have attracted recent scientific attention due to the wearability, flexibility, transparency, and compatibility over curved substrates of integrated electronics (Xue et al. 2017). The poor mechanical strength is a great concern for the individual nanomaterials to be used as sensor. However, scientists have investigated newer preparation and processing methods in order to improve the mechanical strength. As explained, the local deposition of tin dioxide nanoparticles through flame spray pyrolysis was found to be extremely porous and mechanically fragile. Therefore, a new method of preheating the tin dioxide sensing layer and then transferred it onto the contact electrodes via a sacrificial bridge-type zinc oxide layer was adopted to obtain an enhanced stability by locally locate high-quality crystalline tin dioxide layer (Lee et al. 2018). In general, the inorganic and organic polymer nanomaterials possess adequate stability to mechanical stresses. For example, the same sensing response was observed (Fig. 10.15) for ammonia in bent and extending

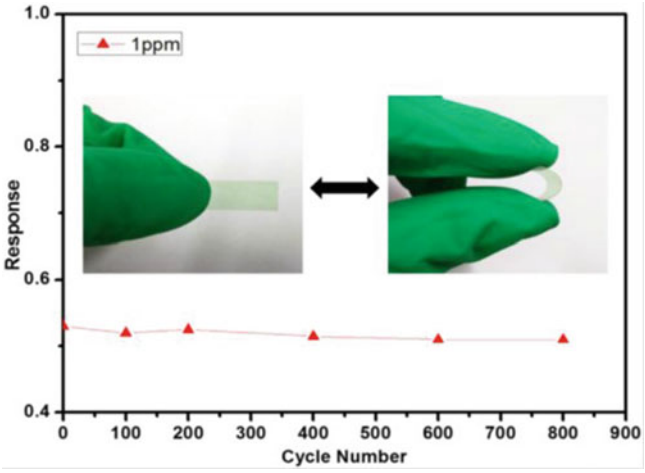

Fig. 10.15 1 ppm ammonia sensing response of the flexible polyaniline–CNT nanocomposite film in bending and extending states. (Reprinted with permission of Elsevier from Xue et al. 2017)

states of polyaniline–CNT nanocomposite at room temperature revealing the reliable and robust flexibility of the device (Xue et al. 2017). However, some of polymer nanomaterials suffer from a drawback of poor mechanical strength due to its brittle nature. The hybrid nanomaterials based on inorganic or organic materials should have close mechanical strength with that of the pristine materials used as matrix. The problems associated with that of the mechanical strength of the sensor element were identified such as braking by a slight shock, braking during ultrasonic wire-bonding process, poor sintering of the material, etc. The problems were often overcome by optimizing the synthesis, processing, or deposition techniques. Therefore, it is possible to improve the material strength which greatly influences the gas sensitivity and performances of the sensor. For example, exploiting the nanomechanical properties of graphene or CNT could lead to increased sensitivity and detection limits especially for the mass sensor transduction approaches (Llobet 2013).

10.4.3 Stability

Environmental stability as well as thermal stability of the nanomaterials in the sensor device is another issue to be considered before selecting the materials as receptor for air pollutant. The thermal stability of inorganic nanomaterials or hybrid nanomaterials based on inorganic materials is very high. However, the thermal stability of organic nanomaterials and hybrid nanomaterials based on organic materials is not so high, but in most of the cases, it is sufficient for the use as sensor layer. For that reason, the ceramic semiconductors have been used for the sensing of air pollutants at very high operating temperature, while the polymer-based sensors have been only used at room temperature. In the polymer matrix nanocomposite temperature, stability is only slightly increased due to incorporation of filler matrix. However, those nanohybrid materials should also be used at room temperature. For example, traditional metal oxides such as tin dioxide, titanium dioxide, zinc oxide, cobalt(II,III) oxide, indium oxide, etc. are widely used to fabricate gas sensors at high temperature of 200–500 °C, while nanocomposites of those metal oxides with conjugated polymer have been used at room temperature for the sensing of same gases (Xu et al. 2018). The considerable environmental stability of polymer with low moisture absorptivity makes them important candidate for the particular applications. But some of the polymers absorb moisture strongly and lose their property in ambient environmental conditions. The inorganic materials generally absorb moisture very weakly and retain their properties after removal of moisture by slight heating. Therefore, the sensing data must be recorded at varying humidity for the sensor to be considered as environmental analysis. As a standard presentation, the stability of the polyaniline@flower-like tungsten trioxide nanocomposite sensor toward 10 ppm ammonia for consecutive 2 weeks at room temperature is shown in Fig. 10.16 (Li et al. 2018a). The stability should be explained by considering the parallel nature of the curve with the axis. Another important parameter in practical application, the long-term stability of the nanomaterials-based sensor, directly affects the service life of the sensor. This type of stability could be checked by observing the change of resistance as well as change of sensing performances of the sensing layer with respect to the time at real optimized

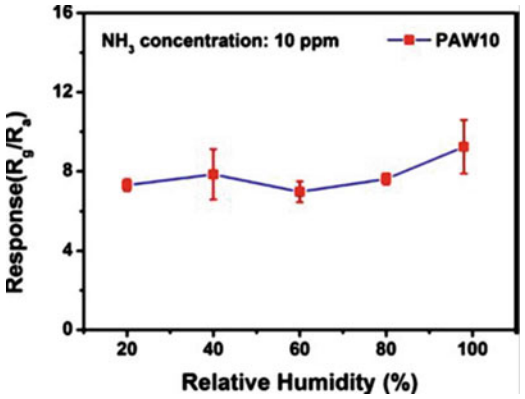

Fig. 10.16 The effect of relative humidity on the response of polyaniline@flower-like tungsten trioxide nanocomposite sensor. (Reprinted with permission of Elsevier from Li et al. 2018a)

conditions. As shown in the figure, similar type of plot should be recorded to explain the long-term stability of sensor in sensing the environment. For example, the resistance and corresponding response toward toluene of tin dioxide-decorated nickel monoxide sensing layer were recorded about 15 and 60 ohms, respectively, at 250 °C in 20 test days (Gao et al. 2018).

10.4.4 Transducer Properties

It is already mentioned that the three general categories of chemical sensors in terms of operating technology of the transducer are (1) electrochemical sensors, (2) mass sensors, and (3) optical sensors. Among those the electrochemical transducer principle implying the transfer of electron or charge during the interaction of chemical analyte with the recognition element is the oldest and widely used strategy. In electrochemical sensor device, the recognition nanomaterials must possess some inherent electrical properties for alter. As a result of electron transfer, the change of electrical properties of the nanomaterials detection layer can be measured with the help of a well-defined electrical circuit by various modes of measurement such as change of voltage in voltammetric, change of current in amperometric, change of conductivity or resistance in conductometric, change of charge in potentiometric, and change of impedance in impediometric. The inorganic nanomaterials either possess the good conducting properties like metallic nanomaterials or possess the semiconducting properties like metal oxide–compound nanomaterials. Nowadays the semiconducting properties have been also introduced in the organic nanomaterials like the conducting polymers or functional ionic polymers. In addition the inherent electronic properties in hybrid nanomaterials may be included by combining the conducting and/or semiconducting inorganic nanomaterials with nonconducting polymers or by combining conducting and/or semiconducting inorganic nanomaterials with conducting polymers.

Change in optical properties of the nanomaterials sensing layer because of interaction with a chemical analyte can provide good sensing response by measuring the absorbance using ultraviolet-visible spectroscopy, surface plasmon resonance, Raman spectroscopy, fluorescence measurements, etc. According to the optical properties of the analyte, the optical chemical sensors in general may be categorized into two types: inherent optical properties and apparent optical properties. In an inherent optical property sensor, the analyte is itself optically active and senses directly some intrinsic optical property such as absorption or luminescence. In apparent optical property sensing systems, a change in the optical response of an analyte is detected by using some optically active analyte-sensitive layer. This latter technique is useful particularly in the case where the analyte has no convenient intrinsic optical property, which is the case for many analytes. In the case of apparent optical property, the possibilities are there to discuss about the analyte-sensitive reagents based on polymer. The optical detection of the apparent optical property can be done by ultraviolet-visible spectroscopy, infrared, surface plasmon resonance, or Raman spectra. Nowadays, the optical fiber sensing technology is the most exploited platform in the development of optical chemical sensors. In fiber optic sensors that utilize surface plasmon resonance techniques and quantum cascade laser spectroscopy as detection system. Fiber-optic sensors are classified according to the role played by the fiber in the operation of the sensor, i.e., passive or active. The fiber's role is considered to be passive if the fiber only acts to transport the optical signal to and from the sensing environment. An active fiber-optic sensor utilizes a fiber that has been modified so as to impart intrinsic analyte sensitivity to the fiber, and here the optical properties of the fiber are in some way changed during the interaction with analyte. An interaction of analytes which oxidize/reduce or protonate/deprotonate of organic nanomaterials or alter the plasmon resonance of inorganic nanomaterials can be a simple principle in an optical sensor. In hybrid nanomaterials the inherent optical property or apparent optical property may be imparted from either of the inorganic or organic component or both the components.

Mass sensing, which is a popular method for chemical analysis, transform the change of most fundamental physical property, i.e., mass, after the interaction with analyte into a change of a property of the sensor detection element. The principles used in the devices to measure the mass sensitivity during the interaction with analyte are quartz crystal microbalances and surface acoustic wave resonators. Quartz crystal microbalance sensors are a kind of piezoelectric quartz crystal with a selective coating deposited on the surface to serve as an adsorptive surface capable of measuring an extremely small mass change. Piezoelectric devices used mainly in gaseous phase, but also in solutions, are based on the measurement of the frequency change of the quartz oscillator plate caused by adsorption of a mass of the analyte at the oscillator. If a piezoelectric substance is incorporated in an oscillating electronic circuit, a surface acoustic wave is formed across the substance. Any change in velocity of these waves, due to the change in mass of the coating on the sensor by an absorbing species, will alter the resonant frequency of the wave. The oscillations are applied to the sensor through a set of metallic electrodes formed on the piezoelectric surface, over which a selective coating is deposited. The change of mass is

possible for any recognized sensing layer made of inorganic, organic, or hybrid nanomaterials provided that the layer is interacting with the analyte.

10.4.5 Operating Temperature

The operating temperature is also an important parameter for the air pollution sensor and it should be room temperature as the best one. Inorganic nanomaterials especially metal oxide layers have been extensively used for this purpose, and some of those are also commercialized. However, the major drawback with inorganic nanomaterials is that metal oxide sensors need high operating temperatures for sensing. Moreover, at high operating temperature, the layer of inorganic nanomaterials often reacts with the analyte. Here is the advantage of organic nanomaterials as sensing layer as the interaction of organic nanomaterials-based sensing layer with chemical analyte is rather strong at room temperature. The hybrid nanomaterials with inorganic matrices should have high operating temperature as it is close to matrix materials. In addition, hybrid nanomaterials with organic especially polymer matrices should have operating temperature at room temperature. For example, a hydrogen gas sensor array employing vertically aligned titanium dioxide nanotube was operated at 100 °C temperature (Lee et al. 2011a), while both polyaniline nanofiber (Sadek et al. 2007) and polyaniline–titanium dioxide nanocomposite (Srivastava et al. 2011) were operated at room temperature.

10.5 Sensing of Air Pollutant by Nanomaterials

As explained earlier, the sensing of gas molecules is important to environmental monitoring, control of chemical processes, and agricultural and medical applications. In addition, the detection of industrial toxic gases such as carbon monoxide, oxides of nitrogen, ammonia, hydrocarbons like LPG, and volatile organic compounds is critical for many industries in order to control air pollution. In recent decades the sensing of gases like carbon dioxide, sulfur dioxide, oxygen, ozone, hydrogen, moisture, and several organic vapors is important for controlling industrial and vehicle emissions, household security, and environmental monitoring. All three types of nanomaterials are employed to develop the devices for the successful sensing of those air pollutants. In this section, the studies on the sensing of main types of gaseous air pollutants using nanomaterials have been reviewed exclusively.

10.5.1 Oxides of Carbon

The main types of oxides of carbons are carbon monoxide and carbon dioxide. The carbon dioxide is released as complete combustion product of any types of fuel,

while the carbon monoxide is produced by incomplete burning, e.g., a major source of those oxides is emission from vehicle exhaust. The exposure of carbon monoxide in the air above threshold limit value of 25 ppm is especially dangerous as it becomes explosive and deadly poisonous for animals. The carbon monoxide may also help to form smog, a secondary pollutant. However, carbon dioxide, which causes global warming by increasing greenhouse effect, is not such dangerous like carbon monoxide.

In general, the sensing study of carbon monoxide has been attempted more than that of carbon dioxide. The highly sensitive tin dioxide nanowire fabricated by self-organized highly ordered porous alumina template was reported to sense the carbon monoxide and oxygen successfully (Kolmakov et al. 2003). As shown in Fig. 10.17, the sensing mechanism was explained with the help of electron depletion by oxygen, whereas electron withdrawal was explained by reducing gas like carbon monoxide (Kolmakov et al. 2003). The influence of humidity for carbon monoxide sensing using tin dioxide hybrid with two doping agents, palladium and platinum, has been demonstrated at an operating temperature of 450 °C (Ménini et al. 2004). The shell-shaped carbon nanoparticle-based carbon monoxide and hydrogen sensor at low concentrations were examined at room temperature both in air and inert atmosphere (Kim et al. 2011). The accurate measure of 1–15% carbon dioxide with a CNT-based resonator-frequency sensor was designed by Zribi et al. (2005). As shown in Fig. 10.18, up to 10 ppm carbon monoxide in the air up was detected selectively over hydrogen, acetone, ammonia, and ethanol at temperature below 50 °C using tin dioxide nanocomposite with gold (Manjula et al. 2011). The sensing response was optimized for tin dioxide nanocomposite with 1.5 weight percentage gold in terms of optimum catalytic effect of well-dispersed gold nanoparticles within the tin dioxide matrix (Manjula et al. 2011). The tin dioxide nanocomposite doped with 5.0 weight percentage of samarium oxide was reported to have selective sensing for carbon monoxide over ethanol at 200 °C operating temperature (Habibzadeh et al. 2010). A highly porous and nanostructured cupric oxide–zinc oxide composite electrodes having high surface-to-volume

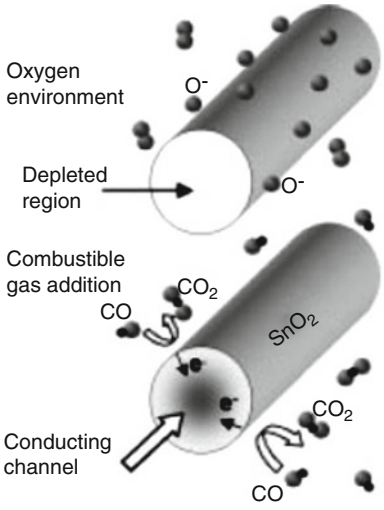

Fig. 10.17 Sensing mechanism of tin dioxide nanowire for oxygen and carbon monoxide. (Reprinted with permission of John Wiley and Sons from Kolmakov et al. 2003)

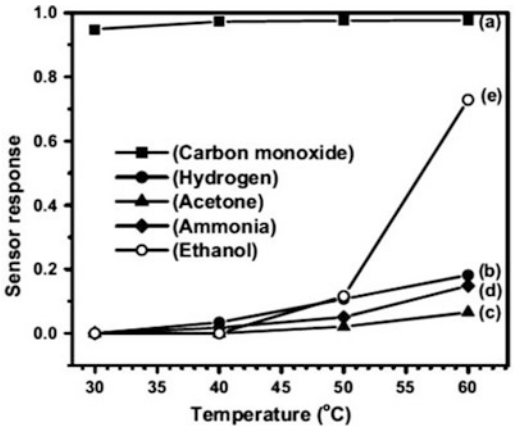

Fig. 10.18 Sensor response with temperature variation toward 10% gas concentration on 1.5 wt% gold–tin dioxide nanocomposite layer. (Reprinted with permission of Elsevier from Manjula et al. 2011)

ratio as well as improved thermal stability were used as solid-state electrochemical sensor for the high-temperature online detection of carbon monoxide (Wu et al. 2005). The gold nanoparticles adsorbed zinc oxide nanowires hydride material was fabricated for 5, 20, 50 and 100 ppm carbon monoxide sensors at 350 °C (Chang et al. 2008). A room temperature sensing of carbon monoxide gas (1–5 ppm) by change in conductivity of zinc–indium oxide nanowire hybrid was achieved selectively over nitric oxide and nitrous oxide (Singh et al. 2010). The hybrid material of tin dioxide combined with 0.1 weight percentage of MWNT having nearly two times higher specific surface area compared to pure tin dioxide was fabricated by simple in situ method for better carbon monoxide gas sensing at room temperature (Zhao et al. 2007). The low-temperature semiconductor carbon monoxide gas sensor in nitrogen flow was constituted by vanadium–tin oxide nanohybrid prepared by a coprecipitation method (Wang and Chen 2010). A novel amperometric carbon monoxide sensor by cyclic voltammetry measurement was fabricated by MWNT-grafted polydiphenylamine hybrid material. The excellent linear concentration range between 10 and 200 ppm was reported under optimal conditions showing a substantially low detection limit of 0.01 ppm (Santhosh et al. 2007). The carboxylic acid group functionalized CNT composite with polyaniline matrix has shown good reversible response to carbon monoxide at 100–500 ppm concentration range (Wanna et al. 2006). The nanocomposite of CNT with platinum and rhodium metal (Star et al. 2006) or tungsten trioxide (Bittencourt et al. 2006) was capable to detect low level of carbon monoxide gas. Another study focused on the sensing of carbon monoxide gas by the highly organized ultrathin polyaniline/metal oxide such as tin dioxide and/or titanium dioxide nanocomposite films (Ram et al. 2005).

10.5.2 Oxides of Nitrogen

Oxides of nitrogen especially nitrogen dioxide are also a potentially toxic gas that can lead to respiratory symptoms in humans and adversely influence plant growth

(Okano and Totsuka 1986). Moreover, the primary pollutant like oxides of nitrogen may cause secondary pollution like ground-level smog and/or acid rain. The threshold limit value has been set at 3 ppm over 10 h a day for nitrogen dioxide exposure.

The pristine CNT networks without any chemical functionalization might be used as gas sensor with improved performances. For example, bare SWNT drop-cast onto interdigitated electrodes (Li et al. 2003) or CNT film deposited on platinum–substrate (Santucci et al. 2003) was reported for the detection of nitrogen dioxide with low detection limit. The single crystalline particles were only slightly aggregated and directly used for thick film sensor deposition. The tin dioxide nanoparticle synthesized by flame spray pyrolysis followed by drop coating film responded well to both reducing gases like propanal and oxidizing gases like nitrogen dioxide (Sahm et al. 2004). The zinc oxide nanorod was highly responsive to nitrogen dioxide gas with short response and recovery time having a detection limit of 10 ppb at 250 °C (Oh et al. 2009). The high sensitivities to low nitrogen dioxide levels together with fast response times were observed for both tin dioxide and indium oxide materials over that of the tungsten trioxide (Starke et al. 2002). The tin dioxide nanowires were reported to show higher sensitivity for nitrogen dioxide gas compared to tin dioxide powder-based thin films, tin dioxide coating on carbon nanotubes, or single/multiple tin dioxide nanobelts (Choi et al. 2008). The sensitivity of the tube-like zinc oxide toward nitrogen dioxide gas was much higher with shorter response time than that of the flower-like zinc oxide gas sensor (Chen et al. 2011). The details of sensing characteristics as well as sensing parameters were optimized for the three nitrogen oxides: nitrogen dioxide, nitric oxide, and nitrous oxide by using zinc oxide, indium oxide, and tungsten trioxide nanowire receptor (Rout et al. 2006a). All-graphene sensor consisting the material in both sensor electrodes and active sensing area was exhibited selective and reversible responses to nitrogen dioxide at room temperature under high humidity conditions as well as bending strain (Kim et al. 2015). The graphene oxide-based resistive sensor reported low-concentration nitrogen dioxide and ammonia gases in air flow at room temperature (Lu et al. 2009). The ozone-treated graphene sensor was demonstrated to show better sensing performances such as percentage response, detection limit, and response time for extremely low ppb nitrogen dioxide gas concentrations over that of the pristine graphene (Chung et al. 2012). The standard sensing plot as well as correlation between percentage response and concentrations is shown in Fig. 10.19. The nanocomposite films of tungsten films impregnated with CNT showed sensitivity to 500 ppb nitrogen dioxide under ambient conditions (Bittencourt et al. 2006). The poly(ethylene imine)-coated SNWT nanocomposite was introduced as good nitrogen dioxide sensor with the lowest detection limit of 100 ppt (Qi et al. 2003). The SWCNT decorated with metal nanoparticles such as platinum, palladium, gold, silver, etc. has shown unique and improved sensing characteristics for nitric oxide gas in the atmosphere over the bare SWNT networks (Kauffman and Star 2007). The drop-cast CNT–tin dioxide nanocomposite onto a cylindrical ceramic tube at internal heating temperature of 300 °C reported cross sensitivity to nitric acid gas concentrations between 2 and 50 ppm (Liang et al. 2004). The highest response to nitrogen dioxide was observed by zinc oxide–tin dioxide nanocomposite with 1:1 zinc and tin molar ratio via

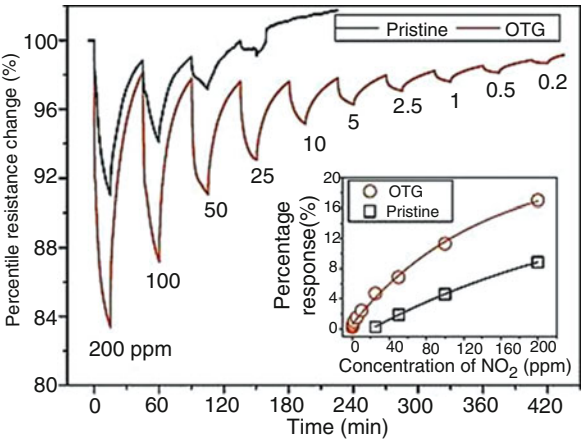

Fig. 10.19 The percentile resistance changes of the ozone-treated graphene (OTG) and pristine graphene (black) sensors for nitrogen dioxide concentration from 200 ppm to 200 ppb. The inset shows the correlation between percentage response and concentrations. (Reprinted with permission of Elsevier from Chung et al. 2012)

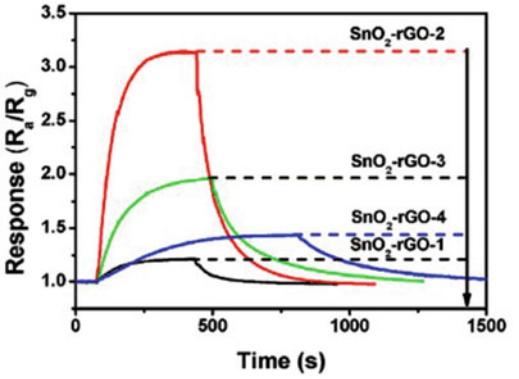

Fig. 10.20 Comparative response curve to 5 ppm nitrogen dioxide concentration at 50 °C for tin dioxide–reduced graphene oxide with different compositions (Reprinted with permission of Elsevier from Zhang et al. 2014a, b)

ultraviolet light stimulation changed 1266-fold to 500 ppb nitrogen dioxide gas at room temperature due to increasing photogenerated electrons (Lu et al. 2012). Tin dioxide nanocomposites with a small amount of strontium oxide, calcium oxide, barium oxide, bismuth oxide, and samarium oxide have been reported for the sensing of nitrous oxide in the concentration range of 10–300 ppm at 500 °C (Kanazawa et al. 2001). The calibration curve of nitrogen dioxide sensing characteristics by tin oxide/reduced graphene oxide nanocomposite-based chemoresistive devices on alumina substrates provided with platinum interdigitated electrodes was reported (Neri et al. 2013). Moreover, improved sensing response was observed for tin dioxide nanoparticles with particular amount of reduced graphene oxide nanocomposites for nitrogen dioxide sensing at 50 °C as shown in Fig. 10.20 (Zhang et al. 2014a, b).

10.5.3 Oxides of Sulfur

Sulfur dioxide is the main type of oxides of sulfur, and it is further oxidized to sulfur trioxide. Sulfur dioxide is originated from human activities like combustion of coal or fuel and petroleum refining and is environmentally harmful as it can aid in the formation of acid rain. The gaseous pollutant can induce respiratory problems in humans above the threshold limit value of 2 ppm.

Semiconductor sensors based on vanadium pentoxide-doped tin dioxide nanocomposite was used for the successful sensing of sulfur dioxide gas with short-term exposure limit of 5 ppm. As shown in Fig. 10.21, the sensing layer of tin dioxide nanocomposite doped with 0.15 weight percentage of vanadium pentoxide responded selectively for sulfur dioxide gas over the other gases like carbon monoxide, methane, and butane (Das et al. 2008). The nanosized tin dioxide-based sensors with various promoters such as vanadium pentoxide, molybdenum trioxide, antimony oxide, aluminum oxide, ceric dioxide, and magnesium oxide were investigated to measure the responses and recovery behaviors in sulfur dioxide gas flow. It was reported that the tin dioxide-based gas sensor with mixture of 5 weight percentage of magnesium oxide and 2 weight percentage of vanadium pentoxide promoters showed a 44 % response at 1 ppm concentration with good repeatability (Lee et al. 2011b).

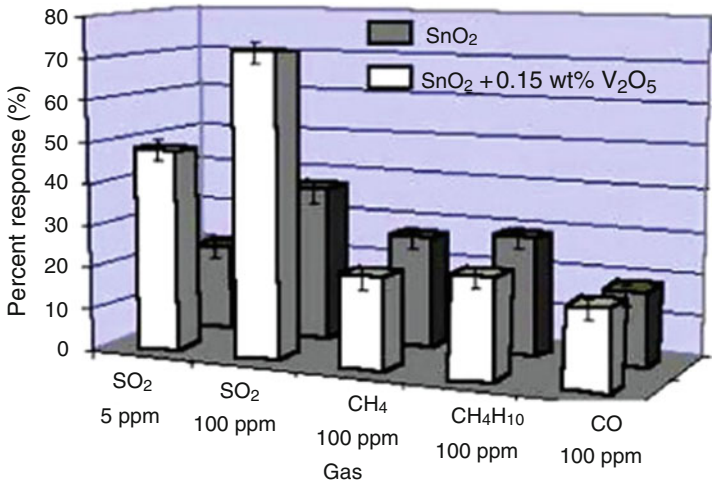

Fig. 10.21 The sensitivity of tin dioxide and tin dioxide weight percentage of vanadium pentoxide toward different gaseous pollutants at 350 °C operating temperature (Reprinted with permission of Elsevier from Das et al. 2008)

10.5.4 Volatile Organic Compounds

The risk of explosion is the primary adverse effect for exposure of hydrogen and hydrocarbon especially methane above the threshold limit value concentration as 4% in atmosphere having high level of oxygen. Moreover, hydrocarbon gas like methane is a much more powerful greenhouse gas even than that of carbon dioxide. The hydrocarbon gases originated from sources such as landfills, fossil fuel production sites, petrochemical industry, and agricultural areas. The important materials used for the sensing of three main types of volatile organic compounds such as alcohol, chlorinated hydrocarbon, and acetone are shown in Table 10.2.

As shown in Fig. 10.22, the tin dioxide nanocomposite doped with 5.0 weight percentage of samarium oxide was reported to have selective sensing for ethanol over carbon monoxide at 300 °C operating temperature (Habibzadeh et al. 2010). The cross sensitivity in presence of other volatile organic compound gases was reported using CNT films to 500 ppm ethanol at 165 °C under dry nitrogen and 80% relative humidity (Cantalini et al. 2003). Similarly, CNT sensors using two transducer mechanisms, resonant frequency and reflectivity changes, reported for the detection of various organic vapors such as methanol, ethanol, isopropyl alcohol, acetone, ethyl acetate, toluene, etc. (Penza et al. 2004a; Penza et al. 2005a, b, c). It was found that indium oxide nanowires exhibited high response, good selectivity, and very short response time to dilute ethanol (Xiangfeng et al. 2004). The layer of thermally treated tin dioxide nanoparticles exhibited good sensitivity with detection limit as low as 1.7 ppm to alcohol vapors like methanol, ethanol, and propanol (Chiu and Yeh, 2007).

A surface aquatic wave sensor fabricated by spray casting CNT solutions with silicon dioxide coating onto quartz substrates was developed to measure ethanol at room temperature with detection limit of 3.9 ppm (Penza et al. 2004b, 2007). The sensitivity to ethanol vapors was described by using tin dioxide-coated CNT devices (Liang et al. 2004), tin dioxide nanocomposite films with CNT (Wisitsoraat et al. 2006), tin dioxide-decorated MWNTs (Liu et al. 2006), and CNT–tin dioxide core–shell nanostructures at 300 °C operating temperature (Chen et al. 2006). The selective sensing of ethanol and methanol vapors over the other volatile organic compounds such as hexane, tetrahydrofuran, cyclohexane, acetone, chloroform, ethyl acetate, methanol, toluene, N,N-dimethyl formamide, and carbon tetrachloride was reported by changing the composition of the aligned CNT–poly(vinyl acetate) nanocomposite (Wei et al. 2006). The nanocomposite of poly(3-methylthiophene)-functionalized CNT showed selectivity to different chloromethane vapors over the other volatile organic compounds like methane, acetone, acetaldehyde, benzaldehyde, tetrahydrofuran, methanol, or ethanol (Santhanam et al. 2005). The nickel oxide-decorated zinc oxide nanowires were proved to provide a promising material platform for the highly sensitive and selective detection of methanol and formaldehyde with a ppb level (Na et al. 2012). As shown in Fig. 10.23, a significantly high selectivity to ethanol vapor was observed by cataluminescence emission from catalytic oxidation of ethanol on the surface of zinc oxide nanoparticles over the

Table 10.2 Sensing data on the three main types of volatile organic compounds such as alcohol, chlorinated hydrocarbon, and acetone

Volatile organic compounds for sensing	Nanomaterials as sensing layer	Remarkable sensing properties	References
Aliphatic alcohols	Poly(m-aminophenol)/ functionalized multi-walled carbon nanotube composite	Considerable response toward methanol and ethanol vapor, whereas it hardly responded to propanol and butanol	Verma et al. (2015)
	Poly(m-aminophenol)–sulfonic acid-functionalized multi-walled carbon nanotube composite	Distinct features of the response for methanol and ethanol, which could be used as a basis for the selective detection	Verma et al. (2017a)
	Poly(m-aminophenol)–amine groups functionalized multi-walled carbon nanotube composite	Significantly selective response for ethanol vapor	Verma et al. (2017b)
	Poly(m-aminophenol)–copper nanocomposite	Selective methanol vapor sensing	Bhuyan et al. (2018)
	Polyaniline–silver nanocomposites	Superior ethanol sensing capacity	Choudhury (2009)
	Poly(methylmethacrylate)/ functionalized multi-walled carbon nanotube composite	Efficient ethanol sensor	Kaur et al. (2015)
	Nanocrystalline barium hexaferrite particles	Promising ethanol sensing characteristics	Karmakar et al. (2014)
	Pseudo-peanut-shaped hematite iron oxide nanoparticles	Promising response toward ethanol and formaldehyde vapors	Das et al. (2016)
	Anatase titania	Temperature-dependent distinctive and systematic sensing performance for detection of 200 ppm ethanol	Das et al. (2017a)
	Rutile phase titania nanoparticles	Higher response of the sensor toward isopropanol than formaldehyde	Das et al. (2017b)
	Graphene-like layers	A stronger response to ethanol than to n-butanol	Gargiulo et al. (2018)
	Functionalized multi-walled carbon nanotubes	Linear response for 1 to 21 ppm alcohol vapor concentrations with detection limit of 0.9 ppm	Sin et al. (2007)
	Palladium–polyaniline nanocomposite	Rapid, reversible, and selective response for methanol even in mixtures of methanol–ethanol and methanol–isopropanol	Athawale et al. (2006)
	Reduced graphene oxide and three-dimensional zinc oxide nanoflower composite	Selectivity toward 2-propanol against interfering neighbors like ethanol, methanol, acetone, and benzene	Acharyya et al. (2018)

(continued)

Table 10.2 (continued)

Volatile organic compounds for sensing	Nanomaterials as sensing layer	Remarkable sensing properties	References
Acetone	Polyaniline–silver nanocomposites	Good response to acetone vapor at any level of vapor concentration	Choudhury et al. (2009)
	Chestnut-like cobalt ferrite @ silicon dioxide @ indium oxide nanocomposite	Superior sensitivity and fast response speed to low-ppm-level acetone	Lin et al. (2018)
	Rh-doped tin dioxide nanofibers	Acetone gas sensor with high gas sensing performance	Kou et al. (2018)
	Perovskite praseodymium ferrite hollow nanofibers	Acetone sensor having high response, good selectivity, long-time stability, low operating temperature of 180 °C, detection limit 10 ppm	Ma et al. (2018)
	Platinum-decorated copper ferrite nanotubes	Acetone sensing at 300 °C showing high response, good selectivity, and long-term stability	Zhao et al. (2018)
	Nanostructured α-ferric oxide–nickel oxide composites	The sensing response of 18.24% to 100 ppm acetone gas at 169 °C	Haq et al. (2018)
	Two-dimensional tin-doped zinc oxide ultrathin nanosheet and silver-doped zinc oxide nanoneedles	Optimization of acetone sensing	Al-Hadeethi et al. (2017a, b)
	Europium-doped tin dioxide nanobelt	Improved gas sensing response to acetone than ethanol, methanol, ethanediol	Chen et al. (2017b)
	Tungsten trioxide–nickel oxide core–shell nanorods	Selectivity and sensitivity for acetone of the tungsten trioxide nanorods enhanced by nickel oxide	Choi et al. (2017)
	Palladium-loaded samarium-doped tin dioxide nanomaterial	94% gas response, better selectivity, faster response, and quicker recovery toward acetone over liquid petroleum gas, ammonia, ethanol, and acetone	Shaikh et al. (2017)
	Carbon-doped tungsten trioxide hollow spheres	High sensitivity to acetone even at 0.2 ppm and lower response to other gases like ethanol, methanol, toluene, ammonia, nitric oxide, and carbon monoxide	Shen et al. (2017)
	Europium-doped α-ferric oxide nanotubes and nanowires	Nanotubes having 2.7 times higher response for selectivity in acetone detection than nanowires	Cheng et al. (2017)

(continued)

Table 10.2 (continued)

Volatile organic compounds for sensing	Nanomaterials as sensing layer	Remarkable sensing properties	References
	Zinc oxide nanosheets	Sensing of 5–1000 ppm acetone vapor at 300 °C with high response, fast response-recovery, and good selectivity	Li et al. (2017)
	Manganese-doped zinc oxide and manganese-doped zinc oxide nanomaterials modified by cadmium oxide	Distinguish the ethanol and acetone concentrations in mixtures with varied ratios	Wang et al. (2017)
	Nanocrystalline barium hexaferrite particles	Promising acetone sensing characteristics	Karmakar et al. (2014)
Halogenated hydrocarbon	Polyaniline–carboxylic acid-functionalized multi-walled carbon nanotube composite	Selectively higher response toward chloroform vapor over chloromethane, dichloromethane, and carbon tetrachloride	Kar and Choudhury (2013)
	Polyaniline–copper nanocomposite	Chloroform vapor sensor	Sharma et al. (2002)

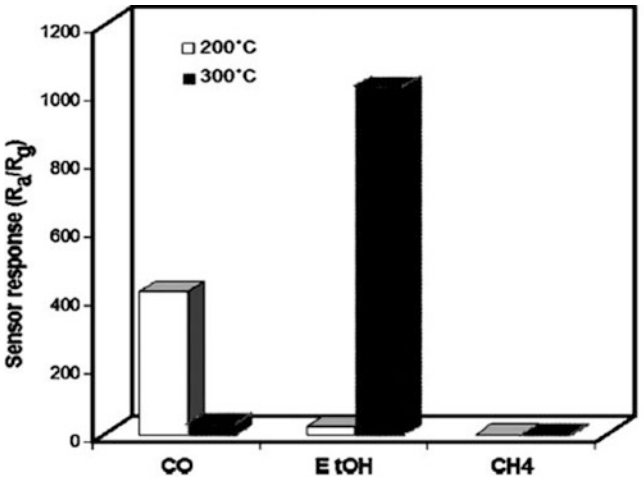

Fig. 10.22 The response of tin dioxide doped with samarium oxide upon exposure to different gases at different temperatures. (Reprinted with permission of Elsevier from Habibzadeh et al. 2010)

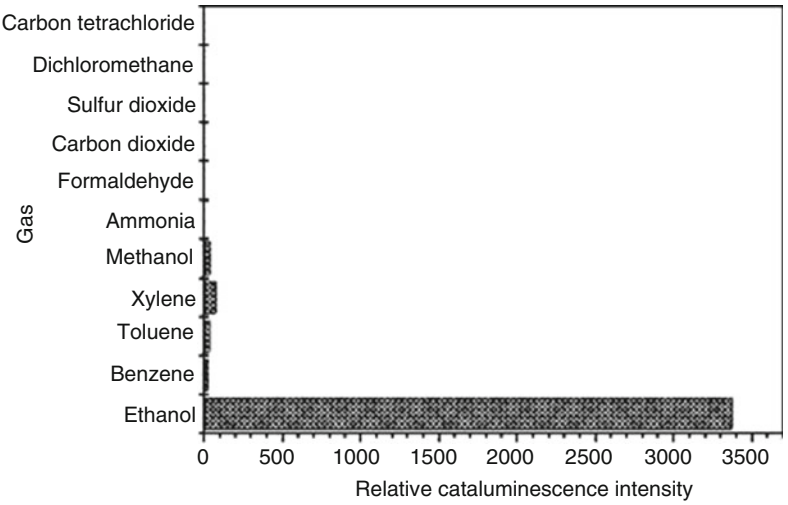

Fig. 10.23 Selectivity of the cataluminescence ethanol sensor on the surface of zinc oxide nanoparticles. (Reprinted with permission of Elsevier from Tang et al. 2007)

gases like ammonia, nitrogen, carbon dioxide, sulfur dioxide, dichloromethane and carbon tetrachloride, benzene, toluene, xylene, and methanol (Tang et al. 2007). The responses of the nanocomposite of poly(m-aminophenol) doped with 2 weight percentage of carboxylic acid-functionalized MWCNT toward aliphatic alcohol vapor were substantially improved compared to pure polymer, and responses/sensitivity for methanol and ethanol was explained as the basis for the selective detection (Verma et al. 2015, 2017a). Further, the selectivity of the poly(m-aminophenol) was further improved toward methanol by using nanocomposite with copper nanoparticles (Bhuyan et al. 2018). Similarly, the nanocomposite of poly (m-aminophenol)/amine group functionalized MWCNT was found to be selective toward ethanol vapor (Verma et al. 2017b). Ultrasensitive reduced graphene oxide and three-dimensional zinc oxide nanoflower composite offered excellent selectivity toward 2-propanol against interfering neighbors like ethanol, methanol, acetone, and benzene (Acharyya et al. 2018).

Polydiacetylene-encapsulated electrospun fiber-based colorimetric sensor has been developed for volatile organic compounds, such as chloroform, tetrahydrofuran, ethyl acetate, and hexane (Yoon et al. 2007). The sensing performance of porous hierarchical indium oxide micro-/nanostructures has been investigated for volatile organic compounds (methanol, toluene, and formaldehyde), and as shown in Fig. 10.24, the sensor was found to have selectivity for methanol gas sensing in terms of better response (Liu et al. 2010). The polyaniline nanocomposite with 2 wt % carboxylic acid group functionalized MWCNT nanocomposite exhibited good selectivity toward chloroform vapor over the other chlorinated methane vapor like chloromethane, dichloromethane, and carbon tetrachloride (Kar and Choudhury 2013). The conducting polyaniline nanofiber was tested as a sensor to the aromatic

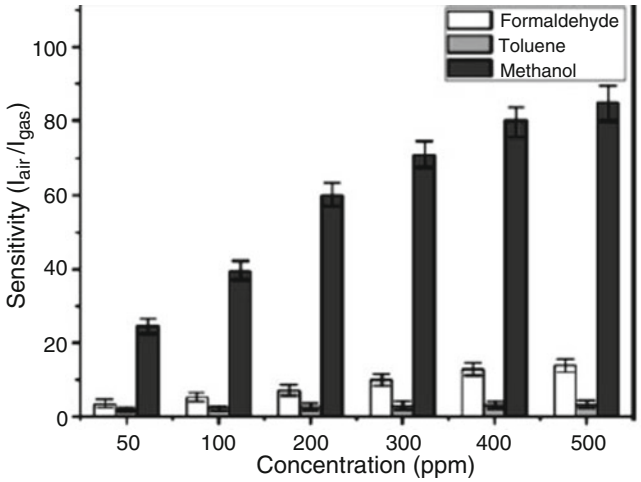

Fig. 10.24 Selectivity of porous hierarchical indium oxide micro-/nanostructures for methanol gas sensing. (Reprinted with permission of American Chemical Society from Liu et al. 2010)

organic compounds in the concentration range of 200–1000 ppm (Li et al. 2009). The polyaniline–silver nanocomposite was employed for the successful sensing of acetone vapor, and the sensor exhibited the fastest response, good reproducibility, and long-term stability in comparison with pure polyaniline sensor (Choudhury et al. 2009). Nanocrystalline barium hexaferrite particles have been revealed as promising sensor for the fast and reproducible detection of acetone and ethanol vapors at concentration as low as 20 ppm (Karmakar et al. 2014).

10.5.5 Ozone

Ozone consisting of three oxygen atoms bound together is unstable and highly reactive. Ozone found in the stratosphere has been called "good" ozone as it protects the earth's surface from dangerous ultraviolet light. Ozone in troposphere, the lowest layer of the atmosphere, is man-made air pollutant released from internal combustion of engines and power plants, and that ozone is often termed "bad" ozone. Ozone can be used as a bleach and a sterilization agent for air and drinking water. However, exposure to ozone has been linked to have significant adverse effects like premature mortality, range of morbidity health, asthma symptom, decrease of vegetation productivity of some crops, injury of flowers and shrubs, etc. Ozone acts as a reactive deodorizing agent and damages synthetic materials, rubber, dyes, paints and coatings, cotton, acetate, nylon, polyester, and other textiles.

Nanosized indium oxide single crystals deposited onto alumina substrates were reported as ozone gas sensor with short response and recovery times even for concentrations as low as 60 ppb (Epifani et al. 2008). A series of nanocrystalline

metal oxides such as tin dioxide, indium oxide, and tungsten trioxide have been tested as ozone detectors for environmental with monitoring applications (Starke and Coles 2002). Among the various zinc oxide nanomaterials, the single-crystal nanorods showed better response for ozone sensing at room temperature in terms of response and recovery time (Chien et al. 2010; Wu et al. 2008). The dependence of ozone sensing performances for zinc oxide nanostructure samples on surface morphology, substrate coverage, and average thickness under ultraviolet irradiation at room temperature has been reported and optimized (Kenanakis et al. 2007). An optical ozone sensor was reported based on the ultrathin layers of indium oxide nanoparticles and an indium gallium nitride–gallium nitride blue light-emitting diode on a single sensor chip for concentrations as low as ~40 ppb (Wang et al. 2007). In a simple optical ozone sensor, the shifting of surface plasmon resonance peak of gold nanoislands was observed with increasing concentration of gaseous ozone (Fig. 10.25) (Pisarenko et al. 2009). Our current results indicate sensing gaseous ozone at concentration of as low as 20 μg/L is achievable at room temperature; gold@titanium dioxide exhibited excellent ozone sensing properties such as fast response and recovery times as well as excellent linearity within concentration range of 0.5–7.0 ppm (Fig. 10.26) (Zhu et al. 2015). The SWCNT-based ozone sensor was reported to have high sensitivity at concentration as low as 50 ppb and fast response time (Park et al. 2009). A new ozone gas sensor based on α-Ag_2WO_4 nanorod was proved as efficient sensor with fast response, short recovery, and good sensitivity even for an ozone concentration as low as 80 ppb at 300 °C operating temperature (daSilva et al. 2014).

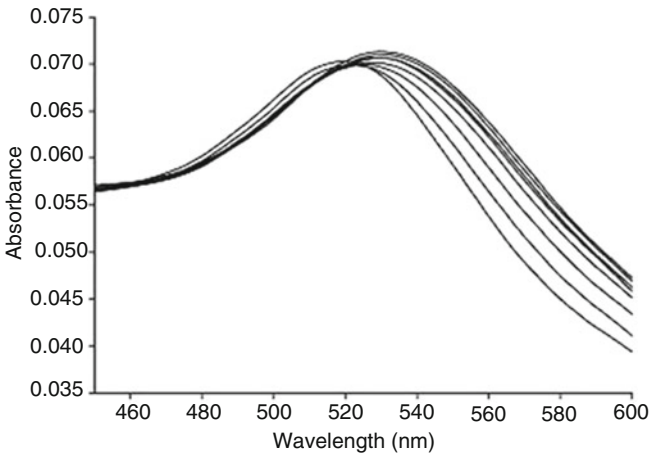

Fig. 10.25 Red-shifting of surface plasmon absorbance max of 25 nm gold nanoisland exposure to ozone vapor of concentration from 20.9 μg/L to 166.1 μg/L. (Reprinted with permission of Elsevier from Pisarenko et al. 2009)

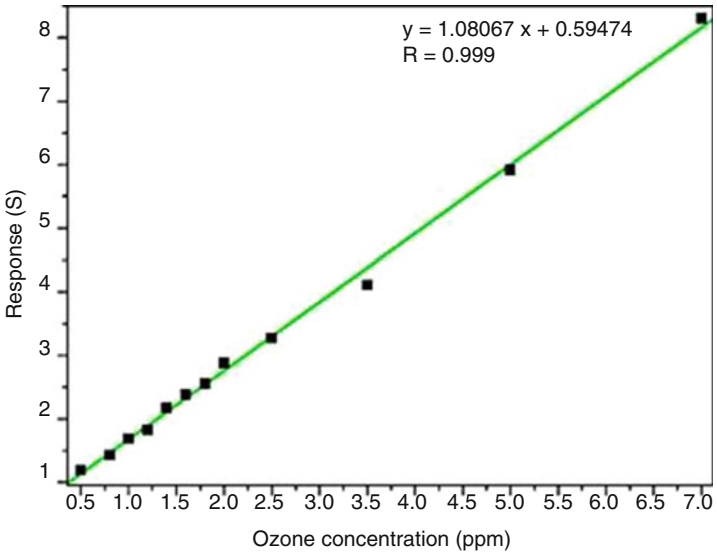

Fig. 10.26 Response of the gold@titanium dioxide from 0.5 to 7.0 ppm ozone gas at room temperature. (Reprinted with permission of Elsevier from Zhu et al. 2015)

10.5.6 Humidity

Humidity in surroundings plays a significant role for biological or non-biological components of the environment. Moreover the strong corrosion effect was observed by the moisture on the materials especially on metals. To have a desirable atmosphere, the ambient humidity has to monitor, detect, and control temperature ranging from low to high. In general, the principal mechanisms of all the humidity sensors may be classified as ionic conduction, electronic conduction, solid electrolyte and capacitive type, chemisorption, physisorption, and capillary condensation processes (Farahani et al. 2014). Few examples of such type of sensing mechanism for different nanomaterials are shown in Table 10.3. The layer-by-layer nano-assembled ultrathin poly(anilinesulfonic acid) film was reported for the sensing of humidity with high-sensitive and rapid response (Nohria et al. 2006). Similarly, deposited nanoblend of sulfonated polystyrene with poly(4-vinylpyridine) on interdigitated gold electrodes was used for the successful sensing of humidity within the range 40–90% only (Li et al. 2018b). The humidity sensing performances including resistance versus relative humidity, humidity hysteresis, response–recover time, and long-term stability have been investigated using composite material made of nanocrystal barium titanate and polymer material quaternary acrylic resin (Wang et al. 2002). The fast and sensitive response to relative humidity in the air up to 90% was studied on a layer of single tin dioxide nanowire at 30 °C (Kuang et al. 2007). Porous vanadium pentoxide micro-/nanotubes were synthesized via a modified chemical vapor deposition process, and a possible growth mechanism was proposed.

Table 10.3 Examples of humidity sensing with different mechanisms for different nanomaterials

Nanomaterials as sensing layer	Sensing mechanism	% Humidity range	References
Poly(diallyldimethylammonium chloride)–graphene oxide nanocomposite	Restive type (electronic conduction)	11–97	Zhang et al. (2014a, b)
Graphene oxide silicon bilayer	Adsorption (surface aquatic wave sensor)	10–90	Le et al. (2018)
Polyaniline–graphene oxide nanocomposite film	Adsorption (quartz crystal microbalance)	0–97	Zhang et al. (2018)
Monolayer graphene oxide and few-layered black phosphorus flakes	Capacitance type (adsorption)	11–97	He et al. (2018)
Two-dimensional titanium dioxide nanosheets	Impedance type (ion conduction)	11–95	Gong et al. (2018)
Nanostructured sulfonated polystyrene-b-poly(4-vinylpyridine)	Impedance type (ion conduction)	40–90	Li et al. (2018b)
Two-dimensional silicon carbide nanosheets	Restive type (electronic conduction)	10–95	Sun et al. (2018)
Graphene oxide	Capacitance type (physisorption)	15–95	Bi et al. (2013)
Hydrophobin-functionalized graphene	Capacitance type (physisorption)	10–50	Tao et al. (2017)
Pyranine modified–reduced graphene oxide	Impedance type (ion conduction)	11–95	Chen et al. (2017a)
Fe-doped tin dioxide nanoparticles and reduced graphene oxide decorated with iron-doped tin dioxide nanoparticles	Restive type (electronic conduction)	0–100	Toloman et al. (2017)
Tin dioxide–reduced graphene oxide nanocomposite	Restive type (electronic conduction)	11–97	Zhang et al. (2016)
Tin oxide hexagonal-shaped nanodiscs and spherical nanoparticles	Restive type (electronic conduction)	5–95	Parthibavarman et al. (2011)
Nickel oxide–tin dioxide nanofibers	Restive type (electronic conduction)	0–100	Pascariu et al. (2016)
Antimony-doped tin dioxide nanowire	Restive type (electronic conduction)	22–44	Zhuo et al. (2013)
Zinc-doped tin dioxide	Restive type (electronic conduction)	40–90	Md Sin et al. (2013)

A fast response and recovery has been recorded for humidity sensing by a single porous vanadium pentoxide micro-/nanotube due to having large surface area in their tubular structure with a porous wall (Yin et al. 2012). The quartz crystal microbalance-type humidity of sensor-based polyacrylic acid–poly(vinyl alcohol) nanofiber composite membranes was found to have two times higher sensitivity than that of the corresponding flat films at 95% room humidity (Wang et al. 2010). An electrochemical humidity sensor was fabricated by nanosized silicon dioxide with poly(2-acrylamido-2-methylpropane sulfonate) matrix, and it was also explained

that the stability of the sensor was increased with increasing silicon dioxide content (Su and Tsai 2004). As reported by the authors, the humidity sensing performance of chemically reduced graphene oxide–poly(diallyldimethylammonium chloride) nanocomposite film was superior over the other reported graphene-based humidity sensor (Zhang et al. 2014a, b). Zinc oxide nanorods and nanowires were reported to have high sensitivity, good long-term stability, and fast response time to a moisture pulse of 97% relative humidity (Zhang et al. 2005). Similarly, high-density single-crystalline zinc oxide nanowires on patterned gallium–silicon dioxide–silicon template electrodes were reported for the sensing of humidity by measuring current–voltage characteristics of the fabricated device at 80 °C (Chang et al. 2010). The humidity sensing response including linearity, hysteresis, response–recovery time, and stability of the titania-loaded mesoporous silica nanocomposite sensor was reported for humid range of 11–98% room humidity at 25 °C (Tomer and Duhan 2015).

10.5.7 Ammonia

The ammonia contamination in the air caused mainly by high agricultural activity; natural waste product of livestock; industrial manufacturing of basic chemicals, metals, textiles, and paper products; automotive emissions; etc. adversely affects human as well as environmental health. High levels of ammonia vapor contamination can result the effects like eye irritation and respiratory tracts of animals, negative impact on wildlife, livestock, and decrease in agricultural productivity (Timmer et al. 2005; Eerden et al. 1998). The threshold limit value has been set at 25 ppm over 10 h a day for exposure of ammonia vapors.

The irreversible response was reported for ammonia sensor using bare SWNT (Quang et al. 2006). The operating temperature of tungsten trioxide sensors for ammonia was decreased down to 150 °C by using tungsten trioxide films impregnated with CNT (Bittencourt et al. 2006). The operating temperature was further decreased down to room temperature for ammonia sensing with detection limit to 10 ppm by using SWNT–tin dioxide nanocomposite (Hoa et al. 2007). The ammonia sensor was developed using nanocomposite of functionalized SWNT with the polymers like poly(m-aminobenzene sulfonic acid) (Bekyarova et al. 2004) or poly (methyl methacrylate) (Li et al. 2007). The ammonia sensor was developed using p–n heterojunction of polyaniline coated on electrospun titanium dioxide fiber, which was 1000 times more sensitive than the best polyaniline sensor for gas (Gong et al. 2010). The polyaniline nanowires deposited on gold electrodes showed a rapid and reversible resistance change upon exposure to ammonia gas even at low concentrations of 0.5 ppm. The oriented single-wire geometry was explained as the reason for instant response and complete recovery by easy adsorption/desorption of gas (Liu et al. 2004). In another study, the effect of polymerization temperature on the gas response of polyaniline–titanium dioxide nanocomposite thin film deposited on a silicon substrate with gold interdigital electrodes was investigated for ammonia

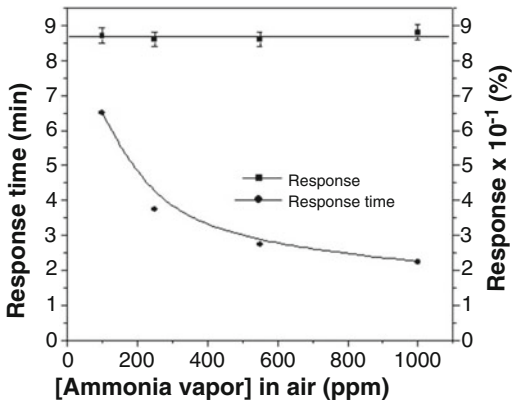

Fig. 10.27 Sensitivity and response time of hydrochloric acid-doped poly(m-aminophenol)–silver nanocomposite at varying concentrations of ammonia in air mixture. (Reprinted with permission of Springer Nature from Kar et al. 2011)

gas sensing application (Tai et al. 2008). It was also reported that the polyaniline–titanium dioxide nanocomposite was found to show the superior sensor for ammonia vapor over carbon monoxide (Tai et al. 2007). The SWNT functionalized with polyaniline nanocomposite network were found to have superior sensitivity of 2.44% resistance change per ppmv ammonia, and the performance was more than 60 times higher than intrinsic SWNT-based sensors with low detection of 50 ppbv as well as good reproducibility (Zhang et al. 2006). The highly porous nanocomposite of polypyrrole-coated titanium dioxide–zinc oxide nanofibrous mat exhibited a fast response over a wide dynamic range of ammonia vapor with a detection limit of 60 ppb (Wang et al. 2009). The stable and reproducible ammonia vapor sensor with average sensitivity of 86.75±2.9% has been reported using poly(m-aminophenol)–silver nanocomposite layer. As shown in Fig. 10.27, the response times were decreased as the concentration of ammonia vapor in the air increased without affecting the response (Kar et al. 2011). Unique thin layers that assembled three-dimensional tin disulfide nanoflower structures were demonstrated as a sensor for ammonia low detection limit of 0.5 ppm with and superb selectivity over carbon dioxide, methane, hydrogen, ethanol, and acetone (Xiong et al. 2018).

10.5.8 LPG and Hydrocarbons

The novel sensor at room temperature for 6–100 ppm methane gas was fabricated by palladium-decorated SWNT (Lu et al. 2004). The hydrocarbon gases like methane, propane, and n-hexane sensing nanocrystalline perovskite oxide lanthanum, neodymium, and samarium ferrite were reported, and it was observed that rare earth elements play the important roles to gas sensitivities of oxides (Giang et al. 2011). Nanowires of tungsten oxide with 2.72 moles of oxygen impregnation by 0.1–1.0% platinum have shown high sensitivity for 2000 ppm of LPG at 200 °C, while the same composition of vanadium pentoxide did not exhibit satisfactory characteristics (Rout et al. 2006b). The nanocomposites of conjugated polymer with metal oxide

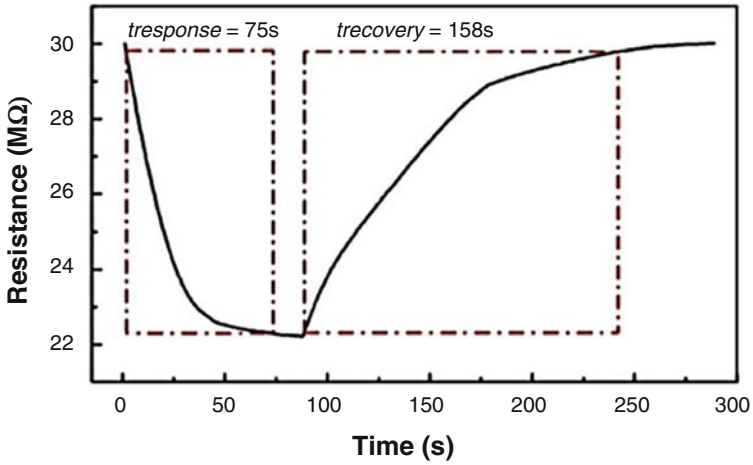

Fig. 10.28 Methane gas sensing performance of vanadium dioxide nanorods. (Reprinted with permission of Elsevier from Li et al. 2016)

nanomaterials were developed on the basic operating principle of heterojunction gas sensor barrier (Dhawale et al. 2008, 2010a, b). For p-type polyaniline nanocomposite with n-type zinc oxide heterojunction has been successfully sense the LPG at room temperature by increasing the barrier height at the interface of nanocomposite heterojunction (Dhawale et al. 2010a). Efficiently enhanced methane gas sensing performance was provided by vanadium dioxide nanorods owing to its special structure with a large specific surface area (Li et al. 2016). For convenience, the sensitivity with response and recovery time of vanadium dioxide nanorods toward 500 ppm methane is shown in Fig. 10.28 (Li et al. 2016). Flexible poly (styrene-butadiene-styrene)–carbon nanotube composite fiber-based sensor has been reported for sensing of cyclohexane with 256% response over acetone vapor with only 19% response for 10% of both the vapors (Wang et al. 2018b). The chitosan–CNT conductive nanocomposites fabricated by spray layer-by-layer technique have been investigated for the successful sensing of polar vapors like water and methanol over nonpolar toluene vapor with high sensitivity (Kumar et al. 2010).

10.5.9 Hydrogen Sulfide

Hydrogen sulfide gas emission is a serious concern for petroleum refineries and coke ovens or from biodegradation site. Hydrogen sulfide is a colorless, flammable, and toxic gas having objectionable bad odor even at very low concentrations. Hydrogen sulfide has short-term toxicity to humans, aquatic life, birds, and animals in extremely low air concentrations. The hydrogen sulfide is dangerous because of its lower explosive limit of 4% and a threshold limit value of 10 ppm (Kauffman and Star 2008).

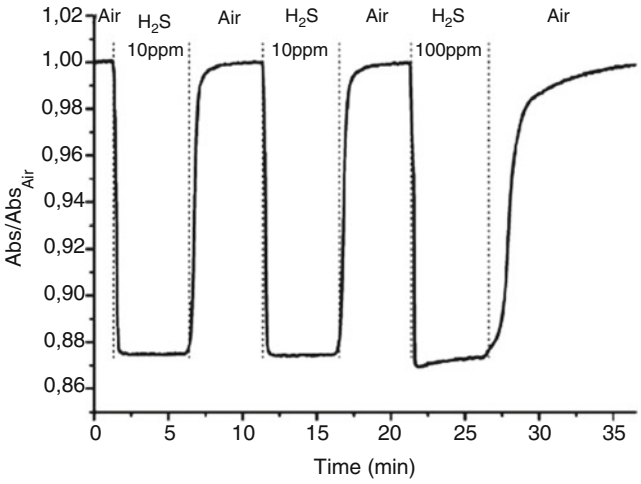

Fig. 10.29 Sensing of hydrogen sulfide by gold–titanium dioxide–nickel oxide nanocomposite. (Reprinted with permission of American Chemical Society from Gaspera et al. 2010)

The palladium metal-decorated SWNT were able to detect 50 ppm hydrogen sulfide in the air (Star et al. 2006). Thin films composed of gold nanoparticles dispersed inside a mixed oxide matrix of titanium dioxide–nickel oxide were used as hydrogen sulfide optical sensors for the absorption of gold-localized surface plasmon resonance by gas exposure (Gaspera et al. 2010). As shown in Fig. 10.29, the sensor was found to have linear response within the concentration range and no interference during simultaneous exposure to carbon monoxide or hydrogen (Gaspera et al. 2010). The single-mode fiber of zinc oxide nanoparticles embedded with poly-methyl-methacrylate matrix composite was found to have changed optical properties by swelling of the polymer matrix during the sensing of hydrogen sulfide at room temperature from 1 ppm to 5 ppm (Kitture et al. 2017).

10.5.10 Others

The SWCNT on an interdigitated electrode have been used for sensing various pollutant gases, and the selectivity to chlorine and hydrochloric acid vapor was demonstrated by coating the SWNT with polymers such as chlorosulfonated polyethylene and hydroxypropyl cellulose (Li et al. 2006b). Thin films of polyaniline nanofibers were found to have sensing performance to vapors of hydrochloric acid and ammonia base with better sensitivity as well as response time than that of the bulk polyaniline film (Huang et al. 2003). The single nanowires of zinc oxide, titanium dioxide, and tungsten 2.72 mole oxide were found to be responsive for the sensing of hydrogen (Rout et al. 2007). In this study it was also reported that the tungsten 2.72 mole oxide nanowire exhibited the highest sensitivity of 22 for 1000 ppm at 298 K. The selective sensing properties toward formaldehyde with

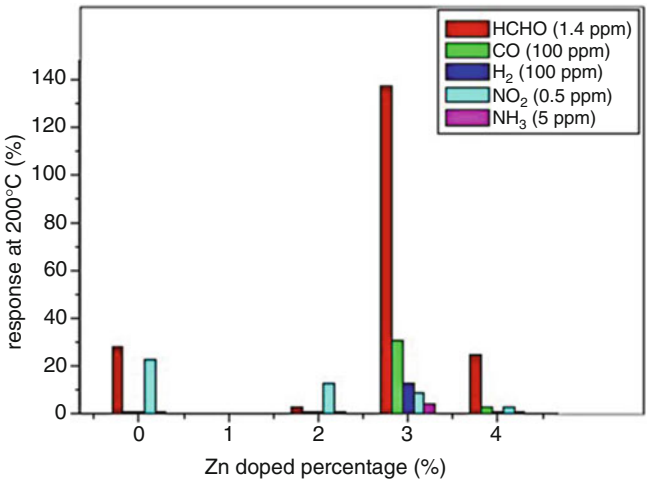

Fig. 10.30 Response of gas sensor based on pure nickel oxide and all zinc-doped nickel oxides toward formaldehyde, carbon monoxide, hydrogen, nitrogen dioxide, and ammonia at 200 °C. (Reprinted with permission of Elsevier from Fomekong et al. 2018)

detection limit of 74 ppb were observed for zinc-doped nickel oxide nanoparticles at optimal operating temperature of 200°C and 10% humidity (Fomekong et al. 2018). As observed from Fig. 10.30, selectivity toward formaldehyde over carbon monoxide, hydrogen, nitrogen dioxide, and ammonia was greatly increased by 3% zinc-doped nickel oxide nanoparticles. Hydrogen gas sensing behavior and response kinetic have been reported by using porous nanocrystalline zinc ferrite sensing elements (Mukherjee and Majumder 2009). Similarly, a nanocrystalline magnesium ferrite powder has been used as sensing materials for successful sensing of hydrogen as well as carbon monoxide (Mukherjee et al. 2010).

10.6 Conclusions

A huge number of various types of sensing devices based on nanomaterials for air pollutants have been explored through the tireless efforts of scientists and researchers. In sensing of air pollutant, the special required properties of the sensing nanomaterials with addition of the general properties of the materials to be considered are as follows:

(a) Simple and miniaturized setup of sensor device.
(b) The materials should be interactive with the analyte at the environmental condition.
(c) The sensing conditions such as temperature, electrical current supply, pressure, moisture, etc. should be as simple as possible.
(d) The sensing response should be reversible, reproducible, reliable, etc.

(e) The maintenance, durability, and cost should be as minimum as possible.
(f) The sensor material should be stable at normal environmental condition like room temperature and room humidity.
(g) The material should interact separately and response selectively for different analytes.
(h) The easy and complete recovery of the material at ambient condition.

Very few commercial nanomaterials-based sensors especially based on inorganic oxide semiconductor nanomaterials are available. However, there are still some serious unresolved problems in using nanomaterials as sensing materials for air pollutants. Researchers in different fields like physics, chemistry, engineering, biology and biochemistry, materials science, and others are trying hard to make nanomaterials as sensor materials as common household utilizer. In that goal, the global research and development on the field of gas sensors has occurred only within the last 50 years. So far, however, they have not fully succeeded due to having the inherent problem to develop a gas sensor like sensitivity, uncontrollable reactions with analyte, poor stability, poor response, etc. Like the gas sensor, nanotechnology developed within last 50–80 years is still in its inefficient developed stage. Moreover, the problems for the use of nanomaterials are associated with the problems in synthesis, problems in reproducibility, problems in processability, problems in mechanical and chemical stability, problems in their size and size distribution, and problems in their surface properties, distribution in the composite, weak properties of the composite, interfacial interaction in their composite, etc. There is still the need for simple techniques that produce high-quality nanomaterials having reproducible properties. Therefore, it is still the goal of sensor science and technology to create nanomaterials that simultaneously increase chemical stability, sensitivity, reproducibility, and selectivity of sensor for real-time air pollution control. These novel nanomaterials-based sensors for air pollution control will progress with time to be as commonplace as the electronic gazettes like TV and refrigerator are today.

References

Acharyya D, Saini A, Bhattacharyya P (2018) Influence of rGO cladding in improving the sensitivity and selectivity of ZnO nanoflowers-based alcohol sensor. IEEE Sensors J 18:1820–1827. https://doi.org/10.1109/JSEN.2018.2790084

Adhikari B, Kar P (2010) Polymers in chemical sensors. In: Korotcenkov G (ed) Chemical sensors, vol 3. Momentum Press LLC, New York, pp 1–76

Al-Hadeethi Y, Umar A, Al-Heniti SH, Kumar R, Kim SH, Zhang X, Raffah BM (2017a) 2D Sn-doped ZnO ultrathin nanosheet networks for enhanced acetone gas sensing application. Ceram Int 43:2418–2423. https://doi.org/10.1016/j.ceramint.2016.11.031

Al-Hadeethi Y, Umar A, Ibrahim AA, Al-Heniti SH, Kumar R, Baskoutas S, Raffah BM (2017b) Synthesis, characterization and acetone gas sensing applications of Ag-doped ZnO nanoneedles. Ceram Int 43:6765–6770. https://doi.org/10.1016/j.ceramint.2017.02.088

Athawale AA, Bhagwat SV, Katre PP (2006) Nanocomposite of Pd–polyaniline as a selective methanol sensor. Sensors Actuators B Chem 114:263–267. https://doi.org/10.1016/j.snb.2005.05.009

Beguin F, Frackowiak E (2010) Carbons for electrochemical energy storage and conversion systems. CRC Press, Boca Raton

Bekyarova E, Davis M, Burch T, Itkis ME, Zhao B, Sunshine S, Haddon RC (2004) Chemically functionalized single-walled carbon nanotubes as ammonia sensors. J Phys Chem B 108:19717–19720. https://doi.org/10.1021/jp0471857

Bergaya F, Lagaly G (2001) Surface modifications of clay minerals. Appl Clay Sci 19:1–3. https://doi.org/10.1016/S0169-1317(01)00063-1

Bhuyan M, Samanta S, Kar P (2018) Selective sensing of methanol by poly(m-aminophenol)/copper nanocomposite. Electron Mater Lett 14:161–172. https://doi.org/10.1007/s13391-018-0010-9

Bi HC, Yin KB, Xie X, Ji J, Wan S, Sun LT, Terrones M, Dresselhaus MS (2013) Ultrahigh humidity sensitivity of graphene oxide. Sci Rep 3:2714–2720. https://doi.org/10.1038/srep02714

Bittencourt C, Felten A, Espinosa EH, Ionescu R, Llobet E, Correig X, Pireaux JJ (2006) WO_3 films modified with functionalised multi-wall carbon nanotubes: morphological, compositional and gas response studies. Sensors Actuators B Chem 115:33–41. https://doi.org/10.1016/j.snb.2005.07.067

Cantalini C, Valentini L, Armentano I, Lozzi L, Kenny JM, Santucci S (2003) Sensitivity to NO_2 and cross-sensitivity analysis to NH_3, ethanol and humidity of carbon nanotubes thin film prepared by PECVD. Sens Actuators B 95:195–202. https://doi.org/10.1016/S0925-4005(03)00418-0

Carotta MC, Cervia A, di Natale V, Gherardi S, Giberti A, Guidi V, Puzzovio D, Vendemiati B, Martinelli G, Sacerdoti M, Calestani D, Zappettini A, Zha M, Zanotti L (2009) ZnO gas sensors: a comparison between nanoparticles and nanotetrapods-based thick films. Sensors Actuators B Chem 137:164–169. https://doi.org/10.1016/j.snb.2008.11.007

Chandra MR, Reddy PSP, Rao TS, Pammi SVN, Kumar KS, Babu KV, Kumar CK, Hemalatha KPJ (2017) Enhanced visible-light photocatalysis and gas sensor properties of polythiophene supported tin doped titanium nanocomposite. J Phys Chem Solids 262:655–663. https://doi.org/10.1016/j.jpcs.2017.02.014

Chang SJ, Hsueh TJ, Chen IC, Huang BR (2008) Highly sensitive ZnO nanowire CO sensors with the adsorption of au nanoparticles. Nanotechnology 19:175502–175506. https://doi.org/10.1088/0957-4484/19/17/175502

Chang SP, Chang SJ, Lu CY, Li MJ, Hsu CL, Chiou YZ, Hsueh TJ, Chen IC (2010) A ZnO nanowire-based humidity sensor. Superlattice Microst 47:772–778. https://doi.org/10.1016/j.spmi.2010.03.006

Chen Y, Zhu C, Wang T (2006) The enhanced ethanol sensing properties of multi-walled carbon nanotubes/SnO_2. Nanotechnology 17:3012–3017. https://doi.org/10.1088/0957-4484/17/12/033

Chen M, Wang Z, Han D, Gu F, Guo G (2011) High-sensitivity NO_2 gas sensors based on flower-like and tube-like ZnO nanomaterials. Sensors Actuators B Chem 157:565–574. https://doi.org/10.1016/j.snb.2011.05.023

Chen Z, Wang Y, Shang Y, Umar A, Xie P, Qi Q, Zhou GF (2017a) One-step fabrication of pyranine modified- reduced graphene oxide with ultrafast and ultrahigh humidity response. Sci Rep 7:2713–2720. https://doi.org/10.1038/s41598-017-02983-8

Chen W, Qin Z, Liu Y, Zhang Y, Li Y, Shen S, Wang ZM, Song HZ (2017b) Promotion on acetone sensing of single SnO_2 nanobelt by Eu doping. Nanoscale Res Lett 12:405–412. https://doi.org/10.1186/s11671-017-2177-7

Cheng Y, Wang Y, Zhang J, Li H, Liu L, Li Y, Du L, Duan H (2017) A comparison of Eu-doped α-Fe_2O_3 nanotubes and nanowires for acetone sensing. Nano 12:1750138–1750148. https://doi.org/10.1142/S1793292017501387

Chien FSS, Wang CR, Chan YL, Lin HL, Chen MH, Wu RJ (2010) Fast-response ozone sensor with ZnO nanorods grown by chemical vapor deposition. Sensors Actuators B Chem 144:120–125. https://doi.org/10.1016/j.snb.2009.10.043

Chiu HC, Yeh CS (2007) Hydrothermal synthesis of SnO_2 nanoparticles and their gas-sensing of alcohol. J Phys Chem C 111:7256–7259. https://doi.org/10.1021/jp0688355

Choi YJ, Hwang IS, Park JG, Choi KJ, Park JH, Lee JH (2008) Novel fabrication of an SnO2 nanowire gas sensor with high sensitivity. Nanotechnology 19:095508–095511. https://doi.org/10.1088/0957-4484/19/9/095508

Choi S, Kyung J, Woo L, Lee S, Lee C (2017) Acetone sensing of multi-networked WO_3-NiO core-shell nanorod sensors. J Korean Phys Soc 71:487–493. https://doi.org/10.3938/jkps.71.487

Choudhury A (2009) Polyaniline/silver nanocomposites: dielectric properties and ethanol vapour sensitivity. Sensors Actuators B Chem 138:318–325. https://doi.org/10.1016/j.snb.2009.01.019

Choudhury A, Kar P, Mukherjee M, Adhikari B (2009) Polyaniline/silver nanocomposite based acetone vapour sensor. Sens Lett 7:592–598. https://doi.org/10.1166/sl.2009.1115

Chung MG, Kim DH, Lee HM, Kim T, Choi JH, Seo DK, Yoo JB, Hong SH, Kang TJ, Kim YH (2012) Highly sensitive NO_2 gas sensor based on ozone treated graphene. Sensors Actuators B Chem 166–167:172–176. https://doi.org/10.1016/j.snb.2012.02.036

Das S, Chakraborty S, Parkash O, Kumar D, Bandyopadhyay S, Samudrala SK, Sen A, Maiti HS (2008) Vanadium doped tin dioxide as a novel sulfur dioxide sensor. Talanta 75:385–389. https://doi.org/10.1016/j.talanta.2007.11.010

Das P, Mondal B, Mukherjee K (2016) Hierarchical zinc oxide nano-tips and micro-rods: hydrothermal synthesis and improved chemi-resistive response towards ethanol. RSC Adv 6:1408–1414. https://doi.org/10.1039/C5RA23203A

Das P, Mondal B, Mukherjee K (2017a) Simultaneous adsorption−desorption processes in the conductance transient of anatase titania for sensing ethanol: a distinctive feature with kinetic perception. J Phys Chem C 121:1146–1152. https://doi.org/10.1021/acs.jpcc.6b10041

Das P, Mondal B, Mukherjee K (2017b) Chemi-resistive response of rutile titania nano-particles towards isopropanol and formaldehyde: a correlation with the volatility and chemical reactivity of vapors. Mater Res Express 4:015503–015512. https://doi.org/10.1088/2053-1591/4/1/015503

daSilva LF, Catto AC, Avansi W, Cavalcante JLS, Andrés J, Aguir K, Mastelaro VR, Longo E (2014) A novel ozone gas sensor based on one-dimensional (1D) α-Ag_2WO_4 nanostructures. Nanoscale 6:4058–4062. https://doi.org/10.1039/C3NR05837A

dePaiva LB, Morales AR, Diaz FRV (2008) Organoclays: properties, preparation and applications. Appl Clay Sci 42:8–24. https://doi.org/10.1016/j.clay.2008.02.006

Deshpande NG, Gudage YG, Sharma R, Vyas JC, Kim JB, Lee YP (2009) Studies on tin oxide-intercalated polyaniline nanocomposite for ammonia gas sensing applications. Sensors Actuators B Chem 138:76–84. https://doi.org/10.1016/j.snb.2009.02.012

Dhawale DS, Salunkhe RR, Patil UM, Gurav KV, More AM, Lokhande CD (2008) Room temperature liquefied petroleum gas (LPG) sensor based on p-polyaniline/n-TiO2 heterojunction. Sensors Actuators B Chem 134:988–992. https://doi.org/10.1016/j.snb.2008.07.003

Dhawale DS, Dubal DP, More AM, Gujar TP, Lokhande CD (2010a) Room temperature liquefied petroleum gas (LPG) sensor. Sensors Actuators B Chem 147:488–494. https://doi.org/10.1016/j.snb.2010.02.063

Dhawale DS, Dubal DP, Jamadade VS, Salunkhe RR, Joshi SS, Lokhande CD (2010b) Room temperature LPG sensor based on n-CdS/p-polyaniline heterojunction. Sensors Actuators B Chem 145:205–210. https://doi.org/10.1016/j.snb.2009.11.063

Eerden LJM, de Visser PHB, van Dijk CJ (1998) Risk of damage to crops in the direct neighbourhood of ammonia sources. Environ Pollut 102:49–53. https://doi.org/10.1016/S0269-7491(98)80014-6

Epifani M, Comini E, Arbiol J, Díaz R, Sergent N, Pagnier T, Siciliano P, Faglia G, Morante JR (2008) Chemical synthesis of In_2O_3 nanocrystals and their application in highly performing ozone-sensing devices. Sensors Actuators B Chem 130:483–487. https://doi.org/10.1016/j.snb.2007.09.025

Farahani H, Wagiran R, Hamidon MN (2014) Humidity sensors principle, mechanism, and fabrication technologies: a comprehensive review. Sensors 14:7881–7939. https://doi.org/10.3390/s140507881

Fomekong RL, Kamta HMT, Lambi JN, Lahem D, Eloy P, Debliquy M, Delcorte A (2018) A sub-ppm level formaldehyde gas sensor based on Zn-doped NiO prepared by a co-precipitation route. J Alloy Comp 731:1188–1196. https://doi.org/10.1016/j.jallcom.2017.10.089

Gao H, Zhao L, Wang L, Sun P, Lu H, Liu F, Chuai X, Lu G (2018) Ultrasensitive and low detection limit of toluene gas sensor based on SnO_2-decorated NiO nanostructure. Sensors Actuators B Chem 255:3505–3515. https://doi.org/10.1016/j.snb.2017.09.184

Gargiulo V, Alfano B, Capua RD, Alfé M, Vorokhta M, Polichetti T, Massera E, Miglietta ML, Schiattarella C, Francia GD (2018) Graphene-like layers as promising chemiresistive sensing material for detection of alcohols at low concentration. J Appl Phys 123:024503–024510. https://doi.org/10.1063/1.5000914

Gaspera ED, Guglielmi M, Agnoli S, Granozzi G, Post ML, Bello V, Mattei G, Martucci A (2010) Au nanoparticles in nanocrystalline TiO_2−NiO films for SPR-based, selective H_2S gas sensing. Chem Mater 22:3407–3417. https://doi.org/10.1021/cm100297q

Giang HT, Duy HT, Ngan PQ, Thai GH, Thu DTA, Thu DT, Toan NN (2011) Hydrocarbon gas sensing of nano-crystalline perovskite oxides $LnFeO_3$ (Ln = La, Nd and Sm). Sensors Actuators B Chem 158:246–251. https://doi.org/10.1016/j.snb.2011.06.013

Gong J, Li Y, Hu Z, Zhou Z, Deng Y (2010) Ultrasensitive NH_3 gas sensor from polyaniline nanograin enchased TiO_2 fibers. J Phys Chem C 114:9970–9974. https://doi.org/10.1021/jp100685r

Gong M, Li Y, Guo Y, Lv X, Dou X (2018) 2D TiO_2 nanosheets for ultrasensitive humidity sensing application benefited by abundant surface oxygen vacancy defects. Sensors Actuators B Chem 262:350–358. https://doi.org/10.1016/j.snb.2018.01.187

Habibzadeh S, Khodadadi AA, Mortazavi Y (2010) CO and ethanol dual selective sensor of Sm_2O_3-doped SnO_2 nanoparticles synthesized by microwave-induced combustion. Sensors Actuators B Chem 144:131–138. https://doi.org/10.1016/j.snb.2009.10.047

Han D, Zhai L, Gu F, Wang Z (2018) Highly sensitive NO2 gas sensor of ppb-level detection based on In2O3 nanobricks at low temperature. Sensors Actuators B Chem 262:655–663. https://doi.org/10.1016/j.snb.2018.02.052

Haq M, Wen Z, Zhang Z, Khan S, Lou Z, Ye Z, Zhu L (2018) A two-step synthesis of nanosheet-covered fibers based on α-Fe_2O_3/NiO composites towards enhanced acetone sensing. Sci Rep 8:1705–17017. https://doi.org/10.1038/s41598-018-20103-y

Hatchett DW, Josowicz M (2008) Composites of intrinsically conducting polymers as sensing nanomaterials. Chem Rev 108:746–769. https://doi.org/10.1021/cr068112h

He P, Brent JR, Ding H, Yang J, Lewis DJ, O'Brien P, Derby B (2018) Fully printed high performance humidity sensors based on two-dimensional materials. Nanoscale 10:5599–5606. https://doi.org/10.1039/C7NR08115D

Hernandez SC, Chaudhuri D, Chen W, Myung NV, Mulchandani A (2007) Single polypyrrole nanowire ammonia gas sensor. Electroanalysis 19:2125–2130. https://doi.org/10.1002/elan.200703933

Hoa ND, Quy NV, Cho YS, Kim D (2007) Nanocomposite of SWNTs and SnO_2 fabricated by soldering process for ammonia gas sensor application. Phys Status Solidi A 204:1820–1824. https://doi.org/10.1002/pssa.200675318

Huang J, Virji S, Weiller BH, Kaner RB (2003) Polyaniline nanofibers: facile synthesis and chemical sensors. J Am Chem Soc 125:314–315. https://doi.org/10.1021/ja028371y

Iravani S (2011) Green synthesis of metal nanoparticles using plants. Green Chem 13:2638–2650. https://doi.org/10.1039/C1GC15386B

Jitianu A, Altindag Y, Zaharescu M, Wark M (2003) New SnO_2 nano-clusters obtained by sol-gel route, structural characterization and their gas sensing applications. J Sol-Gel Sci Technol 26:483–488. https://doi.org/10.1023/A:1020739111

Kanazawa E, Sakai G, Shimanoe K, Kanmura Y, Teraoka Y, Miura N, Yamazoe N (2001) Metal oxide semiconductor N_2O sensor for medical use. Sensors Actuators B Chem 77:72–77. https://doi.org/10.1016/S0925-4005(01)00675-X

Kar P, Choudhury A (2013) Carboxylic acid functionalized multi-walled carbon nanotube doped polyaniline for chloroform sensors. Sensors Actuators B Chem 183:25–33. https://doi.org/10.1016/j.snb.2013.03.093

Kar P, Pradhan NC, Adhikari B (2009) Application of sulfuric acid doped poly (m-aminophenol) as aliphatic alcohol vapor sensor material. Sensors Actuators B Chem 140:525–531. https://doi.org/10.1016/j.snb.2009.05.013

Kar P, Pradhan NC, Adhikari B (2011) Ammonia sensing by hydrochloric acid doped poly (m-aminophenol)–silver nanocomposite. J Mater Sci 46:2905–2913. https://doi.org/10.1007/s10853-010-5165-1

Kar P, Choudhury A, Verma SK (2015) Conjugated polymer nanocomposites-based chemical sensors. In: Saini P (ed) Fundamentals of conjugated polymer blends, copolymers and composites. Wiley-Scrivener, Beverly, pp 621–686. https://doi.org/10.1002/9781119137160.ch12

Karmakar M, Mondal B, Pal M, Mukherjee K (2014) Acetone and ethanol sensing of barium hexaferrite particles: a case study considering the possibilities of non-conventional hexaferrite sensor. Sensors Actuators B Chem 190:627–633. https://doi.org/10.1016/j.snb.2013.09.035

Kauffman DR, Star A (2007) Chemically induced potential barriers at the carbon nanotube−metal nanoparticle interface. Nano Lett 7:1863–1868. https://doi.org/10.1021/nl070330i

Kauffman DR, Star A (2008) Carbon nanotube gas and vapor sensors. Angew Chem Int Ed 47:6550–6570. https://doi.org/10.1002/anie.200704488

Kaur A, Singh I, Kumar J, Bhatnagar C, Dixit SK, Bhatnagar PK, Mathur PC, Covas JA, Paiva MC (2015) Enhancement in the performance of multi-walled carbon nanotube: poly (methylmethacrylate)composite thin film ethanol sensors through appropriate nanotube functionalization. Mater Sci Semicond Process 31:166–174. https://doi.org/10.1016/j.mssp.2014.11.030

Kenanakis G, Vernardou D, Koudoumas E, Kiriakidis G, Katsarakis N (2007) Ozone sensing properties of ZnO nanostructures grown by the aqueous chemical growth technique. Sensors Actuators B Chem 124:187–191. https://doi.org/10.1016/j.snb.2006.12.033

Kim D, Pikhitsa PV, Yang H, Choi M (2011) Room temperature CO and H_2 sensing with carbon nanoparticles. Nanotechnology 22:485501–485507. https://doi.org/10.1088/0957-4484/22/48/485501

Kim YH, Kim SJ, Kim YJ, Shim YS, Kim SY, Hong BH, Jang HW (2015) Self-activated transparent all-graphene gas sensor with endurance to humidity and mechanical bending. ACS Nano 9:10453–10460. https://doi.org/10.1021/acsnano.5b04680

Kitture R, Pawar D, Rao CN, Choubey RK, Kale SN (2017) Nanocomposite modified optical fiber: a room temperature, selective H2S gas sensor: studies using ZnO-PMMA. J Alloy Comp 695:2091–2096. https://doi.org/10.1016/j.jallcom.2016.11.048

Kolmakov A, Zhang Y, Cheng G, Moskovites M (2003) Detection of CO and O_2 using tin oxide nanowire sensors. Adv Mater 15:997–1000. https://doi.org/10.1002/adma.200304889

Kou X, Xie N, Chen F, Wang T, Guo L, Wang C, Wang Q, Ma J, Sun Y, Zhang H, Lu G (2018) Superior acetone gas sensor based on electrospun SnO_2nanofibers by Rh doping. Sensors Actuators B Chem 256:861–869. https://doi.org/10.1016/j.snb.2017.10.011

Kuang Q, Lao C, Wang ZL, Xie Z, Zheng L (2007) High-sensitivity humidity sensor based on a single SnO_2 nanowire. J Am Chem Soc 129:6070–6071. https://doi.org/10.1021/ja070788m

Kumar B, Feller JF, Castro M, Lu J (2010) Conductive bio-polymer nano-composites (CPC): chitosan-carbon nanotube transducers assembled via spray layer-by-layer for volatile organic compound sensing. Talanta 81:908–915. https://doi.org/10.1016/j.talanta.2010.01.036

Labidi A, Gillet E, Delamare R, Maaref M, Aguir K (2006) Ethanol and ozone sensing characteristics of WO_3 based sensors activated by au and Pd. Sensors Actuators B Chem 120:338–345. https://doi.org/10.1016/j.snb.2006.02.015

Le X, Wang X, Pang J, Liu Y, Fang B, Xu Z, Gao C, Xu Y, Xie J (2018) A high performance humidity sensor based on surface acoustic wave and graphene oxide on AlN/Si layered structure. Sensors Actuators B Chem 255:2454–2461. https://doi.org/10.1016/j.snb.2017.09.038

Lee J, Kim DH, Hong SH, Jho JY (2011a) A hydrogen gas sensor employing vertically aligned TiO_2nanotube arrays prepared by template-assisted method. Sensors Actuators B Chem 160:1494–1498. https://doi.org/10.1016/j.snb.2011.08.001

Lee SC, Hwang BW, Lee SJ, Choi HY, Kim SY, Jung SY, Ragupathy D, Lee DD, Kim JC (2011b) A novel tin oxide-based recoverable thick film SO_2 gas sensor promoted with magnesium and vanadium oxides. Sensors Actuators B Chem 160:1328–1334. https://doi.org/10.1016/j.snb.2011.09.070

Lee DH, Kang SK, Pak Y, Lim N, Lee R, Kumaresan Y, Lee S, Lee C, Ham MH, Jung GY (2018) Transfer of preheat-treated SnO_2 via a sacrificial bridge-type ZnO layer for ethanol gas sensor. Sensors Actuators B Chem 255:70–77. https://doi.org/10.1016/j.snb.2017.08.025

Li J, Lu Y, Ye Q, Cinke M, Han J, Meyyappan M (2003) Carbon nanotube sensors for gas and organic vapor detection. Nano Lett 3:929–933. https://doi.org/10.1021/nl034220x

Li B, Sauve G, Iovu MC, Jeffries-EL M, Zhang R, Cooper J, Santhanam S, Schultz L, Revelli JC, Kusne AG, Kowalewski T, Snyder JL, Weiss LE, Fedder GK, McCullough RD, Lambeth DN (2006a) Volatile organic compound detection using nanostructured copolymers. Nano Lett 6:1598–1602. https://doi.org/10.1021/nl060498o

Li J, Lu Y, Meyyappan M (2006b) Nano chemical sensors with polymer-coated carbon nanotubes. IEEE Sensors J 6:1047–1051. https://doi.org/10.1109/JSEN.2006.881018

Li Y, Wang HC, Yang MJ (2007) -type gas sensing characteristics of chemically modified multi-walled carbon nanotubes and PMMA composite. Sensors Actuators B Chem 121:496–500. https://doi.org/10.1016/j.snb.2006.04.074

Li W, Hoa ND, Cho Y, Kim D, Kim JS (2009) Nanofibers of conducting polyaniline for aromatic organic compound sensor. Sensors Actuators B Chem 143:132–138. https://doi.org/10.1016/j.snb.2009.09.006

Li W, Liang J, Liu J, Zhou L, Yang R, Hu M (2016) Synthesis and room temperature CH_4 gas sensing properties of vanadium dioxide nanorods. Mater Lett 173:199–202. https://doi.org/10.1016/j.matlet.2016.03.035

Li SM, Zhang LX, Zhu MY, Ji GJ, Zhao LX, Yin J, Bie LJ (2017) Acetone sensing of ZnO nanosheets synthesized using room-temperature precipitation. Sensors Actuators B Chem 249:611–623. https://doi.org/10.1016/j.snb.2017.04.007

Li S, Lin P, Zhao L, Wang C, Liu D, Liu F, Sun P, Liang X, Liu F, Yan X, Gao Y, Lu G (2018a) The room temperature gas sensor based on Polyaniline@flower-likeWO_3 nanocomposites and flexible PET substrate for NH_3 detection. Sensors Actuators B Chem 259:505–513. https://doi.org/10.1016/j.snb.2017.11.081

Li Y, Zhao H, Jiao M, Yang M (2018b) Sulphonated polystyrene-b-poly(4-vinylpyridine) with nanostructures induced by phase separation as promising humidity sensitive material. Sensors Actuators B Chem 257:1118–1127. https://doi.org/10.1016/j.snb.2017.11.034

Liang YX, Chen YJ, Wang TH (2004) Low-resistance gas sensors fabricated from multiwalled carbon nanotubes coated with a thin tin oxide layer. Appl Phys Lett 85:666–668. https://doi.org/10.1063/1.1775879

Lin G, Wang H, Li X, Lai X, Zou Y, Zhou X, Liu D, Wan J, Xin H (2018) Chestnut-like $CoFe_2O_4$@SiO_2@In_2O_3 nanocomposite microspheres with enhanced acetone sensing property. Sensors Actuators B Chem 255:3364–3373. https://doi.org/10.1016/j.snb.2017.09.163

Liu H, Kameoka J, Czaplewski DA, Craighead HG (2004) Polymeric nanowire chemical sensor. Nano Lett 4:671–675. https://doi.org/10.1021/nl049826f

Liu YL, Yang HF, Yang Y, Liu ZM, Shen GL, Yu RQ (2006) Gas sensing properties of tin dioxide coated onto multi-walled carbon nanotubes. Thin Solid Films 497:355–360. https://doi.org/10.1016/j.tsf.2005.11.018

Liu J, Luo T, Meng F, Qian K, Wan Y, Liu J (2010) Porous hierarchical In_2O_3 micro−/nanostructures: preparation, formation mechanism, and their application in gas sensors for noxious volatile organic compound detection. J Phys Chem C 114:4887–4894. https://doi.org/10.1021/jp911768m

Llobet E (2013) Gas sensors using carbon nanomaterials: a review. Sensors Actuators B Chem 179:32–45. https://doi.org/10.1016/j.snb.2012.11.014

Lu Y, Li J, Han J, Ng HT, Binder C, Partridge C, Meyyappan M (2004) Room temperature methane detection using palladium loaded single-walled carbon nanotube sensors. Chem Phys Lett 391:344–348. https://doi.org/10.1016/j.cplett.2004.05.029

Lu G, Ocola LE, Chen J (2009) Reduced graphene oxide for room-temperature gas sensors. Nanotechnology 20:445502–445510. https://doi.org/10.1088/0957-4484/20/44/445502

Lu G, Xu J, Sun J, Yu Y, Zhang Y, Liu F (2012) UV-enhanced room temperature NO_2 sensor using ZnO nanorods modified with SnO_2 nanoparticles. Sensors Actuators B Chem 162:82–88. https://doi.org/10.1016/j.snb.2011.12.039

Ma L, Ma SY, Shen XF, Wang TT, Jiang XH, Chen Q, Qiang Z, Yang HM, Chen H (2018) $PrFeO_3$ hollow nanofibers as a highly efficient gas sensor for acetone detection. Sensors Actuators B Chem 255:2546–2554. https://doi.org/10.1016/j.snb.2017.09.060

Manjula P, Arunkumar S, Manorama SV (2011) Au/SnO_2 an excellent material for room temperature carbon monoxide sensing. Sensors Actuators B Chem 152:168–175. https://doi.org/10.1016/j.snb.2010.11.059

Md Sin ND, Samsudin N, Ahmad S, Mamat MH, Rusop M (2013) Zn-doped SnO_2 with 3D cubic structure for humidity sensor. Procedia Eng 56:801–806. https://doi.org/10.1016/j.proeng.2013.03.199

Ménini P, Parret F, Guerrero M, Soulantica K, Erades L, Maisonnat A, Chaudret B (2004) CO response of a nanostructured SnO_2 gas sensor doped with palladium and platinum. Sensors Actuators B Chem 103:111–114. https://doi.org/10.1016/j.snb.2004.04.103

Mukherjee K, Majumder SB (2009) Analyses of response and recovery kinetics of zinc ferrite as hydrogen gas sensor. J Appl Phys 106:064912–064920. https://doi.org/10.1063/1.3225996

Mukherjee K, Majumder SB (2010) Reducing gas sensing behavior of nano-crystalline magnesium–zinc ferrite powders. Talanta 81:1826–1832. https://doi.org/10.1016/j.talanta.2010.03.042

Mukherjee K, Bharti DC, Majumder SB (2010) Solution synthesis and kinetic analyses of the gas sensing characteristics of magnesium ferrite particles. Sensors Actuators B Chem 146:91–97. https://doi.org/10.1016/j.snb.2010.02.020

Na CW, Woo HS, Lee JH (2012) Design of highly sensitive volatile organic compound sensors by controlling NiO loading on ZnO nanowire networks. RSC Adv 2:414–417. https://doi.org/10.1039/C1RA01001H

Neri G, Leonardi SG, Latino M, Donato N, Baek S, Conte DE, Russo PA, Pinna N (2013) Sensing behavior of SnO_2/reduced graphene oxide nanocomposites toward NO_2. Sensors Actuators B Chem 179:61–68. https://doi.org/10.1016/j.snb.2012.10.031

Nohria R, Khillan RK, Su Y, Dikshit R, Lvov Y, Varahramyan K (2006) Humidity sensor based on ultrathin polyaniline film deposited using layer-by-layer nano-assembly. Sensors Actuators B Chem 114:218–222. https://doi.org/10.1016/j.snb.2005.04.034

Oh E, Choi HY, Jung SH, Cho S, Kim JC, Lee KH, Kang SW, Kim J, Yun JY, Jeong SH (2009) High-performance NO_2 gas sensor based on ZnO nanorod grown by ultrasonic irradiation. Sensors Actuators B Chem 141:239–243. https://doi.org/10.1016/j.snb.2009.06.031

Okano K, Totsuka T (1986) Absorption of nitrogen dioxide by sunflower plants grown at various levels of nitrate. New Phytol 102:551–562. https://doi.org/10.1111/j.1469-8137.1986.tb00831.x

Park Y, Dong KY, Lee J, Choi J, Bae GN, Ju BK (2009) Development of an ozone gas sensor using single-walled carbon nanotubes. Sensors Actuators B Chem 140:407–411. https://doi.org/10.1016/j.snb.2009.04.055

Parthibavarman M, Hariharan V, Sekar C (2011) High-sensitivity humidity sensorbased on SnO2nanoparticles synthesized by microwave irradiation method. Mater Sci Eng C 31:840–844. https://doi.org/10.1016/j.msec.2011.01.002

Pascariu P, Airinei A, Olaru N, Petrila I, Nica V, Sacarescu L, Tudorache F (2016) Microstructure, electrical and humidity sensor properties of electrospun NiO–SnO_2 nanofibers. Sensors Actuators B Chem 222:1024–1031. https://doi.org/10.1016/j.snb.2015.09.051

Pearce TC, Schiffman SS, Nagle HT, Gardner JW (2003) Handbook of machine olfaction. Wiley-VCH, Weinheim

Penza M, Cassano G, Aversa P, Antolini F, Cusano A, Cutolo A, Giordano M, Nicolais L (2004a) Alcohol detection using carbon nanotubes acoustic and optical sensors. Appl Phys Lett 85:2379–2381. https://doi.org/10.1063/1.1784872

Penza M, Antolini F, Antisari MV (2004b) Carbon nanotubes as SAW chemical sensors materials. Sensors Actuators B Chem 100:47–59. https://doi.org/10.1016/j.snb.2003.12.019

Penza M, Tagliente MA, Aversa P, Cassano G (2005a) Organic-vapor detection using carbon-nanotubes nanocomposite microacoustic sensors. Chem Phys Lett 409:349–354. https://doi.org/10.1016/j.cplett.2005.05.005

Penza M, Cassano G, Aversa P, Cusano A, Cutolo A, Giordano M, Nicolais L (2005b) Carbon nanotube acoustic and optical sensors for volatile organic compound detection. Nanotechnology 16:2536–2547. https://doi.org/10.1088/0957-4484/16/11/013

Penza M, Cassano G, Aversa P, Antolini F, Cusano A, Consales M, Giordano M, Nicolais L (2005c) Syndiotactic polystyrene thin film as sensitive layer for an optoelectronic chemical sensing device. Sensors Actuators B Chem 111–112:171–180. https://doi.org/10.1016/j.snb.2004.02.053

Penza M, Tagliente MA, Aversa P, Re M, Cassano G (2007) The effect of purification of single-walled carbon nanotube bundles on the alcohol sensitivity of nanocomposite Langmuir–Blodgett films for SAW sensing applications. Nanotechnology 18:185502–185513. https://doi.org/10.1088/0957-4484/18/18/185502

Penza M, Rossi R, Alvisi M, Serra E (2010) Metal-modified and vertically aligned carbon nanotube sensors array for landfill gas monitoring applications. Nanotechnology 21:105501–105513. https://doi.org/10.1088/0957-4484/21/10/105501

Peter J, Harris F (1999) Carbon nanotube and related structures, new materials for the twenty first century. University of Cambridge, Cambridge

Pisarenko AN, Spendel WU, Taylor RT, Brown JD, Cox JA, Pacey GE (2009) Detection of ozone gas using gold nanoislands and surface plasmon resonance. Talanta 80:777–780. https://doi.org/10.1016/j.talanta.2009.07.062

Qi P, Vermesh O, Grecu M, Javey A, Wang Q, Dai H, Peng S, Chao KJ (2003) Toward large arrays of multiplex functionalized carbon nanotube sensors for highly sensitive and selective molecular detection. Nano Lett 3:347–351. https://doi.org/10.1021/nl034010k

Quang NH, Trinh MV, Lee BH, Huh JS (2006) Effect of NH_3 gas on the electrical properties of single-walled carbon nanotube bundles. Sensors Actuators B Chem 113:341–346. https://doi.org/10.1016/j.snb.2005.03.089

Ram MK, Yavuz O, Lahsangah V, Aldissi M (2005) CO gas sensing from ultrathin nano-composite conducting polymer film. Sensors Actuators B Chem 106:750–757. https://doi.org/10.1016/j.snb.2004.09.027

Rao PJ, Geckeler KE (2011) Polymer nanoparticles: preparation techniques and size control parameters. Prog Polym Sci 36:887–913. https://doi.org/10.1016/j.progpolymsci.2011.01.001

Rout CS, Ganesh K, Govindaraj A, Rao CNR (2006a) Sensors for the nitrogen oxides, NO_2, NO and N_2O, based on In_2O_3 and WO_3 nanowires. Appl Phys A Mater Sci Process 85:241–246. https://doi.org/10.1007/s00339-006-3707-9

Rout CS, Govindaraj A, Rao CNR (2006b) High-sensitivity hydrocarbon sensors based on tungsten oxide nanowires. J Mater Chem 16:3936–3941. https://doi.org/10.1039/B607012B

Rout CS, Kulkarni GU, Rao CNR (2007) Room temperature hydrogen and hydrocarbon sensors based on single nanowires of metal oxides. J Phys D Appl Phys 40:2777–2782. https://doi.org/10.1088/0022-3727/40/9/016

Sadek AZ, Wlodarski W, Shin K, Kaner RB, Kalantar-zadeh K (2006) A layered surface acoustic wave gas sensor based on a polyaniline/In_2O_3 nanofibre composite. Nanotechnology 17:4488–4492. https://doi.org/10.1088/0957-4484/17/17/034

Sadek AZ, Wlodarski W, Kalantar-zadeh K, Baker C, Kaner RB (2007) Doped and dedoped polyaniline nanofiber based conductometric hydrogen gas sensors. Sensors Actuators A 139:53–57. https://doi.org/10.1016/j.sna.2006.11.033

Sahay PP, Tewari S (2005) Sprayed ZnO thin films for ethanol sensors. J Mater Sci 40:4791–4793. https://doi.org/10.1007/s10853-005-0519-9

Sahm T, Mädler L, Gurlo A, Barsan N, Pratsinis SE, Weimar U (2004) Flame spray synthesis of tin dioxide nanoparticles for gas sensing. Sensors Actuators B Chem 98:148–153. https://doi.org/10.1016/j.snb.2003.10.003

Santhanam KSV, Sangoi R, Fuller L (2005) A chemical sensor for chloromethanes using a nanocomposite of multiwalled carbon nanotubes with poly(3-methylthiophene). Sensors Actuators B Chem 106:766–771. https://doi.org/10.1016/j.snb.2004.09.034

Santhosh P, Manesha KM, Gopalan A, Lee KP (2007) Novel amperometric carbon monoxide sensor based on multi-wall carbon nanotubes grafted with polydiphenylamine—fabrication and performance. Sensors Actuators B Chem 125:92–99. https://doi.org/10.1016/j.snb.2007.01.044

Santucci S, Picozzi S, Gregorio FD, Lozzi L, Cantalini C, Valentini L, Kenny JM, Delley B (2003) NO_2 and CO gas adsorption on carbon nanotubes: experiment and theory. J Chem Phys 119:10904–10910. https://doi.org/10.1063/1.1619948

Shaikh FI, Chikhale LP, Mulla IS, Suryavanshi SS (2017) Synthesis, characterization and enhanced acetone sensing performance of Pd loaded Sm doped SnO_2 nanoparticles. Ceram Int 43:10307–10315. https://doi.org/10.1016/j.ceramint.2017.05.060

Sharma S, Nirkhe C, Pethkar S, Athawale AA (2002) Chloroform vapour sensor based on copper/polyaniline nanocomposite. Sensors Actuators B Chem 85:131–136. https://doi.org/10.1016/S0925-4005(02)00064-3

Shen JY, Zhang L, Ren J, Wang JC, Yao HC, Li ZJ (2017) Highly enhanced acetone sensing performance of porous C-doped WO_3 hollow spheres by carbon spheres as templates. Sensors Actuators B Chem 239:597–607. https://doi.org/10.1016/j.snb.2016.08.069

Shojaee M, Nasresfahani S, Sheikhi MH (2018) Hydrothermally synthesized Pd-loaded SnO_2/partially reducedgraphene oxide nanocomposite for effective detection of carbonmonoxide at room temperature. Sensors Actuators B Chem 254:457–467. https://doi.org/10.1016/j.snb.2017.07.083

Sin MLY, Chow GCT, Wong GMK, Li WJ, Leong PHW, Wong KW (2007) Ultralow-power alcohol vapor sensors using chemically functionalized multiwalled carbon nanotubes. IEEE Trans Nanotechnol 6:571–577. https://doi.org/10.1109/TNANO.2007.900511

Singh N, Yan C, Lee PS (2010) Room temperature CO gas sensing using Zn-doped In_2O_3 single nanowire field effect transistors. Sensors Actuators B 150:19–24. https://doi.org/10.1016/j.snb.2010.07.051

Srivastava S, Kumar S, Singh VN, Singh M, Vijay YK (2011) Synthesis and characterization of TiO2 doped polyaniline composites for hydrogen gas sensing. Int J Hydrog Eng 36:6343–6355. https://doi.org/10.1016/j.ijhydene.2011.01.141

Star A, Joshi V, Skarupo S, Thomas D, Gabriel JCP (2006) Gas sensor array based on metal-decorated carbon nanotubes. J Phys Chem B 110:21014–21020

Starke TKH, Coles GSV (2002) High sensitivity ozone sensors for environmental monitoring produced using laser ablated nanocrystalline metal oxides. IEEE Sensors J 2:14–19. https://doi.org/10.1109/7361.987056

Starke TKH, Coles GSV, Ferkel H (2002) High sensitivity NO_2 sensors for environmental monitoring produced using laser ablated nanocrystalline metal oxides. Sensors Actuators B Chem 85:239–245. https://doi.org/10.1016/S0925-4005(02)00114-4

Su PG, Tsai WY (2004) Humidity sensing and electrical properties of a composite material of nano-sized SiO2 and poly(2-acrylamido-2-methylpropane sulfonate). Sensors Actuators B Chem 100:417–422. https://doi.org/10.1016/j.snb.2004.02.011

Sun L, Wang B, Wang Y (2018) A novel silicon carbide nanosheet for high-performance humidity sensor. Adv Mater Interfaces 5:1701300–1701325. https://doi.org/10.1002/admi.201701300

Sutar DS, Padma N, Aswal DK, Deshpande SK, Gupta SK, Yakhmi JV (2007) Preparation of nanofibrous polyaniline films and their application as ammonia gas sensor. Sensors Actuators B Chem 128:286–292. https://doi.org/10.1016/j.snb.2007.06.015

Tai H, Jiang Y, Xie G, Yu J, Chen X (2007) Fabrication and gas sensitivity of polyaniline–titanium dioxide nanocomposite thin film. Sensors Actuators B Chem 125:644–650. https://doi.org/10.1016/j.snb.2007.03.013

Tai H, Jiang Y, Xie G, Yu J, Chen X, Ying Z (2008) Influence of polymerization temperature on NH3 response of PANI/TiO_2 thin film gas sensor. Sensors Actuators B Chem 129:319–326. https://doi.org/10.1016/j.snb.2007.08.013

Tang H, Li Y, Zheng C, Ye J, Hou X, Lv Y (2007) An ethanol sensor based on cataluminescence on ZnO nanoparticles. Talanta 72:1593–1597. https://doi.org/10.1016/j.talanta.2007.01.035

Tao J, Wang YY, Xiao YJ, Yao P, Chen C, Zhang DH, Pang W, Yang HT, Sun D, Wang ZF, Liu J (2017) One-step exfoliation and functionalization of graphene by hydrophobin for high performance water molecular sensing. Carbon 116:695–702. https://doi.org/10.1016/j.carbon.2017.02.052

Thostenson E, Li C, Chou T (2005) Nanocomposites in context. Compos Sci Technol 65:491–516. https://doi.org/10.1016/j.compscitech.2004.11.003

Timmer B, Olthius W, van den Berg A (2005) Ammonia sensors and their applications – a review. Sensors Actuators B Chem 107:666–677. https://doi.org/10.1016/j.snb.2004.11.054

Toloman D, Popa A, Stan M, Socaci C, Biris AR, Katona G, Tudorache F, Petrila I, Iacomi F (2017) Appl Surf Sci 402:410–417. https://doi.org/10.1016/j.apsusc.2017.01.064

Tomer VK, Duhan S (2015) Nano titania loaded mesoporous silica: preparation and application as high performance humidity sensor. Sensors Actuators B Chem 220:192–200. https://doi.org/10.1016/j.snb.2015.05.072

Verma SK, Kar P, Yang DJ, Choudhury A (2015) Poly(m-aminophenol)/functionalized multi-walled carbon nanotubenanocomposite based alcohol sensors. Sensors Actuators B Chem 219:199–208. https://doi.org/10.1016/j.snb.2015.04.117

Verma SK, Choudhury A, Kar P (2017a) Synthesis, characteristics and aliphatic alcohol sensing behavior of poly(m–aminophenol)/sulfonic acid-functionalized multi-walled carbon nanotube composite. ChemistrySelect 2:3917–3924. https://doi.org/10.1002/slct.201700470

Verma SK, Choudhury A, Kar P (2017b) Selective sensing of ethanol by poly(m-aminophenol)/amine groups functionalized multi-walled carbon nanotube composite. Sens Lett 15:448–456. https://doi.org/10.1166/sl.2017.3826

Virji S, Huang J, Kaner RB, Weiller BH (2004) Polyaniline nanofiber gas sensors: examination of response mechanisms. Nano Lett 4:491–496. https://doi.org/10.1021/nl035122e

Wang CT, Chen MT (2010) Vanadium-promoted tin oxide semiconductor carbon monoxide gas sensors. Sensors Actuators B 150:360–366. https://doi.org/10.1016/j.snb.2010.06.060

Wang J, Lin Q, Zhou R, Xu B (2002) Humidity sensors based on composite material of nano-$BaTiO_3$ and polymer RMX. Sensors Actuators B Chem 81:248–253. https://doi.org/10.1016/S0925-4005(01)00959-5

Wang CY, Cimalla V, Kups T, Röhlig CC, Stauden T, Ambacher O, Kunzer M, Passow T, Schirmacher W, Pletschen W, Köhler K, Wagner J (2007) Integration of In_2O_3 nanoparticle based ozone sensors with GaInN/GaN light emitting diodes. Appl Phys Lett 91:103509–103511. https://doi.org/10.1063/1.2779971

Wang Y, Jia W, Strout T, Schempf A, Zhang H, Li B, Cui J, Lei Y (2009) Ammonia gas sensor using polypyrrole-coated TiO_2/ZnO nanofibers. Electroanalysis 21:1432–1438. https://doi.org/10.1002/elan.200904584

Wang X, Ding B, Yu J, Wang M, Pan F (2010) A highly sensitive humidity sensor based on a nanofibrous membrane coated quartz crystal microbalance. Nanotechnology 21:055502–055507. https://doi.org/10.1088/0957-4484/21/5/055502

Wang J, Yang J, Han N, Zhou X, Gong S, Yang J, Hu P, Chen Y (2017) Highly sensitive and selective ethanol and acetone gas sensors based on modified ZnO nanomaterials. Mater Des 121:69–76. https://doi.org/10.1016/j.matdes.2017.02.048

Wang Q, Kou X, Liu C, Zhao L, Lin T, Liu F, Yang X, Lin J, Lu G (2018a) Hydrothermal synthesis of hierarchical CoO/SnO2 nanostructures for ethanol gas sensor. J Colloid Interface Sci 513:760–766. https://doi.org/10.1016/j.jcis.2017.11.073

Wang X, Li Y, Pionteck J, Zhou Z, Weng W, Luo X, Qin Z, Voit B, Zhu M (2018b) Flexible poly (styrene-butadiene-styrene)/carbon nanotube fiber based vapor sensors with high sensitivity, wide detection range, and fast response. Sensors Actuators B Chem 256:896–904. https://doi.org/10.1016/j.snb.2017.10.028

Wanna Y, Srisukhumbowornchai N, Tauntranont A, Wisitsoraat A, Thavarungkul N, Singjai P (2006) The effect of carbon nanotube dispersion on CO gas sensing characteristics of polyaniline gas sensor. J Nanosci Nanotechnol 6:3893–3896. https://doi.org/10.1166/jnn.2006.675

Wei C, Dai L, Roy A, Tolle TB (2006) Multifunctional chemical vapor sensors of aligned carbon nanotube and polymer composites. J Am Chem Soc 128:1412–1413. https://doi.org/10.1021/ja0570335

Wisitsoraat A, Tuantranont A, Thanachayanont C, Patthanasettakul V, Singjai P (2006) Electron beam evaporated carbon nanotube dispersed SnO_2 thin film gas sensor. J Electroceram 17:45–49. https://doi.org/10.1007/s10832-006-9934-9

Wu N, Zhao M, Zheng JG, Jiang C, Myers B, Li S, Chyu M, Mao SX (2005) Porous CuO–ZnO nanocomposite for sensing electrode of high-temperature CO solid-state electrochemical sensor. Nanotechnology 16:2878–2881. https://doi.org/10.1088/0957-4484/16/12/024

Wu RJ, Lin HL, Chen MH, Wu TM, Chien FSS (2008) Application of nanostructure ZnO for room working temperature ozone sensor. Sens Lett 6:800–802. https://doi.org/10.1166/sl.2008.504

Xiangfeng C, Caihong W, Dongli J, Chenmou Z (2004) Ethanol sensor based on indium oxide nanowires prepared by carbothermal reduction reaction. Chem Phys Lett 399:461–464. https://doi.org/10.1016/j.cplett.2004.10.053

Xiong Y, Xu W, Ding D, Lu W, Zhu L, Zhu Z, Wang Y, Xue Q (2018) Ultra-sensitive NH_3 sensor based on flower-shaped SnS_2 nanostructures with sub-ppm detection ability. J Hazard Mater 341:159–167. https://doi.org/10.1016/j.jhazmat.2017.07.060

Xu K, Fu C, Gao Z, Wei F, Ying Y, Xu C, Fu G (2018) Nanomaterial-based gas sensors: a review. Instrum Sci Technol 46:115–145. https://doi.org/10.1080/10739149.2017.1340896

Xue L, Wang W, Guo Y, Liu G, Wan P (2017) Flexible polyaniline/carbon nanotube nanocomposite film-based electronic gas sensors. Sensors Actuators B Chem 244:47–53. https://doi.org/10.1016/j.snb.2016.12.064

Yan XB, Han ZJ, Yang Y, Tay BK (2007) NO_2 gas sensing with polyaniline nanofibers synthesized by a facile aqueous/organic interfacial polymerization. Sensors Actuators B Chem 123:107–113. https://doi.org/10.1016/j.snb.2006.07.031

Yang W, Thordarson P, Gooding JJ, Ringer SP, Braet F (2007) Carbon nanotubes for biological and biomedical applications. Nanotechnology 18:412001–412013. https://doi.org/10.1088/0957-4484/18/41/412001

Yin H, Yu K, Peng H, Zhang Z, Huang R, Travas-Sejdic J, Zhu Z (2012) Porous V_2O_5 micro/nano-tubes: synthesis via a CVD route, single-tube-based humidity sensor and improved Li-ion storage properties. J Mater Chem 22:5013–5019. https://doi.org/10.1039/C2JM15494C

Yoon J, Chae SK, Kim JM (2007) Colorimetric sensors for volatile organic compounds (VOCs) based on conjugated polymer-embedded electrospun fibers. J Am Chem Soc 129:3038–3039. https://doi.org/10.1021/ja067856+

Zhang Y, Yu K, Jiang D, Zhu Z, Geng H, Luo L (2005) Zinc oxide nanorod and nanowire for humidity sensor. Appl Surf Sci 242:212–217. https://doi.org/10.1016/j.apsusc.2004.08.013

Zhang T, Nix MB, Yoo BY, Deshusses MA, Myung NV (2006) Electrochemically functionalized single-walled carbon nanotube gas sensor. Electroanalysis 18:1153–1158. https://doi.org/10.1002/elan.200603527

Zhang Y, He X, Li J, Miao Z, Huang F (2008) Fabrication and ethanol-sensing properties of micro gas sensor based on electrospun SnO_2 nanofibers. Sensors Actuators B Chem 132:67–73. https://doi.org/10.1016/j.snb.2008.01.006

Zhang H, Feng J, Fei T, Liu S, Zhang T (2014a) SnO_2 nanoparticles-reduced graphene oxide nanocomposites for NO_2 sensing at low operating temperature. Sensors Actuators B 190:472–478. https://doi.org/10.1016/j.snb.2013.08.067

Zhang D, Tong J, Xia B (2014b) Humidity-sensing properties of chemically reduced graphene oxide/polymer nanocomposite film sensor based on layer-by-layer nano self-assembly. Sensors Actuators B Chem 197:66–72. https://doi.org/10.1016/j.snb.2014.02.078

Zhang D, Chang H, Li P, Liu R, Xue Q (2016) Fabrication and characterizationof an ultrasensitive humidity sensor based on metal oxide/graphene hybridnanocomposite. Sensors Actuators B Chem 225:233–240. https://doi.org/10.1016/j.snb.2015.11.024

Zhang D, Wang D, Li P, Zhou X, Zong X, Dong G (2018) Facile fabrication of high-performance QCM humidity sensor based on layer-by-layer self-assembled polyaniline/graphene oxide nanocomposite film. Sensors Actuators B Chem 255:1869–1877. https://doi.org/10.1016/j.snb.2017.08.212

Zhao L, Choi M, Kim HS, Hong SH (2007) The effect of multiwalled carbon nanotube doping on the CO gas sensitivity of SnO_2-based nanomaterials. Nanotechnology 18:445501–445505. https://doi.org/10.1088/0957-4484/18/44/445501

Zhao C, Lan W, Gong H, Bai J, Ramachandran R, Liu S, Wang F (2018) Highly sensitive acetone-sensing properties of Pt-decorated $CuFe_2O_4$ nanotubes prepared by electrospinning. Ceram Int 44:2856–2863. https://doi.org/10.1016/j.ceramint.2017.11.032

Zhu Z, Chang JL, Wu RJ (2015) Fast ozone detection by using a core–shell Au@TiO_2 sensor at room temperature. Sensors Actuators B Chem 214:56–62. https://doi.org/10.1016/j.snb.2015.03.017

Zhuo M, Chen Y, Suna J, Zhang H, Guo D, Zhang H, Li Q, Wang T, Wan Q (2013) Humidity sensing properties of a single Sb doped SnO_2 nanowire field effect transistor. Sensors Actuators B Chem 186:78–83. https://doi.org/10.1016/j.snb.2013.05.043

Zribi A, Knoblock A, Rao R (2005) Enhancement of sensitivity in gas chemiresistors based on carbon nanotube surface functionalized with noble metal (Au, Pt) nanoclusters. Appl Phys Lett 86:203112–203115. https://doi.org/10.1063/1.2722207

Index

A
Abdel-Aziz, H.M.M., 182
Abramian, L., 43
Acharyya, D., 379
Actinobacteria, 195–209
Aghili, R., 170, 172
Agriculture, 97, 168, 177, 205, 317–343
Ahmad, A., 199
Ahmad, M., 20
Ahmad, S., 202
Ai, G., 241
Air pollution, 327, 329, 349–391
Ajmal, A., 38, 40, 47
Alani, F., 199
Alem, A., 69
Al-Hadeethi, Y., 380
Aliabadi, T., 172, 173
Ali, Z., 233
Álvarez, A., 195–209
Amenta, V., 341
Anjali, C.H., 321
Antibacterial activity, 203
Arami, M., 42
Aran, H.C., 75
Arshad, M., 173
Arya, A., 265–311
Asuha, S., 43
Athawale, A.A., 379
Azo dyes, 38, 50, 64, 231

B
Balsara, N.P., 311
Bekkali, C.E., 45
Bhati-Kushwaha, H., 179, 181
Bhuyan, M., 379
Bi, H.C., 386
Binas, V.D., 45
Biotic stress, 167, 175–177
Blin, J.-L., 35–77
Boehm, H., 10
Bonne, M., 35–77
Bosc, F., 69
Boudjemaa, A., 215–251

C
Calza, P., 228
Cambié, D., 73
Campagnoli, A., 183
Cao, H., 18
Chaker, H., 43
Chaniotakis, N.A., 321
Characterization techniques, 3, 7–9, 24, 270, 276–281
Chaves, M.S., 166
Chellam, P.V., 131–159
Chemical and microbial, 120, 320, 334, 337
Chen, C., 43, 233
Cheng, Y., 380
Chen, W., 380
Chen, Y., 45, 106
Chen, Z., 386
Chiarello, G.L., 249
Childress, E.S., 111
Choi, S., 380
Choudhury, A., 379–381
Commercialization, 24, 76, 119, 185, 280, 342

N. Dasgupta et al. (eds.), *Environmental Nanotechnology Volume 4*, Environmental Chemistry for a Sustainable World 32, https://doi.org/10.1007/978-3-030-26668-4

Corradini, E., 322
Costa, D., 195–209
Crop protection, 331, 332

D
Damodar, R.A., 71
Dang, H., 248
Dasgupta, N., 202
Das, P., 379
de Lima, L.B., 45
Desalination, 65, 131–159, 327, 328
Detection, 100, 166, 221, 319, 351
Dhatarwal, P., 292
Dimkpa, C.O., 172, 173
Dinckaya, E., 110
Dong, Y., 115
Do, N.S.T., 302
Doping, 3, 18, 49, 61–63, 75, 77, 111, 141, 221, 222, 228, 229, 232, 241, 243, 245, 357, 373
Du, W.C., 169, 173

E
Eifler, J., 183
Eldin, T.A., 108
Electrical properties, 20, 271, 272, 301, 304, 309, 355, 370
El-Rassy, H., 43
Emrani, A.S., 106
Environmental chemistry, 215–251
Environmental sensor, 351, 354, 369–372, 392
Erceg, M., 293

F
Flow reactor, 44, 72–76
Fomekong, R.L., 391
Font, H., 106
Food safety, 93–120, 182, 183, 334, 341
Food security, 181, 319, 332, 335
Forgacs, E., 39
Frasconi, M., 106
Fu, D., 20
Fu, J., 110
Fujishima, A., 3
Fujita, Y., 335

G
Gandhi, M.P., 131–159
Ganesan, J., 131–159
Ganji, Z., 177
Gao, E., 19
Gao, F., 331
Gargiulo, V., 379
Gaspera, E.D., 390
Gas sensor, 216, 358, 368, 369, 372, 374, 375, 377, 380, 383, 384, 391, 392
Gaudin, P., 35–77
Gawande, S.B., 21
Gehrke, I., 328
Geng, W., 22, 23
Genuino, H.C., 44
Ghasemi, S., 20, 234
Ghosh, T., 20
Gomari, S., 296
Gómez-Ruiz, S., 215–251
Gong, M., 379, 386
Green technology, 197
Grimme, S., 23
Guerrero, J., 195–209
Guo, J., 42
Gupta, V.K., 44

H
Hafeez, A., 171
Haq, M., 380
He, L., 333
He, P., 386
Honda, K., 3
Huanget, J.L., 117
Hummers, W.S., 12
Hussain, H.I., 171
Hu, X., 170
Hwang, S.H., 233

I
Iannone, M.F., 169
Im, J.H., 45
Ing, L.Y., 333
Ion transport mechanism, 288–290

J
Jaberzadeh, A., 171
Jasrotia, P., 165–187
Jiang, G.D., 233
Jiang, X.S., 105
Jonas, F., 35–77
Jones, K.C., 169
Jonsson, A., 183
Jo, Y.K., 333

K
Kahan, D.M., 335, 336
Kalabegishvili, T.L., 199
Kalpana-Sastry, R., 321
Karmakar, M., 379, 381
Kar, P., 349–392
Kasanen, J., 45
Kashyap, P.L., 165–187
Kaur, A., 379
Kezzim, A., 244
Khalid, N., 17, 20
Kheiri, A., 175, 176
Kiarii, E.M., 1–24
Kim, C., 233
Kim, C.H., 20
Kimling, M.C., 42
Kim, S., 296
Kim, Y., 284
Kinsinger, N., 76
Kisalius, D., 76
Klongkan, S., 287
Konate, A., 173, 178, 181
Kottegoda, N., 322
Kou, X., 380
Krishnan, P., 317–343
Kumar, N., 93–120
Kumar, R., 333
Kumar, S., 165–187
Ku, Y., 61
Kuzhikalail, M., 311

L
Lambropoulou, D., 228
Lamsal, K., 333
Larue, C., 169
Lázaro-Navas, S., 234
Lazcka, O., 101, 102
Lebeau, B., 35–77
Lee, E., 233
Lee, W.M., 331
Lee, Y.-C., 15
Lei, Z., 20
Leng, W.H., 237
Le, X., 386
Liang, B., 284
Liang, Y., 233
Li, B., 18, 131–159
Li-ion battery, 266–270, 307, 309
Li, K., 20, 234
Lin, D., 281
Lindstrom, F., 74
Lin, G., 380
Lin, W.C., 45, 54
Lin, Y., 294
Li, S.M., 381
Liu, D., 301
Liu, F., 45
Liu, J., 110, 233, 383
Liu, L., 232, 234
Liu, R., 56
Liu, W., 304, 306
Li, W., 389
Li, X., 74
Li, Y., 12, 54, 386
Li, Y.B., 117
López-Luna, J., 178, 181
Lu, C.M., 330
Lu, D., 20

M
Maalouf, R., 117
Madhavan, J., 228
Maeda, K., 238
Mahlambi, M.M., 54
Mahmoodi, N.M., 42
Mahmoodzadeh, H., 170, 172
Maity, A., 317–343
Mao, X., 334
Ma, Y., 298
McMurray, T.A., 321
Md Sin, N.D., 386
Membrane process, 65–67, 70, 71, 147
Membrane separation, 64, 133, 135
Membrane synthesis, 141, 146, 149, 150
Messih, M.F.A., 233
Messina, P.V., 44
Metal resistance, 201, 207, 354, 355
Miao, A.J., 331
Miao, H., 238
Microbial nanoparticles, 202
Milani, N., 322
Min, Y., 18
Mishra, S., 175, 176
Miwa, T., 249
Mohamed, A.K.S.H., 179, 180
Mohapatra, S.R., 298
Molecular dynamics, 138
Moreno, M., 299
Mozia, S., 67, 68
Mridha, N., 317–343
Mukherjee, A., 317–343
Muller, M., 146
Musante, C., 331

N
Nagendran, M., 131–159
Nair, R., 171
Nair, V., 131–159
Nanobiosensor, 93–120
Nano-biosynthesis, 197, 198
Nanofibers, 64, 153–157, 168, 232, 233, 321, 357, 362, 364, 366, 372, 380, 382, 386, 390
Nanomaterials, 7–10, 14, 37, 38, 54, 77, 102–105, 115, 117, 118, 120, 137, 140, 153, 167–172, 174, 176, 178, 182, 184–187, 197, 203, 204, 215–251, 269, 319–321, 327, 328, 331–335, 337, 338, 340, 342, 349–392
Nanomaterials-based sensor, 349–391
Nanomaterials sensors, 353, 354, 368–372, 379, 385, 386, 389, 392
Nanoparticle properties, 197, 200, 202, 271, 275, 353
Nanoparticles (NPs), 22, 37, 103, 167, 197, 220, 269, 320, 358
Nanoporous desalination, 134, 138, 139, 155, 158
Nanoporous graphene, 151–153
Nanoremediation, 327, 328
Nanosensor, 114, 115, 117–120, 182, 183, 185, 186, 320, 321, 327, 329, 332, 334, 342, 343, 323, 325
Nanotechnology (NT), 1, 102, 133, 167, 197, 216, 318, 392
Naresh Kumar, S., 166
Neethirajan, S., 183
Nguyen-Phan, T.D., 233
Novoselov, K.S., 10

O
Ocsoy, I., 333
Oerke, E.C., 166
Opoku, F., 1–24

P
Pal, P., 282
Pal, S., 109
Paniel, N., 109
Pan, X., 20
Panyuta, O., 173, 175, 176
Papageorgiou, S.K., 69
Parkunan, T., 93–120
Parthibavarman, M., 386
Pascariu, P., 386
Patents, 45, 60, 71, 76, 155–158, 208, 209, 308, 309, 311
Pelaez, M., 41
Peng, Y.G., 43
Pereyra, J., 195–209
Photocatalysis, 2, 37, 216
Photocatalysts, 3–9, 16–22, 24, 35–77, 157, 216, 218, 220–222, 225–230, 233–236, 238, 241, 244, 245, 247, 248, 250, 329
Photodegradation, 1, 5, 6, 16, 18, 19, 41–47, 50, 53–58, 60, 62–64, 67, 69–71, 74–77, 227, 229, 230, 234, 331
Pinto, R.J., 333
Pisarenko, A.N., 384
Pollution sensor, 352, 372
Polu, A.R., 288
Polymer nanocomposites, 265–311
Pradas del Real, A.E., 169
Pramanik, P., 317–343
Prasad, T.N.V.V., 331
Pratt, R.C., 311
Precision farming, 321–323, 325, 326, 342
Production, 3, 64, 94, 157, 166, 197, 216, 267, 318, 378
Protection, 110, 165–187, 321, 331–333, 339, 340, 342
Protocols, 209, 324, 325, 335, 337, 343

Q
Qian, K., 333
Qian, Y., 333

R
Rafique, R., 172
Raghu, H.V., 93–120
Rai, V., 317–343
Ramalingam, C., 202
Ramesh, M., 171, 173
Rasuk, M.V., 195–209
Ren, Y., 15
Riahi-Madvar, A., 171
Rico, C.M., 172
Rico-Oller, B., 234
Rivas, G.A., 115
Roghayyeh, S.M.S., 331
Romero, C.M., 195–209

S
Saharan, V., 333
Sánchez-Muñoz, S., 234

Saran, R., 110
Saravanakumar, B., 20
Sarkar, S., 170
Savi, G.D., 175, 176
Scheufele, D.A., 335
Schneider, J., 228
Schultz, P.C., 44
Sebastián, J., 195–209
Semiconductor, 1–24, 39, 48, 61, 62, 76, 103, 112, 115, 183, 216, 221, 224–227, 234–238, 240, 244, 245, 250, 350, 353, 360, 369, 374, 377, 392
Sener, G., 110
Sengwa, R.J., 293
Sensor, 102, 105, 107–114, 116, 118, 183, 184, 325, 326, 334, 342, 349–391
Shafea, A.A., 174
Shaikh, F.I., 380
Sharma, A.L., 265–311
Sharma, S., 381
Sheng, O., 307
Shen, J.Y., 380
Siegrist, M., 335
Singh, D.P., 165–187
Singh, G.P., 165–187
Singh, M., 311
Singh, S., 182
Sin, M.L.Y., 379
Song, J.Y., 269
Stadler, T., 333
Stathatos, E., 44
Štengl, V.C., 20
Stephan, A.M., 269, 270
Subramaniam, M.N., 56
Sun, D., 173
Sun, L., 386

T
Tang, C., 285
Tang, D., 105
Tang, H., 382
Tang, J., 105
Tan, H., 106
Tao, J., 386
Taran, N., 169, 172, 178, 180
Teekateerawej, S., 75
Teodoro, S., 175
Thakare, S.R., 21
Thejaswini, T.V.L., 43
Titania, 23, 38–53, 55–57, 59–62, 64, 76, 77, 149, 216, 221, 232–234, 379, 387
Titanium dioxide (TiO2), 10, 38, 103, 167, 216, 282, 328, 354
Toloman, D., 386
Torney, F., 321
Tripathi, D.K., 170, 178, 181
Turan, J., 114

U
Ullah, K., 20
Ullah, S., 173

V
Vaez, M., 42
Vamvakaki, V., 321
Varshney, M., 117
Verma, S.K., 379
Vettiger, P., 326

W
Wang, C., 233, 288
Wang, F., 233
Wang, H., 14, 230
Wang, J., 381
Wang, P., 21
Wang, P.F., 234
Wang, R., 116
Wang, Y., 43
Wang, Z., 18, 20
Wan, Y., 117
Water remediation, 16, 23, 227–234, 250
Water-splitting, 57, 216, 225, 226, 234–239, 242–244, 251
Water treatments, 1–24, 37, 38, 41, 54, 55, 64–66, 76, 77, 132, 153, 159, 223, 226, 319, 328, 329
Watson, J.L., 184
Watts, D.J., 331
Wheat, 166, 321
White, J.C., 331
Wild, E., 169
Willmer, I., 76
Wu, C., 21
Wu, J., 183
Wypij, M., 199

X
Xiong, Z., 45
Xu, F., 20, 113
Xu, J.C., 57
Xu, T., 18
Xu, Z.-K., 143

Y
Yang, F.L., 175
Yang, G.J., 116, 117
Yang, J.-W., 15
Yang, L., 331
Yang, X., 21
Yang, Z., 75
Yao, X., 45
Yasmeen, F., 174
Yi, W., 42
Yoo, D.H., 234
Yu, J.C., 220

Z
Zaimenko, N.V., 178, 180
Zeolite membrane, 147–151
Zhang, D., 386
Zhang, F., 182
Zhang, H., 75, 233
Zhang, K., 233
Zhang, L., 331
Zhang, N., 233
Zhang, P., 306
Zhang, S., 238
Zhang, S.S., 270
Zhang, X., 19, 21, 69
Zhang, Y., 299
Zhao, C., 380
Zhao, D., 233
Zhao, T., 45
Zhao, Y., 285
Zhou, F., 21
Zhou, Q., 170
Zhou, W.S., 110
Zhu, J., 14
Zhu, K., 286
Zhuo, M., 386
Zhu, Y., 105
Zhu, Z., 385
Ziaee, M., 177
Zimmerman, M.A., 311
Zou, R., 233